



UNIVERSIDAD DE GRANADA

Facultad de Ciencias

Departamento de Química Orgánica

Programa de Doctorado en Química

*Synthesis of rotaxanes based on vinylsulfonyl "click" chemistry and study of their chiroptical properties.
Study of host-guest chemistry of curved PAHs.*

MEMORIA DE TESIS DOCTORAL

presentada por

ARTHUR H. G. DAVID

para optar al título de

DOCTOR EN QUÍMICA

Con mención INTERNACIONAL

Editor: Universidad de Granada. Tesis Doctorales
Autor: David, Arthur
ISBN: 978-84-1306-656-1
URI: <http://hdl.handle.net/10481/63945>

Acknowledgements

Esta tesis doctoral se ha llevado a cabo en los laboratorios del Departamento de Química Orgánica de la Universidad de Granada, en los grupos “MATERIALES ORGÁNICOS FUNCIONALES” (FQM-367) y “GLYCOCHEMBIO” (FQM-208). Este trabajo ha sido financiado por el Ministerio de Economía y Competitividad (MINECO FEDER CTQ2014-55474-C2-1-R, CTQ2017-85454-C2-1-P y UNGR15-CE-3478), el Ministerio de Ciencia, Innovación y Universidades (PGC2018-101181-B-I00 AEI/FEDER, UE), la Universidad de Granada (los programas: Visiting Scholars PP2016-VS01 y “Intensificación de la Investigación” PP2017-PRI-I-02 de Plan Propio de Investigación) y el European Research Council (ERC-2015-STG-677023).

En primer lugar, quiero agradecer sinceramente a mis directores de tesis, Dr. Victor Blanco Suárez y Dra. Araceli González Campaña, por haberme dado la oportunidad de realizar mi tesis, aquí, en Granada. Muchísimas gracias a vosotros dos por todos vuestros consejos, por haberme transmitido vuestro conocimiento y vuestro entusiasmo, y por vuestro apoyo en el laboratorio y fuera. Sois dos personas extraordinarias y muy inspiradoras, no podía haber soñado con algo mejor que haber hecho mi doctorado aquí con vosotros.

Quiero agradecer a Juanma por sus consejos, su optimismo, por compartir su enorme conocimiento y por abrirnos la mente constantemente durante los seminarios. Gracias a Paco por sus consejos y su apoyo en la investigación. Gracias Luis, Justi, Alba y Sara por vuestros consejos, vuestras sugerencias, vuestra alegría diaria y vuestra buena energía.

También, quiero agradecer a mi vecino de campana, Pablo G.-C., porque eres un tío muy simpático, me has ayudado muchísimas veces en mi vida granadina y también en los distintos proyectos de rotaxanos, gracias por enseñarme palabras y dichos españoles y por todos los momentos en el laboratorio donde siempre lo pasamos genial juntos. Vicente, el tío maldito de Priego, gracias por tu ayuda con el HPLC y el CPL y por los buenos momentos dentro y fuera del laboratorio. Carlos, gracias por la ayuda con el CPL, la voltametría y la síntesis de los nanografenos cuando empecé a sintetizarlos, siempre me acordaré del video clip que vimos juntos un día en el laboratorio. Rafa, gracias por todos los consejos, las discusiones y los debates interminables, por haber compartido conciertos y festivales perfectos juntos. Raquel, gracias por la ayuda con el rotaxano de CPL y por ser una persona muy simpática. Sandra, gracias por haberme enseñado a usar el BuLi y por ser alguien muy atenta con los demás. Irene, gracias por haberme enseñado que había que obtener un resultado excelente en el doctorado cuando empecé el mío. Miguel, gracias por los buenos momentos compartidos, siento que Francia ganara el mundial. Pablo R., gracias por escuchar mi música metal sin quejarte y hablar a veces

en japonés. Ana, gracias por siempre ser una persona muy simpática responder a mis “Holaaaaa” cuando entro en tu laboratorio. Mari, gracias por estar siempre feliz y sonriente. Silvia, gracias por tu simpatía y por los consejos para mi futuro. Edu, gracias por los buenos momentos en el lab y por poner Alestrom para el perro de vez en cuando. Rubén, gracias por ser una persona que siempre dice lo que piensa sin filtro, tanto para lo bueno como para lo malo. Pili, gracias por tu alegría y lo siento por el unicornio. Lucia, gracias por tu energía positiva contagiosa cuando estás en Granada. Karina, gracias por haber preparado muchas veces platos ricos mexicanos. Lola, gracias por autenticidad y por ser alguien amable y muy simpática. Fede, gracias por tu sinceridad, espero que un día podamos tocar la guitarra juntos. Marcos, gracias por compartir canciones muy especiales en el team veggie. Quiero también agradecer al resto de personas de la universidad con quien he tenido el placer de coincidir: Delia, Fernando, Javi, Aida, Paula, Clara, Mario, Felix y Mariano. Espero que los nuevos miembros del grupo, Juampe, Sandra y Jennifer, lo pasen tan bien como yo, aquí, en este maravilloso grupo.

I would like to thanks Prof. David A. Leigh (University of Manchester) for giving me the opportunity to join his group for a three-months stay. I learnt a lot and had so much fun in the lab making very interesting chemistry. I also would like to thank his whole group (Fredrick, Jeff, Julien, Lucian, Dan, Steve, Alberto, Valérie, Javi, ...) for making me feel at home in the laboratory and in Manchester.

Je tiens aussi à remercier sincèrement mes parents, Bruno et Pascale, car ils m’ont toujours été d’un soutien inconditionnel, toujours de bon conseil, toujours présents et à l’écoute. Je vous suis très reconnaissant pour cela et bien plus encore. Vous êtes des parents, des personnes parfaites. Merci pour tout. Je veux aussi remercier mes grand-parents (Henri, Yvette, Gérard et Christiane), Fanfan ainsi que toute ma famille, c’est aussi grâce à vous tous que j’en suis là. Merci aussi à toi Amélie, ma perle rare, mon âme sœur, ma muse, mon amour, la personne qui ensoleille ma vie depuis plus de 3 ans par-delà les montagnes et les océans. Tu es une personne géniale, parfaite, intelligente, gentille, drôle et bienfaitante qui, je l’espère, restera à mes côtés éternellement. Merci à toi aussi Caro, ma grande sœur, pour tout ce que tu fais et as fait pour moi et pour être là quand j’en ai besoin. Tu es géniale, merci simplement d’être toi. Merci aussi à Yves, Sylvain, Rémy, Nico, Yannick, Olivier et Marion. And finally, thank you Kedar, my good friend, I really enjoy every time I have the chance to talk with you about chemistry, life, philosophy and everything.

Dedicated to Gérard David, Yvette Le Blévec

Suzanne Ruelland, Tristan Boursicot

and Marie-Hélène Blain

Resumen

Los resultados presentados en esta tesis doctoral se dividen en dos partes diferenciadas. La primera de ella se centra en el desarrollo de nuevas metodologías sintéticas de rotaxanos y sus aplicaciones, y se divide a su vez en una introducción general y dos capítulos, mientras que la segunda parte consta de un único capítulo en el que se aborda el estudio de la química supramolecular de hidrocarburos aromáticos policíclicos (HAPs) con anillos de siete miembros.

En la primera parte se incluye inicialmente una introducción general en la que se presenta una revisión bibliográfica actualizada sobre los principales avances realizados hasta la fecha en el campo de la síntesis y aplicaciones de rotaxanos. Así, se exponen las posibles estrategias y los numerosos motivos estructurales y efectos plantilla que se han empleado para crear estructuras de tipo rotaxano. Además, se examina una característica clave de los rotaxanos para su aplicación como máquinas moleculares, como es el control de la posición relativa de los diferentes componentes en la estructura así como las aplicaciones que resultan de esta posibilidad.

El primer capítulo se titula "*Synthesis and applications of [2]rotaxanes using click Michael-type addition reactions to the vinyl sulfonyl group*" y está separado en dos bloques. El primero de ellos trata sobre la síntesis de rotaxanos, mientras que el segundo, sobre su desensamblaje. Respecto al primer bloque, se ha realizado un estudio bibliográfico acerca de las reacciones que se han utilizado en la síntesis de rotaxanos y una descripción de la adición de tipo Michael al grupo vinil sulfonilo y sus aplicaciones. A continuación, se presentan los resultados experimentales obtenidos en la aplicación, por primera vez, de esta reacción en la síntesis de rotaxanos basados en diferentes efectos plantilla: interacciones donador- π /aceptor- π , enlaces de hidrógeno y macrociclos de pilar[5]areno, con muy buenos rendimientos (53-91%). Por otra parte, haciendo uso de esta metodología se ha podido preparar un rotaxano de tipo donador- π /aceptor- π basado en un grupo diimida piromelítica y un éter corona aromático (DNP38C10) mediante el uso de iones litio como plantilla. Además, el rotaxano obtenido posee la capacidad de actuar como sensor de cationes metálicos (Li^+ , Sc^{3+} y In^{3+}).

En el segundo bloque de este capítulo se presenta un resumen del concepto de química de acoplamiento-y-desacoplamiento (CAD) adaptado al grupo vinil sulfonato y una descripción de los rotaxanos susceptibles de sufrir fragmentaciones de manera controlada, así como de máquinas moleculares basadas en sistemas entrelazados que exhiben un movimiento direccional de sus componentes, incluidos motores y bombas moleculares. Aquí, se describe el desensamblaje de un rotaxano empleando la química de acoplamiento-y-desacoplamiento del grupo vinil sulfonato. Posteriormente, se describe la aplicación de esta estrategia para controlar el transporte unidireccional

no reversible de un macrociclo a través del componente lineal de un rotaxano mediante un estímulo químico, en este caso la adición de nucleófilos.

El segundo capítulo se titula "*An "ON/OFF" circularly polarized luminescence switch based on a rotaxane architecture*". En la introducción de este capítulo se ha realizado un estudio bibliográfico sobre el fenómeno de emisión de luz polarizada circularmente (CPL), los emisores y los interruptores de CPL, así como ejemplos de rotaxanos quirales y las propiedades quirópticas descritas para estos compuestos. A continuación, se presenta la preparación y el funcionamiento del primer interruptor de CPL basado en un rotaxano. Esta máquina molecular está constituida de un macrociclo fluorescente y un eje que incluye un sistema de interruptor de pH con una estación quiral y una aquiral. La emisión de CPL se basa en una transmisión de la información quiral de un grupo quiral del eje al macrociclo luminiscente. Además, según la posición del macrociclo, la señal de CPL puede estar en modo "ON" o "OFF" manteniendo en todo caso la emisión fluorescente del macrociclo.

Por último, la segunda parte de esta tesis doctoral incluye el tercer capítulo titulado "*Supramolecular chemistry of saddle-shaped heptagon-containing nanographenes*". Este capítulo comienza con una introducción sobre grafeno, nanografenos, sus defectos estructurales y las posibles aplicaciones de moléculas que contengan estos defectos, centrándose en los nanografenos con curvatura negativa. Además, se ha realizado un estudio bibliográfico sobre la química supramolecular de HAPs extendidos planos y curvos, examinando sus propiedades de auto-asociación en disolución, sus propiedades receptor-sustrato y los materiales supramoleculares generados a partir de estos compuestos. De esta revisión se concluye que los nanografenos que contienen anillos heptagonales han sido muy poco explorados en este campo. En este contexto, en este capítulo, se exponen los resultados obtenidos combinando la síntesis y caracterización de nanografenos con estructura tipo silla de montar que incluyen un anillo heptagonal y un estudio de su auto-asociación en disolución y su capacidad para establecer interacciones supramoleculares con distintos sustratos aromáticos, planos y curvos, así como sistemas π -excedentes o π -deficientes. Por otra parte, se describe la síntesis de nanografenos anfífilos distorsionados con anillos de siete miembros, con el objetivo de utilizarlos para una posible aplicación en el autoensamblaje de materiales supramoleculares.

Summary

The results presented in this doctoral thesis are divided in two different parts. The first one, focused on the development of new synthetic methodologies to afford rotaxanes and their applications, is subdivided in a general introduction and two chapters, whereas the second one consists of a single chapter in which the study of the supramolecular chemistry of polycyclic aromatic hydrocarbons (PAHs) with seven-membered rings is discussed.

Firstly, in the first part, a general introduction is included with a literature review of the main advances achieved to date in the field of rotaxane synthesis and applications. Thus, the possible strategies and the numerous structural motifs and template effects employed to create rotaxane structures are displayed. Moreover, the key feature of rotaxanes for their applications as molecular machines, namely the control of the relative position of both components within this architecture, is discussed as well as the resulting applications coming from this possibility.

The first chapter is entitled "*Synthesis and applications of [2]rotaxanes using click Michael-type addition reactions to the vinyl sulfonyl group*" and separated in two blocks. The first one deals with the synthesis of rotaxanes, while the second one, with their disassembly. Regarding the first block, we conducted a literature review about the capping and closing reactions employed in rotaxane synthesis and a description of the Michael type addition to the vinyl sulfonyl group and its applications. Then, the experimental results obtained using, for the first time, this reaction in the synthesis of rotaxane based on π -donor/ π -acceptor interactions, hydrogen bonding and pillar[5]arene macrocycles in very good yield (53-91%) are presented. Moreover, using this methodology, a lithium-templated donor-acceptor rotaxane based on a pyromellitic diimide moiety and a crown ether ring (DNP38C10) has been prepared. Furthermore, this rotaxane can act as a sensor for metal cations (Li^+ , Sc^{3+} y In^{3+}).

In the second section of this chapter, an overview is presented of the coupling-and-decoupling concept (CAD) adapted to the vinyl sulfonate group and a description of rotaxanes able to be cleaved in a controlled manner, as well as molecular machines based on interlocked systems exhibiting a directional movement of their components, including molecular motors and pumps. Here, the disassembly of a rotaxane employing the vinyl sulfonate coupling-and-decoupling chemistry is demonstrated. Subsequently, we describe the application of this strategy to control the nonreversible unidirectional transportation of a macrocycle through the linear component of a rotaxane upon application of a chemical stimulus.

The second chapter is entitled "*An "ON/OFF" circularly polarized luminescence switch based on a rotaxane architecture*". In the introduction of this chapter, we discuss a literature study of the

phenomenon of circularly polarized luminescence (CPL), the CPL emitters and switches, as well as, examples of chiral rotaxanes and chiroptical properties reported for such compounds. Then, the preparation and the operation of the first CPL switch based on a rotaxane. This molecular machine is composed by a fluorescent macrocycle and a pH-driven switching system with both a chiral and an achiral station in the thread. The CPL emission is based on a chiral information transfer from the chiral group of the axle to the luminescent macrocycle. Furthermore, depending on the position of the macrocycle, the CPL signal can be turned “on” or “off”.

Finally, the second part of this doctoral thesis includes the third chapter entitled “*Supramolecular chemistry of saddle-shaped heptagon-containing nanographenes*”. This chapter begins with an introduction to graphene, nanographenes, their structural defects and the possible applications of molecules having such defects focusing on nanographenes with negative curvature. Furthermore, a literature review about the supramolecular chemistry of curved and planar extended PAHs is presented, discussing their self-association properties in solution, their host-guest properties and the supramolecular materials generated with such compounds. From this review, it can be concluded that nanographenes containing heptagonal rings remain unexplored in this field. In this context, within this chapter, the experimental results obtained combine the synthesis and characterisation of saddle-shaped nanographenes including a heptagonal ring with the study of their self-association in solution and their ability to establish supramolecular interactions with different aromatic molecules, planar and curved, as well as electron-rich or poor π -systems. Moreover, we describe the synthesis of three amphiphilic nanographene incorporating this type of curvature with the objective of applying them in possible future applications in self-assembly of supramolecular materials.

Table of contents

Table of contents

Terms and abbreviations	9
--------------------------------------	----------

PART A	15
---------------------	-----------

General introduction	17
-----------------------------------	-----------

1. History of synthetic mechanically interlocked molecules	19
2. Strategies to build rotaxanes.....	21
3. Non-covalent interactions and templates in rotaxane synthesis.....	23
3.1. Hydrogen bonding	23
3.2. π - π interactions	25
3.2.1. π -donor/ π -acceptor interactions	25
3.2.2. Carbon nanostructures.....	27
3.3. Solvophobic forces	28
3.4. Metal coordination.....	30
3.4.1. Passive metal template	30
3.4.2. Active metal template	31
3.5. Other interactions and templates	32
3.5.1. Anion binding template.....	32
3.5.2. Pillar[n]arenes	32
3.5.3. Radical-pair templates.....	33
4. Molecular switches based on rotaxane architectures	34
4.1. pH-driven switches	34
4.2. Redox switches	35
4.3. Photo-switches	38
4.4. Solvent-driven switches.....	41
4.5. Anion switches.....	42

4.6. Cation switches.....	45
5. Molecular machines based on rotaxanes.....	47
5.1. Macroscopic work	48
5.2. Nanovalves	50
5.3. Synthesis.....	51
5.3.1. Peptide synthesizers.....	51
5.3.2. Switchable catalysis.....	52
5.4. Modulation of the fluorescence.....	54
5.5. Logic gates	56

Chapter 1: Synthesis and applications of [2]rotaxanes using click Michael-type addition reactions to the vinyl sulfonyl group 59

1. A new efficient and versatile reaction in rotaxane synthesis	61
1.1 Background.....	61
1.1.1. Reactions for rotaxane synthesis through end-capping.....	61
1.1.2. Michael-type addition reaction of nucleophiles to vinyl sulfonyl groups.....	64
1.2. Objectives	67
1.3. Results and discussion.....	69
1.3.1. Synthesis of rotaxanes based on π -donor/ π -acceptor interactions.....	69
1.3.2. Synthesis of rotaxanes based on hydrogen bonding	74
1.3.2.1. Rotaxanes containing a tetralactam ring	74
1.3.2.2. Rotaxanes containing a crown ether ring.....	80
1.3.3. Synthesis of pillar[5]arene-based rotaxanes	85
1.3.4. A lithium-templated donor-acceptor rotaxane.....	90
1.3.4.1. Synthesis and characterization.....	90
1.3.4.2. Cation sensing	98

1.4. Conclusions.....	105
2. Vinyl sulfonate coupling-and-decoupling chemistry applied to rotaxanes.....	107
2.1. Background.....	107
2.1.1. Coupling-and-decoupling chemistry of the vinyl sulfonate group.....	107
2.1.2. Cleavable rotaxanes	108
2.1.3. Directional transport in rotaxanes	108
2.2. Objectives	115
2.3. Results and discussion.....	117
2.3.1. Chemical disassembly of a [2]rotaxane.....	117
2.3.2. Unidirectional transport of a macrocycle in a [2]rotaxane through CAD chemistry.....	121
2.4. Conclusions.....	137
3. Experimental section.....	139
3.1. General details.....	139
3.2. Synthetic procedures and characterization details.....	140
3.3. UV-Vis studies.....	190
3.4. HPLC method.....	192
3.5. NMR spectra of final compounds.....	193

Chapter 2: An “ON/OFF” circularly polarized luminescence switch based on a rotaxane architecture

..... **223**

1. Background.....	225
1.1. Chiroptical properties.....	225
1.2 CPL emitters.....	227
1.3. CPL switches	228
1.4. Chiral rotaxanes.....	231
1.5. Chiroptical properties of rotaxanes.....	235

2. Objectives	241
3. Results and discussion	243
3.1. Synthesis and characterization	243
3.1.1 Synthesis of the macrocycle	244
3.1.2. Synthesis of the thread precursors	246
3.1.3. Synthesis of threads and rotaxanes	248
3.2. Study and switching of the chiroptical properties	252
4. Conclusions	261
5. Experimental section	263
5.1. General details	263
5.2. Synthetic procedures and characterization details	264
5.3. HPLC method	277
5.4. Photophysical properties	277
5.5. Statistical Analysis of the CPL data	279
5.5.1. Statistical analysis of the CPL spectra of rotaxane (S)-162	279
5.5.1.1. Statistical analysis based on the area	279
5.5.1.2. Statistical analysis based on the intensity	282
5.5.2. Statistical analysis of the CPL data of the operation cycles	283
5.6. Single crystal X-ray diffraction analysis	285
5.7. NMR spectra of key compounds	287

PART B 293

Chapter 3: Supramolecular chemistry of saddle-shaped heptagon-containing nanographenes..... 295

1. Background	297
1.1 Graphene and nanographenes	297
1.2 Defects and distortion in graphene and nanographenes	298

1.3. Supramolecular chemistry of planar and curved PAHs	300
1.3.1. Self-association of HBC derivatives in solution	300
1.3.2. Host-guest properties of PAHs bigger than coronene and corannulene	302
1.3.2.1. PAH-based hosts.....	302
1.3.2.2. PAHs as guests.....	304
1.3.3. PAH-based supramolecular materials	305
1.3.3.1. Liquid crystals	305
1.3.3.2. Supramolecular nanotubular and nanofibrous assemblies	307
1.3.3.3. Supramolecular gels	308
2. Objectives.....	311
3. Results and discussion.....	313
3.1. Self-association and host-guest properties of heptagon-containing nanographenes.....	313
3.1.1. Synthesis and characterization.....	313
3.1.2. Study of the self-association	318
3.1.3. Study of the host-guest properties	321
3.2. Functionalization of saddle-shaped nanographenes towards supramolecular nanostructured assemblies	327
3.2.1. Synthesis and characterization.....	327
3.2.2. Preliminary study to form supramolecular aggregates.....	331
4. Conclusions.....	335
5. Experimental section.....	337
5.1. General details.....	337
5.2. Synthetic procedures and characterization details.....	338
5.3. NMR spectra of target nanographenes	352
5.4. Self-association studies	358
5.5. ^1H and ^{13}C titrations.....	358
5.5.1. PAHs binding NMR studies	358
5.5.2. Fullerenes binding NMR studies.....	358

5.6. Computational methods..... 358

General conclusions..... 361

Terms and abbreviations

18C6	18-Crown-6
aq.	Aqueous
ATP	Adenosine triphosphate
B21C7	Benzo-21-crown-7
BAr^F₄	Tetrakis(3,5-bis(trifluoromethyl)phenyl)borate
BINOL	1,1'-Bi-2-naphthol
Boc	<i>tert</i> -Butoxycarbonyl
BPE	1,2-Bis(4,4-dipyridinium)ethane
BPP34C10	Bis(<i>para</i> -phenylene)-34-crown-10
BPX26C6	Bis- <i>para</i> -xylyl-[26]crown-6
br	Broad
CAD	Coupling-and-Decoupling
CBPQT⁴⁺	Cyclobis(paraquat- <i>para</i> -phenylene)
CD	Circular dichroism
COSY	Bidimensional proton/proton correlation spectroscopy
CPL	Circularly Polarized Luminescence
CuAAC	Copper(I)-catalyzed azide alkyne cycloaddition
d	Doublet
DABCO	1,4-Diazabicyclo[2.2.2]octane
DB24C8	Dibenzo-24-crown-8
dba	Dibenzylideneacetone
DBU	1,8-Diazabicyclo[5.4.0]undec-7-ene
DCB	Dichlorobenzene
DCM	Dichloromethane
DDQ	2,3-Dichloro-5,6-dicyano-1,4-benzoquinone

DEAD	Diethyl azodicarboxylate
DIPEA	N,N-Diisopropylethylamine
DMAP	4-Dimethylaminopyridine
DMF	N,N-Dimethylformamide
DMSO	Dimethyl sulfoxide
DNP38C10	1,5-Dinaphtho-38-crown-10
DOSY	Diffusion ordered spectroscopy
ECD	Electronic circular dichroism
EDCI	N-(3-Dimethylaminopropyl)-N'-ethylcarbodiimide
EI	Electron ionization
Eq.	Equation
equiv.	Equivalent
ESI	Electrospray ionization
Fmoc	Fluorenylmethoxycarbonyl
HBC	Hexa- <i>peri</i> -hexabenzocoronene
hept-HBC	Heptagon-containing hexa- <i>peri</i> -hexabenzocoronene
HMBC	Heteronuclear Multiple Bond Correlation
HMDS	Bis(trimethylsilyl)amine
HOBt	Hydroxybenzotriazole
HPLC	High-performance liquid chromatography
HRMS	High-resolution mass spectrometry
HSQC	Heteronuclear single quantum correlation
Hz	Hertz
J	Coupling constant
m	Multiplet

MALDI	Matrix-assisted laser desorption ionization
MAVS	Michael type Addition to the Vinyl Sulfonyl group
MIMs	Mechanically Interlocked Molecules
MOFs	Metal–organic frameworks
MS	Molecular sieves
ν	Wavelength
NDI	Naphthalene diimide
NMR	Nuclear magnetic resonance
O/N	Overnight
OLED	Organic light-emitting diode
p	Quintet
PAHs	Polycyclic aromatic hydrocarbons
PDI	Perylene diimide
PEM	Photo-elastic modulator
phen	1,10-Phenanthroline
PMT	Photomultiplier tube
Pr	Propyl
QY	Quantum yield
r.t.	Room temperature
s	Singlet
sat	Saturated
STEM	Scanning transmission electron microscope
t	Triplet
TBAF	tetrabutylammonium fluoride
TBDMS	<i>tert</i> -Butyldimethylsilyl

TBTA	Tris((1-benzyl-4-triazolyl)methyl)amine
^tBu	<i>tert</i> -Butyl
terpy	Terpyridine
THF	Tetrahydrofuran
TLC	Thin-layer chromatography
TMS	Trimethylsilane
t_R	Retention time
Trt	Trityl
TTF	Tetrathiafulvalene
XPhos	2-Dicyclohexylphosphino-2',4',6'-triisopropylbiphenyl

PART A

General introduction

1. History of synthetic mechanically interlocked molecules

Mechanically interlocked molecules (MIMs) are a class of molecules that feature a mechanical bond which is an entanglement in space between two components of the compound that cannot be dissociated without breaking a covalent bond. These type of structures include catenanes,¹ which are composed by two or more interlocked rings, knots² and rotaxanes,³ which consist of a dumbbell-shaped molecule owning a ring trapped between its two bulky groups. Thus, in a rotaxane, the only way to take the system apart is to break a covalent bond in the axle or the macrocycle.

Probably the main reason for the relevance and the importance of the synthesis of this type of architectures is the design and preparation of artificial molecular machines, in an attempt to mimic nature.⁴ Indeed, there are numerous molecular machines in living organisms, but also a vast number of MIMs in nature, especially catenanes, such as catenated circular DNA,⁵ proteins⁶ or enzymes.⁷ Consequently, in 2016, Jean-Pierre Sauvage, Sir J. Fraser Stoddart and Bernard L. Feringa received the Nobel Prize in Chemistry for the design and synthesis of molecular machines.⁸

The journey towards these devices started in 1960 when Edle Wasserman synthesized the first MIM: a catenane.⁹ For this purpose, he used a statistical approach and showed that following an acyloin condensation in the presence of a deuterated macrocycle, catenane **1** (Figure 1a) which contained both the deuterium atoms and the acyloin functional group was generated in about 0.0001% yield.¹⁰ Four years later, Schill and Lüttringhaus prepared and isolated their catenane by a directed multistep synthesis method.¹¹ Regarding rotaxanes, their first syntheses were reported in 1967. Thus, Schill and Zollenkopf obtained this structure using a directed multistep synthesis approach¹² while Harrison and Harrison employed a statistical method¹³ (Figure 1b). In both cases, low yields were obtained.

¹ G. Gil-Ramírez, D. A. Leigh, A. J. Stephens, *Angew. Chem., Int. Ed.* **2015**, *54*, 6110-6150.

² S. D. P. Fielden, D. A. Leigh, S. L. Woltering, *Angew. Chem., Int. Ed.* **2017**, *56*, 11166-11194.

³ M. Xue, Y. Yang, X. Chi, X. Yan, F. Huang, *Chem. Rev.* **2015**, *115*, 7398-7501.

⁴ S. Erbas-Cakmak, D. A. Leigh, C. T. McTernan, A. L. Nussbaumer, *Chem. Rev.* **2015**, *115*, 10081-10206.

⁵ B. Hudson, J. Vinograd, *Nature* **1967**, *216*, 647-652.

⁶ W. R. Wikoff, L. Liljas, R. L. Duda, H. Tsuruta, R. W. Hendrix, J. E. Johnson, *Science* **2000**, *289*, 2129-2133.

⁷ Z. Cao, A. W. Roszak, L. J. Gourlay, J. G. Lindsay, N. W. Isaacs, *Structure* **2005**, *13*, 1661-1664.

⁸ *The Nobel Prize in Chemistry 2016—Advanced Information*. Nobelprize.org. Nobel Media AB 2014. Web. October 6, 2016, http://www.nobelprize.org/nobel_prizes/chemistry/laureates/2016/advanced.html.

⁹ E. Wasserman, *J. Am. Chem. Soc.* **1960**, *82*, 4433-4434.

¹⁰ E. Wasserman, *Sci. Am.* **1962**, 94-102.

¹¹ G. Schill, A. Lüttringhaus, *Angew. Chem. Int. Ed. Engl.* **1964**, *3*, 546-547.

¹² G. Schill, H. Zollenkopf, *Nachr. Chem. Techn.* **1967**, *15*, 149-150.

¹³ I. T. Harrison, S. Harrison, *J. Am. Chem. Soc.* **1967**, *89*, 5723-5724.

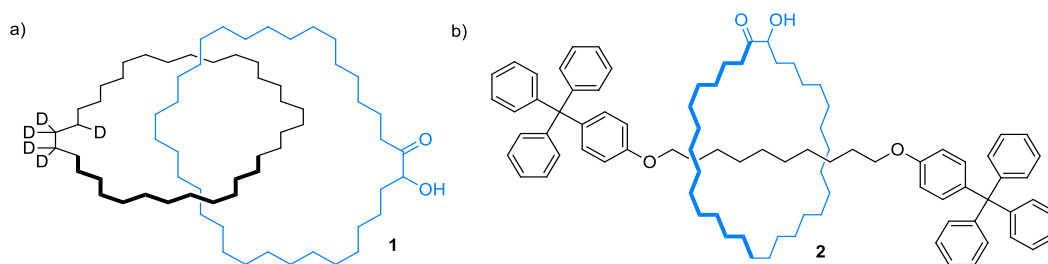
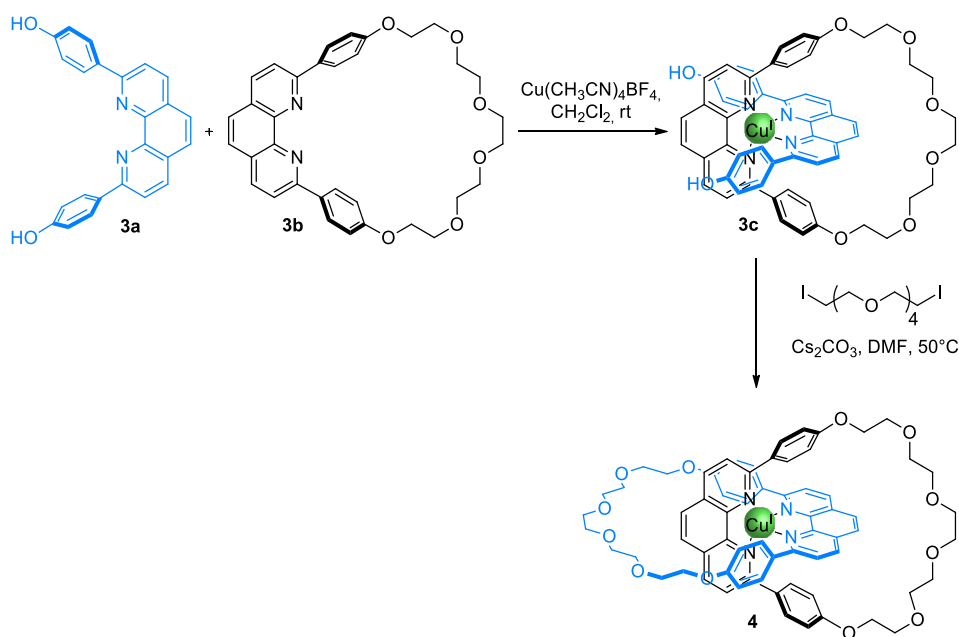


Figure 1. The first synthetic mechanically interlocked molecules: a) The Wasserman catenane (**1**).⁹ b) [2]Rotaxane developed by Harrison and Harrison (**2**).¹³

In 1983, Sauvage and co-workers made a huge breakthrough in the field of supramolecular chemistry by employing the template effect in the synthesis of MIMs. Using a Cu^{I} cation as template and a Williamson reaction, they succeeded to create catenane **4** in a relevant 42% yield (Scheme 1) making the synthesis of MIMs more accessible.¹⁴ Based on the same idea, in 1989, the same group managed to obtain a trefoil knot in 3% yield.¹⁵ Similarly, in 1991, Gibson and co-workers created the first transition metal-templated rotaxane in 42% yield.¹⁶ The same year, Stoddart exploited the π - π interactions to build the first molecular shuttle (**5**· 4PF_6^-) (Scheme 2).¹⁷



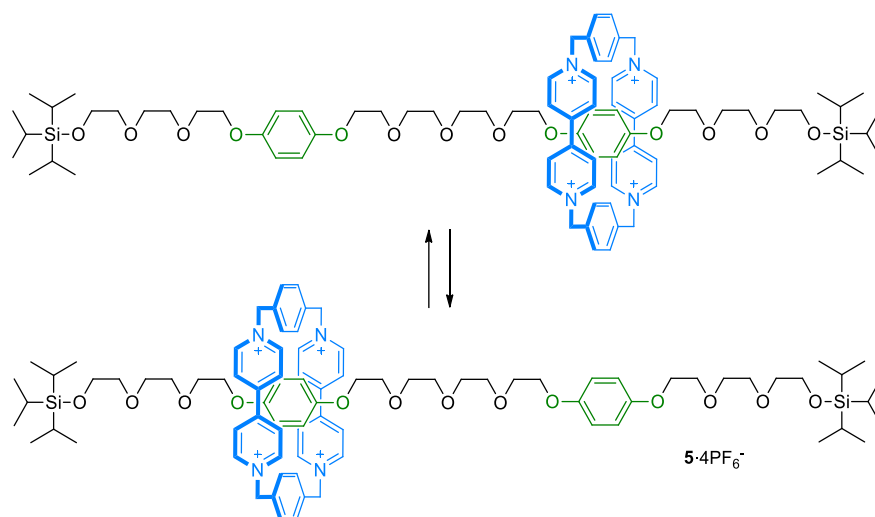
Scheme 1. Metal-templated strategy to afford [2]catenane **4**.¹⁴

¹⁴ C. O. Dietrich-Buchecker, J.-P. Sauvage, J.-P. Kintzinger, *Tetrahedron Lett.* **1983**, *24*, 5095-5098.

¹⁵ C. O. Dietrich-Buchecker, J.-P. Sauvage, *Angew. Chem. Int. Ed. Engl.* **1989**, *28*, 189-192.

¹⁶ C. Wu, P. R. Lecavalier, Y. X. Shen, H. W. Gibson, *Chem. Mater.* **1991**, *3*, 569-572.

¹⁷ P. L. Anelli, N. Spencer, J. F. Stoddart, *J. Am. Chem. Soc.* **1991**, *113*, 5131-5133.



Scheme 2. First bistable molecular shuttle, developed by Stoddart.¹⁷

Following these pioneering works, more and more chemists started to work in this area, developing new strategies to construct rotaxanes, catenanes and knots in order to study their properties and find ways to take advantage of these devices to build molecular machines.^{4,18}

2. Strategies to build rotaxanes

Nowadays, the synthesis of rotaxanes is based on the template effect,¹⁹ in other words, the self-assembly of molecules using non-covalent interactions, such as halogen or hydrogen bonding, metal coordination, van der Waals forces, solvophobic effect or π - π interactions, with the aim of preorganizing the linear and the circular components before undertaking the rotaxane formation reaction. Consequently, various strategies for the formation of rotaxane architectures were described.³

The capping approach is one of the easiest and most useful techniques to obtain rotaxanes. First, a pseudorotaxane, which is the inclusion complex resulting from the interaction between the macrocycle and the thread, is formed. Subsequently, a reaction with a bulky stopper occurs on each side of the linear compound generating the desired rotaxane (Figure 2).^{3,16} Regarding the clipping method, the thread is already blocked on both sides and the macrocycle is built around the axle to give the rotaxane (Figure 2).^{3,17} Another approach is the slipping. Here, the thread possess two specific stoppers that create a steric energetic barrier that lets the ring pass through at high temperature, while at a lower temperature, it hampers its release (Figure 2).^{3,20} More recently, the active metal template

¹⁸ C. J. Bruns, J. F. Stoddart, *The Fundamentals of Making Mechanical Bonds*. John Wiley & Sons: Hoboken, **2016**.

¹⁹ F. Diederich, P. J. Stang, *Templated Organic Synthesis*. Wiley-VCH: Weinheim, **2000**.

²⁰ P. R. Ashton, M. Belohradsky, D. Philp, N. Spencer, J. F. Stoddart, *J. Chem. Soc., Chem. Commun.* **1993**, 1269-1274.

strategy has been developed. In this approach, the macrocycle coordinates a metal center which catalyzes a bond-forming reaction inside the ring in order to build a new covalent bond between two thread precursors, giving rise to a mechanical bond (Figure 2).²¹ A few metal-free versions of the active template method have also been reported.²²

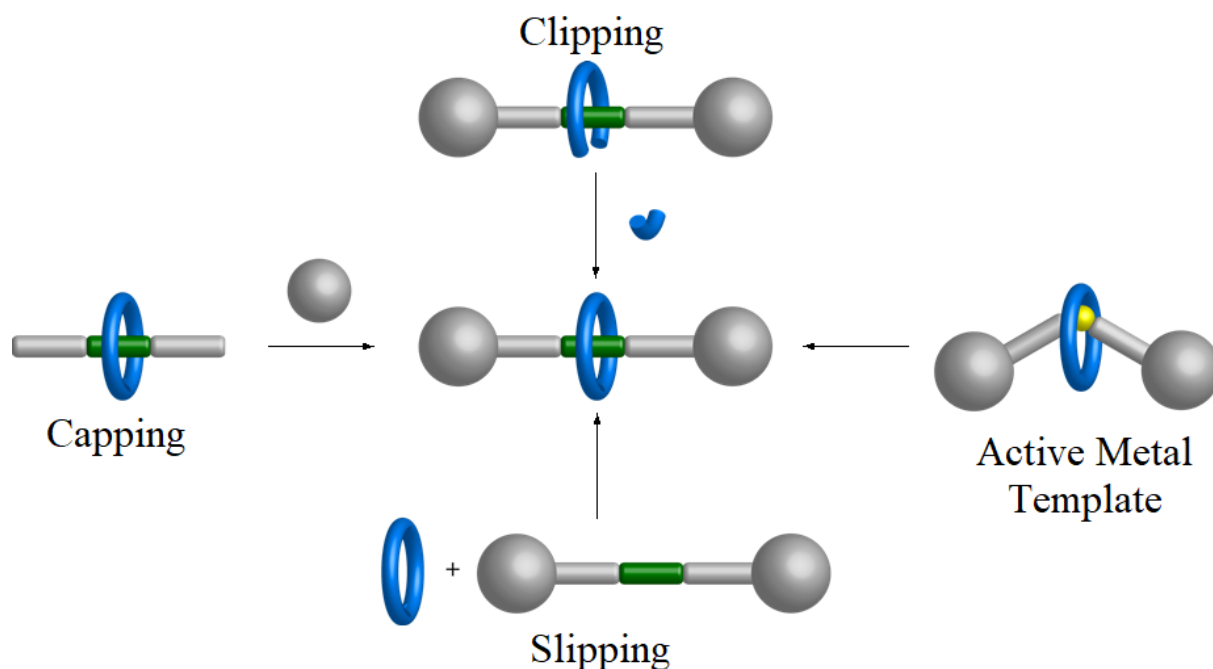


Figure 2. Graphical representation of the most common strategies for rotaxane synthesis.

Furthermore, two other methodologies that engender mechanical bonds exist but have not been extensively used yet. In the shrinking procedure, the axle threaded through the macrocycle. The latter is shrunk in order to reduce its circumference and thus, to disable its exit.²³ On the other side, in the swelling approach, after the threading, one or both stoppers undergo a reaction with the aim of increasing their volume and impeding the dethreading of the macrocycle, thereby generating a rotaxane.²⁴

²¹ a) J. D. Crowley, S. M. Goldup, A.-L. Lee, D. A. Leigh; R. T. McBurney, *Chem. Soc. Rev.* **2009**, *38*, 1530-1541.
b) M. Denis, S. M. Goldup, *Nat. Rev. Chem.* **2017**, *1*, 61.

²² a) X. Hou, C. Ke, J. F. Stoddart, *Chem. Soc. Rev.* **2016**, *45*, 3766-3780. b) S. D. P. Fielden, D. A. Leigh, C. T. McTernan, B. Pérez-Saavedra, I. J. Vitorica-Yrezabal, *J. Am. Chem. Soc.* **2018**, *140*, 6049-6052.

²³ I. Yoon, M. Narita, T. Shimizu, M. Asakawa, *J. Am. Chem. Soc.* **2004**, *126*, 16740-16741.

²⁴ C.-W. Chiu, C.-C. Lai, S.-H. Chiu, *J. Am. Chem. Soc.* **2007**, *129*, 3500-3501.

3. Non-covalent interactions and templates in rotaxane synthesis

3.1. Hydrogen bonding

Typically, there are two families of macrocycles which involve H bonds as the main interaction with different binding sites to create MIMs. The first group are crown ethers, whose synthesis was developed and improved by Pedersen²⁵ and the second one are the amide-based macrocycles.

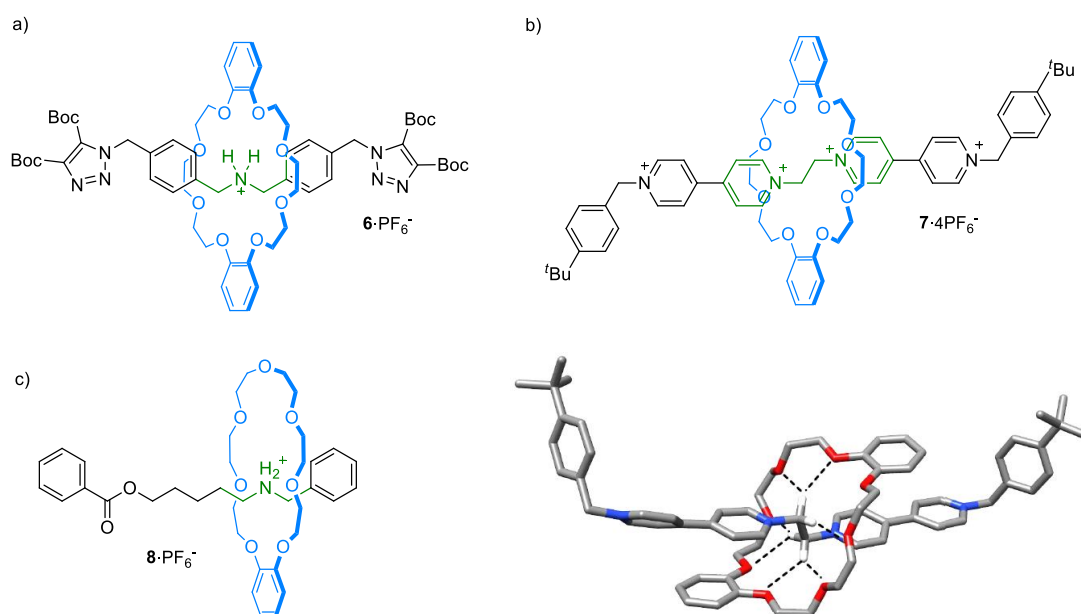


Figure 3. Different rotaxanes based on hydrogen bonds owning a crown ether: a) A dibenzylammonium-based [2]rotaxane reported by Stoddart.^{27a} b) BPE-based [2]rotaxane described by Loeb and its X-ray diffraction structure.³¹ Color coding: C, grey; O, red; N, blue; H, white. c) B21C7 [2]rotaxane reported by Huang.²⁸

In 1996, Stoddart and co-workers showed that DB24C8 is a perfect wheel to bind dialkylammonium salts and generate a pseudorotaxane.²⁶ Based on this system, many rotaxanes with this particular crown ether and an binding motif were created (Figure 3).²⁷ Besides this excellent ring, B21C7²⁸ and other crown ether macrocycles²⁹ were employed with this specific recognition site to generate rotaxanes. In 1998, Loeb reported a new binding motif for DB24C8 called, 1,2-Bis(4,4-

²⁵ a) C. J. Pedersen, *J. Am. Chem. Soc.* **1967**, *89*, 2495-2496. b) C. J. Pedersen, *J. Am. Chem. Soc.* **1967**, *89*, 7017-7036.

²⁶ P. R. Ashton, E. J. T. Chrystal, P. T. Glink, S. Menzer, C. Schiavo, N. Spencer, J. F. Stoddart, P. A. Tasker, A. J. P. White, D. J. Williams, *Chem. Eur. J.* **1996**, *2*, 709-728.

²⁷ Selected examples: a) P. R. Ashton, P. T. Glink, J. F. Stoddart, P. A. Tasker, A. J. P. White, D. J. Williams, *Chem. Eur. J.* **1996**, *2*, 729-736. b) H. Nagai, Y. Suzaki, K. Osakada, *Chem. Lett.* **2016**, *45*, 834-836.

²⁸ C. Zhang, S. Li, J. Zhang, K. Zhu, N. Li, F. Huang, *Org. Lett.* **2007**, *9*, 5553-5556.

²⁹ Selected examples: a) S. J. Cantrill, M. C. T. Fyfe, A. M. Heiss, J. F. Stoddart, A. J. P. White, D. J. Williams, *Chem. Commun.* **1999**, 1251-1252. b) P. T. Glink, A. I. Oliva, J. F. Stoddart, A. J. P. White, D. J. Williams, *Angew. Chem. Int. Ed.* **2001**, *40*, 1870-1875.

dipyridinium)ethane (BPE),³⁰ giving the possibility to access to new interlocked compounds (Figure 3b).³¹

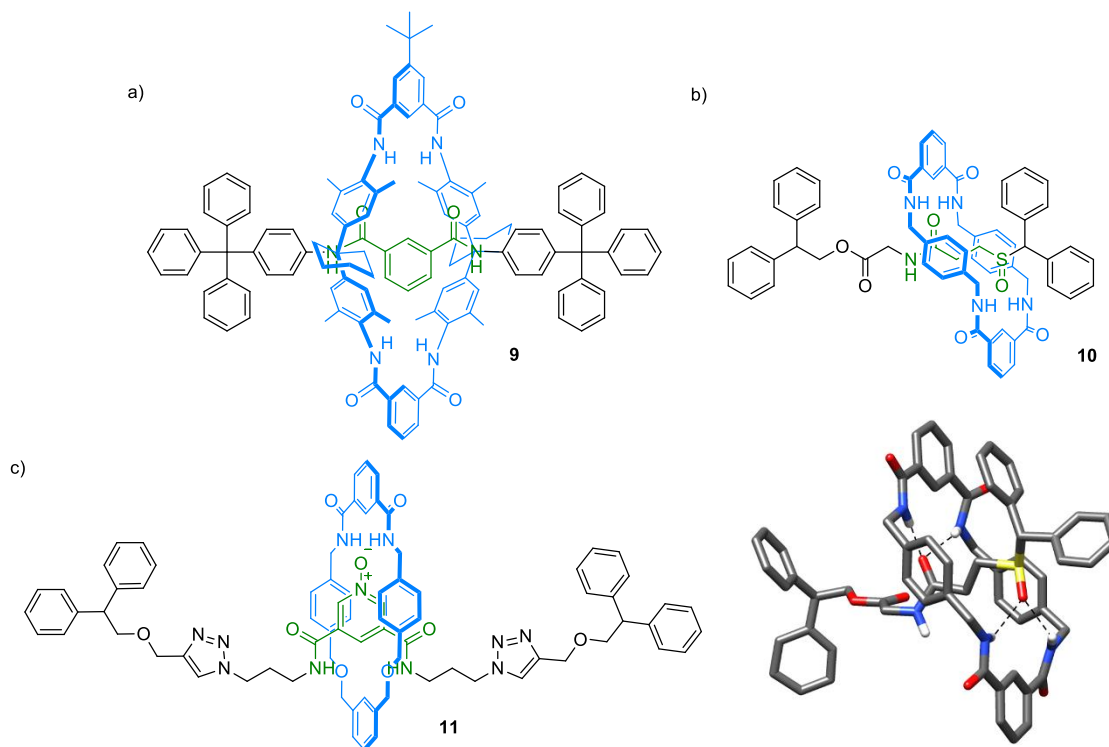


Figure 4. Selected examples of H bonding rotaxanes featuring amide-based macrocycles: a) The first amide-based [2]rotaxane developed by Vögtle.³² b) A sulfoxide [2]rotaxane reported by Leigh and its X-ray diffraction structure.³⁵ Color coding: C, grey; O, red; N, blue; H, white; S, yellow. c) Pyridine-N-oxide isophthalamide [2]rotaxane described by Evans.^{34b}

Regarding rotaxanes incorporating amide-based macrocycles, the first synthesis was achieved in 1995 by Vögtle and co-workers. For this purpose, they used a Hunter/Vögtle-type tetralactam ring and a thread owning amide moieties (Figure 4a).³² After this achievement, other rotaxanes featuring Hunter/Vögtle-type anilide or Leigh-type benzamide macrocycles and different amides as binding motifs were designed.³³ Furthermore, recognition sites other than amides for tetralactam macrocycles were employed in order to get rotaxanes. Indeed, N^+-O^- ,³⁴ $S=O$,³⁵ and $P=O$ ³⁶ groups are hydrogen-bond

³⁰ S. J. Loeb, J. A. Wisner, *Angew. Chem. Int. Ed.* **1998**, *37*, 2838-2840.

³¹ S. J. Loeb, J. A. Wisner, *Chem. Commun.* **1998**, 2757-2758.

³² F. Vögtle, M. Händel, S. Meier, S. Ottens-Hildebrandt, F. Ott, T. Schmidt, *Liebigs Ann./Recl.* **1995**, 739-743.

³³ Selected examples: a) F. Vögtle, R. Jäger, M. Händel, S. Ottens-Hildebrandt, W. Schmidt, *Synthesis* **1996**, 353-356. b) F. G. Gatti, D. A. Leigh, S. A. Nepogodiev, A. M. Z. Slawin, S. J. Teat, J. K. Y. Wong, *J. Am. Chem. Soc.* **2001**, *123*, 5983-5989.

³⁴ a) D. M. D'Souza, D. A. Leigh, L. Mottier, K. M. Mullen, F. Paolucci, S. J. Teat, S. Zhang, *J. Am. Chem. Soc.* **2010**, *132*, 9465-9470. b) N. H. Evans, C. E. Gell, M. J. G. Peach, *Org. Biomol. Chem.* **2016**, *14*, 7972-7981.

³⁵ A. Altieri, V. Aucagne, R. Carrillo, G. J. Clarkson, D. M. D'Souza, J. A. Dunnett, D. A. Leigh, K. M. Mullen, *Chem. Sci.* **2011**, *2*, 1922-1928.

³⁶ R. Ahmed, A. Altieri, D. M. D'Souza, D. A. Leigh, K. M. Mullen, M. Papmeyer, A. M. Z. Slawin, J. K. Y. Wong, J. D. Woollins, *J. Am. Chem. Soc.* **2011**, *133*, 12304-12310.

acceptors efficient enough to act as templates in rotaxane formation (Figure 4) as well as other groups like diketopiperazine,³⁷ squaraine³⁸ or pyridyl-acyl hydrazone³⁹ cores. This versatility expands the range of binding motifs that can be employed and, therefore, the possible designs for their application as, for example, molecular shuttles.

3.2. π - π interactions

3.2.1. π -donor/ π -acceptor interactions

There are mainly two types of macrocycles employed to build rotaxanes involving π -donor/ π -acceptor interactions. The first family contains crown ethers such as bis(*para*-phenylene)-34-crown-10 (BPP34C10) or 1,5-dinaphtho-38-crown-10 (DNP38C10), while the second one includes tetracationic cyclophanes like cyclobis(*para*quat-*para*-phenylene) (CBPQT⁴⁺).

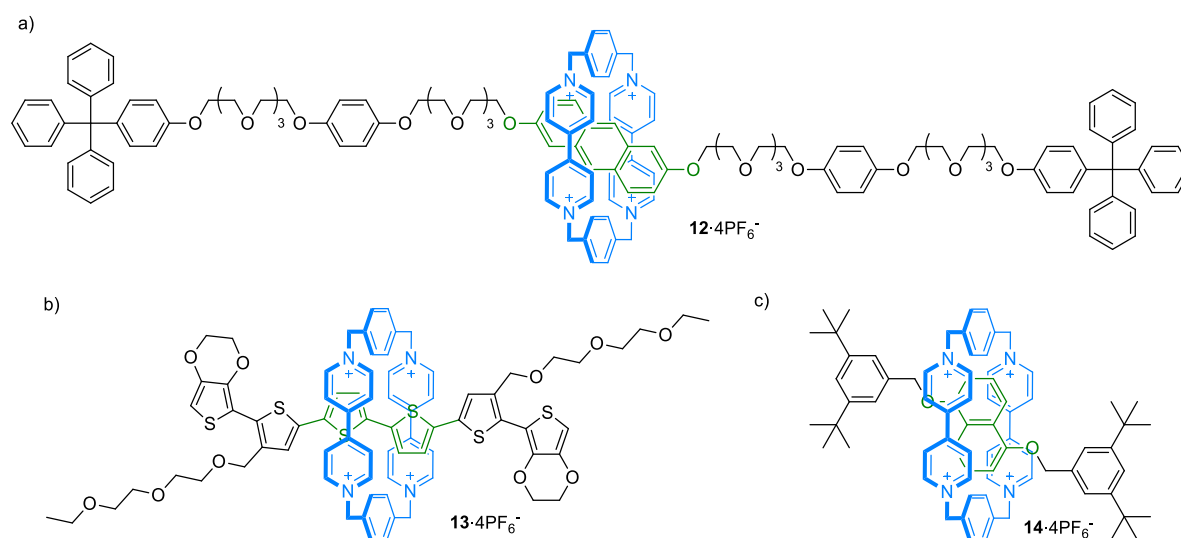


Figure 5. Selected rotaxanes with the CBPQT⁴⁺ ring: a) A 2,6-dialkoxyanthracene-based [2]rotaxane reported by Balzani and Stoddart.⁴⁰ b) [2]Rotaxane incorporating thiophenes reported by Ikeda.⁴³ c) A [2]rotaxane owning a 1,5-dialkoxy naphthalene core described by Jeppesen.⁴¹

Regarding tetracationic cyclophanes, in 1991, Stoddart and co-workers efficiently synthesized the first molecular shuttle (**5**·4PF₆⁻) based on a rotaxane architecture using CBPQT⁴⁺, an electron-poor aromatic ring, and a rod with substituted hydroquinones, an electron-rich group (Scheme 2).¹⁷ Throughout the years, this strategy was extended to other π -electron-rich aromatic rings, such as, 2,6-

³⁷ E. V. Dzyuba, L. Kaufmann, N. L. Löw, A. K. Meyer, H. D. F. Winkler, K. Rissanen, C. A. Schalley, *Org. Lett.* **2011**, *13*, 4838-4841.

³⁸ C. G. Collins, J. M. Baumes, B. D. Smith, *Chem. Commun.* **2011**, *47*, 12352-12354.

³⁹ D. A. Leigh, V. Marcos, T. Nalbantoglu, I. J. Vitorica-Yrezabal, F. T. Yasar, X. Zhu, *J. Am. Chem. Soc.* **2017**, *139*, 7104-7109.

dialkoxyanthracene,⁴⁰ tetrathiafulvalene (TTF),⁴¹ 1,5-dialkoxynaphtalene,⁴¹ benzidine,⁴² biphenol⁴² or thiophene⁴³ (Figure 5).

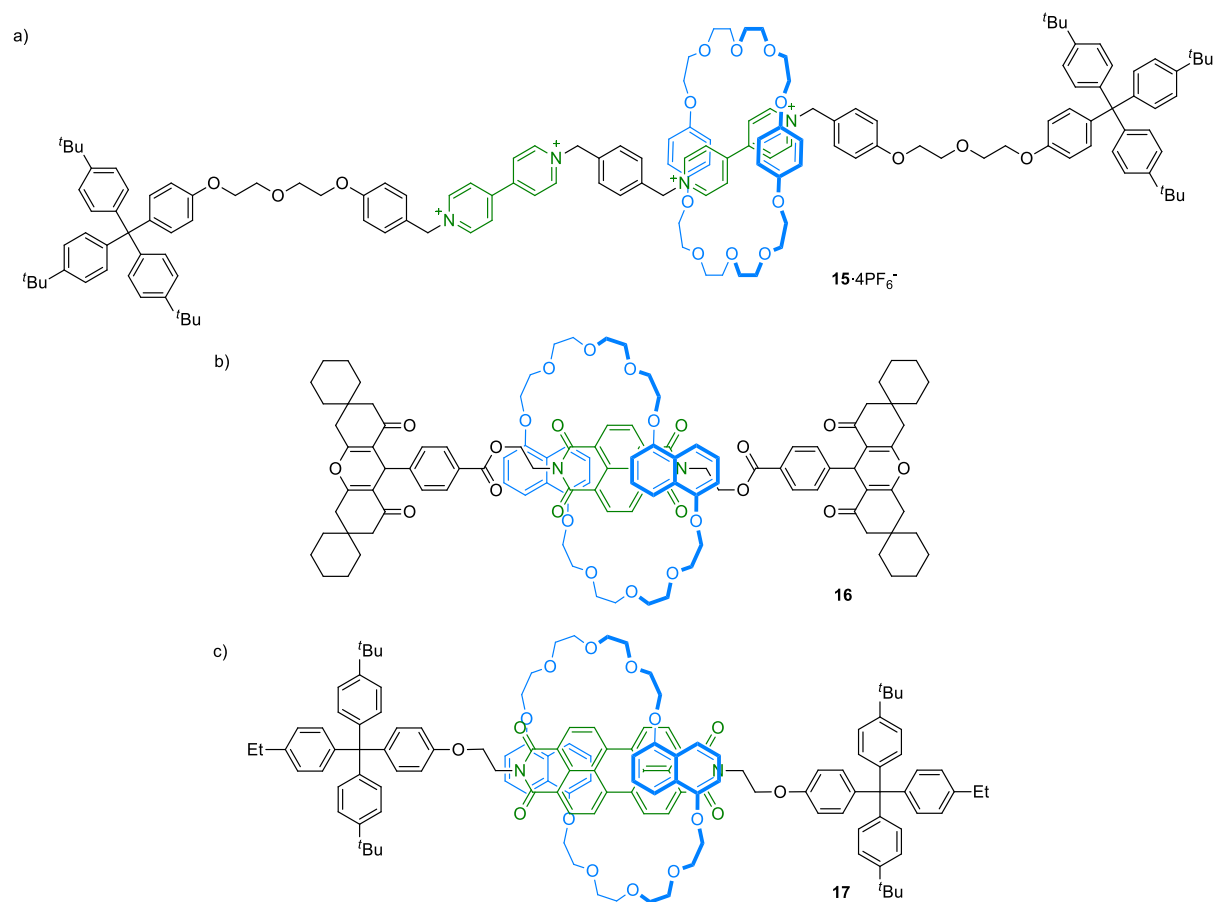


Figure 6. Examples of π -donor/ π -acceptor rotaxanes based on a crown ether macrocycle: a) A viologen-based [2]rotaxane described by Stoddart.⁴⁴ b) NDI-based [2]rotaxane developed by Hamilton.⁴⁵ c) A PDI-based [2]rotaxane reported by Champness.⁴⁸

Conversely, in the case of crown ethers, the electron-rich group is on the macrocycle while the electron-poor one is on the axle. Thus, a [2]rotaxane containing BPP34C10 and a thread with a viologen unit and was synthesized by Stoddart and collaborators (Figure 6a).⁴⁴ Following this example, over the years, this strategy was extended to new designs of electron-poor aromatic binding sites. The most common is naphthalene diimide (NDI), which gives better yields when associated to DNP38C10 (Figure

⁴⁰ R. Ballardini, V. Balzani, W. Dehaen, A. E. Dell'Erba, F. M. Raymo, J. F. Stoddart, M. Venturi, *Eur. J. Org. Chem.* **2000**, 591-602.

⁴¹ S. Nygaard, B. W. Laursen, T. S. Hansen, A. D. Bond, A. H. Flood, J. O. Jeppesen, *Angew. Chem. Int. Ed.* **2007**, *46*, 6093-6097.

⁴² E. Cordova, R. A. Bissell, N. Spencer, P. R. Ashton, J. F. Stoddart, A. E. Kaifer, *J. Org. Chem.* **1993**, *58*, 6550-6552.

⁴³ T. Ikeda, M. Higuchi, D. G. Kurth, *J. Am. Chem. Soc.* **2009**, *131*, 9158-9159.

⁴⁴ P. R. Ashton, D. Philp, N. Spencer, J. F. Stoddart, *J. Chem. Soc., Chem. Commun.*, **1992**, 1124-1128.

⁴⁵ A. M. Cagulada, D. G. Hamilton, *J. Am. Chem. Soc.* **2009**, *131*, 902-903.

6b).⁴⁵ In addition, rotaxanes were also designed with diazapyrenium,⁴⁶ diazaperopyrenium⁴⁷ or perylene diimide⁴⁸ cores (Figure 6c).

3.2.2. Carbon nanostructures

Since the detection of fullerenes in 1985 by Kroto⁴⁹ and the discovery of carbon nanotubes in 1991 by Iijima,⁵⁰ some rotaxane structures incorporating one of these two carbon nanostructures have been designed.⁵¹ Regarding C₆₀, it was first introduced as a stopper by Diederich and Sauvage,⁵² leading to numerous architectures, then it was placed on the macrocycle,⁵³ and finally Guldi and von Delius employed it as recognition site for a [10]cycloparaphenylene ring (Figure 7).⁵⁴

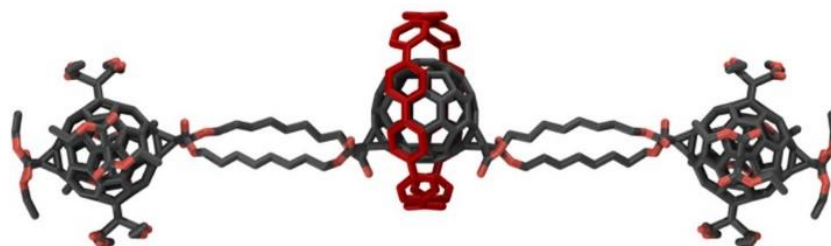


Figure 7. DFT calculated geometry of the [2]rotaxane developed by Guldi and von Delius.⁵⁴ Reprinted with permission from ref 54. Copyright 2018 American Chemical Society.

The use of carbon nanotubes has been more limited so far. In 2014, Pérez and co-workers reported the first mechanically interlocked single-wall carbon nanotube. Thus, they were capable to wrap and close a π -extended tetrathiafulvalene macrocycle around the nanotube using a ring-closing metathesis reaction (Figure 8).⁵⁵ In addition, this methodology was extended to different types of rings, such as

⁴⁶ P. R. Ashton, S. E. Boyd, A. Brindle, S. J. Langford, S. Menzer, L. Pérez-García, J. A. Preece, F. M. Raymo, N. Spencer, J. F. Stoddart, A. J. P. White, D. J. Williams, *New J. Chem.* **1999**, *23*, 587-602.

⁴⁷ A. N. Basuray, H.-P. Jacquot de Rouville, K. J. Hartlieb, T. Kikuchi, N. L. Strutt, C. J. Bruns, M. W. Ambrogio, A.-J. Avestro, S. T. Schneebeli, A. C. Fahrenbach, J. F. Stoddart, *Angew. Chem. Int. Ed.* **2012**, *51*, 11872-11877.

⁴⁸ B. J. Slater, E. S. Davies, S. P. Argent, H. Nowell, W. Lewis, A. J. Blake, N. R. Champness, *Chem. Eur. J.* **2011**, *17*, 14746-14751.

⁴⁹ H. W. Kroto, J. R. Heath, S. C. O'Brien, R. F. Curl, R. E. Smalley, *Nature* **1985**, *318*, 162-163.

⁵⁰ S. Iijima, *Nature* **1991**, *354*, 56-58.

⁵¹ M. Barrejón, A. Mateo-Alonso, M. Prato, *Eur. J. Org. Chem.* **2019**, 3371-3383.

⁵² F. Diederich, C. Dietrich-Buchecker, J.-F. Nierengarten, J.-P. Sauvage, *J. Chem. Soc., Chem. Commun.* **1995**, 781-782.

⁵³ N. Watanabe, N. Kihara, Y. Furusho, T. Takata, Y. Araki, O. Ito, *Angew. Chem. Int. Ed.* **2003**, *42*, 681-683.

⁵⁴ Y. Xu, R. Kaur, B. Wang, M. B. Minameyer, S. Gsänger, B. Meyer, T. Drewello, D. M. Guldi, M. von Delius, *J. Am. Chem. Soc.* **2018**, *140*, 13413-13420.

⁵⁵ A. de Juan, Y. Pouillon, L. Ruiz-González, A. Torres-Pardo, S. Casado, N. Martín, Á. Rubio, E. M. Pérez, *Angew. Chem. Int. Ed.* **2014**, *53*, 5394-5400.

pyrene-,⁵⁶ naphthalene diimide-,⁵⁷ cycloparaphenyleneacetylene-⁵⁸ or porphyrin-containing⁵⁹ macrocycles. It is worth noting that these wheels are unable to dethread the nanotube due to its length.

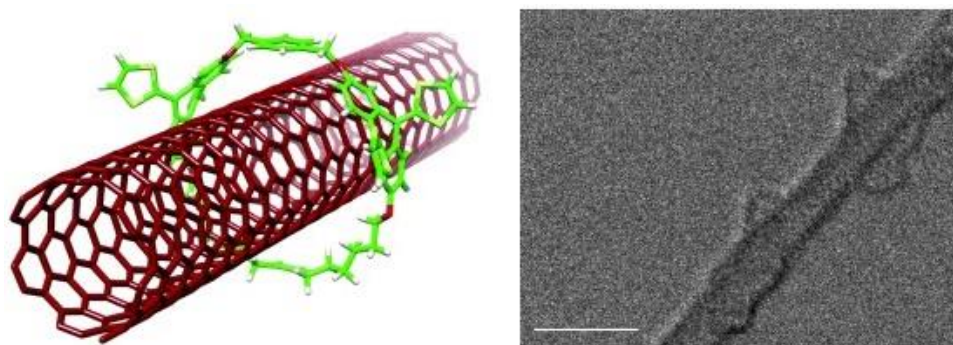


Figure 8. Calculated DFT geometry of a molecular model of the first mechanically interlocked single-wall carbon nanotube reported by Pérez (left) and High-resolution STEM bright-field image of a single single-wall carbon nanotube enveloped by two macrocycles (scale bar is 2 nm) (right).⁵⁵ Reprinted with permission from ref 55. Copyright 2014 John Wiley and Sons.

3.3. Solvophobic forces

When rotaxanes are synthesized taking advantage of solvophobic forces, the designs are usually based on macrocycles owning a hydrophobic cavity and the rotaxane synthesis is achieved in polar solvents, usually in aqueous media. Therefore, in this case, the main driving forces are hydrophobic. Cyclodextrins, a group of cyclic oligosaccharides, or cucurbiturils, which are macrocycles composed by glycoluril units linked by two methylene bridges, have been the macrocycles most widely used.

As it can be noticed from the literature, most cyclodextrin rotaxanes are built with α -cyclodextrin, the smallest one, with 6 units of glucose. Thus, in 1991, Kaifer and co-workers assembled a [2]rotaxane by capping using α -cyclodextrin, an alkane chain as binding motif and a ferrocene and a naphthalene unit as stoppers.⁶⁰ This alkane recognition site was widely explored. However, over the years, new binding motifs were discovered. The most commonly used are azobenzene,⁶¹ stilbene⁶² and diphenylacetylene⁶² (Figure 9). Although, it is possible to prepare a rotaxane with β -cyclodextrin using diphenylacetylene,⁶² stilbene⁶² and azobenzene⁶¹ as hydrophobic sites, yields are clearly higher employing α -cyclodextrin. Alternatively, the synthesis of β -cyclodextrin rotaxanes can be performed

⁵⁶ A. López-Moreno, E. M. Pérez, *Chem. Commun.* **2015**, 51, 5421-5424.

⁵⁷ S. Leret, Y. Pouillon, S. Casado, C. Navío, Á. Rubio, E. M. Pérez, *Chem. Sci.* **2017**, 8, 1927-1935.

⁵⁸ K. Miki, K. Saiki, T. Umeyama, J. Baek, T. Noda, H. Imahori, Y. Sato, K. Suenaga, K. Ohe, *Small* **2018**, 14, 1800720

⁵⁹ L. de Juan-Fernández, P. W. Münich, A. Puthiyedath, B. Nieto-Ortega, S. Casado, L. Ruiz-González, E. M. Pérez, D. M. Guldi, *Chem. Sci.* **2018**, 9, 6779-6784.

⁶⁰ R. Isnin, A. E. Kaifer, *J. Am. Chem. Soc.* **1991**, 113, 8188-8190.

⁶¹ S. Anderson, T. D. W. Claridge, H. L. Anderson, *Angew. Chem Int. Ed. Engl.* **1997**, 36, 1310-1313.

⁶² C. A. Stanier, M. J. O'Connell, W. Clegg, H. L. Anderson, *Chem. Commun.* **2001**, 493-494.

with biphenyl,⁶³ anthracene,⁶⁴ thiophene⁶⁵ or bisphenol A⁶⁶ (Figure 9). Apart from that, a big part of the research in this area is focused on polyrotaxanes. A majority of them are exploiting polyethylene glycol chain to occlude the hydrophobic cavity of the cyclodextrin.⁶⁷

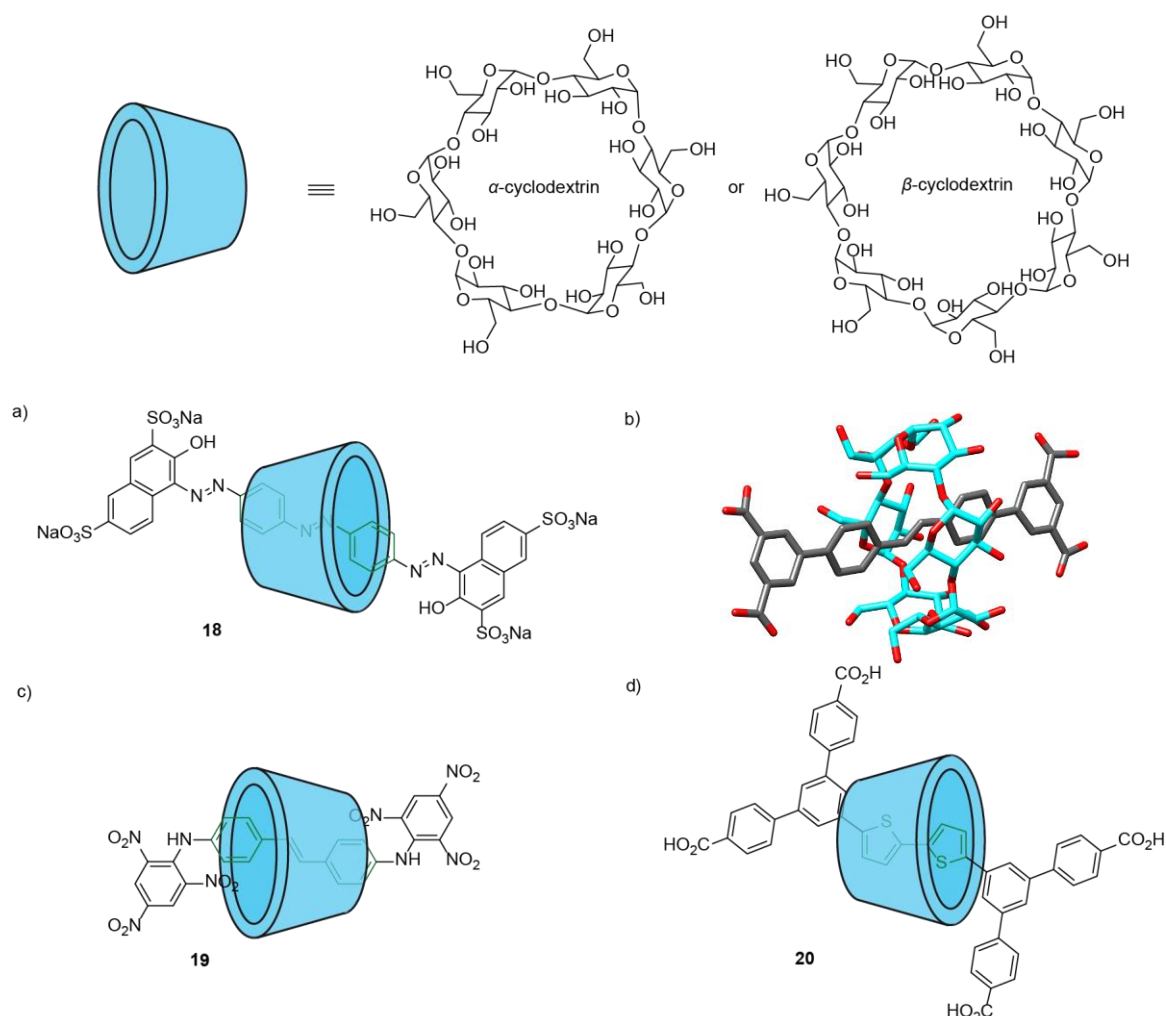


Figure 9. Various cyclodextrin-based rotaxanes: a) Azobenzene-based [2]rotaxane with an α -cyclodextrin developed by Anderson.⁶¹ b) X-ray diffraction structure of a stilbene-containing [2]rotaxane.⁶² Color coding: C, grey or blue; O, red. c) A [2]rotaxane possessing a stilbene motif with an α -cyclodextrin reported by Easton.⁶⁸ d) Thiophene-based [2]rotaxane with a β -cyclodextrin.⁶⁵

When it comes to cucurbiturils, their host-guest properties are similar to those of cyclodextrins. Indeed, they display a hydrophobic cavity capable of binding diverse lipophilic compounds.⁶⁹ Thus,

⁶³ G. Chen, J. Xia, Z. Li, G.-A. Yu, S. Jin, S. H. Liu, *J. Organomet. Chem.* **2010**, 695, 323-326.

⁶⁴ M. T. Stone, H. L. Anderson, *Chem. Commun.* **2007**, 2387-2389.

⁶⁵ L. Zalewski, M. Wykes, S. Brovelli, M. Bonini, T. Breiner, M. Kastler, F. Dötzt, D. Beljonne, H. L. Anderson, F. Cacialli, P. Samori, *Chem. Eur. J.* **2010**, 16, 3933-3941.

⁶⁶ S. Teka, K. Hriz, N. Jaballah, D. Kreher, F. Mathevet, N. Jarroux, M. Majdoub, *Mater. Sci. Semicond. Process.* **2015**, 34, 189-197.

⁶⁷ A. Hashidzume, H. Yamaguchi, A. Harada, *Eur. J. Org. Chem.* **2019**, 3344-3357.

⁶⁸ H. Onagi, B. Carrozzini, G. L. Cascarano, C. J. Easton, A. J. Edwards, S. F. Lincoln, A. D. Rae, *Chem. Eur. J.* **2003**, 9, 5971-5977.

⁶⁹ S. J. Barrow, S. Kasera, M. J. Rowland, J. del Barrio, O. A. Scherman, *Chem. Rev.* **2015**, 115, 12320-12406.

cucurbit[6]uril-based rotaxanes were prepared with spermine groups on the rod⁷⁰ or *via* a metal-free active template procedure by performing an azide-alkyne Huisgen cycloaddition whose final product is a 1,4-disubstituted triazole.^{22a} Cucurbit[7]uril was also exploited since it exhibits a wider range of recognition unit to yield rotaxanes: oligoaniline,⁷¹ bis(pyridinium)-1,4-xylylene,⁷² *para*-xylylene-bisaminium salt,⁷³ viologen⁷⁴ and bis(pyridinium)-4,4'-bitolyl.⁷⁵ Finally, for cucurbit[8]uril, rotaxanes featuring a viologen moiety were reported.⁷⁶

3.4. Metal coordination

3.4.1. Passive metal template

In rotaxane synthesis, the use of metal coordination has been very important and allowed the construction of a great variety of interlocked structures.⁷⁷ From an historical point of view, the first efficient synthesis of a MIM was carried following the strategy developed by Sauvage based on a tetrahedral Cu^I complex with two 1,10-phenanthroline (phen) ligands. Hence, many of these earlier rotaxanes are bearing this exact unit, however, their stoppers vary typically from trityl to porphyrin units.^{16,78} Later, this strategy was extended to the use of other metals and coordination geometries. Thus, Sauvage employed an octahedral Ru^{II} complex with a 2,2'-bipyridine and two phen ligands⁷⁹ and Leigh established a general procedure for the preparation of rotaxanes through imine bond formation employing octahedral metals, such as Co^{II}, Ni^{II}, Zn^{II}, Mn^{II}, *etc* (Figure 10).⁸⁰ Furthermore, a square-planar metal-coordinated rotaxane was constructed through a clipping approach using Pd^{II} with 2,6-dicarboxyamidopyridine ligand on the macrocycle and a pyridine unit on the axle.⁸¹ Recently, the synthesis of rotaxanes templated by alkali metal ions, mainly by Li⁺ and Na⁺, is generating increasing interest. These recognition systems are generally composed by oligo(ethylene glycol), amide and urea subunits.⁸²

⁷⁰ Y.-M. Jeon, D. Whang, J. Kim, K. Kim, *Chem. Lett.* **1996**, 503-504.

⁷¹ R. Eelkema, K. Maeda, B. Odell, H. L. Anderson, *J. Am. Chem. Soc.* **2007**, *129*, 12384-12385.

⁷² V. Sindelar, K. Moon, A. E. Kaifer, *Org. Lett.* **2004**, *6*, 2665-2668.

⁷³ C. J. Bruns, H. Liu, M. B. Francis, *J. Am. Chem. Soc.* **2016**, *138*, 15307-15310.

⁷⁴ L. Zhu, H. Yan, X.-J. Wang, Y. Zhao, *J. Org. Chem.* **2012**, *77*, 10168-10175.

⁷⁵ I. Neira, A. Blanco-Gómez, J. M. Quintela, C. Peinador, M. D. García, *Org. Lett.* **2019**, *21*, 8976-8980.

⁷⁶ V. Ramalingam, A. R. Urbach, *Org. Lett.* **2011**, *13*, 4898-4901.

⁷⁷ J. E. Beves, B. A. Blight, C. J. Campbell, D. A. Leigh, R. T. McBurney, *Angew. Chem. Int. Ed.* **2011**, *50*, 9260-9327.

⁷⁸ Selected examples: a) J.-C. Chambron, V. Heitz, J.-P. Sauvage, *J. Chem. Soc., Chem. Commun.* **1992**, 1131-1133.

b) J.-C. Chambron, V. Heitz, J.-P. Sauvage, *J. Am. Chem. Soc.* **1993**, *115*, 12378-12384.

⁷⁹ D. Pomeranc, D. Jouvenot, J.-C. Chambron, J.-P. Collin, V. Heitz, J.-P. Sauvage, *Chem. Eur. J.* **2003**, *9*, 4247-4254

⁸⁰ L. Hogg, D. A. Leigh, P. J. Lusby, A. Morelli, S. Parsons, J. K. Y. Wong, *Angew. Chem. Int. Ed.* **2004**, *43*, 1218-1221.

⁸¹ A.-M. Fuller, D. A. Leigh, P. J. Lusby, I. D. H. Oswald, S. Parsons, D. B. Walker, *Angew. Chem. Int. Ed.* **2004**, *43*, 3914-3918.

⁸² A. Inthasot, S.-T. Tung, S.-H. Chiu, *Acc. Chem. Res.* **2018**, *51*, 1324-1337.

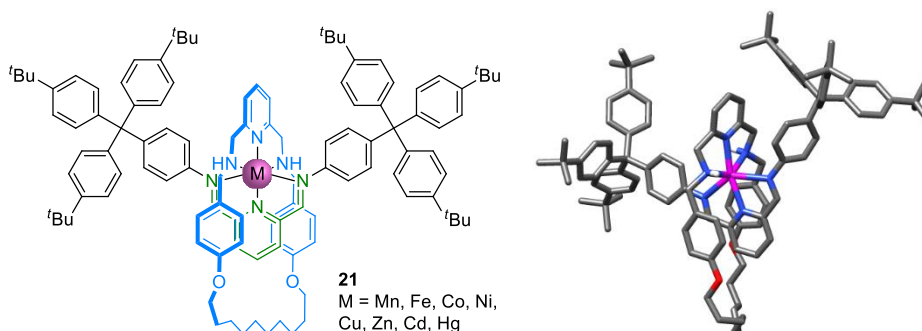
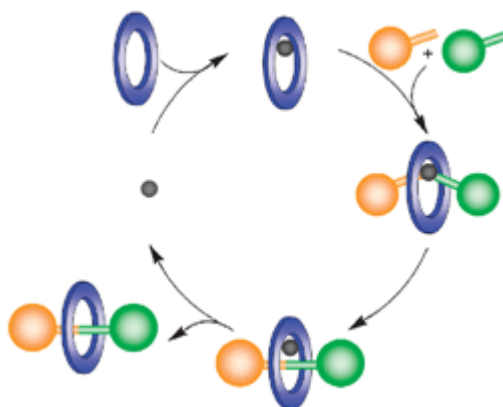


Figure 10. [2]rotaxanes obtained with different octahedral metal templates and the X-ray diffraction structure of **21-Cd^{II}**.⁸⁰ Color coding: C, grey; O, red; N, blue; H, white; Cd, magenta.

3.4.2. Active metal template

The active metal template strategy²¹ was first reported in 2006 by David A. Leigh. For this purpose, he used a 2,6-disubstituted pyridine macrocycle to perform a CuAAC reaction and afford a [2]rotaxane. Indeed, the ring incorporated a ligand capable of coordinating the metal catalyst which performed the reaction between two groups of the thread precursors inside the cavity of the macrocycle to yield a MIM.⁸³ This methodology was extended to other types of macrocycles with different ligands for Cu^I, used for the same reaction⁸⁴ or for other metal centres able to catalyze a variety of reactions such as the Glaser coupling,⁸⁵ the oxidative Heck cross-couplings,⁸⁶ Cu^{II} or Zn^{II} catalyzed Diels-Alder reactions⁸⁷ or nickel-catalyzed sp³-sp³ couplings⁸⁸ (Scheme 3).



Scheme 3. Schematic illustration of the catalytic cycle for the formation of a [2]rotaxane by active-metal template.^{21a} Reprinted with permission from ref 21a. Copyright 2009 Royal Society of Chemistry.

⁸³ V. Aucagne, K. D. Hänni, D. A. Leigh, P. J. Lusby, D. B. Walker, *J. Am. Chem. Soc.* **2006**, *128*, 2186-2187.

⁸⁴ Selected examples: a) V. Aucagne, J. Berná, J. D. Crowley, S. M. Goldup, K. D. Hänni, D. A. Leigh, P. J. Lusby, V. E. Ronaldson, A. M. Z. Slawin, A. Viterisi, D. B. Walker, *J. Am. Chem. Soc.* **2007**, *129*, 11950-11963. b) J. E. M. Lewis, R. J. Bordoli, M. Denis, C. J. Fletcher, M. Galli, E. A. Neal, E. M. Rochette, S. M. Goldup, *Chem. Sci.* **2016**, *7*, 3154-3161.

⁸⁵ M. J. Langton, J. D. Matichak, A. L. Thompson, H. L. Anderson, *Chem. Sci.* **2011**, *2*, 1897-1901.

⁸⁶ J. D. Crowley, K. D. Hänni, A.-L. Lee, D. A. Leigh, *J. Am. Chem. Soc.* **2007**, *129*, 12092-12093.

⁸⁷ J. D. Crowley, K. D. Hänni, D. A. Leigh, A. M. Z. Slawin, *J. Am. Chem. Soc.* **2010**, *132*, 5309-5314.

⁸⁸ S. M. Goldup, D. A. Leigh, R. T. McBurney, P. R. McGonigal, A. Plant, *Chem. Sci.* **2010**, *1*, 383-386.

3.5. Other interactions and templates

3.5.1. Anion binding template

The use of halide anions templates for the synthesis of MIMs relies on hydrogen and halogen bonds. Thus, in 2002, Beer and co-workers reported the first chloride anion-templated synthesis of a [2]rotaxane (**22**) featuring a simple isophthalamide ligand on the wheel and a pyridinium derivative on the thread (Figure 11). In this case, the formation of the pseudorotaxanes relies on the establishment of hydrogen bonds between the chloride anion and the amide groups on the thread and the macrocycle.⁸⁹ The same concept was extended to the use of other groups capable of interacting with anions such as triazolium,⁹⁰ iodotriazolium⁹¹ groups placed in the axle or, in the case of the latter, in both components of the structure.⁹² Besides halide anions, very few examples of template by other inorganic anions, such as nitrate⁹³ or hexafluorophosphate,⁹⁴ have been described in rotaxane synthesis. It is worth noting that most of these rotaxanes are obtained following a clipping methodology using ruthenium-catalyzed ring-closing metathesis or the formation of two amide bonds from the isophthalamide group.

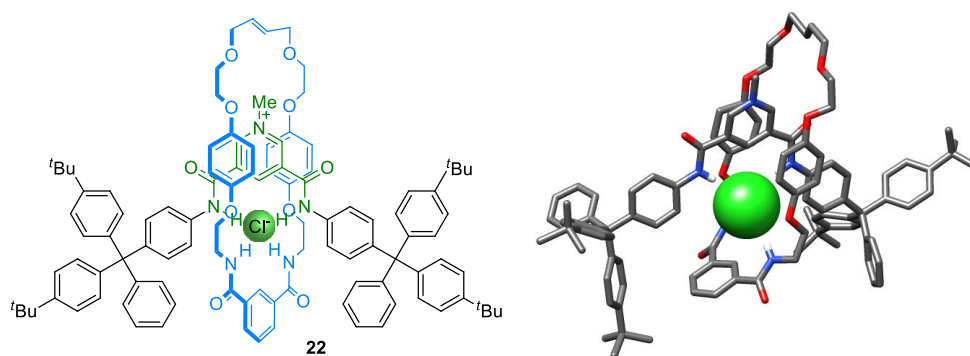


Figure 11. An anion-templated [2]rotaxane reported by Beer and its X-ray diffraction structure.⁸⁹ Color coding: C, grey; O, red; N, blue; H, white; Cl, green.

3.5.2. Pillar[n]arenes

Pillar[n]arenes are macrocycles formed by hydroquinone units bridged, in *para* position, by methylene groups. They were described for the first time by Tomoki Ogoshi in 2008.⁹⁵ They display very interesting

⁸⁹ J. A. Wisner, P. D. Beer, M. G. B. Drew, M. R. Sambrook, *J. Am. Chem. Soc.* **2002**, *124*, 12469-12476.

⁹⁰ K. M. Mullen, J. Mercurio, C. J. Serpell, P. D. Beer, *Angew. Chem.* **2009**, *121*, 4875-4878.

⁹¹ N. L. Kilah, M. D. Wise, C. J. Serpell, A. L. Thompson, N. G. White, K. E. Christensen, P. D. Beer, *J. Am. Chem. Soc.* **2010**, *132*, 11893-11895.

⁹² B. R. Mullaney, A. L. Thompson, P. D. Beer, *Angew. Chem. Int. Ed.* **2014**, *53*, 11458-11462.

⁹³ M. J. Langton, L. C. Duckworth, P. D. Beer, *Chem. Commun.* **2013**, *49*, 8608-8610.

⁹⁴ A. Brown, K. M. Mullen, J. Ryu, M. J. Chmielewski, S. M. Santos, V. Felix, A. L. Thompson, J. E. Warren, S. I. Pascu, P. D. Beer, *J. Am. Chem. Soc.* **2009**, *131*, 4937-4952.

⁹⁵ T. Ogoshi, S. Kanai, S. Fujinami, T. Yamagishi, Y. Nakamoto, *J. Am. Chem. Soc.* **2008**, *130*, 5022-5023.

host-guest properties resulting from a mixture of interactions, mainly hydrogen bondings, π - π interactions and solvophobic effect.

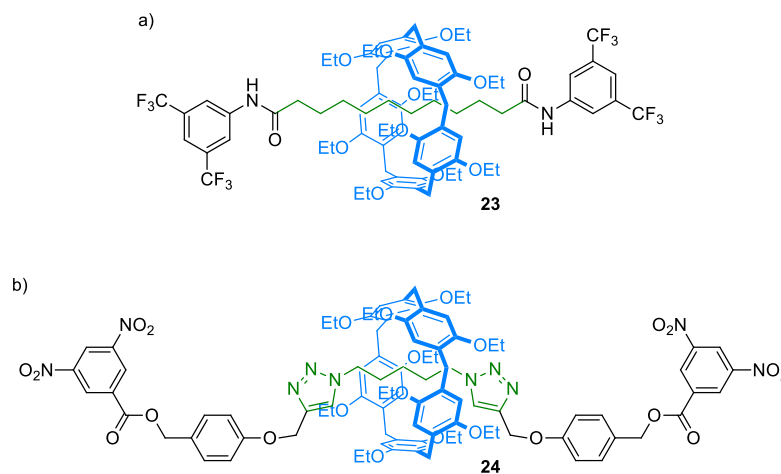


Figure 12. Different pillar[5]arene-based rotaxanes: a) [2]Rotaxane bearing an alkane chain recognition site reported by Nierengarten.^{96b} b) [2]Rotaxane possessing an alkane functionalized with triazole moieties described by Huang.⁹⁸

The most commonly used pillar[n]arenes for MIM synthesis are pillar[5]arenes since their preparation is easier and their host-guest properties broader. Thus, pillar[5]arene rotaxanes with recognition motifs such as an aliphatic chain,⁹⁶ alkanes functionalized with an imidazolium salt,⁹⁷ triazole⁹⁸ or pyridinium salts⁹⁹ were reported (Figure 12). Nevertheless, it is possible to make pillar[6]arene-based rotaxanes but only a couple of examples have been reported, with designs bearing a pyridinium,¹⁰⁰ a bipyridinium¹⁰¹ or a di(1,2,3-triazol-1-yl)butane¹⁰² station.

3.5.3. Radical-pair templates

In 2010, Stoddart and co-workers demonstrated that radical-pairing interactions could template the formation of rotaxanes. Indeed, the reduction of a CBPQT⁴⁺ ring and a viologen derivative to their diradical cation and radical cation, respectively, induced the formation of an inclusion complex that

⁹⁶ Selected examples: a) N. L. Strutt, R. S. Forgan, J. M. Spruell, Y. Y. Botros, J. F. Stoddart, *J. Am. Chem. Soc.* **2011**, *133*, 5668-5671. b) R. Milev, A. Lopez-Pacheco, I. Nierengarten, T. M. N. Trinh, M. Holler, R. Deschenaux, J.-F. Nierengarten, *Eur. J. Org. Chem.* **2015**, 479-485.

⁹⁷ S. Dong, J. Yuan, F. Huang, *Chem. Sci.* **2014**, *5*, 247-252.

⁹⁸ P. Wei, X. Yan, J. Li, Y. Ma, Y. Yao, F. Huang, *Tetrahedron* **2012**, *68*, 9179-9185.

⁹⁹ C. Ke, N. L. Strutt, H. Li, X. Hou, K. J. Hartlieb, P. R. McGonigal, Z. Ma, J. Iehl, C. L. Stern, C. Cheng, Z. Zhu, N. A. Vermeulen, T. J. Meade, Y. Y. Botros, J. F. Stoddart, *J. Am. Chem. Soc.* **2013**, *135*, 17019-17030.

¹⁰⁰ T. Ogoshi, D. Yamafuji, T. Aoki, T. Yamagishi, *Chem. Commun.* **2012**, *48*, 6842-6844.

¹⁰¹ X. Hou, C. Ke, C. Cheng, N. Song, A. K. Blackburn, A. A. Sarjeant, Y. Y. Botros, Y.-W. Yang, J. F. Stoddart, *Chem. Commun.* **2014**, *50*, 6196-6199.

¹⁰² T. Ogoshi, D. Kotera, S. Fa, S. Nishida, T. Kakuta, T. Yamagishi, A. M. Brouwer, *Chem. Comm.* **2020**, doi:10.1039/D0CC03945D.

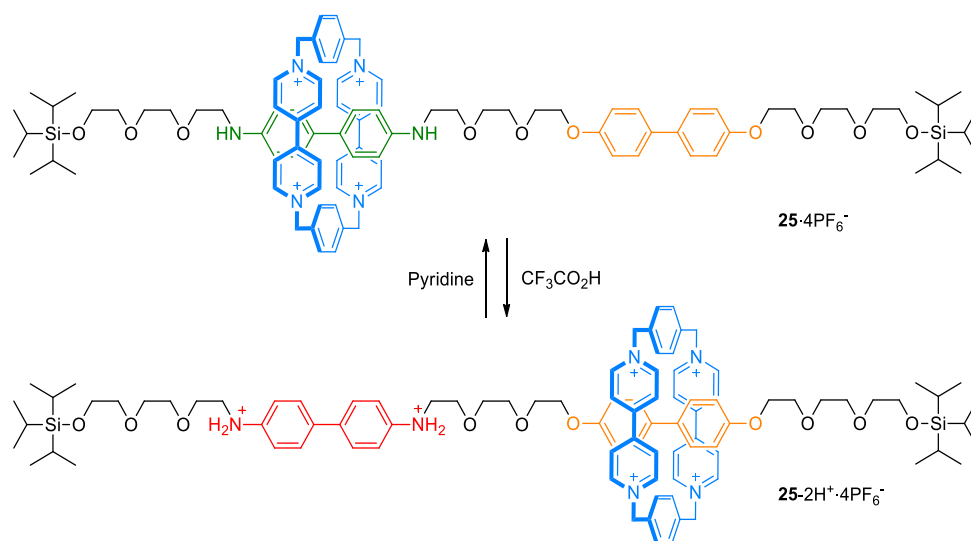
lead to the synthesis of a series of rotaxanes.¹⁰³ Furthermore, they proved that the radical cation of a 4,4'-bipyridinium unit was stabilized against oxidation by this rotaxane architecture.¹⁰⁴

4. Molecular switches based on rotaxane architectures

Throughout the years the operation of molecular switches through the use of external stimuli have been reported in a variety of structures, mainly rotaxanes and catenanes, but also in non-interlocked molecules. Here, we will focus on switches based on rotaxanes where the translation of the macrocycle along the axle can be controlled by external stimuli.

4.1. pH-driven switches

The first pH-switchable molecular shuttle was reported by Stoddart in 1994, using a [2]rotaxane (**25**·4PF₆⁻) including a CBPQT⁴⁺ ring, a biphenol and a benzidine unit as recognition sites on the thread. The addition of acid, CF₃CO₂H, creates a benzidinium group, which generates a repulsive interaction with the CBPQT⁴⁺ macrocycle, resulting in the migration of the latter to the biphenol station. When a base is added, it deprotonates the nitrogen atoms of the benzidinium unit and, therefore, CBPQT⁴⁺ goes back to the benzidine station due to its higher π-electron rich character (Scheme 4).¹⁰⁵



Scheme 4. The first pH-switchable molecular shuttle reported by Stoddart.¹⁰⁵

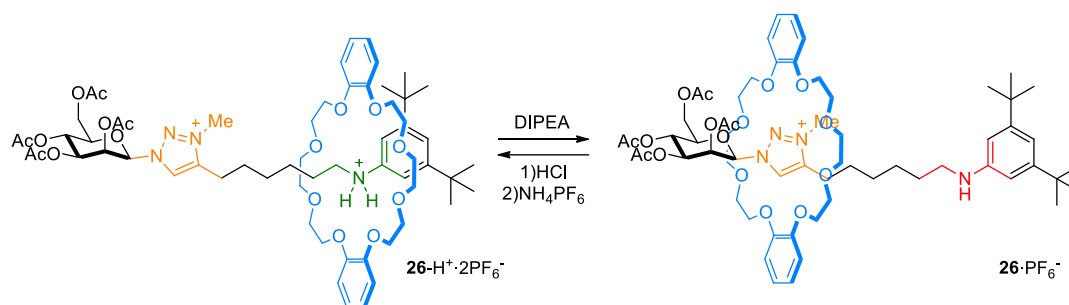
Later, in 1997, Stoddart synthesized the first pH-responsive hydrogen bonding-based molecular shuttle. The [2]rotaxane design shows a DB24C8 ring, a dibenzylammonium and a 4,4'-bipyridinium

¹⁰³ H. Li, A. C. Fahrenbach, S. K. Dey, S. Basu, A. Trabolsi, Z. Zhu, Y. Y. Botros, J. F. Stoddart, *Angew. Chem. Int. Ed.* **2010**, *49*, 8260-8265.

¹⁰⁴ H. Li, Z. Zhu, A. C. Fahrenbach, B. M. Savoie, C. Ke, J. C. Barnes, J. Lei, Y.-L. Zhao, L. M. Lilley, T. J. Marks, M. A. Ratner, J. F. Stoddart, *J. Am. Chem. Soc.* **2013**, *135*, 456-467.

¹⁰⁵ R. A Bissell, E. Córdova, A. E. Kaifer, J. F. Stoddart, *Nature* **1994**, *369*, 133-137.

group as thread stations. In acidic medium, the ammonium salt is protonated, therefore the macrocycle encircles this unit, whereas in basic medium, because of the deprotonation of the ammonium salt, the ring shuttles to the bipyridinium station. This operation was carried out by means of the addition of $\text{CF}_3\text{CO}_2\text{H}$ and DIPEA.¹⁰⁶ Over the years, this system was employed in many architectures, however, it is also possible to use another secondary station, such as BPE¹⁰⁷ or a triazolium salt¹⁰⁸ (Scheme 5). The latter has become very popular and can be found in a great number of molecular machines.¹⁰⁹



Scheme 5. Molecular switch bearing a triazolium secondary station developed by Coutrot.¹⁰⁸

Furthermore, it was possible to build a pH-controllable shuttle thanks to a Pd-coordinated [2]rotaxane using a 4-dimethylaminopyridine (DMAP) and a pyridine station. In basic media, the Pd-complexed macrocycle is situated on the more coordinating DMAP station, whereas after the addition of TsOH, the Pd-complexed ring moves to the pyridine station due to the protonation of the more basic DMAP derivative. It is important to highlight that this operation proceeds at high temperature (110 °C) since the system needs to be under thermodynamic control to operate, which requires that the Pd–N bond becomes labile.¹¹⁰

4.2. Redox switches

In 1994, Stoddart and co-workers operated and controlled the first electrochemically switchable molecular shuttle based on the same [2]rotaxane structure as the first pH switchable shuttle (**25**·4PF₆⁻). When the benzidine unit is oxidized, the macrocycle moves to the biphenol station due to a repulsive interaction.¹⁰⁵ Later, this system was modified since it was found that the electrochemical switch of the position of the macrocycle could be achieved with a high degree of control by the oxidation of a tetrathiofulavene (TTF) derivative. This unit associated with a 1,5-dialkoxynaphthalene secondary

¹⁰⁶ M.-V. Martinez-Diaz, N. Spencer, J. F. Stoddart, *Angew. Chem. Int. Ed. Engl.* **1997**, *36*, 1904-1907.

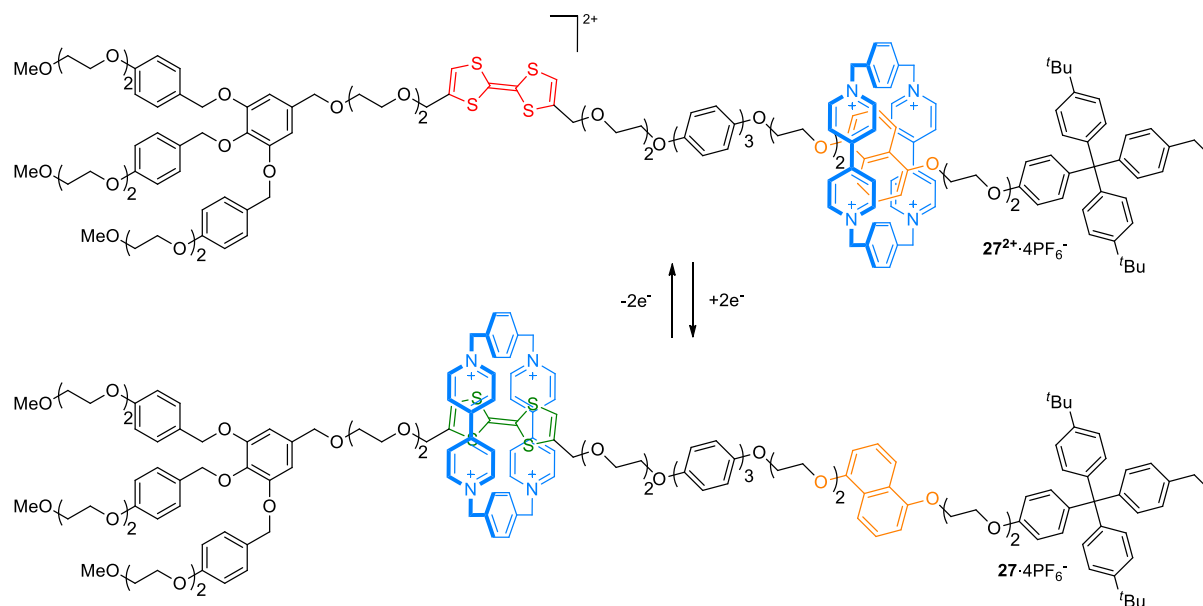
¹⁰⁷ A. M. Elizarov, S.-H. Chiu, J. F. Stoddart, *J. Org. Chem.* **2002**, *67*, 9175-9181.

¹⁰⁸ F. Coutrot, E. Busseron, *Chem. Eur. J.* **2008**, *14*, 4784-4787.

¹⁰⁹ F. Coutrot, *ChemistryOpen* **2015**, *4*, 556-576.

¹¹⁰ J. D. Crowley, D. A. Leigh, P. J. Lusby, R. T. McBurney, L.-E. Perret-Aebi, C. Petzold, A. M. Z. Slawin, M. D. Symes, *J. Am. Chem. Soc.* **2007**, *129*, 15085-15090.

station, was employed by Stoddart a large number of times in the development of molecular switches (Scheme 6).¹¹¹



Scheme 6. A redox switch owning a TTF/1,5-dialkoxynaphthalene system.¹¹¹

It is also feasible to operate a redox switch by reducing a station. This was accomplished in a rotaxane featuring a CBPQT⁴⁺ macrocycle, a 4,4'-bipyridinium and a 1,5-dioxynaphthalene group. When the three 4,4'-bipyridinium derivatives are reduced to their radical cation form, the macrocycle migrates to the 4,4'-bipyridinium station (in its radical cation form) due to the establishment of radical pair interactions.¹¹² In addition, the switching of a DNP38C10 wheel in a rotaxane can be carried out by the reduction of a NDI station to NDI^{•-} with a pyromellitic diimide or a triazole secondary station (Scheme 7).¹¹³

As for tetralactam macrocycle-based switches, the control of the shuttling between a succinamide station and a naphthalimide or NDI stopper can be performed electrochemically by the reduction of this stopper, which induces a translation of the ring towards the reduced unit of the axle.¹¹⁴ Moreover, the position of the macrocycle on the thread can also be regulated using a glycyglycine recognition

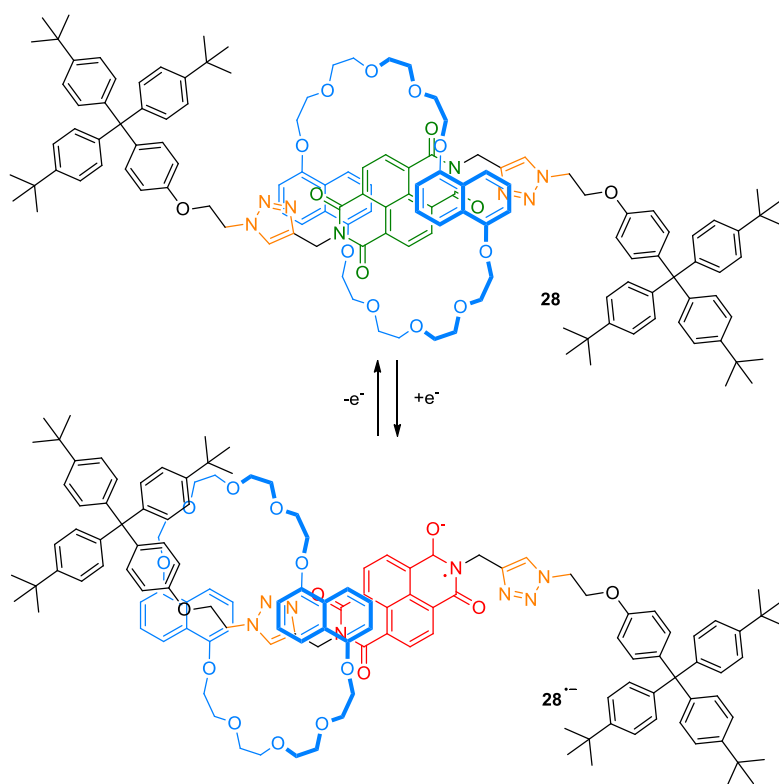
¹¹¹ H.-R. Tseng, S. A. Vignon, P. C. Celestre, J. Perkins, J. O. Jeppesen, A. Di Fabio, R. Ballardini, M. T. Gandolfi, M. Venturi, V. Balzani, J. F. Stoddart, *Chem. Eur. J.* **2004**, *10*, 155-172.

¹¹² A. Trabolsi, N. Khashab, A. C. Fahrenbach, D. C. Friedman, M. T. Colvin, K. K. Cotí, D. Benítez, E. Tkatchouk, J.-C. Olsen, M. E. Belowich, R. Carmielli, H. A. Khatib, W. A. Goddard III, M. R. Wasielewski, J. F. Stoddart, *Nature Chem.* **2010**, *2*, 42-49.

¹¹³ a) T. Iijima, S. A. Vignon, H.-R. Tseng, T. Jarrosson, J. K.M. Sanders, F. Marchioni, M. Venturi, E. Apostoli, V. Balzani, J. F. Stoddart, *Chem. Eur. J.* **2004**, *10*, 6375-6392. b) H.-P. Jacquot de Rouville, J. Iehl, C. J. Bruns, P. L. McGrier, M. Frasconi, A. A. Sarjeant, J. F. Stoddart, *Org. Lett.* **2012**, *14*, 5188-5191.

¹¹⁴ A. M. Brouwer, C. Frochot, F. G. Gatti, D. A. Leigh, L. Mottier, F. Paolucci, S. Roffia, G. W. H. Worpel, *Science* **2001**, *291*, 2124-2128.

motif and C₆₀ as stopper. Indeed, when three radical anions are formed on the fullerene, the ring shuttles towards it.¹¹⁵ Finally, this control can be achieved *via* chemical redox processes employing a sulphur-succinamide³⁵ or a azodicarboxamide station.¹¹⁶



Scheme 7. NDI-based electrochemical switch.^{113b}

Electrochemical switches can also be obtained with rotaxanes synthesized by transition metal template. In 1994, Sauvage and co-workers made a significant breakthrough since they were able to control the switching of a [2]catenane containing two phen ligands and a terpyridine (terpy) secondary ligand on one of the macrocycles. By modifying the oxidation state of the 4-coordinate Cu^I cation, its coordination geometry changes to a 5-coordinate Cu^{II} species. Consequently, the new preferred coordination geometry destabilizes the phen complex and allows the pirouetting of the macrocycle featuring the terpy derivative to enable the formation of a 5-coordinate complex.¹¹⁷ Later, this exact same strategy was extended to rotaxane-based switches possessing a phen or a bipyridine group to control either the pirouetting¹¹⁸ (Scheme 8) or the translation movements of the macrocycle.¹¹⁹

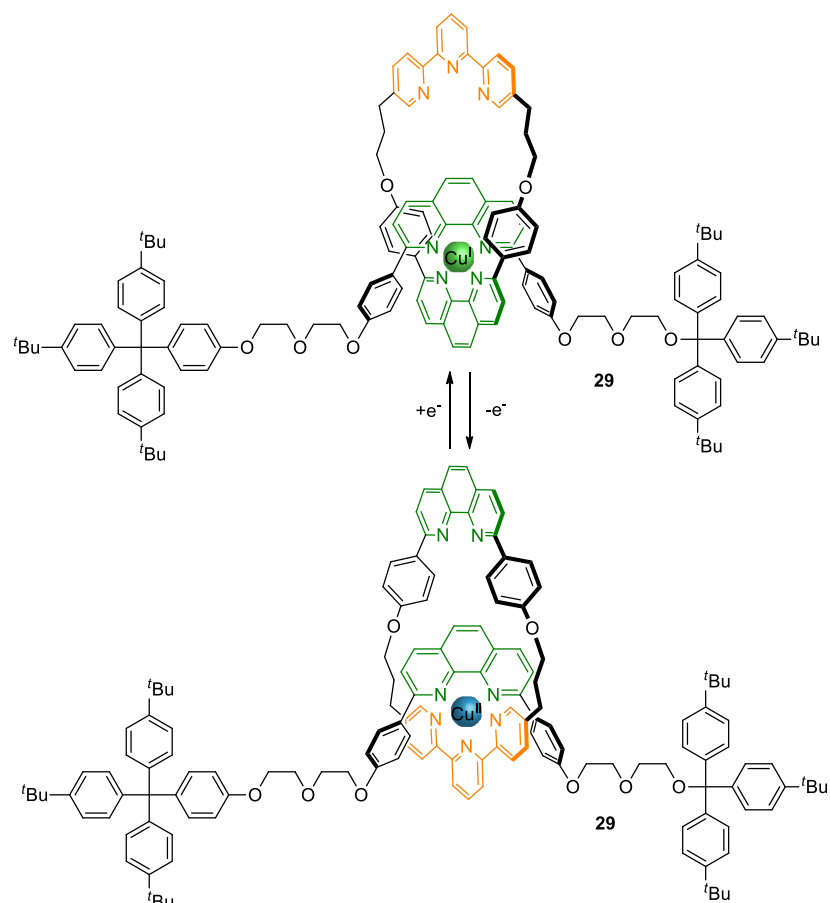
¹¹⁵ A. Mateo-Alonso, G. Fioravanti, M. Marcaccio, F. Paolucci, G. M. A. Rahman, C. Ehli, D. M. Guldi, M. Prato, *Chem. Commun.* **2007**, 1945-1947.

¹¹⁶ J. Berná, M. Alajarín, R.-A. Orenes, *J. Am. Chem. Soc.* **2010**, *132*, 10741-10747.

¹¹⁷ A. Livoreil, C. O. Dietrich-Buchecker, J.-P. Sauvage, *J. Am. Chem. Soc.* **1994**, *116*, 9399-9400.

¹¹⁸ L. Raehm, J.-M. Kern, J.-P. Sauvage, *Chem. Eur. J.* **1999**, *5*, 3310-3317.

¹¹⁹ a) N. Armaroli, V. Balzani, J.-P. Collin, P. Gaviña, J.-P. Sauvage, B. Ventura, *J. Am. Chem. Soc.* **1999**, *121*, 4397-4408. b) F. Durola, J.-P. Sauvage, *Angew. Chem. Int. Ed.* **2007**, *46*, 3537-3540.



Scheme 8. A pirouetting rotaxane-based molecular switch by Sauvage.¹¹⁸

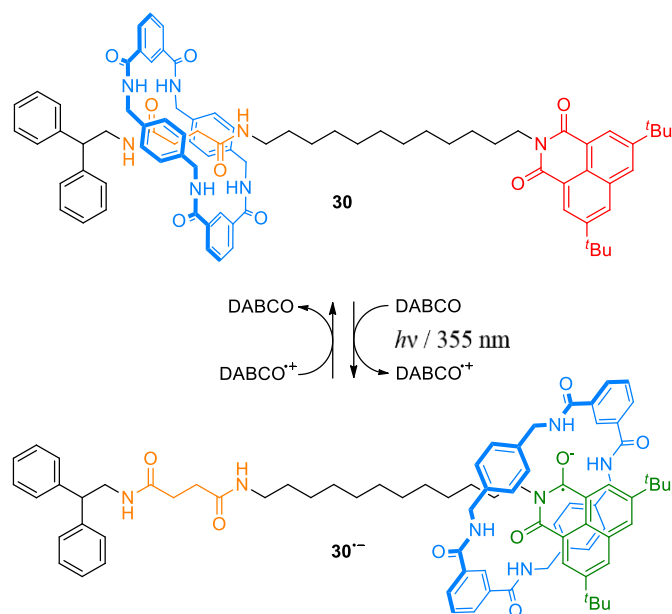
4.3. Photo-switches

In order to obtain photo-driven switches based on MIMs, there are mainly two different strategies: the photoisomerization and the photoinduced electron transfer. Regarding the latter, Benniston and Harriman demonstrated that the laser excitation of a π -donor/ π -acceptor [2]rotaxane incorporating a CBPQT⁴⁺ macrocycle, a substituted hydroquinone core and ferrocene stoppers can act like a shuttle because of the formation of radical cations. One is formed on one of the bipyridine unit of the macrocycle while another one is generated on the hydroquinone subunit of the axle. Then, the radical cation of the thread is transferred to one of the ferrocene stopper resulting in the shuttling of the macrocycle between the opposite stopper and the hydroquinone station.¹²⁰ Later, the translation of a macrocycle in a Cu^I-templated rotaxane by the photo-oxidation of the Cu^I center to Cu^{II} in the presence of *para*-nitrobenzyl bromide was reported.¹²¹ Subsequently, Leigh and Wurpel succeeded to construct a photo-switch employing a benzylic amide macrocycle-based [2]rotaxane (**30**) containing a succinamide station and a naphthalimide stopper. Although, this work can be performed

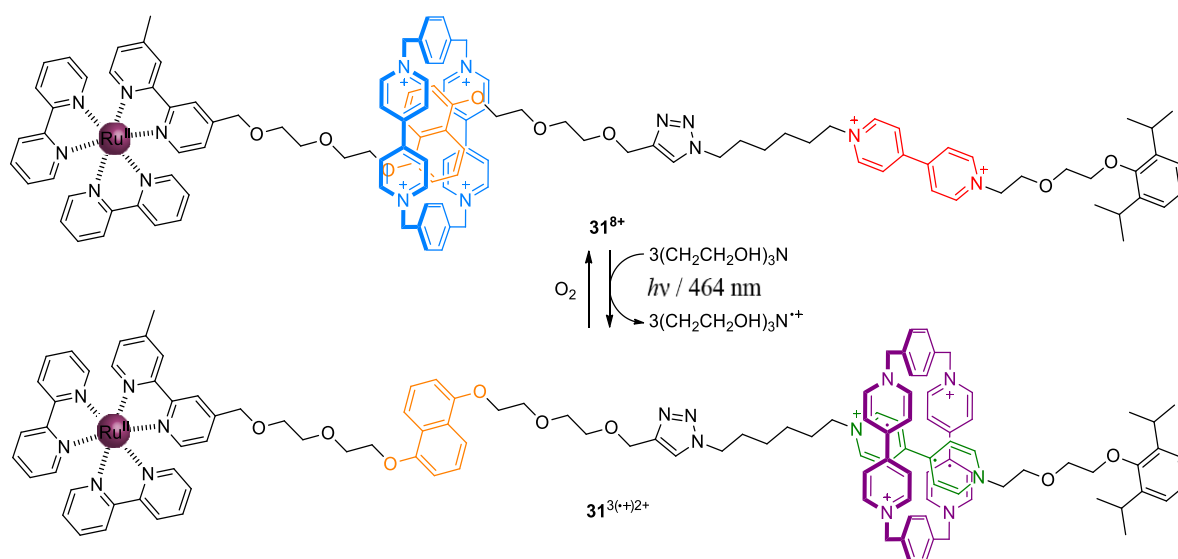
¹²⁰ A. C. Benniston, A. Harriman, *Angew. Chem., Int. Ed. Engl.* **1993**, *32*, 1459-1461.

¹²¹ N. Armaroli, V. Balzani, J.-P. Collin, P. Gaviña, J.-P. Sauvage, B. Ventura, *J. Am. Chem. Soc.* **1999**, *121*, 4397-4408.

electrochemically, the laser-induced excitation of the naphthalimide moiety in the presence an electron donor, such as 1,4-diazabicyclo[2.2.2]octane (DABCO), generates a radical cation on the naphthalimide group which leads the macrocycle towards it (Scheme 9).¹¹⁴



Scheme 9. Photo-driven switch based on a benzylic amide [2]rotaxane.¹¹⁴



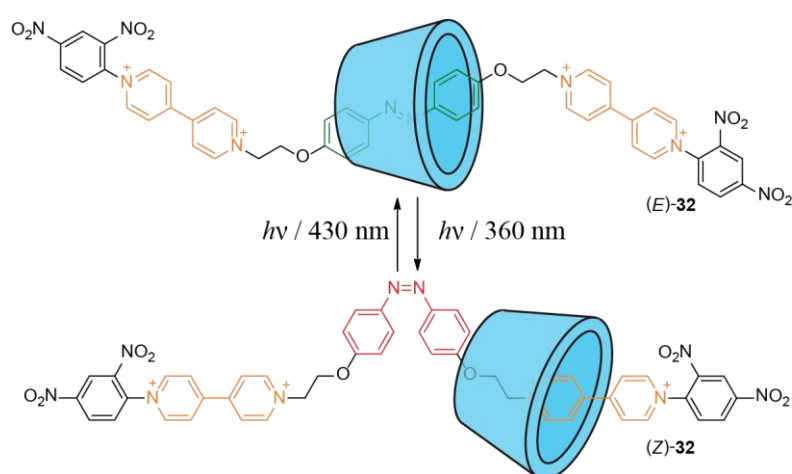
Scheme 10. A photo-switch based on photoinduced electron transfer described by Sauvage and Stoddart.¹²²

Following this work, Balzani, Credi and Stoddart showed that a [2]rotaxane featuring a BPP34C10/4,4'-bipyridinium/3,3'-dimethyl-4,4'-bipyridinium system with a Ru^{II} complex as stopper could operate as a

¹²² H. Li, A. C. Fahrenbach, A. Coskun, Z. Zhu, G. Barin, Y.-L. Zhao, Y. Y. Botros, J.-P. Sauvage, J. F. Stoddart, *Angew. Chem. Int. Ed.* **2011**, *50*, 6782–6788.

switch thanks to the photo-excitation of the Ru^{II} center.¹²³ Similarly, using a CBPQT⁴⁺/4,4'-bipyridinium/1,5-dialkoxynaphthalene system, the photo-excited Ru^{II} stopper can transfer one electron to each of the three bipyridinium groups, in the presence of a sacrificial electron donor molecule, triethanolamine, resulting in the translation of the macrocycle from the dialkoxynaphthalene unit to the bipyridinium radical cation station through radical pair interactions (Scheme 10).¹²²

The synthesis of the first photo-driven switch based on photo-isomerization was accomplished by Nakashima in 1997. For this purpose, he made α -cyclodextrin [2]rotaxane (*E*)-**32** with an azobenzene recognition site and a viologen secondary station. Then, he used the ability of the azobenzene unit to photo-isomerize between its *trans* and *cis* form. Thus, by irradiating the rotaxane with UV light (360 nm), he obtained the *cis*-azobenzene group and, as a result the macrocycle, initially on the *trans*-azobenzene unit, had to move to the viologen station due to steric hindrance. Finally, he recovered the *trans*-azobenzene group by irradiating the rotaxane at 430 nm and, therefore, the ring went back to its original position (Scheme 11).¹²⁴ Since then, the *E/Z* photoisomerization of azobenzene and, similarly, stilbene has been employed in numerous examples of photo-switches, including a variety of examples based on α -cyclodextrin rotaxanes.¹²⁵



Scheme 11. Azobenzene-based photo-switch developed by Nakashima.¹²⁴

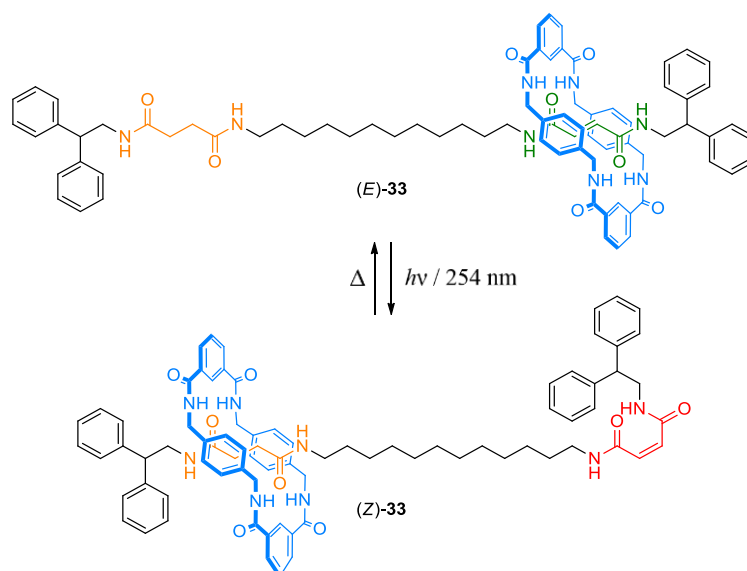
In 2003, Leigh and Zerbetto demonstrated the control of a shuttle (**33**) possessing a benzylic amide macrocycle between a fumaramide station and different secondary stations based on succinamide analogues through the photoisomerization of the alkene of the fumaramide moiety (*E*) to a maleamide

¹²³ V. Balzani, M. Clemente-León, A. Credi, B. Ferrer, M. Venturi, A. H. Flood, J. F. Stoddart, *Proc. Natl. Acad. Sci. U.S.A.* **2006**, *103*, 1178-1183.

¹²⁴ H. Murakami, A. Kawabuchi, K. Kotoo, M. Kunitake, N. Nakashima, *J. Am. Chem. Soc.* **1997**, *119*, 7605-7606.

¹²⁵ C. A. Stanier, S. J. Alderman, T. D. W. Claridge, H. L. Anderson, *Angew. Chem. Int. Ed.* **2002**, *41*, 1769-1772.

group (Z) (Scheme 12).¹²⁶ This system, or an alternative one featuring a glycyglycine secondary station, has been exploited in various switch architectures.¹²⁷ Recently, the regulation of the translation of a tetralactam macrocycle was achieved *via* the photoisomerization of a pyridyl-acyl hydrazone station. This switching system improved the distribution of the macrocycle between both stations of the thread since the photoisomerization of the pyridyl-acyl hydrazone unit is more efficient than that of the fumaramide moiety.³⁹



Scheme 12. A molecular photoswitch based on a [2]rotaxane owning a benzylic amide ring reported by Leigh and Zerbetto.¹²⁶

4.4. Solvent-driven switches

The main mechanism for the design of solvent-driven switches is the disruption of hydrogen bonding. An example of this strategy is [2]rotaxane **34**, containing a benzylic amide macrocycle and a glycyglycine station. In CHCl_3 , the ring is situated on the glycyglycine station because of the establishment of hydrogen bondings, while in DMSO H bonds are broken and therefore, the rotaxane can adopt different co-conformations. Usually, in DMSO, the tetralactam macrocycle will shuttle to an aliphatic chain of the rotaxane¹²⁸ (Scheme 13) or to a fullerene stopper.¹²⁹

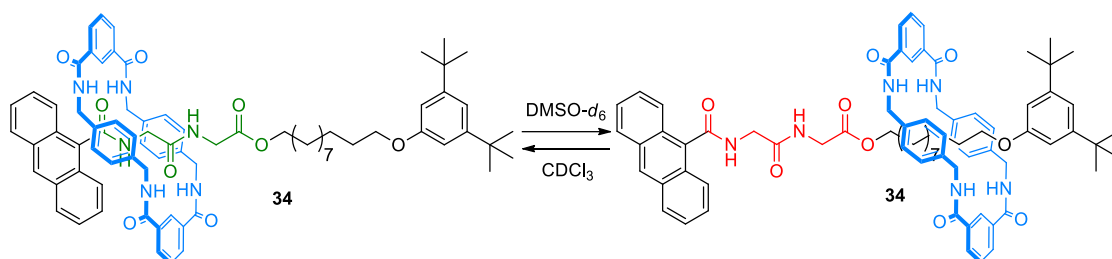
¹²⁶ A. Altieri, G. Bottari, F. Dehez, D. A. Leigh, J. K. Y. Wong, F. Zerbetto, *Angew. Chem. Int. Ed.* **2003**, *42*, 2296-2300.

¹²⁷ Selected examples: a) E. M. Pérez, D. T. F. Dryden, D. A. Leigh, G. Teobaldi, F. Zerbetto, *J. Am. Chem. Soc.* **2004**, *126*, 12210-12211. b) Y. Li, H. Li, Y. Li, H. Liu, S. Wang, X. He, N. Wang, D. Zhu, *Org. Lett.* **2005**, *7*, 4835-4838.

¹²⁸ D. A. Leigh, M. Á. F. Morales, E. M. Pérez, J. K. Y. Wong, C. G. Saiz, A. M. Z. Slawin, A. J. Carmichael, D. M. Haddleton, A. M. Brouwer, W. J. Buma, G. W. H. Wurpel, S. León, Francesco Z., *Angew. Chem. Int. Ed.* **2005**, *44*, 3062-3067.

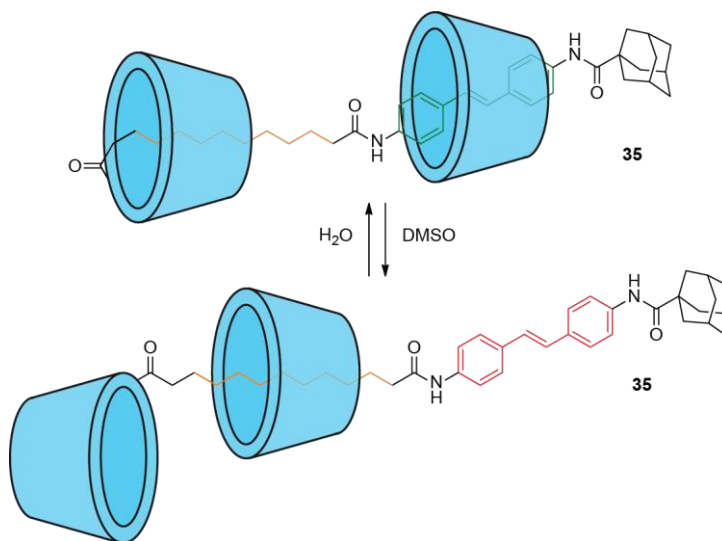
¹²⁹ A. Mateo-Alonso, G. Fioravanti, M. Marcaccio, F. Paolucci, D. C. Jagesar, A. M. Brouwer, M. Prato, *Org. Lett.* **2006**, *8*, 5173-5176.

In addition, it is possible to control the position of a macrocycle by means of solvation effect in an α -cyclodextrin-based [2]rotaxane possessing an alkane chain, a stilbene station and an α -cyclodextrin stopper. Indeed, in water, the cyclodextrin stopper is obstructed by the alkane chain of the thread, and the other ring encircles the stilbene recognition site, while in DMSO, the cyclodextrin stopper is not occluded and the macrocycle is situated on the alkane chain binding site (Scheme 14).¹³⁰



Scheme 13. A solvent-driven shuttle based on a tetralactam macrocycle.¹²⁸

Finally, in a pillar[5]arene-based [2]rotaxane owning a functionalized alkane chain with an imidazolium recognition site, the wheel is displaced from the imidazolium binding site to the alkane chain by increasing the proportion of DMSO in CDCl_3 due to the solvation effect of DMSO on the imidazolium salt.⁹⁷



Scheme 14. A solvent-driven switch based on an α -cyclodextrin-containing [2]rotaxane.¹³⁰

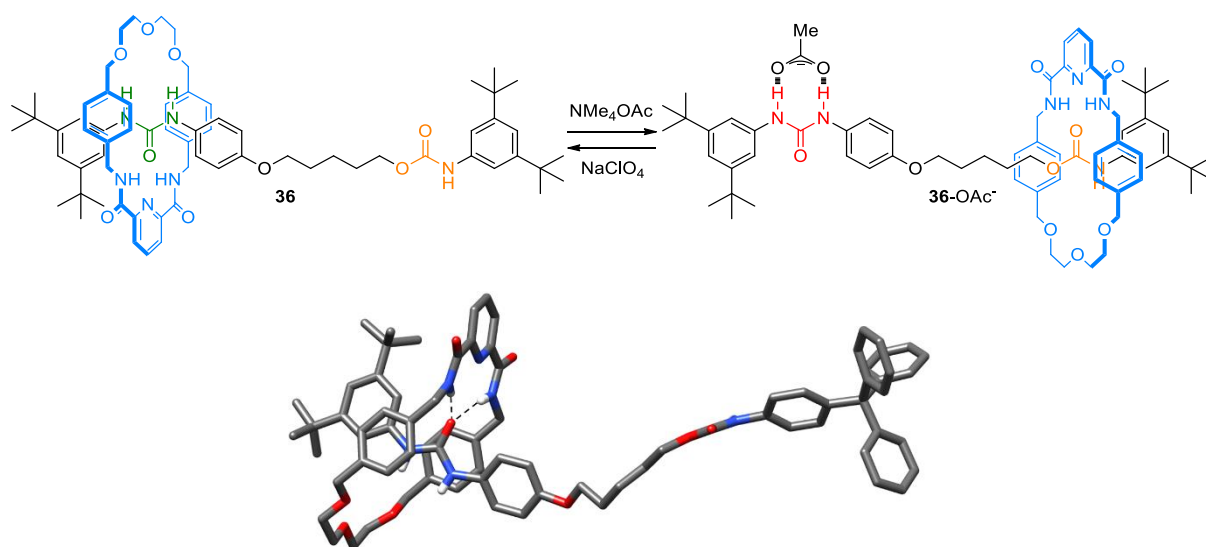
4.5. Anion switches

The two predominant manners that can be distinguished to operate an anion switch are the binding of an anion to both axle and macrocycle that induces a motion of the ring and the binding of an anion

¹³⁰ K. Yamauchi, A. Miyawaki, Y. Takashima, H. Yamaguchi, A. Harada, *J. Org. Chem.* **2010**, *75*, 1040-1046.

on the preferential recognition site of the macrocycle on the thread displacing the ring towards a secondary station.

Regarding the strategy involving the binding of an anion on the main binding site of the macrocycle, in 2007, Chui operated a hydrogen bonding-based [2]rotaxane (**36**) as an anion switch. The design displayed a urea recognition site, a carbamate secondary station and a macrocycle incorporating a diethylene glycol and a 2,6-pyridine dicarboxamide unit. Indeed, in the presence of an acetate anion, this interacts with the urea and therefore hampers the approach of the macrocycle, which has to migrate to the carbamate moiety (Scheme 15).¹³¹ The same methodology was exploited employing a urea primary station and a phosphine oxide secondary.¹³²



Scheme 15. An anion switch based on a [2]rotaxane and its X-ray diffraction structure.¹³¹ Color coding: C, grey; O, red; N, blue; H, white.

Furthermore, the control of the position of a bis-*para*-xylyl-[26]crown-6 (BPX26C6) wheel in a [2]rotaxane featuring a guanidinium primary station and a carbamate secondary station can be achieved thanks to the use of phosphate anions, since they coordinate to the guanidinium unit.¹³³ It was also reported that in the case of a pyridinium secondary station, chloride anions lead the crown ether to the pyridinium binding site.¹³⁴ Finally, in a hydrazodicarboxamide-based [2]rotaxane, the

¹³¹ Y.-L. Huang, W.-C. Hung, C.-C. Lai, Y.-H. Liu, S.-M. Peng, S.-H. Chiu, *Angew. Chem. Int. Ed.* **2007**, *46*, 6629-6633.

¹³² L. Liu, Y. Liu, P. Liu, J. Wu, Y. Guan, X. Hu, C. Lin, Y. Yang, X. Sun, J. Ma, L. Wang, *Chem. Sci.* **2013**, *4*, 1701-1706.

¹³³ Y.-C. You, M.-C. Tzeng, C.-C. Lai, S.-H. Chiu, *Org. Lett.* **2012**, *14*, 1046-1049.

¹³⁴ T.-C. Lin, C.-C. Lai, S.-H. Chiu, *Org. Lett.* **2009**, *11*, 613-616.

benzylic amide ring is displaced using benzoate anions as they coordinate to the hydrazodicarboxamide unit.¹³⁵ This switch can work using a naphthalimide radical anion.¹³⁶

Regarding the motion induced by the interaction of an anion with both the wheel and the thread, it was demonstrated for the first time by Smith in 2010. Employing a squaraine-based [2]rotaxane, he showed that the use of chloride anions can displace the tetralactam macrocycle to the triazole moiety.¹³⁷ One year later, Beer and co-workers reported that a macrocycle owning an ethylene glycol chain and a isophthalamide group can shuttle from an amide binding site to a 2,6-bis-imidazolium-pyridine recognition site on the thread in the presence of chloride anions due to the establishment of four hydrogen bondings between the 2,6-bis-imidazolium-pyridine group, the macrocycle and the anion.¹³⁸ The same strategy can be applied to [2]rotaxanes possessing the same type of ring but containing a naphthalimide or a NDI unit and a triazolium group as recognition sites on the axle. Thus, after the addition of chloride anions, the wheel migrates from the naphthalimide or the NDI station to the triazolium binding site.¹³⁹ Furthermore, in the case of a rotaxane featuring a triazolium and a iodotriazolium station (**37**·2PF₆⁻), the macrocycle encircles the triazolium group, however by addition of iodide anions, the ring moves to the iodotriazolium due to the establishment of halogen and hydrogen bonding (Scheme 16).¹⁴⁰

¹³⁵ J. Berná, C. Franco-Pujante, M. Alajarín, *Org. Biomol. Chem.* **2014**, *12*, 474-478.

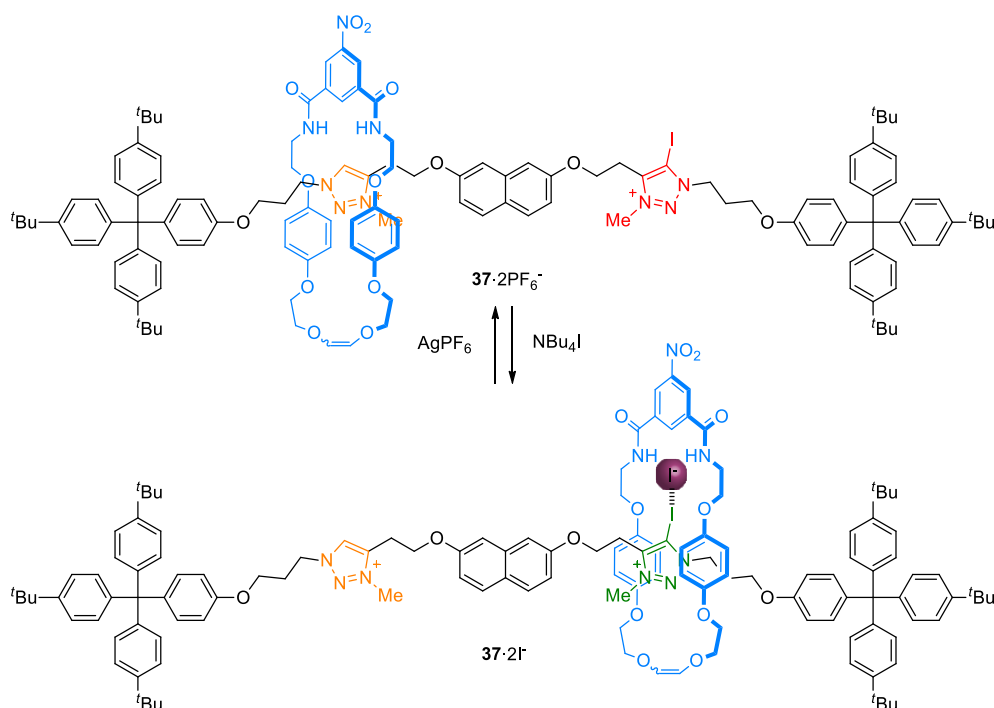
¹³⁶ A. Martinez-Cuezva, A. Pastor, G. Cioncoloni, R.-A. Orenes, M. Alajarin, M. D. Symes, J. Berná, *Chem. Sci.* **2015**, *6*, 3087-3094.

¹³⁷ J. J. Gassensmith, S. Matthys, J.-J. Lee, A. Wojcik, P. V. Kamat, B. D. Smith, *Chem. Eur. J.* **2010**, *16*, 2916-2921.

¹³⁸ C. J. Serpell, R. Chall, A. L. Thompson, P. D. Beer, *Dalton Trans.* **2011**, *40*, 12052–12055.

¹³⁹ a) G. T. Spence, M. B. Pitak, P. D. Beer, *Chem. Eur. J.* **2012**, *18*, 7100-7108. b) T. A. Barendt, I. Rašović, M. A. Lebedeva, G. A. Farrow, A. Auty, D. Chekulaev, I. V. Sazanovich, J. A. Weinstein, K. Porfyrakis, P. D. Beer, *J. Am. Chem. Soc.* **2018**, *140*, 1924-1936.

¹⁴⁰ A. Caballero, L. Swan, F. Zapata, P. D. Beer, *Angew. Chem. Int. Ed.* **2014**, *53*, 11854-11858.



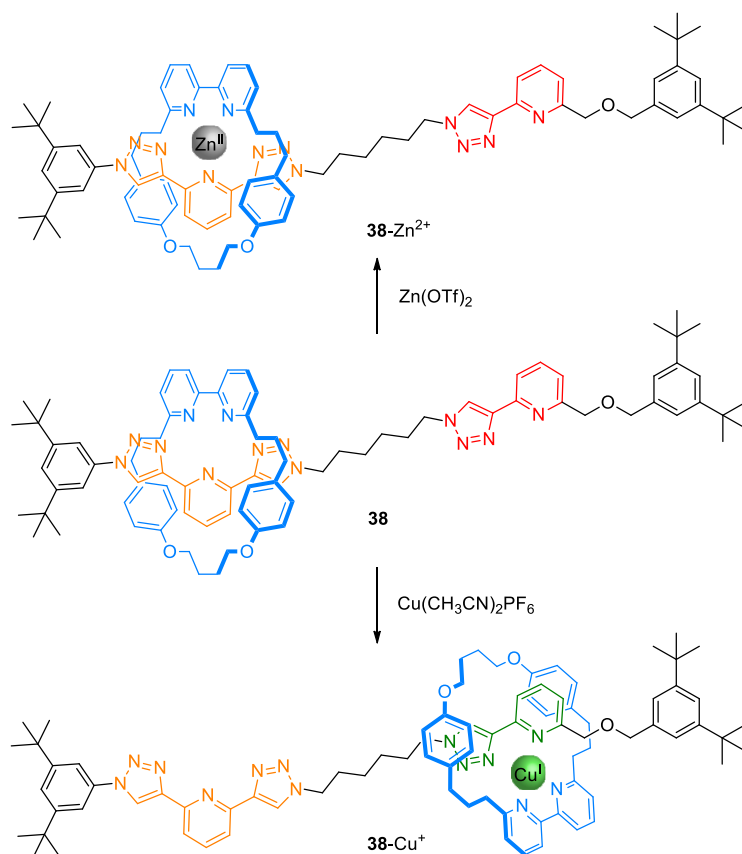
Scheme 16. An iodide anion-based shuttle reported by Beer.¹⁴⁰

4.6. Cation switches

In 2000, Sauvage and co-workers prepared a transition metal-driven switch based on a daisy chain architecture. The system was synthesized employing a Cu^{I} complex with two phen ligands with a terpy ligand as secondary station. After demetallation, the translation can be carried out using Zn^{II} as it forms a 5-coordinate complex with the terpy ligand of the axle and the phen unit of the ring.¹⁴¹ Similarly, Goldup employed a 2,2'-bipyridine macrocycle and a thread containing a bistriazolopyridine and monotriazolopyridine derivatives to control the translation of the wheel *via* the addition of transition metals. Thus, using Cu^{I} , the ring, which was previously situated on the bistriazolopyridine ligand, migrates to the monotriazolopyridine station, however with Zn^{II} , it stays on the same position (Scheme 17).^{84b} Alternatively, Leigh developed a switchable [2]rotaxane operating through allosteric control. Thus, the binding of Cd^{II} to a bis(picoly)amine stopper triggered a translation of a tetralactam ring along the thread from a succinamide to a succinic amide ester station due to a conformational change induced by metal chelation.¹⁴²

¹⁴¹ M. C. Jiménez, C. Dietrich-Buchecker, J.-P. Sauvage, *Angew. Chem. Int. Ed.* **2000**, *39*, 3284-3287.

¹⁴² D. S. Marlin, D. G. Cabrera, D. A. Leigh, A. M. Z. Slawin, *Angew. Chem. Int. Ed.* **2006**, *45*, 1385-1390.

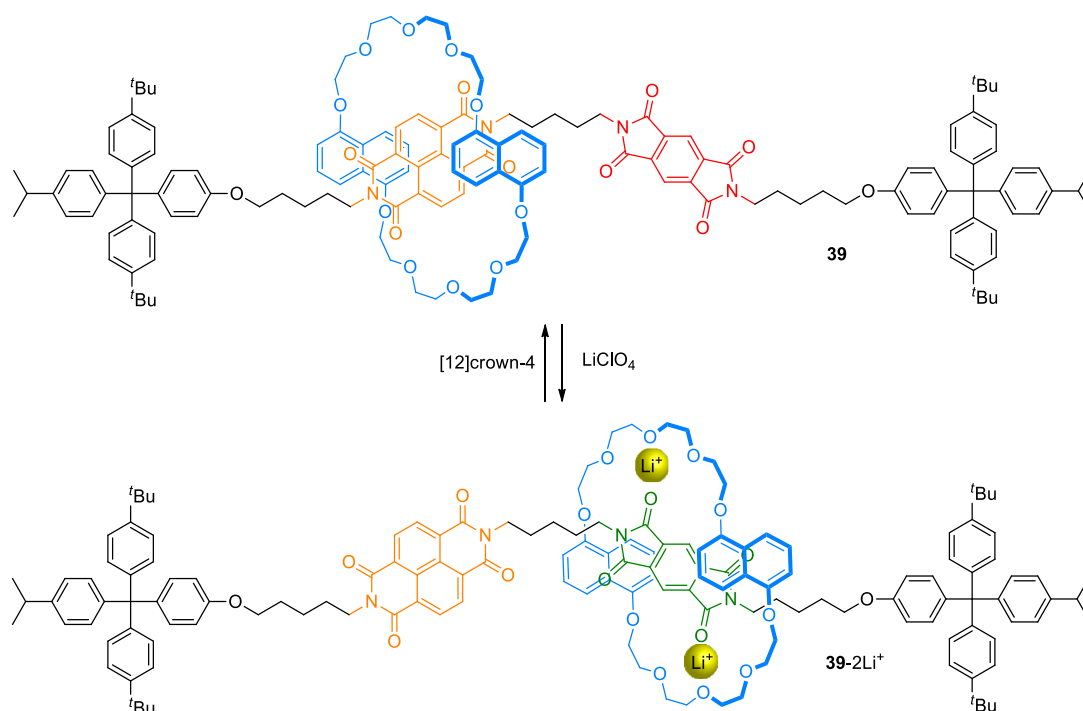


Scheme 17. Cu^I and Zn^{II} templated switch reported by Goldup.^{84b}

The first alkali metal cation switch was designed by Sanders and Stoddart, where they used the ability of Li⁺ to form a complex with a DNP38C10 ring and a pyromellitic diimide moiety. Thus, in a NDI-based [2]rotaxane with a pyromellitic diimide secondary binding site (**39**), the addition of 2 equivalents of LiClO₄ leads DNP38C10 from the NDI to the pyromellitic station. Subsequently, lithium cations are removed with an excess of [12]crown-4 and the crown ether macrocycle returns to its original position (Scheme 18).¹⁴³ Later, Leigh and co-workers employed this ion to induce the switching of a bipyridine macrocycle in a rotaxane featuring an aniline recognition site and DMAP secondary station. Thus, in the presence of Li⁺, the wheel shuttles from the aniline to the DMAP station. In addition, this system can work the same way through the addition of *para*-toluenesulfonic acid.¹⁴⁴

¹⁴³ S. A. Vignon, T. Jarrosson, T. Iijima, H.-R. Tseng, J. K. M. Sanders, J. F. Stoddart, *J. Am. Chem. Soc.* **2004**, *126*, 9884-9885.

¹⁴⁴ J. Berná, S. M. Goldup, A.-L. Lee, D. A. Leigh, M. D. Symes, G. Teobaldi, F. Zerbetto, *Angew. Chem. Int. Ed.* **2008**, *47*, 4392-4396.



Scheme 18. A lithium ion template switch reported by Sanders and Stoddart.¹⁴³

As Chui showed in 2010, Na⁺ ions can also be the trigger for a rotaxane switch containing a squaraine derivative and a macrotricyclic crown ether ring, which encircles a viologen binding site. Thus, upon addition of two equivalents of Na⁺, the wheel is situated on the squaraine station while after their removal with [2.2.2]cryptand, it returns to its initial position.¹⁴⁵ Similarly, this operation can be accomplished with potassium cations when the rotaxane features an anthraquinone secondary station.¹⁴⁶ Finally, barium ions can also control the motion of a macrocycle in a rotaxane. Indeed, Beer and co-workers demonstrated that in a rotaxane having an isophthalamide macrocycle crowned by a calix[4]arene derivative, the pirouetting¹⁴⁷ or the translation¹⁴⁸ of its ring can be achieved by the addition of Ba²⁺.

5. Molecular machines based on rotaxanes

Over the years, the research in the field of synthetic molecular machines has increased considerably. Switches based on rotaxane architectures have attracted much attention and have been employed in various artificial molecular machines since they exhibited a very interesting and highly efficient behaviour.⁴ These applications result mainly from the control of the translation movement of the

¹⁴⁵ S.-Y. Hsueh, C.-C. Lai, S.-H. Chiu, *Chem. Eur. J.* **2010**, *16*, 2997-3000.

¹⁴⁶ Z. Menga, C.-F. Chen, *Org. Biomol. Chem.* **2014**, *12*, 6937-6943.

¹⁴⁷ L. M. Hancock, P. D. Beer, *Chem. Commun.* **2011**, *47*, 6012-6014.

¹⁴⁸ A. V. Leontiev, C. A. Jemmett, P. D. Beer, *Chem. Eur. J.* **2011**, *17*, 816-825.

macrocycle along the thread in order to perform a task. Here, we will discuss some selected examples of molecular machines and their applications.

5.1. Macroscopic work

In 2005, Ho and Stoddart came up with the idea of attaching [3]rotaxanes to a gold surface by their macrocycles with the aim of bending the surface. Thus, they synthesized a redox switch (40^{8+}) containing the TTF/1,5-dialkoxynaphthalene system and two units of a CBPQT $^{4+}$ derivative functionalized with disulphide moieties to allow the union to the surface. Applying redox stimuli, both macrocycles moved from the TTF to the 1,5-dialkoxynaphthalene stations. Since these macrocycles were attached to a surface with a short linker, this translation induced the bending of the surface to accommodate the shorter distance between the macrocycles in the oxidized state. Using this strategy, they successfully bent the surface for 25 complete cycles (Figure 13).¹⁴⁹

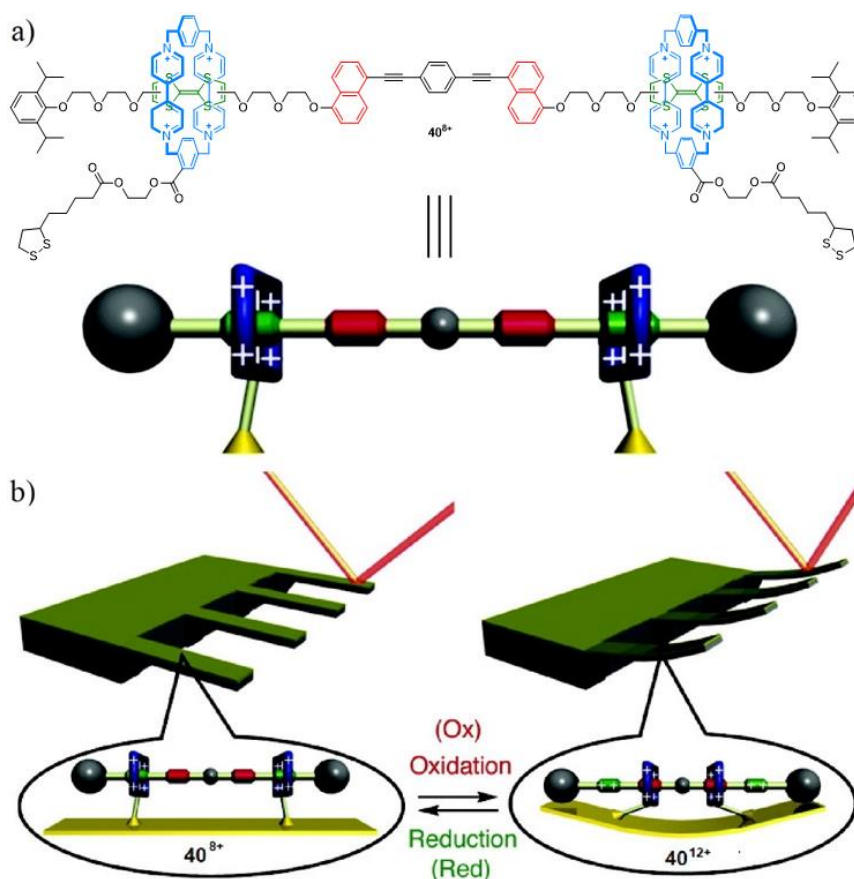


Figure 13. An artificial muscle reported by Ho and Stoddart: a) Structure of the switch (40^{8+}) and its graphical representation. b) Cartoon showing the proposed mechanism to induce the bending of the surface.¹⁴⁹ Reprinted with permission from ref 149. Copyright 2005 American Chemical Society.

¹⁴⁹ Y. Liu, A. H. Flood, P. A. Bonvallet, S. A. Vignon, B. H. Northrop, H.-R. Tseng, J. O. Jeppesen, T. J. Huang, B. Brough, M. Baller, S. Magonov, S. D. Solares, W. A. Goddard, C.-M. Ho, J. F. Stoddart, *J. Am. Chem. Soc.* **2005**, *127*, 9745-9759.

The same year, Leigh, Rudolf and Zerbetto managed to control the motion of droplets of diiodomethane on a gold surface. For this purpose, they adsorbed on this surface switches based on a [2]rotaxane with a tetrafluorosuccinamide/fumaramide system. Their irradiation with UV light causes the macrocycle to migrate from the fumaramide to the tetrafluorosuccinamide station due to the isomerisation of the former to maleamide and, therefore, to change the surface polarity. Indeed, the polarophobic surface turns to more polarophilic due to the encapsulation of the fluoroalkane units. Thanks to this modification, a drop of diiodomethane is capable of moving on a flat surface and climbing a 12° incline from the polarophobic to the polarophilic part of the surface.¹⁵⁰

More recently, Giuseppone prepared a polymeric gel containing daisy chains with an ammonium salt/triazolium salt system with the purpose of contracting and expanding the gel. Indeed, the length of the daisy chain decreases by the addition of an acid and then increases if a base is added. Consequently, the observation of a contraction and an expansion of the gel can be achieved macroscopically (Figure 14).¹⁵¹ The same phenomenon was observed in a polymeric gel incorporating daisy chains formed by α -cyclodextrins and stilbene recognition sites employing the *cis/trans* photoisomerization of the stilbene units. In this case, they demonstrated the bending of this hydrogel upon UV irradiation.¹⁵²

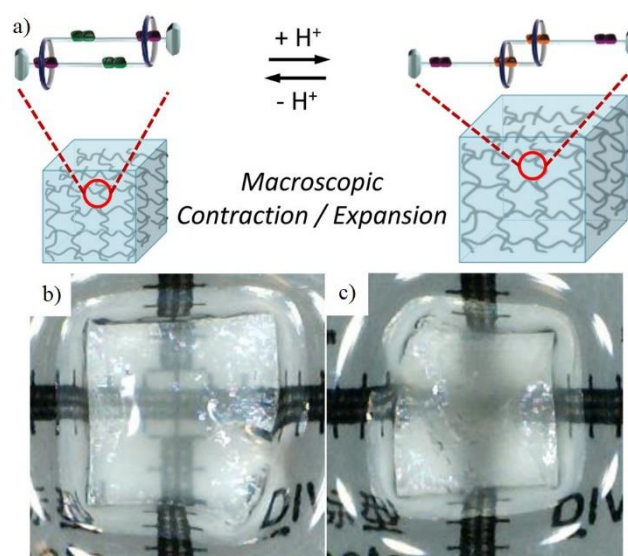


Figure 14. a) Graphical representation of the work induced by the addition of acid and base to the gel reported by Giuseppone. b) Picture of the expanded gel. c) Picture of the contracted gel.¹⁵¹ Reprinted with permission from ref 151. Copyright 2017 American Chemical Society.

¹⁵⁰ J. Berná, D. A. Leigh, M. Lubomska, S. M. Mendoza, E. M. Pérez, P. Rudolf, G. Teobaldi, F. Zerbetto, *Nat. Mat.* **2005**, *4*, 704-710.

¹⁵¹ A. Goujon, T. Lang, G. Mariani, E. Moulin, G. Fuks, J. Raya, E. Buhler, N. Giuseppone, *J. Am. Chem. Soc.* **2017**, *139*, 14825-14828.

¹⁵² S. Ikejiri, Y. Takashima, M. Osaki, H. Yamaguchi, A. Harada, *J. Am. Chem. Soc.* **2018**, *140*, 17308-17315.

5.2. Nanovalves

In 2005, Stoddart and Zink built the first supramolecular nanovalve based on a [2]rotaxane structure. These MIMs were attached to mesostructured silica particles containing nanopores and its design was based on a CBPQT⁴⁺ macrocycle, which encircles a TTF derivative, and a 1,5-dialkoxynaphthalene secondary station. Through a redox control, they were able to load, unload and recharge the nanopores with different luminescent probe molecules by changing the position of the macrocycle of the thread, blocking and unblocking the nanopores (Figure 15).¹⁵³

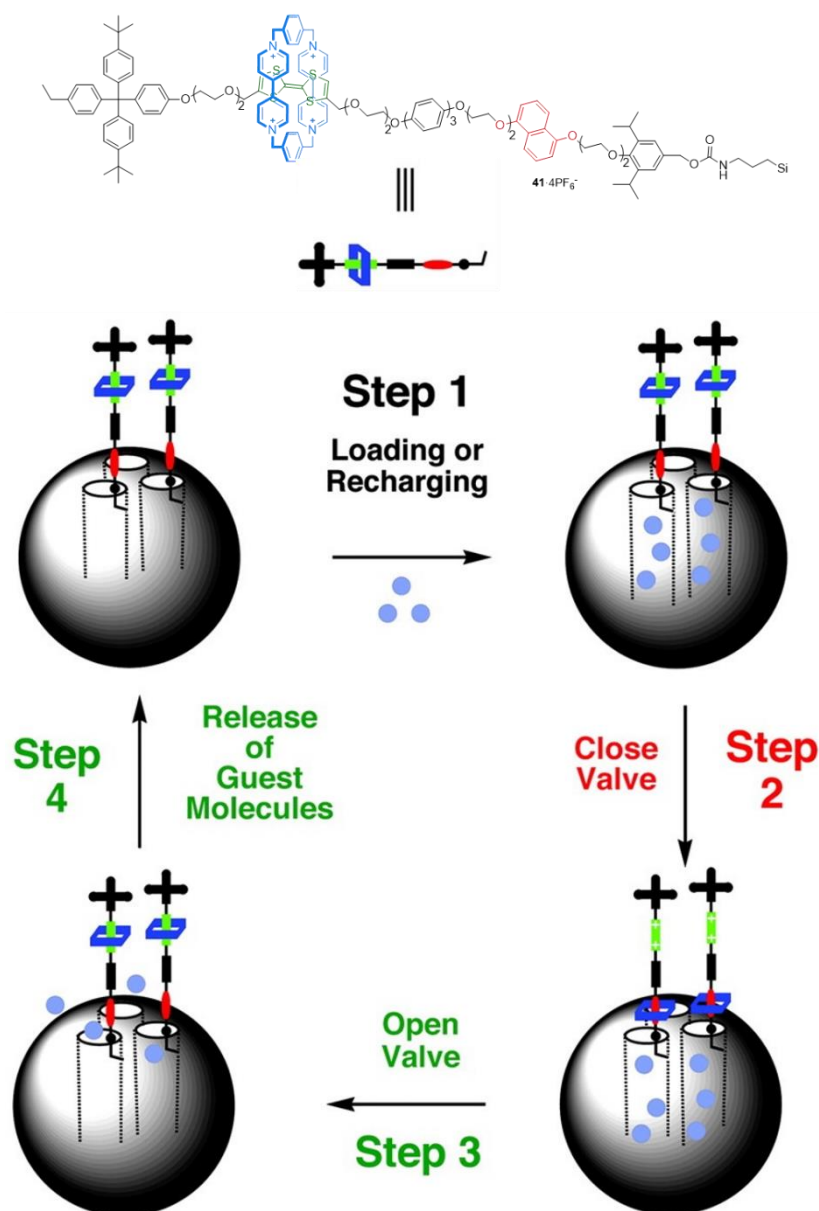


Figure 15. Graphical representation and operation mechanism of the nanovalve system described by Stoddart and Zink.¹⁵³ Reprinted with permission from ref 153. Copyright 2005 National Academy of Sciences.

¹⁵³ T. D. Nguyen, H.-R. Tseng, P. C. Celestre, A. H. Flood, Y. Liu, J. F. Stoddart, J. I. Zink, *Proc. Natl. Acad. Sci. U.S.A.* **2005**, *102*, 10029-10034.

In a similar way, a nanovalve based on an α -cyclodextrin [2]rotaxane was grafted to mesoporous silica. This structure possesses an adamantane stopper connected by an amide or an ester group to the axle. In order to unlock the pores, an enzyme was employed to cleave the amide or the ester bond, leading to the release of the α -cyclodextrin macrocycle and the fluorescent molecules captured in the nanopores.¹⁵⁴

Recently, Berná and co-workers demonstrated the efficiency of their light-responsive nanovalve. Their system featured a fumaramide/glycylglycine switching motif for a benzylic amide macrocycle. By irradiation at 254 nm and 365 nm, they were able to respectively close and open the valve, resulting in the load and delivery of dye cargo molecules.¹⁵⁵

5.3. Synthesis

5.3.1. Peptide synthesizers

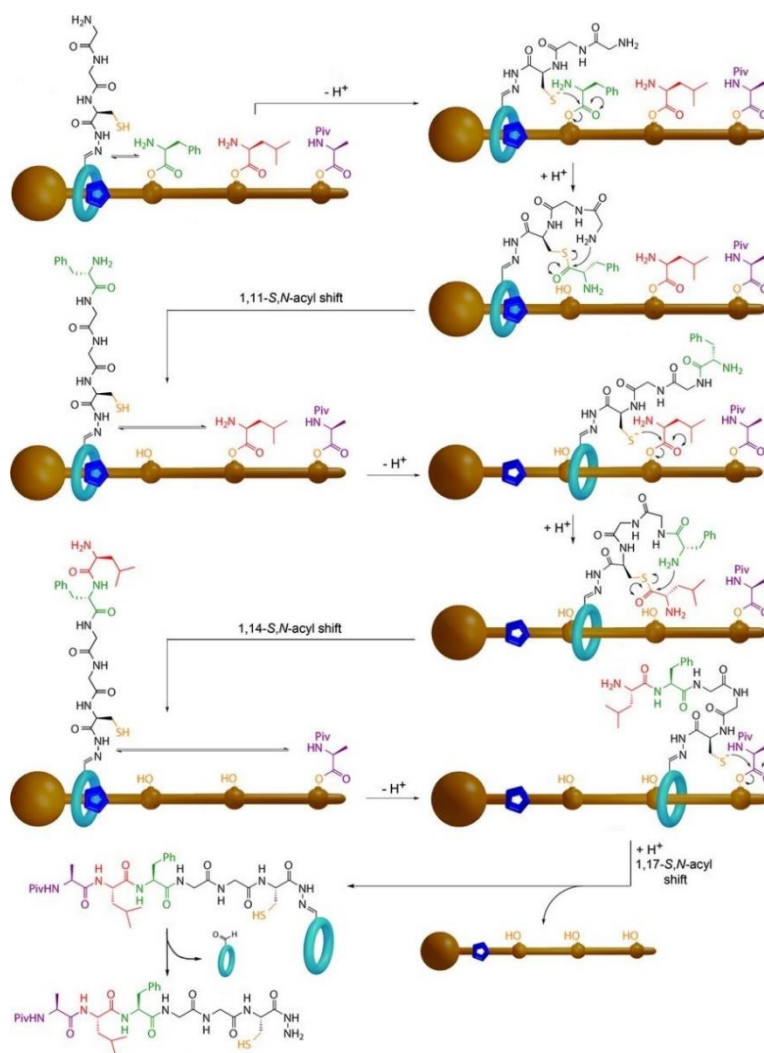
With the intention of mimicking the action of ribosomes, Leigh and co-workers synthesized, by the active metal template strategy, a [2]rotaxane featuring amino acid gates and a macrocycle with a short peptide containing a S-trityl protected cysteine moiety. After deprotection of the thiol, the resulting thiolate cleaves the first amino acid gate and transfers it to the N-terminal amino acid of the macrocycle peptide through a native chemical ligation mechanism. This process occurred for each amino acid on the axle and yielded a peptide whose sequence was defined by the order of the amino acids on the thread (Scheme 19).¹⁵⁶ Following the same strategy, longer peptides and a β -amino acid peptide have been synthesized.¹⁵⁷

¹⁵⁴ K. Patel, S. Angelos, W. R. Dichtel, A. Coskun, Y.-W. Yang, J. I. Zink, J. F. Stoddart, *J. Am. Chem. Soc.* **2008**, *130*, 2382-2383.

¹⁵⁵ A. Martinez-Cuezva, S. Valero-Moya, M. Alajarin, J. Berná, *Chem. Commun.* **2015**, *51*, 14501-14504.

¹⁵⁶ B. Lewandowski, G. De Bo, J. W. Ward, M. Papmeyer, S. Kuschel, M. J. Aldegunde, P. M. E. Gramlich, D. Heckmann, S. M. Goldup, D. M. D'Souza, A. E. Fernandes, D. A. Leigh, *Science* **2013**, *339*, 189-193.

¹⁵⁷ a) G. De Bo, S. Kuschel, D. A. Leigh, B. Lewandowski, M. Papmeyer, J. W. Ward, *J. Am. Chem. Soc.* **2014**, *136*, 5811-5814. b) G. De Bo, M. A. Y. Gall, M. O. Kitching, S. Kuschel, D. A. Leigh, D. J. Tetlow, J. W. Ward, *J. Am. Chem. Soc.* **2017**, *139*, 10875-10879. c) G. De Bo, M. A. Y. Gall, S. Kuschel, J. De Winter, P. Gerbaux, D. A. Leigh, *Nat. Nanotechnol.* **2018**, *13*, 381-385.



Scheme 19. Mechanism of the peptide synthesis by a molecular machine described by Leigh.¹⁵⁶ Reprinted with permission from ref 156. Copyright 2013 The American Association for the Advancement of Science.

5.3.2. Switchable catalysis

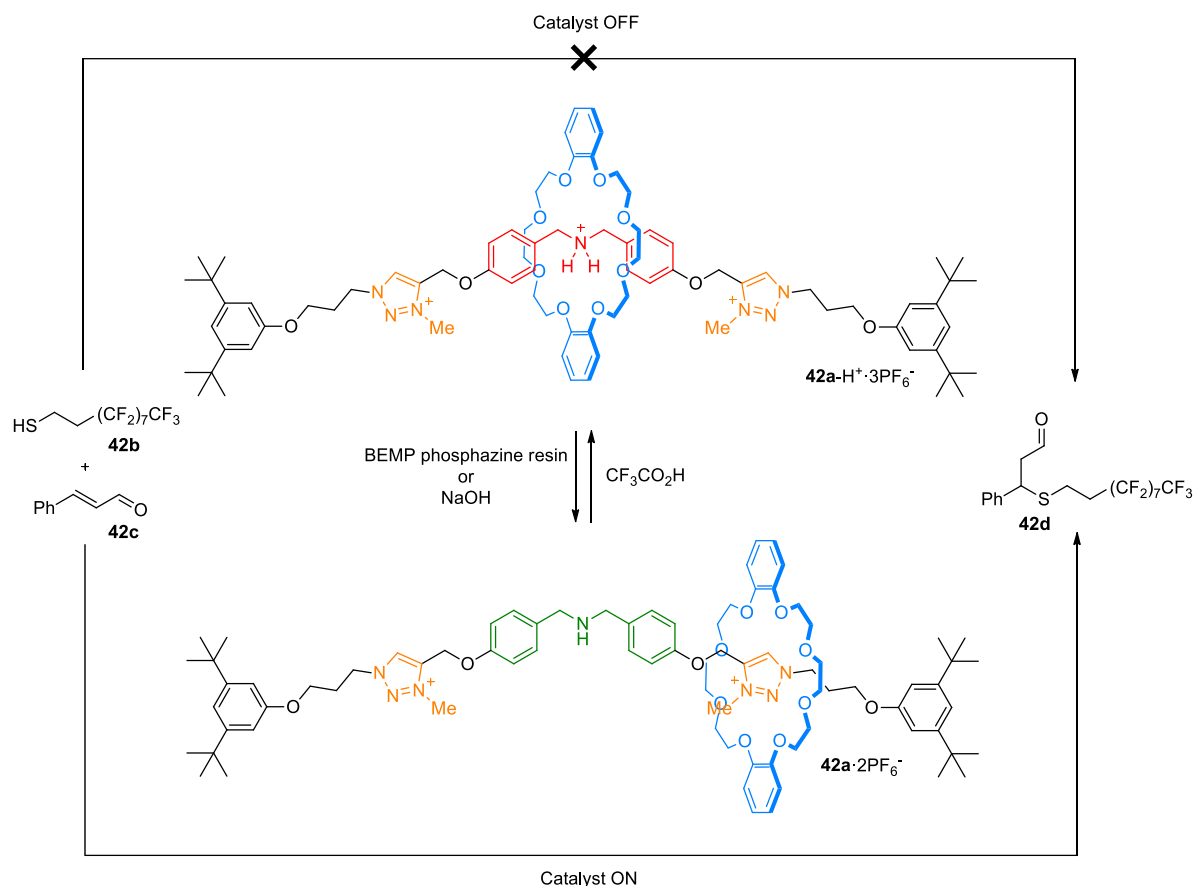
Over the years, a great number of rotaxane catalysts¹⁵⁸ and switchable catalysts¹⁵⁹ were reported. Thus, in 2012, Leigh and co-workers combined both concepts and built the first rotaxane-based switchable catalyst for a Michael addition reaction. This [2]rotaxane was designed as a pH switch containing a dibenzylammonium/triazolium system and a DB24C8 macrocycle. In acidic media, the crown ether encircles the ammonium salt resulting in the concealment of the catalytic site and an absence of catalysis, whereas in basic media, the amine is free and the macrocycle shuttles towards the triazolium ring so the catalytic site is exposed and, therefore, the catalysis occurs (Scheme 20).¹⁶⁰ Later on, they investigated the application of this rotaxane in other organocatalytic reactions, such as

¹⁵⁸ a) D. A. Leigh, V. Marcos, M. R. Wilson, *ACS Catal.* **2014**, *4*, 4490-4497. b) A. Martinez-Cuezva, A. Saura-Sanmartin, M. Alajarin, J. Berna, *ACS Catal.* **2020**, *10*, 7719-7733.

¹⁵⁹ V. Blanco, D. A. Leigh, V. Marcos, *Chem. Soc. Rev.* **2015**, *44*, 5341-5370.

¹⁶⁰ V. Blanco, A. Carlone, K. D. Hänni, D. A. Leigh, B. Lewandowski, *Angew. Chem. Int. Ed.* **2012**, *51*, 5166-5169

enamine catalysis, iminium catalysis, tandem iminium-enamine catalysis, trienamine and anion-binding catalysis.¹⁶¹



Scheme 20. An ON/OFF switchable catalyst employed for a Michael addition reported by Leigh.¹⁶⁰

Following these works, other structures were synthesized for enamine¹⁶² or Michael addition catalysis,¹⁶³ even with two distinct active sites.¹⁶⁴ Furthermore, the asymmetric Michael addition catalysis,¹⁶⁵ the asymmetric aldol reaction catalysis,^{165b} the action of a photo-switch cocatalyst to increase the diastereomeric ratio in a Baylis–Hillman reaction¹⁶⁶ and the control of the stereochemistry

¹⁶¹ a) V. Blanco, D. A. Leigh, U. Lewandowska, B. Lewandowski, V. Marcos, *J. Am. Chem. Soc.* **2014**, *136*, 15775-15780. b) K. Eichstaedt, J. Jaramillo-Garcia, D. A. Leigh, V. Marcos, S. Pisano, T. A. Singleton, *J. Am. Chem. Soc.* **2017**, *139*, 9376-9381.

¹⁶² Y.-J. Lee, K.-S. Liu, C.-C. Lai, Y.-H. Liu, S.-M. Peng, R. P. Cheng, S.-H. Chiu, *Chem. Eur. J.* **2017**, *23*, 9756-9760.

¹⁶³ C. M. Álvarez, H. Barbero, D. Miguel, *Eur. J. Org. Chem.* **2015**, 6631-6640.

¹⁶⁴ J. Beswick, V. Blanco, G. De Bo, D. A. Leigh, U. Lewandowska, B. Lewandowski, K. Mishiro, *Chem. Sci.* **2015**, *6*, 140-143.

¹⁶⁵ a) V. Blanco, D. A. Leigh, V. Marcos, J. A. Morales-Serna, A. L. Nussbaumer, *J. Am. Chem. Soc.* **2014**, *136*, 4905-4908. b) M. Calles, J. Puigcerver, D. A. Alonso, M. Alajarin, A. Martinez-Cuezva, J. Berna, *Chem. Sci.* **2020**, *11*, 3629-3635.

¹⁶⁶ A. Martinez-Cuezva, A. Saura-Sanmartin, T. Nicolas-Garcia, C. Navarro, R.-A. Orenes, M. Alajarin, J. Berna, *Chem. Sci.* **2017**, *8*, 3775-3780.

of an asymmetric enamine catalysis by the position of the macrocycle¹⁶⁷ were described with the involvement of a rotaxane shuttle. It is also possible to use pulses of chemical fuel¹⁶⁸ to regulate the position of the macrocycle in a pH-driven switch in order to generate a dissipative catalyst. Indeed, a [2]rotaxane-based switch, owning a dibenzylammonium/thiourea system and a DB24C8 ring whose position is regulated by pulses of chemical fuel, can catalyze the reduction of an alkene by transfer hydrogenation employing the thiourea moiety as catalytic site when the crown ether encircles the dibenzylammonium.¹⁶⁹

5.4. Modulation of the fluorescence

One of the earliest examples of the controlled modulation of the fluorescence response in a rotaxane was reported by Tian and co-workers employing an emissive naphthalimide stopper and a stilbene/ α -cyclodextrin switching system. The photoisomerization of the stilbene unit induced a translation of the cyclodextrin towards the fluorescent stopper accompanied by an increase of the fluorescence response.¹⁷⁰ Using the same principle in an α -cyclodextrin-based [2]rotaxane with an azobenzene core and two different fluorescent naphthalimide stoppers, they were able to regulate the emission intensity of the shuttle.¹⁷¹

Furthermore, in 2004, Leigh and Zerbetto described a photo-switchable [2]rotaxane featuring a fumaramide/glycylglycine system and an anthracene stopper located next to the glycylglycine station. The photoisomerization of the fumaramide unit resulted in a quenching of the anthracene fluorescence due to the electron transfer between the anthracene stopper and the pyridinium moieties of the macrocycle (Scheme 21).^{127a} Using the same quenching strategy in a solvent-driven switch, they were able to create a logic gate.¹²⁸ Furthermore, triazolium salts have the ability to quench the anthracene fluorescence through photoinduced electron transfer. Therefore, rotaxanes owning a dibenzylammonium/triazolium switching system and a DB24C8 macrocycle were found to be effective in the modulation of their emission response since the crown ether ring inhibits the electron transfer when it encircles the triazolium salt.¹⁷²

¹⁶⁷ M. Dommaschk, J. Echavarren, D. A. Leigh, V. Marcos, T. A. Singleton, *Angew. Chem. Int. Ed.* **2019**, *58*, 14955-14958.

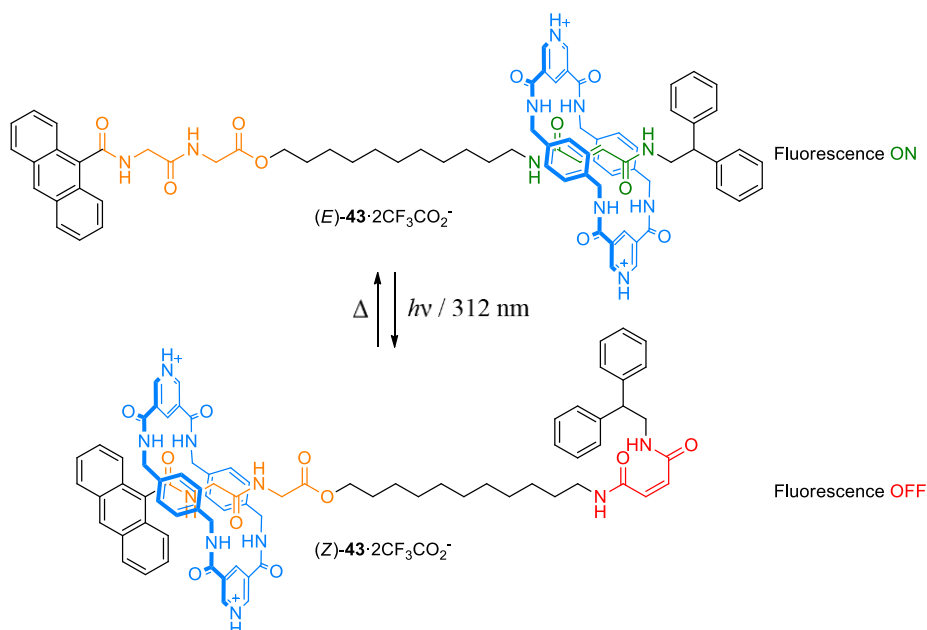
¹⁶⁸ C. Biagini, S. Di Stefano, *Angew. Chem., Int. Ed.* **2020**, *59*, 8344-8354.

¹⁶⁹ C. Biagini, S. D. P. Fielden, D. A. Leigh, F. Schaufelberger, S. Di Stefano, D. Thomas, *Angew. Chem. Int. Ed.* **2019**, *58*, 9876-9880.

¹⁷⁰ Q.-C. Wang, D.-H. Qu, J. Ren, K. Chen, H. Tian, *Angew. Chem. Int. Ed.* **2004**, *43*, 2661-2665.

¹⁷¹ D.-H. Qu, Q.-C. Wang, J. Ren, H. Tian, *Org. Lett.* **2004**, *6*, 2085-2088.

¹⁷² a) W. Yang, Y. Li, J. Zhang, Y. Yu, T. Liu, H. Liu, Y. Li, *Org. Biomol. Chem.* **2011**, *9*, 6022-6026. b) C.-S. Kwan, A. S. C. Chan, K. C.-F. Leung, *Org. Lett.* **2016**, *18*, 976-979. c) A. Ghosh, I. Paul, M. Adlung, C. Wickleder, M. Schmittel, *Org. Lett.* **2018**, *20*, 1046-1049.



Scheme 21. Modulation of the fluorescence in a rotaxane.^{127a}

Recently, Qu and co-workers prepared a switch with a dibenzylammonium/triazolium system and a DB24C8 macrocycle possessing two ferrocene derivatives. This [2]rotaxane was stoppered by one fluorescent naphthalimide unit located next to the triazolium station. Thus, when the macrocycle was encircling the triazolium salt, a strong photoinduced electron transfer was established between the naphthalimide and the ferrocene groups which quenched the emission. On the contrary, when the ring was on the dibenzylammonium station, the photoinduced electron transfer was weak and a strong luminescence was recovered.¹⁷³ Using this quenching method, they were able to modulate the fluorescence of SiO₂ nanoparticles¹⁷⁴ and polymers¹⁷⁵ by attaching this switch on these materials. Moreover, this strategy was employed to switch between the emission of a naphthalimide and a perylene diimide dye.¹⁷⁶ Similarly, they could control the fluorescence of a [3]rotaxane owning the same switching system and macrocycles but featuring a perylene diimide group as emitter.¹⁷⁷

It is also possible to control the luminescence in a [2]rotaxane-based solvent-driven switch using the fluorescence resonance energy transfer (FRET) between a donor and an acceptor coumarin derivative, located on the stopper and the macrocycle respectively.¹⁷⁸ In addition, the control of the phosphorescence in a [2]rotaxane switch was reported for a system composed by an anthracene

¹⁷³ H. Zhang, J. Hu, D.-H. Qu, *Org. Lett.* **2012**, *14*, 2334-2337.

¹⁷⁴ Z.-Q. Cao, Q. Miao, Q. Zhang, H. Li, D.-H. Qu, H. Tian, *Chem. Commun.* **2015**, *51*, 4973-4976.

¹⁷⁵ Z.-Q. Cao, Z.-L. Luan, Q. Zhang, R.-R. Gu, J. Ren, D.-H. Qu, *Polym. Chem.* **2016**, *7*, 1866-1870.

¹⁷⁶ Y. Liu, Q. Zhang, W.-H. Jin, T.-Y. Xu, D.-H. Qu, H. Tian, *Chem. Commun.* **2018**, *54*, 10642-10645.

¹⁷⁷ Z.-Q. Cao, H. Li, J. Yao, L. Zou, D.-H. Qu, H. Tian, *Asian J. Org. Chem.* **2015**, *4*, 212-216.

¹⁷⁸ H. Onagi, J. Rebek Jr., *Chem. Commun.* **2005**, 4604-4606.

stopper and a Pt^{II} porphyrin group placed on the macrocycle.¹⁷⁹ Finally, the luminescence properties of polymers containing rotaxanes with fluorescent macrocycles can be controlled through the stretching of the material since when it is relaxed it is almost not emissive.¹⁸⁰

5.5. Logic gates

Since molecular switches based on [2]rotaxanes possess typically two stations, they can be suitable devices to code or store information in the form of binary digits. Thus, in 1999, Heath employed one of Stoddart's [2]rotaxanes, based on π -donor/ π -acceptor interactions, to create an electronically configurable logic gates.¹⁸¹ Later, they built an electronic memory with a bistable [2]rotaxane based on a TTF/1,5-dialkoxynaphthalene system.¹⁸² In addition, a logic gate can also be constructed with a photo-switch based on photoinduced electron transfer featuring a Ru^{II} stopper and a CBPQT⁴⁺/4,4'-bipyridinium/1,5-dialkoxynaphthalene switching system.¹⁸³

Furthermore, as discussed in section 5.4., in a polymer, the modulation of the fluorescence in a solvent-driven switch can afford a logic gate.¹²⁸ Finally, cyclodextrin-based [2]rotaxanes containing a stilbene and an azobenzene switch as well as naphthalimide stoppers can act like a logic gate through UV-Vis absorption and fluorescence modulation. The controlled photoisomerization of the stilbene or the azobenzene groups is performed at different wavelength. When one of these two units is photoisomerized, the change of fluorescence intensity is high while the absorbance change is low but when both photo-switches are photoisomerized, it is the opposite. Taking advantage of these changes, this [2]rotaxane can act as a logic gate (Scheme 22).¹⁸⁴

¹⁷⁹ X. Ma, J. Zhang, J. Cao, X. Yao, T. Cao, Y. Gong, C. Zhao, H. Tian, *Chem. Sci.* **2016**, *7*, 4582-4588.

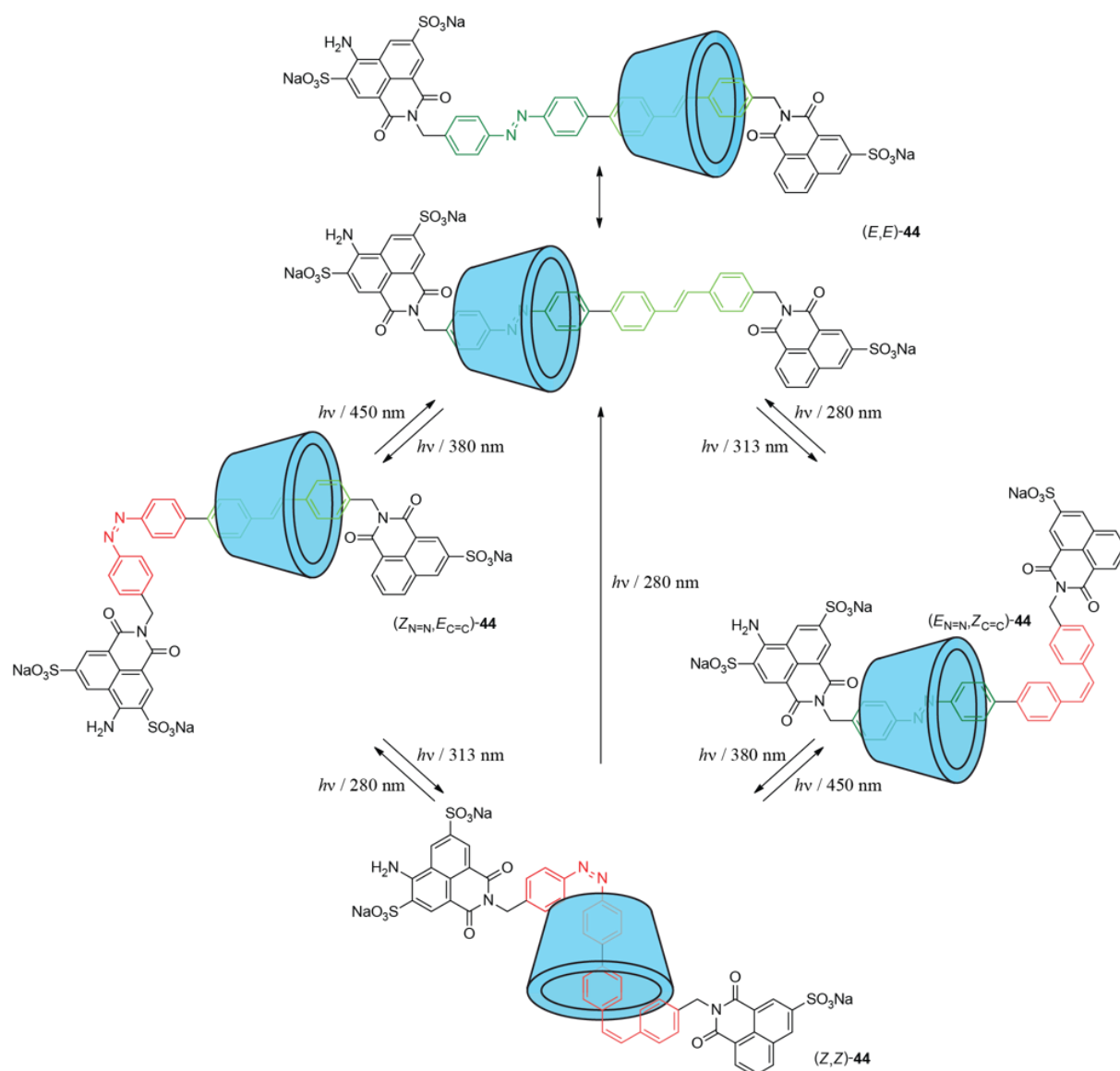
¹⁸⁰ Y. Sagara, M. Karman, A. Seki, M. Pannipara, N. Tamaoki, C. Weder, *ACS Cent. Sci.* **2019**, *5*, 874-881.

¹⁸¹ C. P. Collier, E. W. Wong, M. Belohradsky, F. M. Raymo, J. F. Stoddart, P. J. Kuekes, R. S. Williams, J. R. Heath, *Science* **1999**, *285*, 391-394.

¹⁸² J. E. Green, J. W. Choi, A. Boukai, Y. Bunimovich, E. Johnston-Halperin, E. Delonno, Y. Luo, B. A. Sheriff, K. Xu, Y. S. Shin, H.-R. Tseng, J. F. Stoddart, J. R. Heath, *Nature* **2007**, *445*, 414-417.

¹⁸³ C. Jia, H. Li, J. Jiang, J. Wang, H. Chen, D. Cao, J. F. Stoddart, X. Guo, *Adv. Mater.* **2013**, *25*, 6752-6759.

¹⁸⁴ D.-H. Qu, Q.-C. Wang, H. Tian, *Angew. Chem. Int. Ed.* **2005**, *44*, 5296-5299.



Input 1 (380 nm)	Input 1 (313 nm)	Output 1 (ΔA)	Output 2 (ΔF)	Binary Sum
0	0	0	0	00
1	0	0	1	01
0	1	0	1	01
1	1	1	0	10

Scheme 22. An α -cyclodextrin-based molecular switch that can act like a logic gate through the photoisomerization of its stilbene and azobenzene unit.¹⁸⁴

In addition to these synthetic molecular machines, artificial molecular motors and pumps were developed based on rotaxane switches throughout the years. This topic will be discussed in this thesis in the background section of chapter 1 (section 2.1.3.).

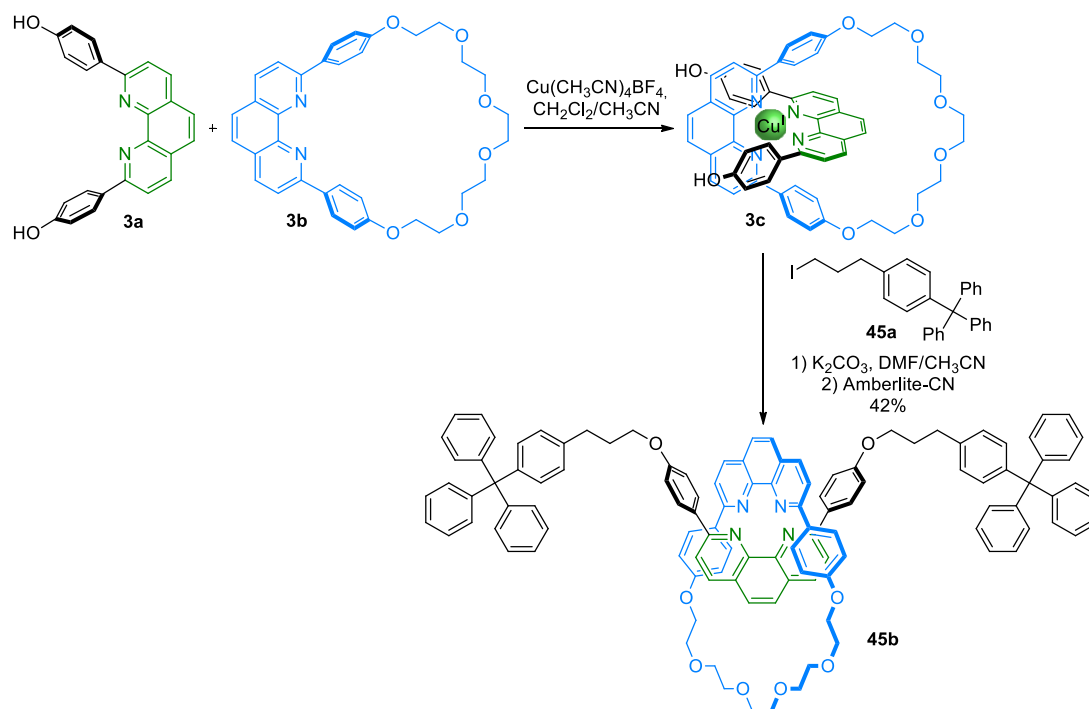
**Chapter 1: Synthesis and applications of [2]rotaxanes
using click Michael-type addition reactions to the vinyl
sulfonyl group**

1. A new efficient and versatile reaction in rotaxane synthesis

1.1 Background

1.1.1. Reactions for rotaxane synthesis through end-capping

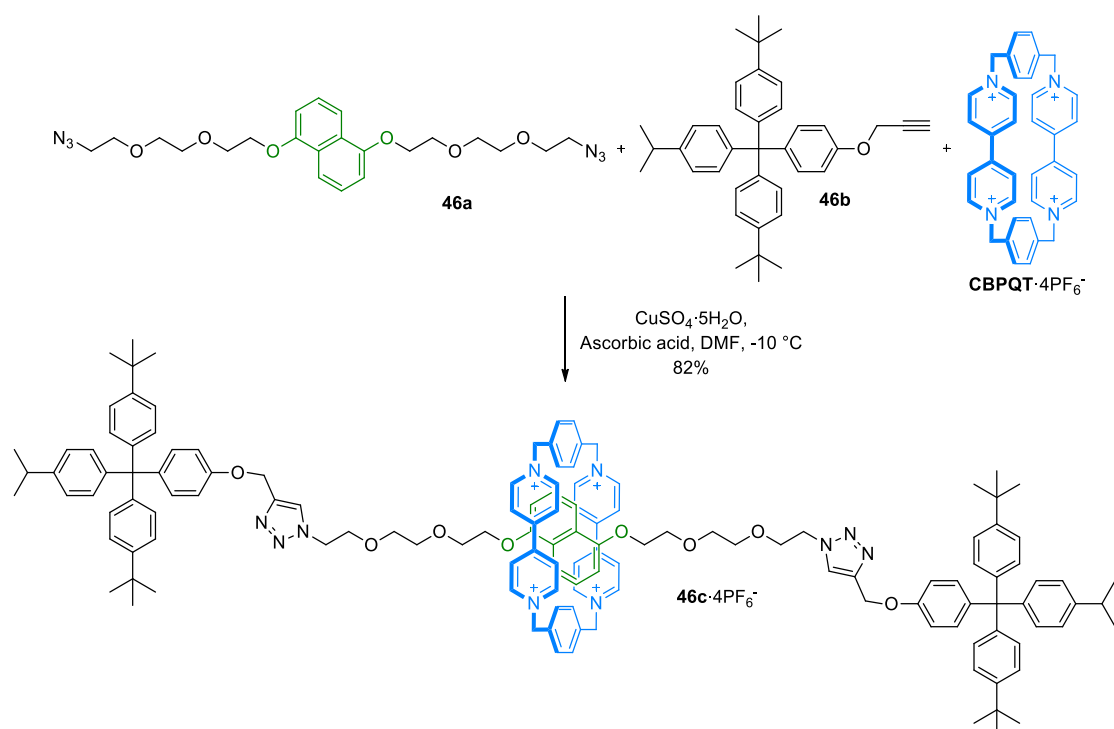
As shown in the general introduction, the incredible complexity and diversity of rotaxanes and their application as molecular machines has been attained through the development of innovative and varied synthetic strategies. The most useful approaches to generate rotaxanes are the capping and the clipping strategies. It is important to consider that these methodologies require to perform the rotaxane formation reaction without significantly altering the complexation equilibrium between both components of the rotaxane to maintain the supramolecular complex. Consequently, the reactions employed need to be efficient and proceed under mild conditions. In this chapter, we will focus mainly on the capping method to afford rotaxanes.



Scheme 23. End-capping synthesis of rotaxane **45b** developed by Gibson.¹⁶

In the early years of MIMs synthesis, Gibson reported the first example of a rotaxane synthesized through a capping protocol involving a Williamson reaction (Scheme 23).¹⁶ It is important to highlight that this reaction needs high temperatures to proceed, which decreases the yield. Indeed, in the related synthesis of Sauvage's original catenane,¹⁴ the use of a mild reaction, the ring-closing metathesis, instead of the Williamson reaction drastically increased the yield of the catenane

formation from 42% to 92%.¹⁸⁵ Since then, rotaxanes have been achieved using other capping reactions including thermal Huisgen 1,3-dipolar cycloadditions,^{27a} the formation of a bipyridinium,⁴⁴ a carbamate,⁹⁷ a thiourea¹⁶⁹ or an ester group,¹⁸⁶ the Suzuki cross-coupling,⁶² the creation of a urea moiety through the nucleophilic attack of an amine to an isocyanate stopper^{29a,187} or the reversible cleavage of disulphide bond.¹⁸⁸ However, the most commonly used reactions in rotaxane synthesis are click reactions,¹⁸⁹ alkene metathesis, especially for the clipping approach,¹⁹⁰ and the formation of an amide^{32,191} or an imine group^{75,192} which have in common the fact that they proceed under mild conditions, usually at room temperature or below.



Scheme 24. One of the earliest examples of a [2]rotaxane synthesized *via* CuAAC.¹⁹³

In this sense, the emergence of the click chemistry concept by Sharpless in 2001 had major repercussions in the field. Indeed, the goal of those reactions is to create larger molecules by joining

¹⁸⁵ M. Weck, B. Mohr, J.-P. Sauvage, R. H. Grubbs, *J. Org. Chem.* **1999**, *64*, 5463-5471.

¹⁸⁶ A. Arduini, R. Ferdani, A. Pochini, A. Secchi, F. Ugozzoli, *Angew. Chem. Int. Ed.* **2000**, *39*, 3453-3456.

¹⁸⁷ S. J. Cantrill, D. A. Fulton, M. C. T. Fyfe, J. F. Stoddart, A. J. P. White, D. J. Williams, *Tetrahedron Lett.* **1999**, *40*, 3669-3672.

¹⁸⁸ T. Yoshii, Y. Kohsaka, T. Moriyama, T. Suzuki, Y. Koyama, T. Takata, *Supramol. Chem.* **2011**, 65-68.

¹⁸⁹ A. C. Fahrenbach, J. F. Stoddart, *Chem. Asian J.* **2011**, *6*, 2660-2669.

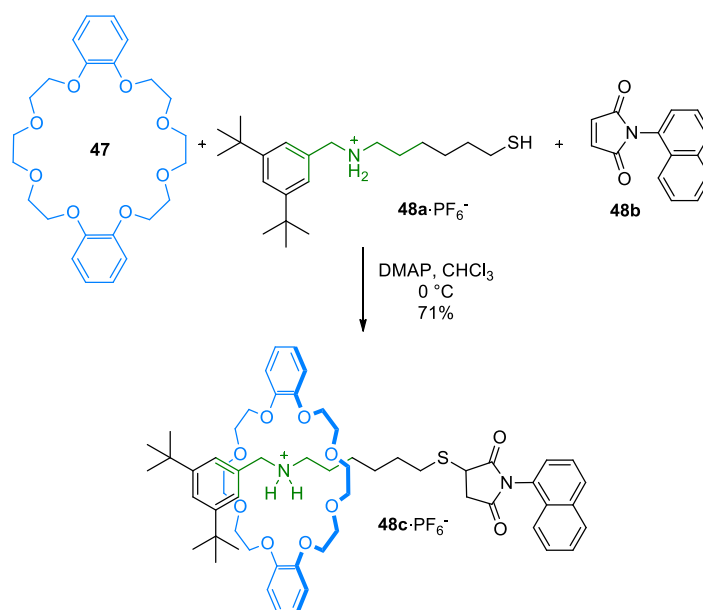
¹⁹⁰ a) Jeffrey S. Hannam, Timothy J. Kidd, David A. Leigh, Andrew J. Wilson, *Org. Lett.* **2003**, *5*, 1907-1910. b) Y. Suzuki, K. Osakada, *Dalton Trans.* **2007**, 2376-2383. c) D. Quaglio, G. Zappia, E. De Paolis, S. Balducci, B. Botta, F. Ghirga, *Org. Chem. Front.* **2018**, *5*, 3022-3055.

¹⁹¹ R. Jäger, S. Baumann, M. Fischer, O. Safarowsky, M. Nieger, F. Vögtle, *Liebigs Ann.* **1997**, 2269-2273.

¹⁹² A. G. Cheetham, T. D. W. Claridge, H. L. Anderson, *Org. Biomol. Chem.* **2007**, *5*, 457-462.

¹⁹³ W. R. Dichtel, O. Š. Miljanić, J. M. Spruell, J. R. Heath, J. F. Stoddart, *J. Am. Chem. Soc.* **2006**, *128*, 10388-10390.

smaller units together. These reactions must “be modular, wide in scope, stereospecific, give very high yield and generate only inoffensive byproducts”.¹⁹⁴ Thus, they fulfil the specific criteria of a perfect capping reaction, which is why their use has been intensified over the last two decades.¹⁸⁹ Among those reactions, one of them in particular, attracted a lot of attention, namely the copper(I)-catalyzed azide alkyne cycloaddition (CuAAC) which affords 1,4-disubstituted triazoles by the reaction of terminal alkynes with organic azides.¹⁹⁵ This reaction has been extensively employed due to its versatility in many rotaxane architectures, containing different recognition sites based on different interactions (Scheme 24).¹⁹⁶ Moreover, the fact that a triazolium salt, which is a great secondary station for crown ether-based switches,¹⁰⁹ can be prepared easily with this tool has significantly increased its impact.



Scheme 25. First use of a thiol maleimide reaction in rotaxane synthesis.^{199a}

Although the triumph of the CuAAC reaction is undeniable in organic synthesis and especially in the fields of MIMs, it is of key importance to develop new click reactions with the purpose of offering various alternatives to efficiently prepare a given rotaxane structure and access any potential design.¹⁹⁷ In this context, other click reactions have successfully afforded rotaxanes in good yields,¹⁸⁹ such as

¹⁹⁴ H. C. Kolb, M. G. Finn, K. B. Sharpless, *Angew. Chem. Int. Ed.* **2001**, *40*, 2004-2021.

¹⁹⁵ a) C. W. Tornøe, C. Christensen, M. Meldal, *J. Org. Chem.* **2002**, *67*, 3057-3064. b) V. V. Rostovtsev, L. G. Green, V. V. Fokin, K. B. Sharpless, *Angew. Chem. Int. Ed.* **2002**, *41*, 2596-2599.

¹⁹⁶ K. D. Hänni, D. A. Leigh, *Chem. Soc. Rev.* **2010**, *39*, 1240-1251.

¹⁹⁷ C. R. Becer, R. Hoogenboom, U. S. Schubert, *Angew. Chem. Int. Ed.* **2009**, *48*, 4900-4908.

Diels-Alder reactions,¹⁹⁸ the thiol-maleimide Michael addition (Scheme 25),^{73,199} the radical thiol-ene/yne²⁰⁰ and nitrile oxide cycloadditions.²⁰¹

1.1.2. Michael-type addition reaction of nucleophiles to vinyl sulfonyl groups

In this group of alternative click reactions, the Michael-type addition reaction of nucleophiles to vinyl sulfonyl groups (MAVS), appears as an attractive alternative to the CuAAC. Among the three vinyl sulfonyl groups, vinyl sulfonamides, vinyl sulfones and vinyl sulfonates (Figure 16), this reaction has been particularly more explored with vinyl sulfone or vinyl sulfonate groups.

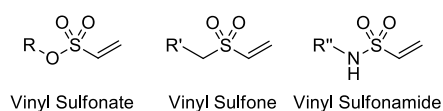
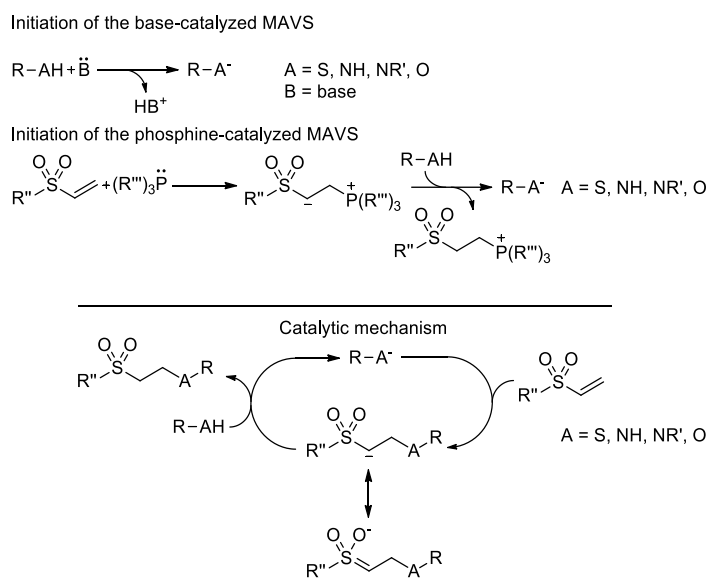


Figure 16. The three vinyl sulfonyl groups.



Scheme 26. Mechanism of the MAVS.

The MAVS satisfies the click criteria since it proceeds in a wide variety of solvents, including water, under mild experimental conditions (room temperature or even at 4 °C) and affords very good yields while creating almost no undesirable byproducts. Furthermore, it is usually catalyzed by a substoichiometric amount of mild bases, such as Et₃N or K₂CO₃, or simple phosphines like PPh₃ (Scheme

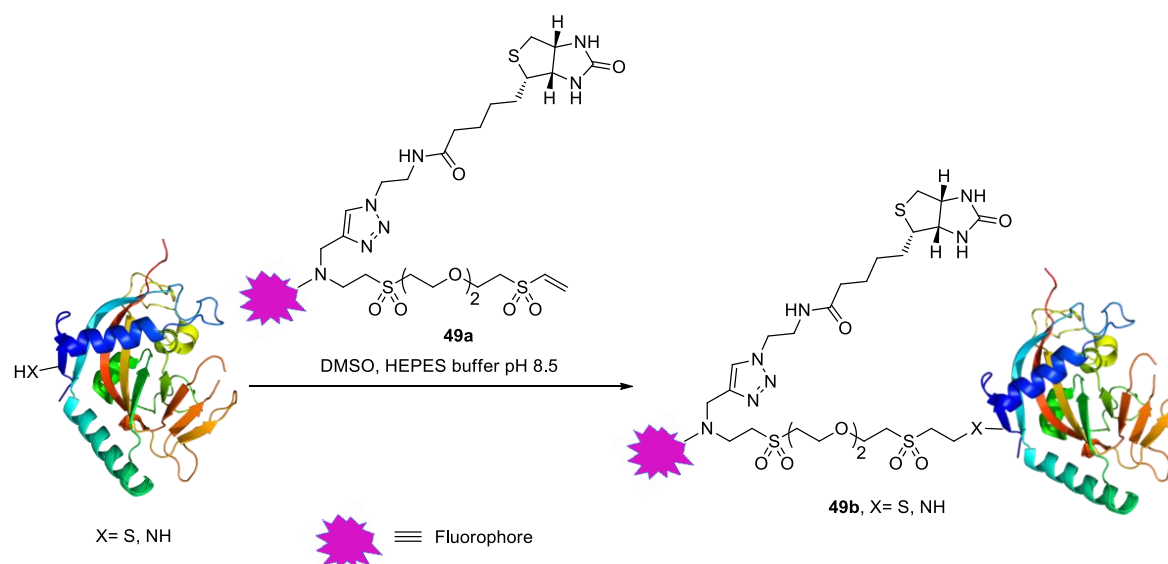
¹⁹⁸ a) H. Sasabe, N. Kihara, Y. Furusho, K. Mizuno, A. Ogawa, T. Takata, *Org. Lett.* **2004**, *6*, 3957-3960. b) C.-C. Hsu, N.-C. Chen, C.-C. Lai, Y.-H. Liu, S.-M. Peng, S.-H. Chiu, *Angew. Chem. Int. Ed.* **2008**, *47*, 7475-7478.

¹⁹⁹ a) K. Nakazono, T. Oku, T. Takata, *Tetrahedron Lett.* **2007**, *48*, 3409-3411. b) U. Choudhary, B. H. Northrop, *Org. Lett.* **2012**, *14*, 2082-2085.

²⁰⁰ a) W. Zhou, H. Zheng, Y. Li, H. Liu, Y. Li, *Org. Lett.* **2010**, *12*, 4078-4081. b) H. Zheng, Y. Li, C. Zhou, Y. Li, W. Yang, W. Zhou, Z. Zuo, H. Liu, *Chem. Eur. J.* **2011**, *17*, 2160-2167.

²⁰¹ a) T. Matsumura, F. Ishiwari, Y. Koyama, T. Takata, *Org. Lett.* **2010**, *12*, 3828-3831. b) Y. Koyama, T. Matsumura, T. Yui, O. Ishitani, T. Takata, *Org. Lett.* **2013**, *15*, 4686-4689.

26). Therefore, it was classified as a click reaction.²⁰² Regarding the reaction mechanism, after being deprotonated the nucleophile attacks the vinyl sulfonyl group generating an anion which is stabilized by resonance. This anion can catch a proton from the nucleophile, which starts again the catalytic cycle, but also from the protonated form of the base or protic solvent molecules, regenerating the base or forming a solvent anion which also have the ability to deprotonate the nucleophile (Scheme 26).



Vinyl sulfones are usually synthesized through a mono-Michael-type addition of thiol, amine or alcohol to divinyl sulfone or by oxidation of thioethers. They can react with proteins since the latter possess thiol and amine moieties, enabling MAVS reactions that proceed under mild conditions.²⁰³ This tool was exploited, by our group and many more, as a bioconjugation reaction with the aim of tagging²⁰⁴ and immobilizing²⁰⁵ proteins (Scheme 27), or inhibiting the activity of enzymes.²⁰⁶ Moreover, it can

²⁰² a) M. van Dijk, D. T. S. Rijkers, R. M. J. Liskamp, C. F. van Nostrum, W. E. Hennink, *Bioconjugate Chem.* **2009**, *20*, 2001-2016. b) M. H. Stenzel, *ACS Macro Lett.* **2013**, *2*, 14-18. c) D. P. Nair, M. Podgórski, S. Chatani, T. Gong, W. Xi, C. R. Fenoli, C. N. Bowman, *Chem. Mater.* **2014**, *26*, 724-744.

²⁰³ M. S. Masri, M. Friedman, *J. Protein Chem.* **1988**, *7*, 49-54.

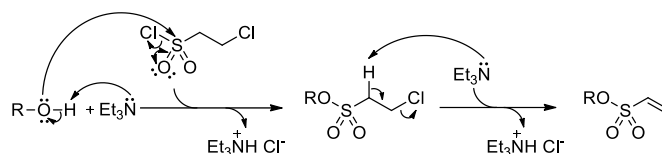
²⁰⁴ a) J. Morales-Sanfrutos, F. J. Lopez-Jaramillo, F. Hernandez-Mateo, F. Santoyo-Gonzalez, *J. Org. Chem.* **2010**, *75*, 4039-4047. b) J. Morales-Sanfrutos, F. J. Lopez-Jaramillo, M. Ortega-Muñoz, A. Megia-Fernandez, F. Perez-Balderas, F. Hernandez-Mateo, F. Santoyo-Gonzalez, *Org. Biomol. Chem.* **2010**, *8*, 667-675.

²⁰⁵ M. Ortega-Muñoz, J. Morales-Sanfrutos, A. Megia-Fernandez, F. J. Lopez-Jaramillo, F. Hernandez-Mateo, F. Santoyo-Gonzalez, *J. Mater. Chem.* **2010**, *20*, 7189-7196.

²⁰⁶ a) B. A. Frankel, M. Bentley, R. G. Kruger, D. G. McCafferty, *J. Am. Chem. Soc.* **2004**, *126*, 3404-3405. b) F. M. Tomlin, U. I. M. Gerling-Driessen, Y.-C. Liu, R. A. Flynn, J. R. Vangala, C. S. Lentz, S. Clauder-Muenster, P. Jakob, W. F. Mueller, D. Ordoñez-Rueda, M. Paulsen, N. Matsui, D. Foley, A. Rafalko, T. Suzuki, M. Bogyo, L. M. Steinmetz, S. K. Radhakrishnan, C. R. Bertozzi, *ACS Cent. Sci.* **2017**, *3*, 1143-1155.

serve to functionalize sugars²⁰⁷ but also allow to design complex carrier systems.^{207b,208} Furthermore, the click MAVS has been extensively applied in materials chemistry, especially for the preparation of polymers.²⁰⁹

When it comes to vinyl sulfonates, their synthesis may seem harder, however, they are easy to generate in very good yields *via* the attack of an alcohol to 2-chloroethanesulfonyl chloride in the presence of Et₃N at 0 °C in a chlorinated solvent (Scheme 28). In addition, their reactivity as Michael acceptors is similar to that of vinyl sulfones.²¹⁰ Hence, this unit has been employed in the production of polymers,²¹¹ the inhibition of enzymes²¹² and for coupling-and-decoupling chemistry.²¹⁰



Scheme 28. Mechanism of the generation of a vinyl sulfonate moiety.

²⁰⁷ a) F. J. Lopez-Jaramillo, M. Ortega-Muñoz, A. Megia-Fernandez, F. Hernandez-Mateo, F. Santoyo-Gonzalez, *Bioconjugate Chem.* **2012**, *23*, 846-855. b) T. del Castillo, J. Marales-Sanfrutos, F. Santoyo-González, S. Magez, F. J. Lopez-Jaramillo, J. A. Garcia-Salcedo, *ChemMedChem* **2014**, *9*, 383-389.

²⁰⁸ a) M. D. Giron-Gonzalez, A. Morales-Portillo, A. Salinas-Castillo, F. J. Lopez-Jaramillo, F. Hernandez-Mateo, F. Santoyo-Gonzalez, R. Salto-Gonzalez, *Bioconjugate Chem.* **2014**, *25*, 1151-1161. b) E. De los Reyes-Berbel, R. Salto-Gonzalez, M. Ortega-Muñoz, F. J. Reche-Perez, A. B. Jodar-Reyes, F. Hernandez-Mateo, M. D. Giron-Gonzalez, F. Santoyo-Gonzalez, *Bioconjugate Chem.* **2018**, *29*, 2561-2575.

²⁰⁹ a) Y. Suzuki, T. Higashihara, S. Ando, M. Ueda, *Macromolecules* **2012**, *45*, 3402-3408. b) S. Chatani, C. Wang, M. Podgórski, C. N. Bowman, *Macromolecules* **2014**, *47*, 4949-4954. c) M. Podgórski, E. Becka, S. Chatani, M. Claudino, C. N. Bowman, *Polym. Chem.* **2015**, *6*, 2234-2240.

²¹⁰ C. M. Cruz, M. Ortega-Muñoz, F. J. López-Jaramillo, F. Hernández-Mateo, V. Blanco, F. Santoyo-González, *Adv. Synth. Catal.* **2016**, *358*, 3394-3413.

²¹¹ a) S. Chatani, M. Podgórski, C. Wang, C. N. Bowman, *Macromolecules* **2014**, *47*, 4894-4900. b) J. Sinha, M. Podgórski, S. Huanga, C. N. Bowman, *Chem. Commun.* **2018**, *54*, 3034-3037.

²¹² a) S. Liu, B. Zhou, H. Yang, Y. He, Z.-X. Jiang, S. Kumar, L. Wu, Z.-Y. Zhang, *J. Am. Chem. Soc.* **2008**, *130*, 8251-8260. b) N. N. Gushwa, S. Kang, J. Chen, J. Taunton, *J. Am. Chem. Soc.* **2012**, *134*, 20214-20217.

1.2. Objectives

In this context, we hypothesize that the Michael-type addition of thiols and amines to vinyl sulfonyl groups, such as vinyl sulfone and vinyl sulfonate, could be a suitable tool for rotaxane synthesis *via* a capping protocol. Thus, we propose to prepare series of rotaxanes based on different binding motifs involving distinct types of interactions, such as hydrogen bonding or π -donor/ π -acceptor interactions.

For this purpose, we plan to synthesize stoppers possessing a thiol or an amine moiety, as well as, axes with various recognition sites owning vinyl sulfone or vinyl sulfonate units. Subsequently, we suggest to mix the rod with the adequate macrocycle, in order to form the pseudorotaxane and try the capping through a MAVS reaction to afford a [2]rotaxane (Figure 17).

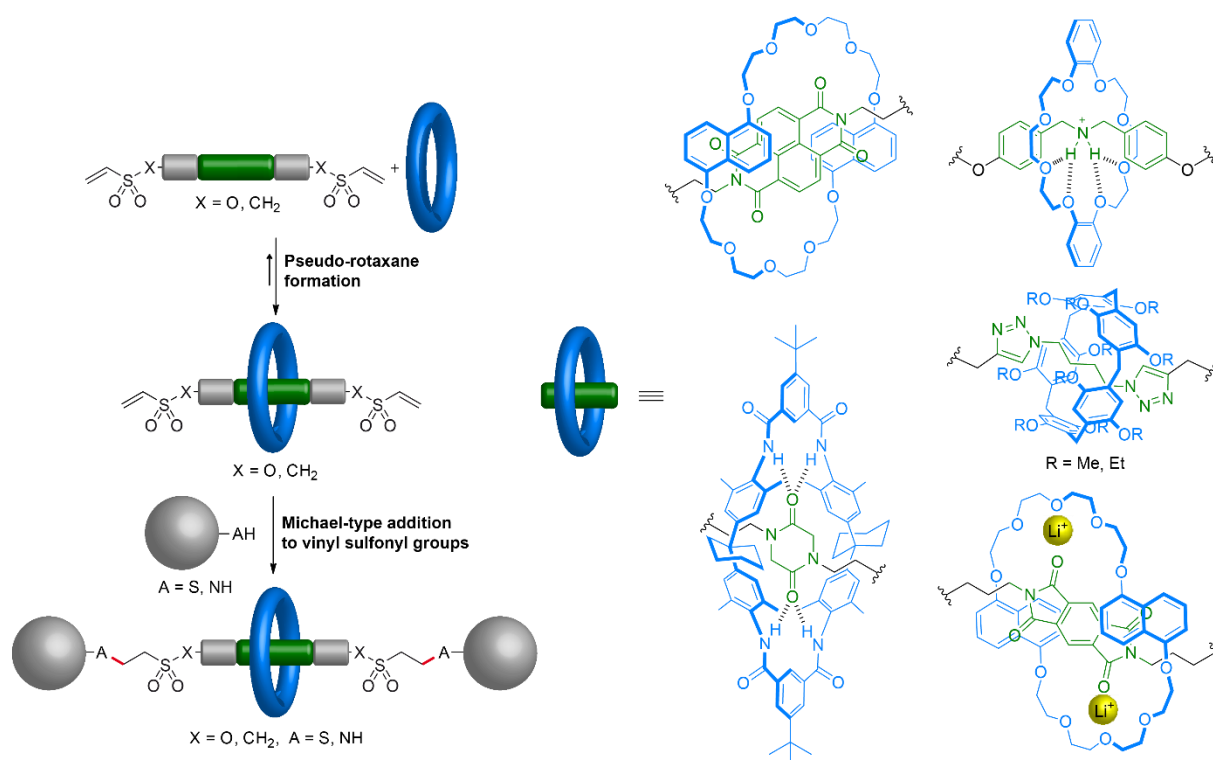


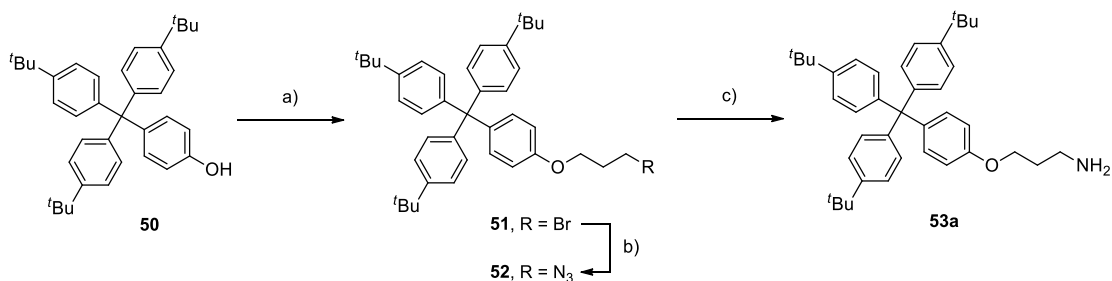
Figure 17. Proposed synthetic strategy for building [2]rotaxanes *via* click MAVS reactions.

1.3. Results and discussion

1.3.1. Synthesis of rotaxanes based on π -donor/ π -acceptor interactions

As an initial stage, we decided to try out our methodology for rotaxanes based on π -donor/ π -acceptor interactions. To this end, we chose the DNP38C10/NDI system. The NDI recognition motif has been widely used to create MIMs and displays a relatively good association constant with the macrocycle: $K_a \approx 1 \times 10^2 \text{ M}^{-1}$ in $\text{CHCl}_3/\text{MeOH}$ (98:2).²¹³ In addition, to the best of our knowledge, for this particular motif the CuAAC did not prove to be highly efficient, as rotaxanes were obtained following this approach in relatively modest yields (18-48%).^{113b,214} Only the thiol-maleimide,^{199b} or a barely used Si–O bond formation reaction between a salicylic acid derivative and a pentacoordinate hydrosilane²¹⁵ afforded high yields (65% and 84%, respectively).

In this context, we want to prepare bulky stopper derivatives functionalized with an amine and a thiol, as well as, axles bearing vinyl sulfonate or vinyl sulfone units. Thus, to prepare amine stopper **53a**, the synthesis started with a Mitsunobu reaction with 3-bromo-1-propanol and phenol **50**, resulting in compound **51** whose bromide group was substituted with an azide unit by reaction with NaN_3 in the presence of a catalytic amount of KI in good yield (81%). Subsequently, the azide group in **52** was reduced to an amine by hydrogenation using palladium on carbon as catalyst and yielding the amine stopper **53a** in 98% yield (Scheme 29).



Scheme 29. Synthesis of amine stopper **53a**. Reagents and conditions: a) 3-Bromo-1-propanol, PPh_3 , DEAD, 0 °C to r.t., 18 h, 77%. b) NaN_3 , $\text{KI}_{(\text{cat.})}$, DMF, 70 °C, 18 h, 81%. c) H_2 , Pd/C, $\text{CH}_2\text{Cl}_2/\text{MeOH}$ (2:1), r.t., 18 h, 98%.

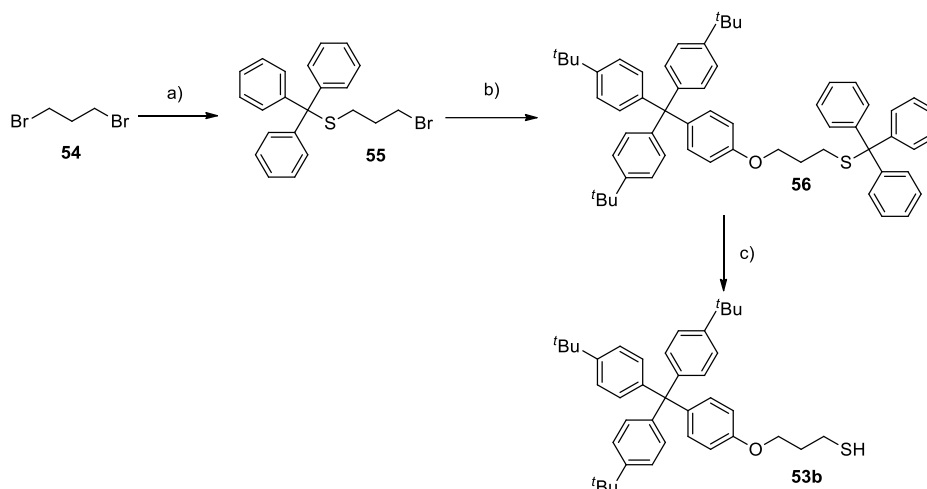
Regarding the thiol stopper **53b**, the thiolate of trityl thiol was generated in THF using LiHMDS, in order to attack 1,3-dibromopropane and form compound **55** in excellent yield (99%). The latter was reacted with phenol **50** through a Williamson reaction to afford **56** in excellent yield (99%). Finally, the thiol

²¹³ S. I. Pascu, C. Naumann, G. Kaiser, A. D. Bond, J. K. M. Sanders, T. Jarrosson, *Dalton Trans.* **2007**, 3874-3884.

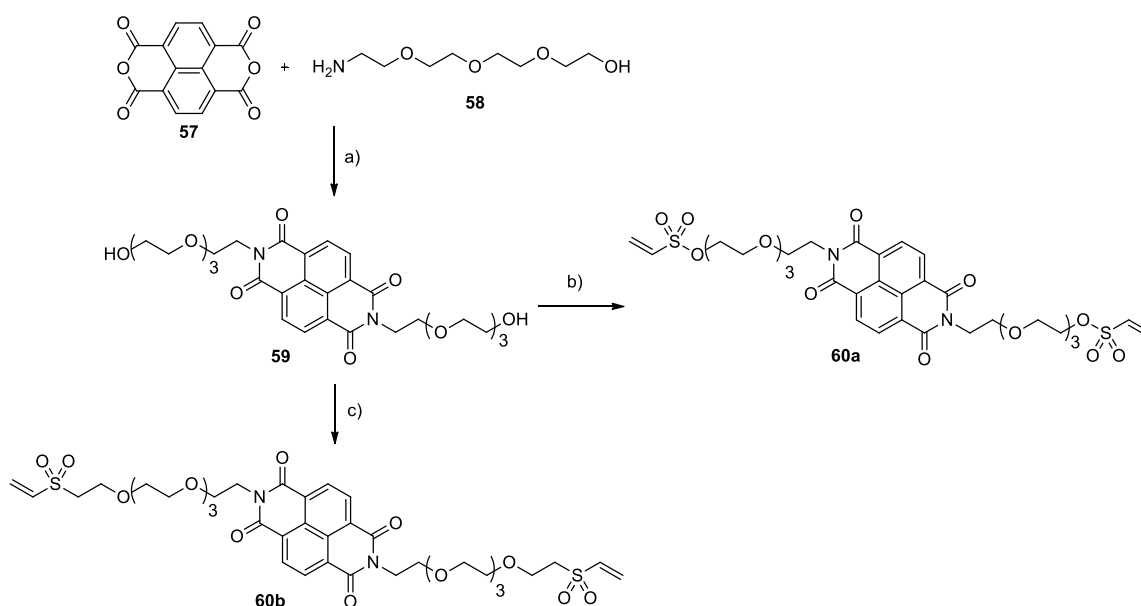
²¹⁴ a) H. Wilson, S. Byrne, N. Bampos, K. M. Mullen, *Org. Biomol. Chem.* **2013**, *11*, 2105-2115. b) H.-G. Li, G.-W. Wang, *J. Org. Chem.* **2017**, *82*, 6341-6348. c) Y. Sagara, M. Karman, E. Verde-Sesto, K. Matsuo, Y. Kim, N. Tamaoki, C. Weder, *J. Am. Chem. Soc.* **2018**, *140*, 1584-1587.

²¹⁵ Y. Domoto, S. Sase, K. Goto, *Chem. Eur. J.* **2014**, *20*, 15998-16005.

was deprotected with $\text{CF}_3\text{CO}_2\text{H}$ and Et_3SiH to give the thiol stopper **53b** in very good yield (94%) (Scheme 30).



Scheme 30. Synthesis of thiol stopper **53b**. Reagents and conditions: a) Trityl thiol, LiHMDS (1 M in THF), THF, 0 °C to r.t., 1 h, 99%. b) **50**, Cs_2CO_3 , DMF, 90 °C, 3 d, 99%. c) $\text{CF}_3\text{CO}_2\text{H}$, Et_3SiH , r.t., 4 h, 94%.

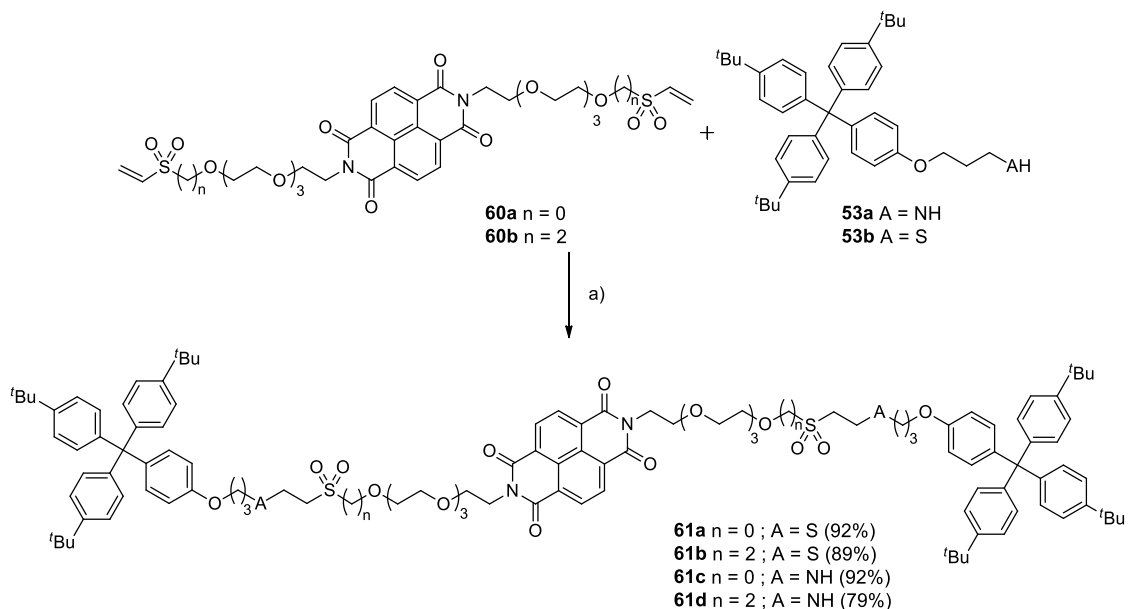


Scheme 31. Synthesis of NDI axles **60a,b**. Reagents and conditions: a) DMF, 90 °C, 3 d, 76%. b) 2-chloroethanesulfonyl chloride, Et_3N , CH_2Cl_2 , 0 °C, 1 h, 99%. c) Divinyl sulfone, $^t\text{BuOK}$, THF, r.t., 5 h, 71%.

With both stoppers in hand, we decided to synthesize vinyl sulfonyl-functionalized NDI axles **60a,b**. For this purpose, diol **59** was prepared from 1,4,5,8-naphthalenetetracarboxylic dianhydride (**57**) and a tetraethylene glycol amine **58**. This product reacted with 2-chloroethanesulfonyl chloride to create the NDI rod functionalized with vinyl sulfonate groups **60a** in excellent yield (99%). Michael addition to divinyl sulfone in the presence of a catalytic amount of $^t\text{BuOK}$ afforded axle **60b** in 71% yield (Scheme

31). Meanwhile, macrocycle DNP38C10 (**62**) was constructed following a recent straightforward 4-step strategy reported by Stoddart and co-workers, which only requires a final column chromatography.²¹⁶

Having synthesized the necessary building blocks to obtain our target rotaxanes, we began with the preparation of the four threads **61a-d**, combining the amine or the thiol stoppers **53a,b** with the sulfonate or the sulfone axles **60a,b**, with the aim of testing the MAVS reactions. Furthermore, the free threads are very important as reference both in the purification process of the crude material from the reaction of the rotaxane formation and in the analysis of the ¹H NMR spectrum of the interlocked compound, where the comparison with the non-interlocked species is essential to visualize the interaction between both components. Thus, we tackled this reaction, using Et₃N as catalyst, obtaining excellent yields: 89-92% for the thia-Michael addition and 79-92% for the aza-Michael addition (Scheme 32). As expected, the efficiency of the click MAVS reactions in these mild conditions makes it a suitable candidate for rotaxane synthesis.

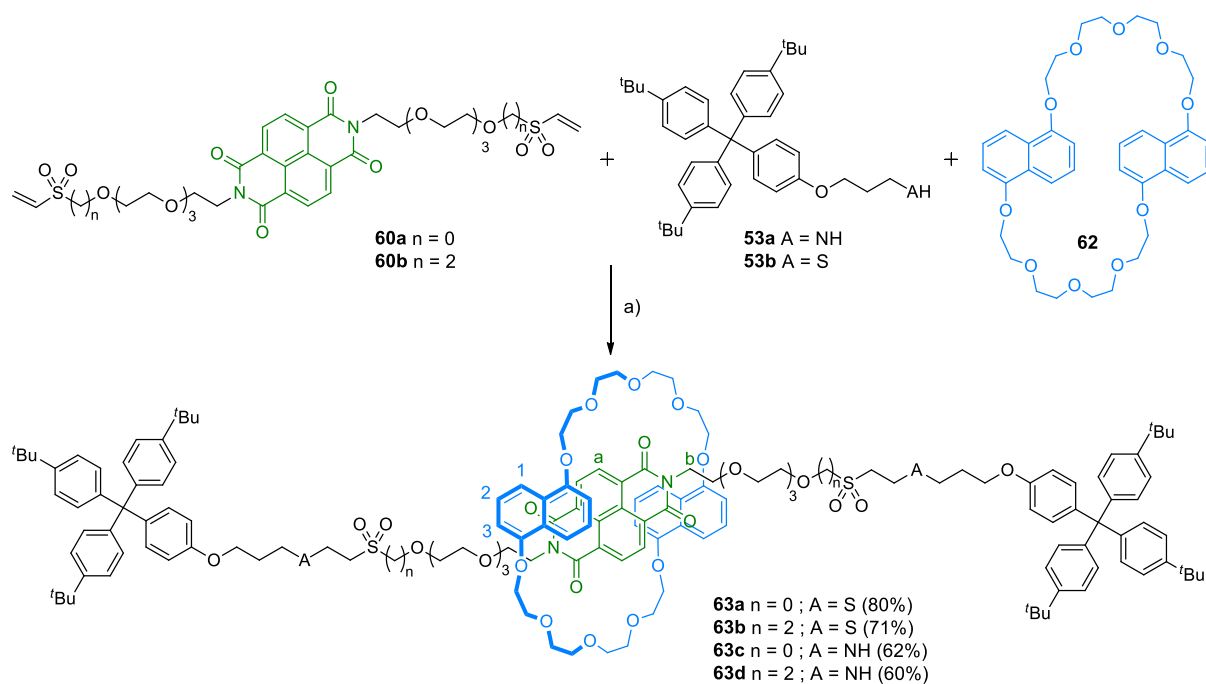


Scheme 32. Synthesis of threads **61a-d**. Reagents and conditions: a) for A = S: Et₃N, CHCl₃/2-propanol, r.t., 18-72 h, 89-92%; for A = NH: Et₃N, CHCl₃/MeOH, r.t., 4-24 h, 79-92%.

In the view of these promising results, we attempted the rotaxane formation employing the same experimental conditions. However, we previously mixed the axle with macrocycle **62** with the intention of forming the pseudorotaxane. Thus, we obtained rotaxanes **63a-d** in very good yields (60-80%) (Scheme 33), which are similar in the case of the thia-Michael addition to the best yield reported for this system,²¹⁵ slightly higher than the NDI rotaxane afforded with the thiol maleimide reaction^{199b} and significantly better than those achieved using a click CuAAC reaction.²¹⁴ It can be noticed that the thia-

²¹⁶ C. J. Bruns, S. Basu, J. F. Stoddart, *Tetrahedron Lett.* **2010**, *51*, 983-986.

Michael addition gives better yields than the aza-Michael addition. We attribute this difference to the purification process of these [2]rotaxanes. Indeed, the purification of **63a** only required a preparative TLC. Nevertheless, **63b-d** needed an initial column chromatography followed by successive runs of gel permeation chromatography²¹⁷ due to the very close retention factor of rotaxane and thread on silica gel, which precluded their separation by normal phase column chromatography or preparative TLC.



Scheme 33. Synthesis of rotaxanes **61a-d** via MAVS reactions. Reagents and conditions: a) $\text{Et}_3\text{N}(\text{cat})$, $\text{CHCl}_3/\text{MeOH}$ (1:1) or $\text{CHCl}_3/\text{PrOH}$ (99:1), r.t., 16-72 h.

The [2]rotaxanes **63a-d** were characterized by NMR spectroscopy. The ^1H NMR spectra exhibit an upfield shift for the signals of the aromatic H of the NDI group and the macrocycle ($\Delta\delta_{\text{Ha}} = -0.48$ ppm, $\Delta\delta_{\text{H1}} \approx -0.95$ ppm, $\Delta\delta_{\text{H2}} = -0.53$ ppm, $\Delta\delta_{\text{H3}} = -0.40$ ppm) (Figure 18). This shielding phenomenon is due to the formation of π -donor/ π -acceptor interactions between the NDI core and the naphthalene derivatives of the ring. This interaction can also be observed with the naked eye since threads are yellow and rotaxanes are red due to the appearance of a charge-transfer band centered at 499 nm ($\epsilon = 735 \text{ L mol}^{-1} \text{ cm}^{-1}$). Moreover, the interlocked character of **63b** was studied by DOSY NMR experiment, which shows that the signals from the rod or the wheel display the same diffusion coefficient (Figure 19). Finally, HRMS spectra confirmed the existence of these rotaxanes given that the experimental exact masses and isotopic distributions of the signals observed in their match perfectly the calculated ones for the proposed structures (Figure 20 for **63a**).

²¹⁷ The purification of **63b** required two runs of size exclusion chromatography while for **63c,d** 5 runs were needed to achieve full purification.

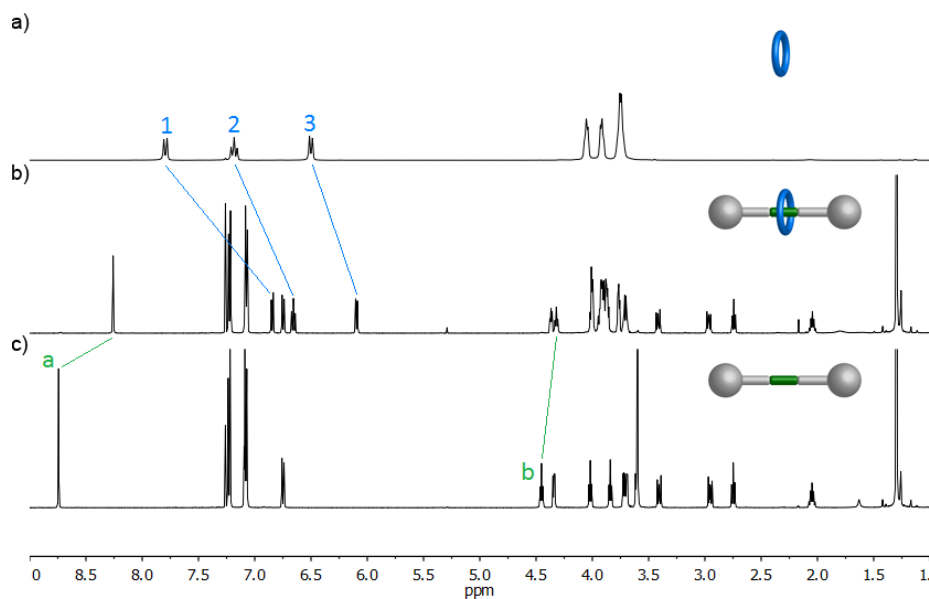


Figure 18. ^1H NMR spectra of: a) Macrocycle **62** (300 MHz, CDCl_3). b) Rotaxane **63a** (500 MHz, CDCl_3). c) Thread **61a** (500 MHz, CDCl_3). Lettering coding is defined in Scheme 33.

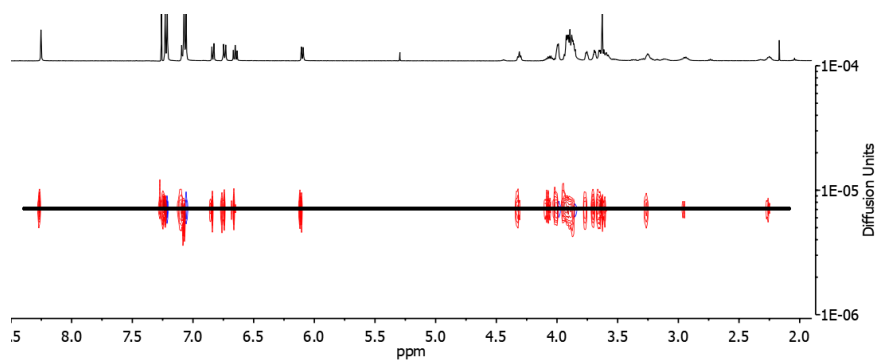


Figure 19. DOSY NMR (500 MHz, CDCl_3) spectrum of **63b**.

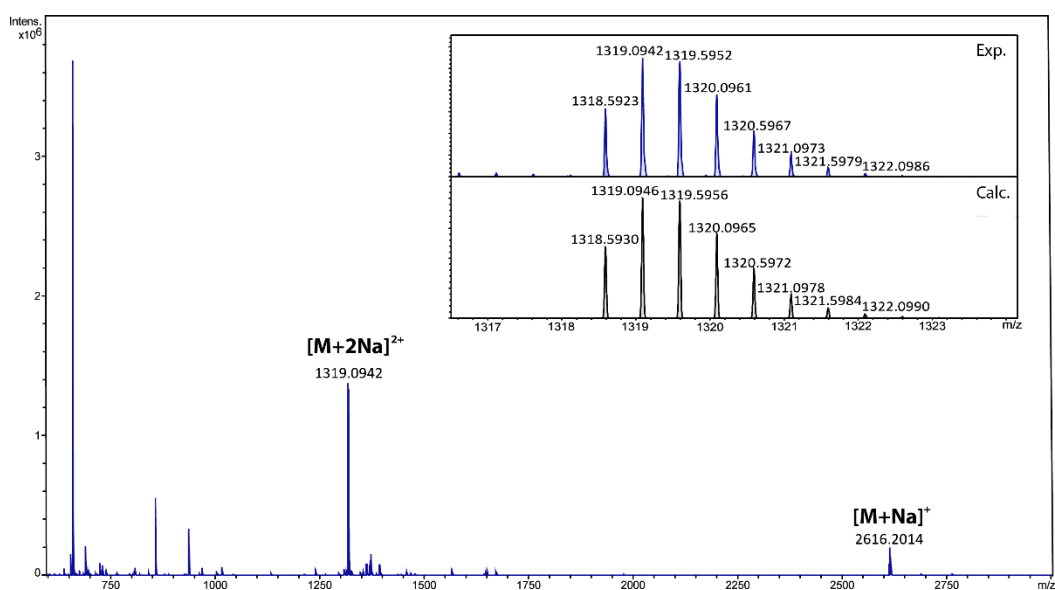


Figure 20. HRMS (ESI $^+$) spectrum of **63a**. Inset: Observed (top) and calculated (bottom) isotopic distribution for $[\mathbf{63a}+2\text{Na}]^{2+}$.

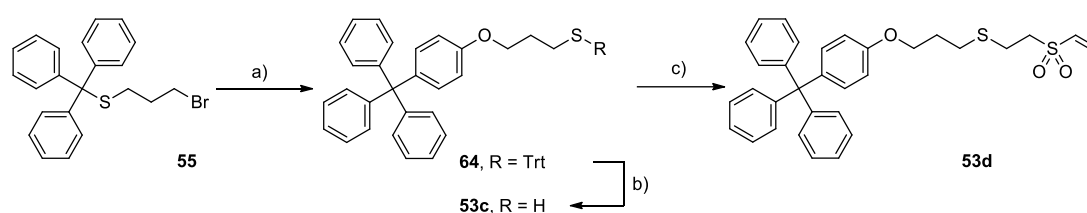
1.3.2. Synthesis of rotaxanes based on hydrogen bonding

Motivated by the good results gathered for the click MAVS reactions in π -donor/ π -acceptor rotaxanes, we chose to go further and try out our methodology with hydrogen bonding-based rotaxanes. As described on the general introduction (see Section 3.1.), there are two families of macrocycles that generate rotaxanes through this interaction which are amide-based macrocycles and crown ethers.

1.3.2.1. Rotaxanes containing a tetralactam ring

Regarding tetralactam rings, we decided to select a Hunter/Vögtle-type anilide macrocycle and a diketopiperazine derivative as recognition site. Indeed, this system exhibits a high binding constant, $K_a = (1.08 \pm 0.09) \times 10^4 \text{ M}^{-1}$ in CDCl_3 at 233 K.³⁷ Rotaxanes owning this particular motif have been prepared by CuAAC in 29-75% yields.^{37,218} Moreover, since the thia-Michael addition seems to be more efficient than the aza-Michael addition and the amine stopper needs a solvent mixture containing an alcohol to be dissolved, we will only focus on the thia-Michael addition reaction thereafter.

First, thiol stopper **53c** and vinyl sulfonyl-functionalized stoppers **53d,e** were synthesized in order to test if the rotaxane formation would work if the vinyl sulfonyl groups were located either on the stopper or on the axle precursor. The synthesis began with the alkylation of 4-tritylphenol by **55** to generate compound **64** displaying a trityl thiol unit in excellent yield (99%). The latter was deprotected affording the thiol stopper **53c** in good very good yield (89%),²¹⁹ which then underwent a click MAVS reaction with an excess of divinyl sulfone to give the vinyl sulfone-functionalized stopper **53d** in 86% yield (Scheme 34). With respect to **53e**, its synthesis was achieved with a Williamson reaction between phenol **50** and 3-bromo-1-propanol yielding intermediate **65** in 80% yield. This reacted with 2-chloroethanesulfonyl chloride in basic medium producing the desired vinyl sulfonate-functionalized stopper **53e** in very good yield 93% (Scheme 35).

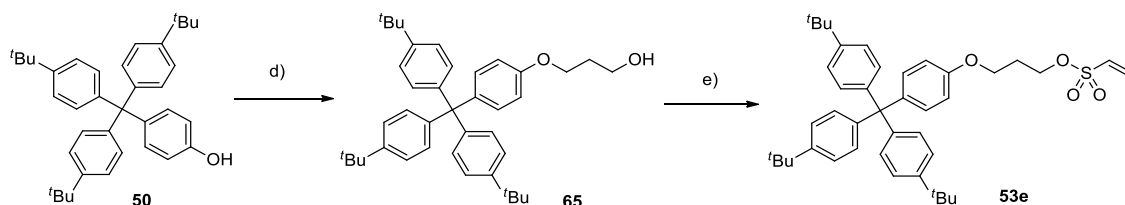


Scheme 34. Synthesis of stoppers **53c,d**. Reagents and conditions: a) 4-Tritylphenol, K_2CO_3 , DMF, 90 °C, 24 h, 99%. b) $\text{CF}_3\text{CO}_2\text{H}$, Et_3SiH , r.t., 4 h, 89%. c) divinyl sulfone, Et_3N , CH_2Cl_2 , r.t., 20 h, 86%.

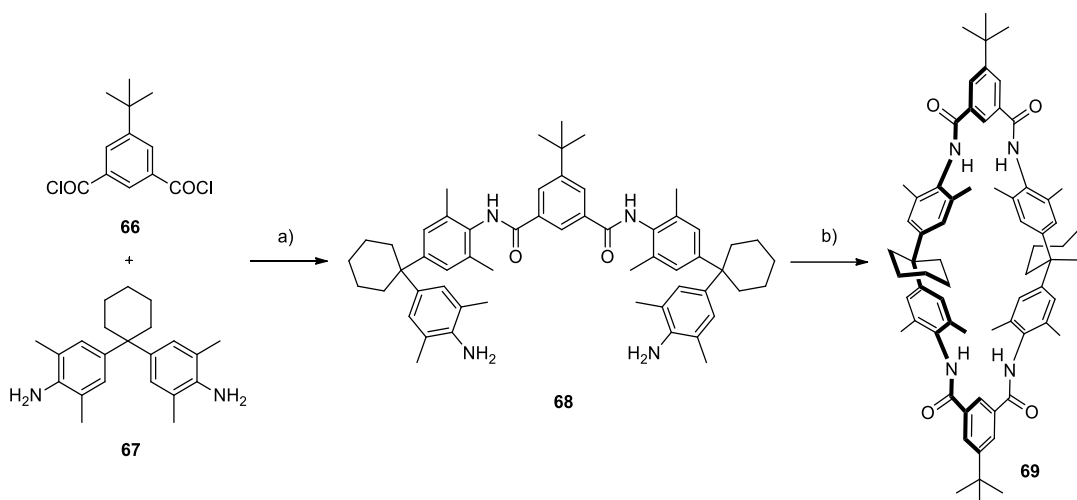
²¹⁸ T. Heinrich, C. H. H. Traulsen, M. Holzweber, S. Richter, V. Kunz, S. K. Kastner, S. O. Krabbenborg, J. Huskens, W. E. S. Unger, C. A. Schalley, *J. Am. Chem. Soc.* **2015**, *137*, 4382-4390.

²¹⁹ This compound was prepared following a procedure already described in our group: P. García-Cerezo, Aplicación de química "click" basada en reacciones de adición de Michael a grupos vinilsulfonilo en el desarrollo de estructuras supramoleculares y sistemas funcionales, BSc dissertation, Universidad de Granada, Granada, Spain, **2016**.

Subsequently, we tackled the preparation of the amide-based macrocycle **69**. The diacyl chloride **66** was reacted with an excess of the diamine **67** to form intermediate **68** in good yield (81%). Diluted solutions of the latter and the diacyl chloride **66** were added simultaneously at a low rate to the reaction medium using a syringe pump in order to maximize the formation of macrocycle **69**, which was attained in 24% yield (Scheme 36).

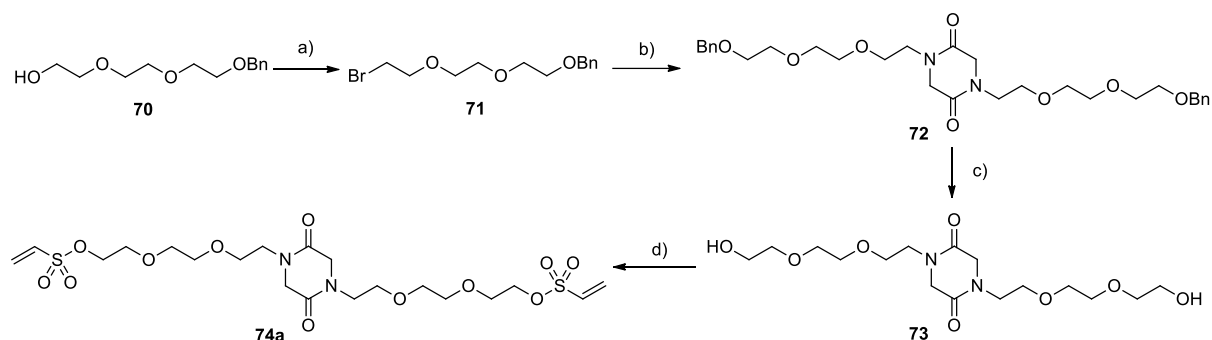


Scheme 35. Synthesis of stopper **53e**. Reagents and conditions: a) 3-bromo-1-propanol, Cs₂CO₃, DMF, 90 °C, 3 d, 80%. b) 2-chloroethanesulfonyl chloride, Et₃N, CH₂Cl₂, 0 °C, 2 h, 93%.



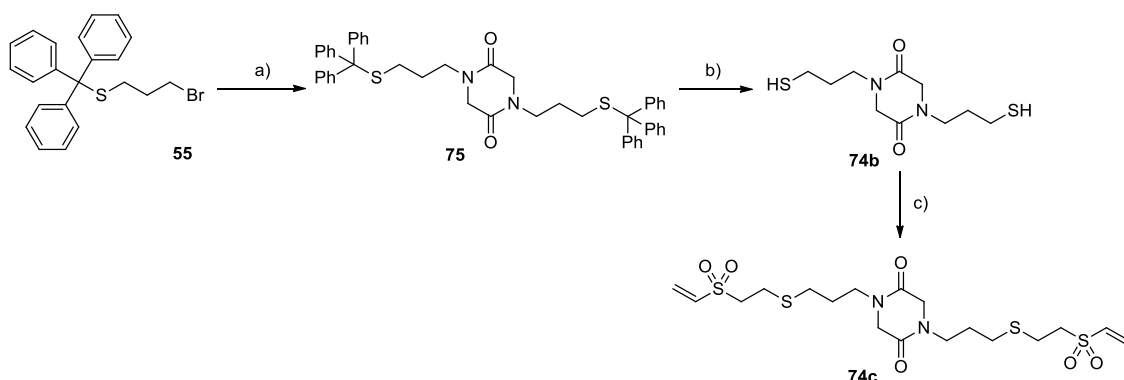
Scheme 36. Synthesis of macrocycle **69**. Reagents and conditions: a) Et₃N, CH₂Cl₂, r.t., O/N, 81%. b) **66**, Et₃N, CH₂Cl₂, r.t., 25 h, 24%.

The synthesis of axles **74a-c** was carried out using two different routes. The first route started with the submission of triethylene glycol derivative **70** to an Appel reaction to obtain **71** owning a bromide group and an alcohol group protected with a benzyl derivative in good yield (84%). Subsequently, glycine anhydride was alkylated with **71** using NaH as base giving intermediate **72** in 64% yield. Then, the benzyl groups were removed by hydrogenation to generate diol **73** in excellent yield (99%). The latter was treated with 2-chloroethanesulfonyl chloride in the presence of Et₃N to afford the diketopiperazine axle **74a**, functionalized with vinyl sulfonate groups in good yield (80%) (Scheme 37).



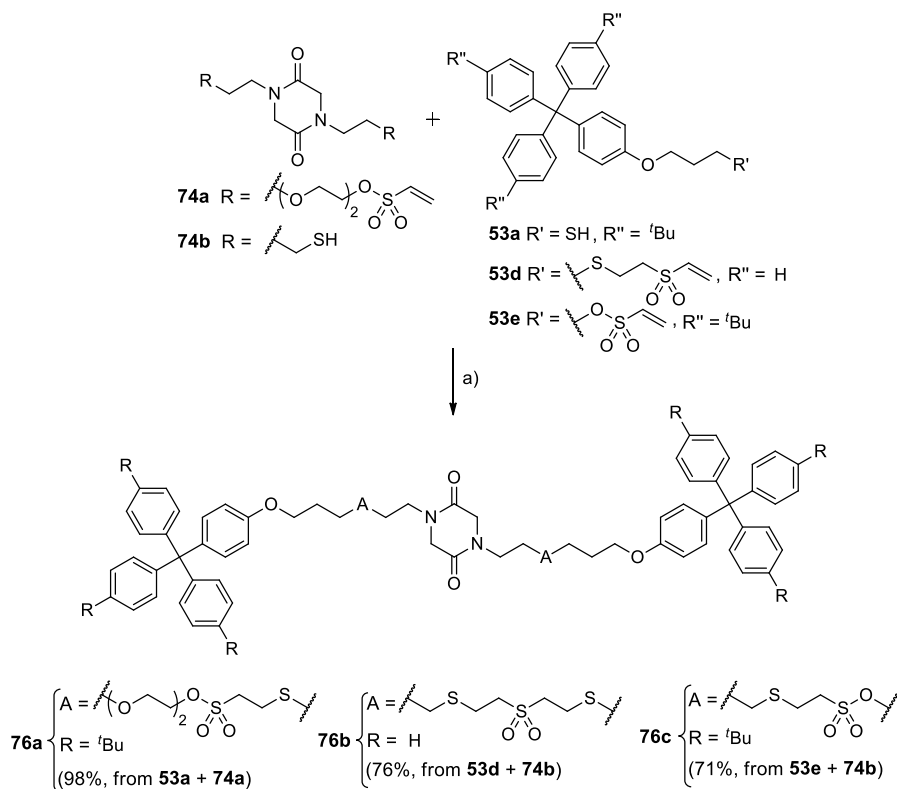
Scheme 37. Synthesis of axle **74a**. Reagents and conditions: a) CBr_4 , PPh_3 , CH_2Cl_2 , 0°C to r.t., 2 h, 84%. b) Glycine anhydride, NaH , DMF , 0°C to r.t., 25 min; Then **71**, $\text{NBu}_4\text{I}(\text{cat.})$, DMF , r.t., O/N, 64%. c) H_2 (5 atm), Pd/C , MeOH , r.t., 72 h, 99%. d) 2-chloroethanesulfonyl chloride, Et_3N , CH_2Cl_2 , 0°C , 2 h, 80%.

The second route started with the alkylation of glycine anhydride with **55** to afford compound **75** containing trityl thiol units in 75% yield. This was treated with $\text{CF}_3\text{CO}_2\text{H}$ and Et_3SiH in order to deprotect the thiol and generate diketopiperazine axle **74b** functionalized with two thiol groups in good yield (88%). **74b** underwent a click MAVS reaction with divinyl sulfone to yield the target diketopiperazine axle **74c** functionalized with vinyl sulfone moieties in moderate yield (60%) (Scheme 38).



Scheme 38. Synthesis of axles **74b,c**. Reagents and conditions: a) Glycine anhydride, NaH , DMF , 0°C to r.t., 30 min; Then **55**, $\text{NBu}_4\text{I}(\text{cat.})$, $\text{DMF}/\text{CH}_2\text{Cl}_2$, r.t., 18 h, 75%. b) $\text{CF}_3\text{CO}_2\text{H}$, Et_3SiH , r.t., 4 h, 88%. c) Divinyl sulfone, Et_3N , CH_2Cl_2 , r.t., 22 h, 60%.

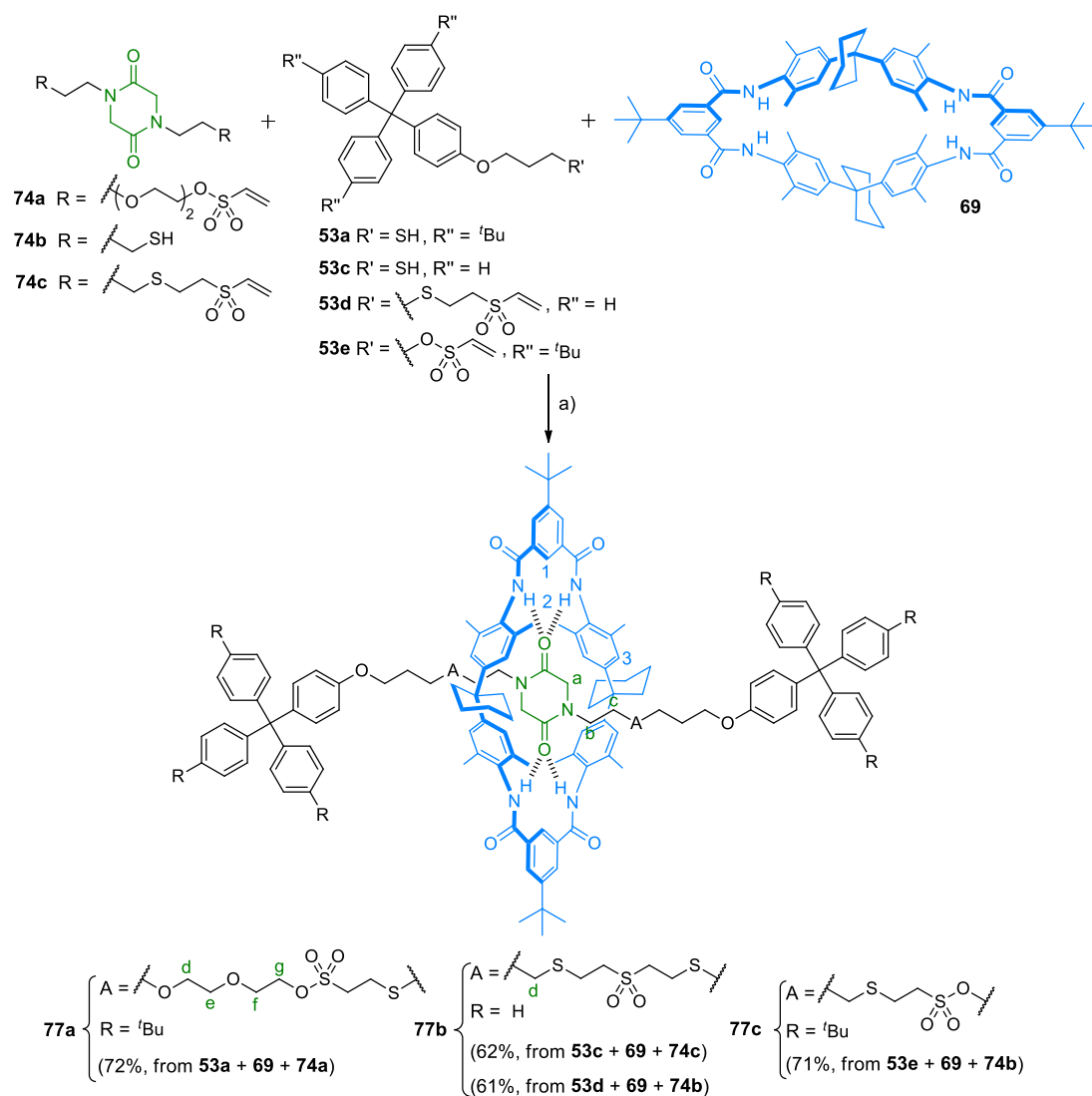
With every component of the target interlocked molecules in hand, we performed the synthesis of the corresponding free threads **76a-c**. Thus, we synthesized threads **76a-c** in good yields (71-98%) employing the thia-Michael addition (Scheme 39). We observed that the reaction is also efficient using the thiol-functionalized diketopiperazine axle and the vinyl sulfonyl stoppers. In addition, we realized that the reaction yield was higher when using a non-anhydrous solvent. It indeed makes sense that traces of water in the solvent helps the catalysis since water is a protic molecule.



Scheme 39. Synthesis of the free threads **76a–c** by a MAVS reaction to sulfonyl groups placed on the stopper or on the rod precursor. Reagents and conditions: a) Et₃N, CHCl₃, r.t., O/N.

Finally, we attempted the click MAVS reactions to obtain the desired rotaxanes **77a–c**. With this aim, first the pseudorotaxanes were generated by mixing together macrocycle **69** and the corresponding axle, and subsequently, the thia-Michael addition was performed employing the appropriate stopper. We attained very good yields (62–72%), which are similar to those previously reported by Schalley and co-workers using the CuAAC reaction. Moreover, we demonstrated that the click MAVS reaction is equally effective when the vinyl sulfone derivative is situated on the rod precursor or on the stopper since the yield of **77b** is almost identical employing both approaches (61–62%) (Scheme 40).

These [2]rotaxanes were characterized by means of NMR spectroscopy. These spectra show that the protons from the macrocycle, especially the amide ones, are shifted downfield due to the hydrogen bonds established ($\Delta\delta_{\text{H1}}=0.44\text{--}0.46$ ppm and $\Delta\delta_{\text{H2}}=1.02\text{--}1.11$ ppm), whereas the signals of those from the axle, especially those of the diketopiperazine H atoms which also become broad, are shielded due to the effect of the aromatic units of the macrocycle ($\Delta\delta_{\text{Ha}}=-1.29\text{--}1.38$ ppm) (Figures 21 and 22). Furthermore, DOSY NMR spectra of **77a** and **77b** demonstrate that both sets of signals from the rod and the ring have a single diffusion coefficient (Figure 23). This is another proof that attests to the existence of a mechanical bond. Finally, the exact masses and isotopic distributions of the signals detected by HRMS are fully consistent with the theoretical ones (Figure 24 for **77b**).



Scheme 40. Synthesis of diketopiperazine-based [2]rotaxanes **77a–c** by MAVS reaction to sulfonyl units placed either on the stopper or on the axle precursor. Reagents and conditions: a) Et_3N , CHCl_3 , r.t., O/N.

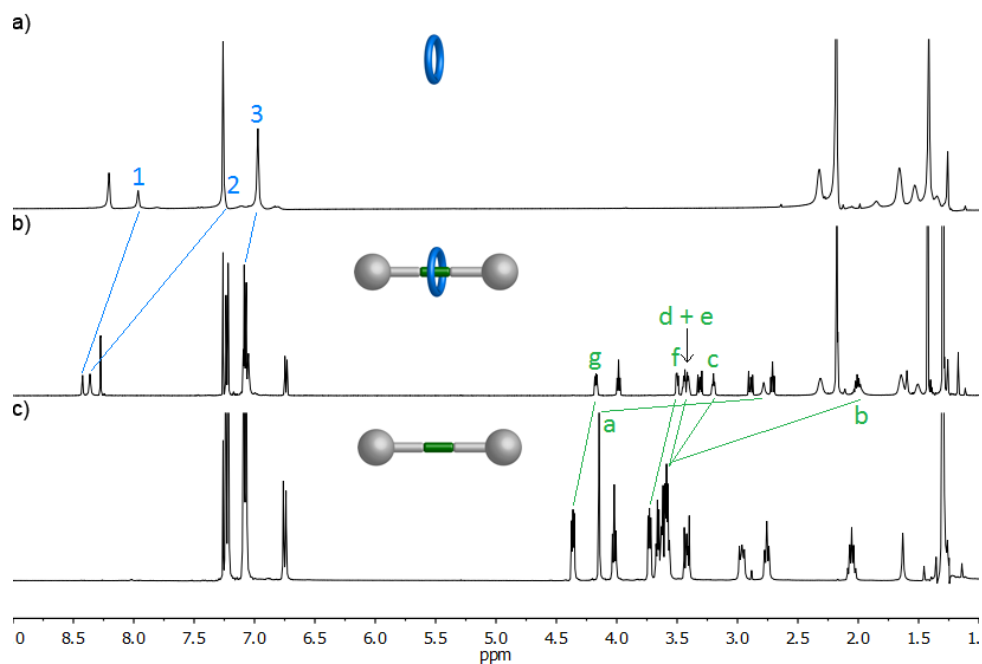


Figure 21. ¹H NMR spectra of: a) Macrocycle **69** (500 MHz, CDCl₃). b) Rotaxane **77a** (500 MHz, CDCl₃). c) Thread **76a** (400 MHz, CDCl₃). Lettering coding is defined in Scheme 40.

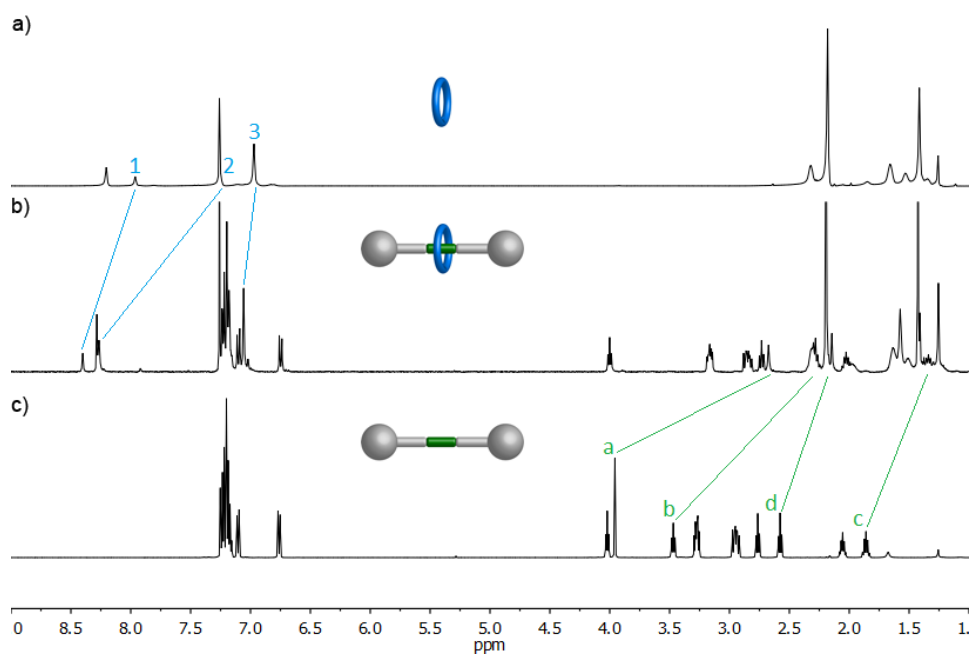


Figure 22. ¹H NMR spectra of: a) Macrocycle **69** (500 MHz, CDCl₃). b) Rotaxane **77b** (400 MHz, CDCl₃). c) Thread **76b** (500 MHz, CDCl₃). Lettering coding is defined in Scheme 40.

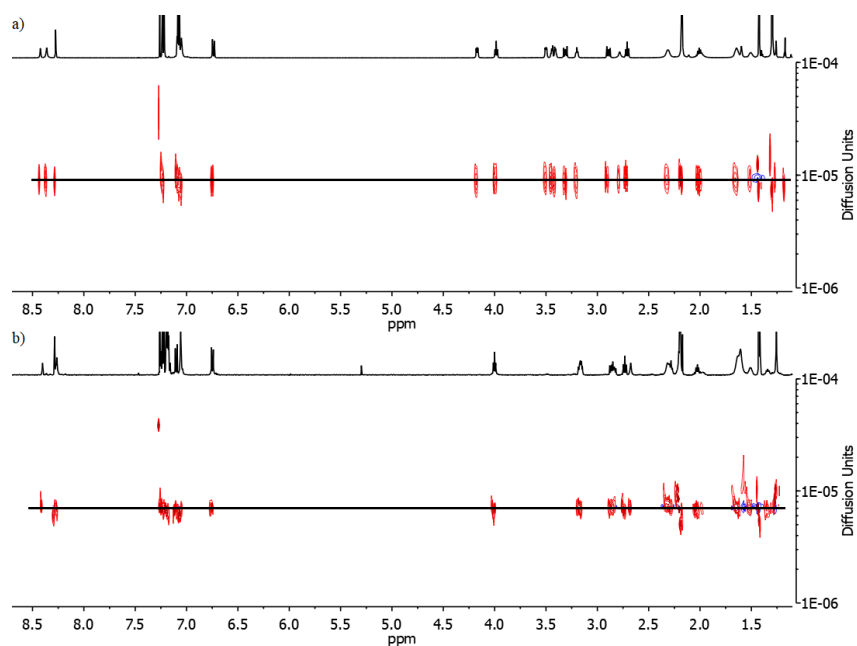


Figure 23. DOSY NMR spectra of: a) Rotaxane **77a** (500 MHz, CDCl_3). b) Rotaxane **77b** (400 MHz, CDCl_3).

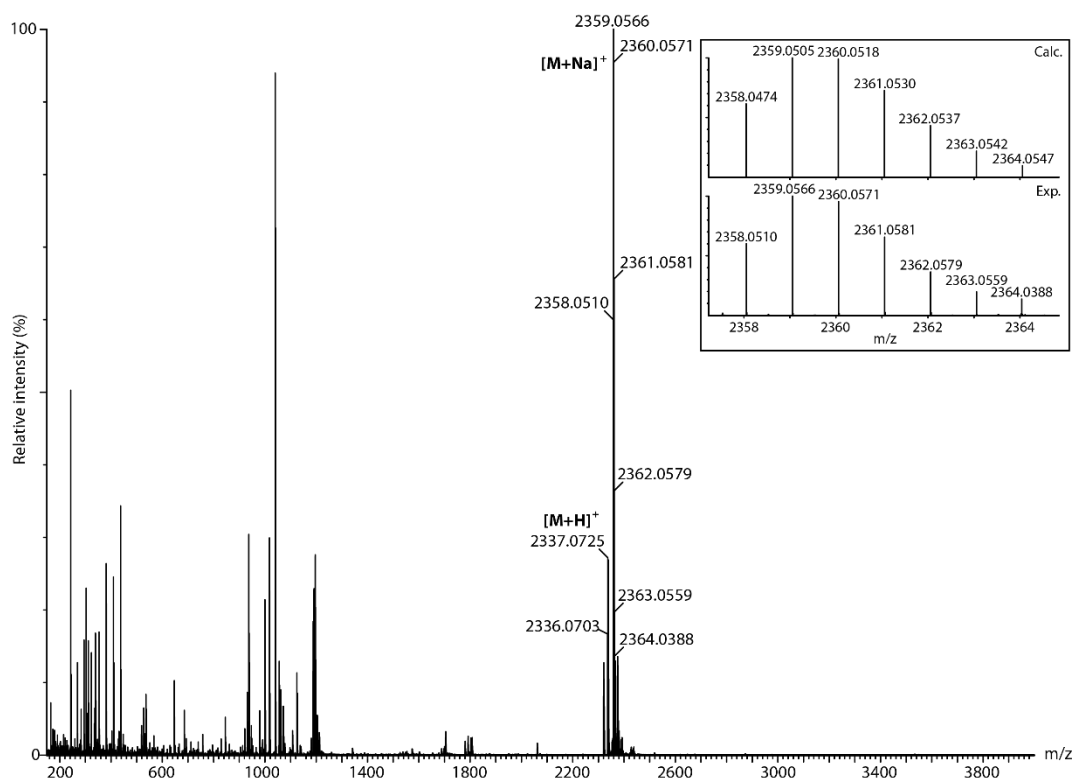


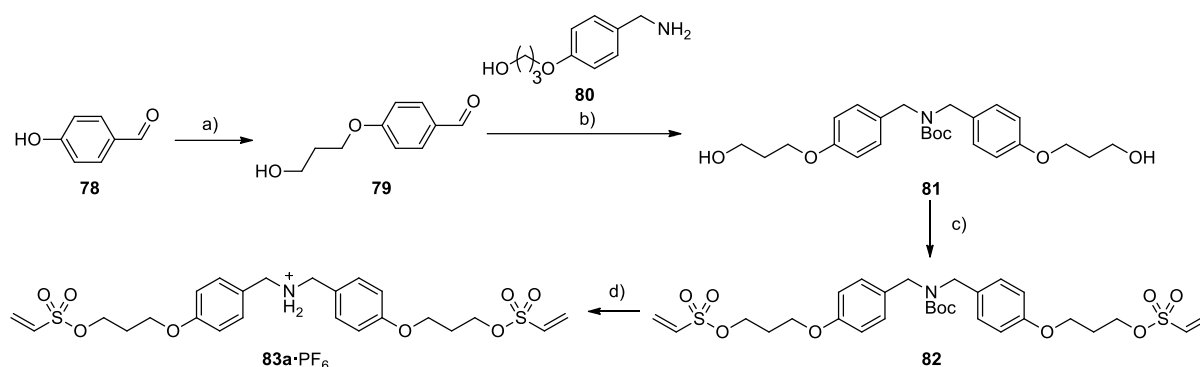
Figure 24. HRMS (ESI^+) spectrum of **77b**. Inset: Observed (bottom) and theoretical (top) isotopic distribution for the signal of $[\mathbf{77b}+\text{Na}]^+$.

1.3.2.2. Rotaxanes containing a crown ether ring

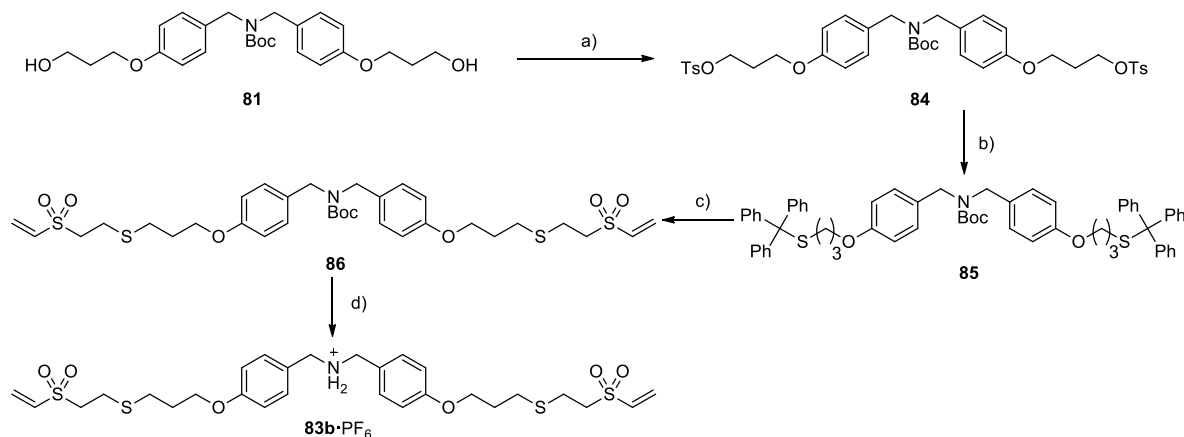
Next, we wanted to study the possibility of creating a rotaxane with the widely used DB24C8/ammonium salt motif. The main drawback of our click MAVS methodology regarding this system is its usual need for a base to be effective. However, the macrocycle only interacts with the

amine when it is protonated as ammonium salt. This causes a dilemma we wanted to address and solve.

Initially, we prepared aldehyde **79**²¹⁹ via a Williamson reaction from 4-hydroxybenzaldehyde (**78**) and 3-bromo-1-propanol. Then, **79** underwent a reductive amination with benzyl amine **80**, followed by a Boc-protection of the generated amine to give **81** in 87% yield. This diol was treated with 2-chloroethanesulfonyl chloride in order to obtain vinyl sulfonate moieties in 67% yield, then Boc-deprotected employing $\text{CF}_3\text{CO}_2\text{H}$, and finally the counterion was changed to PF_6^- , to afford **83a**· PF_6 , the desired rotaxane precursor, in excellent yield (96%) (Scheme 41).



Scheme 41. Synthesis of axle **83a**· PF_6 . Reagents and conditions: a) 3-Bromo-1-propanol, K_2CO_3 , CH_3CN , 75°C , 24 h, 85 %. b) 1. MeOH, r.t., 20 h. 2. NaBH_4 , MeOH, r.t., 18 h. 3. Boc_2O , Et_3N , CH_2Cl_2 , r.t., 24 h, 87%. c) 2-chloroethanesulfonyl chloride, Et_3N , CH_2Cl_2 , 0°C , 1 h, 67%. d) 1. $\text{CF}_3\text{CO}_2\text{H}$, CH_2Cl_2 , r.t., 2 h. 2. HCl (1 M in Et_2O), CH_2Cl_2 , r.t., 2 h. 3. KPF_6 , CH_2Cl_2 , H_2O , acetone, r.t., 24 h, 96%.

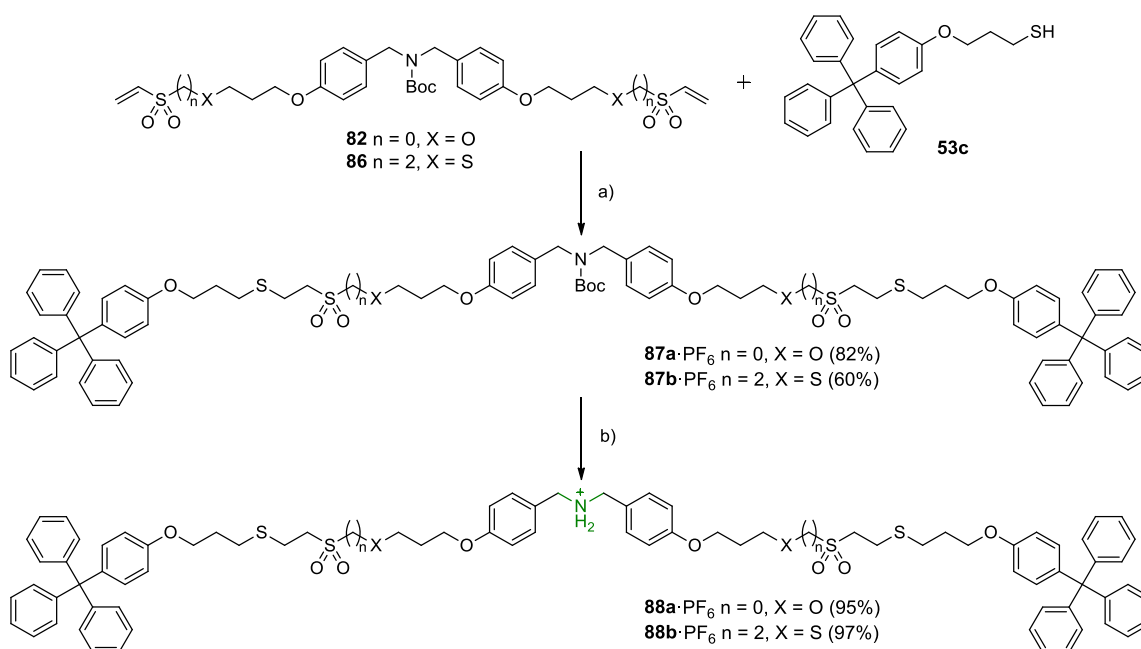


Scheme 42. Synthesis of axle **83b**· PF_6 . Reagents and conditions: a) TsCl , Et_3N , $\text{DMAP}_{(\text{cat.})}$, CH_2Cl_2 , r.t., 18 h, 88%. b) Triphenylmethanethiol, LiHMDS (1 M in THF), THF, 0°C to reflux, 20 h, 93%. c) 1. $\text{CF}_3\text{CO}_2\text{H}$, Et_3SiH , CH_2Cl_2 , r.t., 3 h. 2. Boc_2O , Et_3N , CH_2Cl_2 , r.t., 4 h. 3. divinyl sulfone, Et_3N , CH_2Cl_2 , r.t., 18 h, 56%. d) 1. $\text{CF}_3\text{CO}_2\text{H}$, CH_2Cl_2 , r.t., 2 h. 2. HCl (1 M in Et_2O), CH_2Cl_2 , r.t., 3 h. 3. KPF_6 , CH_2Cl_2 , H_2O , acetone, r.t., 18 h, 89%.

As for the divinyl sulfone-functionalized dibenzylammonium salt, **81** was reacted with TsCl to obtain tosylate **84** in good yield (88%). Subsequently, we carried out the nucleophile substitution of the leaving group of **84** with the thiolate obtained by deprotonation of trityl thiol with LiHMDS to afford

85 in very good yield (93%). The reagents employed for the deprotection of the trityl thiol moieties also removed the Boc protecting group of the amine, so the amine had to be Boc-protected again in order to carry out the subsequent thia-Michael addition in a selective manner. Thus, reaction with Boc_2O followed by treatment with divinyl sulfone yielded the bisvinyl sulfone derivative **86** in moderate yield (56%). The latter was treated with trifluoroacetic acid to generate an ammonium group whose counterion was later changed to PF_6^- to get **83b**· PF_6 in good yield (89%) (Scheme 42).

With the aim of obtaining both reference free threads **88a,b**· PF_6 , we carried out the MAVS reactions with the Boc-protected vinyl sulfonyl-functionalized compounds **82** and **86** and thiol stopper **53c**, followed by a Boc-deprotection employing trifluoroacetic acid and counterion exchange to PF_6^- , to generate **88a,b**· PF_6 (Scheme 43).²²⁰

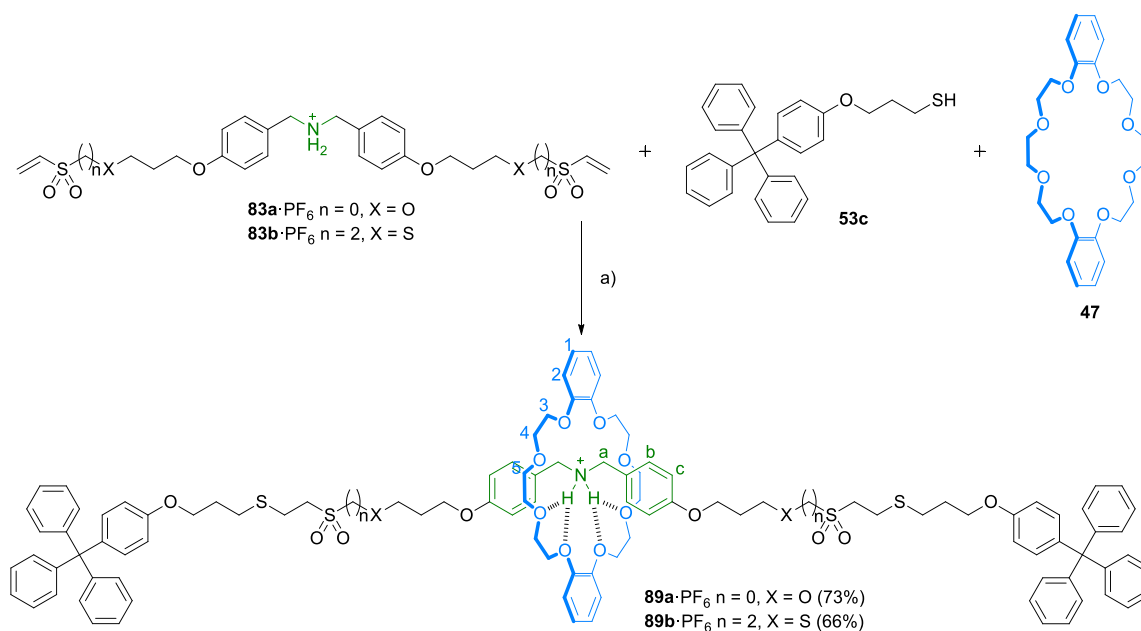


Scheme 43. Synthesis of free threads **88a,b**· PF_6 . Reagents and conditions: a) Et_3N , CH_2Cl_2 , r.t., 18 h. b) 1. $\text{CF}_3\text{CO}_2\text{H}$, CH_2Cl_2 , r.t., 2 h; 2. HCl (1 M in Et_2O), CH_2Cl_2 , r.t., 2-3 h; 3. KPF_6 , CH_2Cl_2 , acetone, H_2O , r.t. 18 h.

Although model studies revealed that the thia-Michael addition is efficiently catalyzed by substoichiometric amounts of Et_3N or PPh_3 , when these conditions were tested for the rotaxane formation, they proved unsuccessful. Thus, employing just 1 equivalent or lower amounts of catalyst, no reaction was observed as we recovered the starting materials. When we used more than 1 equivalent, the MAVS reaction was activated, nonetheless, we obtained the thread and the macrocycle individually with no trace of the target rotaxane. However, Takata and co-workers reported the synthesis of a similar rotaxane through a thiol-maleimide reaction using DMAP as catalyst at 0°C .^{199a}

²²⁰ Compounds **87a** and **88a**· PF_6 were prepared following a procedure already described in our group: P. García-Cerezo, Síntesis de rotaxanos orgánicos mediante Química "click" basada en adiciones de tipo Michael a grupos vinilsulfonilo, MSc dissertation, Universidad de Granada, Granada, Spain, 2017.

Following this strategy, some model studies to adapt these conditions to the MAVS reaction were performed and proved to be efficient. Therefore, the rotaxane formation was carried out using DMAP as catalyst at 0 °C for 3 days, affording rotaxanes **89a,b**·PF₆ in good yields (66-73%) (Scheme 44).



Scheme 44. Synthesis of rotaxanes **89a,b**·PF₆ owning a dibenzylammonium recognition site. Reagents and conditions: a) DMAP, CH₂Cl₂, 0 °C, 72 h.

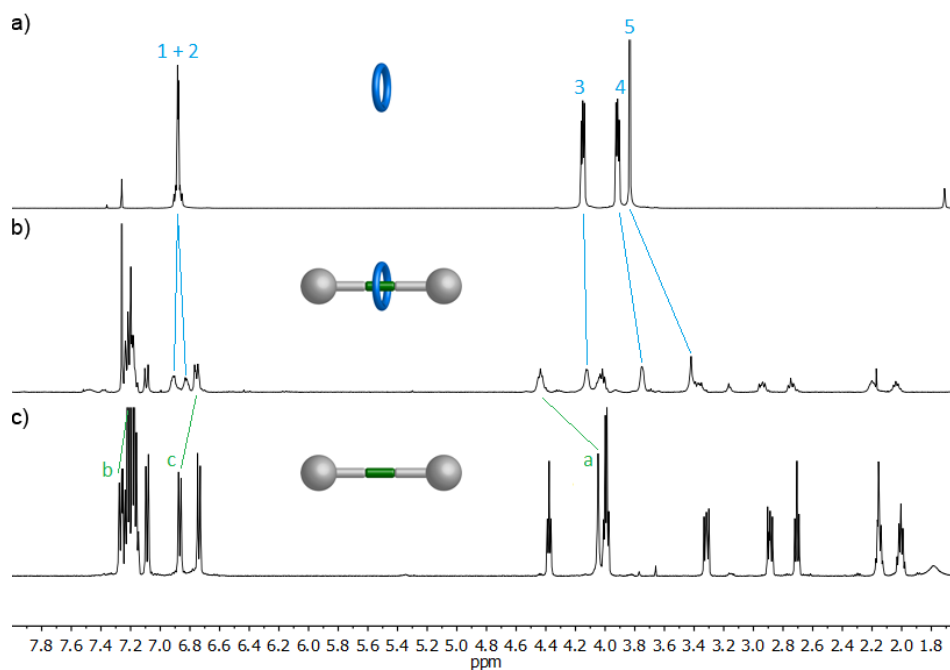


Figure 25. ¹H NMR spectra of: a) Macrocycle **47** (400 MHz, CDCl₃). b) Rotaxane **89a**·PF₆ (400 MHz, CDCl₃). c) Thread **88a**·PF₆ (500 MHz, CDCl₃). Lettering coding is defined in Scheme 44.

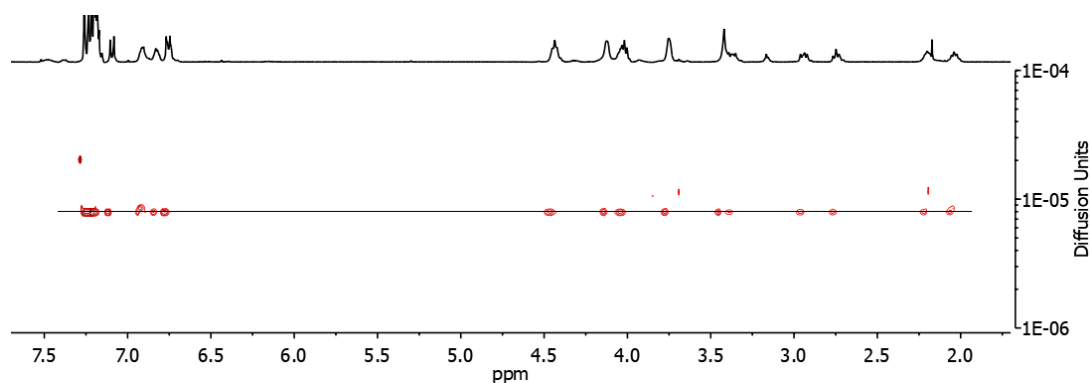


Figure 26. DOSY NMR (400 MHz, CDCl_3) spectrum of **89a**· PF_6 .

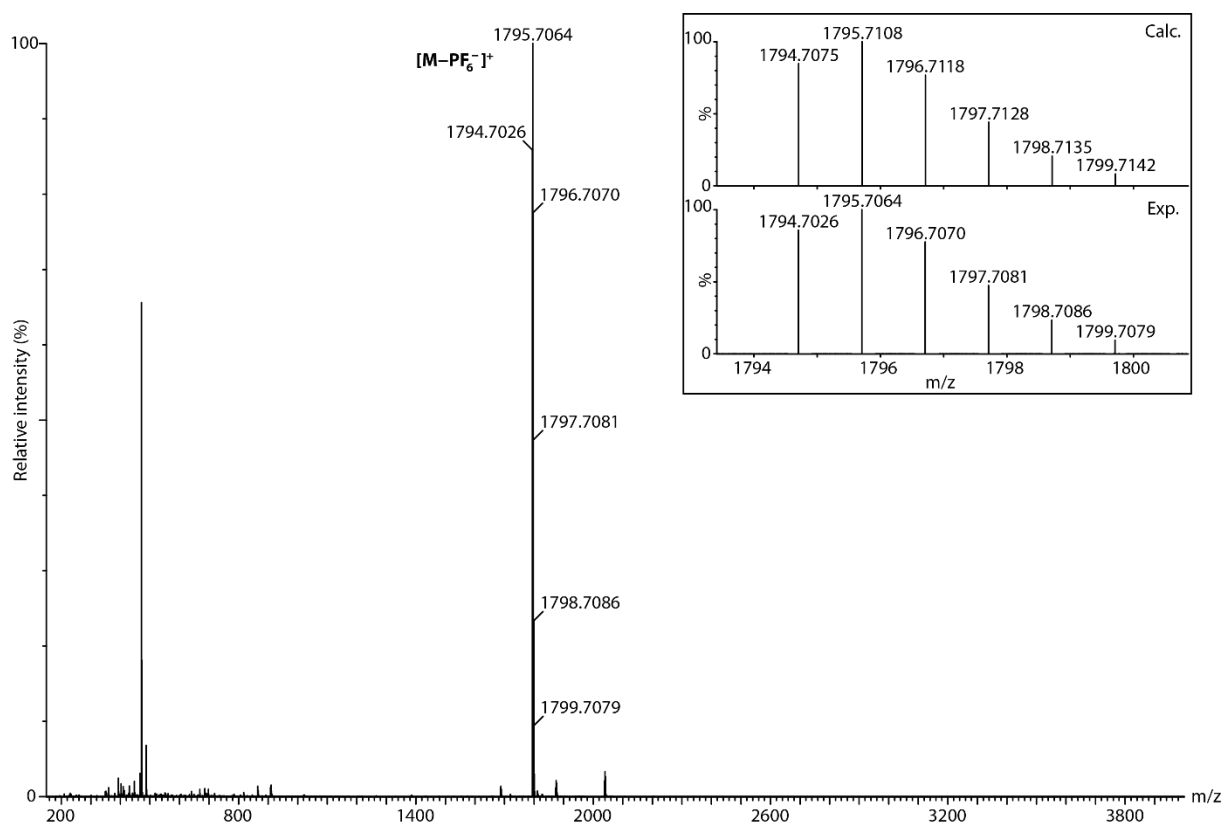


Figure 27. HRMS (ESI^+) spectrum of **89a**. Inset: Observed (bottom) and calculated (top) isotopic distribution for the ion $[\mathbf{89a}-\text{PF}_6]^+$.

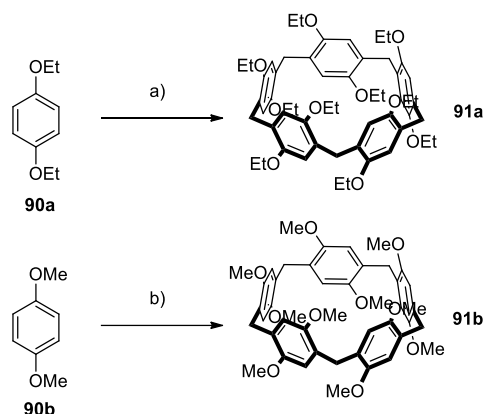
As with previous examples, these dibenzylammonium-based [2]rotaxanes **89a,b**· PF_6 were characterized with the help of NMR spectroscopy. The interlocked nature of the compounds can be easily observed by inspection of the signals of the benzylic protons of the dibenzylammonium salt since they exhibit a downfield shift ($\Delta\delta_{\text{Ha}}=0.39$ ppm) due to the hydrogen bonding which is characteristic for this motif. Moreover, the aromatic H of the macrocycle split into two signals and the CH_2 groups from the macrocycle are shifted upfield ($\Delta\delta_{\text{H5}}=-0.42$ ppm) along with the aromatic protons from the dibenzylammonium salt ($\Delta\delta_{\text{Hc}}=-0.11$ ppm) (Figure 25). This phenomenon is caused by the shielding effect by the aromatic rings from the recognition site and the wheel. In addition, the DOSY NMR

spectrum of **89a**·PF₆ displays a unique diffusion coefficient (Figure 26) and the HRMS confirmed the presence of the target rotaxanes (Figure 27 for **89a**·PF₆).

1.3.3. Synthesis of pillar[5]arene-based rotaxanes

As shown in the general introduction (Section 3.5.2), pillar[n]arenes are a new family of methylene bridged macrocycles that have attracted much interest recently. Consequently, we found relevant to study the formation of pillar[n]arene rotaxanes under click MAVS reactions. In this context we decided to employ a di(1,2,3-triazol-1-yl)butane recognition site for pillar[5]arenes, since it exhibits a high association constant with the per-ethylated pillar[5]arene ($K_a=(1.6 \pm 0.3) \times 10^4 \text{ M}^{-1}$ in CDCl₃ at 298 K).²²¹ With this particular system, the capping approach based on the click CuAAC reaction afforded different [2]rotaxanes in 15%-68% yield.^{221,222}

Initially, we synthesized the per-ethylated pillar[5]arene (**91a**) from 1,4-diethoxybenzene, paraformaldehyde and FeCl₃ in dichloromethane.²²³ Considering that the synthesis was straightforward, we decided to build the per-methylated analogue (**91b**) as well. In this case, we employed 1,4-dimethoxybenzene, paraformaldehyde and BF₃·OEt₂ in 1,2-dichloroethane to obtain the target macrocycle (Scheme 45).



Scheme 45. Synthesis of pillar[5]arenes **91a,b**. Reagents and conditions: a) Paraformaldehyde, FeCl₃, CH₂Cl₂, r.t., 3 h, 69%. b) Paraformaldehyde, BF₃·OEt₂, 1,2-dichloroethane, 30 °C, 30 min, 81%.

Then, the synthesis of axles **97a,b** was achieved taking advantage of the orthogonality of the click MAVS reaction and the click CuAAC reactions.²¹⁰ Thus, diazide **93** was generated in 99% yield employing 1,4-dibromobutane (**92**) and NaN₃.²²⁴ On the other hand, diethylene glycol (**94**) was mono-

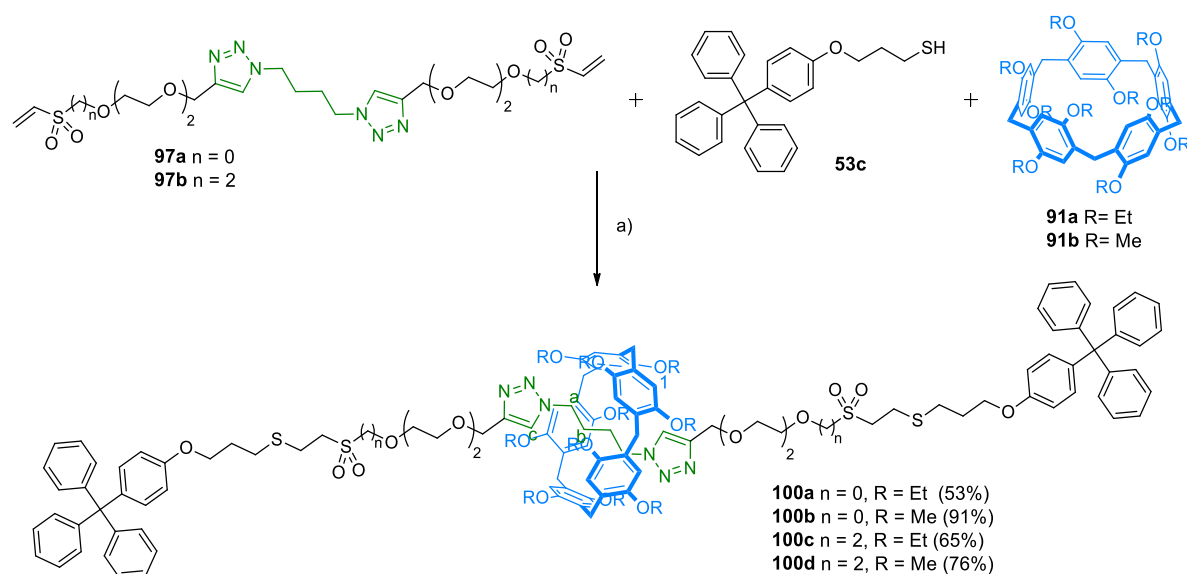
²²¹ T. Ogoshi, R. Iizuka, D. Kotera, T.-A. Yamagishi, *Org. Lett.* **2015**, *17*, 350-353.

²²² T. Ogoshi, D. Kotera, S. Nishida, T. Kakuta, T.-A. Yamagishi, A. M. Brouwer, *Chem. Eur. J.* **2018**, *24*, 6325-6329.

²²³ Compound **91a** was prepared following Meier's procedure: Y. Kou, D. Cao, H. Tao, L. Wang, J. Liang, Z. Chen, H. Meier, *J. Incl. Phenom. Macrocycl. Chem.* **2013**, *77*, 279-289.

²²⁴ Compound **93** was prepared following Rahmani's procedure: S. Rahmani, A. S. Z. Mahani, *Macromol. Res.* **2015**, *23*, 1018-1025.

Once again, the linear fragment and the wheel were mixed before the click MAVS reaction, but this time, the mixture was stirred longer (5 h) since pillar[5]arenes require more time to dissolve in CHCl_3 , especially the per-methylated derivative (**91b**). Afterwards, we performed the thia-Michael addition and obtained the four [2]rotaxanes **100a-d** in remarkable yields (53-91%) (Scheme 48). It can be noticed that the yields of rotaxanes obtained when using the per-ethylated ring **91a** are similar to those reported by Ogoshi.^{221,222} However, surprisingly, the use of the per-methylated pillar[5]arene afforded higher yields, up to 91%. It might be a consequence of its lower solubility in chloroform which promotes the formation of the pseudorotaxanes through solvophobic effect.



Scheme 48. Synthesis of rotaxanes **100a-d** by a thia-Michael addition. Reagents and conditions: a) Et_3N , CH_2Cl_2 , r.t., 16-24 h.

These rotaxanes were characterized by NMR spectroscopy. The interlocked nature of these compound can be assessed using the resonances of the recognition site butane unit as diagnostic signals. Both peaks are significantly shifted upfield ($\Delta\delta_{\text{Ha}} = -2.28$ - 2.33 ppm; $\Delta\delta_{\text{Hb}} = -3.03$ - 3.09 ppm) as well as the H from the triazole group ($\Delta\delta_{\text{Hc}} \approx -0.23$ ppm) (Figures 28 and 29). Furthermore, DOSY NMR spectra show that every signal diffuse with the same diffusion coefficient (Figure 30). High-resolution mass spectrometry of these compounds complete the evidence of the presence of the rotaxane as signals were observed with experimental exact masses and isotopic distributions consistent with the theoretical ones (Figures 31 and 32).

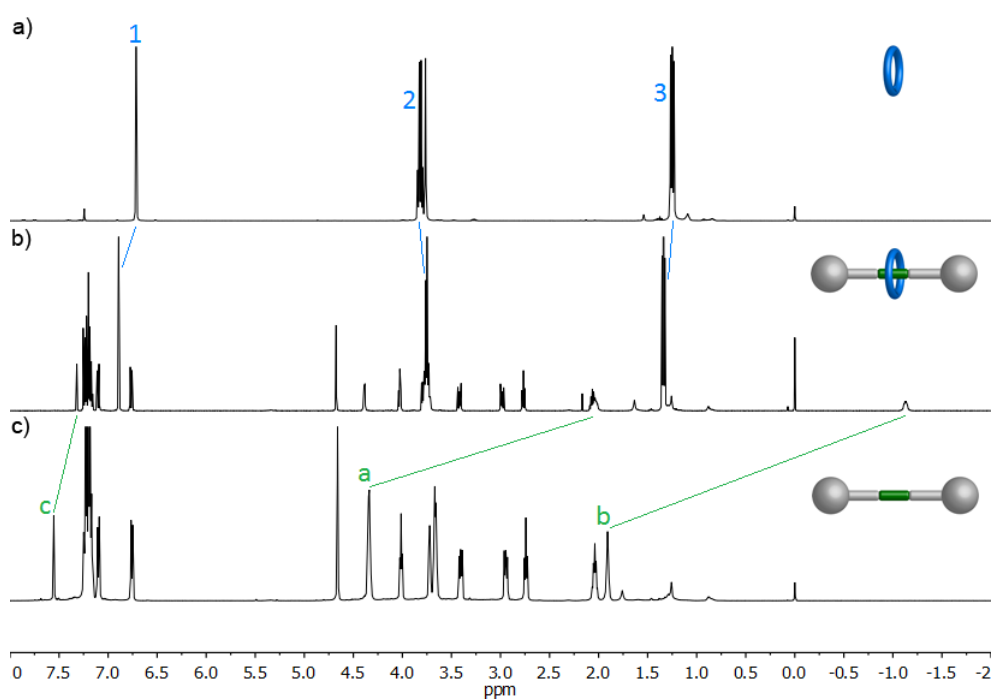


Figure 28. ^1H NMR spectra of: a) Macrocycle **91a** (400 MHz, CDCl_3). b) Rotaxane **100a** (400 MHz, CDCl_3). c) Thread **99a** (500 MHz, CDCl_3). Lettering coding is defined in Scheme 48.

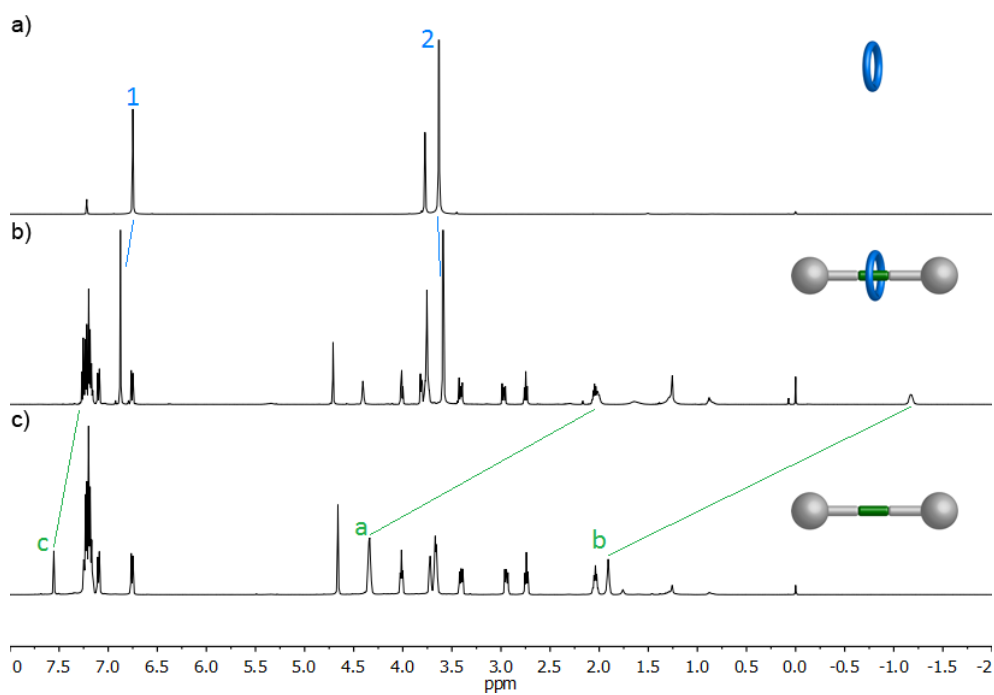


Figure 29. ^1H NMR spectra of: a) Macrocycle **91b** (400 MHz, CDCl_3). b) Rotaxane **100b** (500 MHz, CDCl_3). c) Thread **99a** (500 MHz, CDCl_3). Lettering coding is defined in Scheme 48.

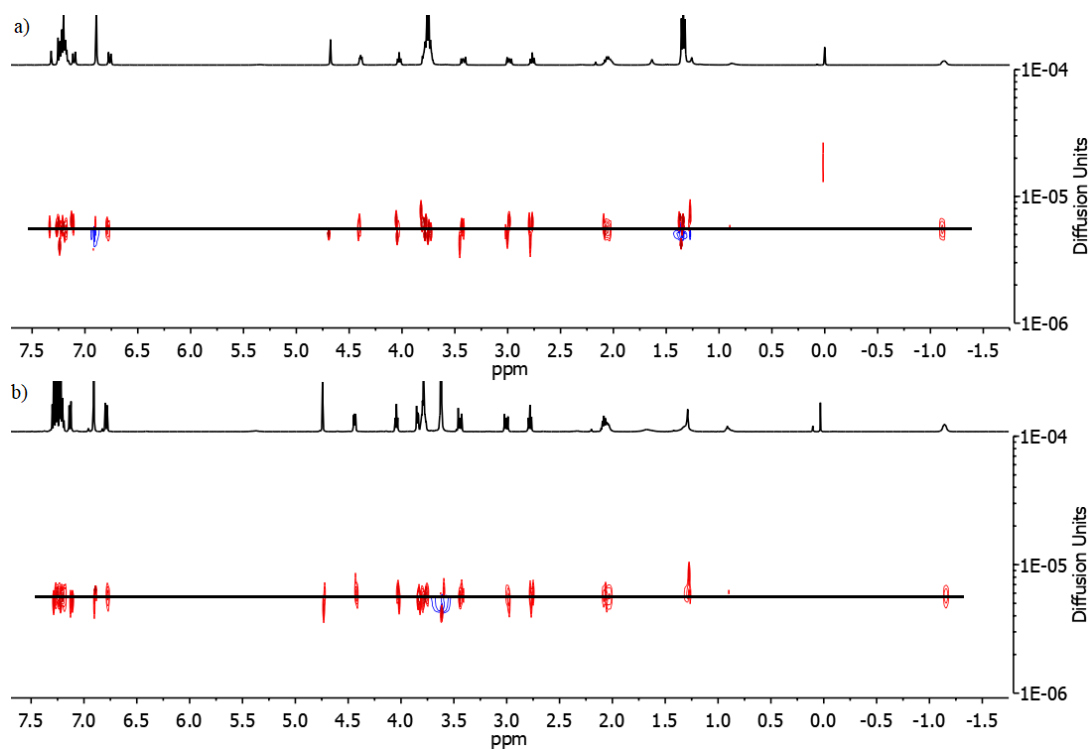


Figure 30. DOSY NMR (500 MHz, CDCl_3) spectra of: a) Rotaxane **100a**. b) Rotaxane **100b**.

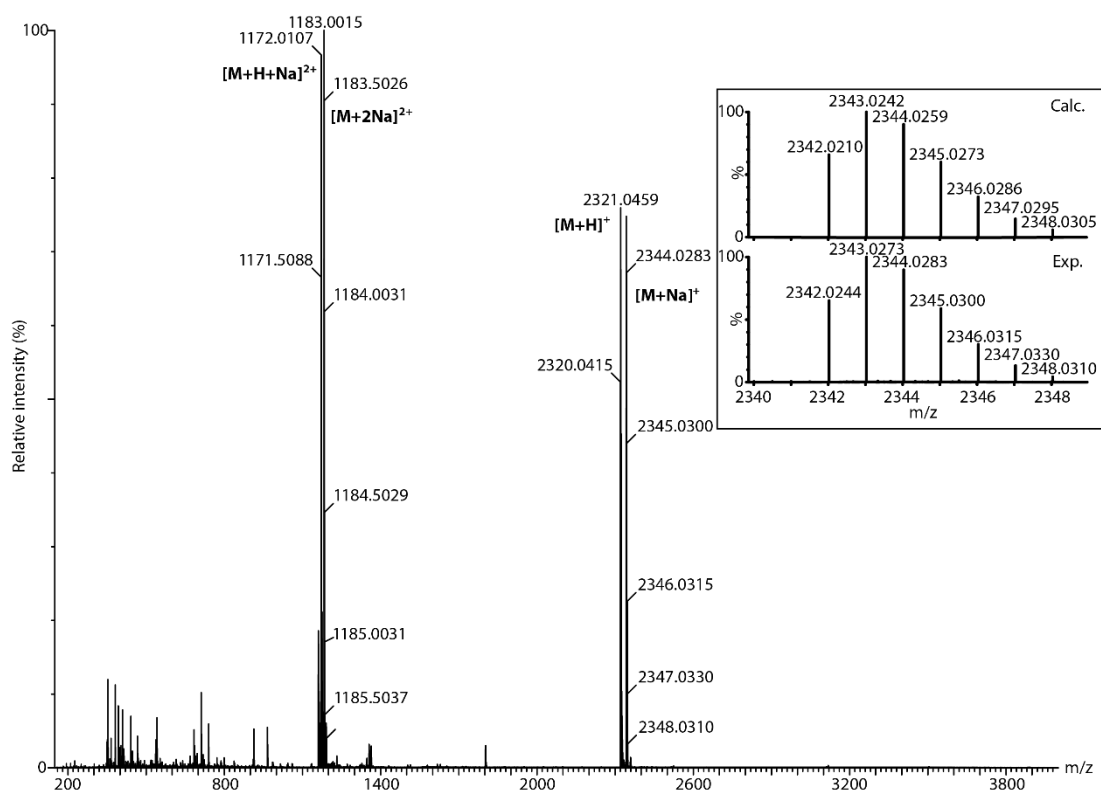


Figure 31. HRMS (ESI^+) spectrum of **100a**. Inset: Observed (bottom) and calculated (top) isotopic distribution for $[\mathbf{100a}+\text{Na}]^+$.

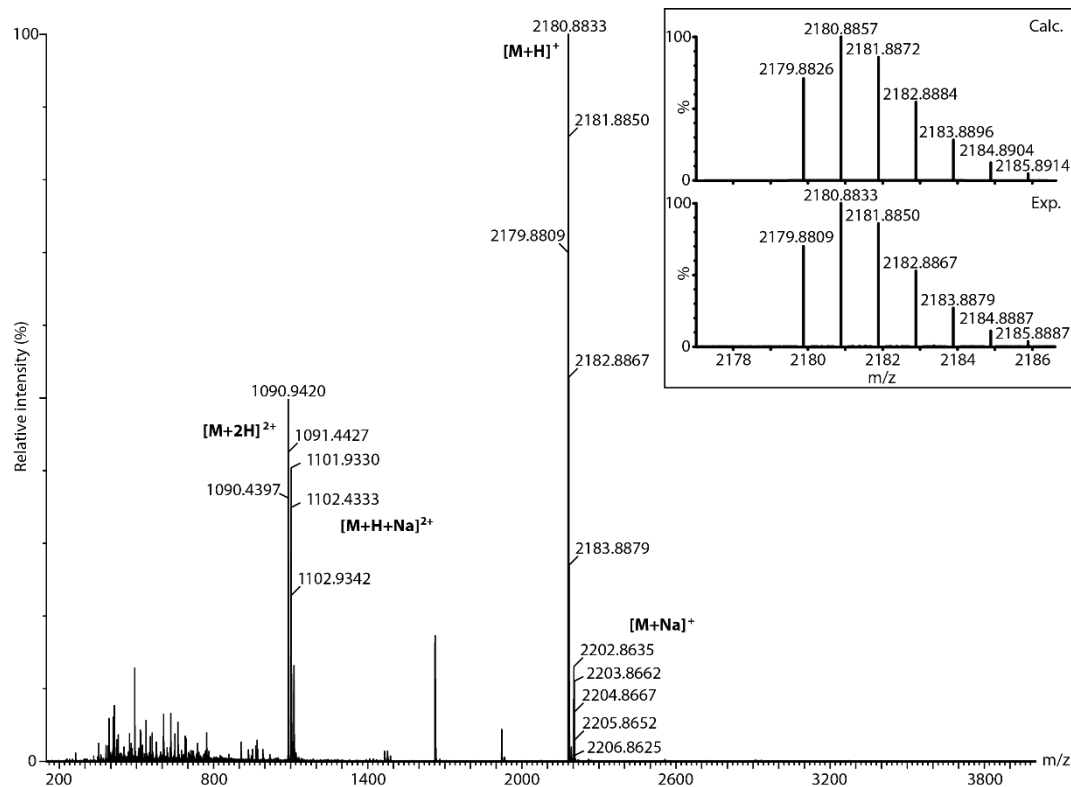


Figure 32. HRMS (ESI⁺) spectrum of **100b**. Inset: Experimental (bottom) and calculated (top) isotopic distribution for [**100b**+H]⁺.

1.3.4. A lithium-templated donor-acceptor rotaxane

1.3.4.1. Synthesis and characterization

Alkali ions have been much less used as template in the synthesis of MIMs than transition metals due to their weaker metal-ligand interactions and less well defined coordination numbers and geometries. However, recently, an increasing number of MIMs templated by those ions have been reported.⁸² Among them, a particular system drew our attention. It consists of a pyromellitic diimide core, a DNP38C10 ring and two Li⁺ ions. Without these cations, the inclusion complex is almost non-existent since the π -donor/ π -acceptor interaction between both aromatic species is very weak. Nonetheless, Li⁺ ions were found to reinforce this inclusion complex²²⁵ due to their coordination to the crown ether and pyromellitic O atoms, as shown by the X-ray structure (Figure 33). As a result, the use of Li⁺ increased the yield of a catenane formation reaction.^{225a} They can also drive the motion of the macrocycle from a NDI recognition site to a pyromellitic secondary station (Scheme 18).^{113a,143} Moreover, this motif was exploited to synthesize a [2]rotaxane displaying two pyromellitic units

²²⁵ a) G. Kaiser, T. Jarrosson, S. Otto, Y.-F. Ng, A. D. Bond, J. K. M. Sanders, *Angew. Chem. Int. Ed.* **2004**, *43*, 1959-1962. b) S. I. Pascu, T. Jarrosson, C. Naumann, S. Otto, G. Kaiser, J. K. M. Sanders, *New J. Chem.* **2005**, *29*, 80-89.

through a slipping method in the presence of LiBr affording the [2]rotaxane in moderate yield (44%), however after heating at 60 °C for 14 d.^{113a}

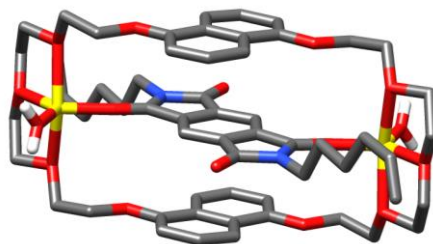
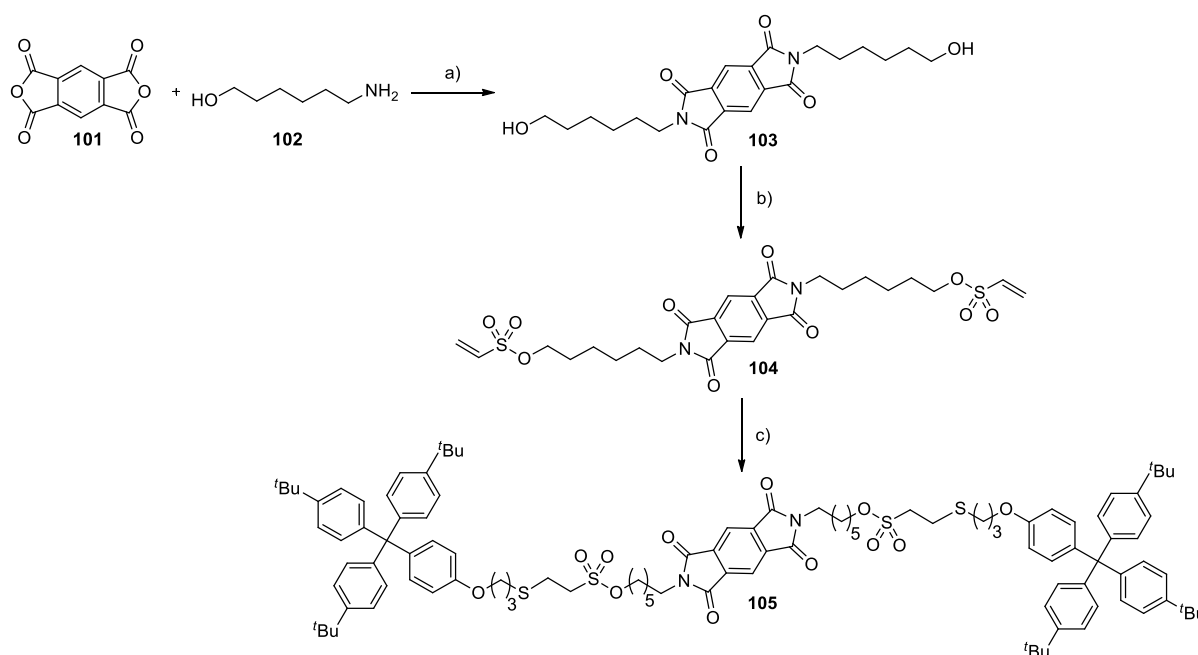


Figure 33. Representation of the X-ray diffraction structure of the inclusion complex formed by a pyromellitic diimide derivative and DNP38C10 coordinated by Li⁺ ions.^{225a} Color coding: C, gray; H, white; O, red; N, blue; Li, yellow.

Considering this background, we envisioned that our MAVS methodology could be an interesting and suitable approach for the synthesis through a capping strategy for the Li⁺-templated synthesis of a π -donor/ π -acceptor rotaxane bearing a DNP38C10 macrocycle and a pyromellitic diimide binding site.

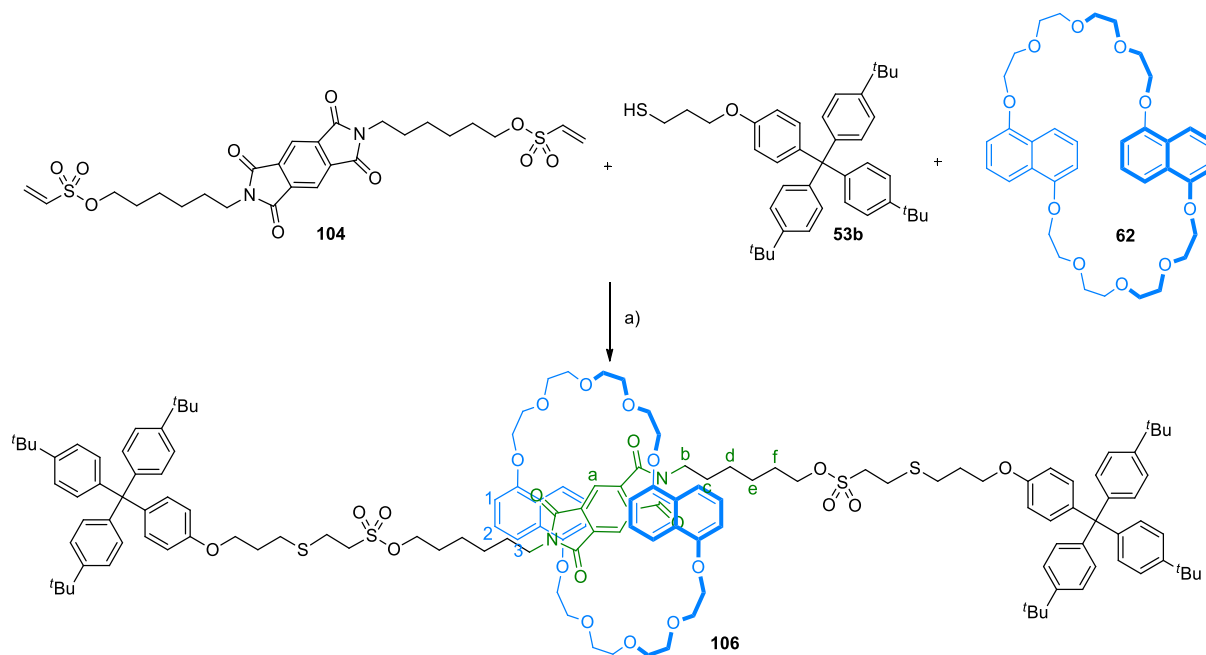


Scheme 49. Synthesis of axle precursor **104** and thread **105**: Reagents and conditions: a) DMF, 20 h, 100 °C, 26%. b) 2-chloroethanesulfonyl chloride, Et₃N, CH₂Cl₂, 2 h, 0 °C, 94%. c) **53b**, Et₃N, CHCl₃, 20 h, r.t., 83%.

We started with the synthesis of pyromellitic derivative **104**, with two vinyl sulfonyl groups and thread **105**. For this purpose, we prepared compound **103** from pyromellitic dianhydride (**101**) and 6-amino-1-hexanol (**102**).²²⁶ Subsequently, this diol was treated with 2-chloroethanesulfonyl chloride in basic medium giving the target vinyl sulfonyl-functionalized axle precursor **104** in excellent yield

²²⁶ Compound **103** was prepared following Ramakrishnan's procedure: S. De and S. Ramakrishnan, *Macromolecules* **2009**, *42*, 8599-8603.

(94%). Bis-vinyl sulfonate **104** and thiol stopper **53b** underwent a thia-Michael addition reaction to afford target thread **105** in 83% yield (Scheme 49).



Scheme 50. Synthesis of rotaxane **106**: General reagents and conditions: a) LiX, Et₃N, CHCl₃/ROH (see Tables 1-6).

With both compounds in hand, we aimed at the synthesis of rotaxane **106** containing a pyromellitic diimide core and a DNP38C10 ring (Scheme 50). First, the reaction was tested without the presence of any Li salt and gave a good overall yield for the MAVS reaction (89%). However, as expected, due to the weak π - π interactions between the macrocycle and the pyromellitic unit, it gave a poor yield for rotaxane **106** (9%) and an excellent yield for thread **105** (80%) (Table 1 – Entry 1). Consequently, we carried out an optimization of the reaction conditions, starting with the study of the effect of different cations in order to increase the yield of rotaxane **106** and the rotaxane:thread ratio.

Therefore, we attempted the synthesis with salts of different alkali, alkaline earth metals, or other metals owning an ionic radius comparable to Li⁺ (Table 1). To this end, we formed the pseudorotaxane from **104** and DNP38C10 (**62**) and then added an excess of the metal salt. The solution changed from yellow to deep orange after the addition of salt in the case of Li⁺, Sc³⁺ and In³⁺ ions. A mixture of chloroform with a small proportion of MeOH was needed as solvent to ensure solubility over time. The best results were obtained with lithium salts, which afforded up to 29% yield for rotaxane **106** combined with a 50:50 rotaxane/thread ratio in the case of LiPF₆. However, the overall yields of these reactions were still quite low (39-69%) (Table 1 – Entries 2, 7 and 9). Conversely, other cations such as, Sc³⁺, In³⁺, Mg²⁺, K⁺ or Na⁺ proved to be less efficient templates since they gave weaker performances than Li⁺ in terms of rotaxane yield and/or rotaxane:thread ratio (Table 1 – Entries 3-6, 8).

Table 1. Effect of metal ions for the synthesis of rotaxane **106**.

Entry	Salt	Yield of thread 105 [%] ^[a]	Yield of rotaxane 106 [%] ^[a]	106/105 Ratio
1	/	80	9	10:90
2	LiOTf	29	10	34:66
3	Sc(OTf) ₃	65	15	19:81
4	In(OTf) ₃	39	2	5:95
5	Mg(OTf) ₂	78	5	6:94
6	KPF ₆	41	5	11:89
7	LiPF ₆	29	29	50:50
8	NaBF ₄	61	7	10:90
9	LiBF ₄	44	25	36:64

[a] Yield of isolated product after purification by column chromatography (SiO₂) and gel permeation chromatography (Bio-Beads® S-X1, CH₂Cl₂). Reactions were carried out using general procedure A.²²⁷

As shown in Table 1, the influence of the counterion of the lithium salt seems to be very important for the rotaxane formation reaction. Thus, we choose to explore the synthesis of rotaxane **106** with various Li⁺ salts (Table 2). It is clear that the yield of rotaxane **106** and the rotaxane/thread ratio was improved by using non-coordinating anions. Thus, the best result was obtained with the salt with the weakest coordinating one, [Li(OEt₂)_n][B(C₆F₅)₄], affording a 44% yield for rotaxane **106** and a 55:45 rotaxane/thread ratio (Table 2 – Entry 13). It should be also noticed that the use of LiI, LiBr and LiOH resulted in the decomposition of the starting materials (Table 2 – Entries 5-7).

Having identified [Li(OEt₂)_n][B(C₆F₅)₄] salt as the more efficient Li⁺ source to enhance the pseudorotaxanes formation, the optimization of the remaining reaction conditions was explored. As starting point, the number of equivalents of Li salt were investigated (Table 3). The best outcome was attained with 3 equivalents reaching 36% yield for rotaxane **106** and a 44:56 rotaxane/thread ratio (Table 3 – Entry 4). When 4 equivalents were added to the solution, a precipitate began to appear after approximately 30 minutes, which resulted in a drastic reduction of the reaction yield (Table 3 – Entry 5).

²²⁷ General procedure A: To a solution of **104** (13 mg, 22 μmol) and **62** (28 mg, 44 μmol) in CHCl₃ (6 mL) were added MeOH (300 μL) and an excess of the indicated salt. The solvent was removed under reduced pressure until the color of the solution was deep orange while ensuring no precipitate was formed (volume of the solution: approximately 1 mL). To this solution under argon were added **53b** (50 mg, 87 μmol) and 2 drops of Et₃N. The solution was stirred for 24 h at room temperature and concentrated to dryness. The crude material was purified by column chromatography (SiO₂, CH₂Cl₂/EtOAc 100:0 to 94:6, to CH₂Cl₂/MeOH 96:4) to afford thread **105** as a white solid and a mixed fraction of macrocycle **62** and rotaxane **106**. The latter was purified by gel permeation chromatography (Bio-Beads® S-X1, CH₂Cl₂) to yield rotaxane **106** as a yellow solid.

Table 2. Li⁺ salt screening for the synthesis of rotaxane **106**.

Entry	Salt	Yield of thread 105 [%] ^[a]	Yield of rotaxane 106 [%] ^[a]	106/105 Ratio
1	-	80	9	10:90
2	LiOTf	29	10	34:66
3	LiBF ₄	44	25	36:64
4	LiPF ₆	29	29	50:50
5	LiI	0	0	-
6	LiBr	0	0	-
7	LiOH ^[b]	0	0	-
8	LiCl	29	2	7:93
9	LiClO ₄	73	4	5:95
10	LiAsF ₆	31	6	16:84
11	LiB(C ₂ O ₄) ₂	66	30	32:68
12	LiSbF ₆	54	39	42:58
13	[Li(OEt ₂) _n][B(C ₆ F ₅) ₄]	36	44	55:45

[a] Yield of isolated product after purification by column chromatography (SiO₂) and gel permeation chromatography (Bio-Beads® S-X1, CH₂Cl₂). [b] Dissolved in H₂O (100 μL). Reactions were carried out using general procedure A.

Table 3. Optimization of reaction conditions for the synthesis of rotaxane **106**: equivalents of Li⁺ salt.

Entry	Equiv. of Li ⁺ salt	Solvent	C [mM]	T	Time [h]	Equiv. of macrocycle 62	Yield of thread 105 [%] ^[a]	Yield of rotaxane 106 [%] ^[a]	106/105 Ratio
1	0	CHCl ₃	18	r.t.	24	2	79	4	5:95
2	1	CHCl ₃	18	r.t.	24	2	66	16	20:80
3	2	CHCl ₃	18	r.t.	24	2	60	21	26:74
4	3	CHCl ₃	18	r.t.	24	2	46	36	44:56
5	4	CHCl ₃	18	r.t.	24	2	9	2	18:82

[a] Yield of isolated product after purification by column chromatography (SiO₂) and gel permeation chromatography (Bio-Beads® S-X1, CH₂Cl₂). Reactions were carried out using general procedure B.²²⁸

²²⁸ General procedure B: To a solution of **104** (11 mg, 18 μmol) and the corresponding amount of **62** in CHCl₃ (6 mL) were added MeOH (600 μL) and [Li(OEt₂)_n][B(C₆F₅)₄]. The solvent was evaporated under reduced pressure. The syrup was dissolved in the indicated solvent. To this solution under argon were added **53b** (43 mg, 72 μmol) and 2 drops of Et₃N. The solution was stirred for 24 h (or 72 h) at the indicated temperature and concentrated to dryness. The crude material was purified by column chromatography (SiO₂, CH₂Cl₂/EtOAc 100:0 to 94:6, to CH₂Cl₂/MeOH 96:4) to afford thread **105** as a white solid and a mixed fraction of macrocycle **62** and rotaxane **106**. The latter was purified by gel permeation chromatography (Bio-Beads® S-X1, CH₂Cl₂) to yield rotaxane **106** as a yellow solid.

Subsequently, the identification of the appropriate solvent to carry out the reaction was examined. Thus, various solvent mixtures were tested to dissolve the pseudorotaxane formed by axle **104** (1 equiv.) and macrocycle **62** (2 equiv.) in the presence of $[\text{Li}(\text{OEt})_n][\text{B}(\text{C}_6\text{F}_5)_4]$ (3 equiv.).²²⁹ Solvent mixtures of a chlorinated solvent and an alcohol (Table 4) and in particular $\text{CHCl}_3/\text{MeOH}$ (95:5) gave the best results, affording rotaxane **106** in 61% yield with a 71:29 rotaxane/thread ratio (Table 4 – Entry 4).

Table 4. Optimization of reaction conditions for the synthesis of rotaxane **106**: solvent mixture.

Entry	Equiv. of Li^+ salt	Solvent	C [mM]	T	Time [h]	Equiv. of macrocycle 62	Yield of thread 105 [%] ^[a]	Yield of rotaxane 106 [%] ^[a]	106/105 Ratio
1	3	CHCl_3	18	r.t.	24	2	46	36	44:56
2	3	$\text{CHCl}_3/\text{PrOH}$ (95:5)	18	r.t.	24	2	34	39	53:47
3	3	$\text{CHCl}_3/\text{EtOH}$ (95:5)	18	r.t.	24	2	28	52	65:35
4	3	$\text{CHCl}_3/\text{MeOH}$ (95:5)	18	r.t.	24	2	25	61	71:29
5	3	$\text{CH}_2\text{Cl}_2/\text{MeOH}$ (95:5)	18	r.t.	24	2	34	7	7:93
6	3	1,2-Dichloroethane /MeOH (95:5)	18	r.t.	24	2	49	16	33:67

[a] Yield of isolated product after purification by column chromatography (SiO_2) and gel permeation chromatography (Bio-Beads® S-X1, CH_2Cl_2). Reactions were carried out using general procedure B.

The effect of concentration was then analysed and 18 mM was identified as the optimum value (Table 5). An attempt to reduce the reaction temperature to 0 °C afforded promising results, nonetheless, the vinyl sulfonate-functionalized axle **104** was not completely consumed after 24 h (Table 6 – Entry 2). Hence, extending the reaction time to 72 h resulted in obtaining a good yield for rotaxane **106** (61%) with a 73:27 rotaxane/thread ratio (Table 6 – Entry 3). Finally, the increase of the equivalents of macrocycle **62** (Table 6 – Entries 3-5), resulted in a rise of the yield of [2]rotaxane **106** with a maximum of 66% isolated yield and a 78:22 rotaxane/thread ratio upon addition of 5 equiv of DNP38C10 (**62**)

²²⁹ In addition to the solvent mixtures from Table 4, we tried different solvents or solvent mixtures which have been found ineffective to dissolve the inclusion complex: MeOH, toluene, CCl_4 , THF, CHCl_3 /toluene (95:5) or (90:10), CHCl_3 /THF (95:5) or (90:10), CCl_4 /MeOH (95:5) or (90:10). On the other hand, when using DMF, CHCl_3 /DMF (95:5), CHCl_3 /PrOH (90:10), CHCl_3 /EtOH (90:10), CHCl_3 /MeOH (90:10), CH_2Cl_2 /PrOH (90:10), CH_2Cl_2 /MeOH (90:10), 1,2-dichloroethane/PrOH (90:10), 1,2-dichloroethane/MeOH (90:10), the pseudorotaxane was soluble. However, the solution became light yellow instead of deep orange showing a decrease of association between the macrocycle and the axle and suggesting that the polarity of the mixture was too high and disrupted the coordination to the Li^+ ion.

(Table 6 – Entry 5). As a summary, to efficiently prepare rotaxane **106**, the reaction needs to be carried out in CHCl₃/MeOH (95:5) at 18 mM and 0 °C for 72 h.

Table 5. Optimization of reaction conditions for the synthesis of rotaxane **106**: concentration.

Entry	Equiv. of Li ⁺ salt	Solvent	C [mM]	T	Time [h]	Equiv. of macrocycle 62	Yield of thread 105 [%] ^[a]	Yield of rotaxane 106 [%] ^[a]	106/105 Ratio
1	3	CHCl ₃ /MeOH (95:5)	50	r.t.	24	2	12	23	66:34
2	3	CHCl ₃ /MeOH (95:5)	30	r.t.	24	2	22	39	64:36
3	3	CHCl ₃ /MeOH (95:5)	18	r.t.	24	2	25	61	71:29
4	3	CHCl ₃ /MeOH (95:5)	10	r.t.	24	2	80	5	6:94

[a] Yield of isolated product after purification by column chromatography (SiO₂) and gel permeation chromatography (Bio-Beads® S-X1, CH₂Cl₂). Reactions were carried out using general procedure B.

This [2]rotaxane was characterized as usual by means of NMR spectroscopy. The ¹H NMR spectrum shows that H signals from the pyromellitic diimide core exhibits an upfield shift ($\Delta\delta_{H_a}=-1.23$ ppm), just like those from the macrocycle naphthalene ring ($\Delta\delta_{H_1}=-0.23$ ppm; $\Delta\delta_{H_2}=-0.41$ ppm; $\Delta\delta_{H_3}=-0.58$ ppm) (Figure 34). This behaviour can be attributed to the π -donor/ π -acceptor interactions existing between the rod and the wheel. Moreover, the DOSY NMR spectrum of the compound displays a unique diffusion coefficient which is consistent with the interlocked nature of the product (Figure 35). Furthermore, the exact mass and isotopic distribution of the peaks of the HRMS spectrum confirmed the existence of the rotaxane (Figure 36).

Table 6. Optimization of reaction conditions for the synthesis of rotaxane **106**: temperature, reaction time and equivalents of macrocycle.

Entry	Equiv. of Li ⁺ salt	Solvent	C [mM]	T	Time [h]	Equiv. of macrocycle 62	Yield of thread 105 [%] ^[a]	Yield of rotaxane 106 [%] ^[a]	106/105 Ratio
1	3	CHCl ₃ /MeOH (95:5)	18	r.t.	24	2	25	61	71:29
2	3	CHCl ₃ /MeOH (95:5)	18	0 °C	24	2	15	48	76:24
3	3	CHCl ₃ /MeOH (95:5)	18	0 °C	72	2	22	61	73:27
4	3	CHCl ₃ /MeOH (95:5)	18	0 °C	72	3	20	61	75:25
5	3	CHCl ₃ /MeOH (95:5)	18	0 °C	72	5	19	66	78:22

[a] Yield of isolated product after purification by column chromatography (SiO₂) and gel permeation chromatography (Bio-Beads® S-X1, CH₂Cl₂). Reactions were carried out using general procedure B.

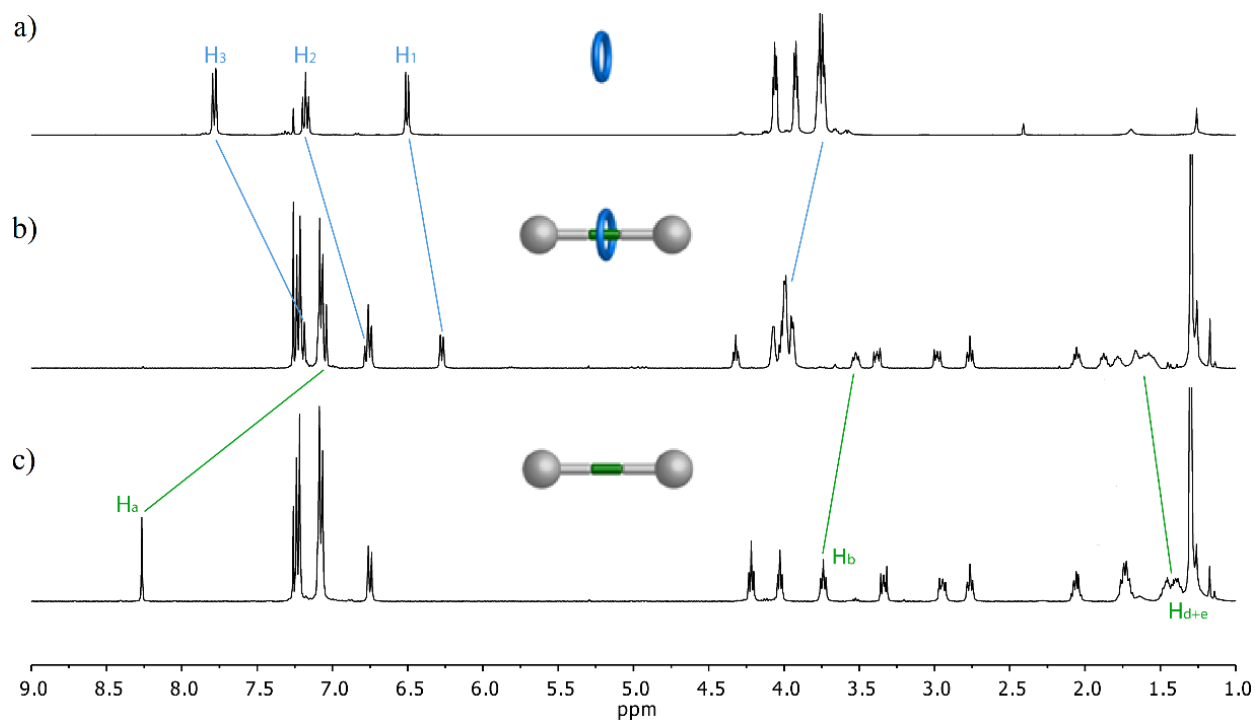


Figure 34. ^1H NMR (400 MHz, CDCl_3) spectra of: a) Macrocycle **62**. b) Rotaxane **106**. c) Thread **105**. Lettering coding is defined in Scheme 50.

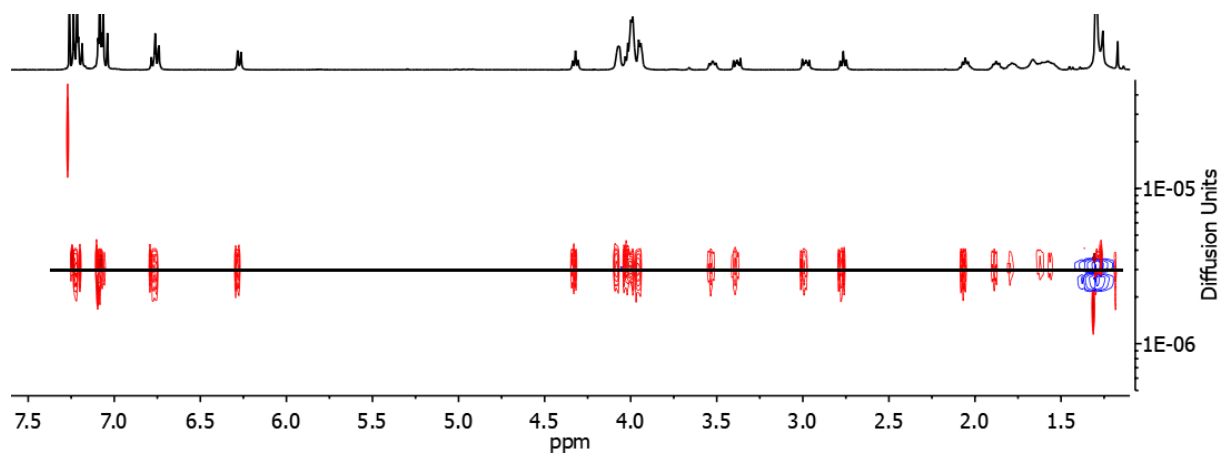


Figure 35. DOSY NMR (500 MHz, CDCl_3) spectrum of **106**.

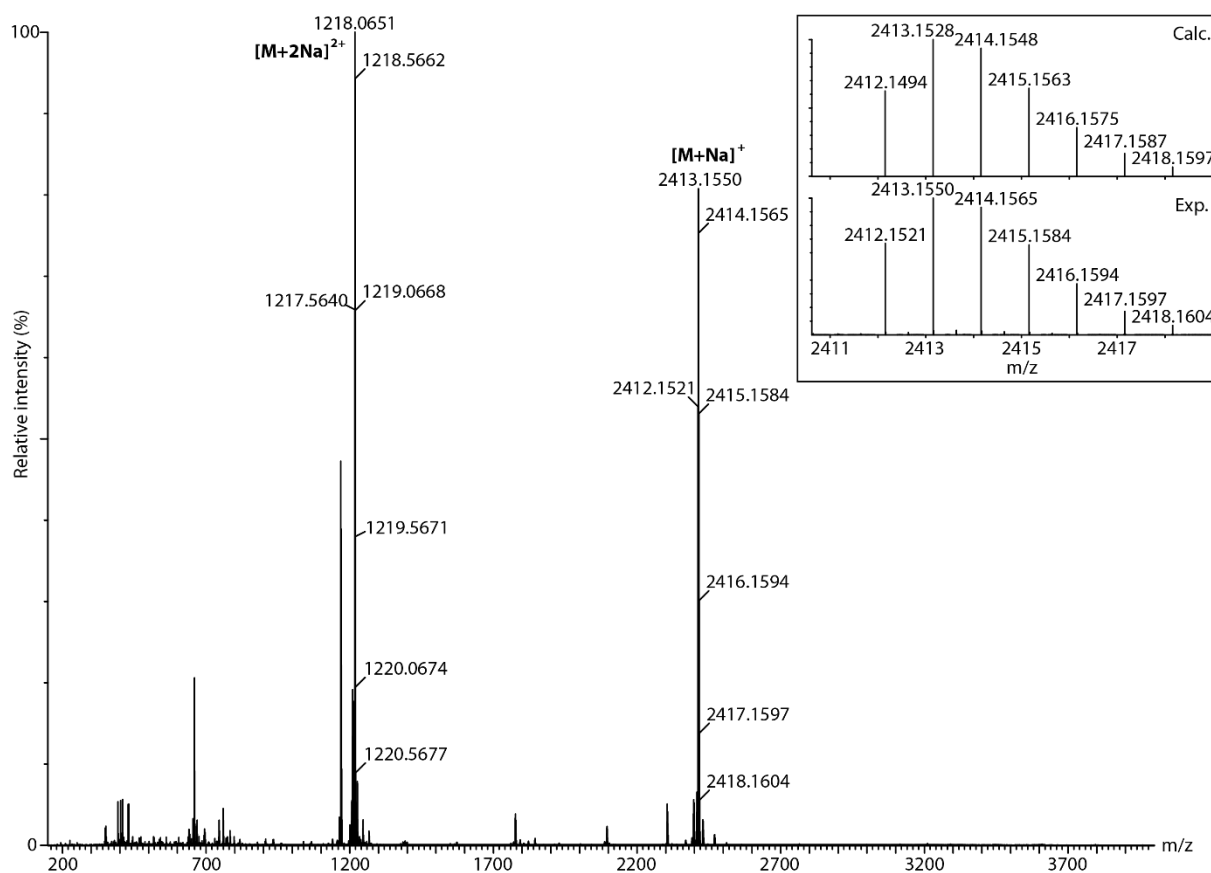


Figure 36. HRMS (ESI⁺) spectrum of **106**. Inset: Observed (bottom) and calculated (top) isotopic distribution for [106+Na]⁺.

1.3.4.2. Cation sensing

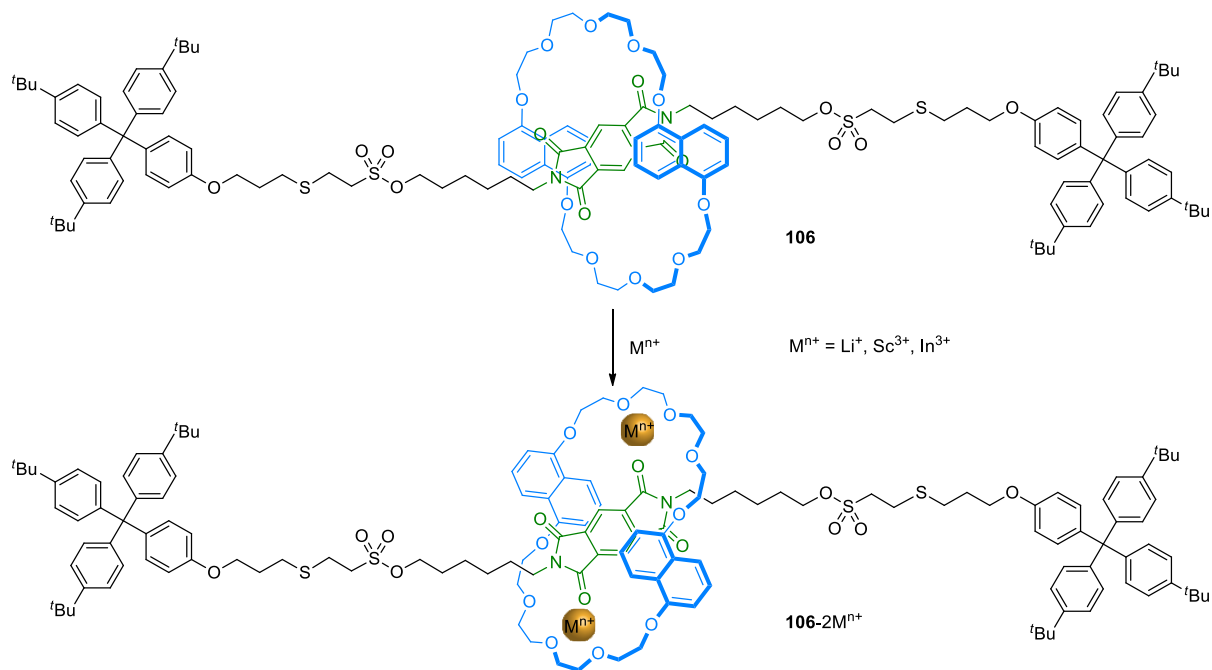
The behaviour of MIMs as ion sensors has been demonstrated over the years. Indeed, their interlocked structures enable the ability to host appropriate ions or ion pairs.²³⁰ Regarding rotaxanes, many probes have been reported exploiting the interlocked nature of the rotaxane to detect alkali,²³¹ alkaline-earth^{231c,d} or transition metal^{231c,e,232} cations. In our case, it was conceivable that [2]rotaxane **106** could act as sensor for Li⁺ (Scheme 51). A subtle hint of this potential behaviour appeared during its purification process. Thus, when the column chromatography (SiO₂) was performed, as a result of the

²³⁰ a) Matthew J. Langton, Paul D. Beer, *Acc. Chem. Res.* **2014**, *47*, 1935-1949. b) K. M. Bāk, K. Porfyrakis, J. J. Davis, P. D. Beer, *Mater. Chem. Front.* **2020**, *4*, 1052-1073.

²³¹ a) K. Hiratani, M. Kaneyama, Y. Nagawa, E. Koyama, M. Kanesato, *J. Am. Chem. Soc.* **2004**, *126*, 13568-13569. b) Y. Nagawa, J.-I. Suga, K. Hiratani, E. Koyama, M. Kanesato, *Chem. Commun.* **2005**, 749-751. c) P. H. Kwan, T. M. Swager, *J. Am. Chem. Soc.* **2005**, *127*, 5902-5909. d) N.-C. Chen, P.-Y. Huang, C.-C. Lai, Y.-H. Liu, Y. Wang, S.-M. Peng, S.-H. Chiu, *Chem. Commun.* **2007**, 4122-4124. e) G. Baggi, S. J. Loeb, *Angew. Chem. Int. Ed.* **2016**, *55*, 12533-12537.

²³² a) A. Tron, P. J. Thornton, B. Kauffmann, J. H. R. Tucker, N. D. McClenaghan, *Supramol. Chem.* **2016**, *28*, 733-741. b) S. Teka, A. Gaiied, N. Jaballah, S. Xiaonan, M. Majdoub, *Mater. Res. Bull.* **2016**, *74*, 248-257. c) M. Denis, J. Pancholi, K. Jobe, M. Watkinson, S. M. Goldup, *Angew. Chem. Int. Ed.* **2018**, *57*, 5310-5314. d) S.-M. Chan, F.-K. Tang, C.-S. Kwan, C.-Y. Lam, S. C. K. Hau, K. C.-F. Leung, *Mater. Chem. Front.* **2019**, *3*, 2388-2396.

lithium salts being strongly retained on the stationary phase, a change of color occurred. The solution changed from deep orange to yellow, the color of a solution of the pure rotaxane.



Scheme 51. Generation of a 1:2 complex between rotaxane **106** and different metal cations.

A first attempt to observe changes induced by the addition of the metal salts was carried out by 1H NMR. Nevertheless, the effect of the addition of cations to rotaxane **106** on its 1H NMR spectrum was minimal. Indeed, apart from the broadening of the signal corresponding to H_a and a small downfield shift of H_1 and H_b , the spectra remained significantly unaltered (Figure 37). However, a color change of the solution was clearly visible.

Therefore, in order to investigate the color change induced by the addition of lithium salts, we firstly analyzed the UV-Vis spectra of [2]rotaxane **106**, thread **105** and macrocycle **62** (Figure 38). Rotaxane **106** possesses a main absorption band between 266 and 369 nm ($\lambda_{max}=288$ nm, $\epsilon=16098$ Lmol $^{-1}$ cm $^{-1}$) and a broad charge-transfer band between 377 and 522 nm whose maximum is located at 440 nm ($\epsilon=1487$ Lmol $^{-1}$ cm $^{-1}$). When it comes to the spectra of thread **105** and macrocycle **62**, they both exhibit bands around the same wavelengths (250–373 nm for **105** and 265–341 nm for **62**) with a maximum centered at 278 nm for **105** ($\epsilon=6413$ Lmol $^{-1}$ cm $^{-1}$) and 299 nm for DNP38C10 (**62**) ($\epsilon=19155$ Lmol $^{-1}$ cm $^{-1}$).

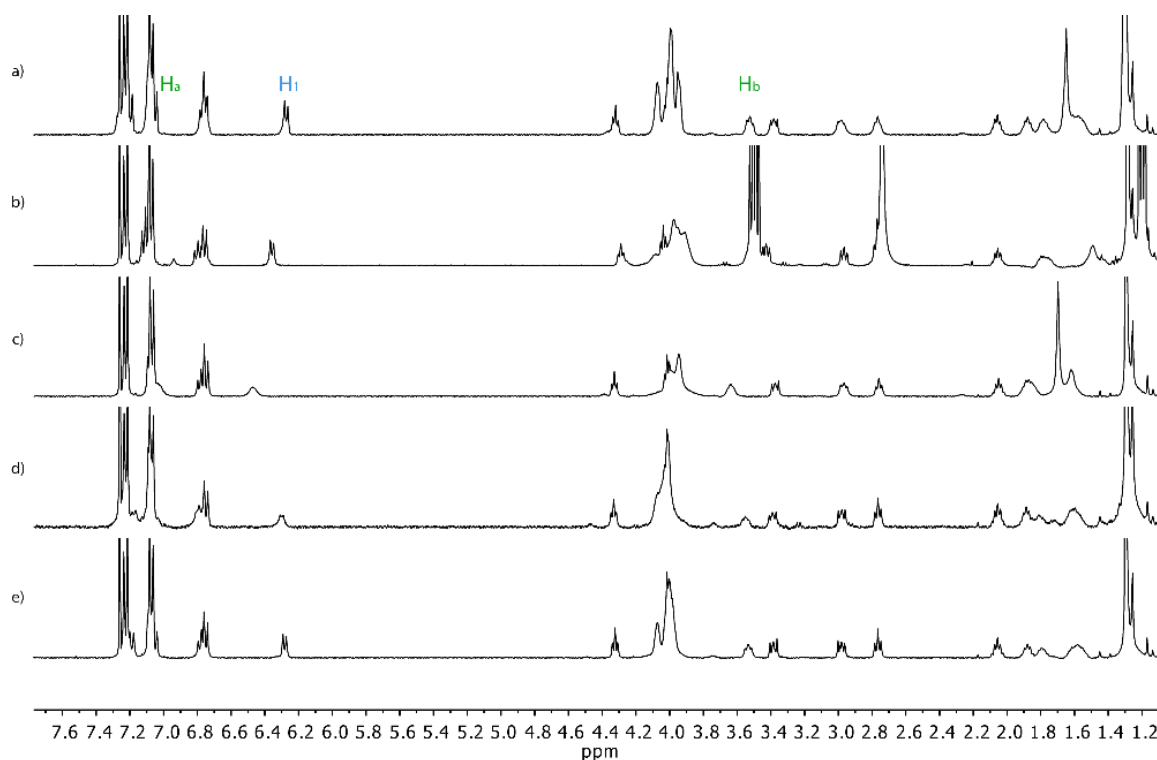


Figure 37. ^1H NMR (400 MHz, CDCl_3) spectra of rotaxane **106** (4 mM): a) in absence of salt; and in the presence of 5 equivalents of: b) $[\text{Li}(\text{OEt}_2)_n][\text{B}(\text{C}_6\text{F}_5)_4]$. c) $\text{Li}(\text{OTf})$. d) $\text{In}(\text{OTf})_3$. e) $\text{Sc}(\text{OTf})_3$. Lettering coding is defined in Scheme 50.

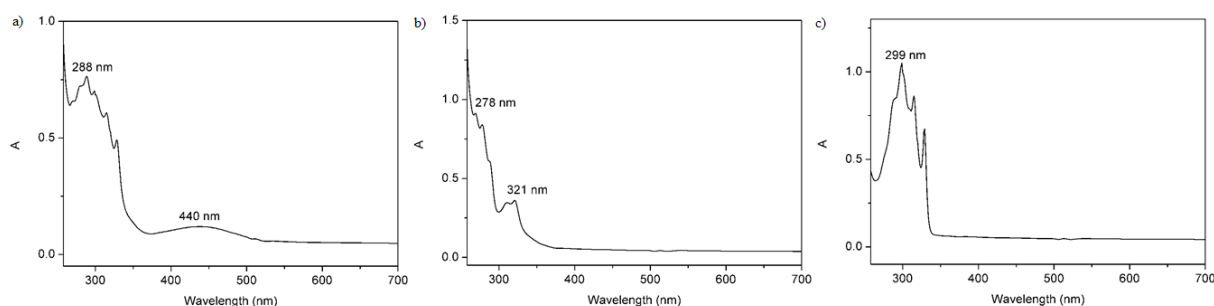


Figure 38. UV Vis spectra recorded at $ca. 5 \times 10^{-5}$ M in CHCl_3 of : a) [2]Rotaxane **106**. b) Thread **105**. c) Macrocycle **62**.

The addition of different salts ($[\text{Li}(\text{OEt}_2)_n][\text{B}(\text{C}_6\text{F}_5)_4]$, $\text{Li}(\text{OTf})$, $\text{Sc}(\text{OTf})_3$, $\text{In}(\text{OTf})_3$) to a solution of rotaxane **106** had the effect to change the color of the solution (Figure 39). The UV-Vis spectra of these solutions shows a bathochromic shift of the charge-transfer band (Figure 40). A screening of different metal salts was conducted to identify those able to induce this change as a result of their binding to rotaxane **106** (Table 7). Thus, by looking at the shift of the charge-transfer band ($\Delta\lambda_{\text{max}}$), the interaction between the cation and the rotaxane can be studied. Indeed, the maximum of the charge-transfer band of rotaxane **106** in the presence of $[\text{Li}(\text{OEt}_2)_n][\text{B}(\text{C}_6\text{F}_5)_4]$, LiPF_6 , LiOTf , $\text{In}(\text{OTf})_3$ and $\text{Sc}(\text{OTf})_3$ shifts (47 nm, 17 nm, 24 nm, 12 nm and 16 nm respectively) while with other salts the changes are almost negligible (Table 7). Furthermore, a control experiment was carried out by mixing thread **105** with the different salts,

showing no significant change in its UV-Vis absorption spectra. This screening demonstrates the interaction of Li^+ as well as In^{3+} and Sc^{3+} with the DNP38C10/pyromellitic diimide-based [2]rotaxane. Therefore, it is clear that the size of the cation is of key importance for its complexation to the system. However, ions displaying an ionic radius similar to Li^+ , such as Zn^{2+} or Mg^{2+} , did not show any interaction with rotaxane **106**, which could be a consequence of weaker metal-ligand interactions or an unfavorable coordination number or geometry.

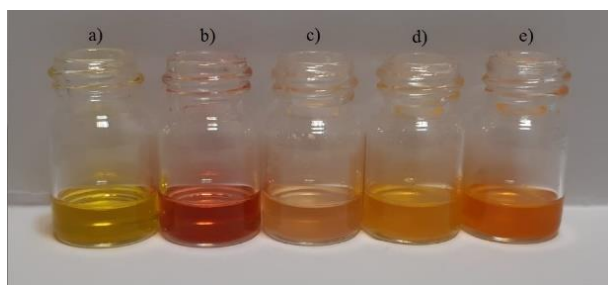


Figure 39. Picture of solutions of rotaxane **106** in CHCl_3 (0.4 mM): a) in absence of salt; and in the presence of 6 equiv. of: b) $[\text{Li}(\text{OEt}_2)_n][\text{B}(\text{C}_6\text{F}_5)_4]$. c) $\text{Li}(\text{OTf})$. d) $\text{Sc}(\text{OTf})_3$. e) $\text{In}(\text{OTf})_3$.

Table 7. $\Delta\lambda_{\text{max}}$ of the charge-transfer band of rotaxane **106** after the addition of different metal salts.

Entry	Metal salt	$\Delta\lambda_{\text{max}}$ [nm]	Entry	Metal salt	$\Delta\lambda_{\text{max}}$ [nm]
1	$[\text{Li}(\text{OEt}_2)_n][\text{B}(\text{C}_6\text{F}_5)_4]$	47	11	$\text{Ba}(\text{OTf})_2$	3
2	LiPF_6	17	12	$\text{Zn}(\text{OTf})_2$	2
3	$\text{LiBF}_4^{[a]}$	2	13	$\text{In}(\text{OTf})_3$	12
4	$\text{LiSbF}_6^{[a]}$	2	14	$\text{Sc}(\text{OTf})_3$	16
5	LiOTf	24	15	$\text{Al}(\text{OTf})_3$	2
6	$\text{NaBF}_4^{[a]}$	2	16	$\text{La}(\text{OTf})_3$	1
7	$\text{KPF}_6^{[a]}$	3	17	$\text{Eu}(\text{OTf})_3$	2
8	CsOMs	2	18	$\text{Er}(\text{OTf})_3$	-2
9	$\text{Mg}(\text{OTf})_2$	0	19	$\text{Yb}(\text{OTf})_3$	0
10	$\text{Ca}(\text{OTf})_2$	2			

[a] The solution was sonicated for 5 min but the salt did not fully dissolve.

Since it is possible to follow the bathochromic shift of the charge-transfer band of **106** caused by the addition Li^+ , Sc^{3+} or In^{3+} salts, we decided to measure their effective association constants K_a by titration of rotaxane **106** with the corresponding cations (Figure 40). It is important to notice that we measure the effective association constant since is also involves the dissociation constant of the salt in chloroform.

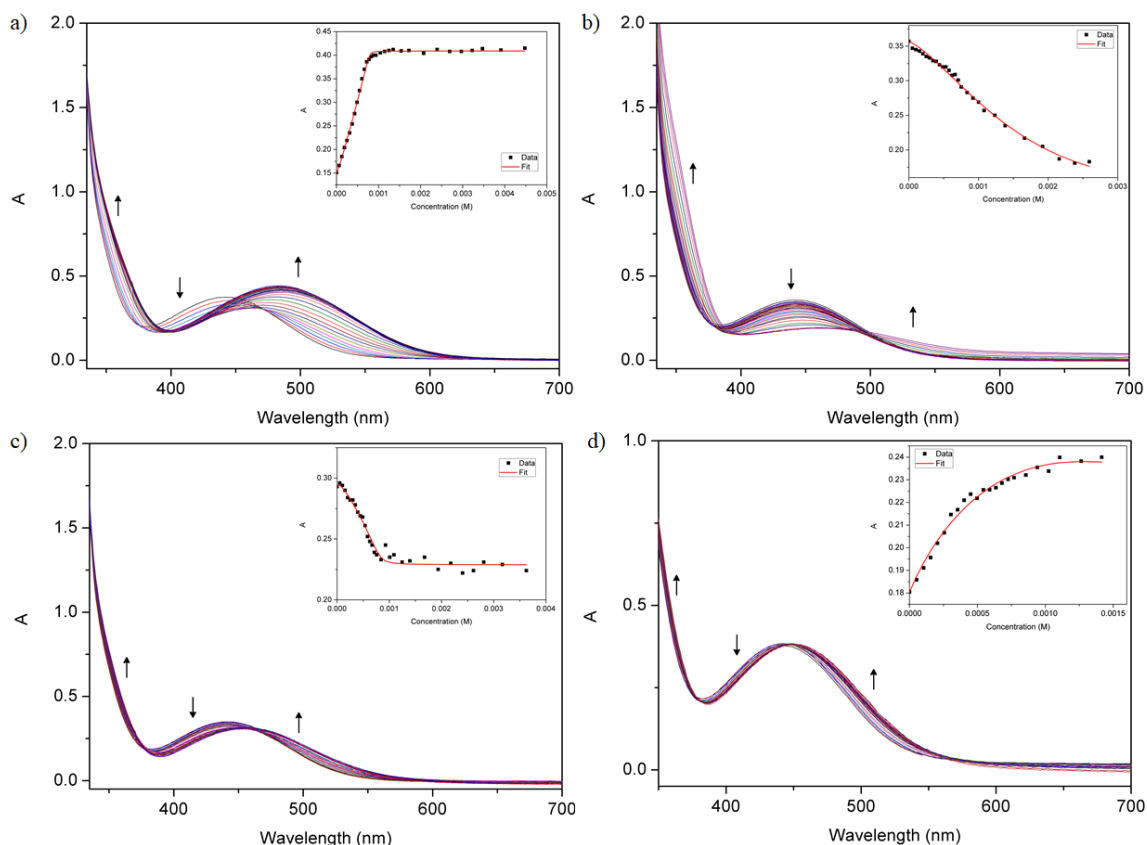


Figure 40. UV-Vis spectra in CHCl_3 at room temperature for the titration of rotaxane **106** with: a) $[\text{Li}(\text{OEt}_2)_n][\text{B}(\text{C}_6\text{F}_5)_4]$. b) LiOTf . c) $\text{Sc}(\text{OTf})_3$. d) $\text{In}(\text{OTf})_3$. Inset: Fitted binding isotherm using a 1:2 association model for the titration of rotaxane **106** with the corresponding salt showing the change of absorbance at: a) 502 nm. b) 439 nm. c) 415 nm. d) 498 nm.

To determine this effective association constants, the analysis of data from the UV-Vis absorption spectra (Figure 40) were carried out using a nonlinear least-squares curve fitting procedure using the online software *Bindfit* (<http://supramolecular.org/>) website with a 1:2 global fitting model (Nelder-Mead method).²³³ Consequently, the value of the 1:1 equilibrium constant (K_{11}) and the 1:2 equilibrium constant (K_{12}) were found, giving us the effective association constant (K_a): $K_a = K_{11} \times K_{12}$ (Table 8).

Table 8. Association constants between rotaxane **106** and the different cations.

Metal salt	$K_{11} [\text{M}^{-1}]$	$K_{12} [\text{M}^{-1}]$	$K_a [\text{M}^{-1}]$
$[\text{Li}(\text{OEt}_2)_n][\text{B}(\text{C}_6\text{F}_5)_4]$	1.15 ± 0.11	$(2.07 \pm 0.18) \times 10^{10}$	$(2.38 \pm 0.43) \times 10^{10}$
LiOTf	$(4.81 \pm 0.05) \times 10^{-1}$	$(1.47 \pm 0.04) \times 10^6$	$(7.07 \pm 0.26) \times 10^5$
$\text{Sc}(\text{OTf})_3$	1.09 ± 0.11	$(2.25 \pm 0.16) \times 10^9$	$(2.45 \pm 0.41) \times 10^9$
$\text{In}(\text{OTf})_3$	1.21 ± 0.02	$(2.09 \pm 0.07) \times 10^6$	$(2.53 \pm 0.13) \times 10^6$

²³³ P. Thordarson, *Chem. Soc. Rev.* **2011**, *40*, 1305-1323.

In general, K_{11} is very low and K_{12} is very high which means that the complex formed between the rotaxane and the metal salt is directly a 1:2 complex and that the 1:1 association is inexistent (Table 8). Nevertheless, its value is still necessary to determine the effective association constant K_a .

Regarding triflate salts the best outcome is obtained by $\text{Sc}(\text{OTf})_3$ whose effective association constant reaches $K_a = (2.45 \pm 0.41) \times 10^9 \text{ M}^{-1}$, however $\text{Li}(\text{OTf})$ and $\text{In}(\text{OTf})_3$ afford also high constants ($K_a = (7.07 \pm 0.26) \times 10^5 \text{ M}^{-1}$, $K_a = (2.53 \pm 0.13) \times 10^6 \text{ M}^{-1}$, respectively). As expected, taking into account the methodology used for the K_a estimation, the counterion has an important role on the dissociation of the salt. Thus, the binding constant with Li^+ increased to $(2.38 \pm 0.43) \times 10^{10} \text{ M}^{-1}$ when $\text{B}(\text{C}_6\text{F}_5)_4^-$ was used as counterion (Table 8). Therefore, the ability of Li^+ , Sc^{3+} and In^{3+} to complex rotaxane **106** with high binding affinities makes it a good sensor for these cations.

1.4. Conclusions

We demonstrated the efficiency and versatility of the click aza- and thia-Michael additions reactions to vinyl sulfone or vinyl sulfonate groups for the synthesis of rotaxanes through the capping approach. Thus, various [2]rotaxanes featuring different recognition sites and macrocycles involving distinct interactions were prepared. This methodology proved to be adequate for the construction of rotaxanes containing well-known recognition motifs, such as NDI/DNP38C10, diketopiperazine/tetralactam macrocycle and di(1,2,3-triazol-1-yl)butane/pillar[5]arene. Furthermore, it provided the opportunity to design a rotaxane whose motif has never been used on its own in the synthesis of such structures through a capping strategy, namely, pyromellitic diimide/DNP38C10/Li⁺. In every case, the click MAVS reaction was carried out under mild conditions, at room temperature or 0 °C and employing a mild base as catalyst, Et₃N or DMAP and afforded these interlocked molecules in high yields, around 60-90%. It is worth noting that these yields are similar or better to those previously reported using other reactions, including the famous and widely used CuAAC.

Moreover, the pyromellitic diimide-based [2]rotaxane, whose synthesis was optimized by the use of Li⁺ template, bound to Li⁺, Sc³⁺ and In³⁺ with remarkable association constants, up to $(2.38 \pm 0.43) \times 10^{10} \text{ M}^{-1}$ for [Li(OEt₂)_n][B(C₆F₅)₄]. Therefore, the ability of this rotaxane system to be used as a cation sensor was proven.

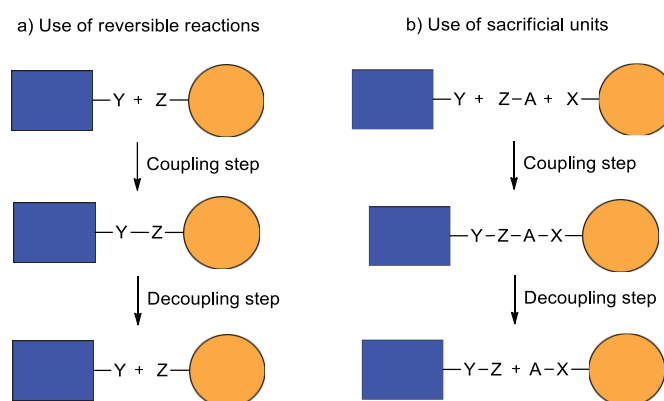
Therefore, the click MAVS reactions demonstrate to be a novel, suitable and efficient tool for rotaxane synthesis that should be stored in the toolbox of organic chemists willing to build new rotaxanes or devices based on this architecture.

2. Vinyl sulfonate coupling-and-decoupling chemistry applied to rotaxanes

2.1. Background

2.1.1. Coupling-and-decoupling chemistry of the vinyl sulfonate group

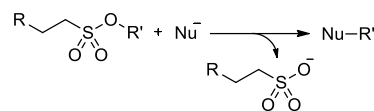
The concept of coupling-and-decoupling chemistry (CAD) was introduced by Bielski and Witczak in 2013. This strategy aims to connect molecular units together and subsequently disconnect them in a controlled manner, in both cases efficiently and, ideally, under mild conditions (Scheme 52). Possible applications resulting from CAD chemistry are vast and range from therapeutic delivery to the detachment from a solid support, as well as targeted release or self-destruction and recycling.²³⁴ It is important to emphasize that the coupling step of the CAD chemistry is widely explored nowadays as it benefited hugely from the click chemistry concept and reactions. However, the reversibility of the latter is not so trivial and remains underdeveloped.



Scheme 52. Schematic representation of the coupling-and-decoupling processes.

Recently, our group revealed that the vinyl sulfonate unit is a promising tool for CAD chemistry.²¹⁰ As shown earlier in chapter 1 (Section 1.), the click Michael-addition reaction of a nucleophile, such as a thiol or an amine, to the vinyl sulfonate group is versatile and efficient. In addition, the sulfonate moiety generated after the MAVS is a suitable group for decoupling chemistry. Indeed, the latter can act as a leaving group and be substituted by a nucleophile, such as an azide, a halide or a thiocyanate salt, as well as, a thiol or an amine, or hydrolysed in very high yields (Scheme 53). Moreover, the vinyl sulfonate group demonstrated a relevant potential for biological systems since it was possible to perform the decoupling reaction with a thiol under mild conditions compatible to those in the living systems.²¹⁰

²³⁴ R. Bielski, Z. Witczak, *Chem. Rev.* **2013**, *113*, 2205-2243.



Scheme 53. Nucleophilic displacement of sulfonate derivative.

2.1.2. Cleavable rotaxanes

Vögtle reported the first examples of rotaxanes that could be cleaved in 1999. He showed that rotaxanes could be disassembled in a controlled manner through the hydrolysis of an ester, a carbonate or an acetal group present on the axle.²³⁵ Later, this process of rupture of a mechanical bond was employed in crown ether [2]rotaxanes and other systems such as cyclodextrin-based polyrotaxanes. In these examples, different reactions like the hydrolysis of vinyl ether bonds²³⁶ or imine bonds,²³⁷ the Fmoc or trityl deprotection of an amine²³⁸ or the cleavage of an ester bond *via* sonication.²³⁹ The relevance of breakable rotaxanes lies on the significant applications they enable, such as the controlled delivery of bioactive molecules,²⁴⁰ the directional transport of a ring,²⁴¹ the regulation of gelation²⁴² or their use as probes for enzyme detection.²⁴³

2.1.3. Directional transport in rotaxanes

One of the most relevant aspects in the field of molecular machines is the directional transport in rotaxane architectures, which allowed the development of molecular motors or pumps,²⁴⁴ key elements in biological systems since they allow them to operate away from the equilibrium. Thus, in our body, these machines conduct essential functions such as long distance transport or the synthesis of ATP through the cell membrane.²⁴⁵ Focusing on synthetic molecular motors and pumps, their crucial feature is the unidirectional movement of a component of the system with respect to another, which induces the achievement of net work. Consequently, numerous systems have been designed where the production of this net transport is achieved following a “Brownian ratchet” mechanism.^{244a} These

²³⁵ C. Reuter, W. Wienand, G. M. Hübner, C. Seel, F. Vögtle, *Chem. Eur. J.* **1999**, *5*, 2692-2697.

²³⁶ S. Loethen, T. Ooya, H. S. Choi, N. Yui, D. H. Thompson, *Biomacromolecules* **2006**, *7*, 2501-2506.

²³⁷ K. C.-F. Leung, W.-Y. Wong, F. Aricó, P. C. Haussmann, J. F. Stoddart, *Org. Biomol. Chem.* **2010**, *8*, 83-89.

²³⁸ L. A. Powers, D. B. Smithrud, *Molecules* **2016**, *21*, 1043.

²³⁹ M. Zhang, G. De Bo, *J. Am. Chem. Soc.* **2019**, *141*, 15879-15883.

²⁴⁰ a) A. Fernandes, A. Viterisi, F. Coutrot, S. Potok, D. A. Leigh, V. Aucagne, S. Papot, *Angew. Chem. Int. Ed.* **2009**, *48*, 6443-6447. b) R. Barat, T. Legigan, I. Tranoy-Opalinski, B. Renoux, E. Péraudeau, J. Clarhaut, P. Poinot, A. E. Fernandes, V. Aucagne, D. A. Leigh, S. Papot, *Chem. Sci.* **2015**, *6*, 2608-2613.

²⁴¹ Z. Meng, J.-F. Xiang, C.-F. Chen, *J. Am. Chem. Soc.* **2016**, *138*, 5652-5658.

²⁴² S.-T. Tung, H.-T. Cheng, A. Inthasot, F.-C. Hsueh, T.-J. Gu, P.-C. Yan, C.-C. Lai, S.-H. Chiu, *Chem. Eur. J.* **2018**, *24*, 1522-1527.

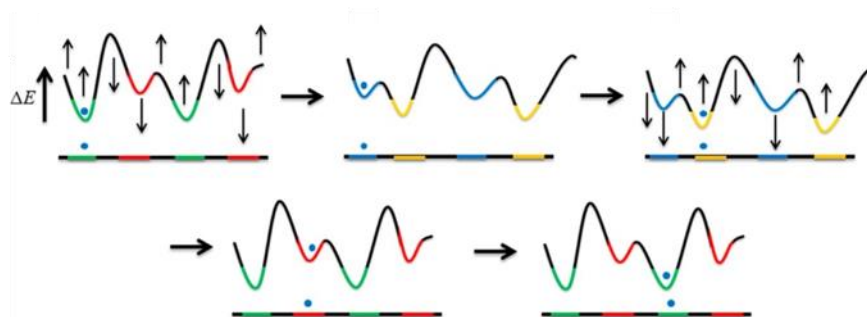
²⁴³ C. C. Slack, J. A. Finbloom, K. Jeong, C. J. Bruns, D. E. Wemmer, A. Pines, M. B. Francis, *Chem. Commun.* **2017**, *53*, 1076-1079.

²⁴⁴ a) S. Kassem, T. van Leeuwen, A. S. Lubbe, M. R. Wilson, B. L. Feringa, D. A. Leigh, *Chem. Soc. Rev.* **2017**, *46*, 2592-2621. b) M. Baroncini, S. Silvi, A. Credi, *Chem. Rev.* **2020**, *120*, 200-268.

²⁴⁵ K. Kinbara, T. Aida, *Chem. Rev.* **2005**, *105*, 1377-1400.

ratchets operate *via* the control of non-symmetrical potential energy profiles, in other words the increase or decrease of the energy barriers and minima, thanks to the use of external energy provided by different stimuli (Figure 41).

Flashing energy ratchet



Information ratchet

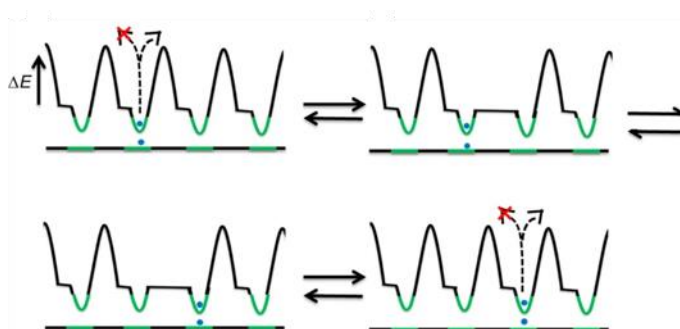
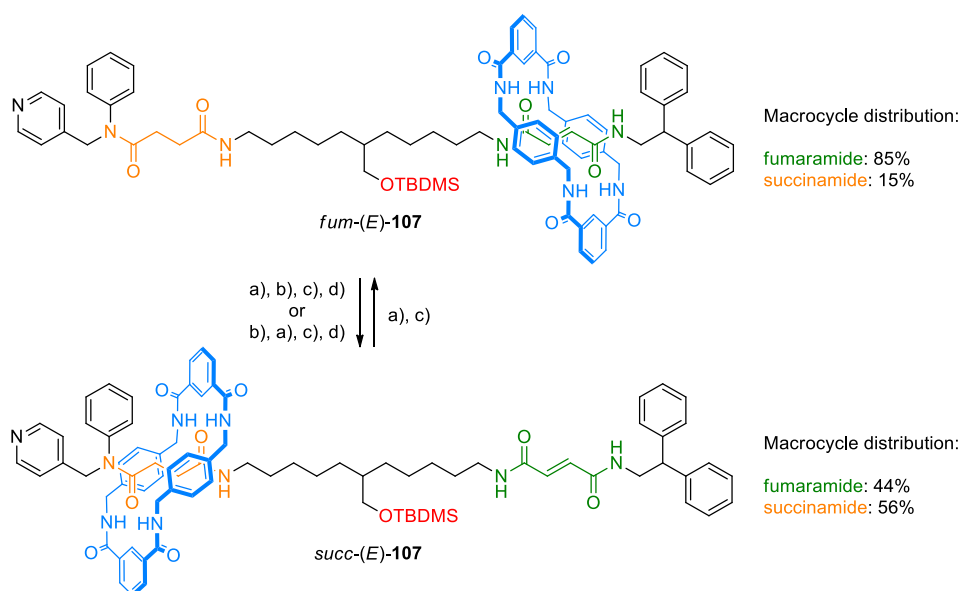
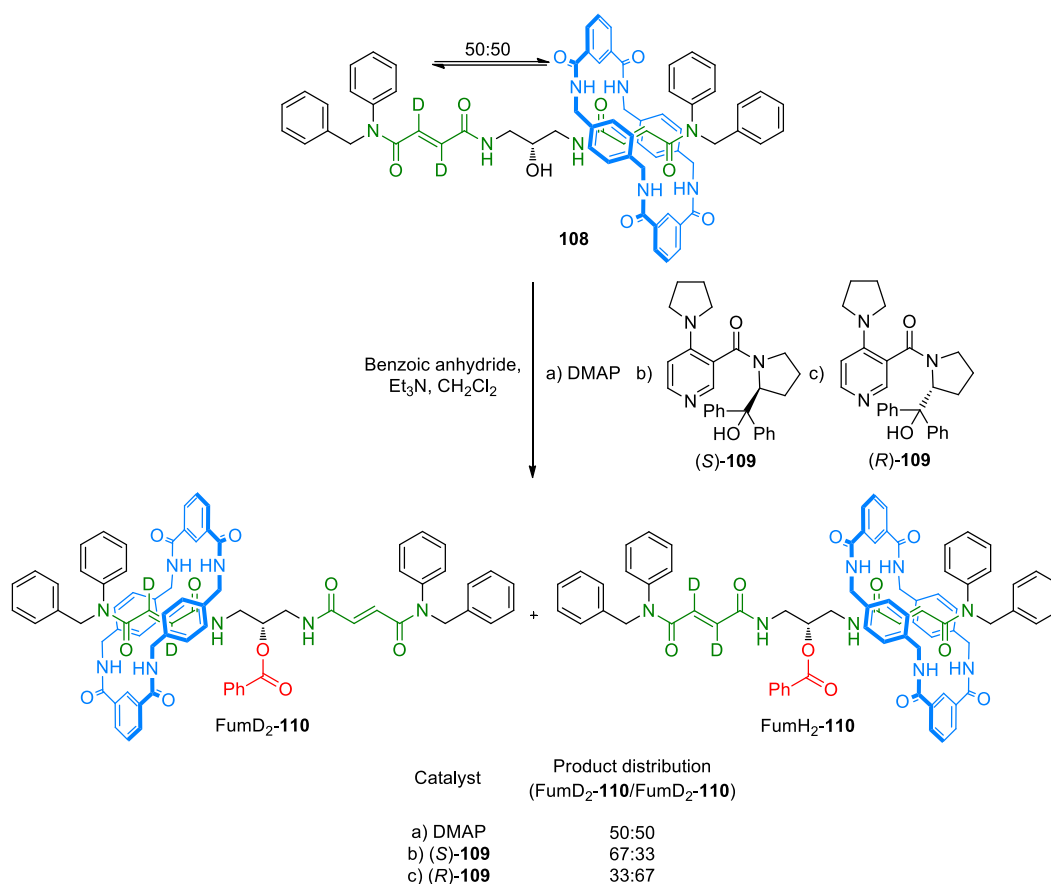


Figure 41. Energy profiles of a flashing energy ratchet (top) and an information ratchet (bottom).⁴ Reprinted with permission from ref.4 Copyright 2015 American Chemical Society.



Scheme 54. The first [2]rotaxane incorporating an energy ratchet mechanism. Operation: a) Desilylation. b) E → Z photoisomerisation. c) Resilylation. d) Z → E thermal isomerisation.²⁴⁶

The first rotaxane including a flashing energy ratchet mechanism was developed by Leigh and collaborators in 2006. This mechanism combines the alteration of the relative binding affinities between the binding stations of the thread and the macrocycle and the control of the shuttling ring between the two stations through the modulation of the energetic barriers for the translocation of the macrocycle. This [2]rotaxane contained a fumaramide/succinamide switching system and a TBDMS silyl ether barrier. This barrier prevented the shuttling of the ring between the two binding sites and created two compartments. Thus, they demonstrated the control of the macrocycle distribution between both compartments through the isomerization of the fumaramide unit and the desilylation/resilylation of the bulky silyl ether barrier (Scheme 54).²⁴⁶



Scheme 55. The first chemically-driven molecular information ratchet based on a [2]rotaxane structure.^{248a}

In a rotaxane-based information ratchet mechanism, the macrocycle distribution between two stations is driven away from the equilibrium without altering the binding affinities of the wheel for the recognition sites. This mechanism was demonstrated for the first time in a rotaxane by Leigh in 2007 through the energy transfer between a photosensitizer unit on the macrocycle and a stilbene group on the axle.²⁴⁷ Later, a chemically-driven information ratchet mechanism was described on benzylic

²⁴⁶ M. N. Chatterjee, E. R. Kay, D. A. Leigh, *J. Am. Chem. Soc.* **2006**, *128*, 4058-4073.

²⁴⁷ V. Serreli, C.-F. Lee, E. R. Kay, D. A. Leigh, *Nature* **2007**, *445*, 523-527.

amide-based [2]rotaxanes owning two or three compartments.²⁴⁸ In rotaxane **108**, the distribution between both fumaramide station is 50:50 while after benzylation using a chiral catalyst, the ratio reaches 33:67 (Scheme 55).^{248a}

The energy ratchet mechanism also led to molecular pumps based on pseudorotaxane or rotaxane architectures. Thus, the motion of DB24C8 through an axle can be directionally controlled employing a linear compound featuring an ammonium salt recognition site functionalized with an azobenzene and a cyclopentane unit. The operation of the system is based on the control of the steric barriers of each side and the affinity of the macrocycle for the binding site. The ring enters from the less hindered azobenzene side of the axle, then a photoisomerization of the azobenzene derivative is induced to yield the *cis* isomer which prevents the release of the ring from this side due to the increased steric hindrance. Finally potassium cations, which exhibit a higher binding affinity for the macrocycle than the ammonium unit, are added to the solution and therefore trigger its delivery through the cyclopentane side of the rod, which now represents the less hindered end (Scheme 56).²⁴⁹ It is worth noting that this operation can be achieved using a slightly different crown ether without the need to include K⁺ to liberate the macrocycle.²⁵⁰ In addition, a solvent- or light-controlled unidirectional transport of a macrocycle through an axle can be accomplished in a system based on a calix[6]arene wheel and a linear compound owning a viologen moiety and a stilbene unit.²⁵¹

Moreover, another pseudorotaxane system regulated through redox control was described. In this case, the system is composed by a CBPQT⁴⁺ ring and an axle owning a 1,5-dialkoxynaphthalene station as well as a steric (2-isopropylphenyl unit) and a coulombic barrier (3,5-dimethylpyridinium group). The macrocycle enters from the steric barrier side of the rod due to electrostatic repulsions between the coulombic barrier and the macrocycle. Subsequently, the ring gets reduced to CBPQT^{(2+)(•+)}. The repulsive interactions between the reduced macrocycle and the 1,5-dialkoxynaphthalene unit led to the dethreading of the ring over the coulombic barrier since it was less sterically hindered than the other and because of the lower repulsive interactions between the pyridinium barrier and the reduced macrocycle with respect to those showed by its tetracationic form.²⁵²

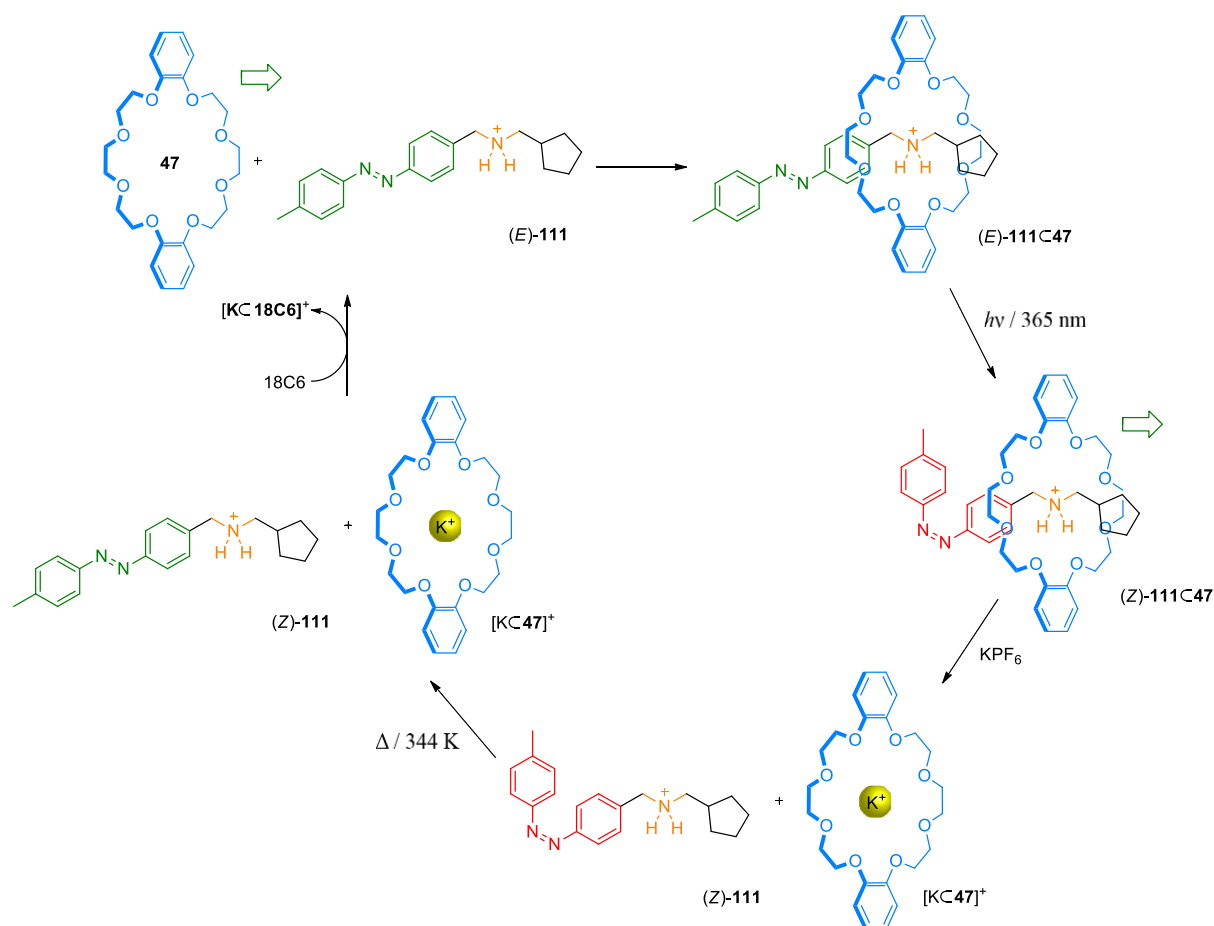
²⁴⁸ a) M. Alvarez-Pérez, S. M. Goldup, D. A. Leigh, A. M. Z. Slawin, *J. Am. Chem. Soc.* **2008**, *130*, 1836-1838. b) A. Carlone, S. M. Goldup, N. Lebrasseur, D. A. Leigh, A. Wilson, *J. Am. Chem. Soc.* **2012**, *134*, 8321-8323.

²⁴⁹ M. Baroncini, S. Silvi, M. Venturi, A. Credi, *Angew. Chem. Int. Ed.* **2012**, *51*, 4223-4226.

²⁵⁰ G. Ragazzon, M. Baroncini, S. Silvi, M. Venturi, A. Credi, *Nat. Nanotech.* **2015**, *10*, 70-75.

²⁵¹ A. Arduini, R. Bussolati, A. Credi, S. Monaco, A. Secchi, S. Silvi, M. Venturi, *Chem. Eur. J.* **2018**, *18*, 16203-16213.

²⁵² H. Li, C. Cheng, P. R. McGonigal, A. C. Fahrenbach, M. Frasconi, W.-G. Liu, Z. Zhu, Y. Zhao, C. Ke, J. Lei, R. M. Young, S. M. Dyar, D. T. Co, Y.-W. Yang, Y. Y. Botros, W. A. Goddard III, M. R. Wasielewski, R. D. Astumian, J. F. Stoddart, *J. Am. Chem. Soc.* **2013**, *135*, 18609-18620.



Scheme 56. A pump based on a pseudorotaxane reported by Venturi and Credi.²⁴⁹

This redox control was also applied in the development of molecular pumps based on the directional movement of macrocycles in a rotaxane. The system is based on a mono-stoppered thread displaying a 4,4'-bipyridinium moiety, a coulombic pyridinium barrier⁴ and the tetracationic cyclophane CBPQT⁴⁺. When this macrocycle and the 4,4'-bipyridinium unit are reduced to CBPQT^{2(•+)} and its radical cation, respectively, the macrocycle can thread the axle because of radical-radical interactions and the ineffective coulombic barrier in this situation. After the oxidation of the three 4,4'-bipyridinium radical cation units, repulsive interactions between the macrocycle and the 4,4'-bipyridinium station led to its translation to the opposite side from the coulombic pyridinium barrier (Figure 42).²⁵³ The main issue of this design was the reversibility of the pumping. However, by inserting a steric barrier in the middle of the rotaxane, the macrocycles can get trapped inside the rotaxane and the pumping process is irreversible.²⁵⁴ It is worth highlighting that recently, a molecular pump based on this strategy generated

²⁵³ C. Cheng, P. R. McGonigal, W.-G. Liu, H. Li, N. A. Vermeulen, C. Ke, M. Frasconi, C. L. Stern, W. A. Goddard III, J. F. Stoddart, *J. Am. Chem. Soc.* **2014**, *136*, 14702-14705.

²⁵⁴ C. Cheng, P. R. McGonigal, S. T. Schneebeli, H. Li, N. A. Vermeulen, C. Ke, J. F. Stoddart, *Nat. Nanotechnol.* **2015**, *10*, 547-553.

a polyrotaxane displaying 10 CBPQT⁴⁺ macrocycles.²⁵⁵ In addition, a rotaxane-based molecular pump regulated by pulses of a chemical fuel was recently reported.²⁵⁶

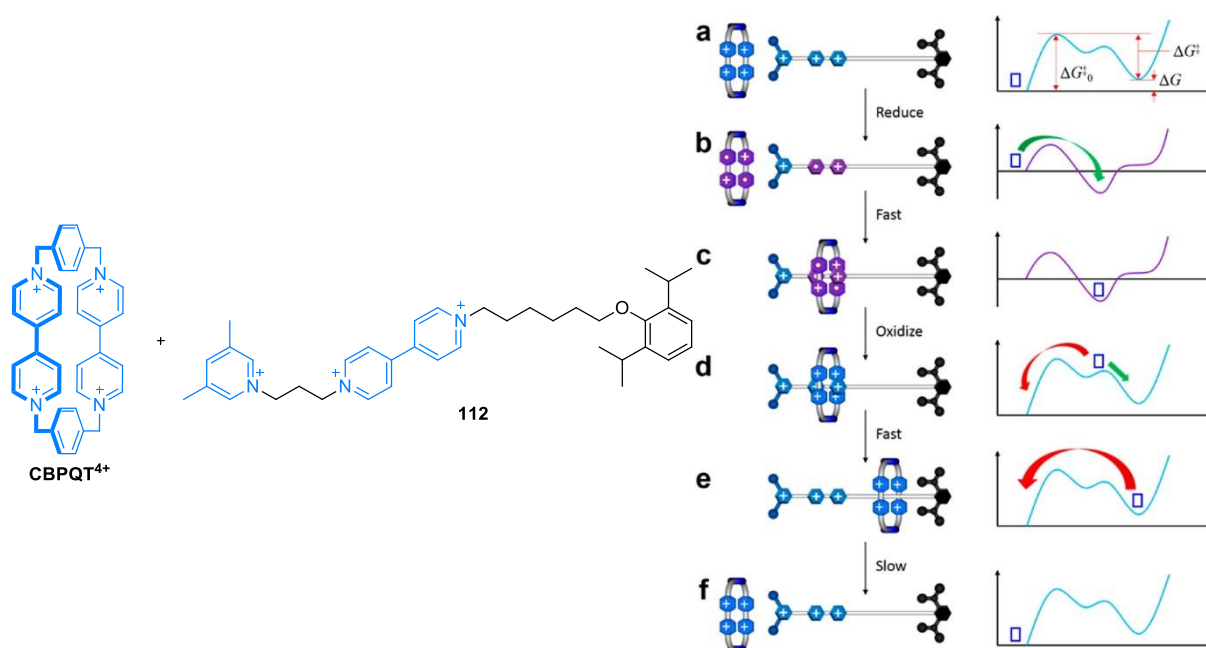


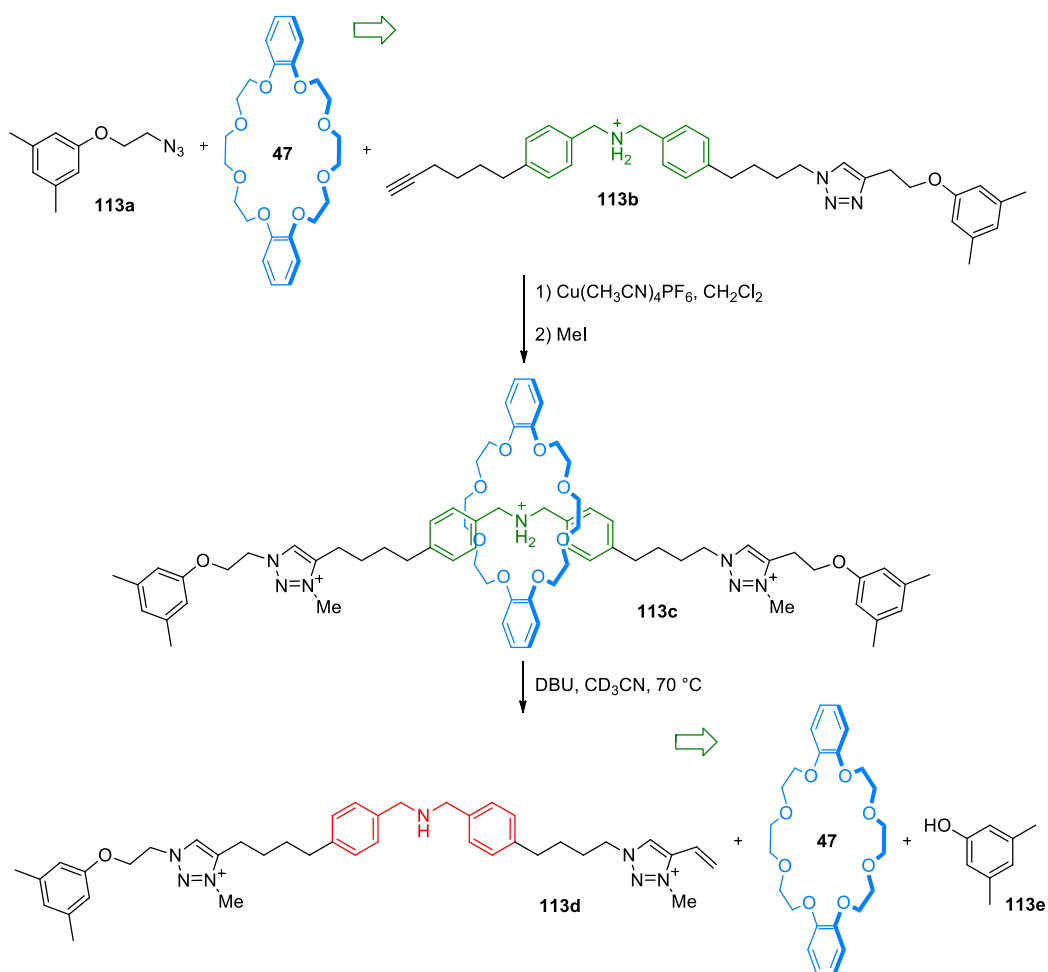
Figure 42. Graphical representation of the pumping mechanism of CBPQT⁴⁺ through axle **112** described by Stoddart and co-workers.²⁵³ Reprinted with permission from ref 253. Copyright 2014 American Chemical Society.

Furthermore, the unidirectional transport of a macrocycle in a rotaxane can be performed using a CAD method through a stopper-leaving strategy. Thus, Chen and co-workers built a non-symmetrical [2]rotaxane with a DB24C8/dibenzylammonium system by a CuAAC reaction on a mono-stoppered axle. After methylation of both triazole units of the axle, a DBU-catalyzed stopper-leaving reaction occurred at 70 °C on the opposite side of the entrance of the macrocycle resulting in the dethreading of the crown ether (Scheme 57).²⁴¹ Another strategy was employed in a helic[6]arene-based [2]rotaxane using the formation a carbamate unit for the capping step of the process and the cleavage of a *tert*-butyldiphenylsilyl group with tetrabutylammonium fluoride in order to liberate the macrocycle.²⁵⁷ These are the only examples a unidirectional transport of a ring in a rotaxane using a stopper-leaving method. Therefore, it could be possible to improve the reaction conditions of this strategy employing the vinyl sulfonate CAD chemistry since the decoupling step could be much milder.

²⁵⁵ Y. Qiu, B. Song, C. Pezzato, D. Shen, W. Liu, L. Zhang, Y. Feng, Q.-H. Guo, K. Cai, W. Li, H. Chen, M. T. Nguyen, Y. Shi, C. Cheng, R. D. Astumian, X. Li, J. F. Stoddart, *Science* **2020**, *368*, 1247-1253.

²⁵⁶ S. Erbas-Cakmak, S. D. P. Fielden, U. Karaca, D. A. Leigh, C. T. McTernan, D. J. Tetlow, M. R. Wilson, *Science* **2017**, *358*, 340-343.

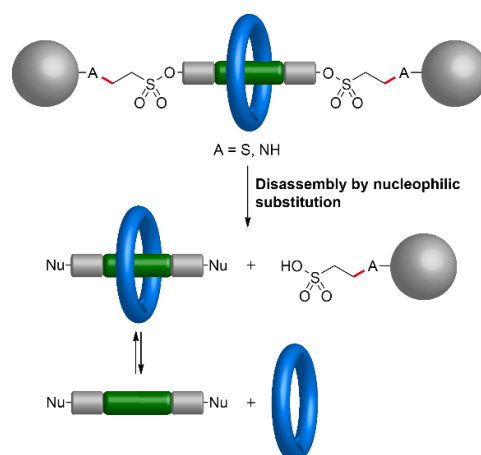
²⁵⁷ H.-Y. Zhou, Y. Han, Q. Shi, C.-F. Chen, *J. Org. Chem.* **2019**, *84*, 5872-5876.



Scheme 57. Unidirectional transport of a crown ether macrocycle in a rotaxane through a stopper-leaving strategy.²⁴¹

2.2. Objectives

In this context, we wanted to apply the usefulness of the CAD chemistry of the vinyl sulfonate group in the field of MIMs to generate cleavable rotaxanes that could undergo chemical disassembly under mild conditions. Therefore, to explore this possibility we propose the cleavage into its components through nucleophilic substitution of [2]rotaxanes obtained by Michael-type addition reactions to vinyl sulfonate groups (Scheme 58).



Scheme 58. Proposed strategy for the disassembly of a [2]rotaxane obtained by a MAVS reaction.

Furthermore, if this strategy proves to be successful, we hypothesize that, taking advantage of the CAD chemistry of the vinyl sulfonate group, we could develop a transport system based on a [2]rotaxane where it would be possible to induce a unidirectional movement of its macrocycle through the thread using a “flashing energy ratchet” mechanism by applying a chemical stimulus. Thus, our proposal would be to follow a similar approach to those previously reported and produce a mono-stoppered axle *via* a thia-Michael addition to a vinyl sulfonate group, followed by a capping step based on our MAVS methodology using a vinyl sulfone group as Michael acceptor to form the corresponding rotaxane. In this way, the macrocycle would enter through one side of the rotaxane and would be released through the opposite side by cleavage of the appropriate stopper (Figure 43).

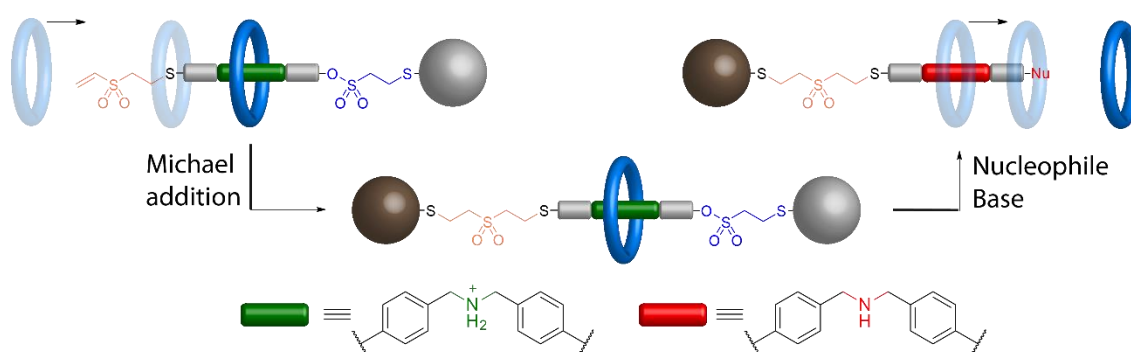


Figure 43. Proposed synthetic strategy employing the MAVS reactions and CAD chemistry of the vinyl sulfonate group to transport a macrocycle in a unidirectional way *via* a “flashing energy ratchet” mechanism.

2.3. Results and discussion

2.3.1. Chemical disassembly of a [2]rotaxane

After studying the formation of rotaxanes *via* MAVS reactions (chapter 1, section 1), we will now examine the cleavage of a [2]rotaxane exploiting the CAD chemistry of the vinyl sulfonate group.

Firstly, it was necessary to investigate that the stability of the rotaxanes is not jeopardized by the presence of a sulfone or a sulfonate group that could enable a retro-Michael addition. Thus, the stability of rotaxanes **63a** and **100d** in solution (CDCl_3) at room temperature was monitored by ^1H NMR spectroscopy over 7 days (Figure 44). These spectra exhibit neither signs of decomposition nor significant changes after a week in solution, which confirms the stability of the [2]rotaxanes prepared either from vinyl sulfonate or vinyl sulfone moieties. Furthermore, a study of the stability in solution (CDCl_3) in the presence of a mild base (Et_3N) was carried out and displayed no signs of retro-Michael addition nor decomposition after 5 days at room temperature (Figure 45). Therefore, the stability of these rotaxanes was demonstrated allowing us to consider their controlled disassembly.

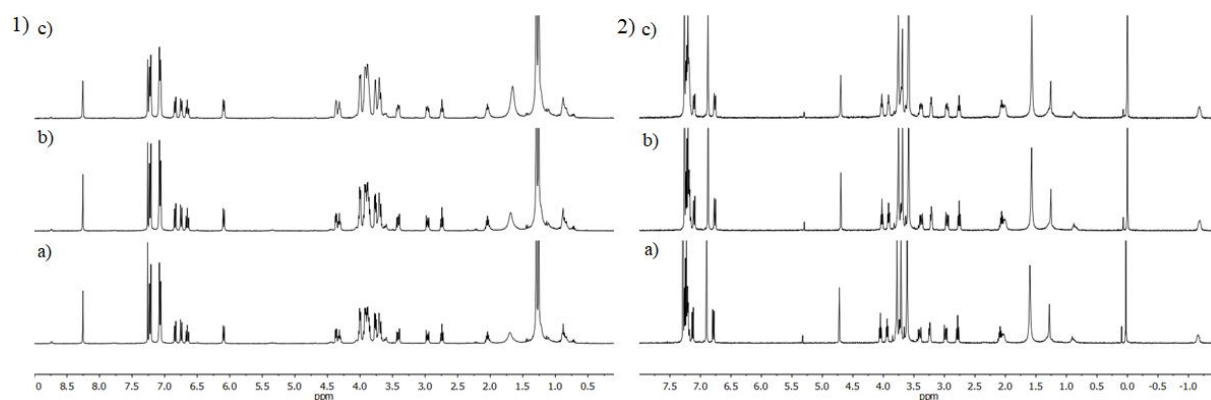


Figure 44. Rotaxane stability experiments at room temperature. ^1H NMR (400 MHz, CDCl_3) spectra of rotaxanes: 1) **63a**; 2) **100d** at (a) $t = 0$ and after: (b) 3 d; (c) 7 d.

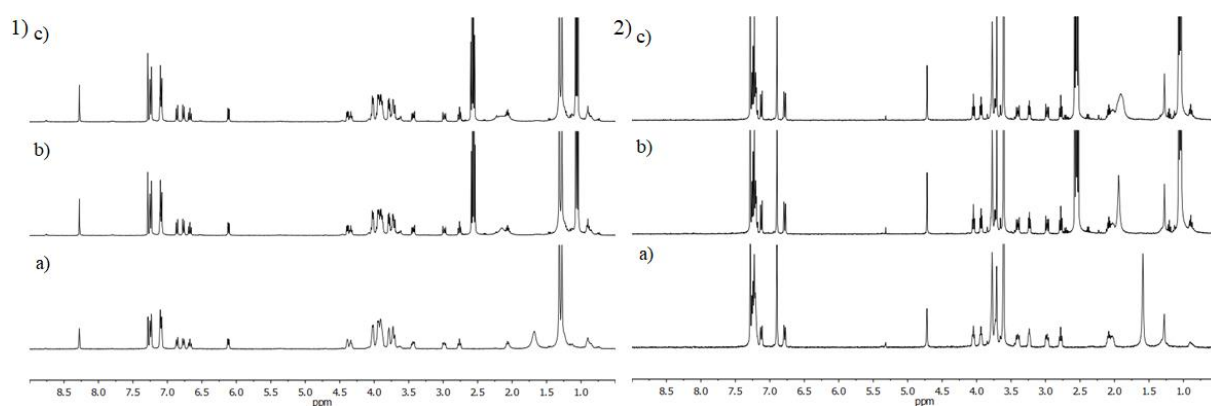
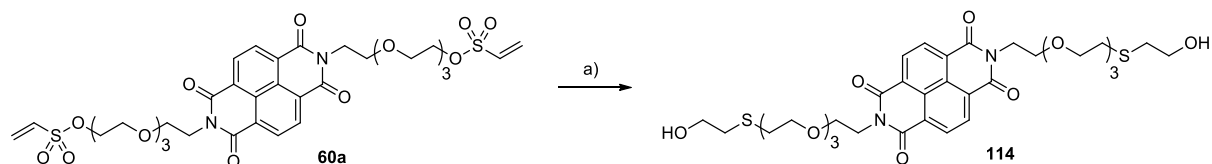
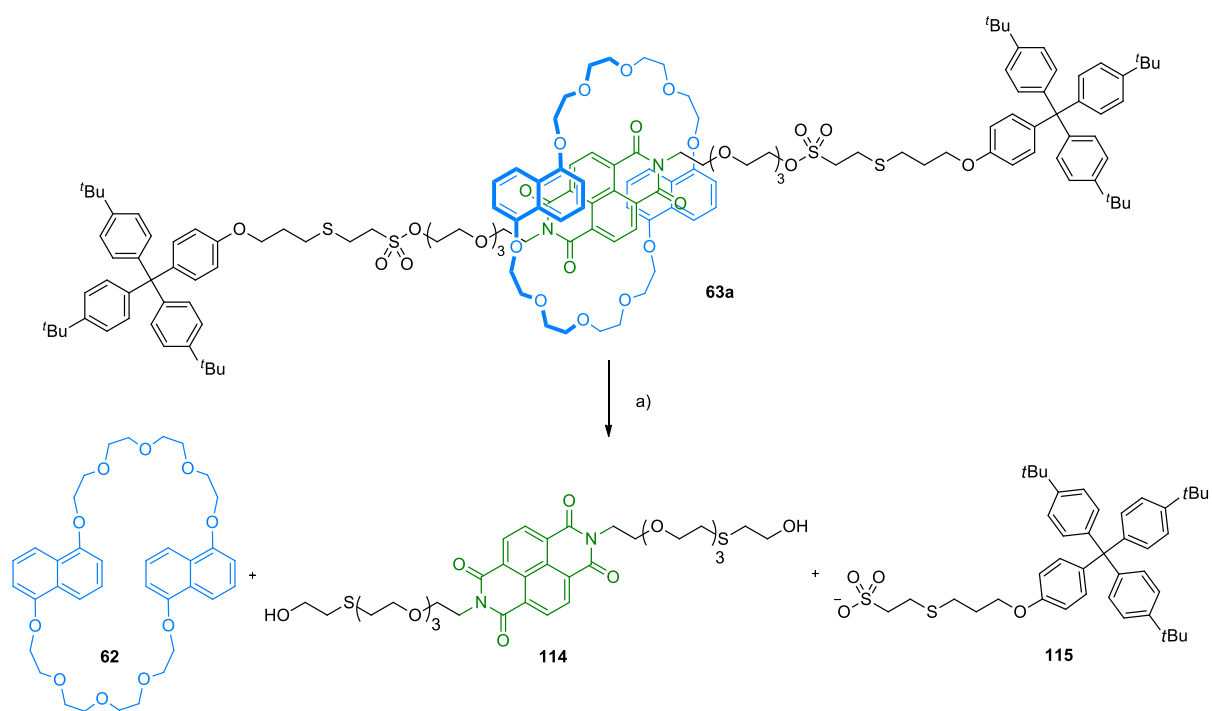


Figure 45. Rotaxane stability experiments in CDCl_3 in the presence of Et_3N at room temperature. ^1H NMR (400 MHz, CDCl_3) spectra of rotaxanes: 1) **63a**; 2) **100d** (a) without Et_3N , and with Et_3N after: (b) 1 d; (c) 5 d.

In this way, we selected the NDI-based [2]rotaxane **63a** to study its chemical disassembly. Among the different nucleophiles previously tested by our group for the nucleophilic substitution-based CAD chemistry of the vinyl sulfonate moiety, we decided to pick 2-mercaptoethanol since this thiol can displace sulfonate moieties at room temperature in DMF in the presence of a mild base such as Cs_2CO_3 . As a first test of the decoupling reaction and to have a reference of the cleaved rod, vinyl sulfonate-functionalized NDI **60a** was treated in the described conditions, affording **114** in a good yield (73%) (Scheme 59).



Scheme 59. Synthesis of cleaved axle **114**. Reagents and conditions: a) 2-Mercaptoethanol, Cs_2CO_3 , DMF, r.t., 3 d, 73%.



Scheme 60. Cleavage of rotaxane **63a**. Reagents and conditions: a) Cs_2CO_3 , DMF, r.t., 48 h.

Following these good results, we submitted rotaxane **63a** to the same reaction conditions, obtaining a mixture of compounds (Scheme 60), which was analyzed by HPLC to prove the selective decoupling and disassembly (Figure 46). Macrocycle **62** ($t_R = 11.347$ min), thread **61a** ($t_R = 11.896$ min), rotaxane **63a** ($t_R = 12.215$ min) and cleaved axle **114** ($t_R = 34.021$ min) were also analyzed as references (Figure 46a-d). Two main signals were observed in the chromatogram of the reaction mixture of the decoupling of rotaxane **63a**. The first peak eluted at a retention time of 11.571 min and a second one

at 34.078 min (Figure 46e). Based on the comparison of their retention time with those of the reference compounds, these peaks were attributed to macrocycle **62** and cleaved axle **114**, respectively. Moreover, an examination of the UV-Vis traces recorded during the HPLC experiments showed a good agreement with the UV-Vis spectra of the corresponding pure compounds (Figure 47). Furthermore, high-resolution mass spectrometry performed on the collected fractions containing the compounds of these two peaks unambiguously certified our assignment since the first fraction showed signals corresponding to the $[\mathbf{62}+\text{NH}_4]^+$ and $[\mathbf{62}+\text{Na}]^+$ ions, while the second fraction displayed a peak associated to $[\mathbf{114}+\text{Na}]^+$ (Figure 48). It is important to point out that no evidences of starting rotaxane or free thread were found in these experiments.

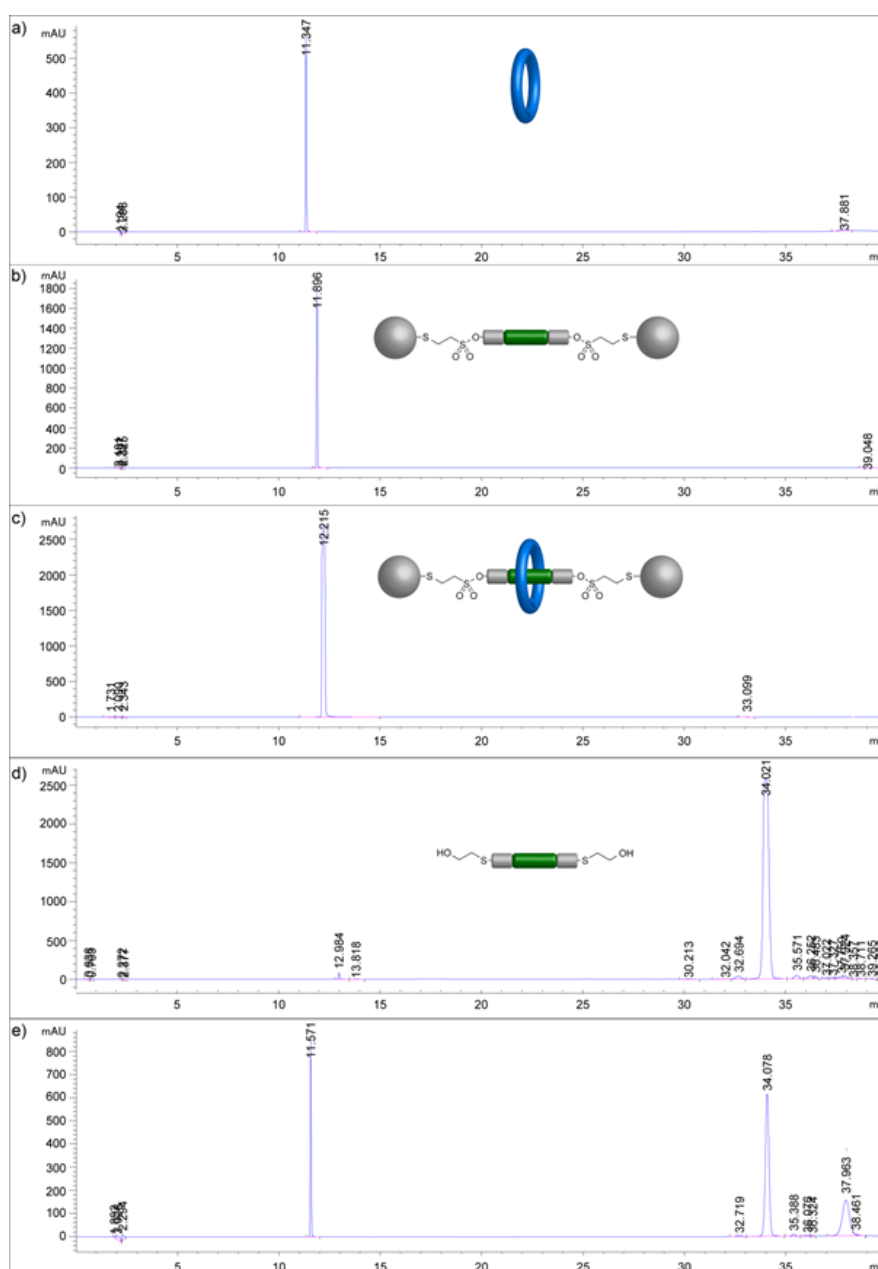


Figure 46. HPLC chromatograms of: a) **62**. b) **61a**. c) **63a**. d) **114**. e) Mixture from the reaction of **63a** and 2-mercaptoethanol for the chemical disassembly of the rotaxane.

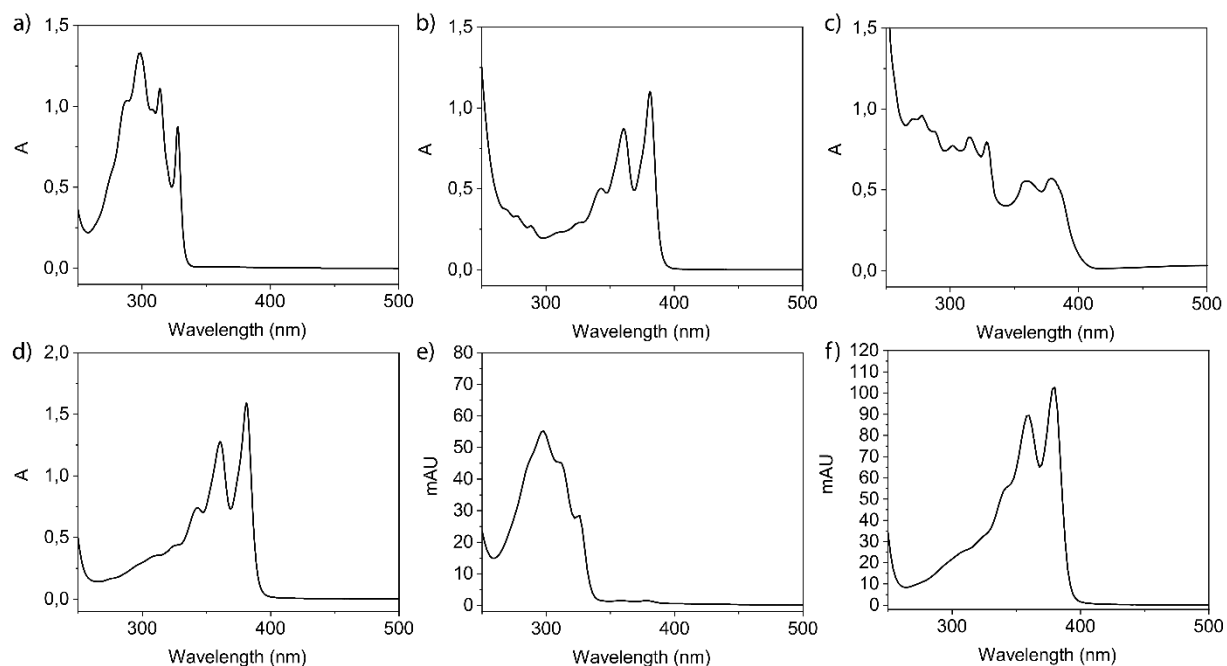


Figure 47. UV-Vis spectrum of: a) Macrocycle **62**. b) Thread **61a**. c) Rotaxane **63a**. d) Cleaved axle **114**. Compounds eluting during the HPLC separation of the mixture obtained from the chemical disassembly of rotaxane **63a**: e) Product eluting at $t_R = 11.571$ min. f) Compound eluting at $t_R = 34.078$ min.

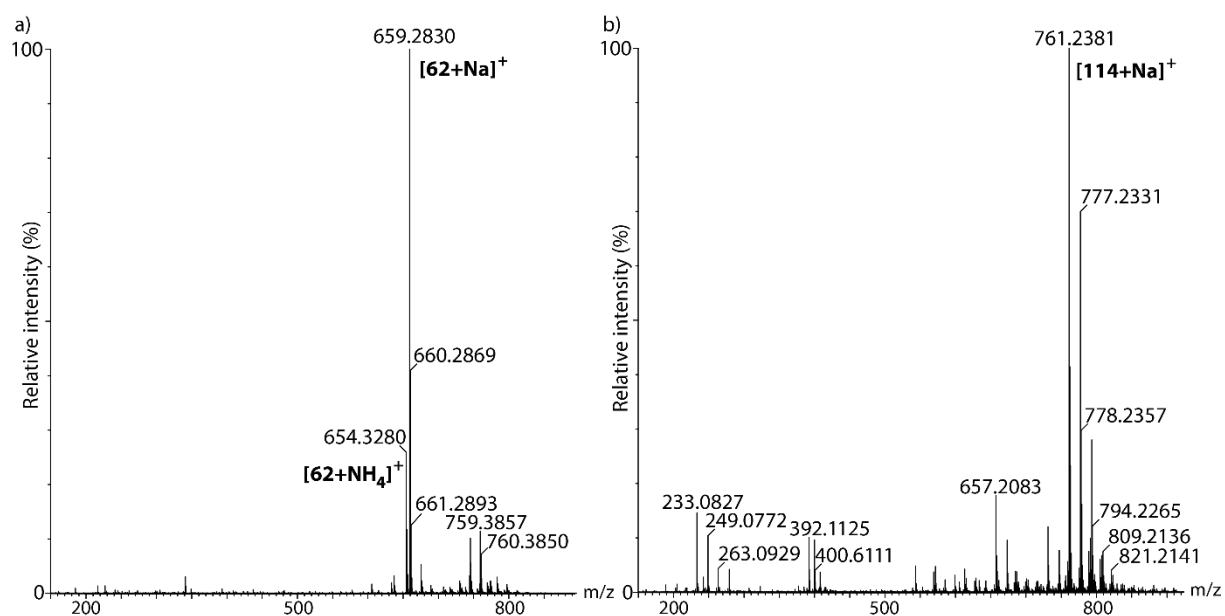


Figure 48. a) HRMS (ESI^+) spectrum of the product eluting at $t_R = 11.571$ min during the HPLC separation, showing peaks corresponding to the $[M+NH_4]^+$ (calc. 654.3273) and $[M+Na]^+$ (calc. 659.2832) ions of macrocycle **62**. b) HRMS (ESI^+) spectrum of the product eluting at $t_R = 34.078$ min during the HPLC separation, showing the peak corresponding to the $[M+Na]^+$ ion of cleaved axle **114**.

In addition, as the stability tests were carried out in the presence of Et_3N , a milder base than Cs_2CO_3 , to check that there was not any undesired decomposition during the decoupling process due to the use of Cs_2CO_3 , rotaxane **63a** was treated with the latter in DMF for 2 days (without the 2-mercaptoethanol). After the work up, the interlocked molecule was undoubtedly recovered

undamaged (Figure 49). Therefore, it can be concluded that rotaxane **63a** was chemically disassembled into its pieces taking advantage of the CAD chemistry of the vinyl sulfonate group.

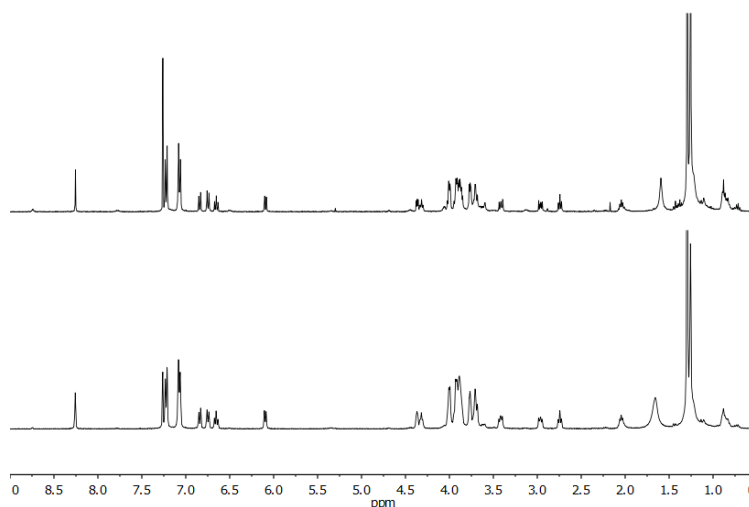
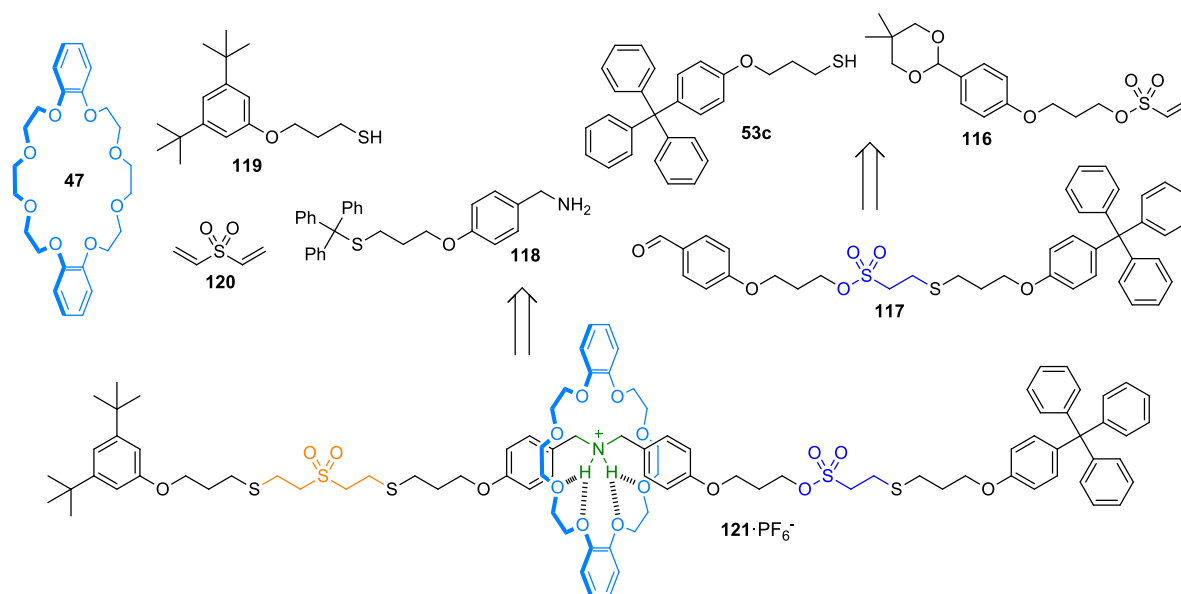


Figure 49. Stability experiment of rotaxane **63a** in DMF in the presence of Cs_2CO_3 at room temperature. ^1H NMR (400 MHz, CDCl_3) spectra of **63a** before (bottom) and after 48 h in DMF with Cs_2CO_3 (crude mixture after work-up) (top).

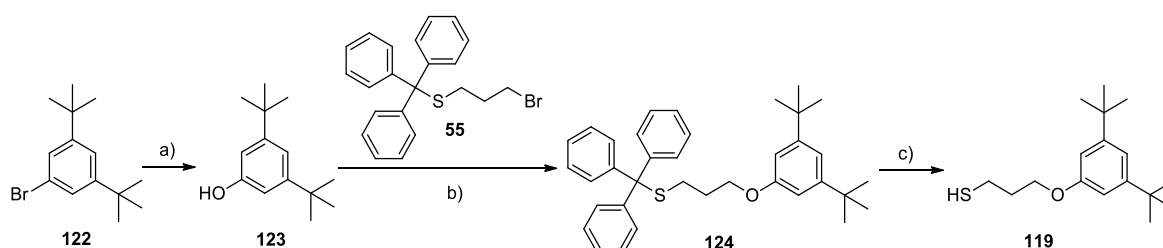
2.3.2. Unidirectional transport of a macrocycle in a [2]rotaxane through CAD chemistry

In view of the successful disassembly of a [2]rotaxane using the CAD chemistry of the vinyl sulfonate group, we decided to extend this methodology to the field of molecular machines. Therefore, we tackled the preparation of a unidirectional transport system employing a “flashing energy ratchet” mechanism and the similarities and differences of the chemistry of both vinyl sulfone and vinyl sulfonate groups. To this end, rotaxane **121**· PF_6^- featuring a sulfone and a sulfonate moiety was designed. This structure could be obtained from the thia-Michael addition of thiol stopper **119** in the presence of DB24C8 (**47**) to a vinyl sulfone-functionalized axle, synthesized by combination of aldehyde **117**, amine **118** and divinyl sulfone. Aldehyde **117** would already feature a sulfonate group coming from the thia-Michael addition between thiol stopper **53c** and vinyl sulfonate-functionalized intermediate **116** (Scheme 61).



Scheme 61. Retrosynthetic plan for the synthesis of rotaxane **121**·PF₆⁻.

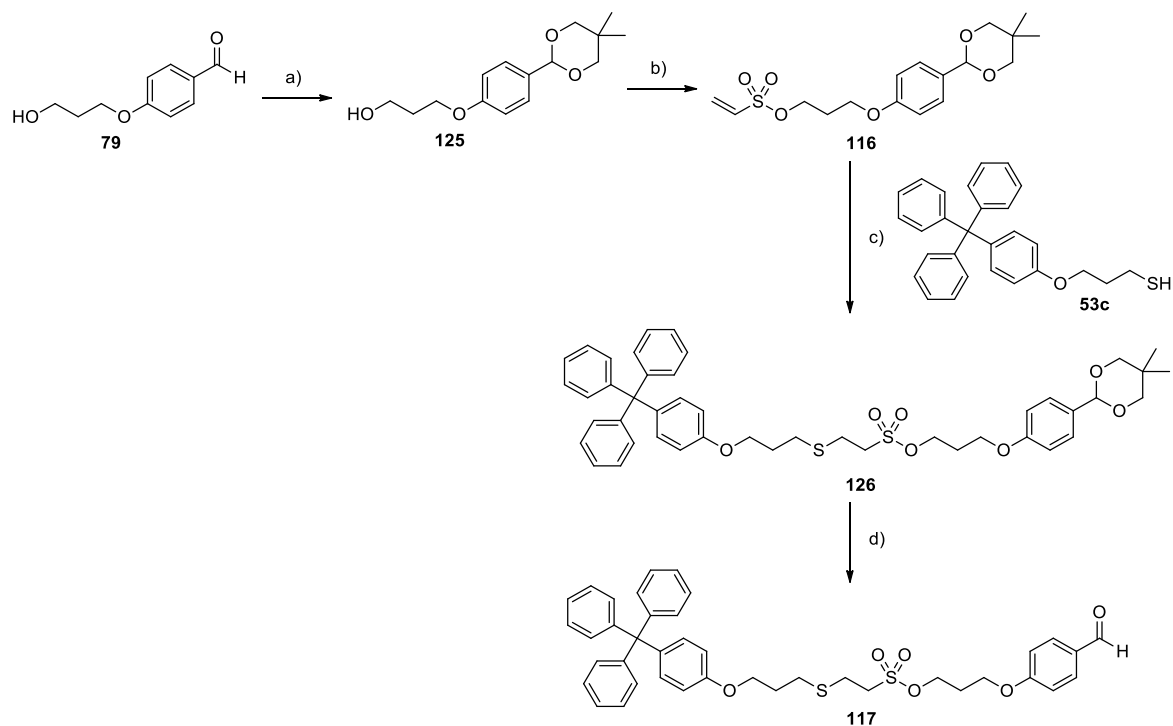
We started with the synthesis of thiol stopper **119**. Thus, aryl bromide compound **122** was transformed into the phenol derivative **123**, which then underwent a Williamson reaction with **55** to afford **124**. The thiol moiety of the latter was deprotected in the presence of CF₃CO₂H and Et₃SiH to yield the target thiol stopper **119** in good yield (79%) (Scheme 62).



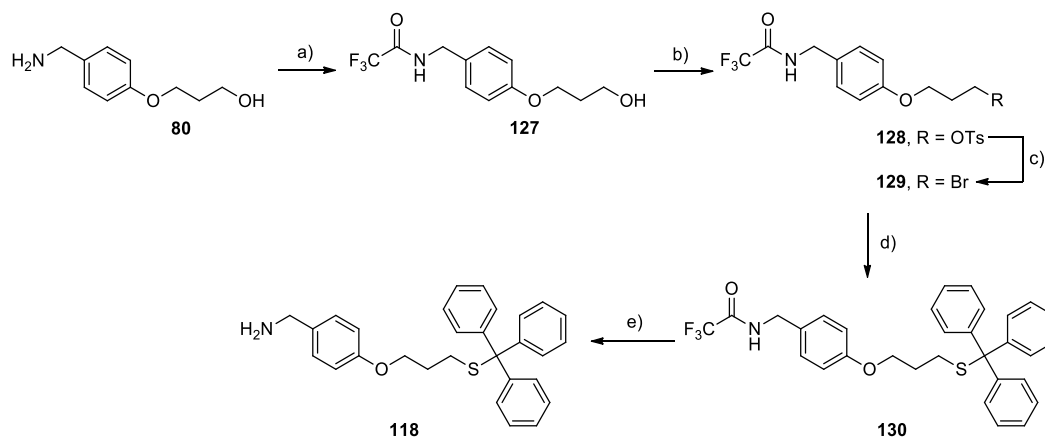
Scheme 62. Synthesis of stopper **119**. Reagents and conditions: a) 1. ⁿBuLi (2.5 M in hexane), THF, -78 °C, 20 min; 2. B(OMe)₃, THF, -78 °C, 20 min, then 0 °C, 2 h; 3. H₂O₂ (33% in H₂O), 0 °C, 30 min, then r.t., 1 h, 61%. b) K₂CO₃, CH₃CN, 75 °C, 22 h, 66 %. c) CF₃CO₂H, Et₃SiH, CH₂Cl₂, r.t., 4 h, 79%.

Subsequently, aldehyde **117** featuring a sulfonate unit was prepared. The synthetic route started with the protection of aldehyde **79** with 2,2-dimethyl-1,3-propanediol, in the presence of 10-camphorsulfonic acid and molecular sieves (3 Å) to afford acetal **125**.²¹⁹ The alcohol group was treated with 2-chloroethanesulfonyl chloride in basic conditions to yield the desired vinyl sulfonate-functionalized compound **116** (80%),²¹⁹ which then underwent the thia-Michael addition of thiol stopper **53c** in the presence of catalytic amounts of Et₃N and PPh₃, giving compound **126**²¹⁹ in excellent

yield (99%).²⁵⁸ Finally, the acetal protecting group was removed in acidic media to get the desired aldehyde **117** in excellent yield (95%) (Scheme 63).²¹⁹



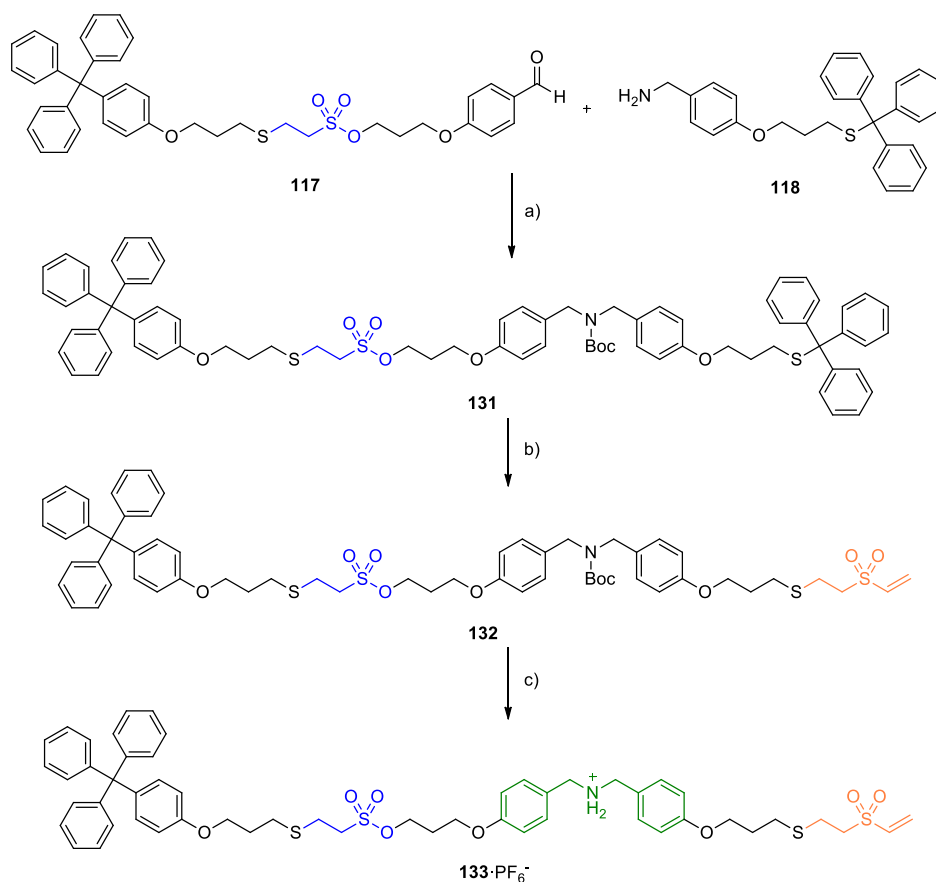
Scheme 63. Synthesis of aldehyde **117**. Reagents and conditions: a) 2,2-dimethyl-1,3-propanediol, 10-camphorsulfonic acid, molecular sieves (3 Å), toluene, 100 °C, 18 h, 73%. b) 2-chloroethanesulfonyl chloride, Et₃N, CH₂Cl₂, 0 °C, 1 h, 80%. c) Et₃N, PPh₃, CH₂Cl₂/iPrOH (8:1), r.t., 24 h, 99%. d) CF₃CO₂H, H₂O, CH₂Cl₂, r.t., 5 h, 95%.



Scheme 64. Synthesis of amine **118**. Reagents and conditions: a) Ethyl trifluoroacetate, Et₃N, MeOH, r.t., 2 h, 89%. b) TsCl, Et₃N, DMAP_(cat.), CH₂Cl₂, r.t., 18 h, 99%. c) LiBr, acetone, reflux, 18 h, 86%. d) Triphenylmethanethiol, LiHMDS (1 M in THF), THF, 0 °C to r.t., 70 min, 85%. e) NaOH, H₂O, MeOH, r.t., 20 h, 76%.

²⁵⁸ The aldehyde group was protected due to the very low yield obtained for the thia-Michael addition with **53c** when the free aldehyde was present.

The next step of the synthetic route was the construction of amine **118**. To this end, amine **80** was protected with a trifluoro acetate group to give **127**. Its alcohol group was then treated with TsCl in basic medium to afford tosylate **128** in excellent yield (99%), which was then converted into a better leaving group employing LiBr in acetone at reflux, yielding bromoalkane **129**. Subsequently, a nucleophilic substitution with trityl thiolate gave compound **130**, incorporating a trityl thiol unit and a protected amine, in very good yield (85%). Finally, the amine was deprotected using sodium hydroxide, affording the target amine **118** in good yield (76%) (Scheme 64).

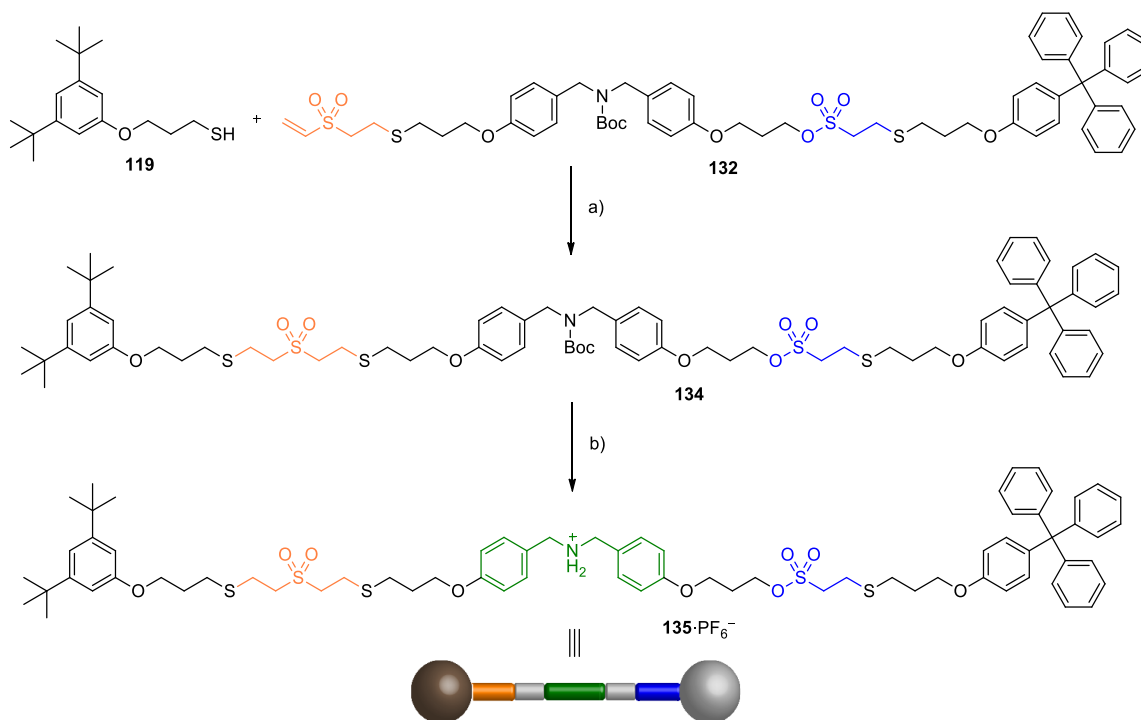


Scheme 65. Synthesis of axle **133**·PF₆⁻. Reagents and conditions: a) 1. MeOH/THF (8:5), r.t., 24 h; 2. NaBH₄, MeOH/THF (8:5), r.t., 24 h; 3. Boc₂O, Et₃N, CH₂Cl₂, r.t., 24 h, 80%. b) 1. CF₃CO₂H, Et₃SiH, CH₂Cl₂, r.t., 6 h; 2. Boc₂O, Et₃N, CH₂Cl₂, r.t., 5 h; 3. Divinyl sulfone, Et₃N, CH₂Cl₂, r.t., 14 h, 52%. c) 1. CF₃CO₂H, CH₂Cl₂, r.t., 5 h; 2. HCl (2 M in Et₂O), CH₂Cl₂, r.t., 3 h; 3. KPF₆, CH₂Cl₂/acetone/H₂O (4:5:5), r.t., 18 h, 84%.

With both compounds in hand, the reductive amination between amine **118** and aldehyde **117** was performed. The resulting amine was subsequently Boc-protected to afford the dibenzylamine derivative **131** in good yield (80%). This compound features both a trityl and a Boc protecting groups. In order to deprotect the trityl moiety, **131** was treated with CF₃CO₂H and Et₃SiH. However, the amine was also deprotected in these conditions. Therefore, this amine had to be protected again as a Boc group to avoid a side aza-Michael addition of the dibenzylamine motif to the vinyl sulfone group during the the MAVS reaction between divinyl sulfone (**120**) and the thiol moiety of the molecule. This

reaction afforded compound **132** in moderate yield (52%). The Boc-protected amine underwent deprotection by using trifluoroacetic acid followed by a counterion exchange to PF_6^- to yield the vinyl sulfone-functionalized dibenzylammonium thread precursor **133**· PF_6^- (Scheme 65).

As common practice, the free thread **135**· PF_6^- was firstly synthesized. Hence, vinyl sulfone **132** and the thiol stopper **119** underwent a MAVS reaction to afford the *tert*-butylcarbamate protected thread **134**, in excellent yield (90%). Treatment with $\text{CF}_3\text{CO}_2\text{H}$ allowed the removal of the Boc protecting group to give the desired ammonium salt on free thread **135**· PF_6^- after counterion exchange (Scheme 66).



Scheme 66. Synthesis of free thread **135**· PF_6^- . Reagents and conditions: a) Et_3N , CHCl_3 , r.t., 18 h, 90%. b) $\text{CF}_3\text{CO}_2\text{H}$, CH_2Cl_2 , r.t., 2 h; 2. HCl (2 M in Et_2O), CH_2Cl_2 , r.t., 3 h; 3. KPF_6 , $\text{CH}_2\text{Cl}_2/\text{acetone}/\text{H}_2\text{O}$ (4:5:5), r.t., 18 h, 83%.

Our proposed strategy for the irreversible unidirectional transport of DB24C8 (**47**) in a rotaxane starts with the generation of the pseudorotaxane from macrocycle **47** and axle **133**· PF_6^- . Thus, the ring will enter from the vinyl sulfone side of the axle since its approach on the other side is impeded by the bulky stopper already present in the structure. Subsequently, macrocycle **47** will be trapped by forming rotaxane **121**· PF_6^- using a thia-Michael addition to the vinyl sulfone group of axle **133**· PF_6^- . Finally, after nucleophilic substitution and the addition of base, the resulting sulfonate moiety of rotaxane **121**· PF_6^- will be displaced promoting the liberation of macrocycle **47** through the opposite side to its entrance (Figure 50).

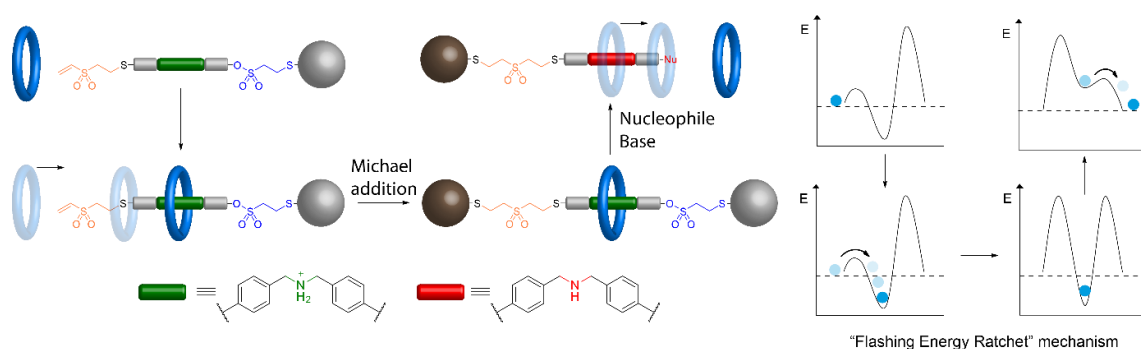
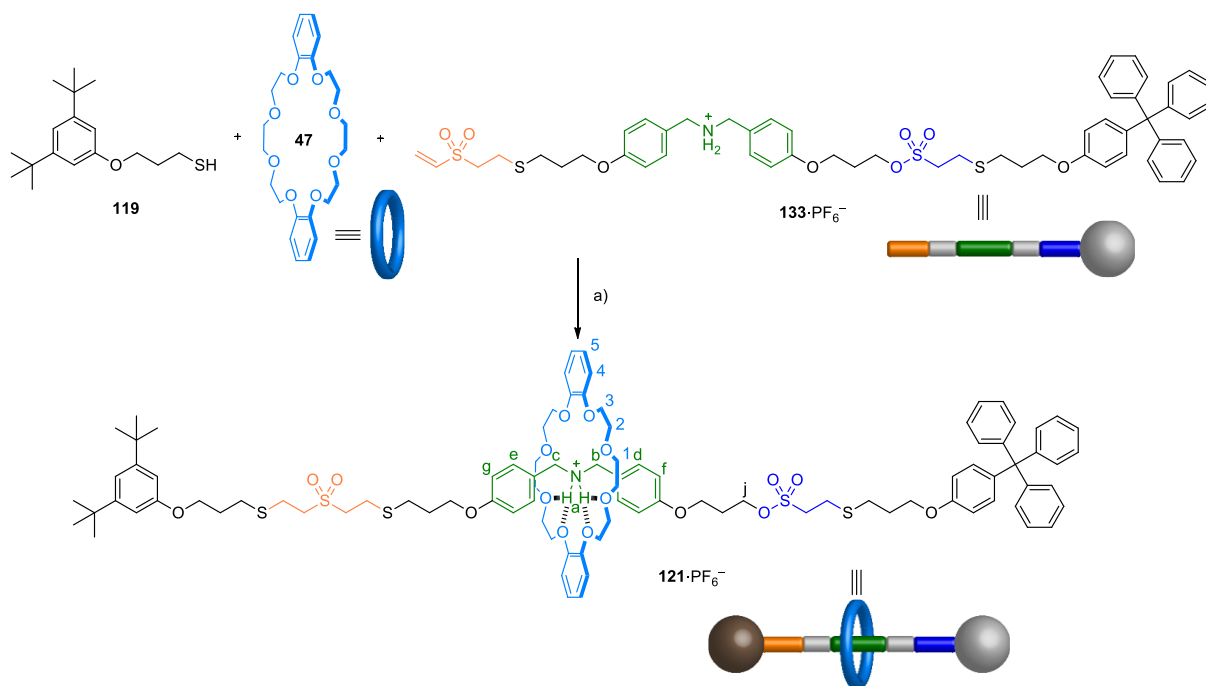


Figure 50. Proposed strategy for the irreversible transportation of a crown ether macrocycle through a linear component in a unidirectional way following a flashing energy ratchet mechanism.

During this process, the formation of the pseudorotaxane would be favored since it would represent a lower energy than the free ring. To form this supramolecular complex, the entrance of macrocycle **47** would take place through the vinyl sulfone side, since the energy barrier would be surmountable while on the other side bulky stoppers would make it impassable. The generation of rotaxane **121**·PF₆⁻ would imply the increase of the potential energy barrier of the vinyl sulfone side. After the cleavage of the sulfonate unit, the energy barrier of this side would drop and the addition of base would destabilize the pseudorotaxane, resulting in the liberation of macrocycle **47** and its unidirectional transportation (Figure 50).



Scheme 67. Synthesis of rotaxane **121**·PF₆⁻. Reagents and conditions: DMAP_(cat.), CHCl₃, 0 °C, 72 h, 66%.

With the different compounds in hand, we firstly attempted a stepwise operation to demonstrate the unidirectional translation of the macrocycle in our system using a flashing energy ratchet mechanism. The first step was the entrance of the macrocycle, that is the formation of [2]rotaxane **121**·PF₆⁻. Hence,

the target rotaxane was prepared by a DMAP-catalyzed Michael-type addition of thiol stopper **119** to the vinyl sulfone group of **133**·PF₆⁻ in the presence of DB24C8 (**47**), which afforded [2]rotaxane **121**·PF₆⁻ in good yield (66%) (Scheme 67).

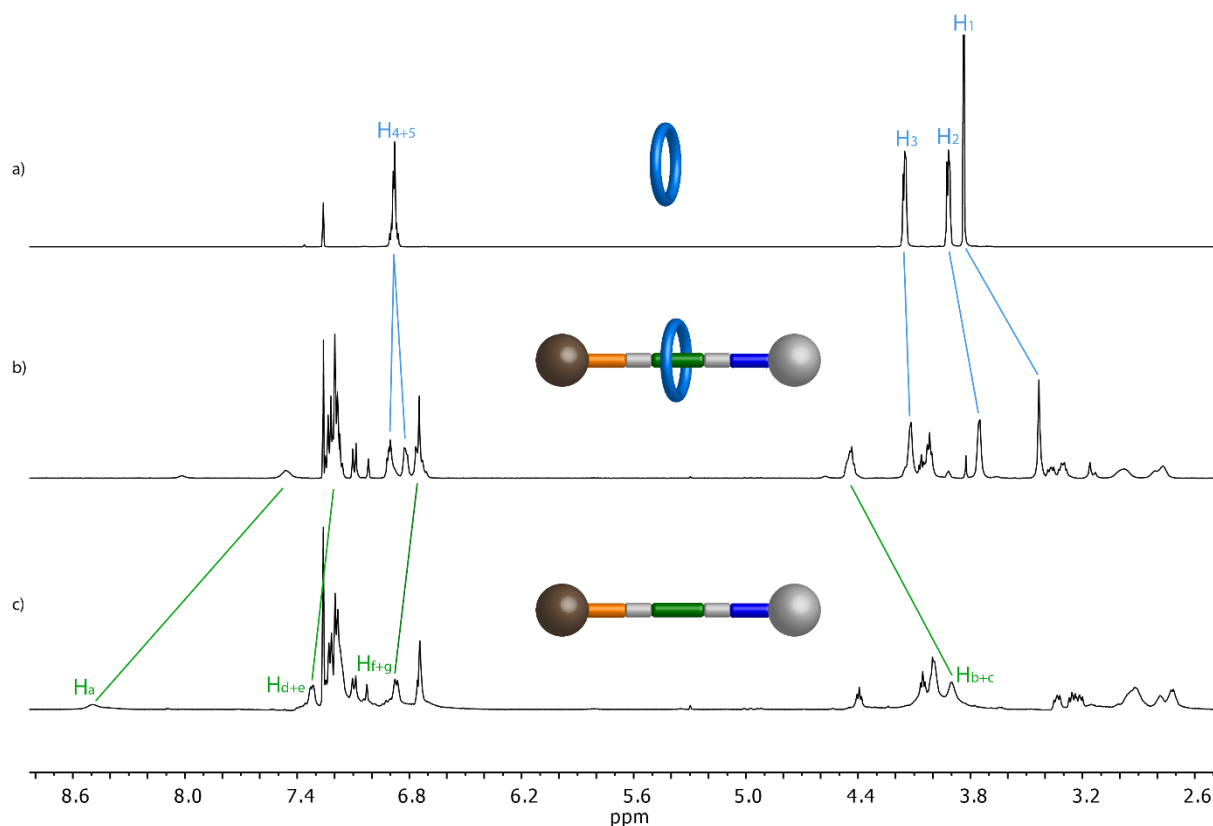


Figure 51. ¹H NMR (500 MHz, CDCl₃) spectra of: a) Macrocycle **47**. b) Rotaxane **121**·PF₆⁻. c) Thread **135**·PF₆⁻. Lettering coding is defined in Scheme 67.

This [2]rotaxane was characterized by means of NMR spectroscopy (Figure 51). Its ¹H NMR spectrum displays an upfield shift for the ammonium H atoms ($\Delta\delta_{\text{Ha}} = -1.03$ ppm) due to their interactions with the crown ether macrocycle. The aromatic protons of the thread are shielded meanwhile the signal of those from the macrocycle split into two new signals. When it comes to the methylene groups, the benzylic CH₂ from the axle suffer a downfield shift ($\Delta\delta_{\text{Hb/c}} = 0.54$ ppm) while those from the crown ether are shielded ($\Delta\delta_{\text{H1}} = -0.40$ ppm; $\Delta\delta_{\text{H2}} = -0.17$ ppm; $\Delta\delta_{\text{H3}} = -0.03$ ppm). These changes in the ¹H NMR spectrum are the typical for this kind of interlocked systems due to the establishment of hydrogen bonding and the shielding effect of the aromatic rings. Furthermore, the DOSY NMR of **121**·PF₆⁻ shows that both the rod and the ring diffuse as a whole which is consistent with the interlocked nature of the product (Figure 52). Finally, the HRMS spectrum confirmed the identity of the [2]rotaxane since the exact mass found for the [M-PF₆]⁺ ions (m/z : 1708.7335) and its isotopic distribution nicely match the theoretical ones (Figure 53).

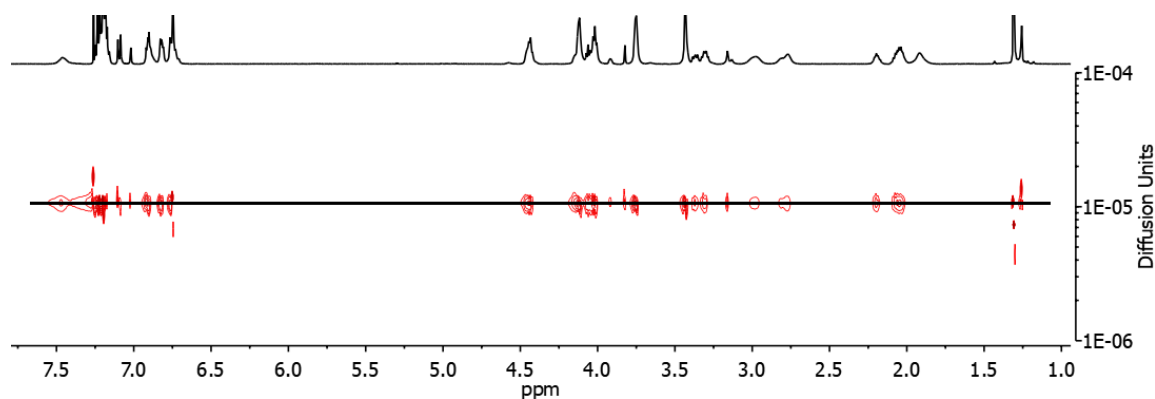


Figure 52. DOSY NMR (500 MHz, CDCl_3) spectrum of $\mathbf{121} \cdot \text{PF}_6^-$.

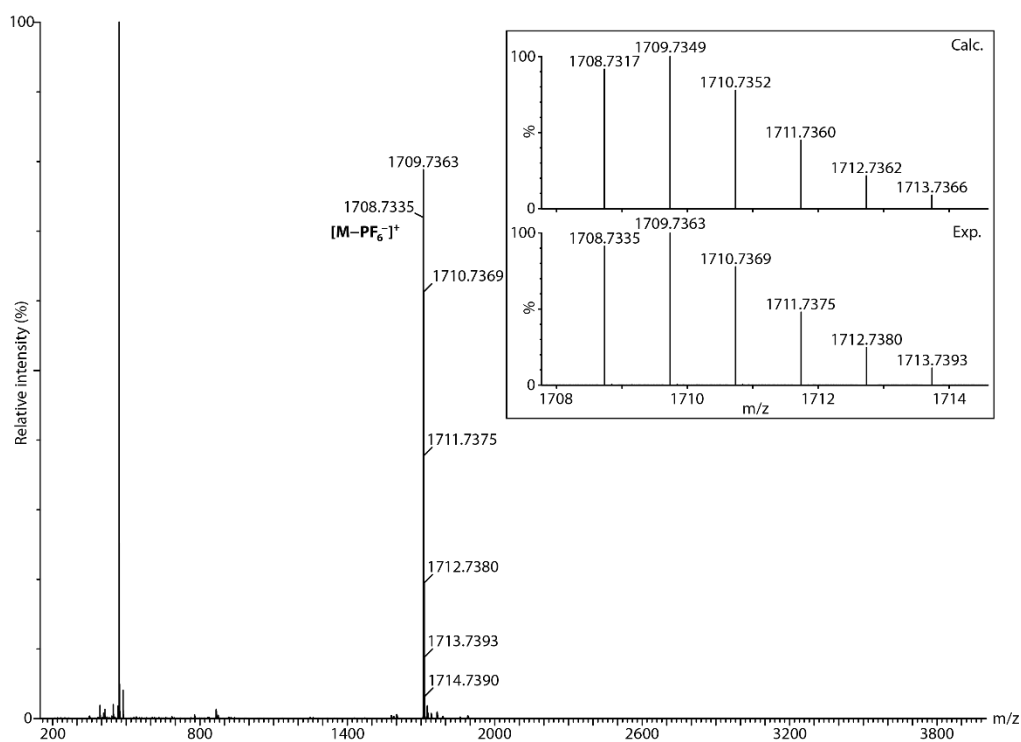
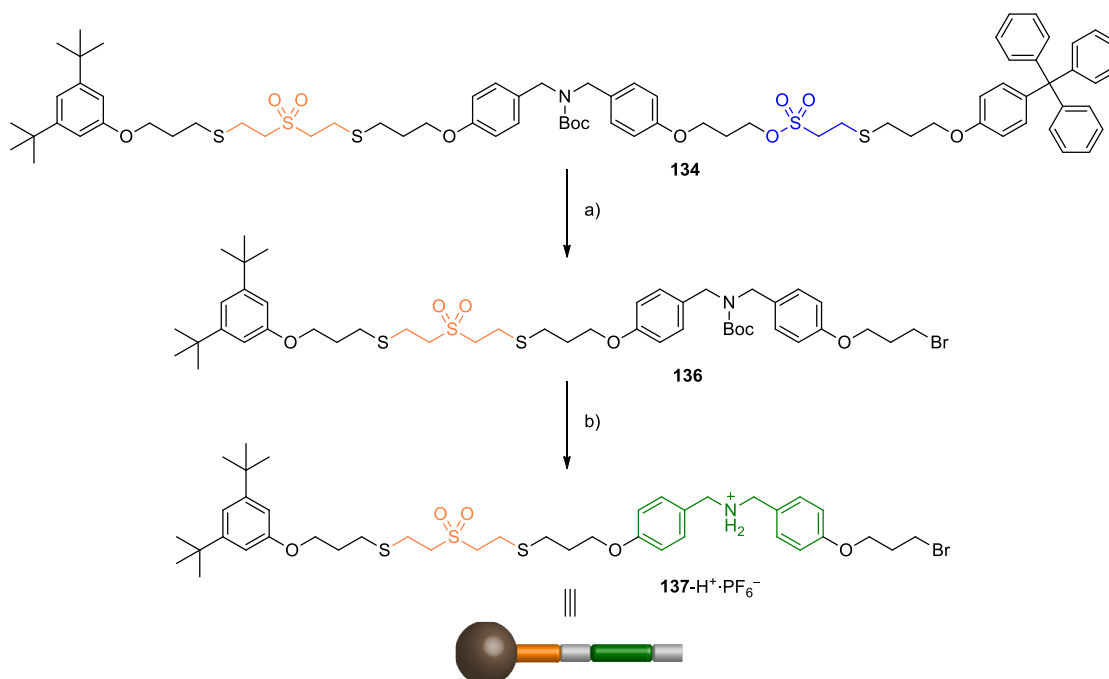


Figure 53. HRMS (ESI⁺) spectrum of rotaxane $\mathbf{121} \cdot \text{PF}_6^-$. Inset: Experimental (bottom) and theoretical (top) isotopic distribution for the $[\text{M}-\text{PF}_6^-]^+$ peak.

The next step was the decoupling reaction and cleavage of rotaxane $\mathbf{121} \cdot \text{PF}_6^-$. For this purpose, a nucleophilic substitution that proceeds at room temperature would be the best tool. Although, the decoupling of the sulfonate in the presence of a thiol and base at room temperature in DMF is efficient for the cleavage of sulfonate rotaxanes, in our system the nucleophilic substitution should ideally take place in a chlorinated solvent at room temperature without the need of a base. This is, in fact, a requirement for an *in situ* operation of the system, as shown in section 2.3.1. After some unsuccessful tests with LiBr, we rediscovered a reaction described by Gore in 1976, rarely used to date.²⁵⁹ Thus, employing MgBr_2 at room temperature in CH_2Cl_2 or CHCl_3 the nucleophilic attack occurs quantitatively,

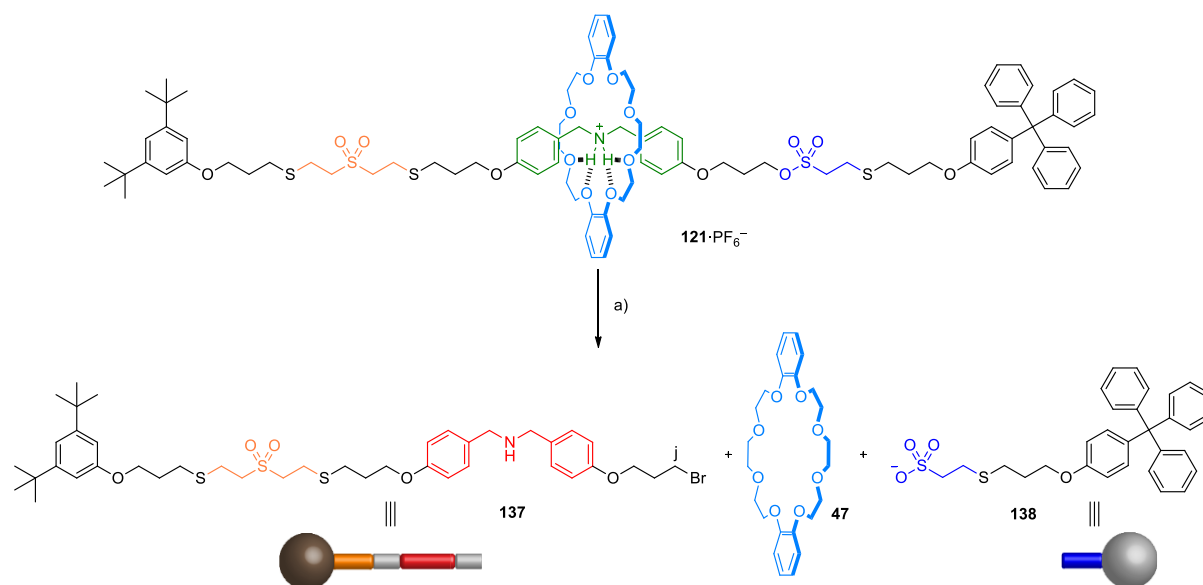
²⁵⁹ P. Place, M. L. Roumestant, J. Gore, *Bull. Soc. Chim. Fr.* **1976**, 169-176.

generating the target bromoalkane. The reaction was then tested on the Boc-protected thread **134**. The substitution of the sulfonate for the bromide takes place, affording **136** in an excellent yield (96%). The resulting thread was Boc-deprotected in acidic medium to obtain after counterion exchanged to PF_6^- generating **137-H⁺·PF₆⁻** (Scheme 68). Compound **137-H⁺·PF₆⁻** will be also used as reference to monitor the operation of the system.



Scheme 68. Cleavage of thread **134**. Reagents and conditions: a) MgBr_2 , CH_2Cl_2 , r.t., 48 h, 96%. b) $\text{CF}_3\text{CO}_2\text{H}$, CH_2Cl_2 , r.t., 2 h; 2. HCl (2 M in Et_2O), CH_2Cl_2 , r.t., 4 h; 3. KPF_6 , $\text{CH}_2\text{Cl}_2/\text{acetone}/\text{H}_2\text{O}$ (4:5:5), r.t., 18 h, 95%.

Having optimized the decoupling reaction, the next step was its application to the controlled cleavage of [2]rotaxane **121·PF₆⁻** to release macrocycle **47**. Thus, the nucleophilic substitution using MgBr_2 was carried out, followed by addition of base (Et_3N) to deprotonate the dibenzylamine moiety and release the crown ether, affording macrocycle **47** and a mixture of compounds **137/138** (1:1) in very good yields (92% and 77% respectively) (Scheme 69).



Scheme 69. Cleavage of rotaxane **121·PF₆⁻**. Reagents and conditions: a) 1. MgBr₂, CHCl₃, r.t., 48 h; 2. Et₃N, CDCl₃, r.t., 10 min, 92% (for **47**) and 77% (for **137/138** (1:1)).

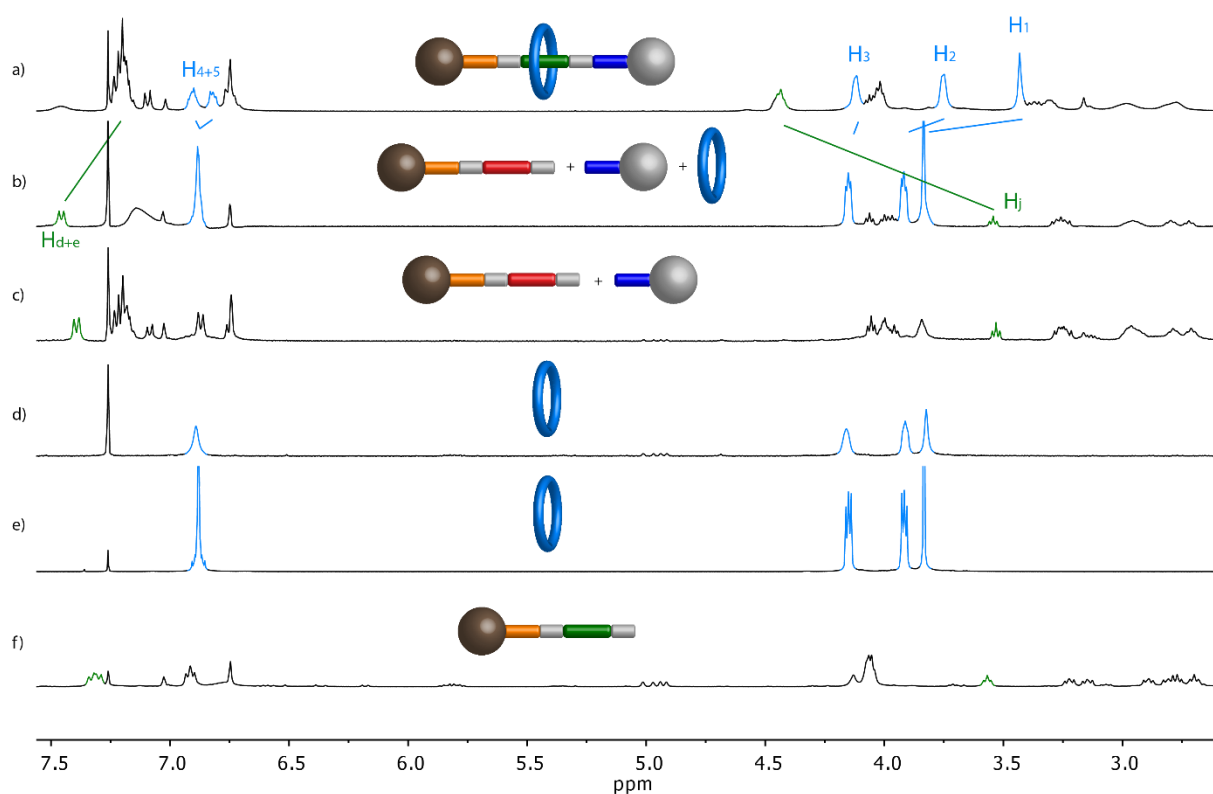
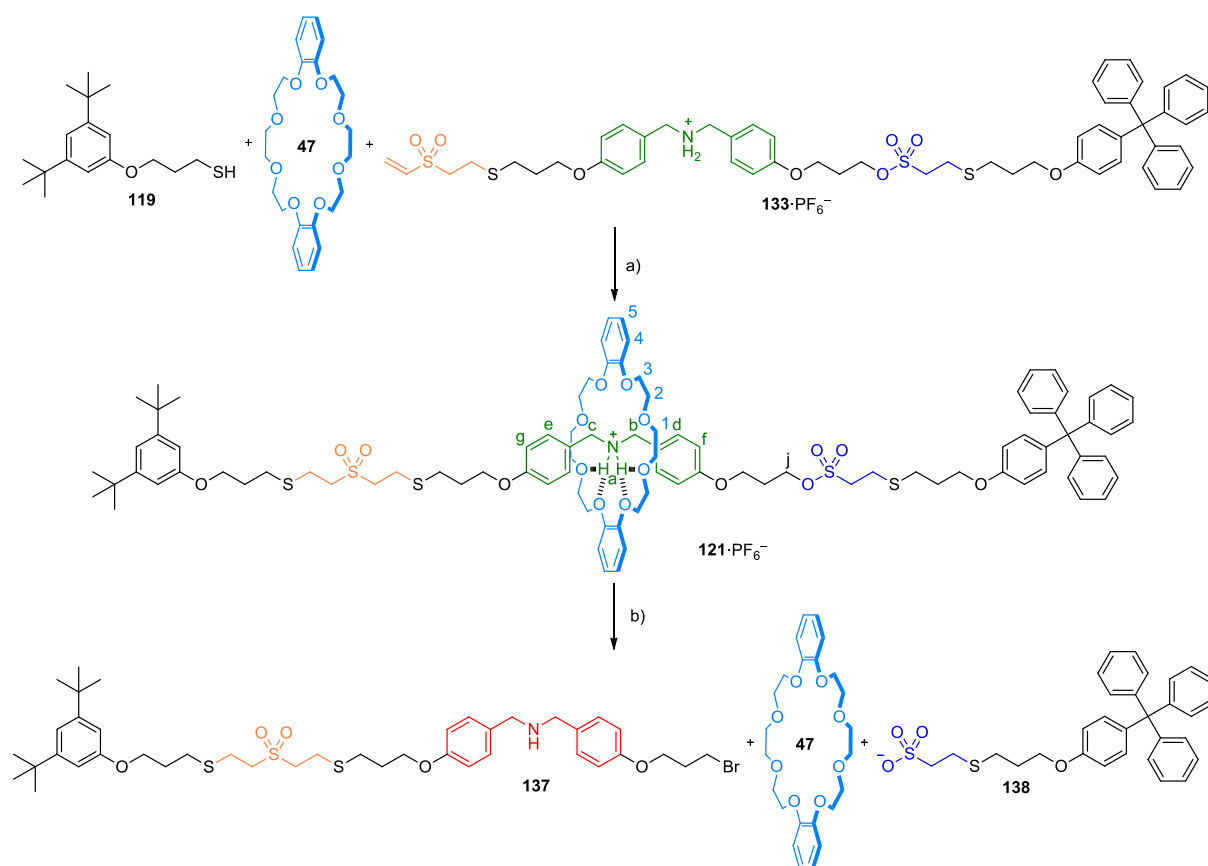


Figure 54. Cleavage and disassembly of rotaxane **121·PF₆⁻**. ¹H NMR (400 MHz, CDCl₃) spectra of: a) Rotaxane **121·PF₆⁻**. b) Crude mixture of the reaction of rotaxane **121·PF₆⁻** with MgBr₂. c) 1:1 Mixture of **137** and stopper **138** obtained after purification of b. d) Macrocycle **47** obtained purification of c. e) Macrocycle **47**. f) Compound **137-H⁺·PF₆⁻**. Lettering coding is defined in Scheme 67.

This stepwise operation was followed by ¹H NMR spectroscopy. On the spectrum recorded from the crude reaction mixture after displacement of the sulfonate unit and basification of the reaction medium, the signals from the macrocycle and the dibenzylammonium unit of the axle shifted

compared to those from the rotaxane and were similar to those from the free ring **47** and cleaved axle **137** (Figure 54a,b,e,f). This indicates the absence of hydrogen bonding interactions between the fragments generated. Moreover, a triplet appeared at 3.54 ppm, the typical chemical shift for a proton of a CH₂-Br group. This signal is also present on axle **137**, supporting the fact that the decoupling reaction occurred (Figure 54b,f). Furthermore, two fractions were isolated during the purification process and were identified as macrocycle **47** and as a 1:1 mixture of axle **137** and stopper **138** since they displayed similar ¹H NMR spectra as those from the reference compounds (Figure 54c-f). In addition, the stepwise transportation of macrocycle **47** along rotaxane **121**·PF₆⁻ was confirmed by HMRS since the exact masses and the isotopic distributions of the signals in the mass spectra of macrocycle **47** (*m/z*: 471.1992 for [M+Na]⁺), thread **137** (*m/z*: 822.2892 for [M+H]⁺) and stopper **138** (*m/z*: 517.1507 [M]⁻) recovered from the reaction were in agreement with the theoretical ones. Therefore, the unidirectional transfer of a macrocycle in a [2]rotaxane employing click MAVS reactions, the CAD chemistry of the vinyl sulfonate group and a flashing energy ratchet mechanism was demonstrated sequentially.



Scheme 70. *In situ* unidirectional transport of macrocycle **47**. Reagents and conditions: a) DMAP_(cat.), CDCl₃, 0 °C, 72 h. b) 1. MgBr₂, CDCl₃, r.t., 48 h; 2. Et₃N, CDCl₃, r.t., 30 min.

Finally, the ultimate goal was to accomplish the *in situ* unidirectional transportation of the crown ether (**45**), that is, the assembly of the pseudorotaxanes, the synthesis of rotaxane **121**·PF₆⁻ *via* a MAVS

reaction, the subsequent decoupling of the sulfonate and the base-mediated disassembly of the rotaxane **121**·PF₆⁻ into its components in one-pot (Scheme 70). Thus, we studied the *in situ* operation performing the sequence of reactions in CDCl₃ employing the methodology optimized for the stepwise operation. The operation was monitored by ¹H NMR spectroscopy and HRMS.

As shown by ¹H NMR spectroscopy, firstly, the pseudorotaxane composed of **133**·PF₆⁻ and **47** was explicitly formed since the ammonium hydrogen atoms H_b and H_c suffered the classic downfield shift while H₁ and H₂ shifted upfield (Figure 55a-c). The absence of a mechanical bond was supported by HRMS since we did not observe a signal for the self-assembled species but peaks for the mixture of free compounds (Figure 56). Then, thiol stopper **119** and a catalytic amount of DMAP were added. As a result, the thia-Michael addition reaction to the vinyl sulfone derivative of **133**·PF₆⁻ took place, yielding rotaxane **121**·PF₆⁻. Indeed, H_b, H_c, H₁, and H₂ showed chemical shifts similar to those of pure rotaxane **121**·PF₆⁻ (Figure 55d). In addition, the presence of rotaxane **121**·PF₆⁻ was demonstrated by HRMS, which showed a signal exhibiting an exact mass (m/z : 1708.7313 for [M-PF₆]⁺) whose isotopic distribution was in good agreement with the theoretical one (Figure 57). Traces of an unknown by-product that seems to feature an alkene unit was detected by NMR spectroscopy in the region between 6.2 and 6.4 ppm. However, the absence of one of the signals of the vinyl sulfone group (that originally located at δ = 6.55 ppm) suggests that this species was not thread precursor **133**·PF₆⁻ (Figure 55d). In fact, neither the vinyl sulfone-functionalized axle **133**·PF₆⁻ nor free thread **135**·PF₆⁻ were detected by HRMS (Figure 54). Subsequently, MgBr₂ was added and the ¹H NMR spectrum recorded 48 h after (Figure 55e). Its analysis revealed the appearance of a triplet at δ = 3.53 ppm, corresponding to H_j, evidencing the creation of the desired CH₂-Br bond and the shifting of the characteristic signals from rotaxane **121**·PF₆⁻ (H_b, H_c, H₁, and H₂). Furthermore, by positive-mode HRMS, a peak corresponding to the exact mass of the cleaved axle **137**-H⁺·PF₆⁻ was observed (m/z : 822.2893 [M-PF₆]⁺) while that of rotaxane **121**·PF₆⁻ was missing (Figure 58). Likewise, in negative mode, a peak belonging to the detached stopper **138** (m/z : 517.1508 [M]⁻) was present (Figure 59). Finally, by addition of Et₃N the ¹H NMR signals from macrocycle **47** shifted back to their initial chemical shifts while those of **137** remained unchanged (Figure 55f). Therefore, it was unambiguously demonstrated that DB24C8 underwent a unidirectional transport along this rotaxane system using the MAVS reactions and the CAD chemistry of the vinyl sulfonate moiety.

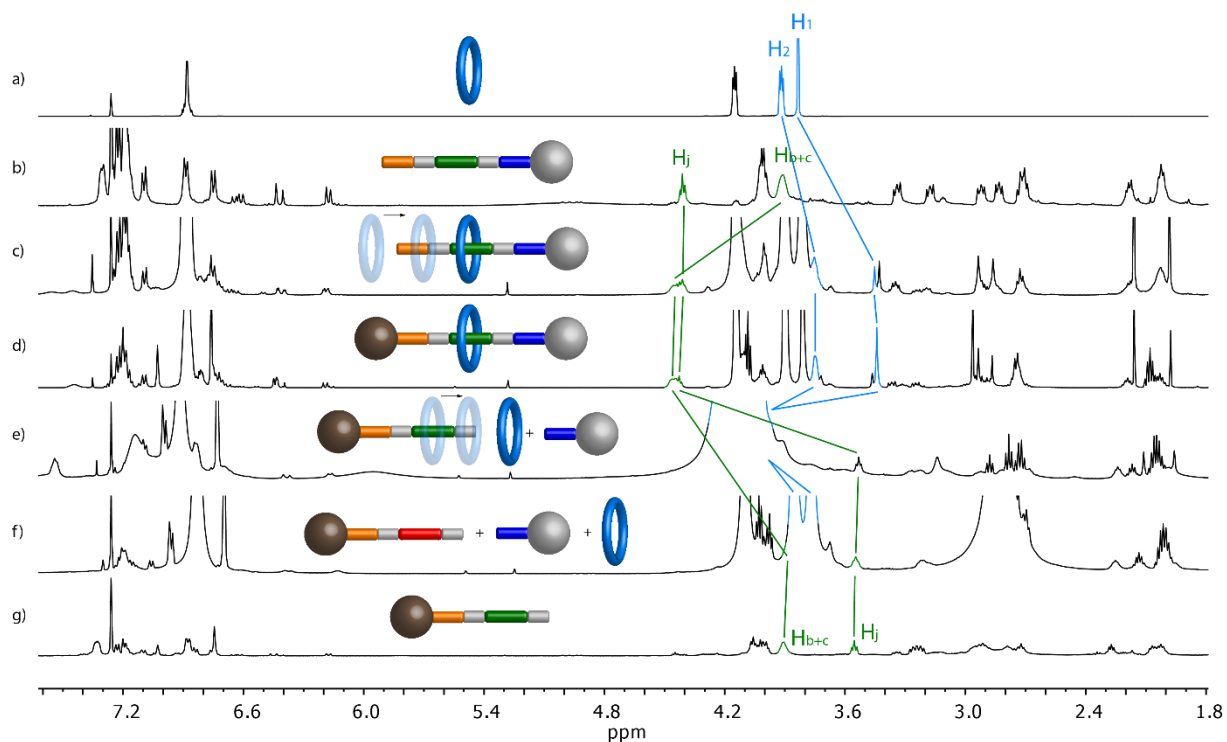


Figure 55. *In situ* unidirectional transport experiment of macrocycle **47**. ^1H NMR (500 MHz, CDCl_3) spectra of: a) Macrocycle **45**. b) Axle $\mathbf{133}\cdot\text{PF}_6^-$. c) Pseudorotaxane formed by $\mathbf{133}\cdot\text{PF}_6^-$ and **47**. d) Mixture c 72 h after the addition of stopper **119** and DMAP. e) Mixture d 48 h after the addition of MgBr_2 . f) Mixture e 30 min after the addition of Et_3N . g) Axle $\mathbf{137}\text{-H}^+\cdot\text{PF}_6^-$. Lettering coding is defined in Scheme 69.

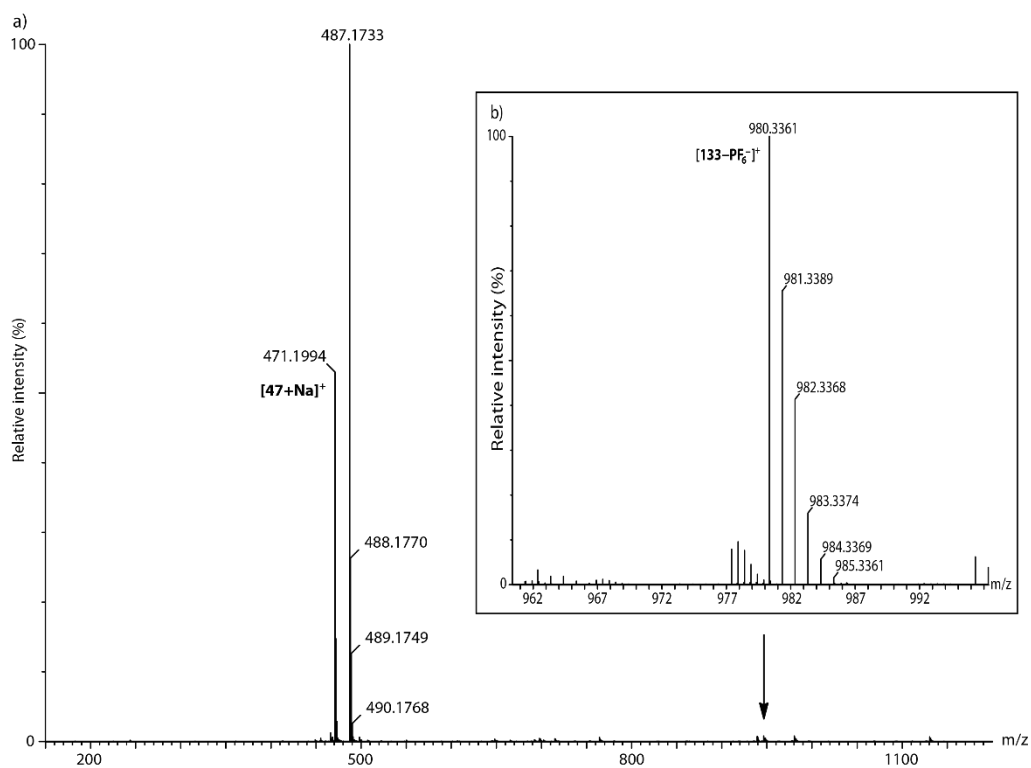


Figure 56. *In situ* unidirectional transport experiment of macrocycle **47**: a) HRMS (ESI^+) spectrum of a mixture of **47** and thread $\mathbf{133}\cdot\text{PF}_6^-$, showing the peaks corresponding to macrocycle **47**: m/z : 471.1994 $[\text{M}+\text{Na}]^+$ (calcd for $\text{C}_{24}\text{H}_{32}\text{NaO}_8$: 471.1995). b) Zoom showing the peaks corresponding to thread $\mathbf{133}\cdot\text{PF}_6^-$: m/z : 980.3361 $[\text{M}-\text{PF}_6]^-$ (calcd for $\text{C}_{54}\text{H}_{62}\text{NO}_8\text{S}_4$: 980.3358).

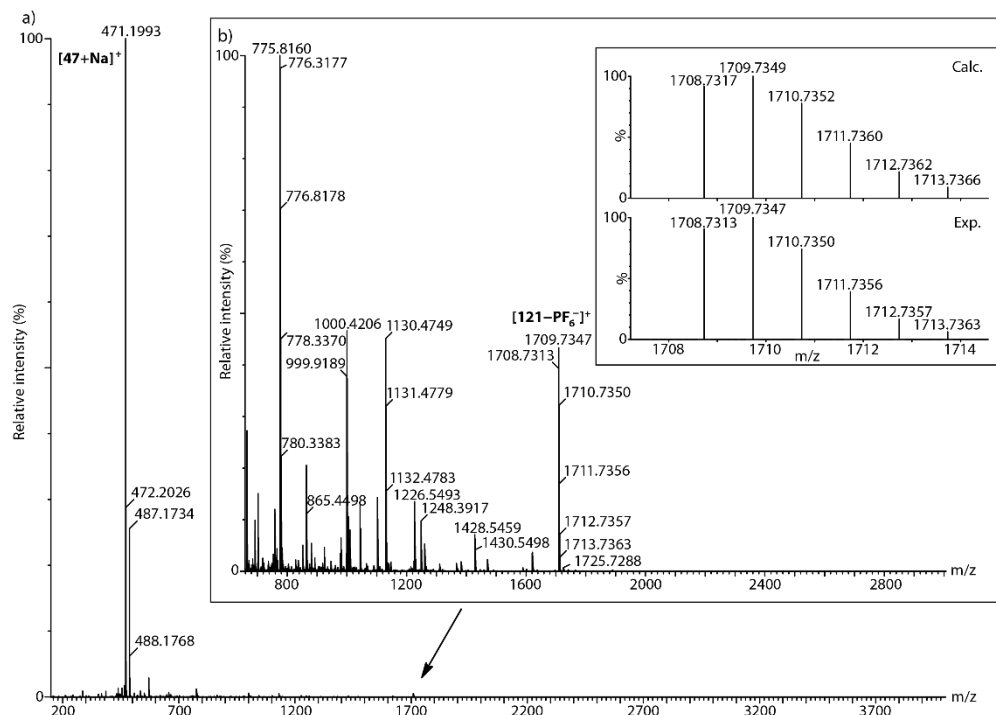


Figure 57. *In situ* unidirectional transport experiment of macrocycle **47**: a) HRMS (ESI⁺) spectrum recorded 72 h after the addition of stopper **119** and DMAP, showing the peaks corresponding to the excess of macrocycle **47**: m/z : 471.1993 [M+Na]⁺ (calcd for C₂₄H₃₂NaO₈: 471.1995). b) Zoom showing the peak corresponding to rotaxane **121**·PF₆⁻: m/z : 1708.7313 [M-PF₆]⁺ (calcd for C₉₅H₁₂₂NO₁₇S₅: 1708.7316). Inset: experimental (bottom) and theoretical (top) isotopic distribution for the [M-PF₆]⁺ peak.

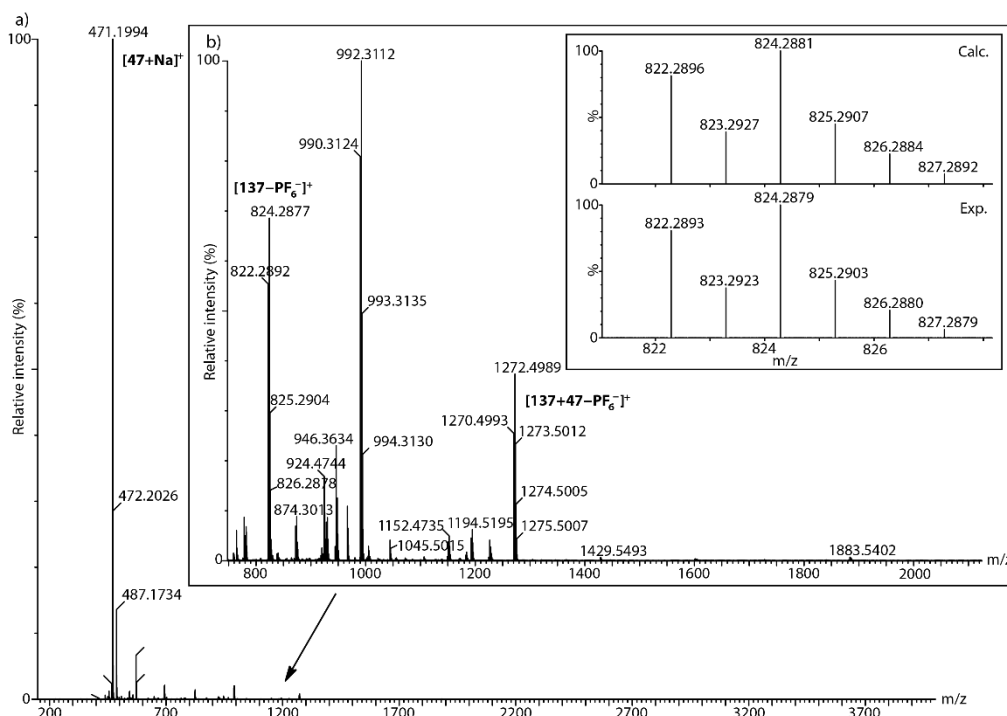


Figure 58. *In situ* unidirectional transport experiment of macrocycle **47**: a) HRMS (ESI⁺) spectrum measured 48 h after the addition of MgBr₂, showing the peaks corresponding to the excess of macrocycle **47**: m/z : 471.1994 [M+Na]⁺ (calcd for C₂₄H₃₂NaO₈: 471.1995). b) Zoom showing the peak corresponding to cleaved thread **137**-H⁺·PF₆⁻ (ESI⁺): m/z : 822.2893 [M-PF₆]⁺ (calcd for C₄₁H₆₁NBrO₅S₂: 822.2896). Inset: experimental (bottom) and calculated (top) isotopic distribution for the [M-PF₆]⁺ peak.

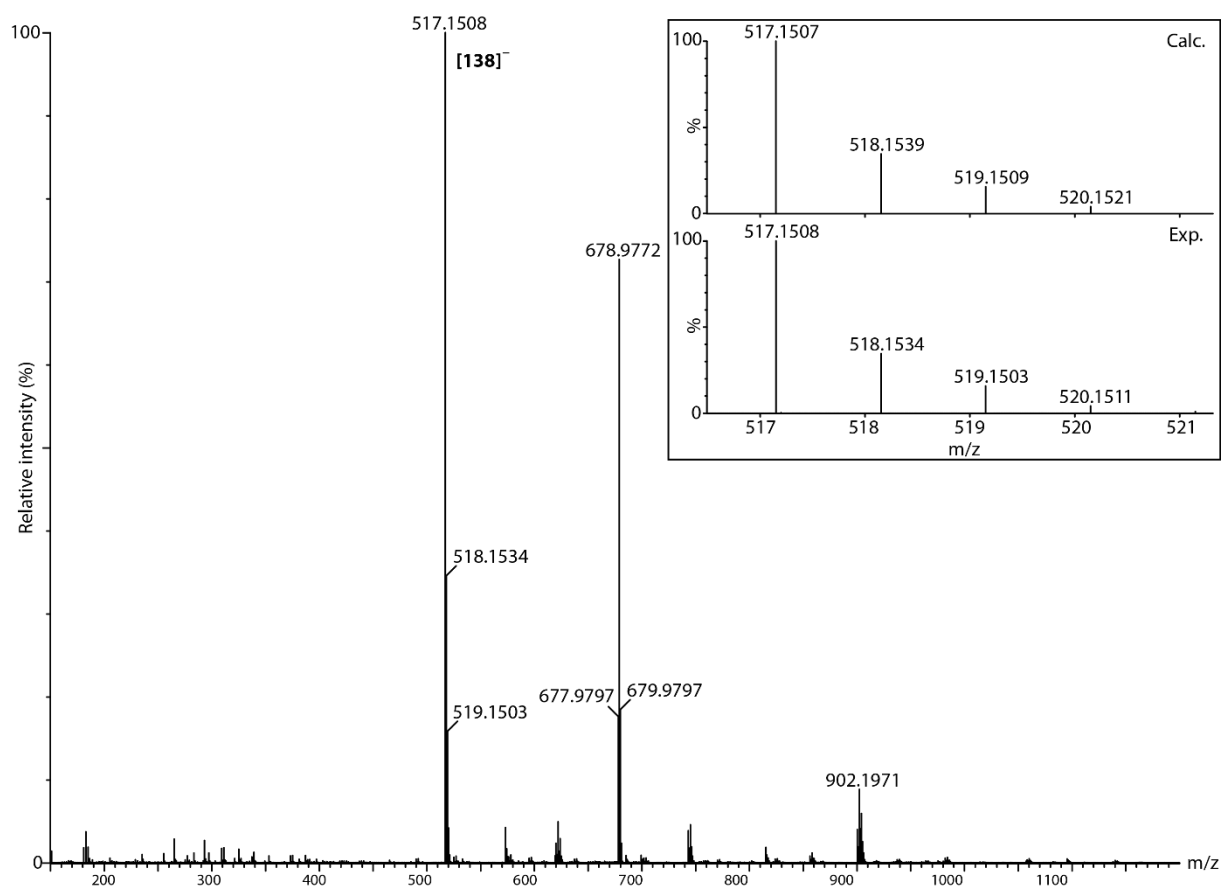


Figure 59. *In situ* unidirectional transport experiment of macrocycle **47**: HRMS (ESI⁻) spectrum recorded 48 h after the addition of MgBr₂, showing the peak corresponding to stopper **138**: *m/z*: 517.1508 [M]⁻ (calcd for C₃₀H₂₉O₄S₂: 517.1507). Inset: experimental (bottom) and calculated (top) isotopic distribution for [M]⁻ peak obtained during the *in situ* unidirectional transport experiment.

2.4. Conclusions

As a starting point, the stability of both sulfonate and sulfone-functionalized [2]rotaxanes was investigated and even in the presence of a mild base (Et_3N), these interlocked molecules stayed intact after a few days in solution. Thus, this behaviour enabled the controlled cleavage of the sulfonate [2]rotaxanes employing the CAD chemistry of the vinyl sulfonate group. In this fashion, [2]rotaxane **63a** has been synthesized *via* a MAVS reaction and subsequently, chemically disassembled efficiently into its component.

Following these results and the specific characteristics of both vinyl sulfone and vinyl sulfonate units, an irreversible transportation system based on a “flashing energy ratchet” mechanism has been designed. Indeed, by capping a [2]rotaxane incorporating a sulfonate moiety *via* a thia-Michael addition to the vinyl sulfone group followed by decoupling of its sulfonate stopper, the macrocycle entered from one side of the rotaxane and was released through the other side, inducing a unidirectional motion or transport of this component with respect to the system. Furthermore, the *in situ* operation of the machine was also demonstrated.

Therefore, it can be concluded that the CAD chemistry of vinyl sulfonate is a promising instrument for the development of cleavable rotaxanes and could lead to more complex molecular machines since it is feasible to incorporate this chemistry to control the translation of a molecular component in interlocked systems through ratchet mechanisms.

3. Experimental section

3.1. General details

Unless otherwise noted, commercially available reagents, solvents and anhydrous solvents were used as purchased without further purification. Anhydrous THF was freshly distilled over Na/benzophenone.

TBTA,²⁶⁰ compounds **50**,²⁶¹ **58**,²⁶² **66**,²⁶³ **67**,²⁶⁴ **70**²⁶⁵ and **80**^{200b} were synthesized according to literature procedures.

TLC was performed on Merck Silica gel 60 F₂₅₄ aluminium sheets or Sigma-Aldrich (silica gel matrix, with fluorescent indicator 254 nm). The TLC plates were stained with potassium permanganate (1% w/v in water), cerium molybdate stain (Hanessian's stain), or ninhydrin (0.3% w/v in ethanol), or observed under UV light when applicable.

Flash column chromatography was performed with Silica gel 60 (Merck, 40-63 μm , 230-400 mesh ASTM, or Scharlab, Spain, Silica gel 60 (230-400 mesh) or VWR, 40-63 μm). Silica gel G preparative TLC plates were purchased from ANALTECH (20×20cm, 2000 micron) or from Silicycle (20×20cm, 1000 micron). Gel permeation chromatography was performed with Biobeads® SX-1 or Biobeads® SX-3 resin beads.

¹H and ¹³C NMR spectra were recorded at room temperature on a Varian Inova Unity (300 MHz), Varian Direct Drive (400 MHz or 500 MHz), Bruker Avance III HD NanoBay (400 MHz) or Bruker Avance Neo (400 MHz or 500 MHz) spectrometers at a constant temperature of 298 K. Chemical shifts are given in ppm and referenced to the signal of the residual protiated solvent (¹H: δ =7.26 for CDCl₃, δ =1.94 for CD₃CN, δ =2.05 for acetone-*d*₆, δ =2.55 for DMSO-*d*₆, and δ =3.31 for CD₃OD at room temperature) or the ¹³C signal of the solvents (¹³C: δ =77.16 for CDCl₃, δ =39.52 for DMSO-*d*₆ and δ =1.32 for CD₃CN) or to the signal of the residual TMS (¹H: δ =0.00). Coupling constant (*J*) values are given in Hz. Abbreviations indicating multiplicity were used as follow: m = multiplet, p = quintet, q = quartet, t = triplet, d = doublet, dd= doublet of doublets, s = singlet, br = broad. Signals were assigned by means of 2D NMR spectroscopy (COSY, HSQC, HMBC).

²⁶⁰ T. R. Chan, R. Hilgraf, K. B. Sharpless, V. V. Fokin, *Org. Lett.* **2004**, *6*, 2853-2855.

²⁶¹ H. W. Gibson, S.-H. Lee, P. T. Engen, P. Lecavalier, J. Sze, Y. X. Shen, M. Bheda, *J. Org. Chem.* **1993**, *58*, 3748-3756.

²⁶² O. M. Martina, S. Mecozzi, *Tetrahedron* **2007**, *63*, 5539-5547.

²⁶³ A. Bugarin, B. T. Connell, *Organometallics* **2008**, *27*, 4357-4369.

²⁶⁴ J. Baggerman, D. C. Jagesar, R. A. L. Vallée, J. Hofkens, F. C. De Schryver, F. Schelhase, F. Vögtle, A. M. Brouwer, *Chem. Eur. J.* **2007**, *13*, 1291-1299.

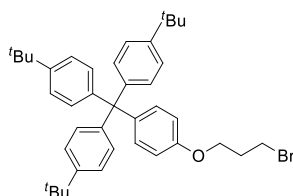
²⁶⁵ M. A. Pilkington-Miksa, S. Sarkar, M. J. Writer, S. E. Barker, P. A. Shamlou, S. L. Hart, H. C. Hailes, A. B. Tabor, *Eur. J. Org. Chem.* **2008**, 2900-2914.

Electrospray (ESI) HRMS spectra were recorded on a Waters Xevo G2-XS QTOF, a Waters SYNAP G2, a WATERS LCT Premier XE or a Bruker Maxis II spectrometer. Electronic impact (EI) HRMS spectra were recorded on a Bruker Maxis II spectrometer. Melting points were measured with a Stuart® melting point apparatus SMP3 and are uncorrected. IR spectra were recorded with a Perkin-Elmer Spectrum Two FTIR ATR spectrometer. UV-Vis spectra were recorded using an Analytik Jena Specord 200 plus.

HPLC experiments were carried out using an HPLC Agilent 1200 Infinity Series with a LiChroCART® 250-4 LiChrospher® 100 RP-8 (5 μm) analytical column. The column temperature was set at 20.0 °C. The wavelength selected for the peak detection was 330 nm and the flow was constant during the operation: 1.000 mL/min.

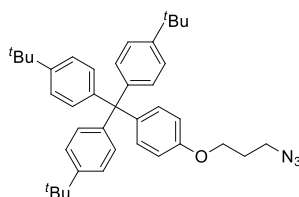
3.2. Synthetic procedures and characterization details

Compound 51:



Under Ar, to a solution of **50** (1.94 g, 3.84 mmol, 1.00 equiv.) in dry THF (120 mL) were added PPh_3 (2.01 g, 7.68 mmol, 2.00 equiv.) and 3-bromo-1-propanol (695 μL , 7.68 mmol, 2.00 equiv.). The mixture was cooled to 0 °C and was added a solution of diethyl azodicarboxylate in THF (40%, 3.00 mL, 7.68 mmol, 2.00 equiv.). The solution was allowed to warm up to room temperature and stirred for 18 h. The solvent was removed under reduced pressure and the crude was dissolved in CH_2Cl_2 (10 mL). Addition of MeOH (100 mL) afforded a precipitate, which was collected to give **51** (1.84 g, 77%) as a white solid. ^1H NMR (300 MHz, CDCl_3) δ =7.26 – 7.17 (m; 6H), 7.12 – 7.02 (m; 8H), 6.76 (d, J = 8.9 Hz; 2H), 4.06 (t, J = 5.8 Hz; 2H), 3.58 (t, J = 6.4 Hz; 2H), 2.29 (m; 2H), 1.29 (s; 27H). Spectral data agree with those previously reported values.⁸⁶

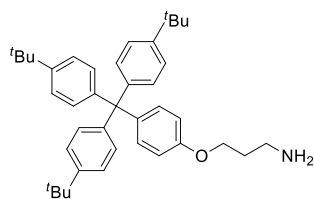
Compound 52:



Under inert atmosphere, to a suspension of **51** (726 mg, 1.16 mmol, 1.00 equiv.) in anhydrous DMF (30 mL) were added NaN_3 (226 mg, 3.48 mmol, 3.00 equiv.) and a catalytic amount of KI. The mixture

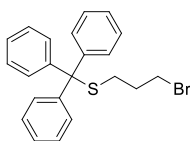
was stirred for 18 h at 70 °C. The resulting mixture was diluted with of CH₂Cl₂/H₂O (1:1, 200 mL). Layers were separated and the aqueous one was extracted with CH₂Cl₂ (2 × 100 mL). The combined organic phases were dried over anhydrous Na₂SO₄ and the solvent was evaporated under vacuum. The crude material was purified by column chromatography (SiO₂, CH₂Cl₂/hexane 1:1) to give **52** (553 mg, 81%) as a white solid. ¹H NMR (300 MHz, CDCl₃) δ=7.27 – 7.19 (m; 6H), 7.13 – 7.04 (m; 8H), 6.74 (d, *J* = 8.7 Hz; 2H), 4.01 (t, *J* = 5.9 Hz; 2H), 3.50 (t, *J* = 6.7 Hz; 2H), 2.02 (m; 2H), 1.30 (s; 27H). Spectral data agree with those previously reported values.²⁶⁶

Compound 53a:



Under an Ar atmosphere, to a solution of **52** (555 mg, 0.940 mmol, 1.00 equiv.) in dry CH₂Cl₂ (50 mL) were added dry MeOH (25 mL) and Pd/C (13%, 70 mg). The atmosphere was changed to H₂ and the mixture was stirred for 18 h at room temperature. Then, the mixture was filtered through a pad of Celite®. The solvent was removed under reduced pressure affording **53a** (518 mg, 98%) as a white solid. ¹H NMR (300 MHz, CD₃OD): δ=7.29 – 7.17 (m; 6H), 7.14 – 7.01 (m; 8H), 6.82 (d, *J* = 8.8 Hz; 2H), 4.10 (t, *J* = 5.5 Hz; 2H), 3.12 (t, *J* = 6.2 Hz; 2H), 2.12 (m; 2H), 1.31 (s; 27H). Spectral data agree with those previously reported values.²⁶⁷

Compound 55:



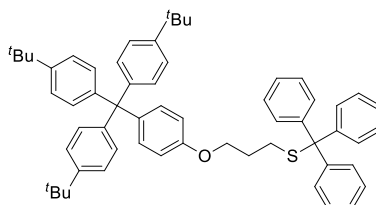
Under inert atmosphere, to a solution of triphenylmethanethiol (1.00 g, 3.61 mmol, 1.00 equiv.) in dry THF (10 mL), cooled in a water-ice bath, was added a solution of LiHMDS in THF (1 M, 3.60 mL, 3.61 mmol, 1.00 equiv.). The solution was stirred until the thiolate precipitated; then, the suspension was allowed to warm up to room temperature. To this suspension, was added 1,3-dibromopropane (480 μL, 4.70 mmol, 1.30 equiv.). The mixture was stirred for 30 minutes at room temperature and the solvent was removed under reduced pressure. The crude was dissolved in EtOAc (100 mL) and subsequently washed with H₂O (3 × 60 mL). The organic phase was dried over anhydrous Na₂SO₄ and

²⁶⁶ J.-P. Collin, J.-P. Sauvage, Y. Trolez, K. Rissanen, *New J. Chem.* **2009**, 33, 2148-2154.

²⁶⁷ H. Zheng, W. Zhou, J. Lv, X. Yin, Y. Li, H. Liu, Y. Li, *Chem. Eur. J.* **2009**, 15, 13253-13262.

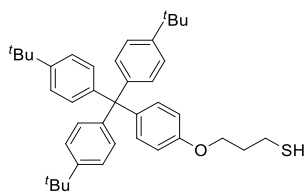
the solvent was evaporated under vacuum to afford **55** (1.43 g, 99%) as a white solid. ^1H NMR (300 MHz, CDCl_3) δ =7.49 – 7.12 (m; 15H), 3.29 (t, J = 6.6 Hz; 2H), 2.31 (t, J = 7.0 Hz; 2H), 1.78 (m; 2H). Spectral data agree with those previously reported values.²⁶⁸

Compound 56:



To a solution of **55** (1.40 g, 3.52 mmol, 2.00 equiv.) in anhydrous DMF (70 mL) were added **50** (890 mg, 1.76 mmol, 1.00 equiv.) and Cs_2CO_3 (2.90 g, 8.80 mmol, 5.00 equiv.) under Ar. The suspension was stirred for 3 days at 90 °C. The solvent was removed under reduced pressure and the crude was dissolved in a mixture of $\text{CH}_2\text{Cl}_2/\text{H}_2\text{O}$ (2:1, 225 mL). Layers were separated and the organic one was washed with H_2O (2 × 75 mL). The organic phase was dried over anhydrous Na_2SO_4 and the solvent was evaporated under vacuum. The crude material was purified by column chromatography (SiO_2 , CH_2Cl_2 /hexane 1:4 to 2:3) to afford **56** (1.44 g, 99%) as a white solid. M.p. 168 °C (decomp). ^1H NMR (500 MHz, CDCl_3) δ =7.50 – 7.45 (m; 6H), 7.33 – 7.12 (m; 23H), 6.74 (d, J = 8.7 Hz; 2H), 3.95 (m; 2H), 2.43 (m; 2H), 1.86 (m; 2H), 1.37 (s; 27H). ^{13}C NMR (126 MHz, CDCl_3) δ =156.70, 148.38, 145.02, 144.33, 139.68, 132.32, 130.87, 129.72, 127.99, 126.73, 124.18, 113.14, 66.72, 66.08, 63.21, 34.43, 31.55, 28.70, 28.55. IR (neat): ν =2960, 2856, 1605, 1504, 1246 cm^{-1} . HR-MS (ESI⁺): m/z : 843.4586 [$\text{M}+\text{Na}$]⁺ (calcd for $\text{C}_{59}\text{H}_{64}\text{NaOS}$: 843.4576).

Compound 53b:

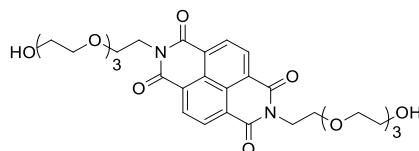


Under Ar, to a solution of **56** (1.40 g, 1.70 mmol, 1.00 equiv.) in dry CH_2Cl_2 (40 mL) were added $\text{CF}_3\text{CO}_2\text{H}$ (20 mL) and Et_3SiH (5 mL). The solution was stirred for 4 h at room temperature. The solvent was removed under reduced pressure and the crude was dissolved in toluene (10 mL) and evaporated again under vacuum. The crude material was purified by column chromatography (SiO_2 , CH_2Cl_2 /hexane 1:4 to 1:1) to afford **53b** (923 mg, 94%) as a white solid. M.p. 227–230 °C. ^1H NMR (400 MHz, CDCl_3) δ =7.25

²⁶⁸ Y. Lina, A. Favre-Réguillon, S. Pellet-Rostaing, M. Lemaire, *Tetrahedron Lett.* **2007**, *48*, 3463-3466.

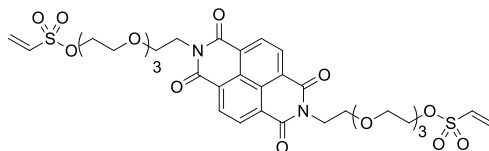
– 7.20 (m; 6H), 7.11 – 7.06 (m; 8H), 6.75 (d, $J = 8.8$ Hz; 2H), 4.04 (t, $J = 5.9$ Hz; 2H), 2.72 (m; 2H), 2.05 (m; 2H), 1.38 (t, $J = 8.1$ Hz; 1H), 1.29 (s; 27H). ^{13}C NMR (101 MHz, CDCl_3) δ =156.76, 148.44, 144.28, 139.87, 132.41, 130.87, 124.17, 113.10, 65.61, 63.21, 34.44, 33.61, 31.54, 21.48. IR (neat): ν =2960, 2855, 1606, 1505, 1245 cm^{-1} . HR-MS (ESI⁺): m/z : 617.3221 $[\text{M}+\text{K}]^+$ (calcd for $\text{C}_{40}\text{H}_{50}\text{KOS}$: 617.3219).

Compound 59:



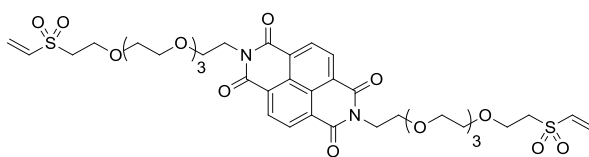
Under inert atmosphere, to a solution of **58** (5.00 g, 25.9 mmol, 2.50 equiv.) in anhydrous DMF (100 mL) was added 1,4,5,8-naphthalenetetracarboxylic dianhydride (2.78 g, 10.4 mmol, 1.00 equiv.). The solution was stirred for 3 days at 90 °C. The solvent was evaporated under reduced pressure and the crude material was purified by column chromatography (SiO_2 , $\text{CH}_2\text{Cl}_2/\text{MeOH}$ 95:5) to give **59** (4.89 g, 76%) as a brown solid. ^1H NMR (400 MHz, CDCl_3): δ =8.59 (s; 4H), 4.33 (t, $J = 5.8$ Hz; 4H), 3.75 (t, $J = 5.8$ Hz; 4H), 3.62 (m; 4H), 3.56 – 3.47 (m; 16H), 3.42 (m; 4H). Spectral data agree with those previously reported values.²⁶⁹

Compound 60a:

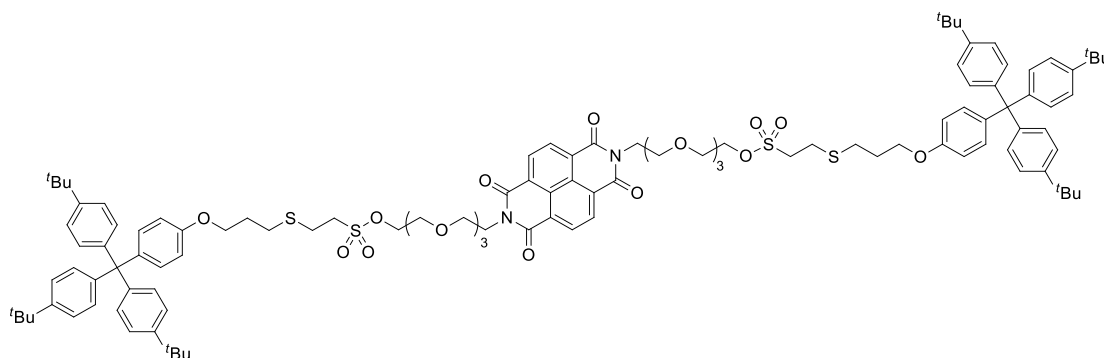


Under Ar, to a solution of **59** (874 mg, 1.41 mmol, 1.00 equiv.) in anhydrous CH_2Cl_2 (10 mL) at 0 – 4 °C, were added Et_3N (2.00 mL, 14.1 mmol, 10.0 equiv.) and a solution of 2-chloroethanesulfonyl chloride (450 μL , 4.23 mmol, 3.00 equiv.) in dry CH_2Cl_2 (10 mL). The solution was stirred for 1 h at 0 - 4 °C and then, the solvent was removed under reduced pressure. The crude material was purified by column chromatography (SiO_2 , $\text{CH}_2\text{Cl}_2/\text{MeOH}$ 98:2) to give **60a** (1.11 g, 99%) as a yellow oil. ^1H NMR (500 MHz, CDCl_3): δ =8.64 (s; 4H), 6.55 (dd, $J = 16.7, 10.0$ Hz; 2H), 6.32 (d, $J = 16.7$ Hz; 2H), 6.07 (d, $J = 10.0$ Hz; 2H), 4.38 (t, $J = 6.0$ Hz; 4H), 4.17 (t, $J = 6.0$ Hz; 4H), 3.79 (t, $J = 6.0$ Hz; 4H), 3.68 – 3.63 (m; 8H), 3.58 – 3.52 (m; 12H). ^{13}C NMR (126 MHz, CDCl_3): δ =162.72, 132.56, 130.88, 130.04, 126.56, 126.46, 70.62, 70.57, 70.50, 70.06, 69.69, 68.68, 67.72, 39.54. IR (neat): ν =2871, 1705, 1664, 1333, 1170, 731 cm^{-1} . HR-MS (ESI⁺): m/z : 799.2075 $[\text{M}+\text{H}]^+$ (calcd for $\text{C}_{34}\text{H}_{43}\text{N}_2\text{O}_{16}\text{S}_2$: 799.2054).

²⁶⁹ J. G. Hansen, N. Feeder, D. G. Hamilton, M. J. Gunter, J. Becher, J. K. M. Sanders, *Org. Lett.* **2000**, 2, 449-452.

Compound 60b:

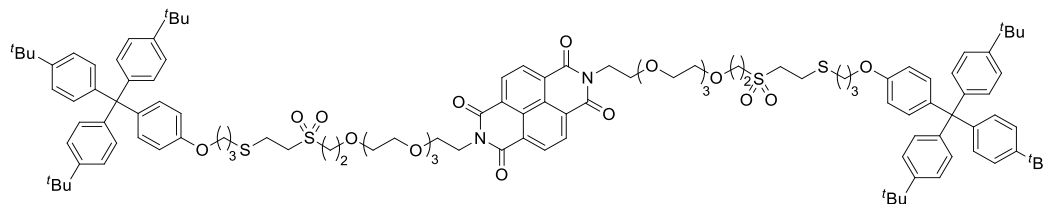
To a solution of **59** (946 mg, 1.53 mmol, 1.00 equiv.) in anhydrous THF (160 mL) were added divinyl sulfone (1.30 mL, 12.2 mmol, 8.00 equiv.) and ^tBuOK (68 mg, 0.61 mmol, 0.40 equiv.) under inert atmosphere. The suspension was stirred for 5 h at room temperature. The solvent was removed under vacuum. The crude material was purified by column chromatography (SiO₂, CH₂Cl₂/MeOH 95:5) to give **60b** (933 mg, 71%) as a yellow oil. ¹H NMR (400 MHz, CDCl₃): δ=8.71 (s; 4H), 6.78 (dd, *J* = 16.6, 9.9 Hz; 2H), 6.34 (d, *J* = 16.6 Hz; 2H), 6.05 (d, *J* = 9.9 Hz; 2H), 4.42 (t, *J* = 5.9 Hz; 4H), 3.89 – 3.79 (m; 8H), 3.68 (m; 4H), 3.61 – 3.52 (m; 20H), 3.22 (t, *J* = 5.7 Hz; 4H). ¹³C NMR (101 MHz, CDCl₃): δ=162.90, 138.09, 131.04, 128.72, 126.80, 126.67, 70.68 (×2), 70.60, 70.56, 70.31, 70.18, 67.85, 64.73, 55.10, 39.66. IR (neat): ν=2872, 1705, 1666, 1315, 1124, 767 cm⁻¹. HR-MS (ESI⁺): *m/z*: 872.2981 [M+NH₄]⁺ (calcd for C₃₈H₅₄N₃O₁₆S₂: 872.2945).

Compound 61a:

Under an Ar atmosphere, to a solution **60a** (20 mg, 0.025 mmol, 1.0 equiv.) in CHCl₃ (6 mL) were added **53b** (58 mg, 0.10 mmol, 4.0 equiv.), a few drops of 2-propanol and 2 drops of Et₃N. The solution was stirred for 18 h at room temperature. The solvent was removed under reduced pressure. The crude material was purified by column chromatography (SiO₂, CH₂Cl₂/MeOH 98:2) to afford **61a** (45 mg, 92%) as a yellow solid. M.p. 199 °C (decomp). ¹H NMR (500 MHz, CDCl₃): δ=8.74 (s; 4H), 7.25 – 7.21 (m; 12H), 7.11 – 7.06 (m; 16H), 6.75 (d, *J* = 8.6 Hz; 4H), 4.45 (t, *J* = 6.0 Hz; 4H), 4.34 (m; 4H), 4.02 (t, *J* = 5.9 Hz; 4H), 3.84 (t, *J* = 6.0 Hz; 4H), 3.74 – 3.68 (m; 8H), 3.63 – 3.58 (m; 12H), 3.41 (m; 4H), 2.95 (m; 4H), 2.75 (t, *J* = 7.2 Hz; 4H), 2.05 (p, *J* = 6.2 Hz; 4H), 1.30 (s; 54H). ¹³C NMR (126 MHz, CDCl₃): δ=162.98, 156.63, 148.43, 144.24, 139.94, 132.41, 131.13, 130.84, 126.89, 126.76, 124.17, 113.07, 70.79, 70.74, 70.27, 69.59, 69.13, 67.95, 65.86, 63.18, 50.81, 39.75, 34.42, 31.52, 29.83, 29.28, 28.98, 25.30. IR (neat):

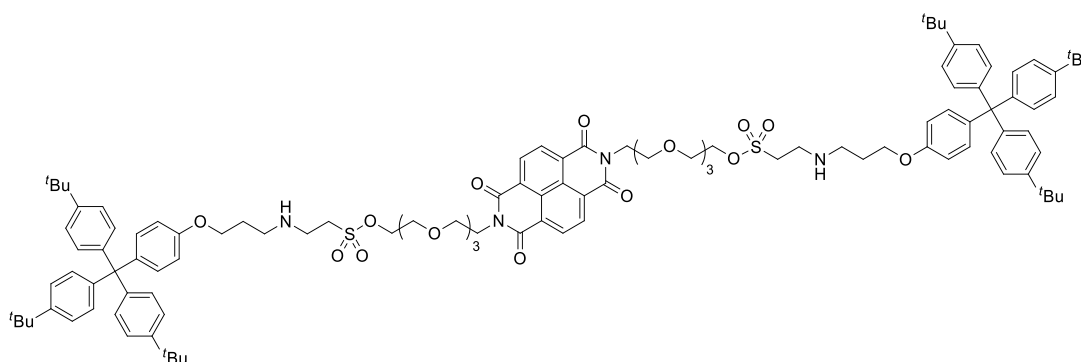
$\nu=2957, 2867, 1706, 1667, 1505, 1245, 823 \text{ cm}^{-1}$. HR-MS (ESI⁺): m/z : 1955.9268 [M+H]⁺ (calcd for C₁₁₄H₁₄₃N₂O₁₈S₄: 1955.9219).

Compound 61b:



Under inert atmosphere, to a solution of **60b** (20 mg, 0.023 mmol, 1.0 equiv.) in CHCl₃ (6 mL) were added **53b** (54 mg, 0.094 mmol, 4.0 equiv.), a few drops of 2-propanol and 2 drops of Et₃N. The solution was stirred for 72 h at room temperature. The solvent was removed under reduced pressure. The crude material was purified by column chromatography (SiO₂, CH₂Cl₂/MeOH 98:2) to afford **61b** (42 mg, 89%) as a yellow solid. M.p. 199–200 °C. ¹H NMR (500 MHz, CDCl₃): $\delta=8.74$ (s; 4H), 7.24 – 7.21 (m; 12H), 7.11 – 7.05 (m; 16H), 6.75 (d, $J = 8.6$ Hz; 4H), 4.45 (t, $J = 6.0$ Hz; 4H), 4.02 (t, $J = 5.9$ Hz; 4H), 3.88 (t, $J = 6.0$ Hz; 4H), 3.83 (t, $J = 6.0$ Hz; 4H), 3.69 (m; 4H), 3.64 – 3.55 (m; 20H), 3.38 (m; 4H), 3.21 (t, $J = 5.9$ Hz; 4H), 2.94 (m; 4H), 2.75 (t, $J = 7.2$ Hz; 4H), 2.05 (p, $J = 6.2$ Hz; 4H), 1.30 (s; 54H). ¹³C NMR (126 MHz, CDCl₃): $\delta=162.98, 156.65, 148.43, 144.25, 139.90, 132.39, 131.13, 130.83, 126.89, 126.75, 124.17, 113.08, 70.75, 70.74, 70.66, 70.37, 70.23, 67.92, 65.88, 64.91, 63.18, 55.08, 54.01, 39.73, 34.42, 31.52, 29.83, 29.27, 28.85, 24.09$. IR (neat): $\nu=2960, 2867, 1706, 1667, 1505, 1245, 1111, 824 \text{ cm}^{-1}$. HR-MS (ESI⁺): m/z : 2011.9944 [M+H]⁺ (calcd for C₁₁₈H₁₅₁N₂O₁₈S₄: 2011.9845).

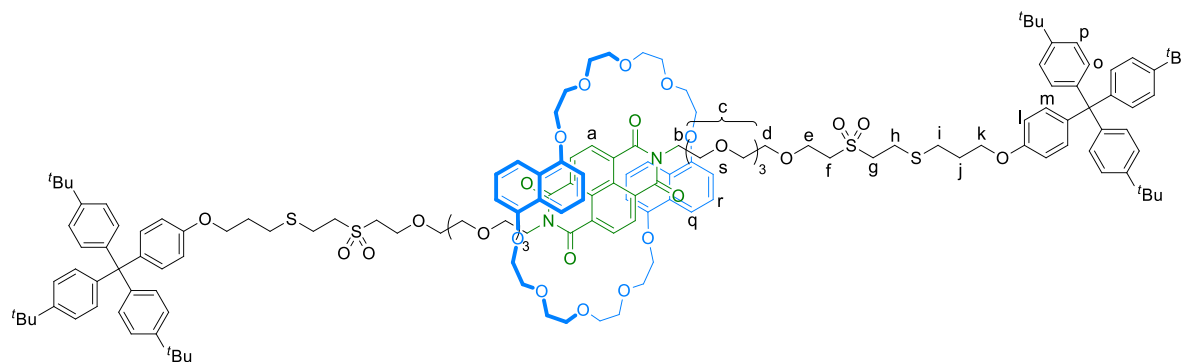
Compound 61c:



Under Ar, to a solution of **60a** (20 mg, 0.025 mmol, 1.0 equiv.) in CHCl₃ (1 mL) were a solution of **53a** (52 mg, 0.092 mmol, 3.7 equiv.) in CHCl₃/MeOH (3:2, 5 mL) and 2 drops of Et₃N. The solution was stirred for 4 h at room temperature. The solvent was evaporated under reduced pressure. The crude material was purified by column chromatography (SiO₂, CH₂Cl₂/MeOH 95:5) to afford **61c** (44 mg, 92%) as a yellow solid. M.p. 219 °C (decomp). ¹H NMR (500 MHz, CDCl₃): $\delta=8.74$ (s; 4H), 7.24 – 7.20 (m; 12H),

A solution of **60a** (15 mg, 0.020 mmol, 1.0 equiv.) and **62** (25 mg, 0.040 mmol, 2.0 equiv.) in CHCl_3 (15 mL) was stirred for 10 minutes at room temperature. The solvent was removed under reduced pressure. The crude was redissolved in CHCl_3 (1 mL). Under Ar, to this solution were added a few drops of 2-propanol, **53b** (46 mg, 0.080 mmol, 4.0 equiv.) and 2 drops of Et_3N . The mixture was stirred for 18 h at room temperature. The solvent was evaporated under reduced pressure. The crude material was purified by a preparative TLC (SiO_2 , $\text{CH}_2\text{Cl}_2/\text{MeOH}$ 99:1) to afford **63a** (39 mg, 80%) as a red solid. M.p. 177–179 °C. ^1H NMR (500 MHz, CDCl_3): δ =8.26 (s; 4H, H_a), 7.24 – 7.20 (m; 12H, H_m), 7.09 – 7.05 (m; 16H, H_{l+k}), 6.84 (d, J = 8.4 Hz; 4H, H_n), 6.75 (d, J = 8.6 Hz; 4H, H_j), 6.65 (t, J = 7.9 Hz; 4H, H_o), 6.09 (d, J = 7.6 Hz; 4H, H_p), 4.37 (m; 4H, H_d), 4.32 (t, J = 6.4 Hz; 4H, H_b), 4.02 – 3.68 (m; 60H, $\text{H}_{\text{macCH}_2+\text{c+i}}$), 3.41 (m; 4H, H_e), 2.96 (m; 4H, H_f), 2.74 (t, J = 7.2 Hz; 4H, H_g), 2.04 (p, J = 6.6 Hz, 4H; H_h), 1.29 (s, 54H; H_{tBu}). ^{13}C NMR (126 MHz, CDCl_3): δ =163.26, 156.66, 153.14, 148.45, 144.25, 139.93, 132.42, 130.85, 130.73, 125.14, 124.88, 124.18, 123.80, 114.24, 113.08, 110.14, 103.63, 71.46, 71.31, 70.99, 70.89, 70.88, 70.39, 70.01, 69.65, 69.22, 67.50, 65.88, 63.19, 50.85, 39.23, 34.44, 31.53, 29.85, 29.30, 29.00, 25.33. IR (neat): ν =2958, 2868, 1662, 1507, 1359, 1268, 766 cm^{-1} . HR-MS (ESI⁺): m/z : 2614.1968 [$\text{M}+\text{Na}$]⁺ (calcd for $\text{C}_{150}\text{H}_{186}\text{N}_2\text{O}_{28}\text{S}_4\text{Na}$: 2614.1967); 1318.5923 [$\text{M}+2\text{Na}$]²⁺ (calcd for $\text{C}_{150}\text{H}_{186}\text{N}_2\text{O}_{28}\text{S}_4\text{Na}_2$: 1318.5930).

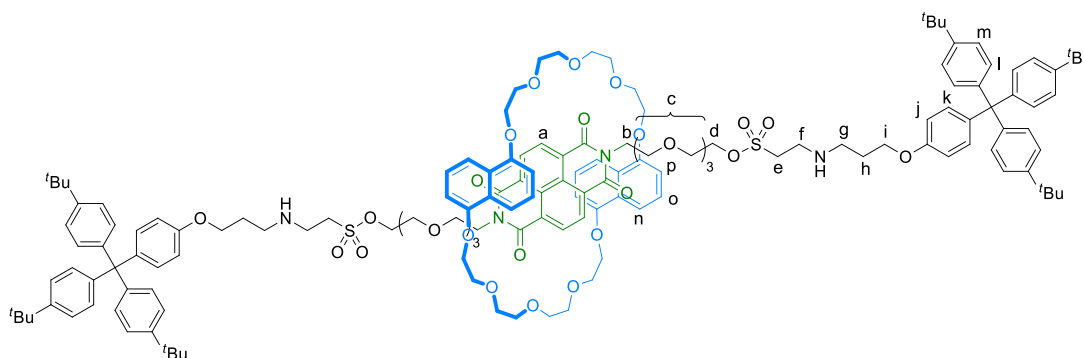
Compound 63b:



A solution of **60b** (19 mg, 0.022 mmol, 1.0 equiv.) and **62** (28 mg, 0.044 mmol, 2.0 equiv.) in CHCl_3 (20 mL) was stirred for 10 minutes at room temperature. The solvent was removed under reduced pressure. The crude was redissolved in CHCl_3 (1 mL). Under Ar, to this solution were added a few drops of 2-propanol, **53b** (51 mg, 0.089 mmol, 4.0 equiv.) and 2 drops of Et_3N . The mixture was stirred for 26 h at room temperature. The solvent was evaporated under reduced pressure. The crude material was purified by column chromatography (SiO_2 , $\text{EtOAc}/2$ -propanol 98:2, to $\text{CH}_2\text{Cl}_2/\text{MeOH}$ 95:5) and subsequently by gel permeation chromatography (Bio-Beads® S-X3, CH_2Cl_2) to afford **63b** (42 mg, 71%) as a red solid. M.p. 175–177 °C. ^1H NMR (500 MHz, CDCl_3): δ =8.25 (s; 4H, H_a), 7.24 – 7.20 (m; 12H, H_p), 7.10 – 7.05 (m; 16H, H_{m+o}), 6.84 (d, J = 8.4 Hz; 4H, H_q), 6.74 (d, J = 8.6 Hz; 4H, H_l), 6.65 (t, J = 8.3 Hz; 4H,

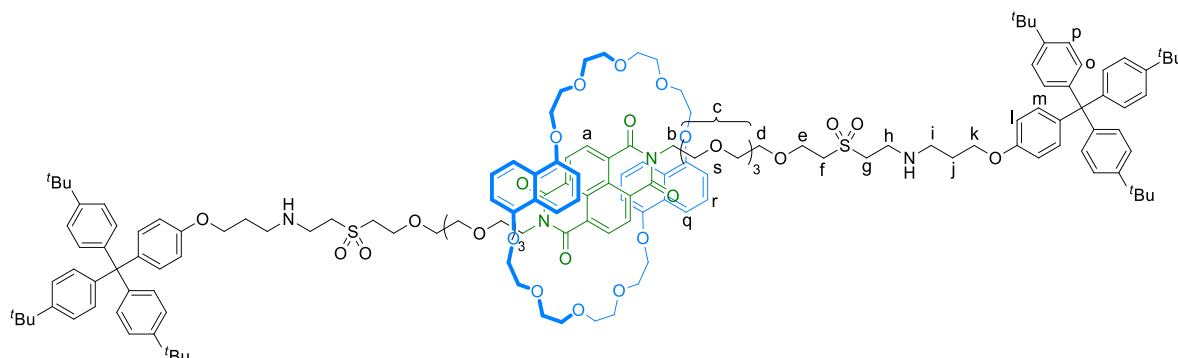
H_r), 6.10 (d, *J* = 7.5 Hz; 4H, H_s), 4.31 (t, *J* = 6.4 Hz; 4H, H_b), 4.07 – 3.54 (m; 72H, H_{macCH2+c+d+e+g+k}), 3.34 – 3.19 (m; 8H, H_{h+lf}), 2.95 (m; 4H, H_l), 2.25 (m; 4H, H_j), 1.29 (s; 54H, H_{tBu}). ¹³C NMR (126 MHz, CDCl₃): δ=163.25, 156.37, 153.12, 148.48, 144.19, 140.24, 132.47, 130.83, 130.72, 125.14, 124.86, 124.19, 124.16, 123.82, 114.24, 113.07, 103.67, 71.48, 71.31, 70.93, 70.87, 70.68, 70.39, 70.35, 70.01, 68.12, 67.53, 65.92, 64.92, 63.20, 54.57, 49.79, 48.46, 43.68, 39.21, 34.43, 31.53, 29.84, 23.04. IR (neat): ν=2924, 2867, 1659, 1387, 1095, 766 cm⁻¹. HR-MS (ESI⁺): *m/z*: 2670.2693 [M+Na]⁺ (calcd for C₁₅₄H₁₉₄N₂O₂₈S₄Na: 2670.2599).

Compound 63c:



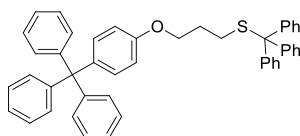
A solution of **60a** (19 mg, 0.024 mmol, 1.0 equiv.) and **62** (30 mg, 0.048 mmol, 2.0 equiv.) in CHCl₃ (22 mL) was stirred for 10 minutes at room temperature. The solvent was removed under reduced pressure. The crude was redissolved in CHCl₃ (1 mL). Under Ar, to this solution were added a solution of **53a** (53 mg, 0.095 mmol, 4.0 equiv.) in CHCl₃/MeOH (1:2, 3 mL) and 2 drops of Et₃N. The mixture was stirred for 16 h at room temperature. The solvent was evaporated under reduced pressure. The crude material was purified by column chromatography (SiO₂, CH₂Cl₂/MeOH 95:5) and subsequently by gel permeation chromatography (Bio-Beads® S-X3, CH₂Cl₂) to afford **63c** (38 mg, 62%) as a red solid. M.p. 238 °C (decomp). ¹H NMR (500 MHz, CDCl₃): δ=8.25 (s; 4H, H_a), 7.24 – 7.19 (m; 12H, H_m), 7.09 – 7.04 (m; 16H, H_{l+k}), 6.83 (d, *J* = 8.4 Hz; 4H, H_n), 6.75 (d, *J* = 8.6 Hz; 4H, H_j), 6.65 (t, *J* = 7.8 Hz; 4H, H_o), 6.10 (d, *J* = 7.7 Hz; 4H, H_p), 4.40 – 4.27 (m; 8H, H_{b+d}), 4.03 – 3.52 (m; 64H, H_{macCH2+c+e+i}), 3.25 (m; 4H, H_f), 2.95 (m; 4H, H_g), 2.04 (m; 4H, H_h), 1.29 (s; 54H, H_{tBu}). ¹³C NMR (126 MHz, CDCl₃): δ=163.26, 156.63, 153.13, 148.42, 144.25, 139.95, 132.38, 130.84, 130.72, 125.13, 124.84, 124.17, 123.83, 123.78, 114.24, 113.10, 103.63, 71.46, 71.30, 70.94, 70.81, 70.77, 70.36, 70.00, 69.09, 68.15, 67.58, 67.52, 65.97, 63.19, 46.98, 43.74, 39.26, 34.43, 31.53, 29.84, 22.83. IR (neat): ν=2958, 2868, 1662, 1507, 1267, 1107, 1084, 766 cm⁻¹. HR-MS (ESI⁺): *m/z*: 2558.2954 [M+H]⁺ (calcd for C₁₅₀H₁₈₉N₄O₂₈S₂: 2558.2930).

Compound 63d:



A solution of **60b** (18 mg, 0.021 mmol, 1.0 equiv.) and **62** (27 mg, 0.042 mmol, 2.0 equiv.) in CHCl_3 (20 mL) was stirred for 10 minutes at room temperature. The solvent was removed under reduced pressure. The crude was redissolved in CHCl_3 (500 μL). Under inert atmosphere, to this solution were added a solution of **53a** (47 mg, 0.084 mmol, 4.0 equiv.) in $\text{CHCl}_3/\text{MeOH}$ (1:1, 2 mL) and 2 drops of Et_3N . The mixture was stirred for 72 h at room temperature. The solvent was evaporated under reduced pressure. The crude material was purified by column chromatography (SiO_2 , $\text{CH}_2\text{Cl}_2/\text{MeOH}$ 95:5) and subsequently by gel permeation chromatography (Bio-Beads[®] S-X3, CH_2Cl_2) to afford **63d** (33 mg, 60%) as a red solid. M.p. 177–179 °C. ^1H NMR (500 MHz, CDCl_3): δ =8.25 (s; 4H, H_a), 7.23 – 7.18 (m; 12H, H_p), 7.09 – 7.03 (m; 16H, H_{m+o}), 6.83 (d, $J = 8.4$ Hz; 4H, H_q), 6.76 (d, $J = 8.7$ Hz; 4H, H_l), 6.65 (t, $J = 7.9$ Hz; 4H, H_r), 6.09 (d, $J = 7.5$ Hz; 4H, H_s), 4.31 (t, $J = 6.4$ Hz; 4H, H_b), 4.06 – 3.48 (m; 72H, $H_{\text{macCH}_2+c+d+e+g+k}$), 3.36 – 3.23 (m; 8H, H_{h+f}), 2.99 (m; 4H, H_i), 2.09 (m; 4H, H_j), 1.29 (s; 54H, $H_{t\text{Bu}}$). ^{13}C NMR (126 MHz, CDCl_3): δ =163.26, 156.61, 153.13, 148.43, 144.24, 139.98, 132.39, 130.83, 130.73, 126.00, 125.14, 124.85, 124.17, 123.81, 114.25, 113.10, 103.65, 71.47, 71.32, 70.92, 70.87, 70.60, 70.56, 70.37, 70.35, 70.00, 67.56, 65.89, 64.88, 63.18, 54.72, 47.64, 46.91, 42.72, 39.23, 34.43, 31.52, 29.84, 19.36. IR (neat): ν =2958, 2868, 1661, 1507, 1267, 1107, 1084, 767 cm^{-1} . HR-MS (ESI⁺): m/z : 2614.3564, $[\text{M}+\text{H}]^+$ (calcd for $\text{C}_{154}\text{H}_{197}\text{N}_4\text{O}_{28}\text{S}_2$: 2614.3556).

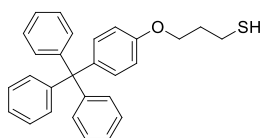
Compound 64:



Under Ar, to a solution of **55** (2.20 g, 5.53 mmol, 2.00 equiv.) in dry DMF (80 mL) were added 4-tritylphenol (1.36 g, 2.76 mmol, 1.00 equiv.) and K_2CO_3 (1.9 g, 14 mmol, 5.0 equiv.). The mixture was stirred for 24 h at 90 °C. The solvent was evaporated under vacuum. The crude was dissolved in $\text{CH}_2\text{Cl}_2/\text{H}_2\text{O}$ (1:1, 200 mL). Layers were separated and the aqueous one was extracted with CH_2Cl_2 (2 \times 100 mL). The combined organic phases were dried over anhydrous Na_2SO_4 and the solvent was

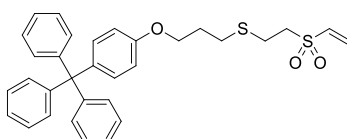
removed under reduced pressure. The crude material was purified by column chromatography (SiO₂, CH₂Cl₂/hexane 1:1) to afford **64** (1.80 g, 99%) as a white solid. M.p. 175–177 °C. ¹H NMR (300 MHz, CDCl₃) δ=7.44 – 7.36 (m; 6H) 7.28 – 7.04 (m; 26H), 6.69 (d, *J* = 8.6 Hz; 2H), 3.88 (t, *J* = 6.0 Hz; 2H), 2.35 (t, *J* = 7.1 Hz; 2H), 1.79 (m; 2H). ¹³C NMR (75 MHz, CDCl₃) δ=156.85, 147.19, 145.00, 139.07, 132.26, 131.24, 129.71, 127.99, 127.55, 126.73, 125.97, 113.39, 66.73, 66.09, 64.44, 28.65, 28.51. IR (neat): ν=3055, 1666, 1490, 1246, 746, 700 cm⁻¹. HR-MS (ESI⁺): *m/z*: 675.2696 [M+Na]⁺ (calcd for C₄₇H₄₀NaOS: 675.2698).

Compound 53c:



Under Ar, to a solution of **64** (1.75 g, 2.68 mmol, 1.00 equiv.) in dry CH₂Cl₂ (30 mL) were added CF₃CO₂H (15 mL) and Et₃SiH (5 mL). The solution was stirred for 4 h at room temperature. The solvent was removed under reduced pressure, then, the crude was dissolved in toluene (10 mL) and evaporated again under vacuum. The crude material was purified by column chromatography (SiO₂, CH₂Cl₂/hexane 30:70) to afford **53c** (979 mg, 89%) as a white solid. M.p. 176–178 °C. ¹H NMR (400 MHz, CDCl₃) δ=7.28 – 7.15 (m; 15H), 7.10 (d, *J* = 8.7 Hz; 2H), 6.77 (m; 2H), 4.04 (t, *J* = 5.9 Hz; 2H), 2.72 (m; 2H), 2.06 (p, *J* = 5.6 Hz; 2H), 1.38 (t, *J* = 8.1 Hz; 1H). ¹³C NMR (101 MHz, CDCl₃) δ=156.88, 147.14, 139.22, 132.33, 131.23, 127.54, 125.97, 113.35, 65.58, 64.43, 33.54, 21.44. IR (neat): ν=3055, 2926, 1666, 1507, 1246, 700 cm⁻¹. HR-MS (ESI⁺): *m/z*: 449.1339 [M+K]⁺ (calcd for C₂₈H₂₆KOS: 449.1341).

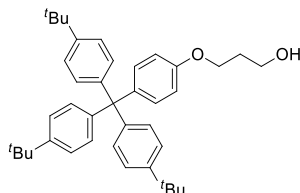
Compound 53d:



Under an Ar atmosphere, to a solution of **53c** (434 mg, 1.05 mmol, 1.00 equiv.) in dry CH₂Cl₂ (25 mL) were added divinyl sulfone (848 μL, 8.45 mmol, 8.00 equiv.) and Et₃N (1.5 mL, 11 mmol, 10 equiv.). The solution was stirred for 20 h at room temperature. The solvent was removed under reduced pressure. The crude was dissolved in the minimum amount of CH₂Cl₂ and MeOH (100 mL) was added. CH₂Cl₂ was removed under reduced pressure allowing the product to precipitate. The solid was collected and washed with cold MeOH to afford **53d** (482 mg, 86%) as a white solid. M.p. 132–133 °C. ¹H NMR (400 MHz, CDCl₃) δ=7.27 – 7.14 (m; 15H), 7.11 (m; 2H), 6.76 (d, *J* = 8.7 Hz; 2H), 6.61 (dd, *J* = 16.6, 9.8 Hz; 1H), 6.42 (d, *J* = 16.6 Hz; 1H), 6.12 (d, *J* = 9.8 Hz; 1H), 4.01 (t, *J* = 5.9 Hz; 2H), 3.23 (m; 2H),

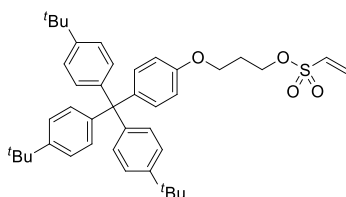
2.87 (m; 2H), 2.73 (t, $J = 7.1$ Hz; 2H), 2.03 (p, $J = 5.6$ Hz; 2H). ^{13}C NMR (101 MHz, CDCl_3) δ =156.69, 147.07, 139.34, 136.06, 132.32, 131.32, 131.17, 127.53, 125.96, 113.31, 65.69, 64.39, 54.48, 29.18, 28.94, 24.32. IR (neat): ν =3055, 2923, 1606, 1507, 1318, 1246, 702 cm^{-1} . HR-MS (ESI⁺): m/z : 551.1710 $[\text{M}+\text{Na}]^+$ (calcd for $\text{C}_{32}\text{H}_{32}\text{NaO}_3\text{S}_2$: 551.1691).

Compound 65:



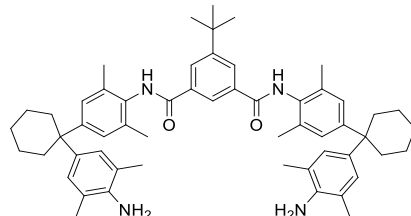
To a solution of **50** (1.62 g, 3.21 mmol, 1.00 equiv.) in dry DMF (130 mL) were added Cs_2CO_3 (5.00 g, 16.0 mmol, 5.00 equiv.) and 3-bromo-1-propanol (580 μL , 6.42 mmol, 2.00 equiv.) under inert atmosphere. The suspension was stirred at 90 °C for 3 days. The solvent was removed under reduced pressure. The crude was then dissolved in a mixture of $\text{CH}_2\text{Cl}_2/\text{H}_2\text{O}$ (1:1, 450 mL). Layers were separated and the organic one was washed with H_2O (2 \times 150 mL). The organic layer was dried over anhydrous Na_2SO_4 and the solvent was evaporated under vacuum. The crude material was purified by column chromatography (SiO_2 , $\text{CH}_2\text{Cl}_2/\text{MeOH}$ 97:3) to afford **65** (1.44 g, 80%) as a white solid. ^1H NMR (300 MHz, CDCl_3) δ =7.25 – 7.20 (m; 6H), 7.11 – 7.05 (m; 8H), 6.77 (d, $J = 8.7$ Hz; 2H), 4.10 (t, $J = 5.9$ Hz; 2H), 3.86 (q, $J = 5.6$ Hz; 2H), 2.03 (m; 2H), 1.78 (t, $J = 5.3$ Hz; 1H), 1.30 (s; 27H). Spectral data agree with those previously reported values.⁸⁶

Compound 53e:

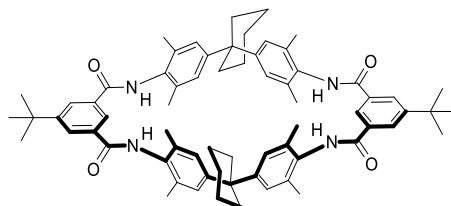


Under an Ar atmosphere, to a solution of **65** (1.44 g, 2.55 mmol, 1.00 equiv.) in anhydrous CH_2Cl_2 (125 mL), cooled in a water-ice bath, were added Et_3N (1.8 mL, 13 mmol, 5.0 equiv.) and a solution of 2-chloroethanesulfonyl chloride (400 μL , 3.84 mmol, 1.50 equiv.) in dry CH_2Cl_2 (50 mL). The solution was stirred for 2 h at 0 – 4 °C. The solvent was removed. The crude material was purified by column chromatography (SiO_2 , CH_2Cl_2) to afford **53e** (1.51 g, 93%) as a white solid. M.p. 225–227 °C. ^1H NMR (300 MHz, CDCl_3) δ =7.26 – 7.19 (m; 6H), 7.12 – 7.05 (m; 8H), 6.73 (d, $J = 8.7$ Hz; 2H), 6.51 – 6.32 (m; 2H), 6.00 (d, $J = 9.2$ Hz; 1H), 4.32 (t, $J = 6.1$ Hz; 2H), 4.03 (t, $J = 5.8$ Hz; 2H), 2.17 (m; 2H), 1.29 (s; 27H). ^{13}C NMR (75 MHz, CDCl_3) δ =156.38, 148.44, 144.19, 140.16, 132.42, 132.33, 130.81, 130.46, 124.18,

113.08, 67.62, 63.18, 63.06, 34.41, 31.52, 29.15. IR (neat): $\nu=2960, 1504, 1363, 1246, 1172, 823 \text{ cm}^{-1}$. HR-MS (ESI⁺): m/z : 675.3478 [M+Na]⁺ (calcd for C₄₂H₅₂NaO₄S: 675.3484).

Compound 68:

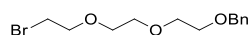
To a solution of **67** (10.0 g, 32.3 mmol, 4.00 equiv.) and Et₃N (1.4 mL) in anhydrous CH₂Cl₂ (50 mL) was added a solution of **66** (2.00 g, 7.72 mmol, 1.00 equiv.) in dry CH₂Cl₂ (100 mL) over 4 h, under inert atmosphere. The solution was stirred overnight at room temperature. Then, the mixture was concentrated to dryness and the crude material was purified by column chromatography (SiO₂, CH₂Cl₂/EtOAc 98:2 to 88/12) to afford **68** (5.21 g, 81%) as brownish solid. ¹H NMR (300 MHz, CDCl₃) $\delta=8.21$ (br; 1H), 8.10 (br; 2H), 7.39 (s; 2H), 7.01 (s; 4H), 6.85 (s; 4H), 3.45 (s; 4H), 2.30 – 2.09 (m; 32H), 1.64 – 1.36 (m; 21H). Spectral data agree with those previously reported values.³²

Compound 69:

In a three-neck round-bottom flask, to anhydrous CH₂Cl₂ (200 mL) were added simultaneously a solution of **68** (166 mg, 0.199 mmol, 1.00 equiv.) and Et₃N (55 μ L) in dry CH₂Cl₂ (20 mL) and a solution of **66** (52.0 mg, 0.199 mmol, 1.00 equiv.) in dry CH₂Cl₂ (20 mL) over 24 h under Ar. After the complete addition of both solutions, the mixture was stirred for 1 h and the solvent was removed under vacuum. The crude material was purified by column chromatography (SiO₂, CH₂Cl₂/EtOAc 90:10) to afford **69** (49 mg, 24%) as white solid. ¹H NMR (500 MHz, CDCl₃) $\delta=8.21$ (br; 4H), 7.96 (br; 2H), 7.25 (s; 4H), 6.97 (s; 8H), 2.32 (br; 8H), 2.18 (s; 24H), 1.74 – 1.49 (m; 12H), 1.42 (s; 18H). ¹³C NMR (126 MHz, CDCl₃) $\delta=165.76, 154.20, 148.18, 135.01, 134.61, 131.11, 128.79, 126.67, 122.56, 45.31, 35.61, 31.36, 29.83, 26.51, 23.08, 19.16$. IR (neat): $\nu=3270$ (br), 2933, 1657, 1591, 1507, 1285, 1257, 684 cm^{-1} . Spectral data agree with those previously reported values.²⁷⁰

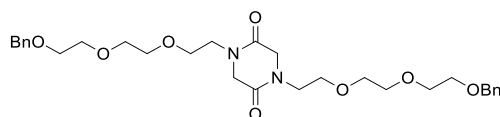
²⁷⁰ C. Fischer, M. Nieger, O. Mogck, V. Böhmer, R. Ungaro, F. Vögtle, *Eur. J. Org. Chem.* **1998**, 155-161.

Compound 71:



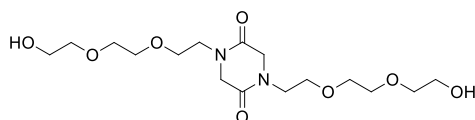
Under inert atmosphere, to a solution of **70** (3.58 g, 14.9 mmol, 1.00 equiv.) in dry CH_2Cl_2 (30 mL) was added CBr_4 (5.93 g, 17.9 mmol, 1.20 equiv.). The solution was cooled to 0°C and PPh_3 (7.81 g, 29.8 mmol, 2.00 equiv.) was added portionwise. The solution was stirred for 2 h at room temperature. The solvent was evaporated under reduced pressure. The crude material was purified by column chromatography (SiO_2 , EtOAc/hexane 30:70) to afford **71** (3.79 g, 84%) as an oil. ^1H NMR (300 MHz, CDCl_3): δ =7.38 – 7.24 (m; 5H), 4.57 (s; 2H), 3.81 (t, J = 6.3 Hz; 2H), 3.72 – 3.59 (m; 8H), 3.46 (t, J = 6.3 Hz; 2H). Spectral data agree with those previously reported values.²⁷¹

Compound 72:



Under inert atmosphere, to anhydrous DMF (10 mL) at 0°C was added NaH (60% dispersion in mineral oil, 401 mg, 10.0 mmol, 2.00 equiv.). The suspension was stirred for 10 minutes at 0°C then glycine anhydride (572 mg, 5.01 mmol, 1.00 equiv.) was added. The mixture was stirred for 5 minutes at 0°C and 20 minutes while allowing it to reach room temperature. To this suspension were added **71** (3.80 g, 12.5 mmol, 2.50 equiv.) and a catalytic amount of $\text{Bu}_4\text{NI}_{(\text{cat})}$. The mixture was stirred overnight at room temperature. Subsequently, H_2O (50 mL) was added and the mixture was extracted with CH_2Cl_2 (3 \times 50 mL). The combined organic phases were dried over anhydrous Na_2SO_4 and the solvent was evaporated under reduced pressure. The crude material was purified by column chromatography (SiO_2 , $\text{CH}_2\text{Cl}_2/\text{MeOH}$ 98:2 to 95:5) to afford **72** (1.80 g, 64%) as an oil. ^1H NMR (400 MHz, CDCl_3): δ =7.36 – 7.24 (m; 10H), 4.56 (s; 4H), 4.12 (s; 4H), 3.68 – 3.58 (m; 20H), 3.54 (t, J = 5.0 Hz; 4H). ^{13}C NMR (101 MHz, CDCl_3): δ =163.97, 138.35, 128.43, 127.80, 127.66, 73.29, 70.77, 70.69, 70.55, 69.54, 69.42, 51.87, 46.21. IR (neat): ν =2857, 1660, 1274, 1095, 715 cm^{-1} . HR-MS (ESI⁺): m/z : 581.2830 [$\text{M}+\text{Na}$]⁺ (calcd for $\text{C}_{30}\text{H}_{42}\text{NaN}_2\text{O}_8$: 581.2839).

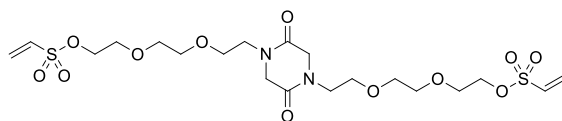
Compound 73:



²⁷¹ T. Sugawara, K. Irie, H. Iwasawa, T. Yoshikawa, S. Okuno, H. K. Watanabe, T. Kato, M. Shibukawa, Y. Ito, *Carbohydr. Res.* **1992**, 230, 117-149.

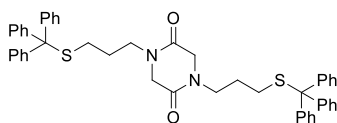
To a solution of **72** (1.80 g, 3.21, 1.00 equiv.) in dry MeOH (20 mL) was added Pd/C (11%, 190 mg). The suspension was stirred under a pressurized H₂ atmosphere (5 atm) for 72 h at room temperature. Then it was filtered through a pad of Celite® and washed with MeOH (100 mL). The solvent was removed under reduced pressure affording **73** (1.30 g, 99%) as a colorless oil. ¹H NMR (400 MHz, CDCl₃): δ=4.25 (s; 4H), 3.69 (q, *J* = 5.0 Hz; 8H), 3.63 – 3.52 (m; 16H). ¹³C NMR (101 MHz, CDCl₃): δ=164.49, 73.02, 70.41, 70.17, 69.42, 61.75, 51.72, 45.75. IR (neat): ν=3407 (br), 2859, 1550, 1111, 1064 cm⁻¹. HR-MS (ESI⁺): *m/z*: 401.1894 [M+H]⁺ (calcd for C₁₆H₃₀NaN₂O₈: 401.1900).

Compound 74a:



Under inert atmosphere, to a solution of **73** (208 mg, 0.492 mmol, 1.00 equiv.) in dry CH₂Cl₂ (10 mL) at 0 °C were added Et₃N (680 μL, 4.92 mmol, 10.0 equiv.) and a solution of 2-chloroethanesulfonyl chloride (156 μL, 1.47 mmol, 3.00 equiv.) in anhydrous CH₂Cl₂ (2 mL). The mixture was stirred for 2 h at 0 °C. The solvent was removed under vacuum. The crude material was purified by column chromatography (SiO₂, CH₂Cl₂/MeOH 95:5) to afford **74a** (235 mg, 80%) as a colorless oil. ¹H NMR (400 MHz, CDCl₃): δ=6.58 (dd, *J* = 16.7, 10.0 Hz; 2H), 6.36 (d, *J* = 16.7 Hz; 2H), 6.10 (d, *J* = 10.0 Hz; 2H), 4.21 (m; 4H), 4.10 (s; 4H), 3.72 – 3.51 (m; 20H). ¹³C NMR (101 MHz, CDCl₃): δ=164.08, 132.57, 130.25, 70.70, 70.31, 69.68, 69.27, 68.80, 51.72, 46.03. IR (neat): ν=2871, 1658, 1351, 1169, 918 cm⁻¹. HR-MS (ESI⁺): *m/z*: 559.1649 [M+H]⁺ (calcd for C₂₀H₃₅N₂O₁₂S₂: 559.1631).

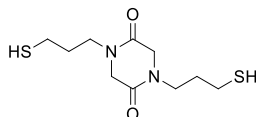
Compound 75:



Under an Ar atmosphere, a suspension of NaH (60% dispersion in mineral oil, 275 mg, 6.86 mmol, 2.0 equiv.) in anhydrous DMF (6 mL) was stirred for 5 minutes at 0 °C. Then, glycine anhydride (392 mg, 3.43 mmol, 1.00 equiv.) was added. The mixture was stirred for 30 minutes allowing it to warm up to room temperature. To this solution were added a solution of **55** (3.41 g, 8.58 mmol, 2.50 equiv.) in dry DMF/CH₂Cl₂ (1:1, 10 mL) and Bu₄Ni_(cat). The mixture was stirred for 18 h at room temperature. H₂O (50 mL) was added to the resulting mixture and was extracted with CH₂Cl₂ (3 × 50 mL). The combined organic phases were dried over anhydrous Na₂SO₄ and the solvent was removed under reduced pressure. The crude material was purified by column chromatography (SiO₂, EtOAc/hexane 1:1 to EtOAc/CH₂Cl₂ 1:1) to afford **75** (1.92 g, 75%) as a white solid. M.p. 208 °C (decomp). ¹H NMR (500 MHz,

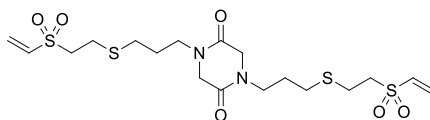
CDCl₃): δ =7.42 – 7.38 (m; 12H), 7.29 – 7.25 (m; 12H), 7.21 – 7.18 (m; 6H), 3.67 (s; 4H), 3.24 (t, J = 7.3 Hz; 4H), 2.16 (t, J = 7.3 Hz; 4H), 1.50 (p, J = 7.3 Hz; 4H). ¹³C NMR (126 MHz, CDCl₃): δ =163.19, 144.79, 129.69, 128.04, 126.82, 67.01, 50.01, 45.38, 29.20, 26.07. IR (neat): ν =3055, 2924, 1667, 1483, 743, 699 cm⁻¹. HR-MS (ESI⁺): m/z : 747.3070, (calcd for C₄₈H₄₇N₂O₂S₂⁺ [M+H]⁺: 747.3079).

Compound 74b:



Under inert atmosphere, to a solution of **75** (196 mg, 262 μ mol, 1.00 equiv.) in dry CH₂Cl₂ (10 mL) were added CF₃CO₂H (3 mL) and Et₃SiH (1 mL). The solution was stirred for 4 h at room temperature. The solvent was removed under reduced pressure and the residue was dissolved in toluene (10 mL) and evaporated again under reduced pressure. The crude material was purified by column chromatography (SiO₂, EtOAc/hexane 4:1 to 1:0) to afford **74b** (61 mg, 88%) as a white syrup. ¹H NMR (500 MHz, CDCl₃): δ =3.96 (s; 4H), 3.50 (t, J = 6.9 Hz; 4H), 2.52 (m; 4H), 1.86 (p, J = 6.9 Hz; 4H), 1.55 (t, J = 8.1 Hz; 2H). ¹³C NMR (126 MHz, CDCl₃): δ =163.62, 50.17, 44.71, 30.78, 21.83. IR (neat): ν =2925, 2548, 1650, 1479, 1334 cm⁻¹. HR-MS (ESI⁺): m/z : 285.0705 [M+H]⁺ (calcd for C₁₀H₁₈NaN₂O₂S₂: 285.0707).

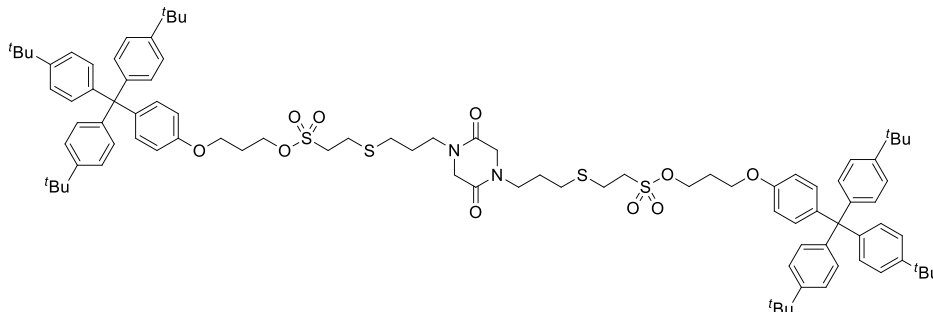
Compound 74c:



Under Ar, to **74b** (43 mg, 0.16 mmol, 1.0 equiv.) in dry CH₂Cl₂ (10 mL) was added divinyl sulfone (165 μ L, 1.64 mmol, 10.0 equiv.) and Et₃N (230 μ L, 1.64 mmol, 10.0 equiv.). The solution was stirred for 22 h at room temperature. The solvent was evaporated under reduced pressure. The crude material was purified by column chromatography (SiO₂, CH₂Cl₂) to afford **74c** (49 mg, 60%) as a white solid. M.p. 99–101 °C. ¹H NMR (500 MHz, CDCl₃): δ =6.67 (dd, J = 16.6, 9.8 Hz; 2H), 6.45 (d, J = 16.6 Hz; 2H), 6.21 (d, J = 9.8 Hz; 2H), 3.97 (s; 4H), 3.48 (t, J = 7.0 Hz; 4H), 3.23 (m; 4H), 2.86 (m; 4H), 2.57 (t, J = 7.3 Hz; 4H), 1.86 (m; 4H). ¹³C NMR (126 MHz, CDCl₃): δ =163.70, 136.12, 131.42, 54.46, 50.33, 45.24, 29.62, 26.49, 24.27. IR (neat): ν =2922, 1655, 1314, 1135, 750 cm⁻¹. HR-MS (ESI⁺): m/z : 499.1063 [M+H]⁺ (calcd for C₁₈H₃₁N₂O₆S₄: 499.1065).

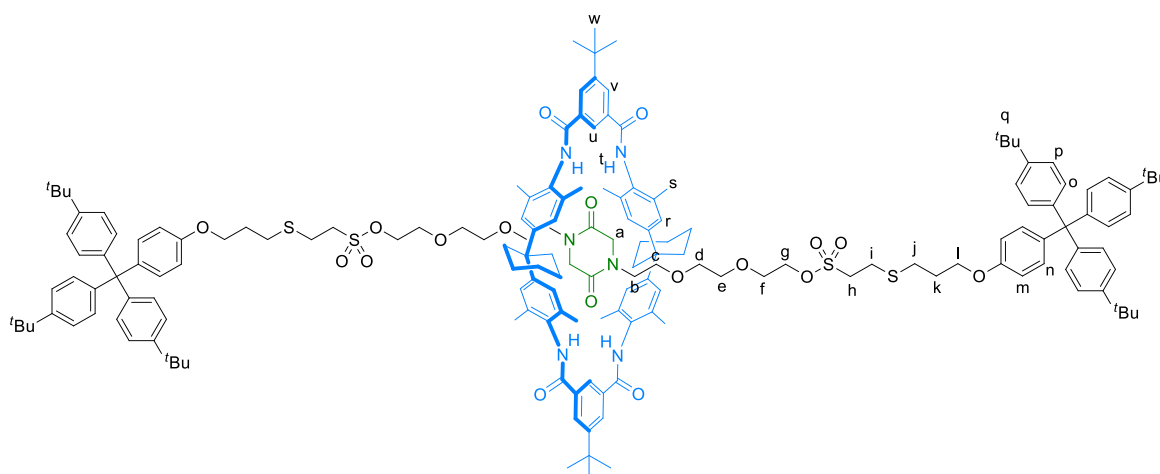
53.77, 50.33, 45.20, 29.76, 29.20, 29.13, 26.47, 24.08, 24.03. IR (neat): $\nu=2924, 1664, 1508, 1320, 1247, 749, 702 \text{ cm}^{-1}$. HR-MS (ESI⁺): m/z : 1341.4298 [M+Na]⁺ (calcd for C₇₄H₈₂NaN₂O₈S₆: 1341.4293).

Compound 76c:



Under Ar, to a solution of **74b** (11 mg, 42 μmol , 1.00 equiv.) in CHCl₃ (6 mL) were added **53e** (106 mg, 0.167 mmol, 4.00 equiv.) and 2 drops of Et₃N. The solution was stirred for 20 h at room temperature. The solvent was removed under reduced pressure. The crude material was purified by column chromatography (SiO₂, CH₂Cl₂) to afford **76c** (57 mg, 88%) as a white solid. M.p. 216 °C (decomp). ¹H NMR (400 MHz, CDCl₃): $\delta=7.25 - 7.20$ (m; 12H), 7.12 – 7.04 (m; 16H), 6.75 (d, $J = 8.6 \text{ Hz}$; 4H), 4.45 (t, $J = 6.2 \text{ Hz}$; 4H), 4.06 (t, $J = 5.8 \text{ Hz}$; 4H), 3.95 (s; 4H), 3.47 (t, $J = 7.1 \text{ Hz}$; 4H), 3.34 (m; 4H), 2.92 (m; 4H), 2.56 (t, $J = 7.1 \text{ Hz}$; 4H), 2.21 (p, $J = 6.0 \text{ Hz}$; 4H), 1.85 (p, $J = 7.1 \text{ Hz}$; 4H), 1.30 (s; 54H). ¹³C NMR (101 MHz, CDCl₃): $\delta=163.63, 156.36, 148.47, 144.19, 140.21, 132.47, 130.84, 124.19, 113.09, 67.33, 63.22, 63.19, 50.66, 50.34, 45.29, 34.44, 31.53, 29.68, 29.46, 26.53, 25.44$. IR (neat): $\nu=2960, 2866, 1665, 1505, 1361, 1166, 823 \text{ cm}^{-1}$. HR-MS (ESI⁺): m/z : 1589.7887 [M+Na]⁺ (calcd for C₉₄H₁₂₂NaN₂O₁₀S₆: 1589.7880).

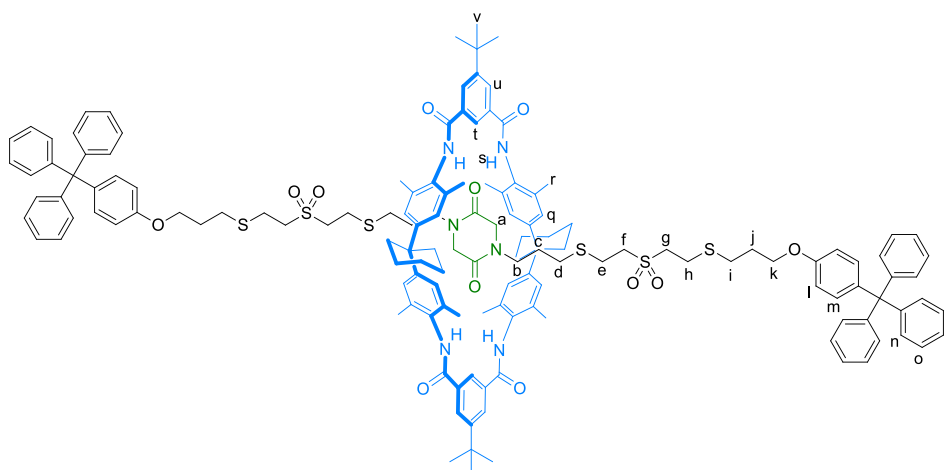
Compound 77a:



Under Ar, to a solution of **74a** (16 mg, 30 μmol , 2.0 equiv.) and **69** (15 mg, 15 μmol , 1.0 equiv.) in CHCl₃ (4 mL) were added **53a** (68 mg, 118 μmol , 8.0 equiv.) and 2 drops of Et₃N. The solution was stirred for 24 h at room temperature. The solvent was removed under reduced pressure. The crude material was

purified by gel permeation chromatography (Bio-Beads® S-X1, CH₂Cl₂) to afford **77a** (29 mg, 72%) as a white solid. M.p. 237 °C (decomp). ¹H NMR (500 MHz, CDCl₃): δ=8.42 (s; 2H, H_u), 8.36 (s; 4H, H_t), 8.27 (d, *J* = 1.5 Hz; 4H, H_v), 7.25 – 7.21 (m; 12H, H_p), 7.10 – 7.03 (m; 24H, H_{n+o+r}), 6.74 (d, *J* = 8.7 Hz; 4H, H_m), 4.17 (m; 4H, H_g), 3.98 (t, *J* = 5.9 Hz; 4H, H_l), 3.50 (m; 4H, H_j), 3.46 – 3.39 (m; 8H, H_{d+e}), 3.31 (m; 4H, H_h), 3.20 (t, *J* = 4.9 Hz; 4H, H_c), 2.89 (m; 4H, H_i), 2.78 (s; 4H, H_a), 2.71 (t, *J* = 7.2 Hz; 4H, H_j), 2.32 (s; 8H, H_{CyCH2}), 2.18 (s; 24H, H_s), 2.06 – 1.95 (m; 8H, H_{b+k}), 1.62 (s; 8H, H_{CyCH2}), 1.51 (s; 4H, H_{CyCH2}), 1.42 (s; 18H, H_w), 1.30 (s; 54H, H_q). ¹³C NMR (126 MHz, CDCl₃): δ=165.81, 163.92, 156.61, 154.12, 148.45, 144.25, 139.96, 135.64, 134.43, 132.42, 132.40, 131.73, 130.85, 129.08, 126.47, 124.18, 122.66, 113.06, 70.70, 70.49, 69.13, 69.11, 69.02, 65.81, 63.19, 50.93, 49.58, 45.34, 44.87, 35.73, 35.56, 34.43, 31.53, 31.45, 29.84, 29.29, 29.01, 25.23, 22.94, 18.85. IR (neat): ν=3342 (br), 2923, 1548, 1505, 1247, 823, 735 cm⁻¹. HR-MS (ESI⁺): *m/z*: 2754.4807 [M+Na]⁺ (calcd for C₁₆₈H₂₁₄NaN₆O₁₈S₄: 2754.4795).

Compound 77b



from **74b**:

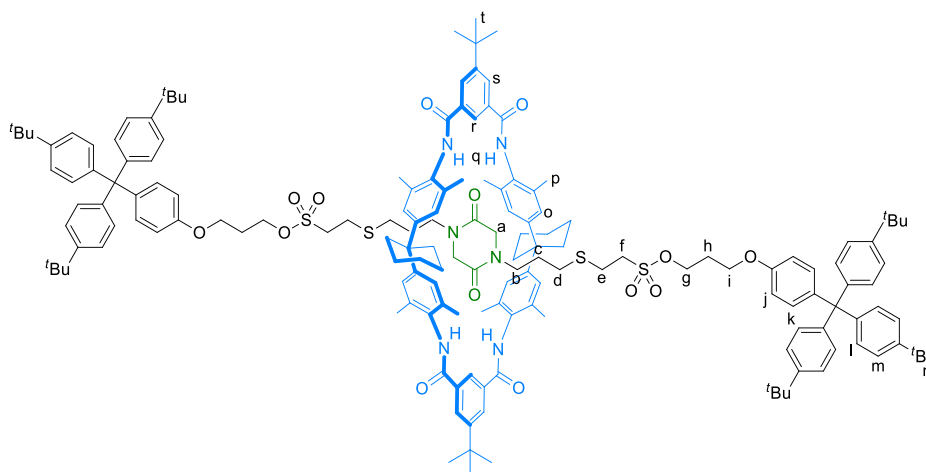
Under inert atmosphere, to a solution of **74b** (5.0 mg, 20 μmol, 2.0 equiv.) and **69** (10 mg, 10 μmol, 1.0 equiv.) in CHCl₃ (8 mL) were added **53d** (41 mg, 79 μmol, 8.0 equiv.) and 2 drops of Et₃N. The solution was stirred for 22 h at room temperature. The solvent was removed under reduced pressure. The crude material was purified by gel permeation chromatography (Bio-Beads® S-X1, CH₂Cl₂) to afford **77b** (14 mg, 61%) as white solid.

from **74c**:

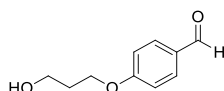
Under an Ar atmosphere, to a solution of **74c** (5.0 mg, 9.8 μmol, 2.0 equiv.) and **69** (5.0 mg, 4.9 μmol, 1.0 equiv.) in CHCl₃ (8 mL) were added **53c** (16 mg, 39 μmol, 8.0 equiv.) and 2 drops of Et₃N. The solution was stirred for 22 h at room temperature. The solvent was removed under reduced pressure. The crude material was purified by gel permeation chromatography (Bio-Beads® S-X1, CH₂Cl₂) to give

77b (7 mg, 62%) as white solid. M.p. 217 °C (decomp). ^1H NMR (400 MHz, CDCl_3): δ =8.40 (s; 2H, H_t), 8.29 – 8.25 (m; 8H, H_{s+u}), 7.25 – 7.15 (m; 30H, H_{n+o+p}), 7.10 (m; 4H, H_m), 7.06 (s; 8H, H_q), 6.75 (d, J = 8.6 Hz; 4H, H_i), 4.00 (t, J = 5.8 Hz; 4H, H_k), 3.16 (m; 8H, H_{f+g}), 2.89 – 2.81 (m; 8H, H_{e+h}), 2.73 (t, J = 7.2 Hz; 4H, H_j), 2.67 (s; 4H, H_a), 2.36 – 2.24 (m; 12H, $\text{H}_{b+\text{CYCH}_2}$), 2.19 (m; 28H, H_{d+r}), 2.03 (m; 4H, H_l), 1.67 – 1.48 (m; 12H, H_{CYCH_2}), 1.43 (s; 18H, H_v), 1.34 (m; 4H, H_c). ^{13}C NMR (126 MHz, CDCl_3): δ =165.72, 163.94, 156.70, 154.14, 147.11, 139.47, 135.55, 134.38, 132.40, 131.95, 131.23, 131.17, 129.21, 127.58, 126.52, 126.02, 122.74, 113.34, 65.75, 64.45, 54.03, 53.79, 45.24, 43.56, 35.76, 35.58, 31.45, 29.85, 29.55, 29.35, 29.23, 26.38, 26.04, 24.19, 23.93, 22.91, 19.17. IR (neat): ν =3334 (br), 2924, 2856, 1655, 1508, 1248, 748, 701 cm^{-1} . HR-MS (ESI $^+$): m/z : 2358.0510 [$\text{M}+\text{Na}$] $^+$ (calcd for $\text{C}_{142}\text{H}_{162}\text{NaN}_6\text{O}_{12}\text{S}_6$: 2358.0473); 2336.0703 [$\text{M}+\text{H}$] $^+$ (calcd for $\text{C}_{142}\text{H}_{163}\text{N}_6\text{O}_{12}\text{S}_6$: 2336.0653).

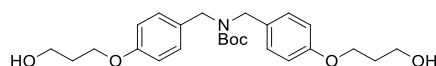
Compound 77c:



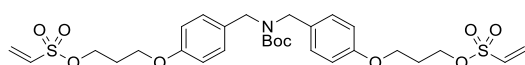
Under inert atmosphere, to a solution of **74b** (5.0 mg, 18 μmol , 2.0 equiv.) and **69** (9.0 mg, 8.8 μmol , 1.0 equiv.) in CHCl_3 (8 mL) were added **53e** (45 mg, 71 μmol , 8.0 equiv.) and 2 drops of Et_3N . The solution was stirred for 20 h at room temperature. The solvent was removed under reduced pressure. The crude material was purified by gel permeation chromatography (Bio-Beads $^{\text{®}}$ S-X1, CH_2Cl_2) to afford **77c** (16 mg, 71%) as white solid. M.p. 200 °C (decomp). ^1H NMR (400 MHz, CDCl_3): δ =8.42 (s; 2H, H_t), 8.32 – 8.28 (m; 8H, H_{q+s}), 7.25 – 7.20 (m; 12H, H_m), 7.12 – 7.02 (m; 24H, H_{k+l+o}), 6.74 (d, J = 8.7 Hz; 4H, H_j), 4.43 (t, J = 6.3 Hz; 4H, H_g), 4.03 (t, J = 5.7 Hz; 4H, H_i), 3.29 (m; 4H, H_f), 2.89 (m; 4H, H_e), 2.57 (s; 4H, H_a), 2.36 – 2.24 (m; 12H, $\text{H}_{\text{CYCH}_2+b}$), 2.19 (s; 28H, H_{h+p}), 1.84 (s; 2H, H_{CYCH_2}), 1.64 (s; 12H, $\text{H}_{\text{CYCH}_2+d}$), 1.51 (s; 2H, H_{CYCH_2}), 1.43 (s; 18H, H_v), 1.29 (m; 58H, H_{c+n}). ^{13}C NMR (101 MHz, CDCl_3): δ =165.72, 164.03, 156.32, 154.15, 148.53, 148.30, 144.20, 140.33, 135.59, 134.37, 132.51, 131.99, 130.86, 129.20, 126.55, 124.21, 122.76, 113.09, 67.48, 63.18, 50.69, 47.85, 45.26, 43.42, 35.81, 34.45, 32.08, 31.53, 31.46, 31.08, 29.86, 29.55, 29.39, 26.86, 25.53, 22.90, 19.13. IR (neat): ν =3341 (br), 2958, 2925, 2861, 1652, 1505, 1249, 1166, 823, 750 cm^{-1} . HR-MS (ESI $^+$): m/z : 2606.4077 [$\text{M}+\text{Na}$] $^+$ (calcd for $\text{C}_{162}\text{H}_{202}\text{NaN}_6\text{O}_{14}\text{S}_4$: 2606.4060).

Compound 79:

To a degassed solution of 4-hydroxybenzaldehyde (1.00 g, 8.19 mmol) in dry CH₃CN (30 mL) were added K₂CO₃ (5.66 g, 41.0 mmol) and 3-bromo-1-propanol (0.960 mL, 10.7 mmol). The suspension was stirred for 24 h at 75 °C. The mixture was cooled to room temperature, filtered and the solvent was evaporated under reduced pressure. The syrup was dissolved in CH₂Cl₂ (50 mL) and washed with H₂O (50 mL). The aqueous layer was extracted with (50 mL) and the combined organic phases were dried over anhydrous Na₂SO₄. The solvent was removed under vacuum and the crude material was purified by column chromatography (SiO₂, CH₂Cl₂/EtOAc 85:15) to yield **79** (1.25 g, 85%) as a colorless oil. ¹H NMR (400 MHz, CDCl₃): δ=9.88 (s, 1H), 7.83 (d, *J* = 8.8 Hz, 2H), 7.01 (d, *J* = 8.8 Hz, 2H), 4.21 (t, *J* = 6.1 Hz, 2H), 3.88 (t, *J* = 5.9 Hz, 2H), 2.08 (p, *J* = 6.0 Hz, 2H). Characterization data are in agreement with those from literature.²⁷²

Compound 81:

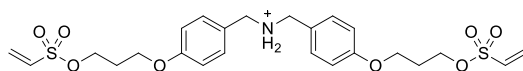
Under Ar, a solution of **79** (1.00 g, 5.52 mmol, 1.00 equiv.) and **80** (1.00 g, 5.52 mmol, 1.00 equiv.) in dry MeOH (50 mL) was stirred for 20 h at room temperature. NaBH₄ (834 mg, 22.1 mmol, 4.00 equiv.) was added and the mixture was further stirred for 18 h at room temperature. H₂O (50 mL) was added to the resulting mixture, which was extracted with CH₂Cl₂ (3 × 300 mL). The combined organic phases were dried over anhydrous Na₂SO₄ and the solvent was removed under reduced pressure. Under inert atmosphere, the solid was dissolved in anhydrous CH₂Cl₂ (100 mL) and Et₃N (2.30 mL, 16.6 mmol, 3.00 equiv.). A solution of Boc₂O (1.60 g, 7.17 mmol, 1.30 eq.) in dry CH₂Cl₂ (30 mL) was added dropwise and the resulting mixture was stirred for 24 h at room temperature. The solvent was evaporated under reduced pressure and the crude material was purified by column chromatography (SiO₂, CH₂Cl₂/MeOH 98:2) to yield **81** (2.17 g, 87%) as a colorless oil. ¹H NMR (300 MHz, CDCl₃) δ=7.09 (br; 4H), 6.83 (d, *J* = 8.6 Hz; 4H), 4.26 (br; 4H), 4.07 (t, *J* = 6.0 Hz; 4H), 3.80 (t, *J* = 5.9 Hz; 4H), 2.79 (s; 2H), 2.00 (p, *J* = 5.9 Hz; 4H), 1.48 (s; 9H). ¹³C NMR (75 MHz, CDCl₃) δ=158.06, 156.03, 130.08, 129.25, 128.79, 114.49, 80.08, 65.48, 59.91, 48.40, 48.15, 32.04, 28.49. Spectral data agree with those previously reported values.²⁰⁰

Compound 82:

²⁷² C. Sirichaiwat, C. Intaraudom, S. Kamchonwongpaisan, J. Vanichtanankul, Y. Thebtaranonth, Y. Yuthavong, *J. Med. Chem.* **2004**, *47*, 345-354.

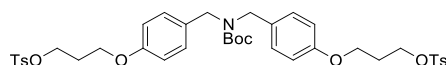
Under an Ar atmosphere, to a solution of **81** (2.06 g, 4.62 mmol, 1.00 equiv.) in dry CH₂Cl₂ (100 mL), cooled in a water-ice bath were added Et₃N (6.50 mL, 46.2 mmol, 10.0 equiv.) and a solution of 2-chloroethanesulfonyl chloride (1.46 mL, 13.9 mmol, 3.00 equiv.) in dry CH₂Cl₂ (20 mL). The mixture was stirred for 1 h at 0 °C. Subsequently, the solvent was removed under vacuum. The crude was dissolved in CH₂Cl₂ (200 mL) and washed with NH₄Cl_(sat) (100 mL). The aqueous layer was extracted with CH₂Cl₂ (200 mL) and the combined organic phases were dried over anhydrous Na₂SO₄ and the solvent was removed under reduced pressure. The crude material was purified by column chromatography (SiO₂, CH₂Cl₂/EtOAc 97:3) to yield **82** (1.94 g, 67%) as a colorless oil. ¹H NMR (400 MHz,): δ=7.12 (br; 4H), 6.83 (m; 4H), 6.53 – 6.36 (m; 4H), 6.09 (d, *J* = 9.5 Hz; 2H), 4.38 – 4.20 (m; 8H), 4.06 (t, *J* = 5.9 Hz; 4H), 2.20 (p, *J* = 6.0 Hz; 4H), 1.50 (s; 9H). ¹³C NMR (101 MHz, CDCl₃): δ=157.84, 156.02, 132.36, 130.66, 130.45, 129.45, 128.97, 114.58, 80.08, 67.56, 63.32, 48.52, 48.31, 29.12, 28.59. IR (neat): ν=2972, 1683, 1510, 1358, 1238, 1165, 941, 832 cm⁻¹. HR-MS (ESI⁺): *m/z*: 648.1907 [M+Na]⁺ (calcd for C₂₉H₃₉NaNO₁₀S₂: 648.1913).

Compound **83a**·PF₆:



To a solution of **82** (652 mg, 1.04 mmol, 1.00 equiv.) in CH₂Cl₂ (30 mL) was added CF₃CO₂H (15 mL). The mixture was stirred for 2 h at room temperature and the solvent was removed under vacuum. The solid was then redissolved in CH₂Cl₂ (50 mL) and a solution of HCl in Et₂O (2 M, 7.82 mL, 15.6 mmol, 15.0 equiv.) was added. The solution was stirred for another 2 h at room temperature and the solvent was evaporated under reduced pressure. The solid was dissolved again in CH₂Cl₂ (15 mL). H₂O (30 mL), acetone (30 mL) and an excess of KPF₆ were added and the suspension was stirred for 24 h at room temperature. The mixture was diluted with H₂O (100 mL) and extracted with CH₂Cl₂ (3 × 100 mL). The combined organic phases were dried over anhydrous Na₂SO₄ and the solvent was removed under reduced pressure to give **83a**·PF₆ (672 mg, 96%) as a white solid. M.p. 82–83 °C. ¹H NMR (400 MHz, CD₃CN): δ=7.39 (d, *J* = 8.7 Hz; 4H), 6.98 (d, *J* = 8.7 Hz; 4H), 6.63 (dd, *J* = 16.6, 10.0 Hz; 2H), 6.34 (d, *J* = 16.7 Hz; 2H), 6.17 (d, *J* = 10.0 Hz; 2H), 4.30 (t, *J* = 6.2 Hz; 4H), 4.18 – 4.06 (m; 8H), 2.17 (p, *J* = 6.1 Hz; 4H). ¹³C NMR (101 MHz, CD₃CN): δ=160.72, 133.07, 132.85, 131.86, 123.52, 115.85, 68.89, 64.69, 51.77, 29.51. IR (neat): ν=3636, 2949, 1515, 1349, 1252, 1166, 831 cm⁻¹. HR-MS (ESI⁺): *m/z*: 526.1567 [M-PF₆⁻]⁺ (calcd for C₂₄H₃₂NO₈S₂: 526.1569).

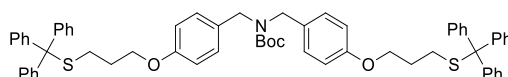
Compound **84**:



Under inert atmosphere, to a solution of **81** (1.07 g, 2.40 mmol, 1.00 equiv.) in CH₂Cl₂ (80 mL) were added Et₃N (2.67 mL, 19.2 mmol, 8.00 equiv.), TsCl (1.83 g, 9.61 mmol, 4.00 equiv.) and a catalytic

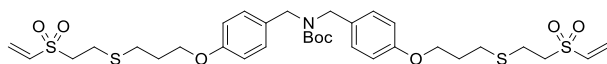
amount of DMAP. The mixture was stirred for 18 h at room temperature. The solvent was removed under vacuum and the crude material was purified by column chromatography (SiO₂, CH₂Cl₂/EtOAc 97:3) to yield **84** (1.60 g, 88%) as a colorless oil. ¹H NMR (400 MHz, CDCl₃): δ=7.76 (d, *J* = 8.3 Hz; 4H), 7.26 (d, *J* = 8.2 Hz; 4H), 7.10 (br; 4H), 6.73 (d, *J* = 8.3 Hz; 4H), 4.36 – 4.20 (m; 8H), 3.95 (t, *J* = 5.8 Hz; 4H), 2.39 (s; 6H), 2.12 (p, *J* = 5.9 Hz; 4H), 1.51 (s; 9H). ¹³C NMR (101 MHz, CDCl₃): δ=157.86, 156.04, 144.90, 132.95, 130.47, 129.96, 129.43, 128.85, 127.99, 114.53, 80.11, 67.22, 63.27, 48.51, 48.20, 29.03, 28.64, 21.77. IR (neat): ν=2973, 1684, 1510, 1359, 1239, 1173, 945, 734 cm⁻¹. HR-MS (ESI⁺): *m/z*: 776.2526 [M+Na]⁺ (calcd for C₃₉H₄₇NaNO₁₀S₂: 776.2539).

Compound 85:

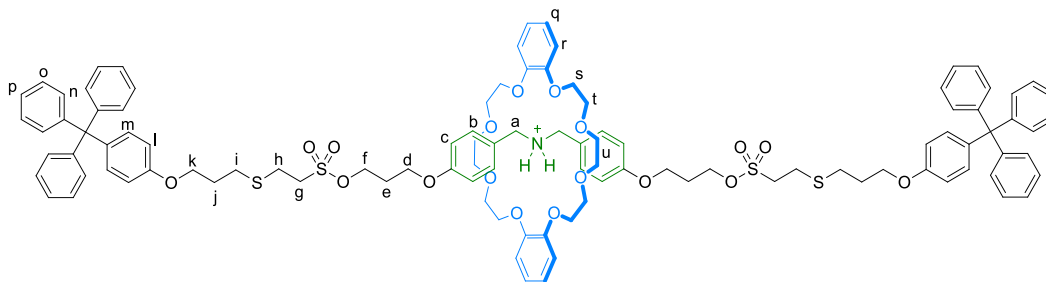


Under Ar, to a solution of triphenylmethanethiol (728 mg, 2.63 mmol, 2.40 equiv.) in THF (7 mL), cooled in a water-ice bath, was added a solution of LiHMDS in THF (1 M, 2.63 mL, 2.63 mmol, 2.40 equiv.). The mixture was stirred at 0 °C until the thiolate precipitates. The suspension was allowed to warm up to room temperature and a solution of **84** (828 mg, 1.10 mmol, 1.00 equiv.) in THF (3 mL) was added. The mixture was then refluxed for another 20 h. The solvent was removed under reduced pressure and the crude was dissolved in CH₂Cl₂ (100 mL). The organic layer was washed with H₂O (2 × 100 mL) and dried over anhydrous Na₂SO₄ and the solvent was removed under vacuum. The crude material was purified by column chromatography (SiO₂, CH₂Cl₂/Hexane 4:1 to CH₂Cl₂) to afford **85** (978 mg, 93%) as a yellow syrup. ¹H NMR (500 MHz, CDCl₃): δ=7.41 (m; 12H), 7.31 – 7.03 (m; 22H), 6.77 (m; 4H), 4.28 (br; 4H), 3.89 (t, *J* = 6.1 Hz; 4H), 2.36 (t, *J* = 7.1 Hz; 4H), 1.80 (p, *J* = 6.6 Hz; 4H), 1.50 (s; 9H). ¹³C NMR (126 MHz, CDCl₃): δ=158.18, 156.09, 145.00, 130.21, 129.73, 129.48, 128.85, 128.00, 126.74, 114.63, 80.02, 66.73, 66.36, 48.40, 48.13, 28.66, 28.64, 28.48. IR (neat): ν=3056, 2926, 1689, 1510, 1240, 1164, 699 cm⁻¹. HR-MS (ESI⁺): *m/z*: 984.4068 [M+Na]⁺ (calcd for C₆₃H₆₃NaNO₄S₂: 984.4096).

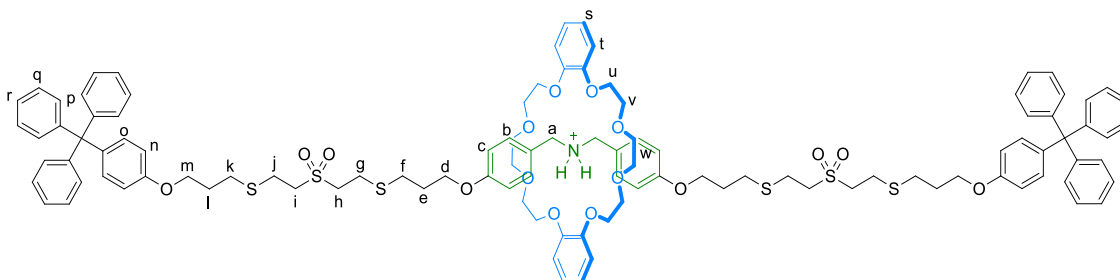
Compound 86:



Under an Ar atmosphere, to a solution of **85** (648 mg, 0.673 mmol, 1.00 equiv.) in dry CH₂Cl₂ (10 mL) were added CF₃CO₂H (4 mL) and Et₃SiH (2 mL). The reaction was stirred for 3 h at room temperature. The solvent was removed under vacuum. The resulting oil was dissolved in toluene (10 mL) and the solvent was evaporated again under reduced pressure. Under Ar, the crude was dissolved in anhydrous CH₂Cl₂ (15 mL) and Et₃N (2 mL) and Boc₂O (147 mg, 0.673 mmol, 1.00 equiv.) were added. The mixture was stirred for 4 h at room temperature and divinyl sulfone (540 μL, 5.38 mmol, 8.00 equiv.) was added. The solution was further stirred for 18 h at room temperature and the solvent was removed

Compound 89a·PF₆:

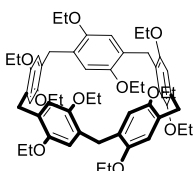
83a·PF₆ (17 mg, 25 μmol, 1.0 equiv.) and **47** (57 mg, 0.13 mmol, 5.0 equiv.) were dissolved in CH₂Cl₂/CH₃CN (2:1, 15 mL). The solvent was removed under reduced pressure and the solid was redissolved in CH₂Cl₂ (0.8 mL). Under Ar, the solution was cooled to 0 °C and was stirred for 1 h. **53c** (42 mg, 0.10 mmol, 4.0 equiv.) and a catalytic amount of DMAP were added. The mixture was stirred for 72 h at 0 °C. The solvent was evaporated under vacuum. The crude material was purified by gel permeation chromatography (Bio-Beads[®] S-X1, CH₂Cl₂, and then Bio-Beads[®] S-X3, CH₂Cl₂). The crude was dissolved in CH₂Cl₂ (20 mL) and washed with HCl (1%, 3 × 20 mL). The organic phase was dried over anhydrous Na₂SO₄ and the solvent was removed under reduced pressure to yield **89a**·PF₆ (36 mg, 73%) as a white solid. M.p. 60–61 °C. ¹H NMR (400 MHz, CDCl₃): δ=7.25 – 7.15 (m; 34H, H_{b+n+o+p}), 7.09 (d, *J* = 8.9 Hz; 4H, H_m), 6.95 – 6.80 (m; 8H, H_{q+r}), 6.75 (m; 8H, H_{c+i}), 4.44 (m; 8H, H_{a+f}), 4.18 – 3.97 (m; 16H, H_{d+k+s/t}), 3.75 (br; 8H, H_{s/t}), 3.46 – 3.31 (m; 12H, H_{g+u}), 2.94 (m; 4H, H_h), 2.75 (m; 4H, H_i), 2.20 (m; 4H, H_e), 2.04 (m; 4H, H_j). ¹³C NMR (126 MHz, CDCl₃): δ=159.28, 156.78, 147.66, 147.12, 139.28, 132.34, 131.22, 130.97, 127.55, 125.98, 124.07, 121.96, 114.72, 113.36, 113.06, 70.84, 70.31, 68.53, 67.38, 65.88, 64.43, 63.59, 52.10, 50.69, 29.83, 29.20, 28.98, 25.33. IR (neat): ν=2922, 1610, 1506, 1250, 1168, 842, 749 cm⁻¹ HR-MS (ESI⁺): *m/z*: 1794.7026 [M-PF₆⁻]⁺ (calcd for C₁₀₄H₁₁₆NO₁₈S₄: 1794.7075).

Compound 89b·PF₆:

83b·PF₆ (16 mg, 21 μmol, 1.0 equiv.) and **47** (47 mg, 0.11 mmol, 5.0 equiv.) were dissolved in CH₂Cl₂/CH₃CN (2:1, 15 mL). The solvent was removed under reduced pressure and the solid was redissolved in CH₂Cl₂ (0.8 mL). Under an Ar atmosphere, the solution was cooled to 0 °C and was stirred for 1 h. **53c** (35 mg, 84 μmol, 4.0 equiv.) and a catalytic amount of DMAP were added. The mixture was stirred for 72 h at 0 °C. The solvent was evaporated under vacuum. The crude material was purified by gel permeation chromatography (Bio-Beads[®] S-X1, CH₂Cl₂, and then Bio-Beads[®] S-X3, CH₂Cl₂). The

crude was dissolved in CH_2Cl_2 (20 mL) and washed with HCl (1%, 3×20 mL). The organic phase was dried over anhydrous Na_2SO_4 and the solvent was removed under reduced pressure to yield **89b**· PF_6 (28 mg, 66%) as white syrup. ^1H NMR (500 MHz, CDCl_3): δ =7.27 – 7.15 (m; 34H, $\text{H}_{b+p+q+r}$), 7.09 (d, $J = 7.6$ Hz; 4H, H_o), 6.95 – 6.72 (m; 16H, $\text{H}_{c+n+s+t}$), 4.44 (br; 4H, H_a), 4.21 – 3.63 (m; 24H, $\text{H}_{d+m+u+v}$), 3.57 – 3.10 (m; 16H, H_{h+i+w}), 3.05 – 2.64 (m; 16H, $\text{H}_{f+g+j+k}$), 2.06 (br; 8H, H_{e+l}). ^{13}C NMR (126 MHz, CDCl_3): δ =159.58, 156.83, 147.73, 147.16, 139.27, 132.37, 131.25, 131.13, 127.57, 125.99, 123.88, 122.05, 115.19, 113.45, 113.31, 71.33, 70.64, 70.09, 69.55, 68.99, 66.08, 64.45, 54.39, 52.21, 29.85, 29.33, 29.24, 29.16, 24.20, 24.11. IR (neat): ν =2926, 1686, 1509, 1320, 1242, 1167, 1118, 747, 702 cm^{-1} . HR-MS (ESI⁺): m/z : 1882.7189 [$\text{M}-\text{PF}_6$]⁺ (calcd for $\text{C}_{108}\text{H}_{124}\text{NO}_{16}\text{S}_6$: 1882.7244).

Compound 91a:



To a solution of 1,4-diethoxybenzene (415 mg, 2.50 mmol, 1.00 eq.) in dichloromethane (100 mL) under argon, were added paraformaldehyde (210 mg, 7.00 mmol, 2.80 eq.) and iron(III) chloride (75 mg, 0.462 mmol, 0.185 eq.). The mixture was stirred for 3h at room temperature. It was, then, washed with water (50 mL) and extracted with dichloromethane (3×25 mL). The organic layer was dried over sodium sulfate and the solvent was evaporated under reduced pressure. The crude material was purified by column chromatography (SiO_2 , dichloromethane/hexane 1:1 to 1:0) to afford **91a** (308 g, 69%) as a white solid. ^1H NMR (400 MHz, CDCl_3) δ = 6.73 (s, 10H), 3.84 (q, $J = 7.0$ Hz, 20H), 3.78 (s, 10H), 1.27 (t, $J = 7.0$ Hz, 30H). ^{13}C NMR (101 MHz, CDCl_3) δ = 150.00, 128.69, 115.31, 63.96, 30.02, 15.19. Spectral data agree with previous reported values.²⁷³

Compound 92b:

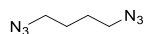


Under inert atmosphere, to a solution of 1,4-dimethoxybenzene (1.38 g, 10.0 mmol, 1.00 equiv.) in 1,2-dichloroethane (20 mL) were added paraformaldehyde (0.93 g, 30 mmol, 3.0 equiv.) and $\text{BF}_3 \cdot \text{Et}_2\text{O}$ (1.25 mL, 10.0 mmol, 1.00 equiv.). The solution was stirred for 30 minutes at 30 °C. MeOH (100 mL) was added to the mixture. A precipitate was formed and was filtered, then washed with MeOH (100 mL). The crude material was purified by column chromatography (SiO_2 , CH_2Cl_2) to afford **92b** (1.219 g,

²⁷³ T. Ogoshi, K. Kitajima, T. Aoki, S. Fujinami, T.-A. Yamagishi, Y. Nakamoto, *J. Org. Chem.* **2010**, *75*, 3268-3273.

81%) as a white solid. ^1H NMR (400 MHz, CDCl_3) δ =6.79 (s; 10H), 3.82 (s; 10H), 3.67 (s; 30H). ^{13}C NMR (101 MHz, CDCl_3) δ =150.90, 128.41, 114.15, 55.90, 29.75. Spectral data agree with those previously reported values.⁹⁵

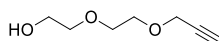
Compound 93:



Caution! Low molecular weight azides can be heat and shock sensitive and **explosive**. Although we did not experience any problem, compound **93** should be handled with care and adequate safety measures should be taken during the synthesis, workup and concentration. Moreover, the reaction should not be scaled up.

Under inert atmosphere, a suspension of 1,4-dibromobutane (1.50 g, 7.00 mmol, 1.00 equiv.) and NaN_3 (1.24 mg, 19.0 mmol, 2.70 equiv.) in anhydrous DMF (10 mL) was stirred for 24 h at 80 °C. The mixture was cooled to room temperature and H_2O (10 mL) was added. The mixture was extracted with Et_2O (3 \times 50 mL) and the combined organic layers were washed with a $\text{NaHCO}_3(\text{sat})$ (2 \times 100 mL). The organic phase was dried over anhydrous Na_2SO_4 and the solvent was evaporated under reduced pressure to give **93** (980 g, 99%) as a colorless oil. ^1H NMR (300 MHz, CDCl_3): δ =3.32 (m; 4H), 1.67 (m; 4H). Spectral data agree with those previously reported values.²⁷⁴

Compound 95:

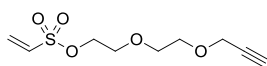


Under Ar, to a solution of *t*BuOK (2.50 g, 22.2 mmol, 1.00 equiv.) in dry THF (50 mL), cooled in a water-ice bath was added diethylene glycol (4.20 mL, 44.4 mmol, 2.00 equiv.). The suspension was stirred for 30 minutes allowing it to reach room temperature and propargyl bromide (80% in THF, 2.40 mL, 22.2 mmol, 1.00 equiv.) was added. The mixture was stirred for 24 h at room temperature. The mixture was diluted with CH_2Cl_2 (50 mL) and filtered. The solvent was removed under reduced pressure. The crude material was purified by column chromatography (SiO_2 , EtOAc) to afford **95** (1.961 g, 61%) as a colorless oil. ^1H NMR (400 MHz, CDCl_3): δ =4.21 (d, J = 2.4 Hz; 2H), 3.79 – 3.67 (m; 6H), 3.61 (m; 2H), 2.44 (t, J = 2.4 Hz; 1H). Spectral data agree with those previously reported values.²⁷⁵

²⁷⁴ Y. Ju, D. Kumar, R. S. Varma, *J. Org. Chem.* **2006**, 71, 6697-6700.

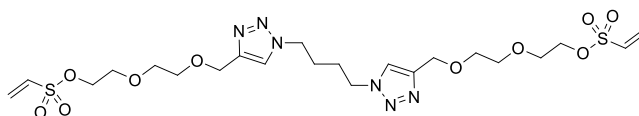
²⁷⁵ J. Diot, M. I. García-Moreno, S. G. Gouin, C. Ortiz Mellet, K. Haupt, J. Kovensky, *Org. Biomol. Chem.* **2009**, 7, 357-363.

Compound 96:



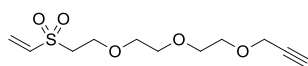
Under an Ar atmosphere, to a solution of **95** (574 mg, 3.98 mmol, 1.00 equiv.) in dry CH₂Cl₂ (20 mL) was added Et₃N (2.70 mL, 19.9 mmol, 5.00 equiv.). The solution was cooled in a water-ice bath and a solution of 2-chloroethanesulfonyl chloride (630 μL, 5.97 mmol, 1.50 equiv.) in dry CH₂Cl₂ (5 mL) was added. The mixture was stirred for 3 h at 0 - 4 °C. The solvent was removed under reduced pressure. The crude material was purified by column chromatography (SiO₂, CH₂Cl₂/EtOAc 95:5) to afford **96** (792 mg, 85%) as a colorless oil. ¹H NMR (400 MHz, CDCl₃): δ=6.60 (dd, *J* = 16.7, 9.9 Hz; 1H), 6.39 (d, *J* = 16.7 Hz; 1H), 6.11 (d, *J* = 9.9 Hz; 1H), 4.25 (m; 2H), 4.17 (d, *J* = 2.4 Hz; 2H), 3.74 (m; 2H), 3.67 (s; 4H), 2.43 (t, *J* = 2.4 Hz; 1H). ¹³C NMR (101 MHz, CDCl₃): δ=132.69, 130.12, 79.57, 74.78, 70.61, 69.75, 69.13, 68.84, 58.49. IR (neat): ν=3363 (br), 2923, 1634, 1352, 1171 cm⁻¹. HR-MS (ESI⁺): *m/z*: 257.0463 [M+Na]⁺ (calcd for C₉H₁₄NaO₅S: 257.0460).

Compound 97a:

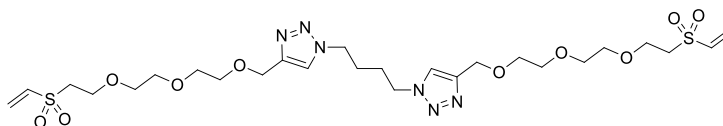


Caution! Low molecular weight azides can be heat and shock sensitive and **explosive**. Although we did not experience any problem, compound **93** should be handled with care and adequate safety measures should be taken during the synthesis, workup and concentration. Moreover, the reaction should not be scaled up.

Under Ar, to a solution of **93** (217 mg, 1.55 mmol, 1.00 equiv.) in anhydrous CH₂Cl₂ (15 mL) were added **96** (1.09 g, 4.65 mmol, 3.00 equiv.), TBTA (164 mg, 0.310 mmol, 0.200 equiv.) and Cu(CH₃CN)₄PF₆ (116 mg, 0.310 mmol, 0.200 equiv.). The solution was stirred for 24 h at room temperature. The resulting mixture was diluted with CH₂Cl₂ (50 mL) and washed with an aqueous solution of Na₄EDTA (0.1 M, 5 × 50 mL). Then, the organic layer was dried over anhydrous Na₂SO₄ and the solvent was evaporated under reduced pressure. The crude material was purified by column chromatography (SiO₂, CH₂Cl₂/MeOH 95:5) to afford **97a** (561 mg, 59%) as a white syrup. ¹H NMR (400 MHz, CDCl₃): δ=7.60 (s; 2H), 6.60 (dd, *J* = 16.7, 9.9 Hz; 2H), 6.40 (d, *J* = 16.7 Hz; 2H), 6.11 (d, *J* = 9.9 Hz; 2H), 4.68 (s; 4H), 4.38 (m; 4H), 4.26 (m; 4H), 3.74 (m; 4H), 3.71 – 3.64 (m; 8H), 1.94 (m; 4H). ¹³C NMR (126 MHz, CDCl₃): δ=145.36, 132.60, 130.32, 122.88, 70.68, 69.86, 69.67, 68.76, 64.69, 49.39, 27.17. IR (neat): ν=3282, 2870, 1351, 1169, 1096, 916, 785 cm⁻¹. HR-MS (ESI⁺): *m/z*: 631.1827 [M+Na]⁺ (calcd for C₂₂H₃₆NaN₁₀O₁₀S₂: 631.1827).

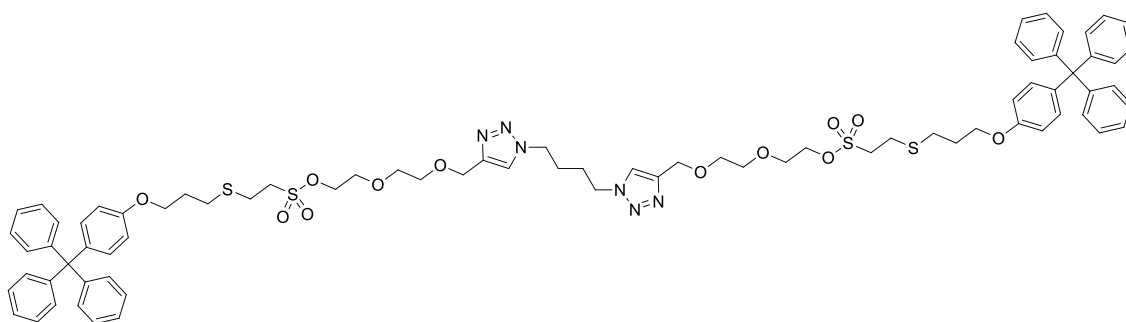
Compound 98:

Under Ar, to a solution of **95** (1.61 g, 14.1 mmol, 1.00 equiv.) in dry THF (40 mL) were added divinyl sulfone (3.5 mL, 35 mmol, 2.5 equiv.) and *t*BuOK (631 mg, 5.63 mmol, 0.400 equiv.). The mixture was stirred for 45 minutes at room temperature. The solvent was removed under reduced pressure and the crude material was purified by column chromatography (SiO₂, EtOAc/hexane 1:1) to afford **98** (1.23 g, 38%) as an oil. ¹H NMR (400 MHz, CDCl₃): δ=6.82 (dd, *J* = 16.6, 9.9 Hz; 1H), 6.39 (d, *J* = 16.6 Hz; 1H), 6.08 (d, *J* = 9.9 Hz; 1H), 4.19 (d, *J* = 2.4 Hz; 2H), 3.90 (t, *J* = 5.7 Hz; 2H), 3.71 – 3.63 (m; 8H), 3.26 (t, *J* = 5.7 Hz; 2H), 2.43 (t, *J* = 2.4 Hz; 1H). ¹³C NMR (101 MHz, CDCl₃): δ=138.19, 128.80, 79.71, 74.75, 70.67, 70.50, 70.42, 69.27, 64.83, 58.56, 55.22. IR (neat): ν=3393 (br), 2925, 1640, 1287, 1115 cm⁻¹. HR-MS (ESI⁺): *m/z*: 285.0774 [M+Na]⁺ (calcd for C₁₁H₁₈NaO₅S: 285.0773).

Compound 97b:

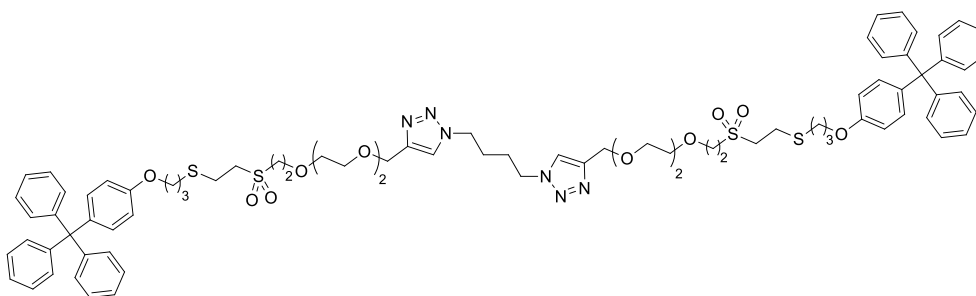
Under inert atmosphere, to a solution of **93** (67 mg, 0.48 mmol, 1.0 equiv.) and **98** (333 mg, 1.43 mmol, 3.00 equiv.) in anhydrous CH₂Cl₂ (8 mL) were added TBTA (51 mg, 96 μmol, 0.20 equiv.) and Cu(CH₃CN)₄PF₆ (36 mg, 96 μmol, 0.20 equiv.). The solution was stirred for 24 h at room temperature. The resulting mixture was diluted with CH₂Cl₂ (50 mL) and washed with an aqueous solution of Na₄EDTA (0.1 M, 5 × 50 mL). Then, the organic layer was dried over anhydrous Na₂SO₄ and the solvent was evaporated under reduced pressure. The crude material was purified by column chromatography (SiO₂, CH₂Cl₂/MeOH 96:4) to afford **97b** (282 mg, 98%) as an oil. ¹H NMR (400 MHz, CDCl₃): δ=7.57 (s; 2H), 6.79 (dd, *J* = 16.6, 9.9 Hz; 2H), 6.30 (d, *J* = 16.6 Hz; 2H), 6.00 (d, *J* = 9.9 Hz; 2H), 4.62 (s; 4H), 4.33 (m; 4H), 3.85 (t, *J* = 5.6 Hz; 4H), 3.68 – 3.55 (m; 16H), 3.21 (t, *J* = 5.6 Hz; 4H), 1.89 (m; 4H). ¹³C NMR (101 MHz, CDCl₃): δ=145.14, 138.07, 128.76, 122.88, 70.51, 70.45, 70.27, 69.76, 64.67, 64.62, 55.09, 49.36, 27.15. IR (neat): ν=3058, 2871, 1312, 1292, 1117, 1089, 731 cm⁻¹. HR-MS (ESI⁺): *m/z*: 687.2454 [M+Na]⁺ (calcd for C₂₆H₄₄NaN₆O₁₀S₂: 687.2458).

Compound 99a:



Under Ar, to a solution of **97a** (20 mg, 32 μmol , 1.0 eq.) in CHCl_3 (3 mL) were added **53c** (53 mg, 0.13 mmol, 4.0 eq.) and 2 drops of Et_3N . The solution was stirred for 16 h at room temperature. The solvent was removed under reduced pressure. The crude material was purified by column chromatography (SiO_2 , $\text{CH}_2\text{Cl}_2/\text{MeOH}$ 96:4) to afford **99a** (44 mg, 94%) as a white syrup. ^1H NMR (500 MHz, CDCl_3): δ =7.55 (s; 2H), 7.27 – 7.14 (m; 30H), 7.10 (d, J = 8.4 Hz; 4H), 6.76 (d, J = 8.4 Hz; 4H), 4.66 (s; 4H), 4.34 (m; 8H), 4.01 (t, J = 5.9 Hz; 4H), 3.74 – 3.63 (m; 12H), 3.41 (m; 4H), 2.94 (m; 4H), 2.74 (t, J = 7.2 Hz; 4H), 2.04 (p, J = 6.5 Hz; 4H), 1.91 (m; 4H). ^{13}C NMR (126 MHz, CDCl_3): δ =156.74, 147.08, 145.31, 139.30, 132.32, 131.18, 127.53, 125.95, 122.72, 113.33, 70.71, 69.73, 69.64, 69.05, 65.84, 64.75, 64.40, 50.80, 49.39, 29.19, 28.92, 27.22, 25.28. IR (neat): ν =2926, 1607, 1507, 1353, 1245, 1165, 921, 701 cm^{-1} . HR-MS (ESI $^+$): m/z : 1451.5262 [$\text{M}+\text{Na}$] $^+$ (calcd for $\text{C}_{78}\text{H}_{88}\text{NaN}_6\text{O}_{12}\text{S}_4$: 1451.5241).

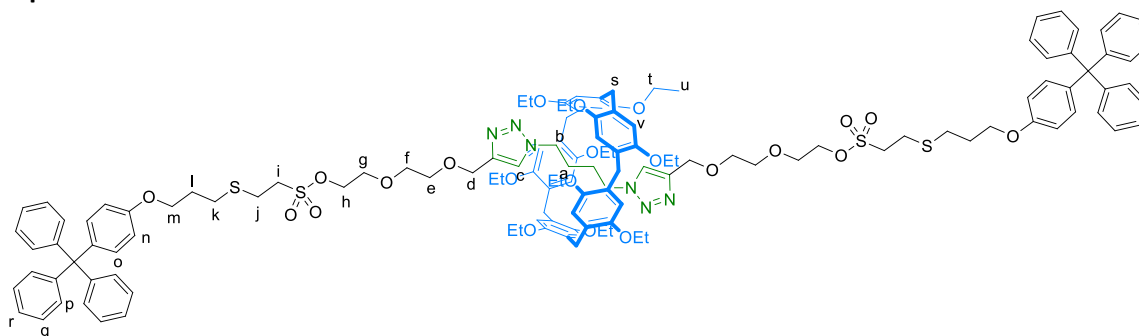
Compound 99b:



Under Ar, to a solution of **97b** (19 mg, 31 μmol , 1.0 equiv.) in CHCl_3 (3 mL) were added **53c** (51 mg, 0.13 mmol, 4.0 equiv.) and 3 drops of Et_3N . The solution was stirred for 18 h at room temperature. The solvent was removed under reduced pressure. The crude material was purified by column chromatography (SiO_2 , $\text{CH}_2\text{Cl}_2/\text{MeOH}$ 96:4) to afford **99b** (35 mg, 82%) as a white syrup. ^1H NMR (400 MHz, CDCl_3): δ =7.56 (s; 2H), 7.27 – 7.14 (m; 30H), 7.10 (d, J = 8.5 Hz; 4H), 6.76 (d, J = 8.5 Hz; 4H), 4.65 (s; 4H), 4.34 (m; 4H), 4.02 (t, J = 5.9 Hz; 4H), 3.89 (m; 4H), 3.70 – 3.58 (m; 16H), 3.38 (m; 4H), 3.20 (m; 4H), 2.92 (m; 4H), 2.74 (t, J = 7.1 Hz; 4H), 2.04 (m; 4H), 1.91 (m; 4H). ^{13}C NMR (101 MHz, CDCl_3): δ =156.79, 147.12, 145.34, 139.28, 132.32, 131.20, 127.55, 125.97, 122.78, 113.35, 70.73, 70.59, 70.40, 69.93, 65.90, 64.93, 64.77, 64.41, 55.07, 53.99, 49.41, 29.18, 28.80, 27.24, 24.09. IR (neat): ν =3055,

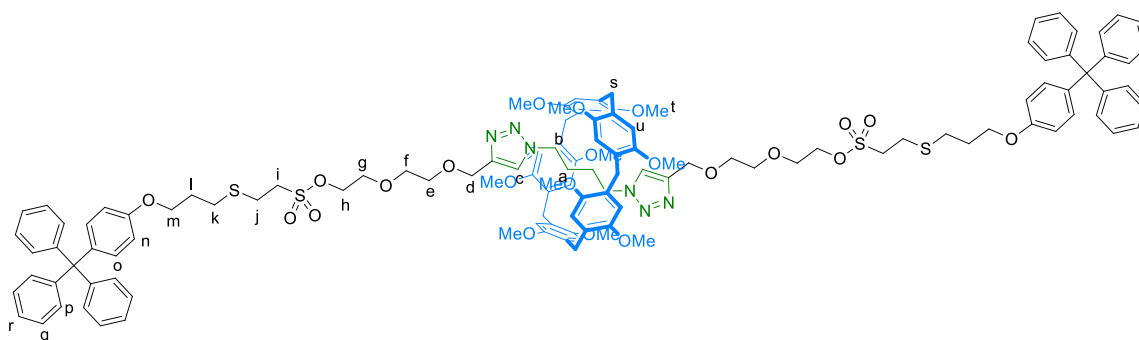
2870, 1607, 1507, 1245, 1113, 731 cm^{-1} . HR-MS (ESI⁺): m/z : 1507.5894 [M+Na]⁺ (calcd for C₈₂H₉₆NaN₆O₁₂S₄: 1507.5867).

Compound 100a:



A solution of **97a** (22 mg, 37 μmol , 1.0 equiv.) and **91a** (166 mg, 186 μmol , 5.00 equiv.) in CHCl_3 (2 mL) was stirred for 5 h at room temperature under an Ar atmosphere. To this mixture were added **53c** (61 mg, 0.15 mmol, 4.0 equiv.) and 2 drops of Et_3N . The solution was stirred for 24 h at room temperature. The solvent was evaporated under reduced pressure. The crude material was purified by two consecutive column chromatographies (firstly, SiO_2 , CH_2Cl_2 /hexane 3:7 to 1:0, to CH_2Cl_2 /MeOH 98:2; then CH_2Cl_2 /MeOH 98:2) to afford **100a** (45 mg, 53%) as a white syrup. ¹H NMR (400 MHz, CDCl_3): δ =7.32 (s; 2H, H_c), 7.27 – 7.15 (m; 30H, H_{p+q+r}), 7.10 (d, J = 8.6 Hz; 4H, H_o), 6.89 (s; 10H, H_v), 6.76 (d, J = 8.6 Hz; 4H, H_n), 4.68 (s; 4H, H_d), 4.39 (m; 4H, H_h), 4.03 (t, J = 5.9 Hz; 4H, H_m), 3.83 – 3.70 (m; 42H, H_{e+f+g+s+t}), 3.42 (m; 4H, H_i), 2.98 (m; 4H, H_j), 2.77 (t, J = 7.2 Hz; 4H, H_k), 2.10 – 1.99 (m; 8H, H_{b+i}), 1.34 (t, J = 6.9 Hz; 30H, H_u), -1.13 (br; 4H, H_a). ¹³C NMR (101 MHz, CDCl_3): δ =156.78, 149.80, 147.13, 143.46, 139.37, 132.38, 131.24, 128.98, 127.56, 125.99, 121.92, 114.81, 113.35, 70.78, 69.75, 69.32, 69.27, 65.84, 64.61, 64.44, 64.04, 50.91, 48.39, 29.29, 29.20, 29.01, 25.33, 24.10, 15.46. IR (neat): ν =2974, 2929, 2870, 1737, 1606, 1498, 1392, 1206, 1050, 701 cm^{-1} . HR-MS (ESI⁺): m/z : 2320.0415 [M+H]⁺ (calcd for C₁₃₃H₁₅₉N₆O₂₂S₄: 2320.0390); 2342.0244 [M+Na]⁺ (calcd for C₁₃₃H₁₅₈NaN₆O₂₂S₄: 2342.0210).

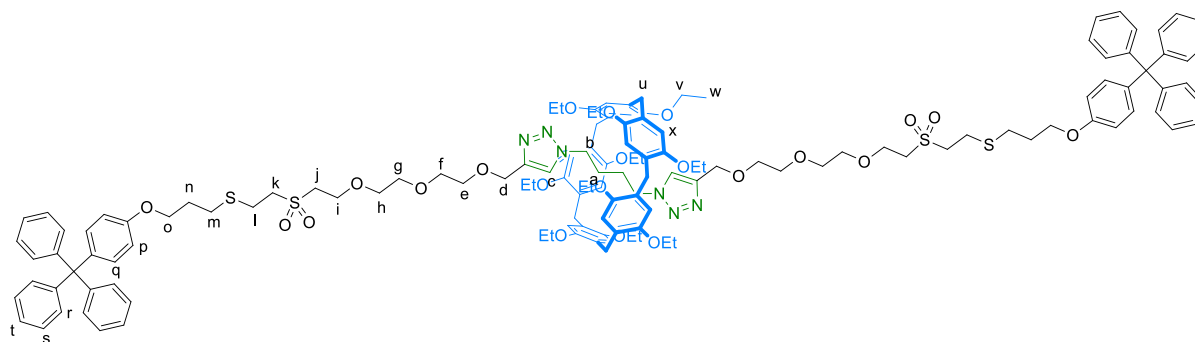
Compound 100b:



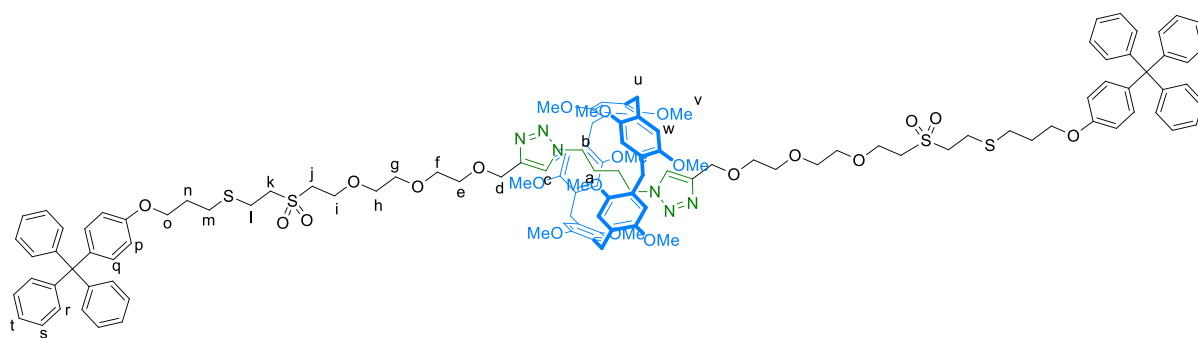
A solution of **97a** (26 mg, 43 μmol) and **91b** (160 mg, 0.21 Mmol,) in CHCl_3 (3 mL) was stirred for 5 h at room temperature under inert atmosphere. Stopper **53c** (70 mg, 0.17 mmol) and 2 drops of

triethylamine were added. The resulting mixture was stirred for 24 h at room temperature. The solvent was evaporated under reduced pressure and the crude purified by two consecutive column chromatographies (firstly, SiO₂, CH₂Cl₂/hexane 30:70 to 100:0, to CH₂Cl₂/MeOH to 49:1; then SiO₂, CH₂Cl₂/MeOH 100:0 to 24:1) to afford **100b** (85 mg, 91%) as a colourless syrup. ¹H NMR (500 MHz, CDCl₃): δ=7.28 – 7.15 (m; 32H, H_{c+p+q+r}), 7.10 (d, *J* = 8.6 Hz; 4H, H_o), 6.88 (s; 10H, H_u), 6.76 (d, *J* = 8.6 Hz; 4H, H_n), 4.71 (s; 4H, H_d), 4.41 (m; 4H, H_h), 4.01 (t, *J* = 5.9 Hz; 4H, H_m), 3.83 – 3.72 (m; 22H, H_{e+f+g+s}), 3.59 (s; 30H, H_t), 3.41 (m; 4H, H_i), 2.97 (m; 4H, H_j), 2.75 (t, *J* = 7.2 Hz; 4H, H_k), 2.08 – 1.97 (m; 8H, H_{b+t}), -1.18 (br; 4H, H_a). ¹³C NMR (126 MHz, CDCl₃): δ=156.77, 150.53, 147.13, 143.86, 139.37, 132.37, 131.23, 128.82, 127.56, 125.99, 122.08, 113.86, 113.35, 70.88, 69.82, 69.31, 69.26, 65.83, 64.77, 64.44, 55.90, 50.92, 48.35, 29.26, 29.20, 29.00, 25.32, 24.16. IR (neat): ν=2932, 1737, 1608, 1497, 1398, 1213, 1044, 703 cm⁻¹. HR-MS (ESI⁺): *m/z*: 2179.8809 [M+H]⁺ (calcd for C₁₂₃H₁₃₉N₆O₂₂S₄: 2179.8825).

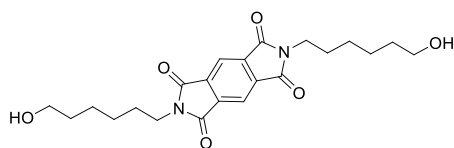
Compound 100c:



A solution of **97b** (22 mg, 33 μmol, 1.0 equiv.) and **91a** (147 mg, 165 μmol, 5.00 equiv.) in CHCl₃ (1 mL) was stirred for 5 h at room temperature under inert atmosphere. To this mixture were added **53c** (54 mg, 0.13 mmol, 4.0 equiv.) and 2 drops of Et₃N. The solution was stirred for 18 h at room temperature. The solvent was evaporated under reduced pressure. The crude material was purified by gel permeation chromatography (Bio-Beads[®] S-X1, CH₂Cl₂) followed by a preparative TLC (SiO₂, CH₂Cl₂/MeOH 97:3) to afford **100c** (51 mg, 65%) as a white syrup. ¹H NMR (500 MHz, CDCl₃): δ=7.31 (s; 2H, H_c), 7.25 – 7.15 (m; 30H, H_{r+s+t}), 7.10 (d, *J* = 8.6 Hz; 4H, H_q), 6.89 (s; 10H, H_x), 6.77 (d, *J* = 8.6 Hz; 4H, H_p), 4.67 (s; 4H, H_d), 4.03 (t, *J* = 5.9 Hz; 4H, H_o), 3.92 (t, *J* = 5.3 Hz; 4H, H_i), 3.79 – 3.65 (m; 46H, H_{e+f+g+h+u+v}), 3.39 (m; 4H, H_k), 3.23 (m; 4H, H_j), 2.97 (m; 4H, H_i), 2.77 (t, *J* = 7.2 Hz; 4H, H_m), 2.11 – 1.98 (m; 8H, H_{b+n}), 1.34 (t, *J* = 6.9 Hz; 30H, H_w), -1.13 (br; 4H, H_a). ¹³C NMR (126 MHz, CDCl₃): δ=156.81, 149.79, 147.14, 143.59, 139.34, 132.37, 131.23, 128.95, 127.57, 126.00, 121.88, 114.77, 113.36, 70.81, 70.64, 70.49, 69.89, 65.86, 64.94, 64.65, 64.44, 64.03, 55.12, 54.02, 48.39, 29.29, 29.27, 28.91, 24.11, 24.05, 15.46. IR (neat): ν=2974, 2928, 2871, 1736, 1607, 1498, 1392, 1206, 1111, 1050, 702 cm⁻¹. HR-MS (ESI⁺): *m/z*: 2376.1057 [M+H]⁺ (calcd for C₁₃₇H₁₆₇N₆O₂₂S₄: 2376.1016); 2398.0881 [M+H]⁺ (calcd for C₁₃₇H₁₆₆NaN₆O₂₂S₄: 2398.0836).

Compound 100d:

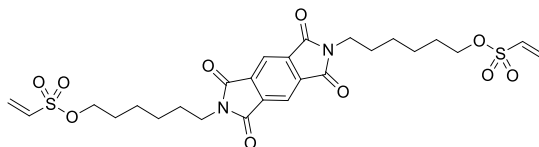
A solution of **97b** (18 mg, 27 μmol , 1.0 equiv.) and **91b** (101 mg, 135 μmol , 5.00 equiv.) in CHCl_3 (6 mL) was stirred for 5 h at room temperature under Ar. To this mixture were added **53c** (44 mg, 0.11 mmol, 4.0 equiv.) and 2 drops of Et_3N . The solution was stirred for 18 h at room temperature. The solvent was evaporated under reduced pressure. The crude material was purified by gel permeation chromatography (Bio-Beads[®] S-X1, CH_2Cl_2) followed by a preparative TLC (SiO_2 , $\text{CH}_2\text{Cl}_2/\text{MeOH}$ 97:3) to afford **100d** (46 mg, 76%) as a white syrup. ^1H NMR (500 MHz, CDCl_3): δ =7.28 – 7.14 (m; 32H, $\text{H}_{\text{C}+\text{r}+\text{s}+\text{t}}$), 7.10 (d, J = 8.7 Hz; 4H, H_q), 6.88 (s; 10H, H_w), 6.76 (d, J = 8.7 Hz; 4H, H_q), 4.70 (s; 4H, H_d), 4.02 (t, J = 5.9 Hz; 4H, H_o), 3.91 (t, J = 5.3 Hz; 4H, H_i), 3.79 – 3.66 (m; 26H, $\text{H}_{\text{e}+\text{f}+\text{g}+\text{h}+\text{u}}$), 3.59 (s; 30H, H_v), 3.38 (m; 4H, H_k), 3.21 (t, J = 5.3 Hz; 4H, H_j), 2.95 (m; 4H, H_l), 2.76 (t, J = 7.1 Hz; 4H, H_m), 2.09 – 1.96 (m; 8H, $\text{H}_{\text{b}+\text{n}}$), -1.18 (br; 4H, H_a). ^{13}C NMR (126 MHz, CDCl_3): δ =156.78, 150.49, 147.12, 143.99, 139.32, 132.34, 131.21, 128.78, 127.55, 125.97, 122.01, 113.81, 113.35, 70.80, 70.73, 70.50, 69.98, 65.87, 64.92, 64.81, 64.43, 55.89, 55.11, 53.98, 48.35, 29.83, 29.26, 29.20, 28.91, 24.06. IR (neat): ν =2931, 1736, 1608, 1497, 1398, 1213, 1044, 749, 703 cm^{-1} . HR-MS (ESI⁺): m/z : 2257.9287 [$\text{M}+\text{Na}$]⁺ (calcd for $\text{C}_{127}\text{H}_{146}\text{NaN}_6\text{O}_{22}\text{S}_4$: 2257.9271); 2235.9478 [$\text{M}+\text{H}$]⁺ (calcd for $\text{C}_{127}\text{H}_{147}\text{N}_6\text{O}_{22}\text{S}_4$: 2235.9451).

Compound 103:

Under Ar, to a suspension of pyromellitic dianhydride (1.06 g, 4.83 mmol) in anhydrous DMF (10 mL) was added 6-amino-1-hexanol (1.19 g, 10.1 mmol). The solution was stirred for 20 h at 100 °C. The solution was poured into water and filtered. Subsequently, the precipitate was washed with MeOH (40 mL), dried and collected to give **103** (519 mg, 26%) as a white solid. M.p. 202 – 203 °C. ^1H NMR (400 MHz, CDCl_3): δ =8.27 (s, 2H), 3.75 (t, J = 7.2 Hz, 4H), 3.64 (t, J = 6.5 Hz, 4H), 1.78 – 1.34 (m, 16H). IR (neat): ν =3390 (br), 2937, 2860, 1700, 1403, 1367, 1059, 730 cm^{-1} . HR-MS (ESI⁺): m/z : 439.1847

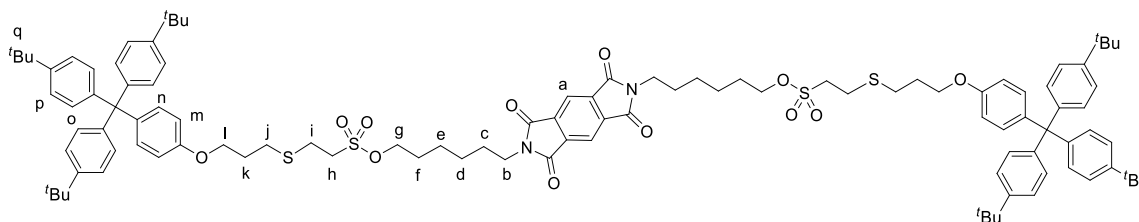
$[M+Na]^+$ (calcd for $C_{22}H_{28}N_2O_6Na$: 439.1845). Spectral data agree with those previously reported values.²²⁶

Compound 104:



To a degassed suspension of **103** (198 mg, 0.475 mmol) in dry CH_2Cl_2 (15 mL), in a water-ice bath, were added Et_3N (660 μL , 4.75 mmol) and a degassed solution of 2-chloroethanesulfonyl chloride (150 μL , 1.43 mmol) in anhydrous CH_2Cl_2 (3 mL). The mixture was stirred for 2 h at 0 °C and the solvent was removed under vacuum. The crude material was purified by column chromatography (SiO_2 , CH_2Cl_2 to $CH_2Cl_2/MeOH$ 98:2) to afford **104** (267 mg, 94%) as a white solid. M.p. 130 – 133 °C. 1H NMR (400 MHz, $CDCl_3$): δ =8.26 (s, 2H), 6.52 (dd, J = 16.6, 9.8 Hz, 2H), 6.39 (d, J = 16.7 Hz, 2H), 6.12 (d, J = 9.8 Hz, 2H), 4.10 (t, J = 6.4 Hz, 4H), 3.73 (t, J = 7.2 Hz, 4H), 1.71 (m, 8H), 1.51 – 1.32 (m, 8H). ^{13}C NMR (101 MHz, $CDCl_3$): δ =166.39, 137.35, 132.62, 130.21, 118.33, 70.76, 38.57, 28.93, 28.33, 26.33, 25.13. IR (neat): ν =2940, 2861, 1706, 1394, 1354, 1265, 1169, 952, 920, 748, 730 cm^{-1} . HR-MS (ESI⁺): m/z : 619.1393 $[M+Na]^+$ (calcd for $C_{26}H_{32}N_2O_{10}S_2Na$: 619.1396).

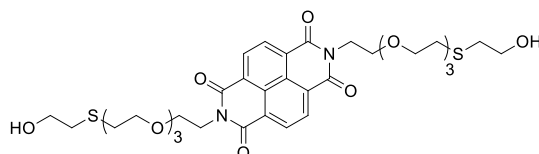
Compound 105:



Under an Ar atmosphere, to a solution of **104** (14 mg, 23 μmol) in $CHCl_3$ (5 mL) were added **53b** (40 mg, 70 μmol) and 2 drops of Et_3N . The solution was stirred for 20 h at room temperature. The solvent was evaporated under reduced pressure. The crude material was purified by column chromatography (SiO_2 , $CH_2Cl_2/EtOAc$ 96:4) to yield **105** (34 mg, 83%) as a white solid. M.p. 183 – 185 °C. 1H NMR (400 MHz, $CDCl_3$): δ = 8.27 (s, 2H, H_a), 7.23 (d, J = 8.6 Hz, 12H, H_p), 7.08 (m, 16H, H_{n+o}), 6.75 (d, J = 8.9 Hz, 4H, H_m), 4.22 (t, J = 6.4 Hz, 4H, H_g), 4.03 (t, J = 5.9 Hz, 4H, H_l), 3.74 (t, J = 7.2 Hz, 4H, H_b), 3.34 (m, 4H, H_n), 2.95 (m, 4H, H_i), 2.77 (t, J = 7.1 Hz, 4H, H_j), 2.06 (p, J = 7.6, 7.0 Hz, 4H, H_k), 1.73 (m, 8H, H_{c+f}), 1.51 – 1.22 (s, 62H, H_{d+e+q}). ^{13}C NMR (126 MHz, $CDCl_3$): δ =166.38, 156.63, 148.46, 144.25, 139.99, 137.37, 132.44, 130.85, 124.18, 118.36, 113.08, 70.03, 65.83, 63.20, 50.79, 38.56, 34.44, 31.53, 29.29, 29.23, 29.09,

δ =166.40, 156.63, 153.78, 148.46, 144.24, 139.98, 133.64, 132.43, 130.85, 125.61, 124.27, 124.18, 115.91, 114.18, 113.08, 104.67, 71.41, 71.35, 70.21, 69.68, 68.11, 65.83, 63.20, 50.85, 38.01, 34.44, 31.53, 29.54, 29.29, 29.12, 28.76, 26.90, 25.42, 25.36. IR (neat): ν =2956, 2867, 1715, 1507, 1359, 1267, 1082, 823, 776, 730 cm^{-1} . HR-MS (ESI⁺): m/z : 2412.1521 [M+Na]⁺ (calcd for C₁₄₂H₁₇₆N₂O₂₂S₄Na: 2412.1495).

Compound 114:



Under Ar, to a solution of **60a** (99 mg, 0.12 mmol, 1.0 equiv.) in anhydrous DMF (10 mL) were added 2-mercaptoethanol (180 μL , 2.5 mmol, 20 equiv.) and Cs₂CO₃ (0.32 g, 0.98 mmol, 8.0 equiv.). The suspension was stirred for 3 days at room temperature. The solvent was removed under reduced pressure. The crude was dissolved in a mixture of CH₂Cl₂/H₂O (1:1, 100 mL). Layers were separated and the aqueous one was extracted with CH₂Cl₂ (2 \times 50 mL). The combined organic phases were dried over anhydrous Na₂SO₄ and the solvent was evaporated under reduced pressure. The crude material was purified by column chromatography (SiO₂, CH₂Cl₂/MeOH 96:4) to afford **114** (67 mg, 73%) as an oil. ¹H NMR (400 MHz, CDCl₃): δ =8.73 (s; 4H), 4.44 (t, J = 5.9 Hz; 4H), 3.84 (t, J = 5.9 Hz; 4H), 3.72 – 3.66 (m; 8H), 3.63 – 3.52 (m; 16H), 2.75 – 2.64 (m; 8H). ¹³C NMR (101 MHz, CDCl₃): δ =162.99, 131.09, 126.85, 126.73, 71.36, 70.73, 70.63, 70.41, 70.26, 67.93, 61.12, 39.74, 35.98, 31.53. IR (neat): ν =3407, 2868, 1704, 1662, 1332, 1244, 1092, 767 cm^{-1} . HR-MS (ESI⁺): m/z : 739.2578 [M+H]⁺ (calcd for C₃₄H₄₇N₂O₁₂S₂: 739.2570).

Stability experiments of rotaxanes **63a** and **100d**:

a) Stability in solution

Samples for the stability experiments were prepared by dissolving the corresponding rotaxanes **63a** or **100d** in CDCl₃ (600 μL) in a NMR tube stored at room temperature. The solutions were monitored by ¹H NMR over 7 days.

b) Stability in solution in the presence of Et₃N

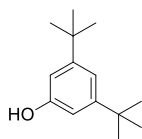
Samples for the stability experiments of rotaxanes in the presence of a mild base were prepared by dissolving rotaxanes **63a** or **100d** in CDCl₃ (600 μL) in a NMR tube. Subsequently, Et₃N (10 μL) was added and the samples were stored at room temperature. The solutions were monitored by ¹H NMR for 5 days.

Chemical disassembly of rotaxane 63a:

Under an Ar atmosphere, to a solution of rotaxane **63a** (16 mg, 6.2 μmol , 1.0 equiv.) in dry DMF (500 μL) was added 2-mercaptoethanol (2.0 μL , 31 μmol , 5 equiv.) and Cs_2CO_3 (10 mg, 31 μmol , 5.0 equiv.). The suspension was stirred for 48 hours at room temperature under an Ar atmosphere. $\text{LiCl}_{(\text{aq})}$ (5%, 25 mL) was added to the resulting mixture which was extracted with dichloromethane (3×25 mL). The combined organic phases were dried over anhydrous Na_2SO_4 and the solvent was evaporated under reduced pressure. The resulting crude mixture was analyzed by HPLC.

Control for the chemical disassembly of rotaxane 63a:

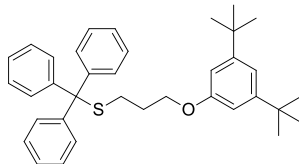
Rotaxane **63a** (10 mg) was dissolved in DMF (1 mL). Subsequently, Cs_2CO_3 (15 mg) was added and the suspension was stirred for 48 h at room temperature under inert atmosphere. To this mixture was added an aqueous solution of LiCl (5%, 25 mL) and the aqueous layer was extracted with CH_2Cl_2 (2×25 mL). The combined organic phases were dried over anhydrous Na_2SO_4 and the solvent was evaporated under reduced pressure. The residue was dissolved in CDCl_3 (600 μL) and analyzed by ^1H NMR.

Compound 123:

To a degassed solution of 1-bromo-3,5-di-*tert*-butylbenzene (1.29 g, 4.79 mmol) in freshly distilled THF (15 mL) at -78 $^{\circ}\text{C}$ was added $^n\text{BuLi}$ (2.5 M in hexane, 2.30 mL, 5.75 mmol) dropwise. The solution was stirred for 20 min at -78 $^{\circ}\text{C}$ and trimethyl borate (800 μL , 7.19 mmol) was added. The solution was stirred for 25 min at -78 $^{\circ}\text{C}$. The mixture was allowed to warm up to 0 $^{\circ}\text{C}$ and was further stirred for 2 h at 0 $^{\circ}\text{C}$. Subsequently, H_2O_2 (33% in H_2O , 875 μL , 9.58 mmol) was added and the resulting mixture was stirred for 30 min at 0 $^{\circ}\text{C}$ then, 1 h at room temperature. The reaction mixture was cooled in a water-ice bath and was slowly treated with an aqueous solution of Na_2SO_3 (0.63 M, 15 mL). The mixture was then stirred for 15 min at 0 $^{\circ}\text{C}$ and 5 min at room temperature. The resulting mixture was extracted with EtOAc (3×50 mL) and the combined extracts were washed with H_2O (2×100 mL) and brine (2×100 mL). The organic layer was dried over anhydrous Na_2SO_4 and the solvent was evaporated under vacuum. The crude material was purified by column chromatography (SiO_2 , EtOAc/Hexane 10:90) to give **123** (599 mg, 61%) as a white solid. ^1H NMR (400 MHz, CDCl_3): δ =7.06 (s, 1H), 6.76 (s, 2H), 5.59

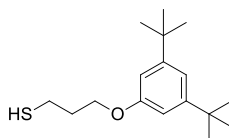
(br, 1H), 1.34 (s, 18H). HR-MS (ESI⁻): m/z : 205.1593 [M-H]⁻ (calcd for C₁₄H₂₁O: 205.1592). Characterization data are in agreement with those from literature.²⁷⁶

Compound 124:



To a degassed solution of **123** (520 mg, 2.52 mmol) in anhydrous CH₃CN (30 mL) were added **55** (2.00 g, 5.03 mmol) and K₂CO₃ (1.74 g, 12.6 mmol). The suspension was stirred for 22 h at 75 °C. The solvent was evaporated under reduced pressure and the solid was dissolved in CH₂Cl₂/H₂O (1:1, 200 mL). Layers were separated and the aqueous one was extracted with CH₂Cl₂ (50 mL). The combined extracts were dried over anhydrous Na₂SO₄ and the solvent was removed under vacuum. The crude material was purified by column chromatography (SiO₂, CH₂Cl₂/Hexane 20:80) to yield **124** (864 mg, 66%) as a colorless oil. ¹H NMR (400 MHz, CDCl₃): δ= 7.43 (m, 6H), 7.28 – 7.15 (m, 9H), 7.01 (s, 1H), 6.69 (s, 2H), 3.92 (m, 2H), 2.38 (m, 2H), 1.84 (m, 2H), 1.31 (s, 18H). ¹³C NMR (101 MHz, CDCl₃): δ=158.50, 152.21, 145.05, 129.75, 127.98, 126.71, 115.02, 108.95, 66.77, 66.14, 35.11, 31.62, 28.75. IR (neat): ν=2958, 2866, 1591, 1443, 1427, 1299, 1053, 744, 699 cm⁻¹. HR-MS (ESI⁺): m/z : 545.2856 [M+Na]⁺ (calcd for C₃₆H₄₂ONaS: 545.2854).

Compound 119:

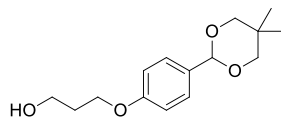


Under argon, to a solution of **124** (800 mg, 1.53 mmol) in dry CH₂Cl₂ (10 mL) were added CF₃CO₂H (2 mL) and Et₃SiH (1 mL). The solution was stirred for 4 h at room temperature and the solvent was removed under reduced pressure. Subsequently, the solid was dissolved in toluene (20 mL) and the solvent was evaporated under vacuum. The crude material was purified by column chromatography (SiO₂, CH₂Cl₂/Hexane 20:80) to afford **119** (340 mg, 79%) as a colorless oil. ¹H NMR (400 MHz, CDCl₃): δ=7.07 (t, J = 1.7 Hz, 1H), 6.80 (d, J = 1.7 Hz, 2H), 4.12 (t, J = 5.9 Hz, 2H), 2.79 (q, J = 7.1 Hz, 2H), 2.12 (p, J = 6.5 Hz, 2H), 1.45 (t, J = 8.1 Hz, 1H), 1.35 (s, 18H). ¹³C NMR (101 MHz, CDCl₃): δ=158.52, 152.35, 115.21, 108.92, 65.51, 35.12, 33.76, 31.59, 21.50. IR (neat): ν=2956, 2866, 1591, 1427, 1298, 1217,

²⁷⁶ O. Kwon, K. V. N. Esguerra, M. Glazerman, L. Petitjean, Y. Xu, X. Ottenwaelder and J.-P. Lumb, *Synlett* **2017**, 28, 1548-1553.

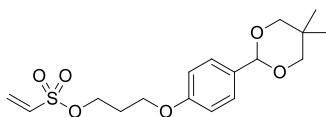
1203, 1061, 863, 764, 750, 707 cm^{-1} . HR-MS (ESI⁺): m/z : 303.1754 [M+Na]⁺ (calcd for C₁₇H₂₈ONaS: 303.1753).

Compound 125:



To a degassed solution of **79** (6.45 g, 35.8 mmol) in dry toluene (300 mL) were added 2,2-dimethyl-1,3-propanediol (5.59 g, 53.7 mmol), dl-10-camphorsulfonic acid (1.66 g, 7.16 mmol) and MS 3Å (10 g). The suspension was stirred for 18 h at 100 °C. The resulting mixture was cooled to room temperature and Et₃N (15 mL) was added. The solution was concentrated to dryness and the crude material was purified by column chromatography (SiO₂, EtOAc/CH₂Cl₂ 15:85) to afford **125** (6.92 g, 73%) as a white solid. M.p. 55–57 °C. ¹H NMR (500 MHz, CDCl₃): δ =7.42 (d, J = 8.7 Hz, 2H), 6.89 (d, J = 8.7 Hz, 2H), 5.34 (s, 1H), 4.11 (t, J = 6.0 Hz, 2H), 3.83 (t, J = 5.9 Hz, 2H), 3.75 (d, J = 11.3 Hz, 2H), 3.63 (d, J = 10.5 Hz, 2H), 2.02 (p, J = 6.0 Hz, 2H), 1.29 (s, 3H), 0.79 (s, 3H). ¹³C NMR (126 MHz, CDCl₃): δ =159.29, 131.40, 127.58, 114.40, 101.76, 77.79, 65.90, 60.55, 32.08, 30.31, 23.18, 22.02. IR (neat): ν =3400 (br), 2953, 2858, 1614, 1516, 1387, 1245, 1097, 1059, 1036, 1012, 987, 827, 764, 749 cm^{-1} . HR-MS (ESI⁺): m/z : 289.1415 [M+Na]⁺ (calcd for C₁₅H₂₂O₄Na: 289.1416).

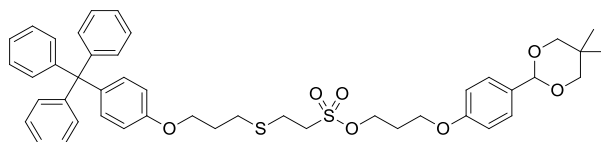
Compound 116:



Under an argon atmosphere, to a solution of **125** (2.29 g, 8.58 mmol) in anhydrous CH₂Cl₂ (250 mL), in a water-ice bath, were added Et₃N (5.96 mL, 42.9 mmol) and a solution of 2-chloroethanesulfonyl chloride (1.35 mL, 12.9 mmol) in anhydrous CH₂Cl₂ (25 mL). The solution was stirred for 1 h at 0 °C. Subsequently, the mixture was diluted with CH₂Cl₂ (50 mL) and washed with H₂O (250 mL). The aqueous layer was then extracted with CH₂Cl₂ (250 mL). The combined organic phases were dried over anhydrous Na₂SO₄ and the solvent was removed under reduced pressure. The crude material was purified by column chromatography (SiO₂, EtOAc/Hexane 35:65) to yield **116** (2.46 g, 80%) as a white solid. M.p. 57–58 °C. ¹H NMR (400 MHz, CDCl₃): δ =7.43 (d, J = 8.7 Hz, 2H), 6.87 (d, J = 8.7 Hz, 2H), 6.50 – 6.36 (m, 2H), 6.06 (d, J = 9.3 Hz, 1H), 5.34 (s, 1H), 4.32 (t, J = 6.1 Hz, 2H), 4.06 (t, J = 5.9 Hz, 2H), 3.75 (d, J = 11.2 Hz, 2H), 3.64 (d, J = 10.5 Hz, 2H), 2.19 (p, J = 6.0 Hz, 2H), 1.29 (s, 3H), 0.79 (s, 3H). ¹³C NMR (101 MHz, CDCl₃): δ =158.96, 132.31, 131.69, 130.46, 127.66, 114.34, 101.67, 77.78, 67.49, 63.28,

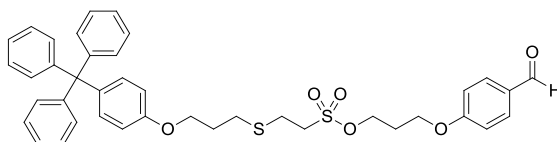
30.30, 29.04, 23.17, 22.00. IR (neat): $\nu=2954, 2848, 1614, 1516, 1358, 1244, 1169, 1097, 974, 944, 828, 761 \text{ cm}^{-1}$. HR-MS (ESI⁺): m/z : 379.1188 [M+Na]⁺ (calcd for C₁₇H₂₄O₆SNa: 379.1191).

Compound 126:

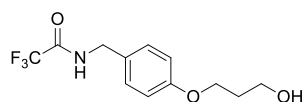


To a degassed solution of **116** (1.15 g, 3.23 mmol) in CH₂Cl₂/PrOH (8:1, 90 mL) were added **53c** (2.15 g, 5.24 mmol), Et₃N (225 μ L, 1.62 mmol) and PPh₃ (169 mg, 0.646 mmol). The solution was stirred for 24 h at room temperature. The solvent was then evaporated under reduced pressure and the crude material was purified by column chromatography (SiO₂, CH₂Cl₂/EtOAc 98:2) to give **126** (2.46 g, 99%) as a white solid. M.p. 70–73 °C. ¹H NMR (400 MHz, CDCl₃): $\delta=7.43$ (d, $J = 8.7$ Hz, 2H), 7.30 – 7.14 (m, 15H), 7.11 (d, $J = 8.9$ Hz, 2H), 6.88 (d, $J = 8.7$ Hz, 2H), 6.76 (d, $J = 8.9$ Hz, 2H), 5.33 (s, 1H), 4.44 (t, $J = 6.2$ Hz, 2H), 4.08 (t, $J = 5.9$ Hz, 2H), 3.99 (t, $J = 5.9$ Hz, 2H), 3.74 (d, $J = 11.2$ Hz, 2H), 3.62 (d, $J = 10.6$ Hz, 2H), 3.34 (m, 2H), 2.92 (m, 2H), 2.69 (t, $J = 7.2$ Hz, 2H), 2.21 (p, $J = 6.0$ Hz, 2H), 2.01 (p, $J = 6.4$ Hz, 2H), 1.28 (s, 3H), 0.79 (s, 3H). ¹³C NMR (101 MHz, CDCl₃): $\delta=158.95, 156.79, 147.15, 139.32, 132.36, 131.77, 131.24, 127.70, 127.56, 125.99, 114.38, 113.36, 101.66, 77.78, 67.05, 65.81, 64.45, 63.41, 50.66, 30.31, 29.30, 29.19, 29.01, 25.37, 23.19, 22.03$. IR (neat): $\nu=3055, 2956, 2849, 1611, 1508, 1244, 1167, 1099, 828, 734, 702 \text{ cm}^{-1}$. HR-MS (ESI⁺): m/z : 789.2890 [M+Na]⁺ (calcd for C₄₅H₅₀NaO₇S₂: 789.2896).

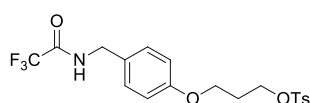
Compound 117:



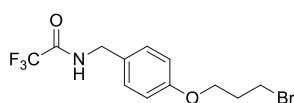
Under argon, to a solution of **126** (2.28 g, 2.97) in CH₂Cl₂ (50 mL) were added CF₃CO₂H (20 mL) and H₂O (2 mL). The solution was stirred for 5 h at room temperature and concentrated to dryness. The crude material was purified by column chromatography (SiO₂, CH₂Cl₂/EtOAc 99:1) to afford **117** (1.93 g, 95%) as a white solid. M.p. 91–93 °C. ¹H NMR (400 MHz, CDCl₃): $\delta=9.87$ (s, 1H), 7.82 (d, $J = 8.7$ Hz, 2H), 7.26 – 7.15 (m, 15H), 7.10 (d, $J = 8.9$ Hz, 2H), 6.99 (d, $J = 8.7$ Hz, 2H), 6.75 (d, $J = 8.9$ Hz, 2H), 4.45 (t, $J = 6.1$ Hz, 2H), 4.16 (t, $J = 5.9$ Hz, 2H), 4.00 (t, $J = 5.8$ Hz, 2H), 3.44 (m, 2H), 2.92 (m, 2H), 2.71 (t, $J = 7.2$ Hz, 2H), 2.25 (p, $J = 6.0$ Hz, 2H), 2.02 (p, $J = 6.4$ Hz, 2H). ¹³C NMR (101 MHz, CDCl₃): $\delta=190.82, 163.54, 156.73, 147.11, 139.42, 132.38, 132.16, 131.22, 130.43, 127.56, 126.00, 114.87, 113.34, 66.67, 65.78, 64.44, 63.80, 50.76, 29.27, 29.22, 29.07, 25.41$. IR (neat): $\nu=2929, 1688, 1600, 1508, 1357, 1253, 1162, 1035, 942, 831, 750, 703 \text{ cm}^{-1}$. HR-MS (ESI⁺): m/z : 703.2158 [M+Na]⁺ (calcd for C₄₀H₄₀NaO₆S₂: 703.2164).

Compound 127:

To a degassed solution of **80** (2.61 g, 14.4 mmol) in dry MeOH (90 mL) were added Et₃N (2.00 mL, 14.4 mmol) and ethyl trifluoroacetate (2.22 mL, 18.7 mmol). The solution was stirred for 2 h at room temperature. The resulting solution was diluted with H₂O (100 mL) and brine (150 mL) and then extracted with EtOAc (3 × 250 mL). The combined organic layers were dried over anhydrous Na₂SO₄ and the solvent was removed under vacuum. The crude material was purified by column chromatography (SiO₂, CH₂Cl₂/MeOH 96:4) to afford **127** (3.55 g, 89%) as a white solid. M.p. 81–84 °C. ¹H NMR (400 MHz, CDCl₃): δ=7.20 (d, *J* = 8.6 Hz, 2H), 6.88 (d, *J* = 8.6 Hz, 2H), 6.72 (br, 1H), 4.44 (d, *J* = 5.7 Hz, 2H), 4.10 (t, *J* = 6.0 Hz, 2H), 3.84 (t, *J* = 5.9 Hz, 2H), 2.03 (p, *J* = 6.0 Hz, 2H), 1.85 (br, 1H). ¹³C NMR (101 MHz, CDCl₃): δ=158.93, 157.18 (q, *J* = 37.2 Hz), 129.59, 128.26, 116.01 (q, *J* = 287.8 Hz), 115.08, 65.87, 60.41, 43.56, 32.05. IR (neat): ν=3300, 2948, 2878, 1697, 1555, 1513, 1188, 1167, 1061 cm⁻¹. HR-MS (ESI⁺): *m/z*: 300.0824 [M+Na]⁺ (calcd for C₁₂H₁₄NO₃F₃Na: 300.0823).

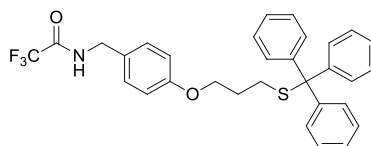
Compound 128:

To a degassed solution of **127** (3.38 g, 12.2 mmol) in anhydrous CH₂Cl₂ (150 mL) were added Et₃N (6.80 mL, 48.8 mmol), TsCl (4.65 g, 24.4 mmol) and a catalytic amount of DMAP. The solution was stirred for 18 h at room temperature and concentrated to dryness. The crude material was purified by column chromatography (SiO₂, CH₂Cl₂, to CH₂Cl₂/MeOH 98:2) to yield **128** (5.24 g, 99%) as a white solid. M.p. 122–125 °C. ¹H NMR (500 MHz, CDCl₃): δ=7.76 (d, *J* = 8.3 Hz, 2H), 7.27 (d, *J* = 8.5 Hz, 2H), 7.19 (d, *J* = 8.7 Hz, 2H), 6.77 (d, *J* = 8.6 Hz, 2H), 6.48 (br, 1H), 4.46 (d, *J* = 5.7 Hz, 2H), 4.24 (t, *J* = 6.0 Hz, 2H), 3.96 (t, *J* = 5.9 Hz, 2H), 2.39 (s, 3H), 2.12 (p, *J* = 6.0 Hz, 2H). ¹³C NMR (126 MHz, CDCl₃): δ= 158.69, 157.13 (q, *J* = 37.3 Hz), 144.95, 133.01, 129.98, 129.55, 128.32, 128.01, 116.01 (q, *J* = 287.9 Hz), 115.07, 67.09, 63.42, 43.59, 29.02, 21.76. IR (neat): ν=3323, 2934, 1688, 1517, 1358, 1251, 1166, 951, 749 cm⁻¹. HR-MS (ESI⁺): *m/z*: 454.0912 [M+Na]⁺ (calcd for C₁₉H₂₀NF₃O₅SNa: 454.0912).

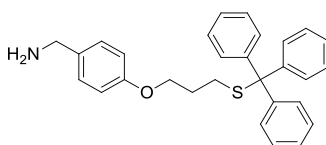
Compound 129:

Under an argon atmosphere, to a solution of **128** (2.92 g, 6.77 mmol) in dry acetone (180 mL) was added LiBr (5.88 g, 67.7 mmol). The suspension was stirred for 18 h at reflux and concentrated to dryness. The resulting solid was dissolved in CH₂Cl₂/H₂O (1:1, 500 mL). Layers were separated and the aqueous one was extracted with CH₂Cl₂ (2 × 250 mL). The combined organic phases were dried over anhydrous Na₂SO₄ and the solvent was evaporated under vacuum. The crude material was purified by column chromatography (SiO₂, CH₂Cl₂) to give **129** (1.97 g, 86%) as a white solid. M.p. 106–109 °C. ¹H NMR (400 MHz, CDCl₃): δ=7.22 (d, *J* = 8.6 Hz, 2H), 6.90 (d, *J* = 8.6 Hz, 2H), 6.50 (br, 1H), 4.46 (d, *J* = 5.7 Hz, 2H), 4.11 (t, *J* = 5.8 Hz, 2H), 3.60 (t, *J* = 6.4 Hz, 2H), 2.32 (p, *J* = 6.1 Hz, 2H). ¹³C NMR (126 MHz, CDCl₃): δ=158.89, 157.12 (q, *J* = 36.9 Hz), 129.64, 128.30, 116.00 (q, *J* = 287.9 Hz), 115.17, 65.56, 43.61, 32.40, 30.01. IR (neat): ν=3288, 1698, 1551, 1515, 1248, 1181, 1159, 823, 754 cm⁻¹. HR-MS (ESI⁻): *m/z*: 338.0003 [M-H]⁻ (calcd for C₁₂H₁₂NO₂F₃Br: 338.0004).

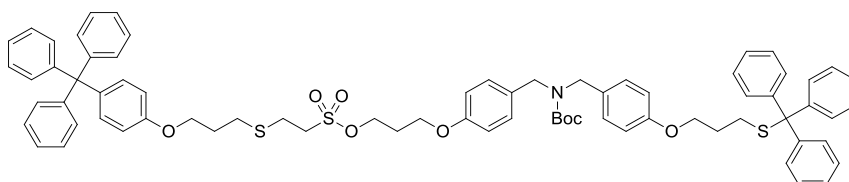
Compound 130:



To a degassed solution of triphenylmethanethiol (955 mg, 3.46 mmol) in anhydrous THF (9 mL), in a water-ice bath, was added LiHMDS (1 M in THF, 3.50 mL, 3.46 mmol). The mixture was stirred at 0 °C until the thiolate precipitates (approximately 10 min). Subsequently, the suspension was allowed to warm up to room temperature and a degassed solution of **129** (980 mg, 2.88 mmol) in dry THF (4 mL) was added. The mixture was further stirred for 1 h at room temperature and was concentrated to dryness. The resulting syrup was dissolved in CH₂Cl₂ (100 mL) and washed with H₂O (2 × 100 mL). The organic layer was dried over anhydrous Na₂SO₄ and the solvent was removed under reduced pressure. The crude material was purified by column chromatography (SiO₂, Hexane/CH₂Cl₂ 20:80) to give **130** (1.31 g, 85%) as a white solid. M.p. 111–113 °C. ¹H NMR (500 MHz, CDCl₃): δ=7.44 (m, 6H), 7.34 – 7.19 (m, 11H), 6.84 (d, *J* = 8.6 Hz, 2H), 6.58 (br, 1H), 4.46 (d, *J* = 5.7 Hz, 2H), 3.92 (t, *J* = 6.2 Hz, 2H), 2.39 (t, *J* = 7.1 Hz, 2H), 1.84 (p, *J* = 6.7 Hz, 2H). ¹³C NMR (126 MHz, CDCl₃): δ=158.97, 157.09 (q, *J* = 36.9 Hz), 144.95, 129.70, 129.51, 127.99, 126.75, 115.99 (q, *J* = 287.9 Hz), 115.11, 66.76, 66.44, 43.60, 28.54, 28.38. IR (neat): ν=3307, 3058, 2932, 1705, 1512, 1443, 1246, 1202, 1172, 1033, 743, 700 cm⁻¹. HR-MS (ESI⁺): *m/z*: 558.1691 [M+Na]⁺ (calcd for C₃₁H₂₈NO₂SF₃Na: 558.1691).

Compound 118:

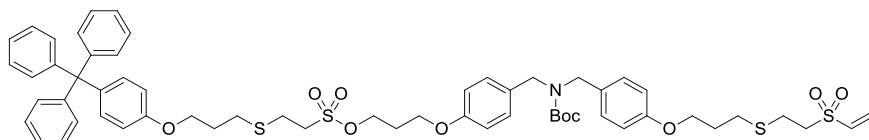
130 (1.95 g, 3.64 mmol) was dissolved in MeOH (30 mL) upon sonication, then, a solution of NaOH (728 mg, 18.2 mmol) in H₂O (8 mL) was added. The mixture was stirred for 20 h at room temperature. MeOH was evaporated under reduced pressure and the resulting mixture was diluted with H₂O/CH₂Cl₂ (2:3, 150 mL). Layers were separated and the aqueous one was extracted with CH₂Cl₂ (2 × 100 mL). The combined extracts were dried over anhydrous Na₂SO₄ and the solvent was removed under reduced pressure. The crude material was purified by column chromatography (SiO₂, CH₂Cl₂/MeOH 95:5, to CH₂Cl₂/MeOH/NH₃ (30% in H₂O) 90:10:2) to yield **118** (1.21 g, 76%) as a light yellow oil. ¹H NMR (400 MHz, CDCl₃): δ=7.44 (m, 6H), 7.31 – 7.19 (m, 11H), 6.80 (d, *J* = 8.6 Hz, 2H), 3.90 (t, *J* = 6.2 Hz, 2H), 3.80 (s, 2H), 2.38 (t, *J* = 7.1 Hz, 2H), 2.29 (br, 2H), 1.82 (p, *J* = 6.8 Hz, 2H). ¹³C NMR (101 MHz, CDCl₃): δ=157.96, 144.96, 129.68, 128.49, 127.95, 126.70, 114.71, 66.70, 66.39, 45.71, 28.58, 28.45. IR (neat): ν=3056, 2925, 1609, 1510, 1488, 1444, 1243, 1033, 764, 748, 700 cm⁻¹. HR-MS (ESI⁺): *m/z*: 462.1869 [M+Na]⁺ (calcd for C₂₉H₂₉NOSNa: 462.1868); 440.2042 [M+H]⁺ (calcd for C₂₉H₃₀NOS: 440.2048)

Compound 131:

117 (1.66 g, 2.44 mmol) and **118** (1.07 g, 2.44 mmol) were dissolved in degassed anhydrous MeOH/THF (8:5, 65 mL) upon sonication. Then, the solution was stirred for 24 h at room temperature. NaBH₄ (369 mg, 9.76 mmol) was added and the solution was further stirred for 24 h at room temperature. H₂O (50 mL) was added, the mixture was stirred for 15 min and diluted with brine (100 mL). The resulting mixture was extracted with CH₂Cl₂ (3 × 150 mL). The combined extracts were dried over anhydrous Na₂SO₄ and the solvent was removed under vacuum. Subsequently, the solid was dissolved in degassed CH₂Cl₂ (60 mL); Et₃N (1.00 mL, 7.19 mmol) and a solution of Boc₂O (691 mg, 3.17 mmol) in CH₂Cl₂ (5 mL) were added dropwise. The solution was stirred for 24 h at room temperature and was concentrated to dryness. The crude material was purified by column chromatography (SiO₂, CH₂Cl₂, to CH₂Cl₂/EtOAc 96:4) to yield **131** (2.34 g, 80%) as a light yellow oil. ¹H NMR (500 MHz, CDCl₃): δ=7.42 (m, 6H), 7.29 – 7.07 (m, 30H), 6.85 (d, *J* = 8.6 Hz, 2H), 6.77 (m, 4H), 4.45 (t, *J* = 6.2 Hz, 2H), 4.28 (br d, *J* = 42.0 Hz, 4H), 4.07 (t, *J* = 5.8 Hz, 2H), 4.01 (t, *J* = 5.9 Hz, 2H), 3.91 (t, *J* = 6.1 Hz, 2H), 3.35 (m, 2H), 2.94

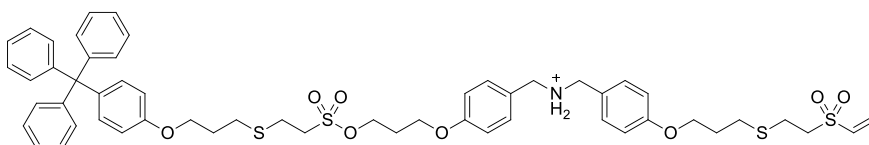
(m, 2H), 2.73 (t, $J = 7.2$ Hz, 2H), 2.37 (t, $J = 7.1$ Hz, 2H), 2.22 (p, $J = 6.0$ Hz, 2H), 2.03 (p, $J = 6.6$ Hz, 2H), 1.82 (p, $J = 6.7$ Hz, 2H), 1.50 (s, 9H). ^{13}C NMR (126 MHz, CDCl_3): $\delta = 158.19, 157.81, 156.74, 156.06, 147.12, 144.98, 139.36, 132.37, 131.22, 130.77, 130.14, 129.72, 129.56, 128.00, 127.56, 126.74, 125.99, 114.64, 114.60, 113.34, 80.06, 67.13, 66.73, 66.35, 65.76, 64.43, 63.38, 50.67, 48.45, 48.37, 48.16, 48.09, 29.39, 29.20, 29.02, 28.64, 28.47, 25.37$. IR (neat): $\nu = 2928, 1688, 1610, 1510, 1364, 1244, 1166, 764, 749, 702$ cm^{-1} . HR-MS (ESI⁺): m/z : 1226.4707 [M+Na]⁺ (calcd for $\text{C}_{74}\text{H}_{77}\text{NO}_8\text{S}_3\text{Na}$: 1226.4709).

Compound 132:



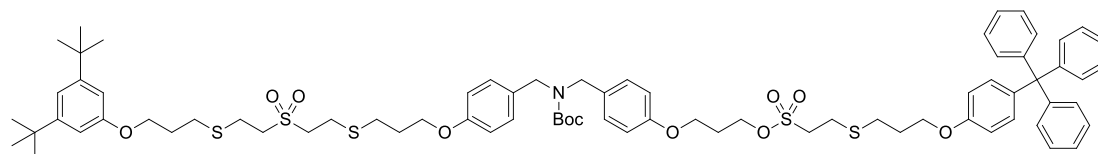
Under an argon atmosphere, to a solution of **131** (2.16 g, 1.79 mmol) in anhydrous CH_2Cl_2 (80 mL) were added $\text{CF}_3\text{CO}_2\text{H}$ (15 mL) and Et_3SiH (7 mL). The solution was stirred for 6 h at room temperature and was concentrated to dryness. The crude was dissolved in toluene (70 mL) and the solvent was evaporated under reduced pressure. Then, the solid was dissolved in degassed CH_2Cl_2 (80 mL) and Et_3N (8 mL) and Boc_2O (391 mg, 1.79 mmol) were added. The mixture was stirred for 5 h at room temperature. Subsequently, divinyl sulfone (1.40 mL, 14.3 mmol) was added and the solution was stirred for another 14 h at room temperature. The solvent was evaporated under vacuum and the crude material was purified by column chromatography (SiO_2 , CH_2Cl_2 , to $\text{CH}_2\text{Cl}_2/\text{EtOAc}$ 98:2) to afford **132** (1.01 g, 52%) as a light yellow oil. ^1H NMR (500 MHz, CDCl_3): $\delta = 7.27 - 7.08$ (m, 21H), 6.85 (d, $J = 8.6$ Hz, 4H), 6.76 (d, $J = 8.9$ Hz, 2H), 6.64 (dd, $J = 16.6, 9.8$ Hz, 1H), 6.45 (d, $J = 16.6$ Hz, 1H), 6.17 (d, $J = 9.8$ Hz, 1H), 4.45 (t, $J = 6.1$ Hz, 2H), 4.28 (br d, $J = 36.3$ Hz, 4H), 4.09 – 3.99 (m, 6H), 3.35 (m, 2H), 3.24 (m, 2H), 2.92 (m, 4H), 2.74 (m, 4H), 2.22 (p, $J = 5.9$ Hz, 2H), 2.05 (m, 4H), 1.50 (s, 9H). ^{13}C NMR (126 MHz, CDCl_3): $\delta = 158.06, 157.82, 156.73, 156.03, 147.10, 139.35, 136.13, 132.35, 131.31, 131.20, 130.72, 130.47, 129.51, 128.97, 127.53, 125.97, 114.60, 113.33, 80.08, 67.12, 65.92, 65.77, 64.42, 63.40, 54.54, 50.66, 48.50, 48.19, 29.81, 29.37, 29.19, 29.00, 28.96, 28.62, 25.35, 24.34$. IR (neat): $\nu = 2928, 1685, 1610, 1510, 1318, 1241, 1164, 764, 750, 703$ cm^{-1} . HR-MS (ESI⁺): m/z : 1102.3708 [M+Na]⁺ (calcd for $\text{C}_{59}\text{H}_{69}\text{NO}_{10}\text{NaS}_4$: 1102.3702).

Compound 133·PF₆⁻:



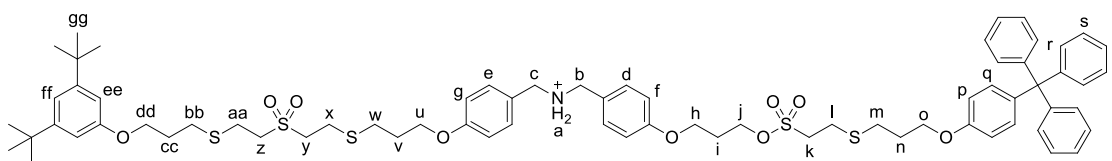
To a solution of **132** (519 mg, 0.480 mmol) in CH₂Cl₂ (30 mL) was added CF₃CO₂H (6 mL). The solution was stirred for 5 h at room temperature and was concentrated to dryness. The solid was then dissolved in CH₂Cl₂ (20 mL) and HCl (2 M in Et₂O, 3.6 mL, 7.2 mmol) was added. The mixture was stirred for 3 h at room temperature. The solvent was evaporated under reduced pressure. The resulting solid was dissolved in CH₂Cl₂/acetone/H₂O (4:5:5, 70 mL) and an excess of KPF₆ was added. The mixture was stirred for 18 h at room temperature and was diluted with H₂O (35 mL). The resulting mixture was extracted with CH₂Cl₂ (3 × 50 mL) and the combined organic phases were dried over anhydrous Na₂SO₄. The solvent was removed under reduced pressure to give **133**·PF₆⁻ (456 mg, 84%) as a white solid. M.p. 154–156 °C (decomp.). ¹H NMR (500 MHz, CDCl₃): δ=8.49 (br, 2H), 7.33 – 7.14 (m, 19H), 7.10 (d, *J* = 8.8 Hz, 2H), 6.89 (d, *J* = 8.2 Hz, 4H), 6.75 (d, *J* = 8.6 Hz, 2H), 6.63 (dd, *J* = 16.6, 9.9 Hz, 1H), 6.42 (d, *J* = 16.6 Hz, 1H), 6.18 (d, *J* = 9.9 Hz, 1H), 4.41 (t, *J* = 6.2 Hz, 2H), 4.05 – 3.87 (m, 10H), 3.34 (m, 2H), 3.18 (m, 2H), 2.92 (m, 2H), 2.83 (m, 2H), 2.72 (m, 4H), 2.28 (m, 2H), 2.02 (m, 4H). ¹³C NMR (126 MHz, CDCl₃): δ=159.82, 159.60, 156.76, 147.14, 139.41, 136.02, 132.39, 131.69, 131.51, 131.24, 127.58, 126.01, 122.35, 122.20, 115.33, 113.37, 66.98, 65.98, 65.84, 64.46, 63.52, 54.46, 53.12, 50.74, 49.48, 49.43, 29.33, 29.23, 29.05, 28.80, 25.38, 24.34. IR (neat): ν=2932, 1655, 1611, 1515, 1250, 829, 749, 702 cm⁻¹. HR-MS (ESI⁺): *m/z*: 980.3353 [M-PF₆⁻]⁺ (calcd for C₅₄H₆₂NO₈S₄: 980.3358).

Compound 134:



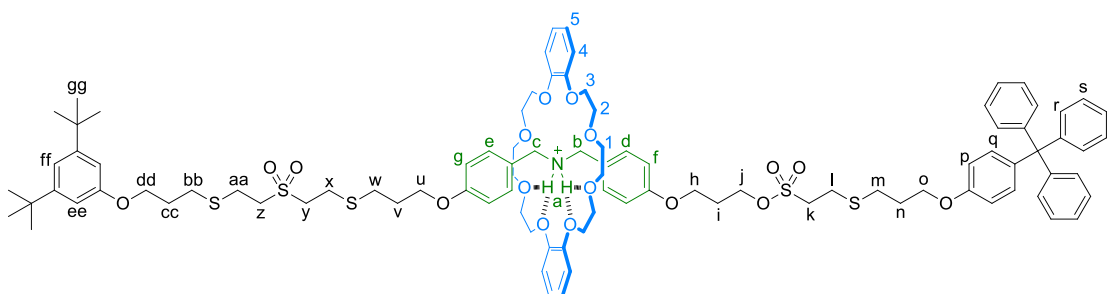
To a degassed solution **132** (54 mg, 0.049 mmol) and **119** (28 mg, 0.10 mmol) in CHCl₃ (3 mL) was added 2 drops of Et₃N. The solution was stirred for 18 h at room temperature and was concentrated to dryness. The crude material was purified by column chromatography (SiO₂, CH₂Cl₂, to CH₂Cl₂/EtOAc 97:3) to afford **134** (61 mg, 90%) as a white syrup. ¹H NMR (500 MHz, CDCl₃): δ=7.27 – 7.07 (m, 21H), 7.04 (t, *J* = 1.7 Hz, 1H), 6.85 (d, *J* = 8.6 Hz, 4H), 6.77 (m, 4H), 4.45 (t, *J* = 6.1 Hz, 2H), 4.28 (br d, *J* = 38.2 Hz, 4H), 4.10 – 3.98 (m, 8H), 3.35 (m, 2H), 3.28 (m, 4H), 2.95 (m, 6H), 2.83 – 2.70 (m, 6H), 2.22 (p, *J* = 6.0 Hz, 2H), 2.05 (m, 6H), 1.50 (s, 9H), 1.32 (s, 18H). ¹³C NMR (126 MHz, CDCl₃): δ=158.39, 158.07, 157.82, 156.74, 156.03, 152.41, 147.11, 139.35, 132.35, 131.21, 130.74, 130.47, 129.52, 128.97, 127.54, 125.98, 115.33, 114.61, 113.34, 108.90, 80.07, 67.12, 65.95, 65.77, 65.72, 64.43, 63.40, 53.83, 53.81, 50.68, 48.49, 48.15, 35.12, 31.58, 29.82, 29.40, 29.23, 29.20, 29.12, 29.01, 28.63, 25.37, 24.12, 24.07. IR (neat): ν=2948, 1687, 1608, 1591, 1510, 1242, 1164, 1119, 1038, 828, 703 cm⁻¹. HR-MS (ESI⁺): *m/z*: 1382.5573 [M+Na]⁺ (calcd for C₇₆H₉₇NO₁₁S₅Na: 1382.5563).

Compound 135·PF₆⁻:



To a solution of **134** (7 mg, 5.1 μmol) in CH₂Cl₂ (2 mL) was added CF₃CO₂H (500 μL). The solution was stirred for 2 h at room temperature and was concentrated to dryness. The solid was then dissolved in CH₂Cl₂ (3 mL) and HCl (2 M in Et₂O, 40 μL, 80 μmol) was added. The solution was stirred for 3 h at room temperature. The solvent was removed under reduced pressure. The resulting solid was dissolved in CH₂Cl₂/acetone/H₂O (4:5:5, 14 mL) and an excess of KPF₆ was added. The mixture was stirred for 18 h at room temperature and was diluted with H₂O (10 mL). The resulting mixture was extracted with CH₂Cl₂ (3 × 10 mL) and the combined organic layers were dried over anhydrous Na₂SO₄. The solvent was evaporated under vacuum to give **135·PF₆⁻** (6 mg, 83%) as a white solid. M.p. 151–153 °C (decomp.). ¹H NMR (500 MHz, CDCl₃): δ=8.49 (br, 2H, H_a), 7.35 – 7.14 (m, 19H, H_{d+e+r+s+t}), 7.10 (d, *J* = 8.5 Hz, 2H, H_q), 7.03 (s, 1H, H_{ff}), 6.87 (d, *J* = 6.7 Hz, 4H, H_{f+g}), 6.75 (m, 4H, H_{p+ee}), 4.39 (t, *J* = 6.1 Hz, 2H, H_j), 4.10 – 3.83 (m, 12H, H_{b+c+h+o+u+dd}), 3.34 (m, 2H, H_k), 3.28 – 3.19 (m, 4H, H_{y+z}), 3.00 – 2.86 (m, 6H, H_{l+x+aa}), 2.82 – 2.66 (m, 6H, H_{m+w+bb}), 2.17 (m, 2H, H_i), 2.10 – 1.97 (m, 6H, H_{n+v+cc}), 1.31 (s, 18H, H_{gg}). ¹³C NMR (126 MHz, CDCl₃): δ=158.45, 156.78, 152.45, 147.15, 147.10, 139.42, 136.40, 132.45, 132.39, 131.86, 131.81, 131.25, 127.58, 126.02, 115.36, 115.28, 113.40, 108.97, 67.01, 66.02, 65.88, 65.81, 64.48, 63.54, 53.79, 50.79, 49.40, 35.16, 32.08, 31.61, 29.86, 29.51, 29.46, 29.35, 29.26, 29.08, 28.97, 25.38, 24.09, 24.05, 22.84. IR (neat): ν=2920, 2850, 1608, 1514, 1275, 1256, 843, 764, 750 cm⁻¹. HR-MS (ESI⁺): *m/z*: 1260.5226 [M–PF₆⁻]⁺ (calcd for C₇₁H₉₀NO₉S₅: 1260.5219).

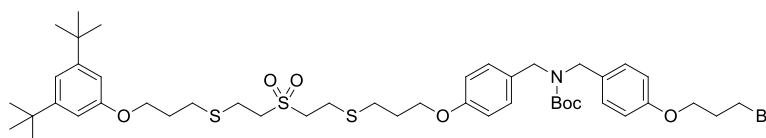
Compound 121·PF₆⁻:



133·PF₆⁻ (22 mg, 20 μmol) and **47** (44 mg, 98 μmol) were dissolved in CHCl₃ (7 mL) upon sonication. The solvent was removed under vacuum and the syrup was dissolved in degassed CHCl₃ (700 μL). The mixture was cooled to 0 °C and stirred for 1 h. To this solution were added a degassed solution of **119** (11 mg, 39 μmol) in CHCl₃ (100 μL) and a catalytic amount of DMAP. The solution was stirred for 72 h

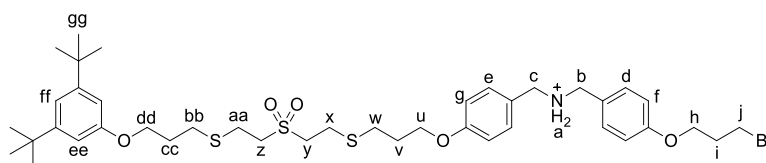
at 0 °C. Then, the solvent was evaporated under reduced pressure and the crude material was purified by gel permeation chromatography (Bio-Beads® S-X1, CH₂Cl₂) to yield **121**·PF₆⁻ (24 mg, 66%) as a white solid. M.p. 165–168 °C (decomp.). ¹H NMR (500 MHz, CDCl₃): δ= 7.46 (br, 2H, H_a), 7.25 – 7.15 (m, 19H, H_{e+d+r+s+t}), 7.09 (d, *J* = 8.8 Hz, 2H, H_q), 7.02 (t, *J* = 1.6 Hz, 1H, H_{ff}), 6.93 – 6.80 (m, 8H, H₄₊₅), 6.76 (m, 8H, H_{f+g+p+ee}), 4.44 (m, 6H, H_{j+b+c}), 4.17 – 3.99 (m, 16H, H_{3+h+o+u+dd}), 3.75 (m, 8H, H₂), 3.46 – 3.26 (m, 14H, H_{1+k+y+z}), 3.18 – 2.72 (m, 12H, H_{l+m+w+x+aa+bb}), 2.19 (m, 2H, H_i), 2.06 (m, 6H, H_{n+v+cc}), 1.31 (s, 18H, H_{gg}). ¹³C NMR (126 MHz, CDCl₃): δ= 159.52, 159.29, 158.45, 156.78, 152.38, 148.97, 147.67, 147.13, 139.31, 132.35, 131.22, 130.96, 127.56, 125.98, 124.11, 123.87, 121.97, 121.62, 115.25, 114.72, 113.37, 113.05, 108.95, 71.31, 70.84, 70.31, 70.07, 69.43, 68.53, 67.34, 66.19, 65.88, 64.44, 63.57, 53.92, 53.83, 52.13, 50.72, 35.13, 31.60, 29.83, 29.43, 29.27, 29.09, 28.97, 28.80, 25.32, 23.96, 23.85. IR (neat): ν=2937, 1655, 1590, 1506, 1275, 1256, 1214, 1180, 1121, 1055, 951, 841, 764, 750 cm⁻¹. HR-MS (ESI⁺): *m/z*: 1708.7335 [M–PF₆⁻]⁺ (calcd for C₉₅H₁₂₂NO₁₇S₅: 1708.7316).

Compound 136:



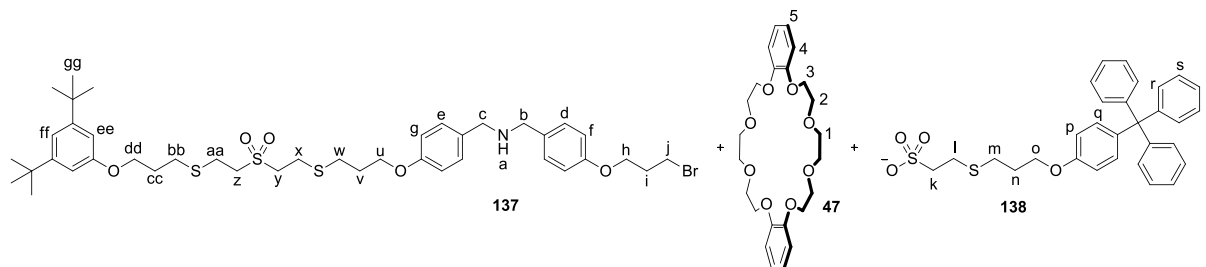
Under Ar, to a solution of **134** (20 mg, 15 μmol) in dry CH₂Cl₂ (2 mL) was added MgBr₂ (27 mg, 0.15 mmol). The suspension was stirred for 48 h at room temperature. The solvent was evaporated under reduced pressure and the crude material was purified by column chromatography (SiO₂, CH₂Cl₂/EtOAc 96:4) to afford **136** (13 mg, 96%) as a white syrup. ¹H NMR (500 MHz, CDCl₃): δ=7.13 (br, 4H), 7.03 (t, *J* = 1.7 Hz, 1H), 6.85 (m, 4H), 6.75 (d, *J* = 1.7 Hz, 2H), 4.28 (d, *J* = 37.0 Hz, 4H), 4.12 – 4.02 (m, 6H), 3.61 (t, *J* = 6.4 Hz, 2H), 3.27 (m, 4H), 2.97 (br, 4H), 2.79 (m, 4H), 2.32 (p, *J* = 6.1 Hz, 2H), 2.07 (p, *J* = 6.3 Hz, 4H), 1.50 (s, 9H), 1.31 (s, 18H). ¹³C NMR (126 MHz, CDCl₃): δ=158.41, 158.08, 156.08, 152.44, 130.54, 129.54, 128.98, 115.35, 114.68, 114.62, 108.92, 80.09, 65.97, 65.75, 65.50, 53.87, 53.84, 48.49, 48.20, 35.15, 32.54, 31.60, 30.17, 29.43, 29.26, 29.22, 29.15, 28.65, 24.15, 24.11. IR (neat): ν=2959, 2923, 1688, 1610, 1591, 1511, 1299, 1241, 1164, 1119, 1037 cm⁻¹. HR-MS (ESI⁺): *m/z*: 944.3236 [M+Na]⁺ (calcd for C₄₆H₆₈NO₇S₃NaBr: 944.3239).

Compound 137-H⁺·PF₆⁻:



To a solution of **136** (11 mg, 12 μmol) in CH_2Cl_2 (2 mL) was added $\text{CF}_3\text{CO}_2\text{H}$ (500 μL). The solution was stirred for 2 h at room temperature and was concentrated to dryness. The solid was then dissolved in CH_2Cl_2 (2 mL) and HCl (2 M in Et_2O , 90 μL , 0.18 mmol) was added. The solution was stirred for 4 h at room temperature. The solvent was removed under reduced pressure. The resulting solid was dissolved in $\text{CH}_2\text{Cl}_2/\text{acetone}/\text{H}_2\text{O}$ (4:5:5, 14 mL) and an excess of KPF_6 was added. The mixture was stirred for 18 h at room temperature and was diluted with H_2O (10 mL). The resulting mixture was extracted with CH_2Cl_2 (3 \times 20 mL) and the combined organic extracts were dried over anhydrous Na_2SO_4 . The solvent was evaporated under vacuum to yield **137** $\cdot\text{H}^+\cdot\text{PF}_6^-$ (11 mg, 95%) as a white solid. M.p. 173–175 $^\circ\text{C}$ (decomp.). ^1H NMR (500 MHz, CDCl_3): δ =8.43 (br, 2H, H_a), 7.33 (m, 4H, H_{d+e}), 7.03 (br, 1H, H_{ff}), 6.88 (d, J = 5.8 Hz, 4H, H_{f+g}), 6.75 (br, 2H, H_{ee}), 4.09 – 3.97 (m, 6H, H_{h+u+dd}), 3.91 (m, 4H, H_{b+c}), 3.55 (t, J = 6.4 Hz, 2H, H_j), 3.24 (m, 4H, H_{y+z}), 2.99 – 2.68 (m, 8H, $\text{H}_{w+x+aa+bb}$), 2.27 (p, J = 6.0 Hz, 2H, H_i), 2.10 – 1.99 (m, 4H, H_{v+cc}), 1.31 (s, 18H, H_{gg}). ^{13}C NMR (126 MHz, CDCl_3): δ =159.61, 158.29, 152.30, 147.00, 131.66, 131.10, 127.43, 122.16, 115.22, 115.13, 113.24, 108.81, 65.85, 65.66, 65.39, 53.68, 53.65, 35.00, 32.22, 31.93, 31.46, 29.36, 29.11, 28.94, 28.84, 28.51, 23.95, 23.92, 22.69. IR (neat): ν =2919, 1611, 1515, 1275, 1260, 1180, 1030, 843, 764, 750 cm^{-1} . HR-MS (ESI $^+$): m/z : 822.2895 [$\text{M}\cdot\text{PF}_6^-$] $^+$ (calcd for $\text{C}_{41}\text{H}_{61}\text{NO}_5\text{S}_3\text{Br}$: 822.2895).

Compounds **47**, **137** and **138** from the cleavage of rotaxane **121** $\cdot\text{PF}_6^-$:



Under an Ar atmosphere, to a solution of **121** $\cdot\text{PF}_6^-$ (18 mg, 9.7 μmol) in CHCl_3 (2 mL) was added MgBr_2 (18 mg, 97 μmol). The suspension was stirred for 48 h at room temperature. The solvent was removed under vacuum. The resulting solid was dissolved in CDCl_3 (1 mL) and Et_3N (14 μL , 97 μmol) was added. The solvent solution was stirred for 10 min and filtered through a 0.22 μm filter. The solvent was evaporated under reduced pressure and the crude was purified by gel permeation chromatography (Bio-Beads $^\circledR$ S-X1, CH_2Cl_2) to yield an equimolar fraction of **137/138** (10 mg, 77%) as a white solid and a mixed fraction of **47** with Et_3N . The latter was purified by column chromatography (SiO_2 , $\text{CH}_2\text{Cl}_2/\text{MeOH}$ 95:5) to afford **47** (4 mg, 92%) as a white solid.

47: ^1H NMR (500 MHz, CDCl_3): δ =6.89 (s, 4H, H_{4+5}), 4.16 (br, 4H, H_3), 3.91 (t, J = 4.3 Hz, 4H, H_2), 3.82 (s, 4H, H_1). HR-MS (ESI $^+$): m/z : 471.1992 [$\text{M}+\text{Na}$] $^+$ (calcd for $\text{C}_{24}\text{H}_{32}\text{O}_8\text{Na}$: 471.1995). Characterization data matches that of commercially available compound.

137: HR-MS (ESI⁺): m/z : 822.2892 [M+H]⁺ (calcd for C₄₁H₆₁NBrO₅S₃: 822.2895).

138: HR-MS (ESI⁻): m/z : 517.1507 [M]⁻ (calcd for C₃₀H₂₉O₄S₂: 517.1507).

137/138 (1:1): ¹H NMR (500 MHz, CDCl₃): δ = 9.19 (br, 1H, H_a), 7.40 (d, J = 8.1 Hz, 4H, H_{d+e}), 7.25 – 7.14 (m, 15H, H_{r+s+t}), 7.08 (d, J = 8.9 Hz, 2H, H_q), 7.03 (t, J = 1.7 Hz, 1H, H_{ff}), 6.88 (m, 4H, H_{f+g}), 6.75 (m, 4H, H_{p+ee}), 4.09 – 3.94 (m, 8H, H_{h+o+u+dd}), 3.85 (br, 4H, H_{b+c}), 3.53 (t, J = 6.4 Hz, 2H, H_j), 3.30 – 3.09 (m, 6H, H_{k+y+z}), 3.04 – 2.66 (m, 12H, H_{l+m+w+x+aa+bb}), 2.25 (p, J = 6.1 Hz, 2H, H_i), 2.04 (m, 6H, H_{n+v+cc}), 1.31 (s, 18H, H_{gg}).

***In situ* unidirectional transport of the macrocycle 47:**

Under Ar, **133**·PF₆⁻ (36 mg, 32 μ mol) and **47** (71 mg, 0.16 mmol) were dissolved in CDCl₃ (1.5 mL) upon sonication. The solution was cooled to 0 °C and stirred for 1 h. To this solution were added a degassed solution of **119** (18 mg, 64 μ mol) in CDCl₃ (100 μ L) and a catalytic amount of DMAP. The solution was stirred for 72 h at 0 °C. The resulting solution was allowed to warm up to room temperature and MgBr₂ (59 mg, 0.32 mmol) was added. The suspension was stirred for 48 h at room temperature. Subsequently, to this suspension was added Et₃N (44 μ L, 0.32 mmol) and the mixture was stirred for 30 min at room temperature.

The unidirectional transport process was monitored and analyzed by ¹H NMR and HRMS throughout the experiment. After the addition of MgBr₂, aliquots were prepared by filtering them through a 0.22 μ m filter in order to have a clear solution to analyze.

3.3. UV-Vis studies

Molar extinction coefficient (ϵ)

For the calculation of the molar extinction coefficient, solutions of each compound were prepared in HPLC grade CHCl₃. The absorbance spectra were measured from 250 to 700 nm. The absorbance on the different maxima was plotted obtaining the value of the molar extinction coefficient at each wavelength from the slope.

Metal salt screening

For the metal salt screening, a stock solution of rotaxane **106** in CHCl₃ (4.32 \times 10⁻⁴ M) have been prepared using a 50 mL volumetric flask. In a vial, to the metal salt (5 equiv.) was added the stock solution of rotaxane **106** (2 mL). Subsequently, the mixture was sonicated for 1 min and the UV-Vis spectrum was recorded.

For the control experiment of the addition of salt in the presence of thread **105**, a stock solution of thread **105** in CHCl_3 (2.9×10^{-4} M) have been prepared using a 50 mL volumetric flask. In a vial, to the metal salt (5 equiv.) was added the stock solution of thread **105** (2 mL). Subsequently, the mixture was sonicated for 1 min and the UV-Vis spectrum was recorded.

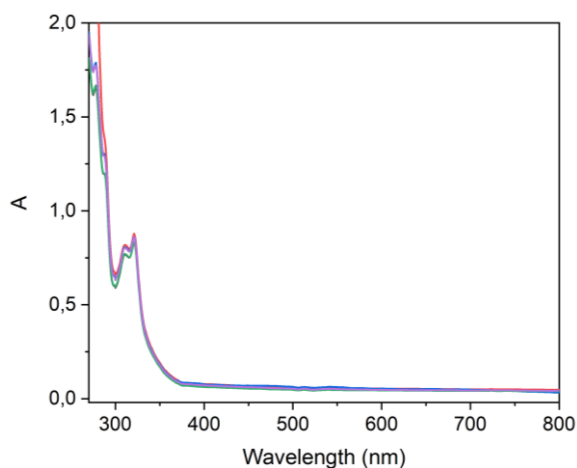


Figure 60. UV-Vis spectra (CHCl_3) of thread **105** (black), thread **105** with a 5 equiv. of $[\text{Li}(\text{OEt}_2)_n][\text{B}(\text{C}_6\text{F}_5)_4]$ (red), LiOTf (blue), $\text{Sc}(\text{OTf})_3$ (green) and $\text{In}(\text{OTf})_3$ (purple) showing no difference of absorption.

UV-Vis titrations

For the following titrations, a stock solution of rotaxane **106** was prepared in CHCl_3 (3.80×10^{-4} M) using a volumetric flask. Then, the solution of desired metal salt was prepared in another volumetric flask using the stock solution of rotaxane **106** in CHCl_3 in order to obtain a constant concentration of the rotaxane during the titration experiment. The addition of the solution of the metal salt in the rotaxane solution (2 mL) was achieved with Hamilton® syringes using typically the following order: $16 \times 12 \mu\text{L}$, $4 \times 24 \mu\text{L}$, $2 \times 48 \mu\text{L}$, $6 \times 96 \mu\text{L}$, $1 \times 192 \mu\text{L}$ and $1 \times 288 \mu\text{L}$. After each addition, the solution was shaken for 10 seconds and the UV-Vis spectrum was recorded from 250 nm to 800 nm.

Table 9. Concentration of the solution of the corresponding salt used for the titration.

salt	Concentration of the salt [mM]
$[\text{Li}(\text{OEt}_2)_n][\text{B}(\text{C}_6\text{F}_5)_4]$	10.7
LiOTf	8.59
$\text{Sc}(\text{OTf})_3$	8.66
$\text{In}(\text{OTf})_3$	8.79

3.4. HPLC method

The mobile phase gradient used is shown in the following table:

Table 10. Solvent gradient used for the HPLC analysis.

Time (min)	CH ₂ Cl ₂	Methanol
0	100	0
1	99	1
15	98	2
25	97	3
30	96	4
32	95	5
34	93	7
36	90	10
38	95	5
40	100	0

3.5. NMR spectra of final compounds

Compound 61a:

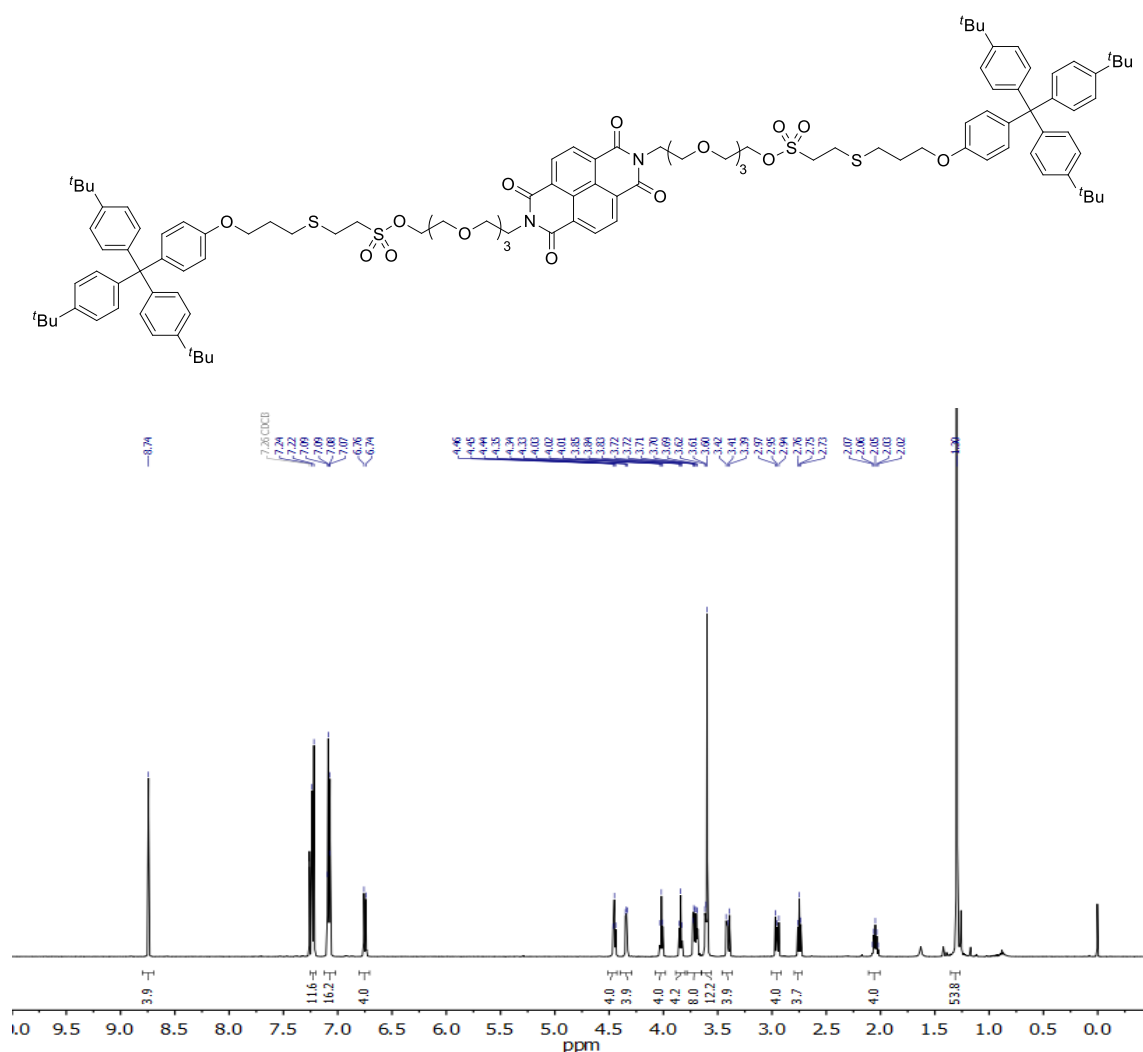


Figure 61. ¹H NMR (500 MHz, CDCl₃) spectrum of 61a.

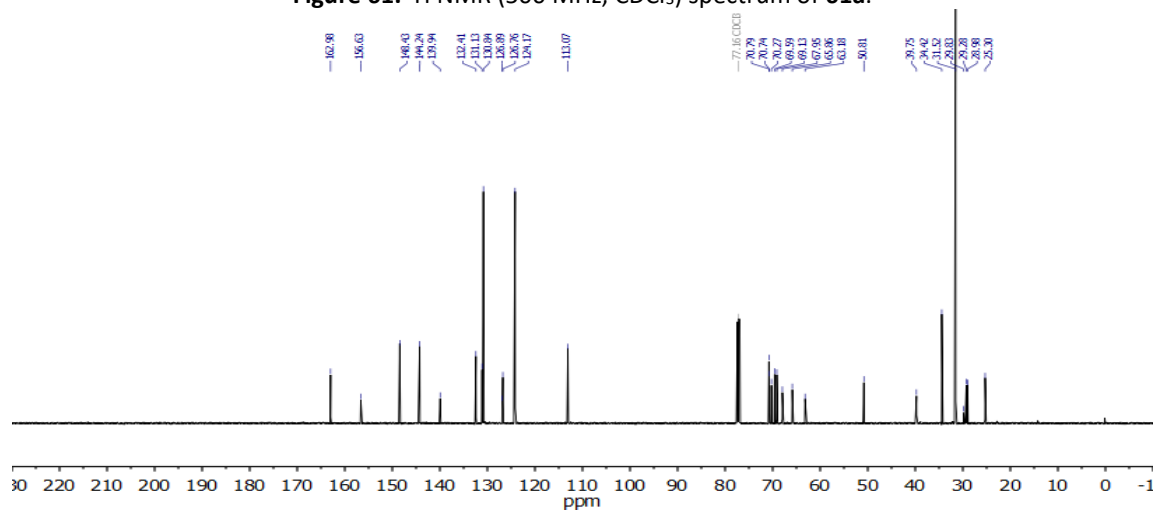
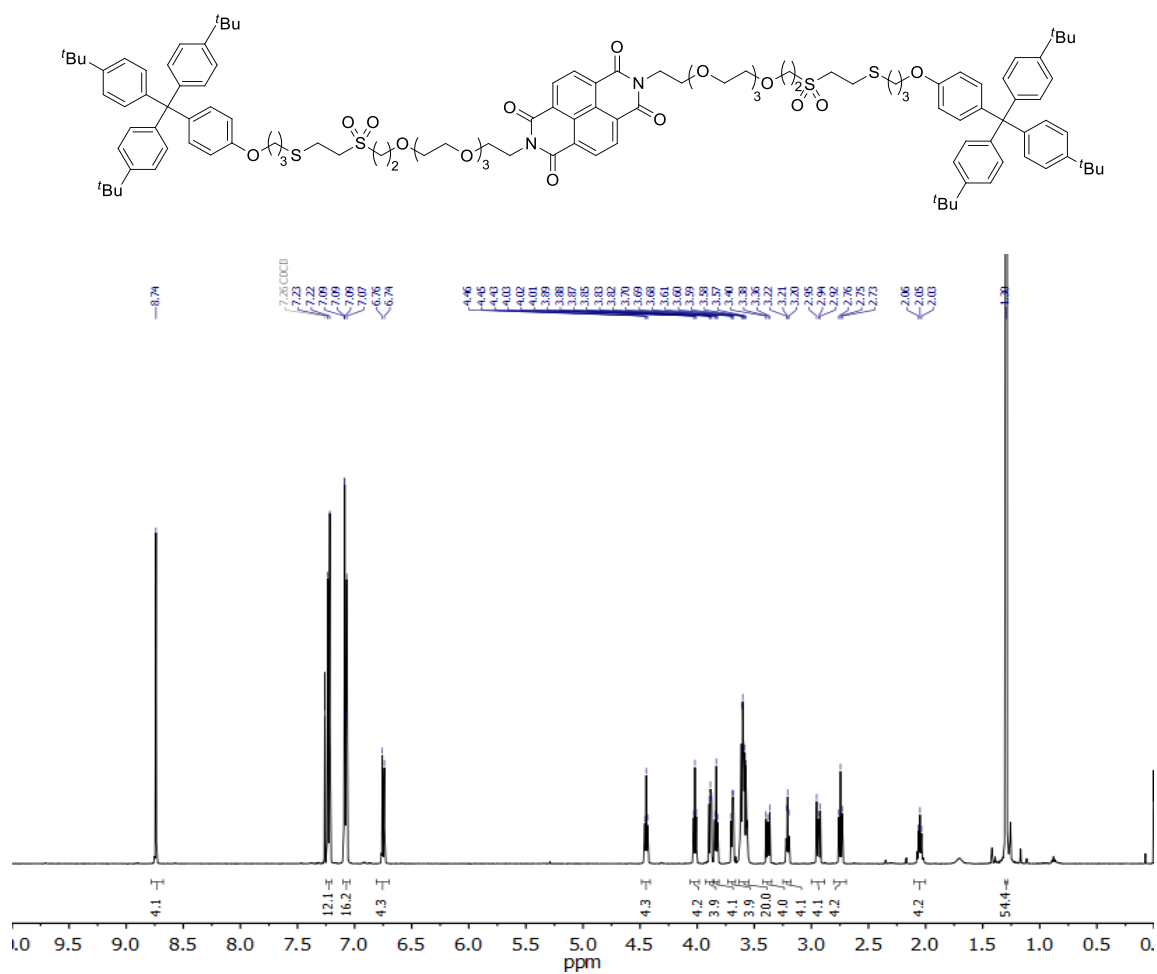
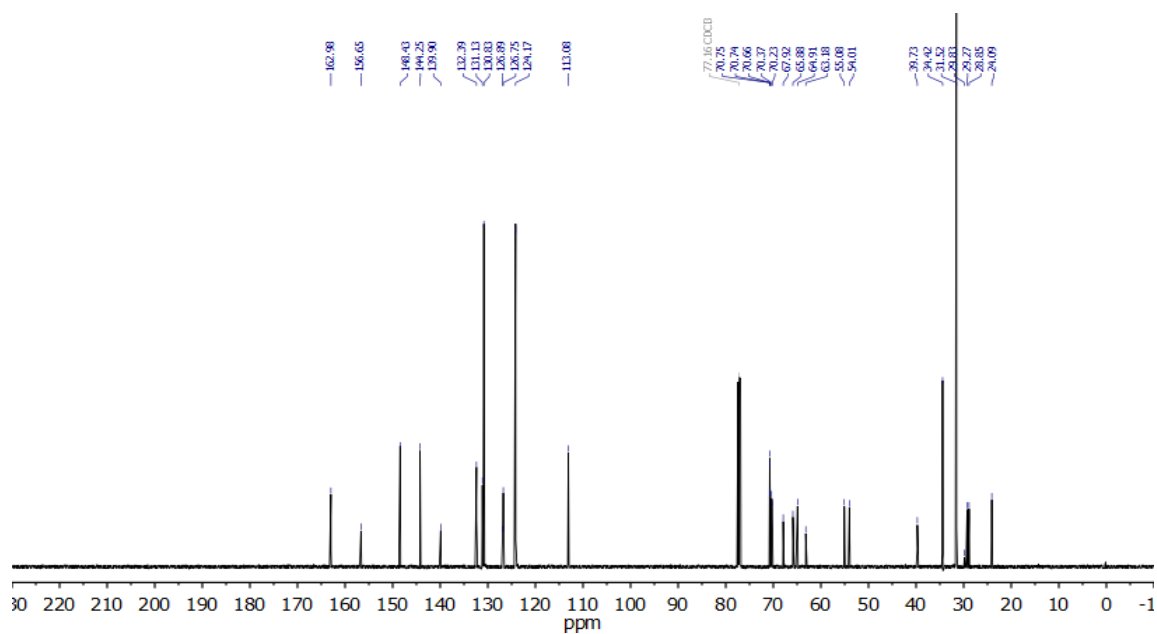


Figure 62. ¹³C NMR (126 MHz, CDCl₃) spectrum of 61a.

Compound 61b:

Figure 63. ¹H NMR (500 MHz, CDCl₃) spectrum of 61b.Figure 64. ¹³C NMR (126 MHz, CDCl₃) spectrum of 61b.

Compound 61c:

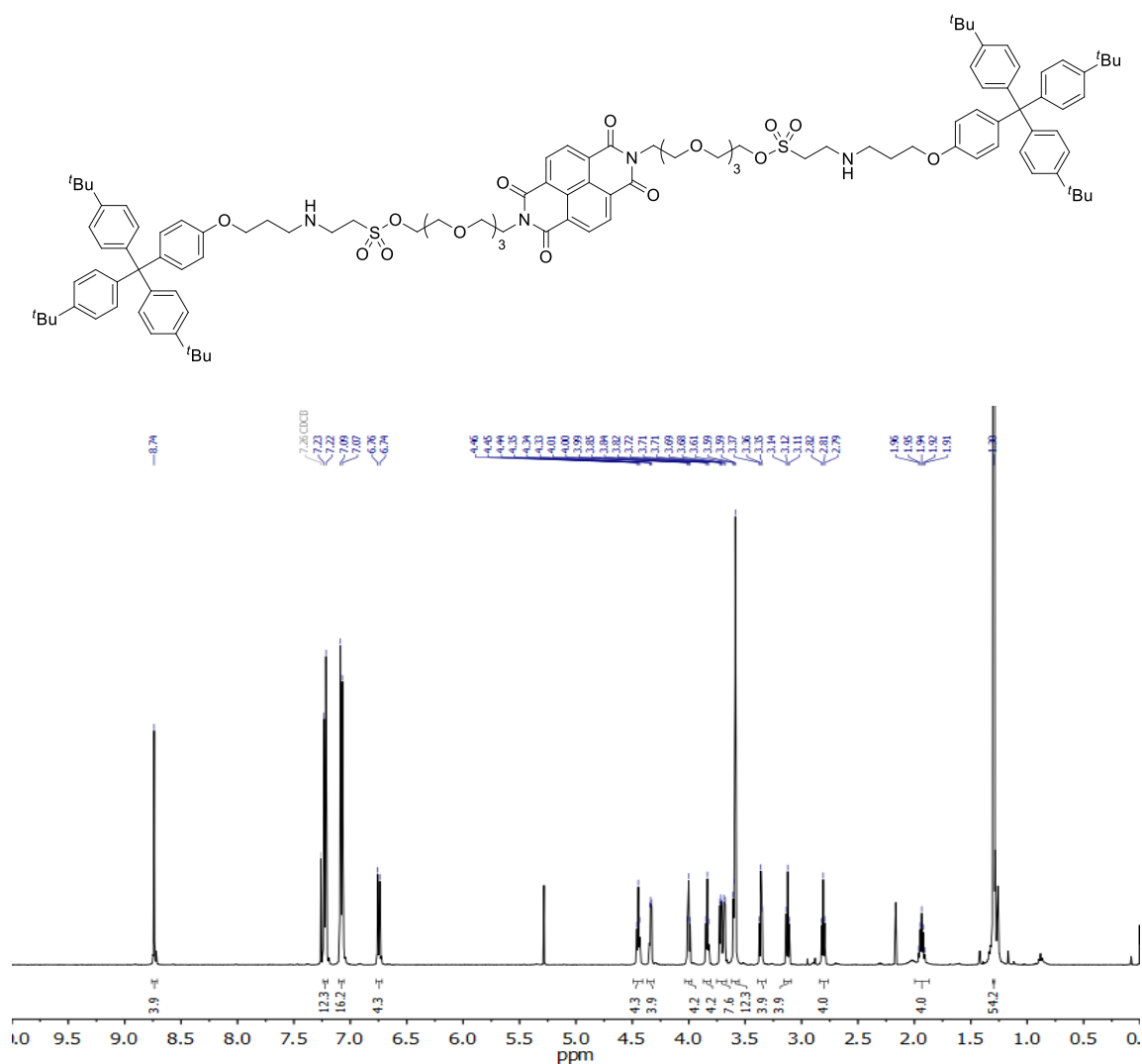


Figure 65. ¹H NMR (500 MHz, CDCl₃) spectrum of 61c.

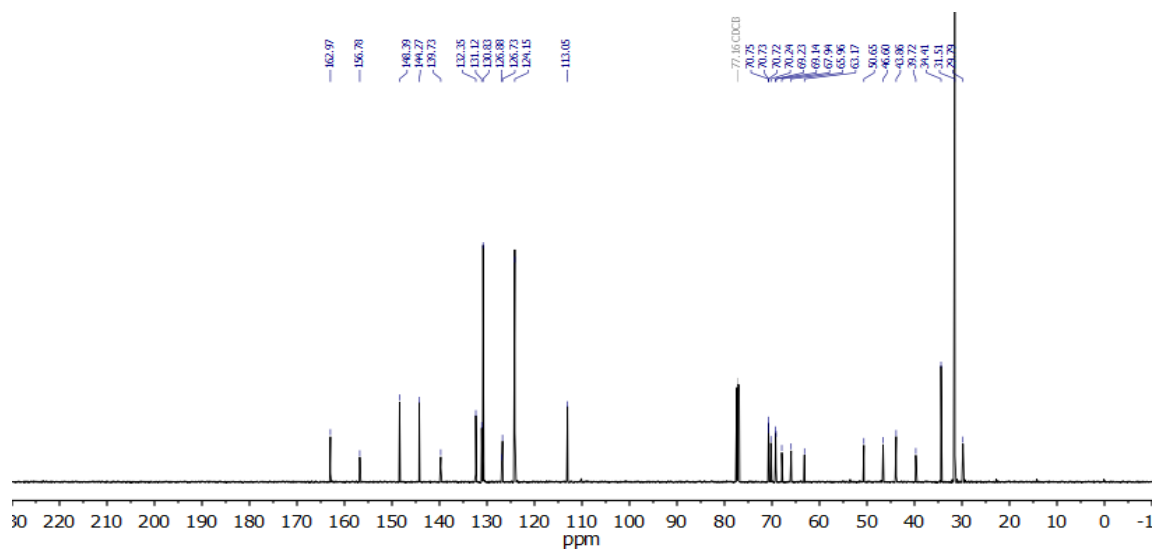
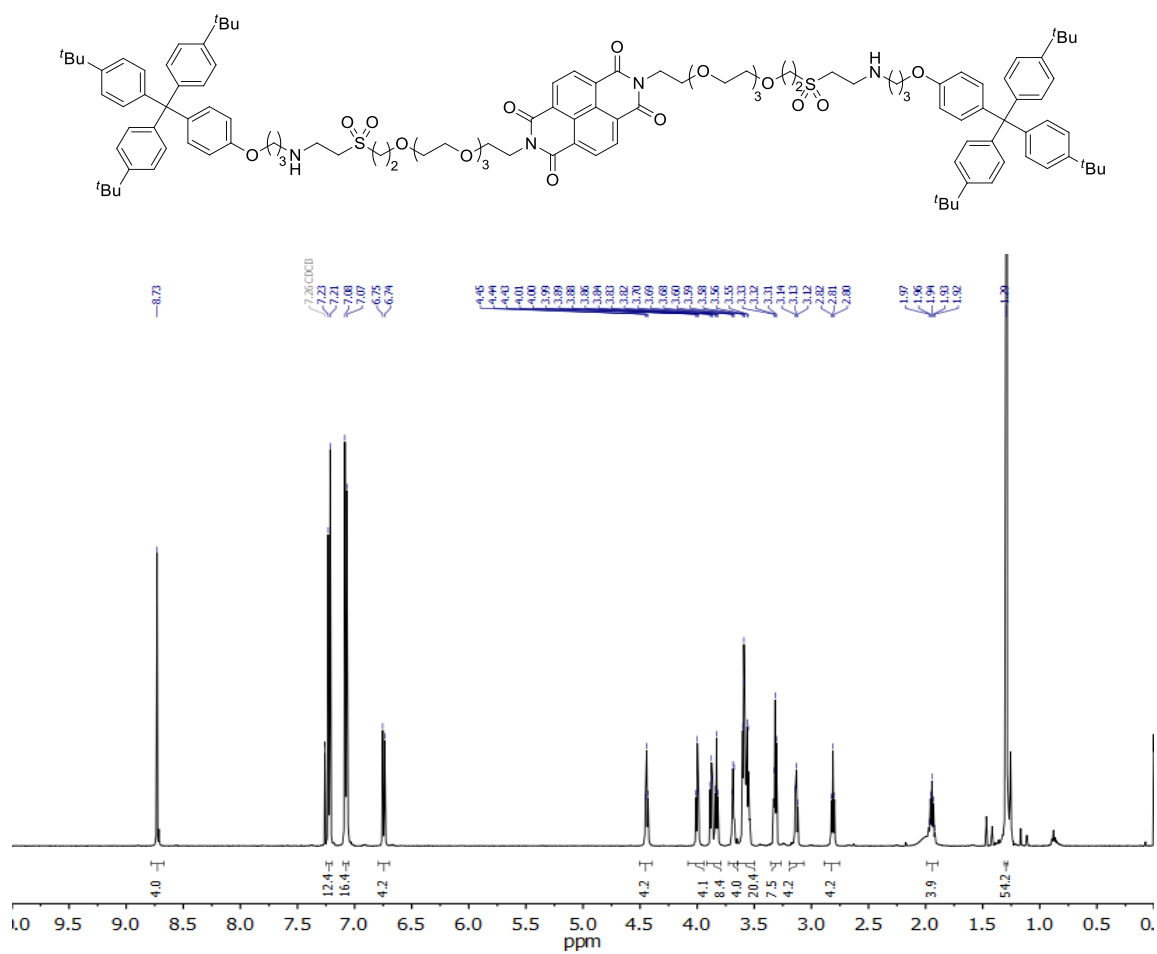
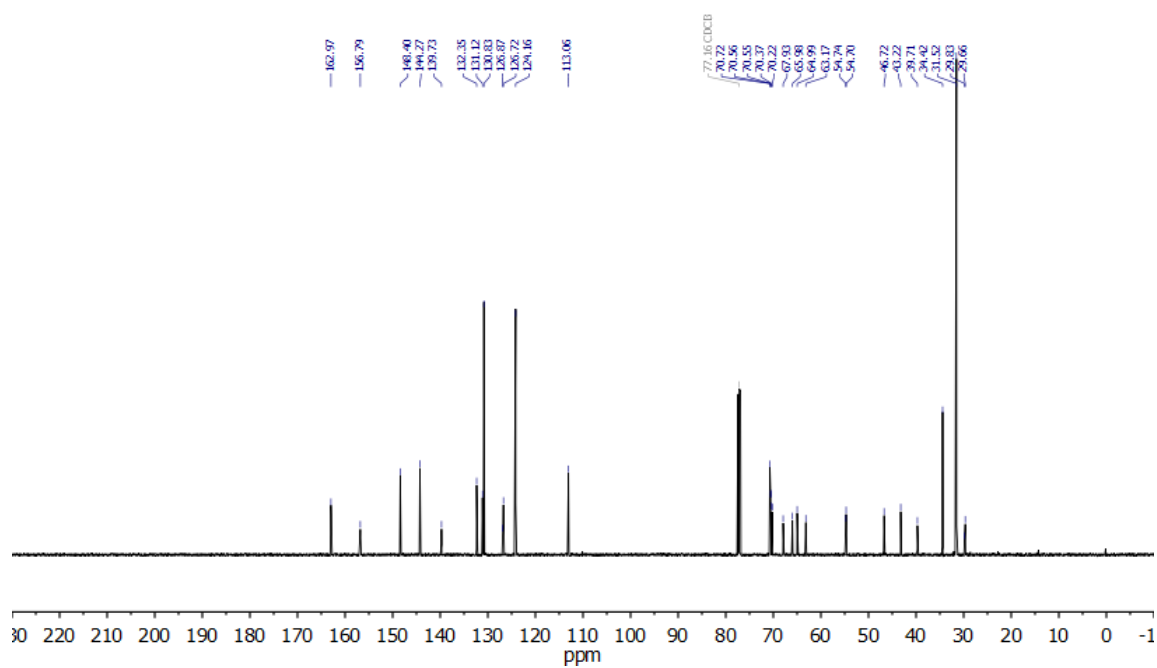


Figure 66. ¹³C NMR (126 MHz, CDCl₃) spectrum of 61c.

Compound 61d:

Figure 67. ^1H NMR (500 MHz, CDCl_3) spectrum of 61d.Figure 68. ^{13}C NMR (126 MHz, CDCl_3) spectrum of 61d.

Compound 63a:

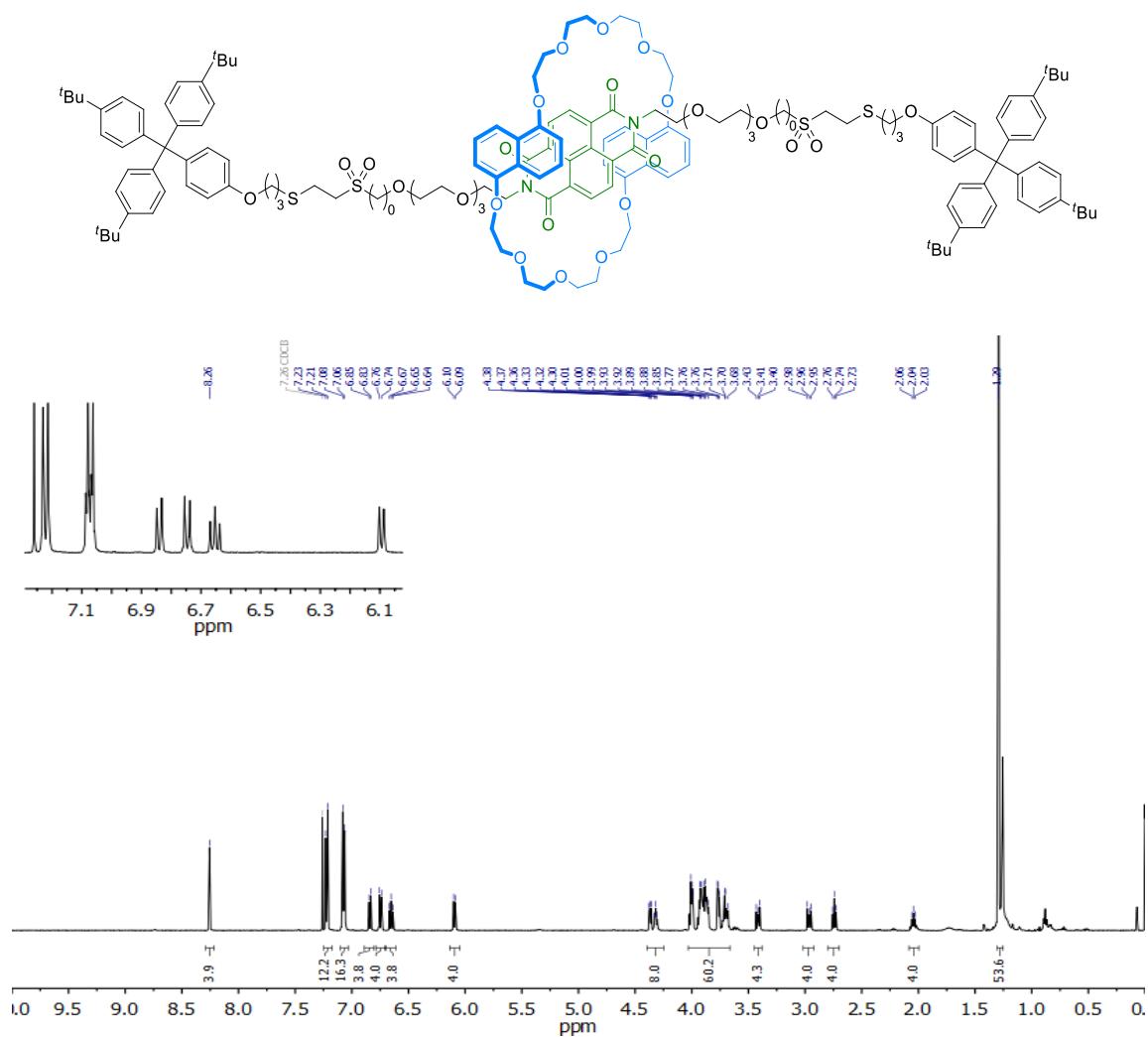


Figure 69. ¹H NMR (500 MHz, CDCl₃) spectrum of 63a.

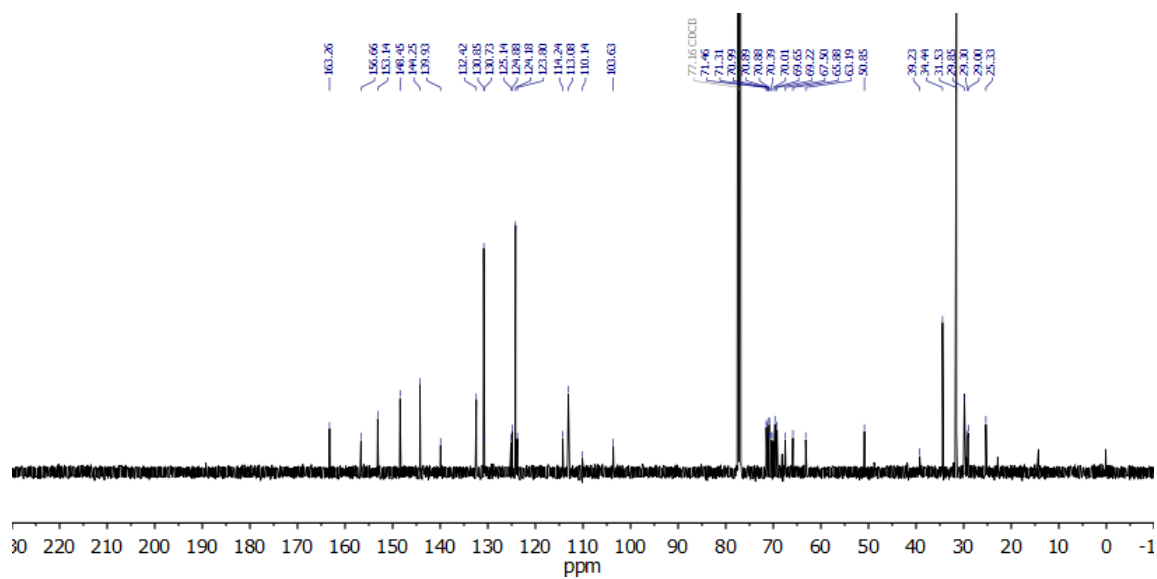
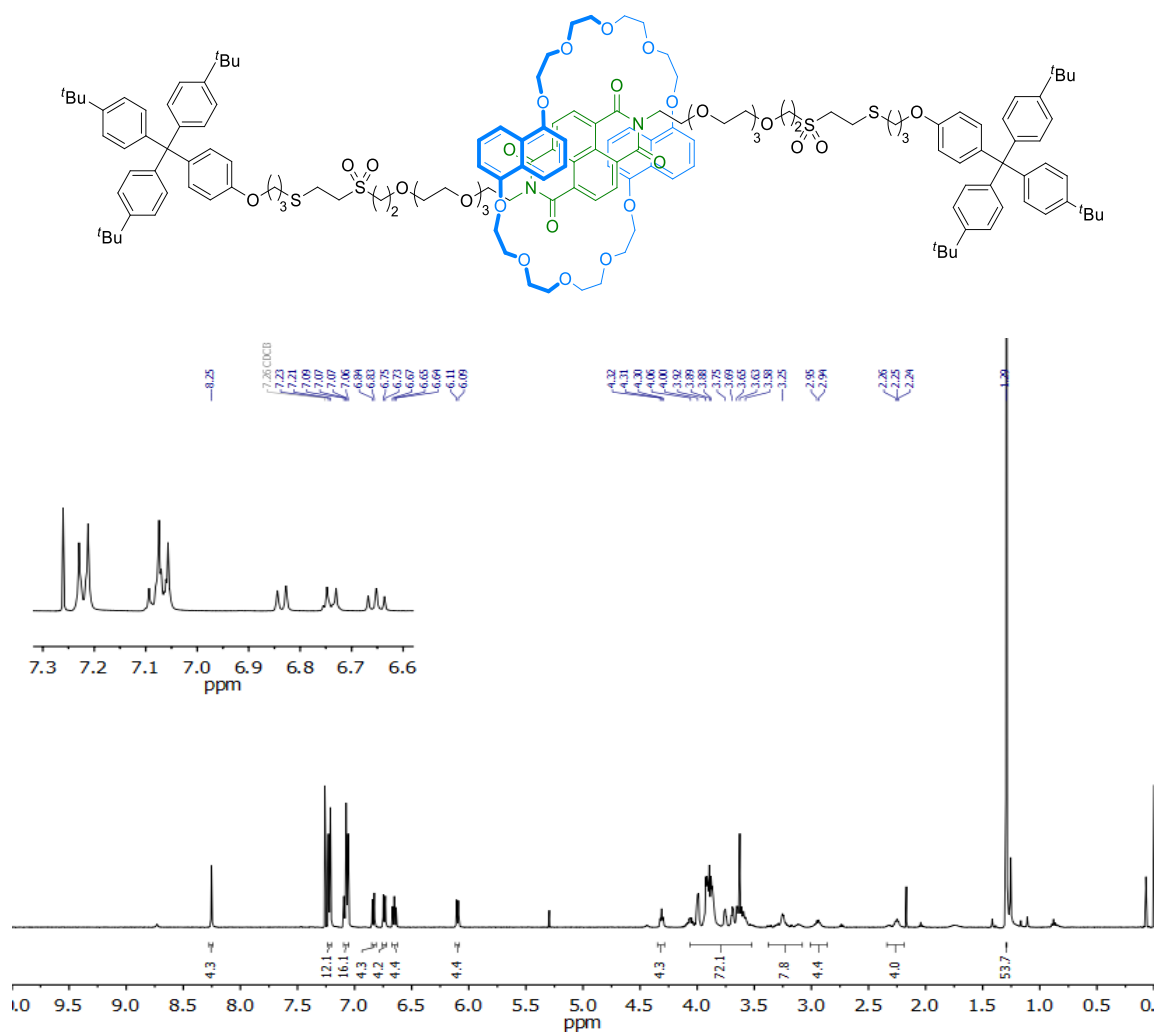
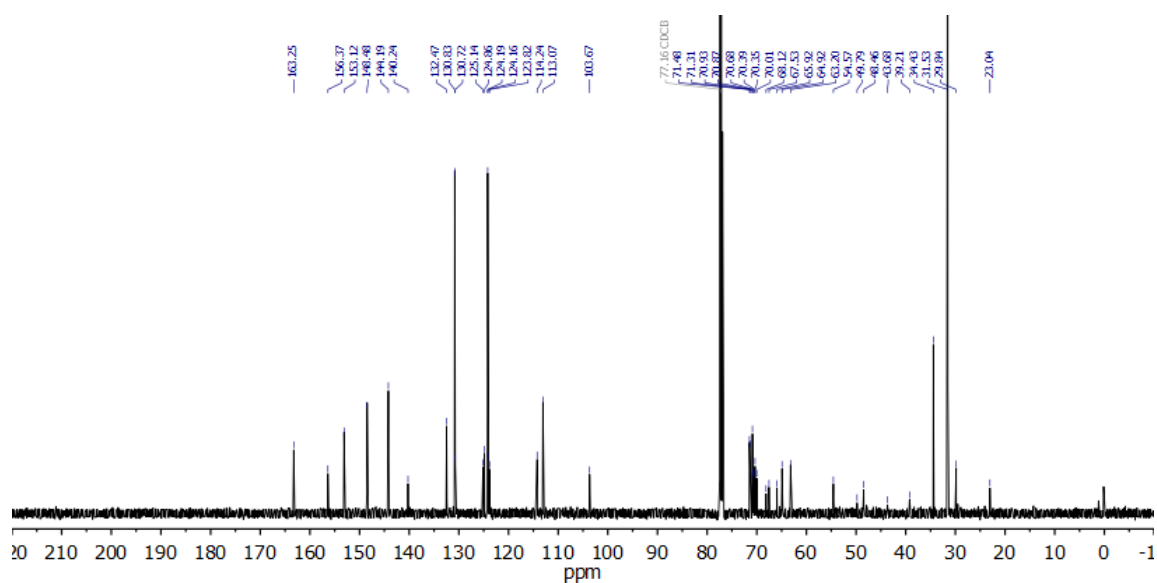


Figure 70. ¹³C NMR (126 MHz, CDCl₃) spectrum of 63a.

Compound 63b:

Figure 71. $^1\text{H NMR}$ (500 MHz, CDCl_3) spectrum of 63b.Figure 72. $^{13}\text{C NMR}$ (126 MHz, CDCl_3) spectrum of 63b.

Compound 63c:

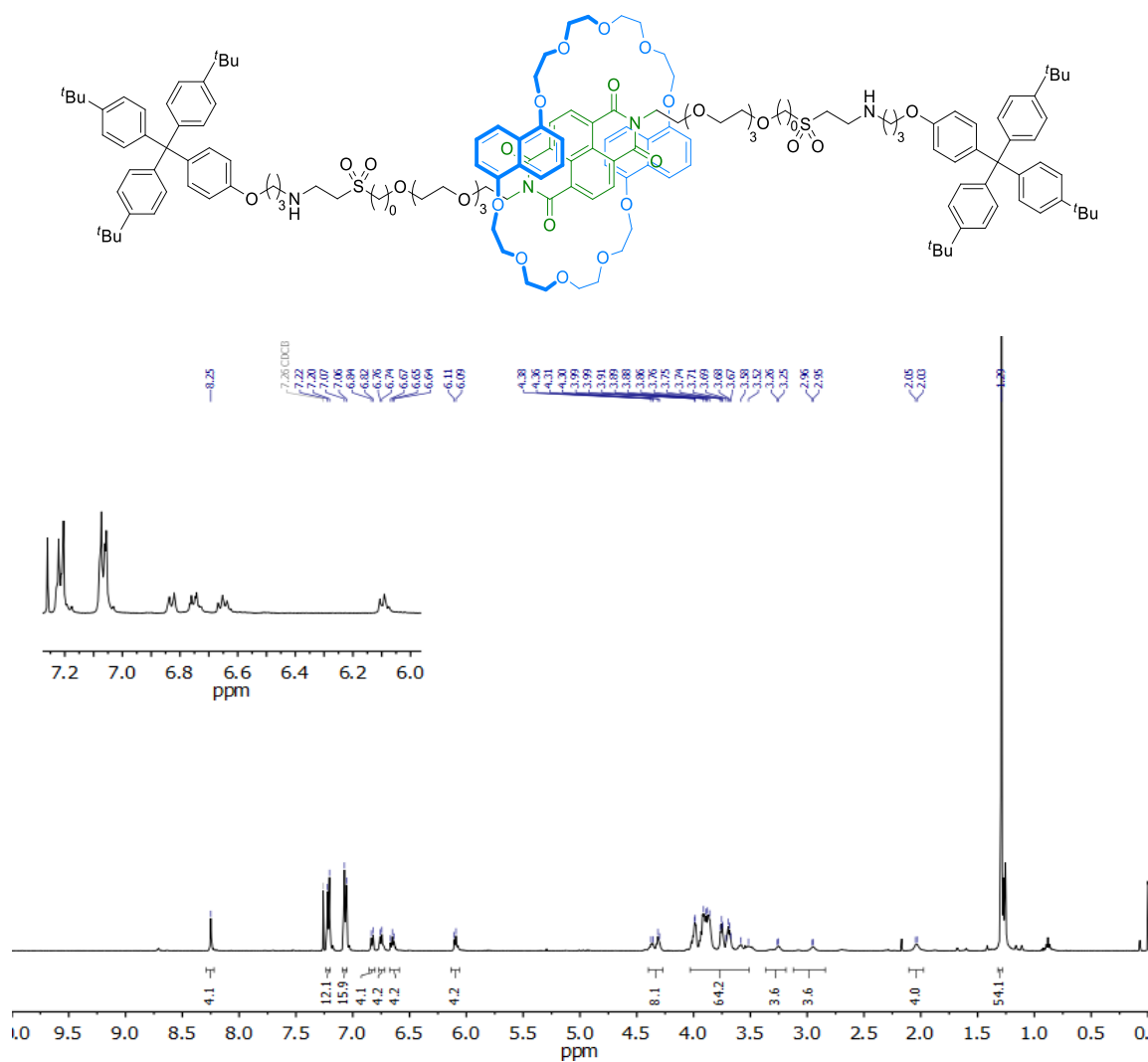
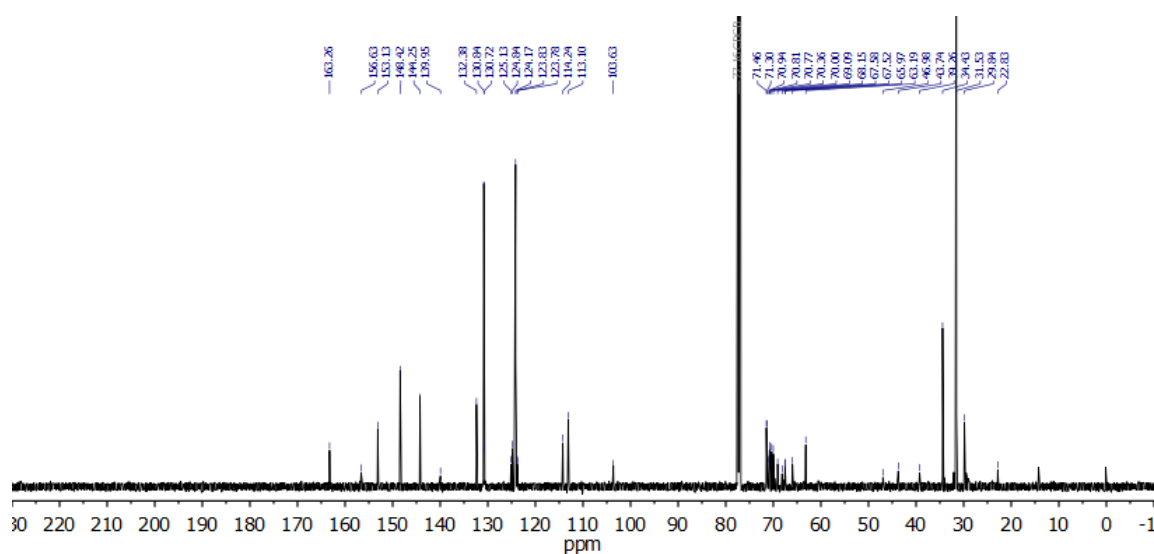
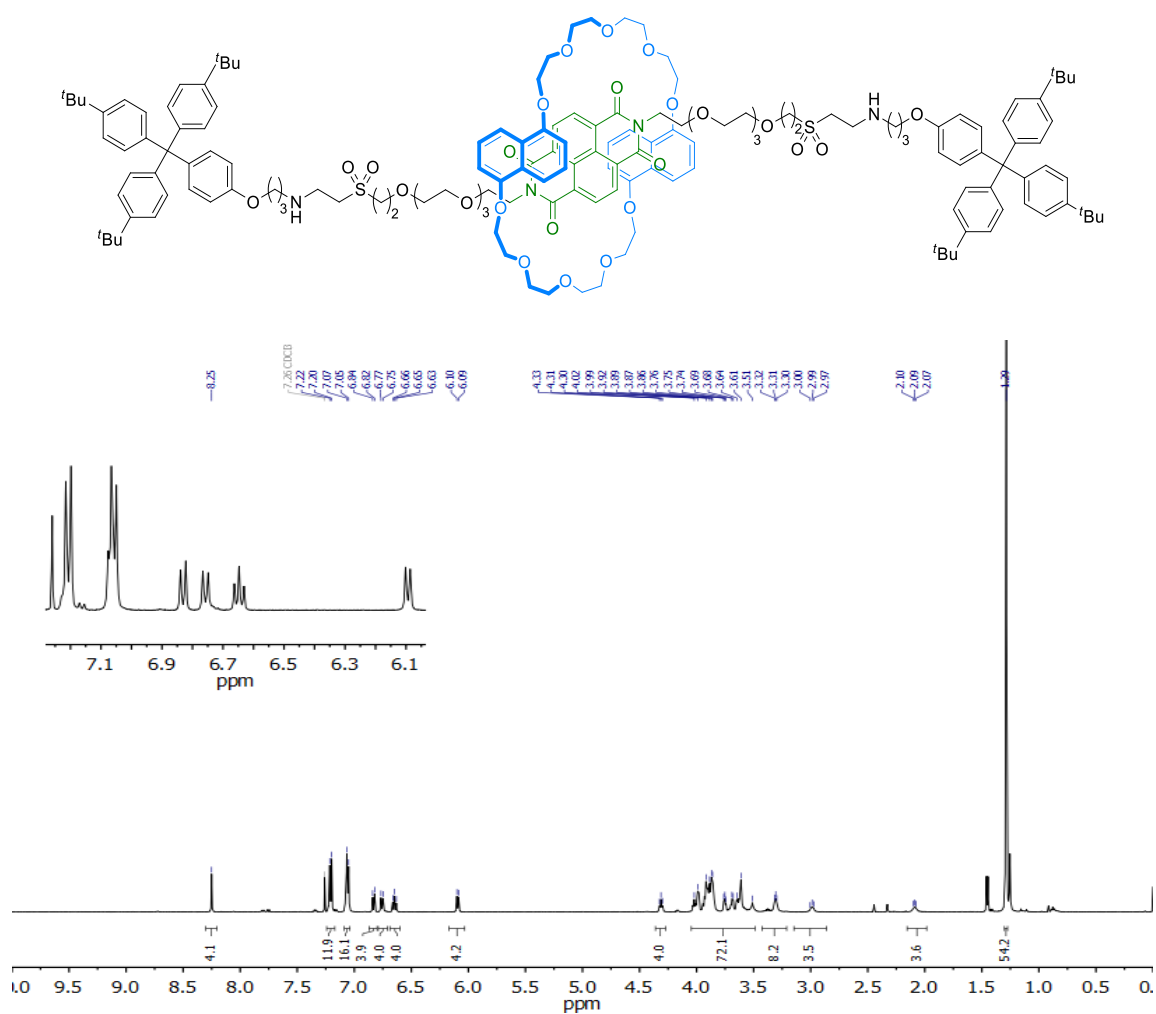
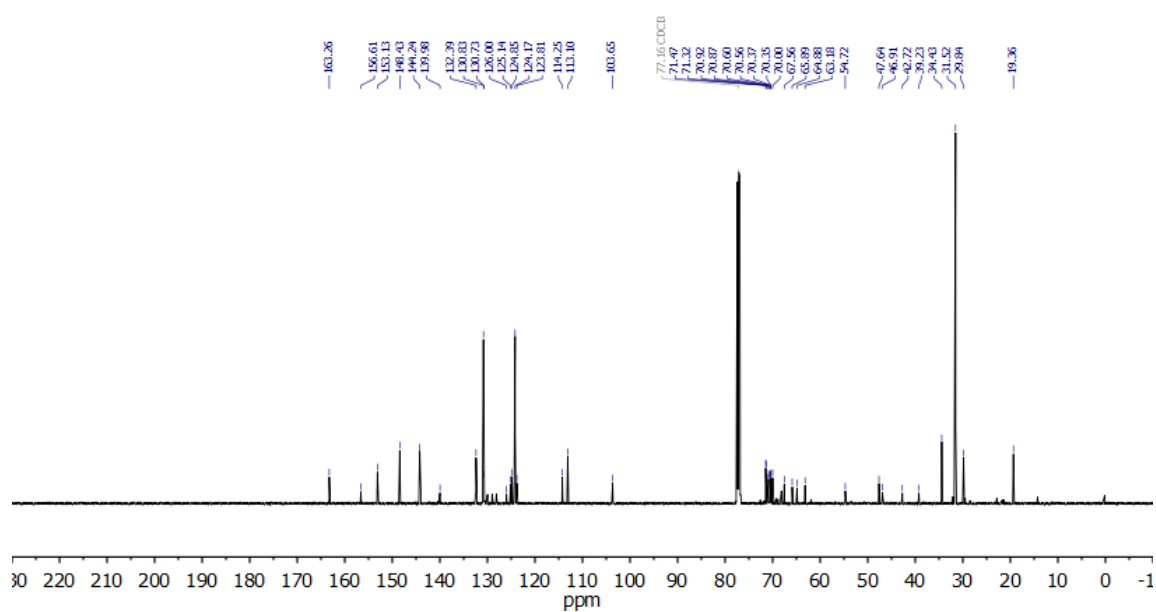


Figure 73. ^1H NMR (500 MHz, CDCl_3) spectrum of 63c.



Compound 63d:

Figure 75. ^1H NMR (500 MHz, CDCl_3) spectrum of 63d.Figure 76. ^{13}C NMR (126 MHz, CDCl_3) spectrum of 63d.

Compound 76a:

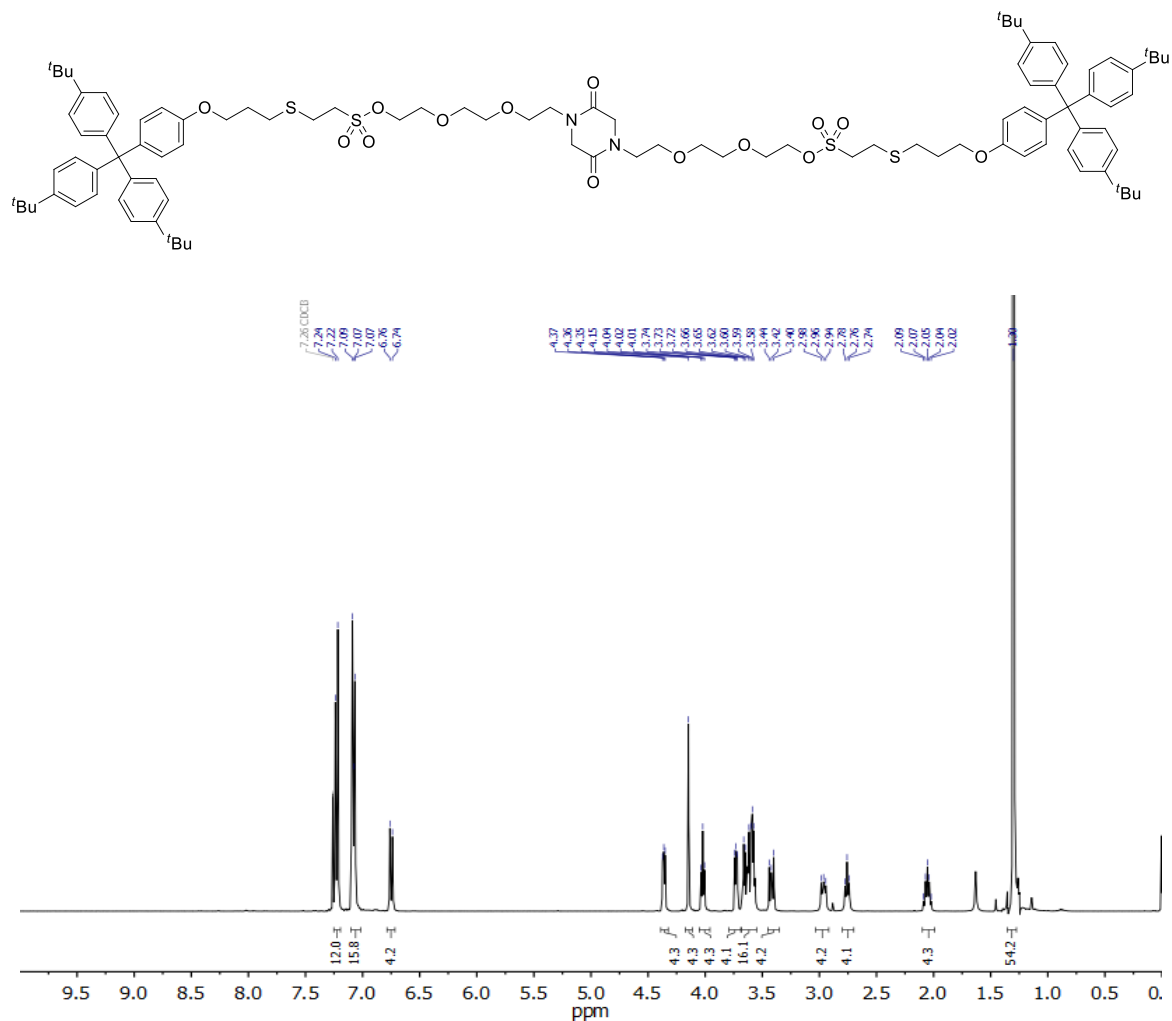


Figure 77. ¹H NMR (400 MHz, CDCl₃) spectrum of 76a.

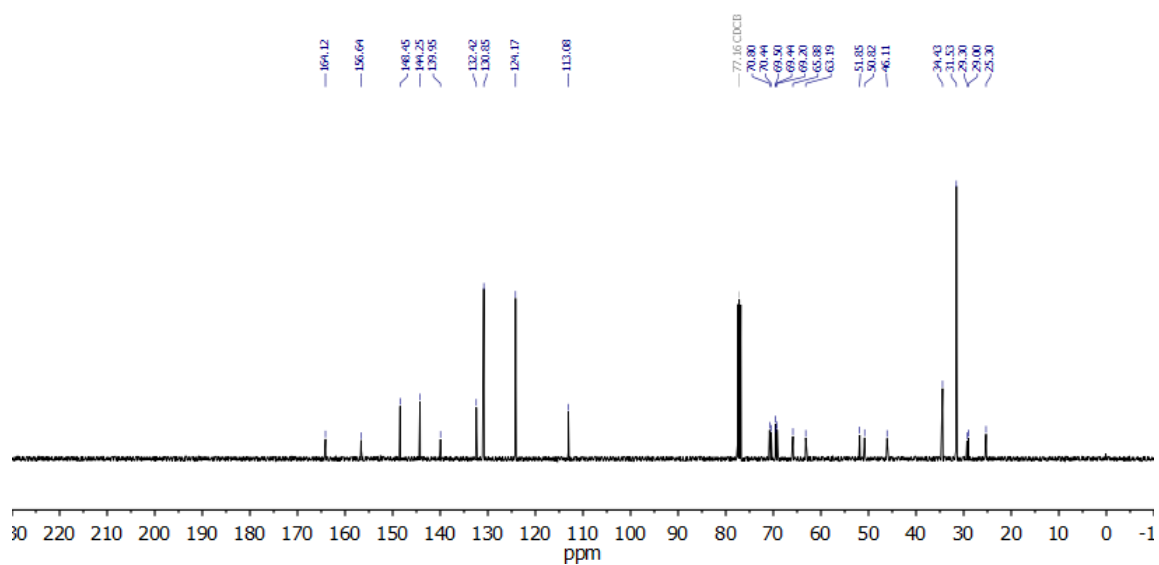
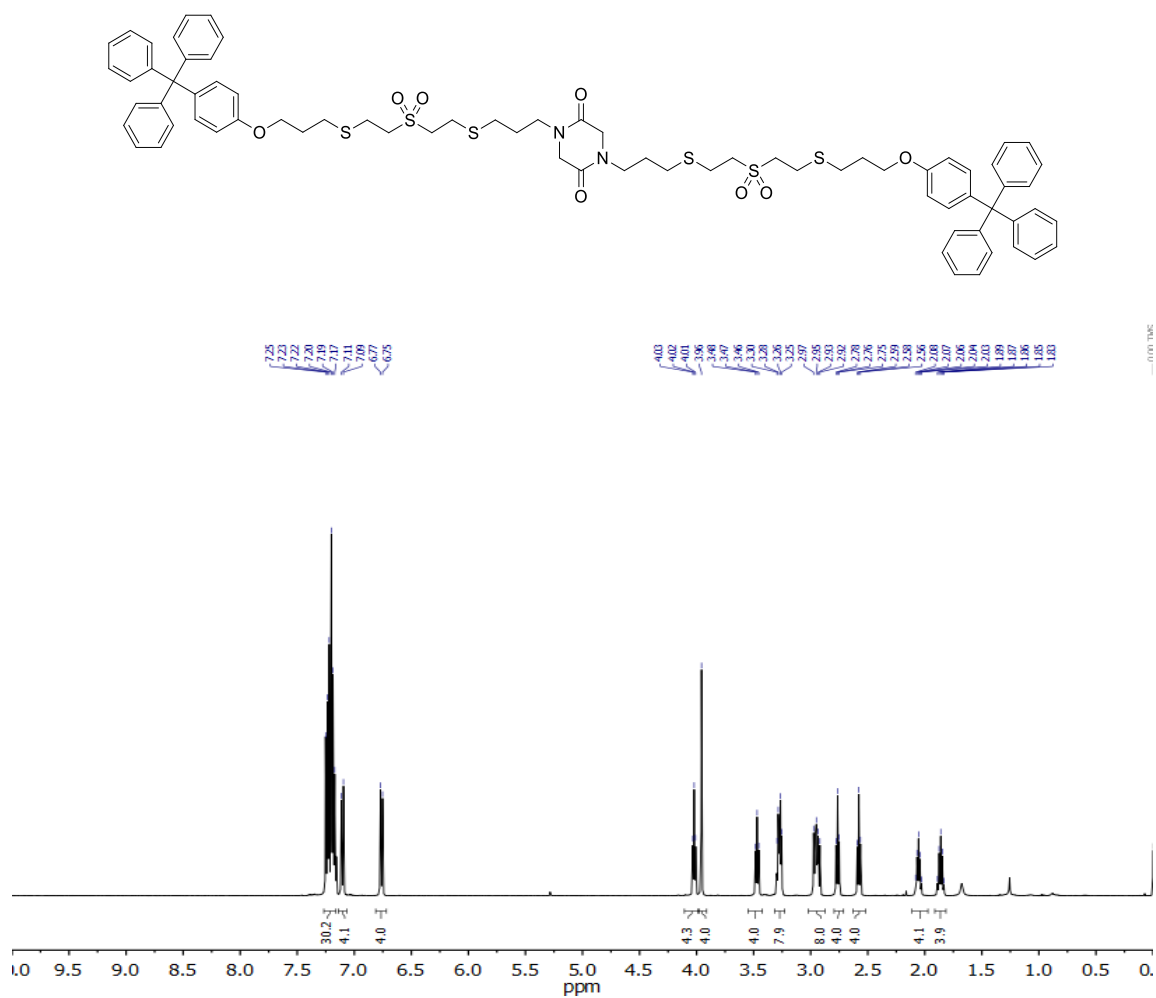
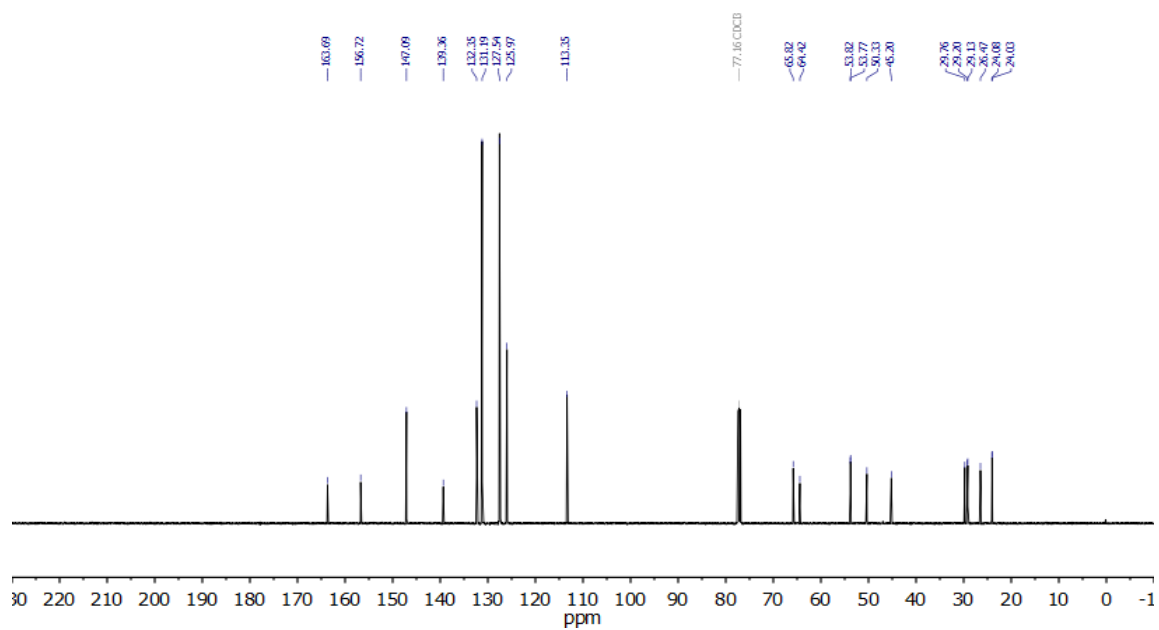


Figure 78. ¹³C NMR (101 MHz, CDCl₃) spectrum of 76a.

Compound 76b:

Figure 79. ^1H NMR (500 MHz, CDCl_3) spectrum of 76b.Figure 80. ^{13}C NMR (126 MHz, CDCl_3) spectrum of 76b.

Compound 76c:

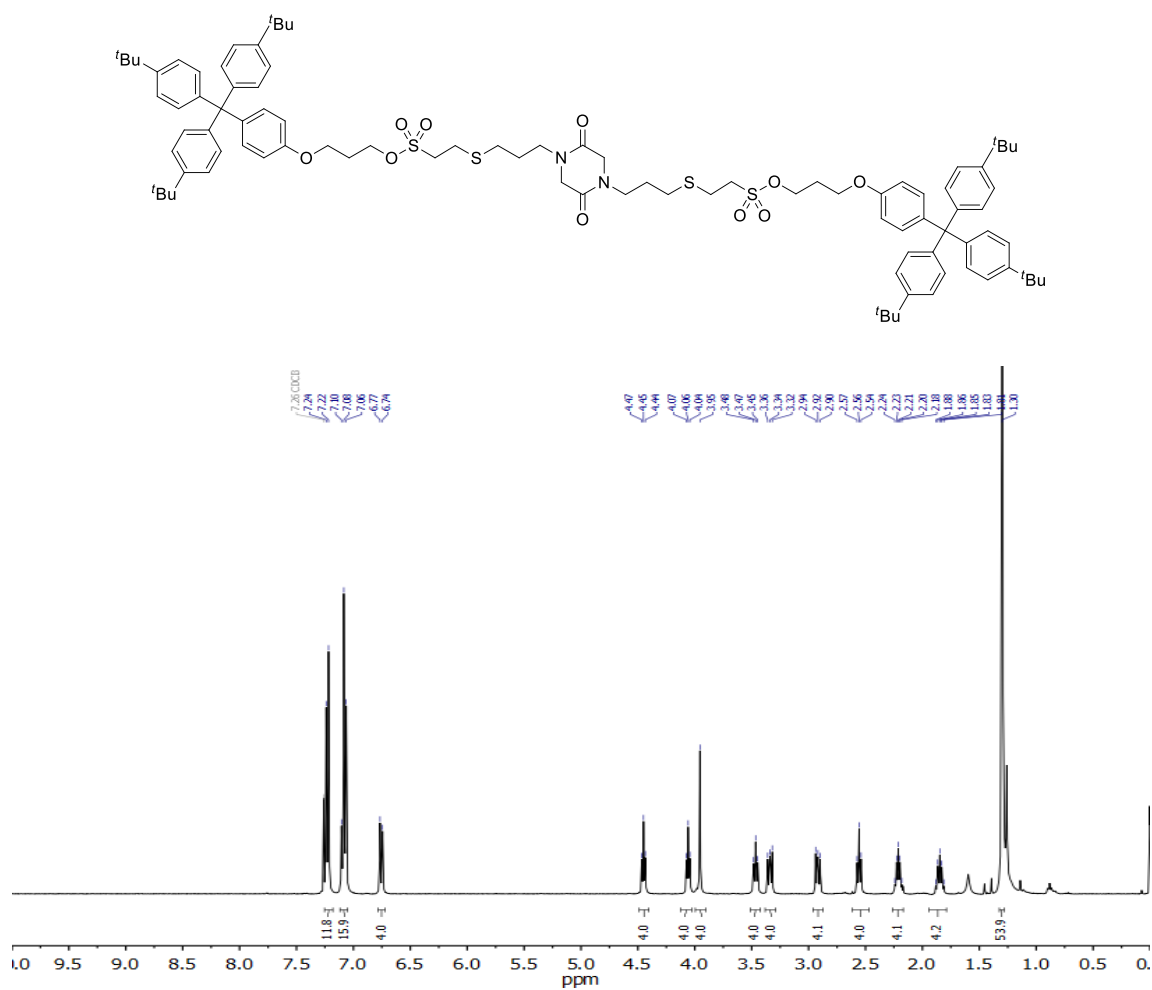


Figure 81. ¹H NMR (400 MHz, CDCl₃) spectrum of 76c.

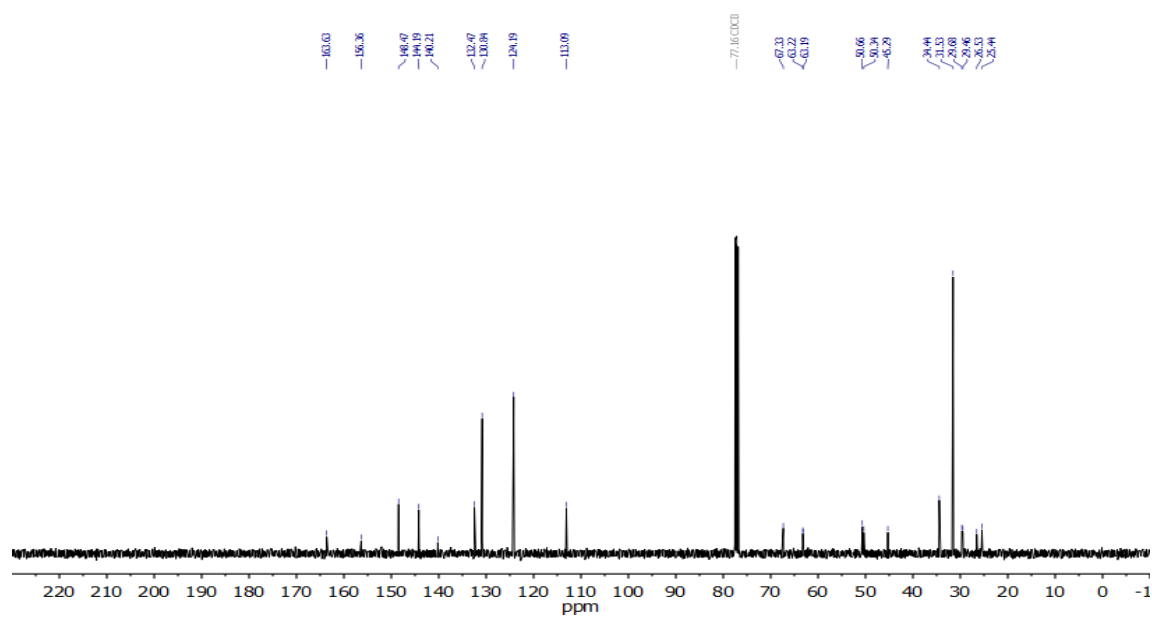
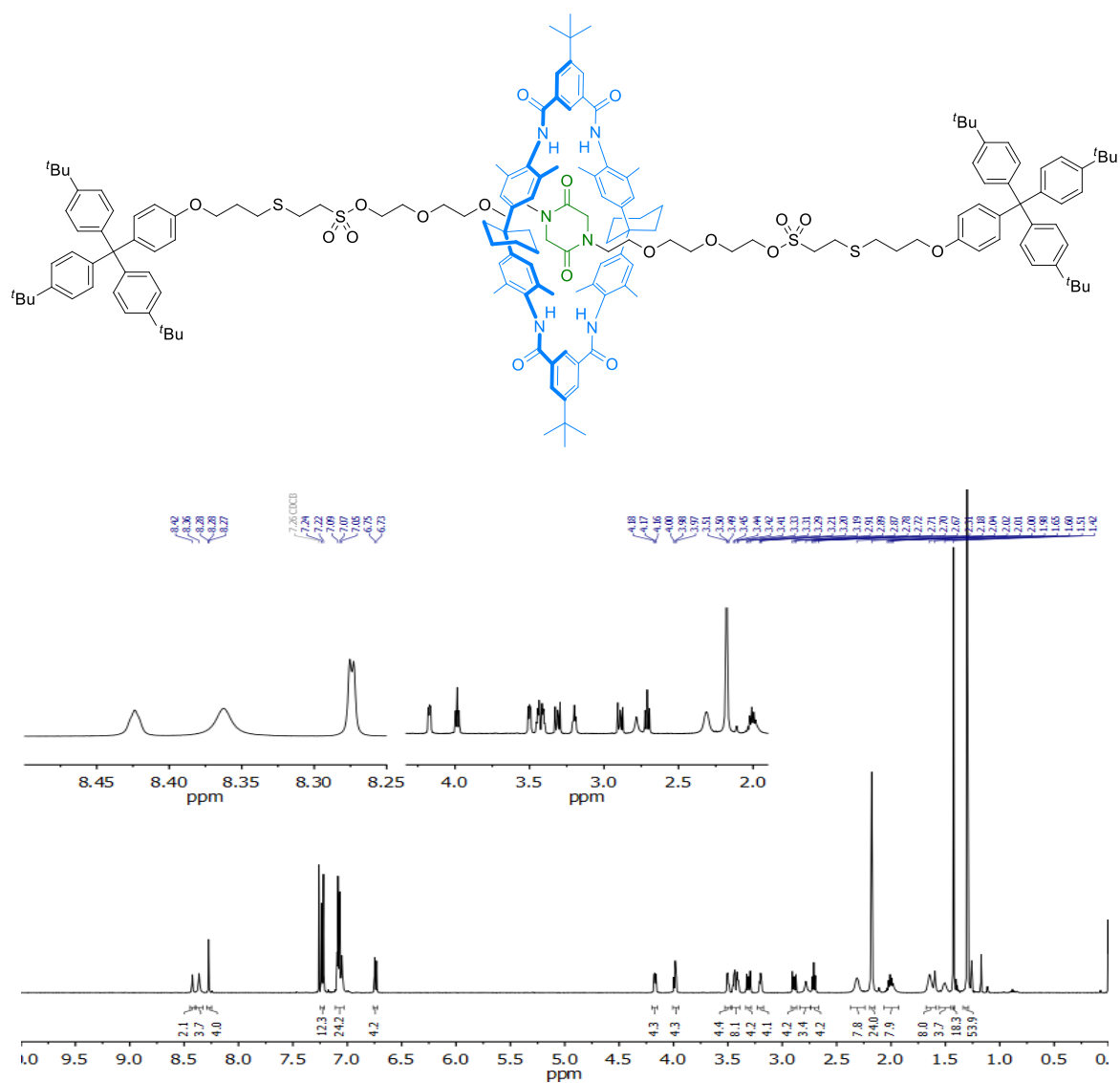
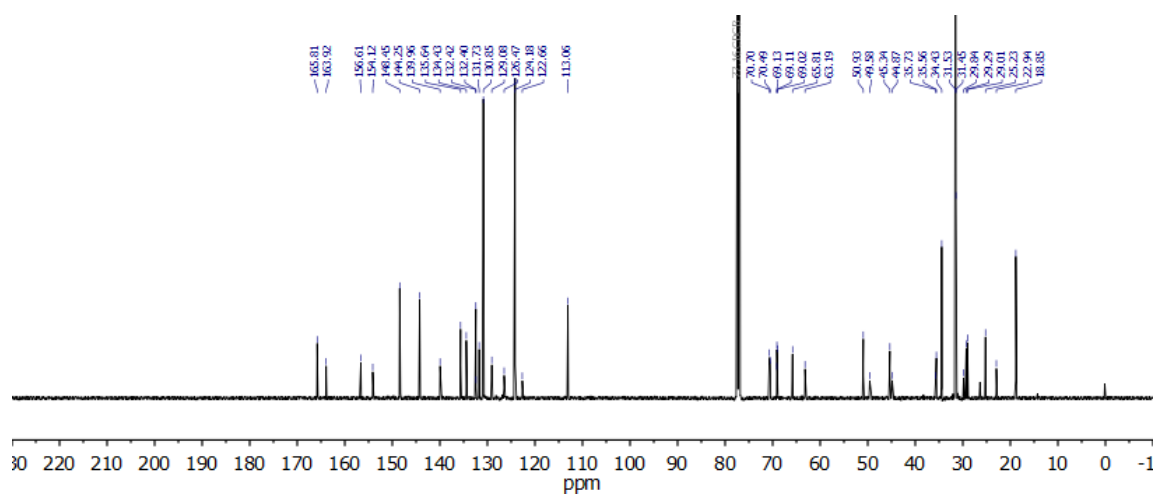


Figure 82. ¹³C NMR (101 MHz, CDCl₃) spectrum of 76c.

Compound 77a:

Figure 83. ^1H NMR (500 MHz, CDCl_3) spectrum of 77a.Figure 84. ^{13}C NMR (126 MHz, CDCl_3) spectrum of 77a.

Compound **77b**:

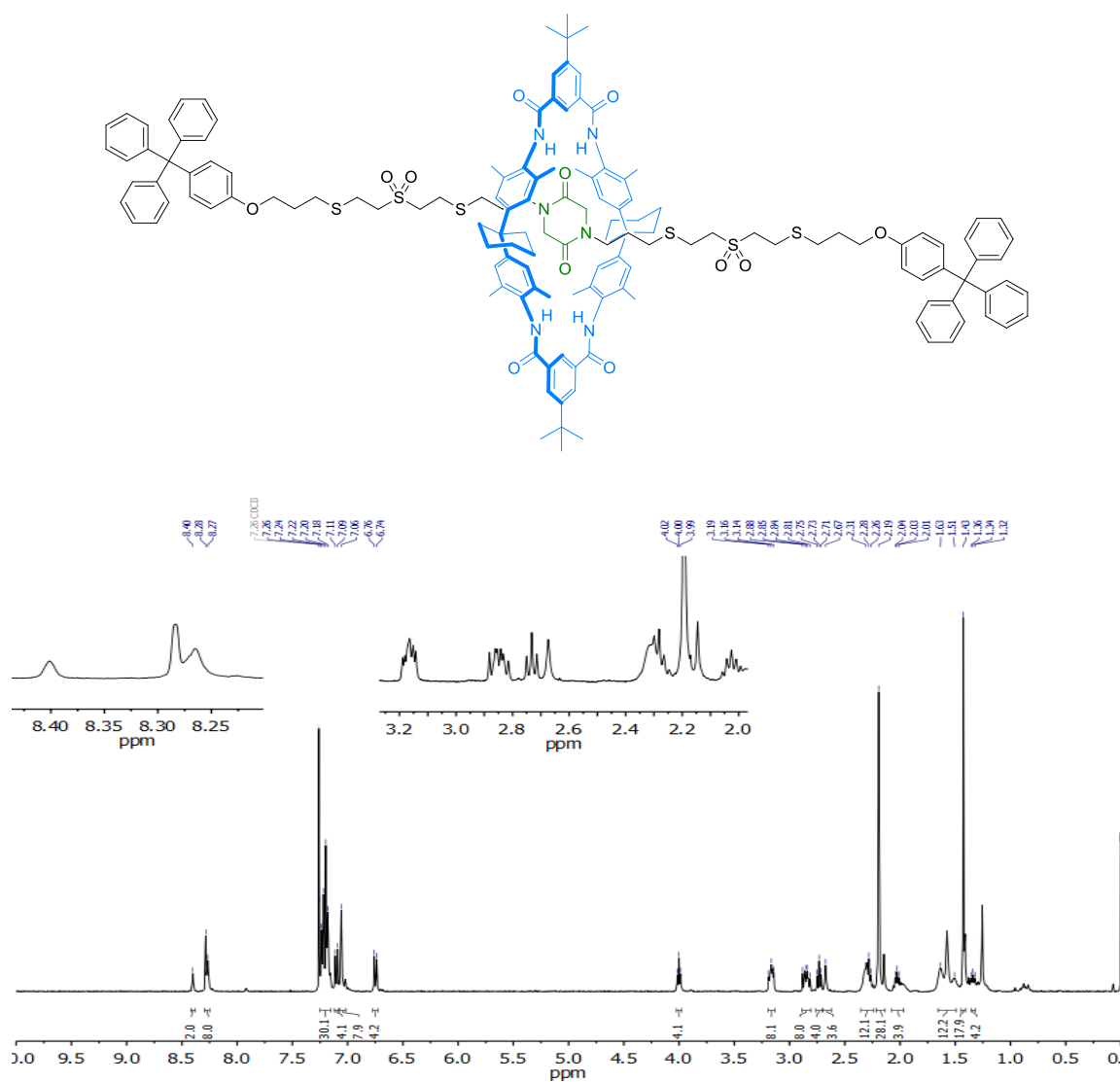


Figure 85. ¹H NMR (400 MHz, CDCl₃) spectrum of **77b**.

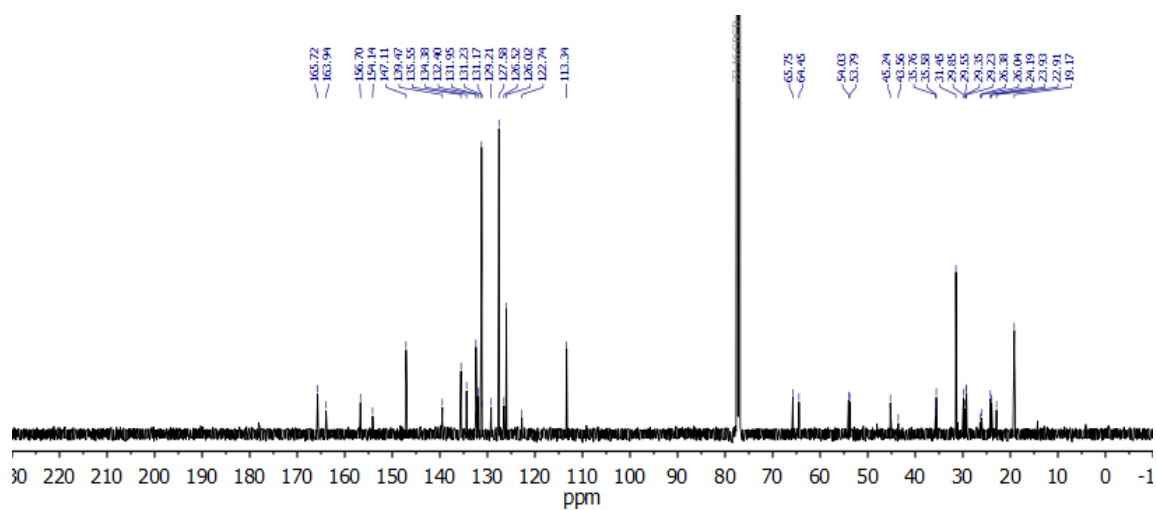
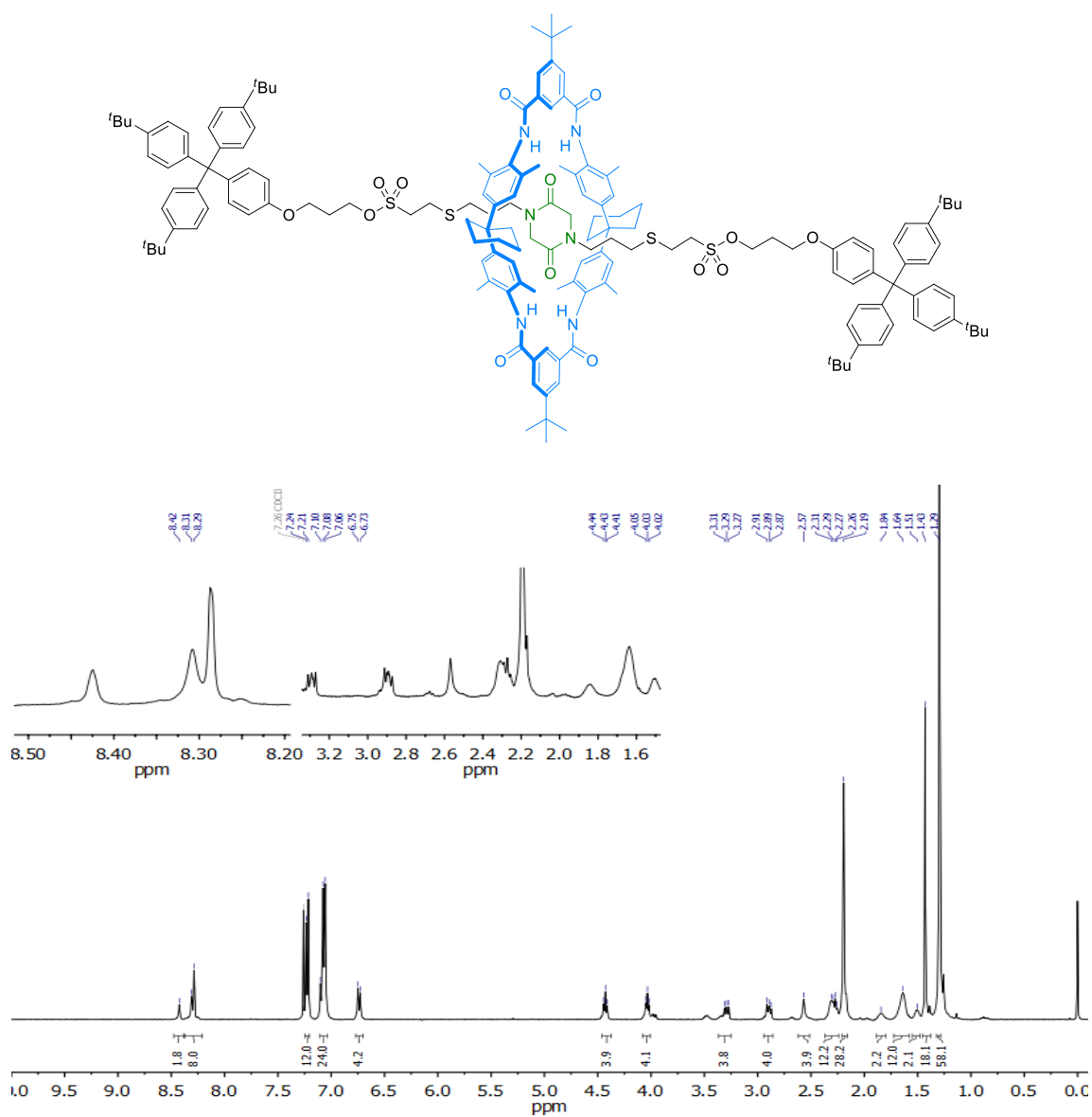
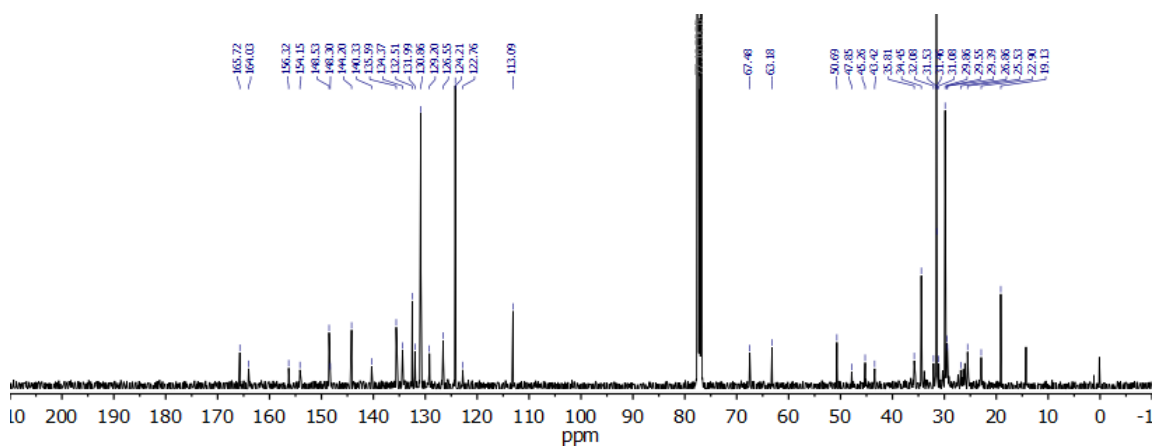


Figure 86. ¹³C NMR (101 MHz, CDCl₃) spectrum of **77b**.

Compound 77c:

Figure 87. ^1H NMR (400 MHz, CDCl_3) spectrum of 77c.Figure 88. ^{13}C NMR (101 MHz, CDCl_3) spectrum of 77c.

Compound 88a·PF₆:

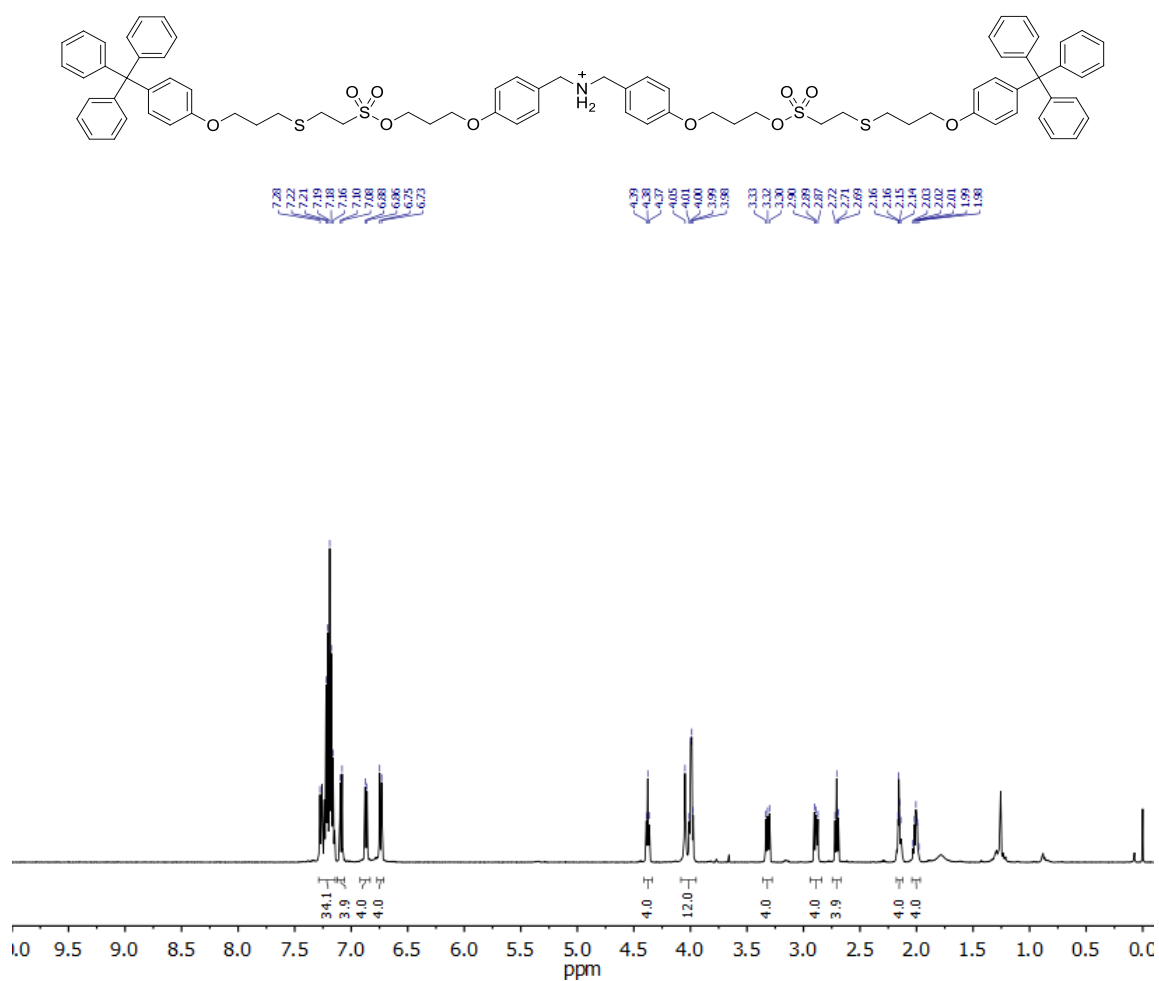


Figure 89. ¹H NMR (500 MHz, CDCl₃) spectrum of 88a·PF₆.

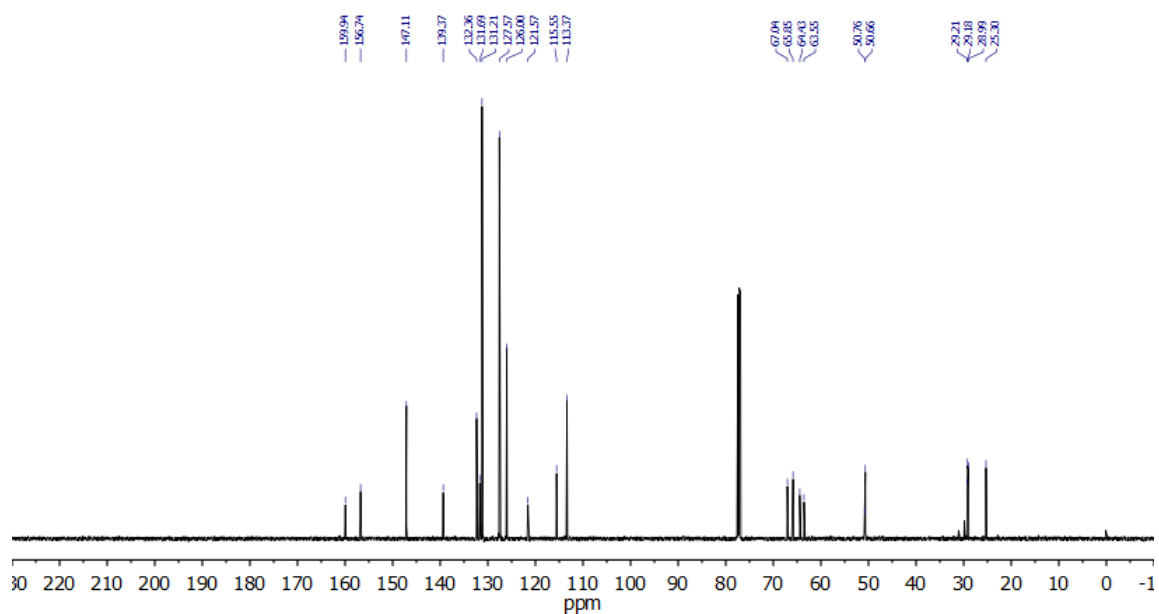


Figure 90. ¹³C NMR (126 MHz, CDCl₃) spectrum of 88a·PF₆.

Compound 89a·PF₆:

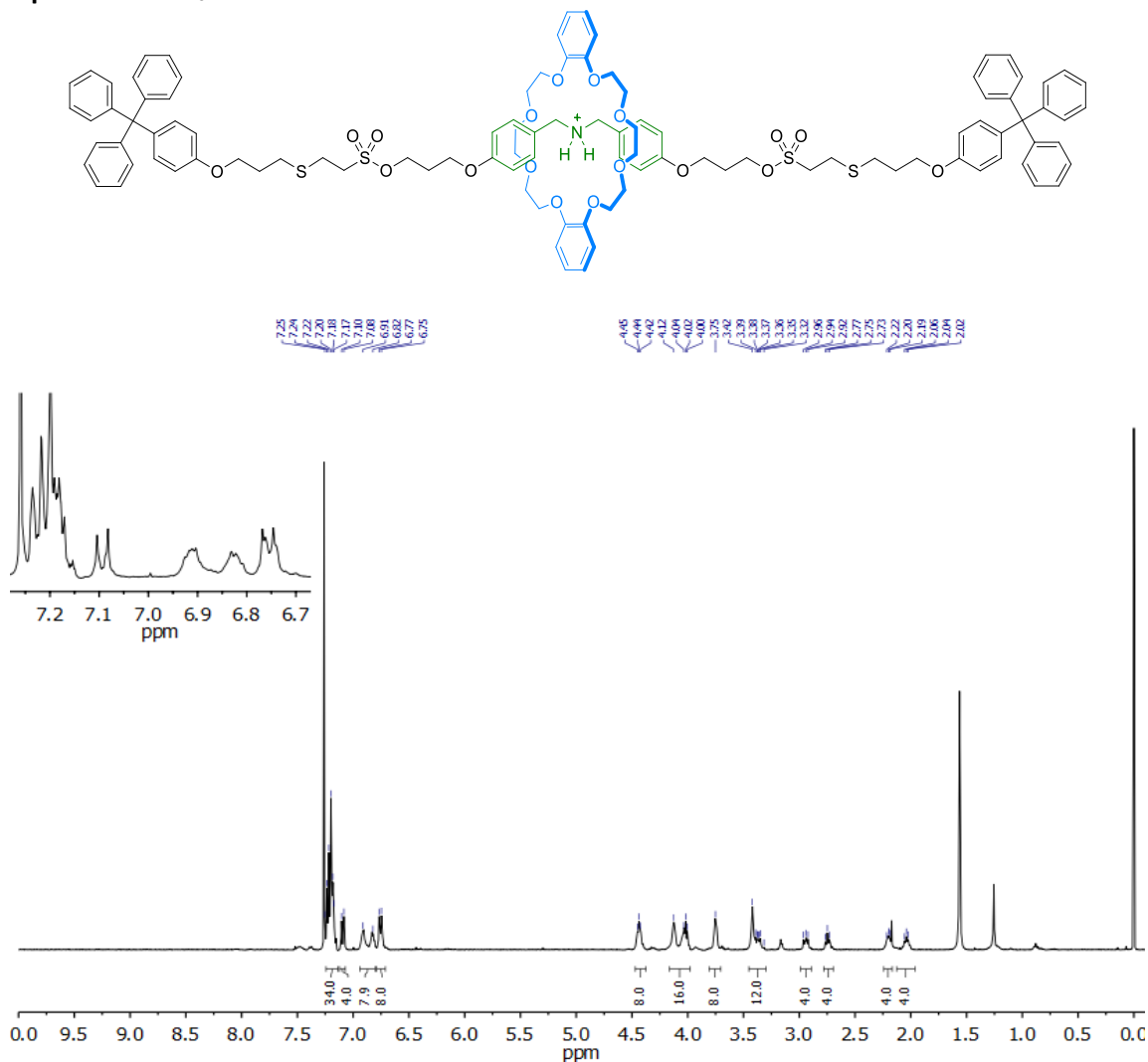


Figure 93. ¹H NMR (400 MHz, CDCl₃) spectrum of 89a·PF₆.

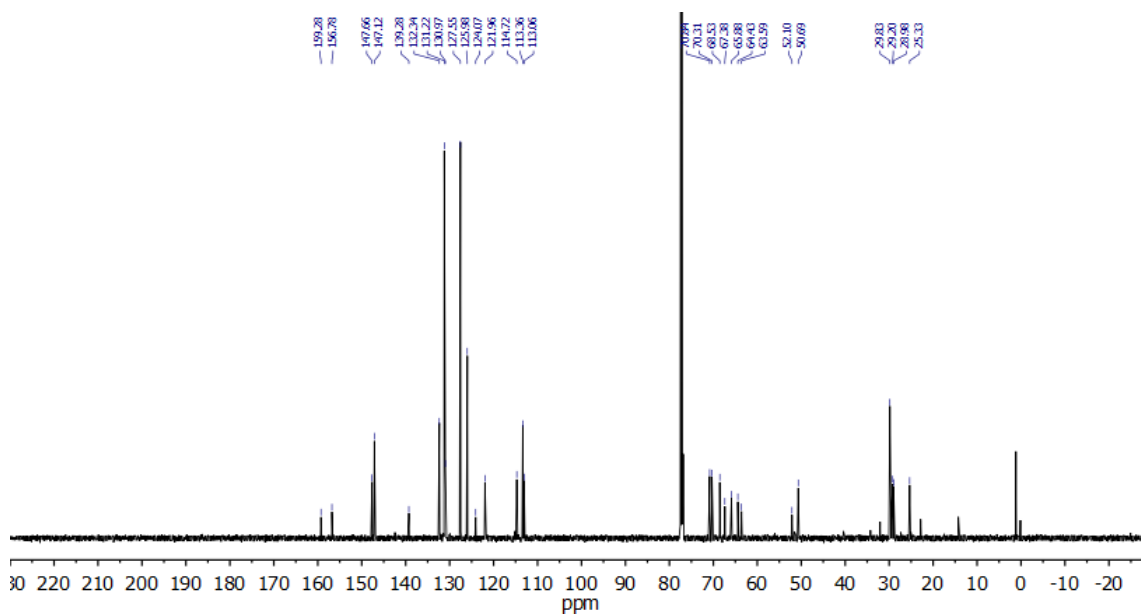
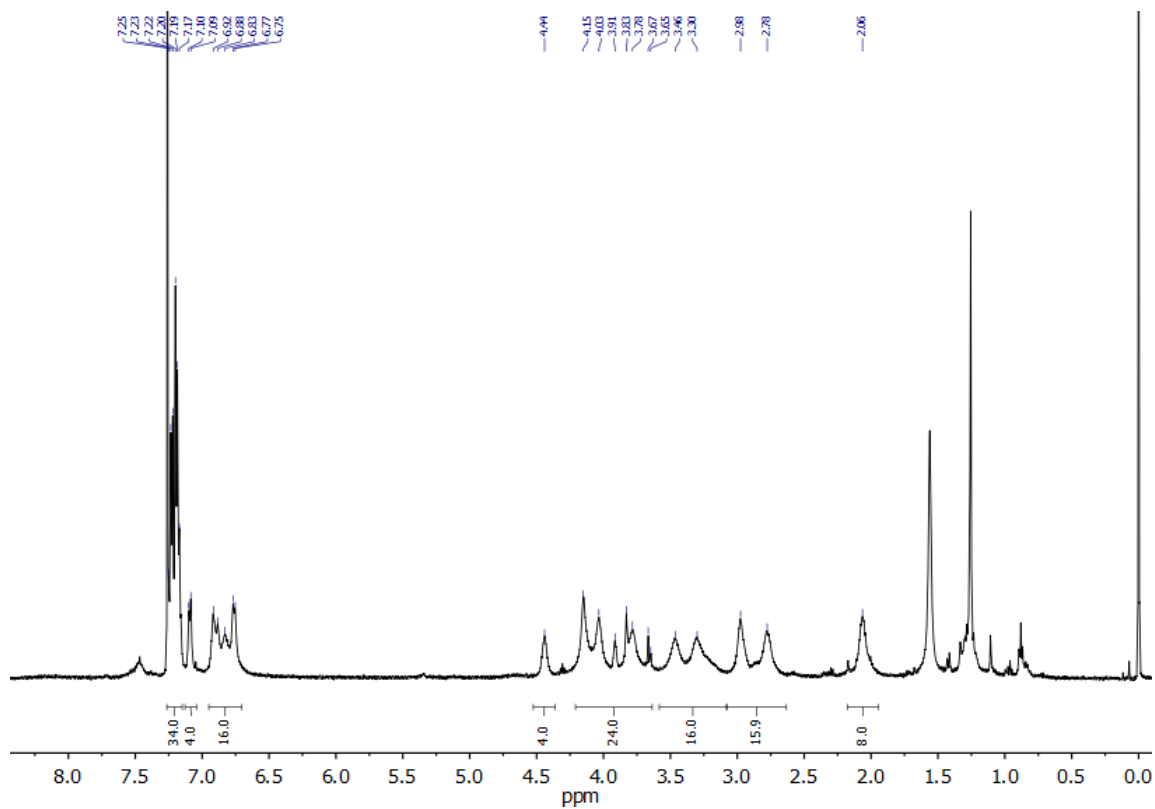
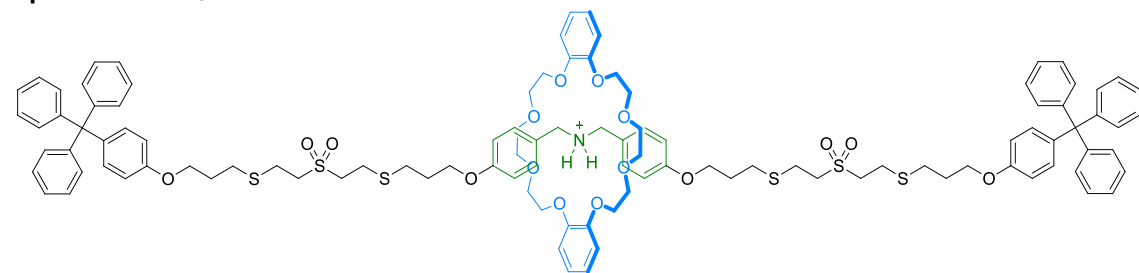
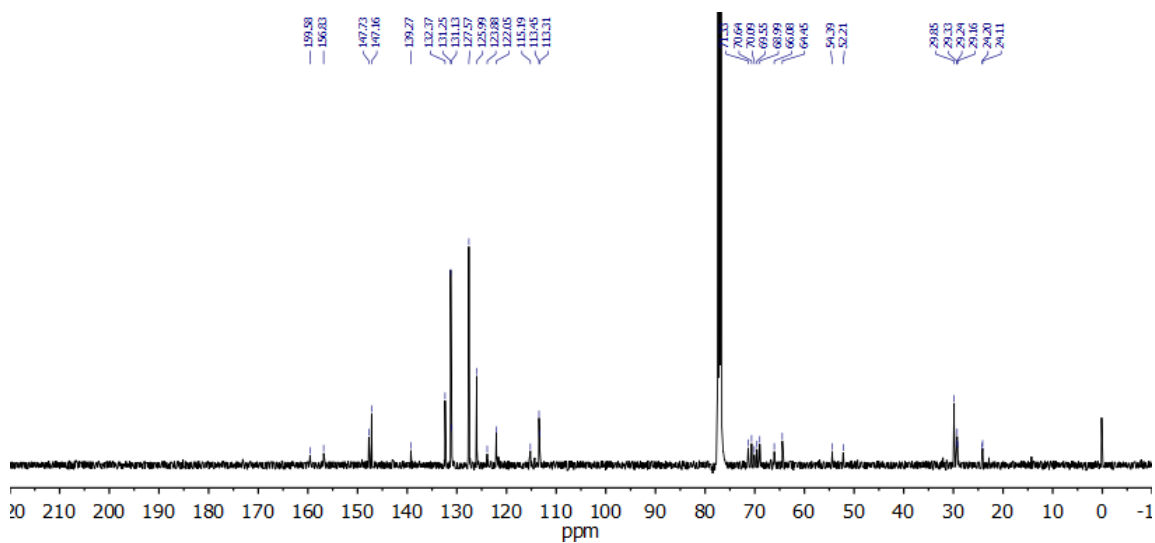


Figure 94. ¹³C NMR (101 MHz, CDCl₃) spectrum of 89a·PF₆.

Compound 89b·PF₆:Figure 95. ¹H NMR (500 MHz, CDCl₃) spectrum of 89b·PF₆.Figure 96. ¹³C NMR (126 MHz, CDCl₃) spectrum of 89b·PF₆.

Compound 99a:

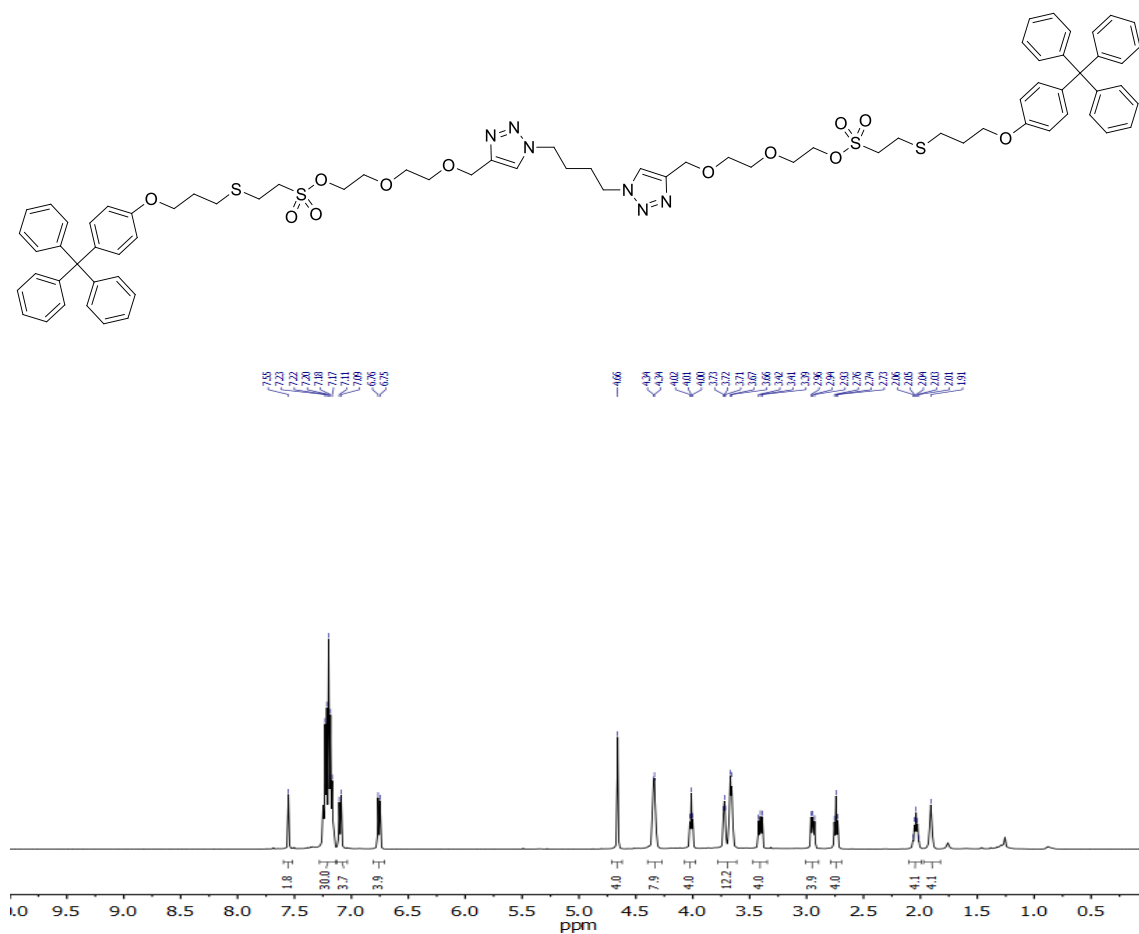


Figure 97. ¹H NMR (500 MHz, CDCl₃) spectrum of 99a.

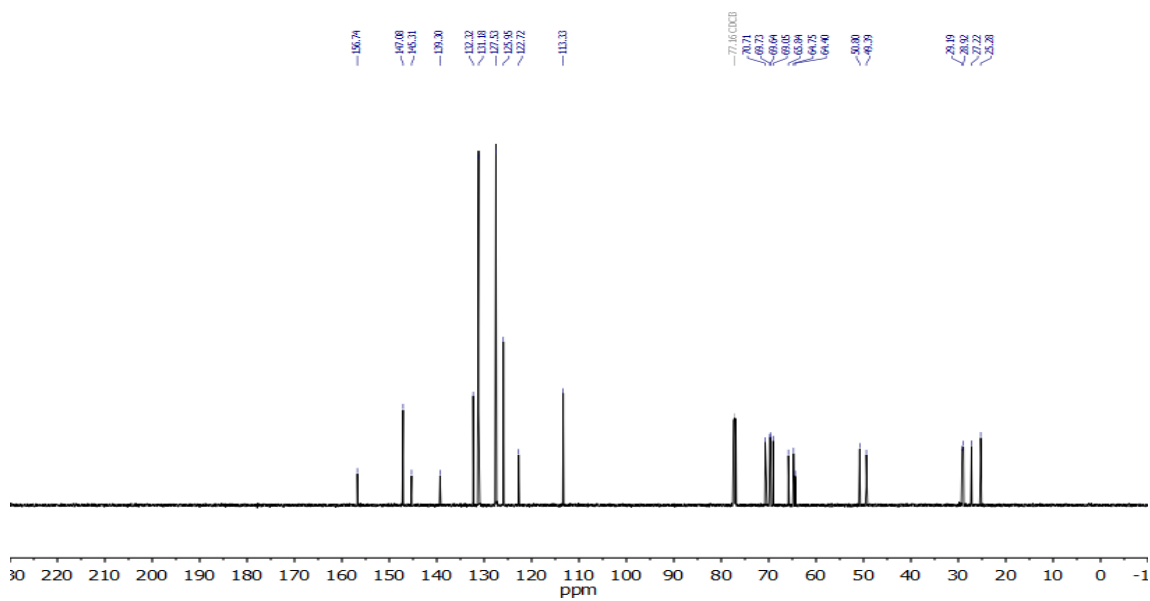
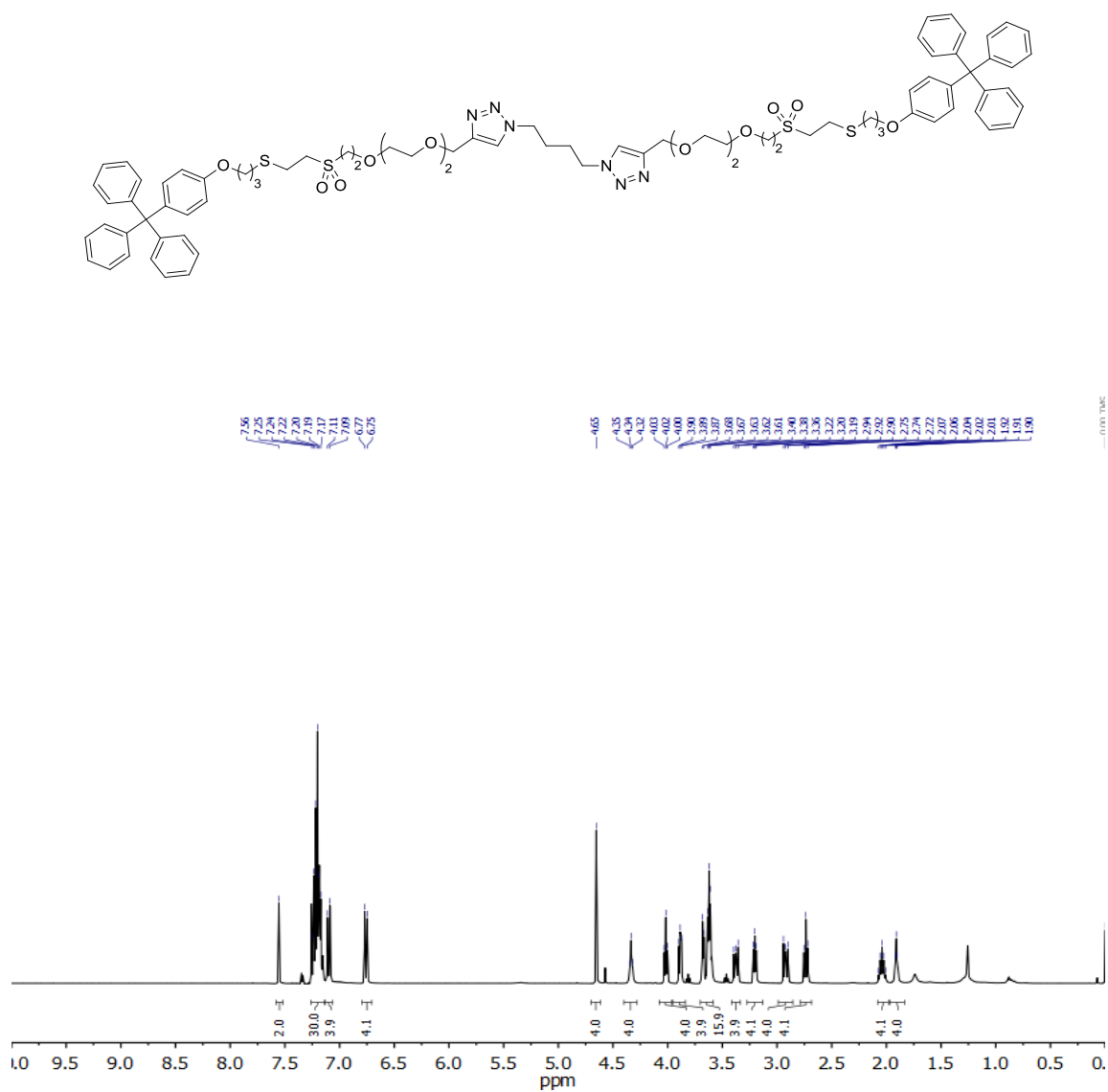
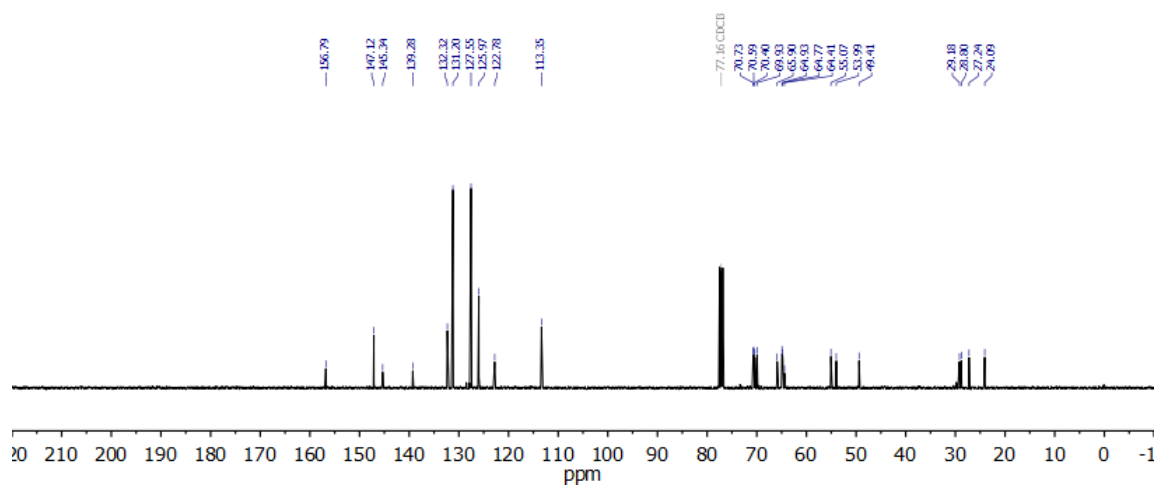


Figure 98. ¹³C NMR (126 MHz, CDCl₃) spectrum of 99a.

Compound 99b:

Figure 99. ^1H NMR (400 MHz, CDCl_3) spectrum of 99b.Figure 100. ^{13}C NMR (101 MHz, CDCl_3) spectrum of 99b.

Compound 100a:

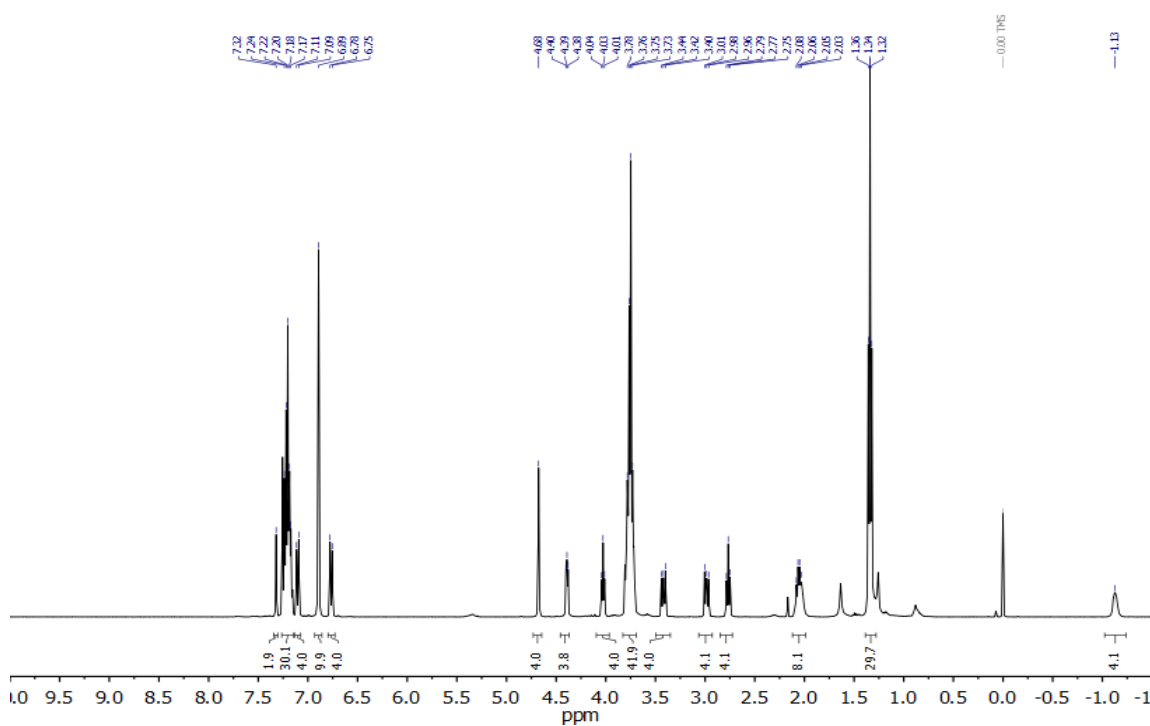
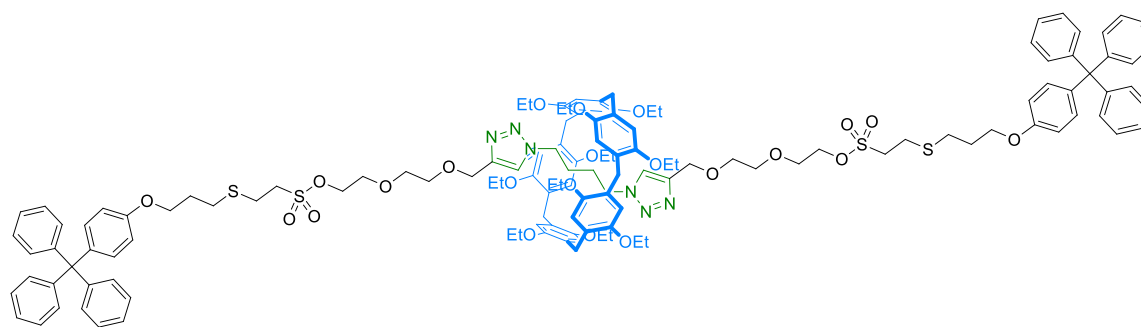


Figure 101. ^1H NMR (400 MHz, CDCl_3) spectrum of 100a.

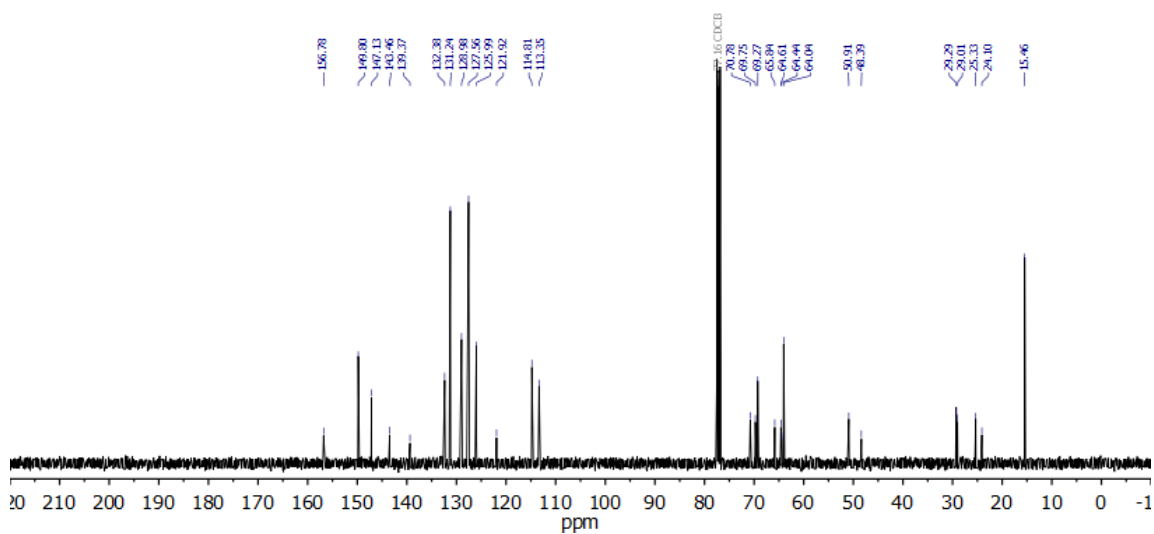
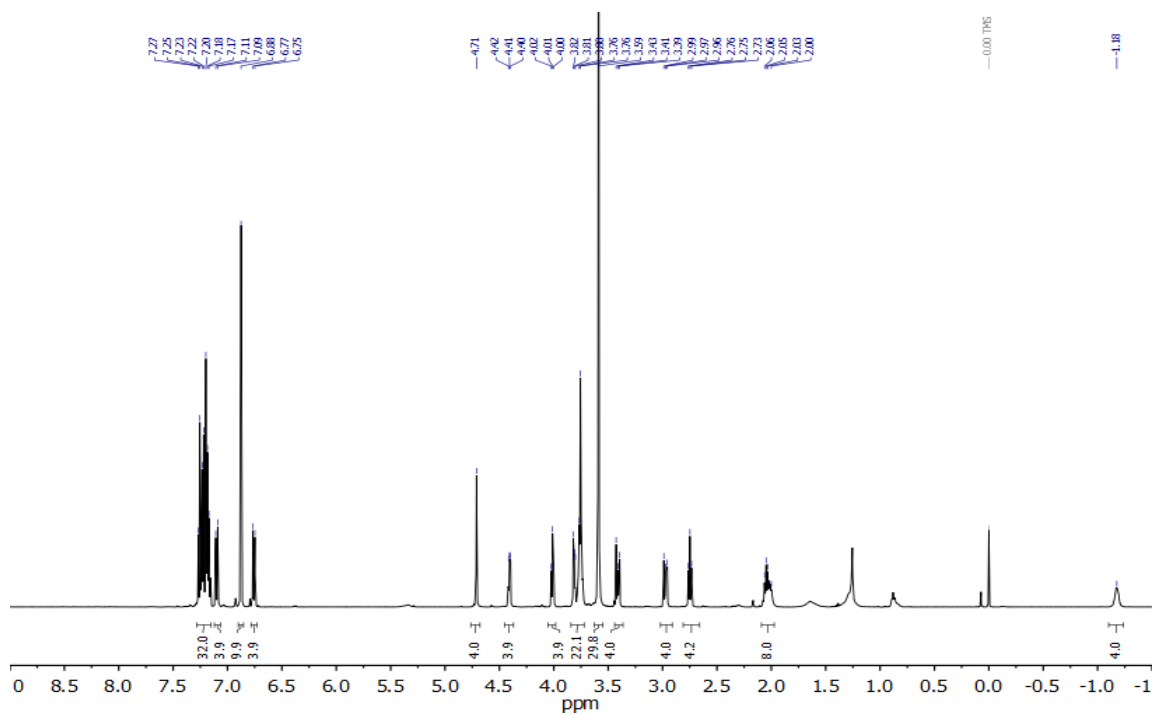
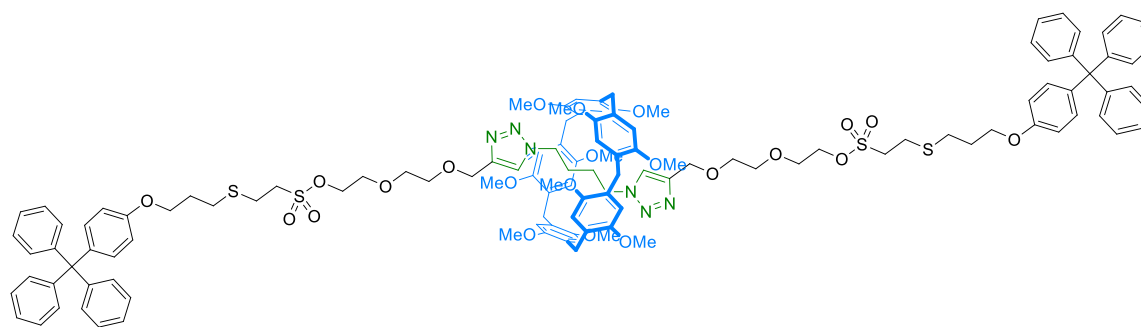
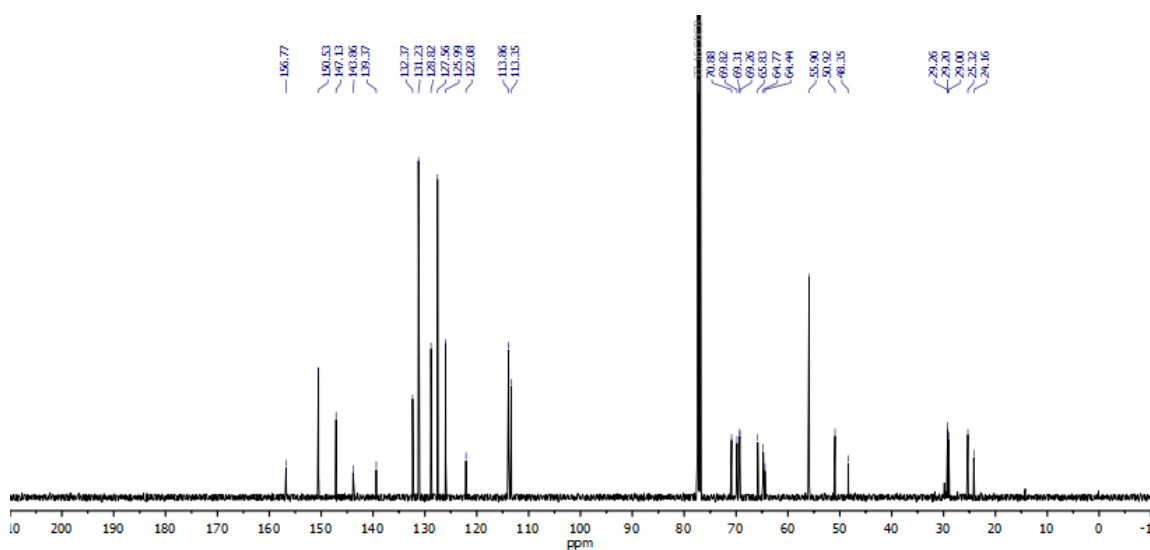


Figure 102. ^{13}C NMR (101 MHz, CDCl_3) spectrum of 100a.

Compound 100b:

Figure 103. ^1H NMR (500 MHz, CDCl_3) spectrum of 100b.Figure 104. ^{13}C NMR (126 MHz, CDCl_3) spectrum of 100b.

Compound 100c:

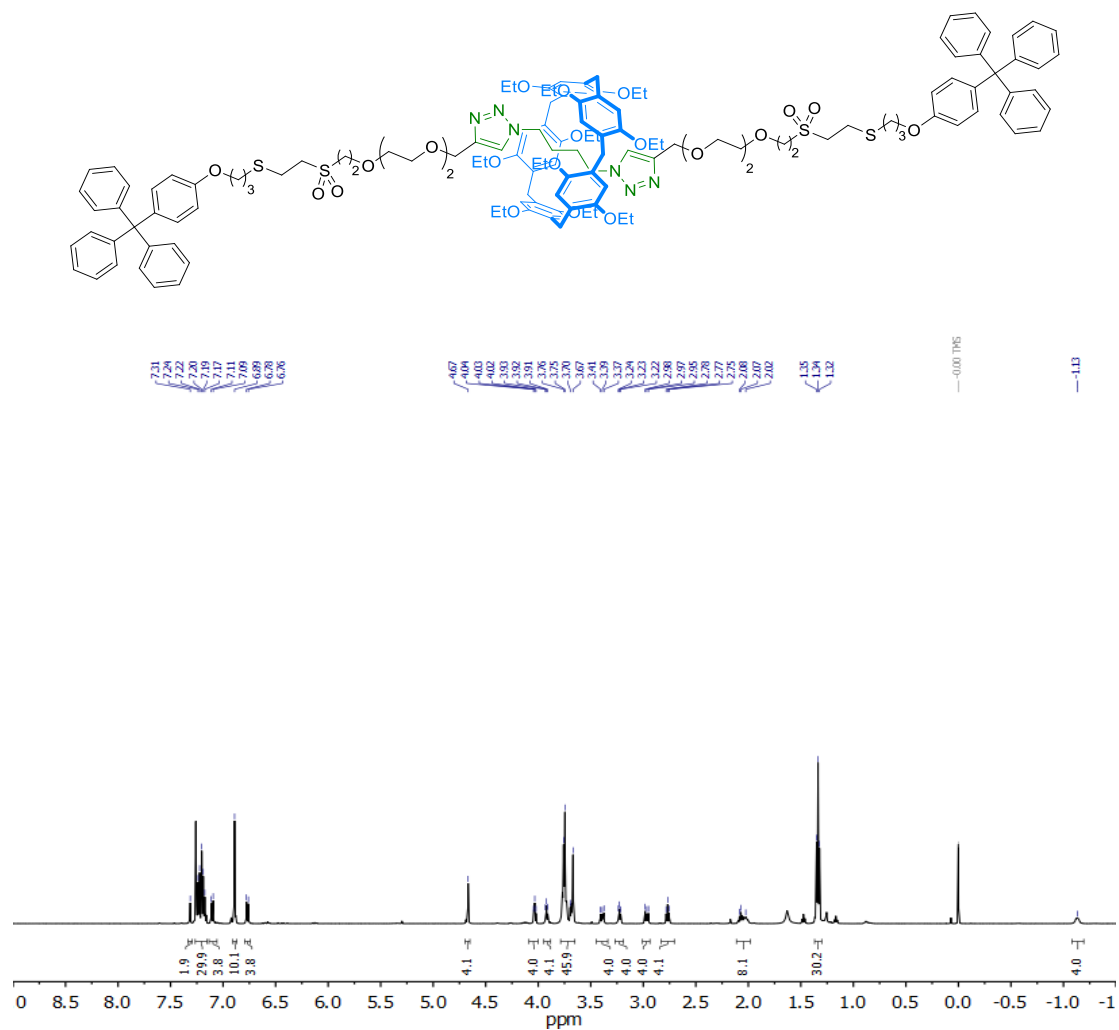


Figure 105. ¹H NMR (500 MHz, CDCl₃) spectrum of 100c.

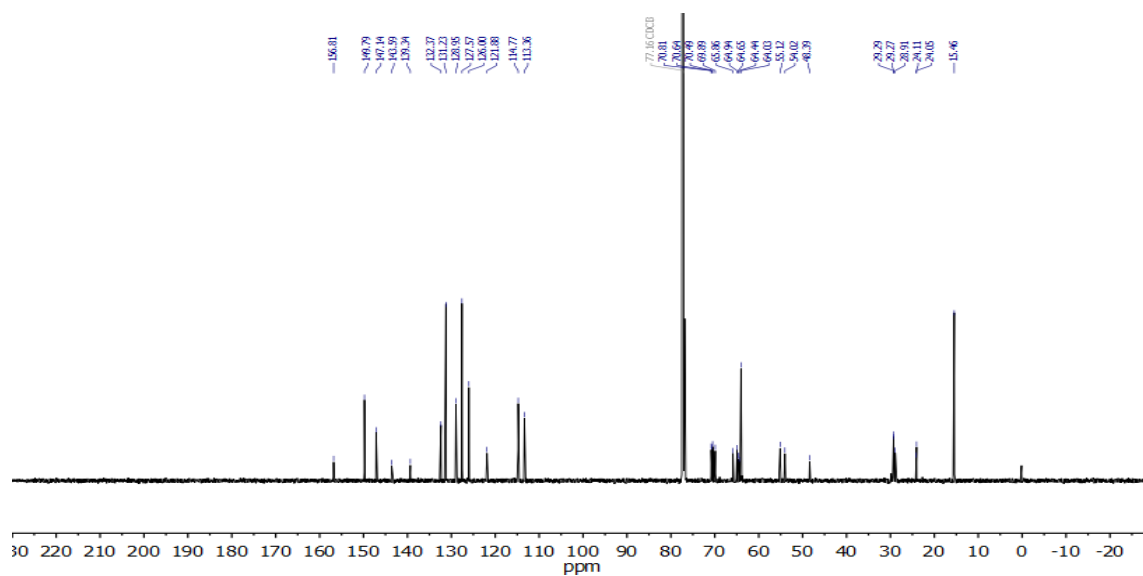
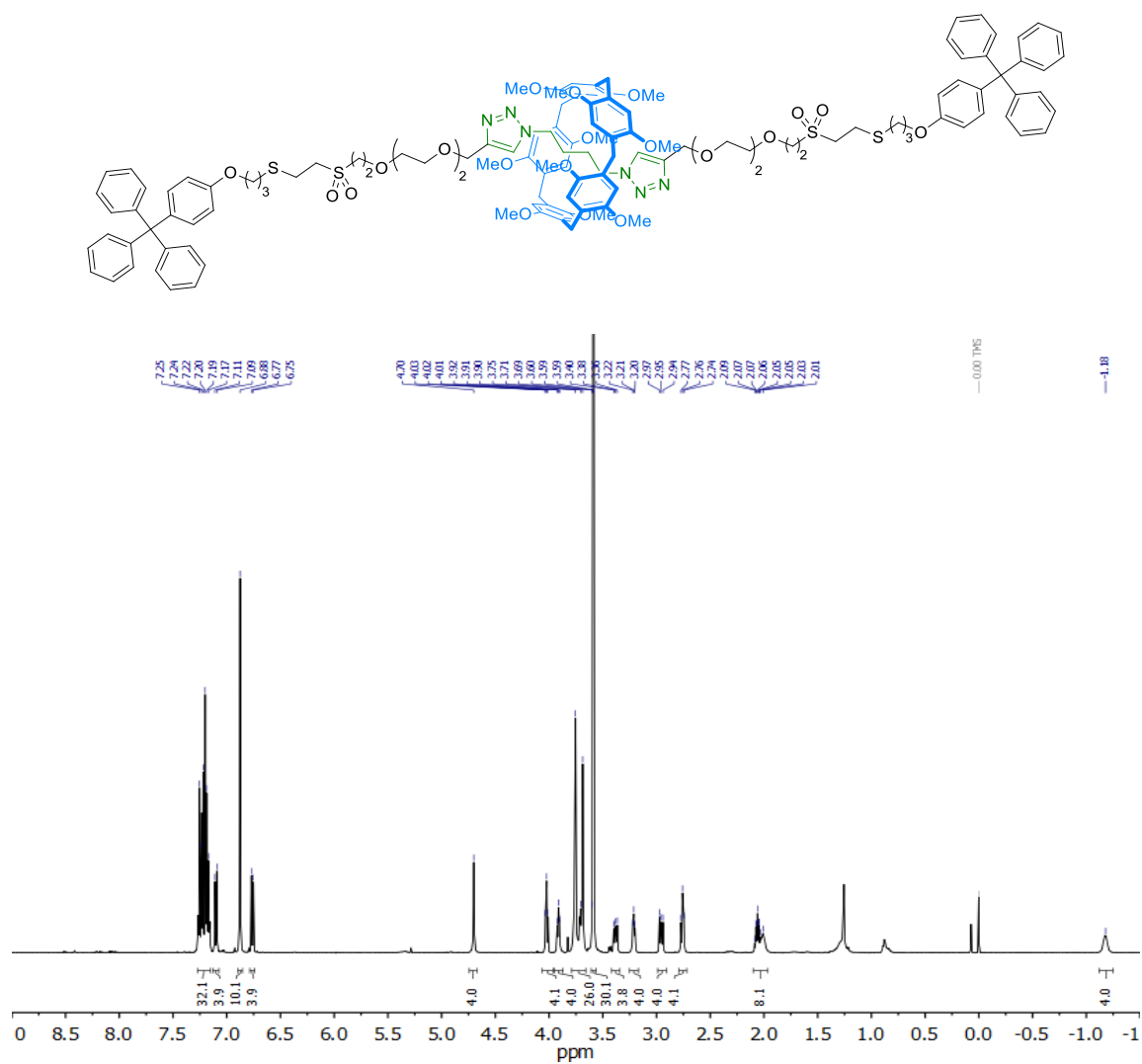
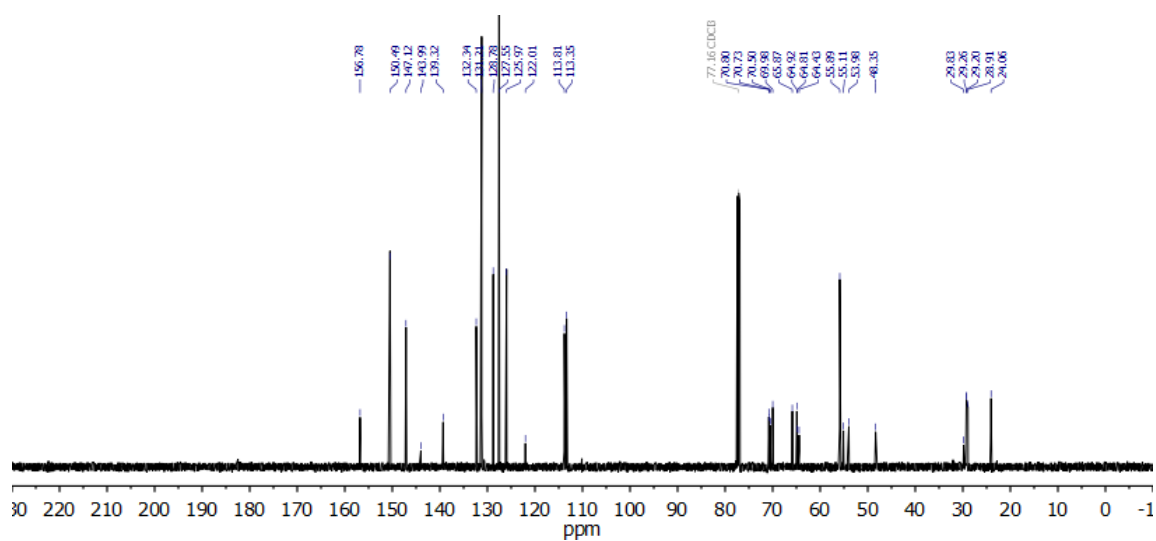
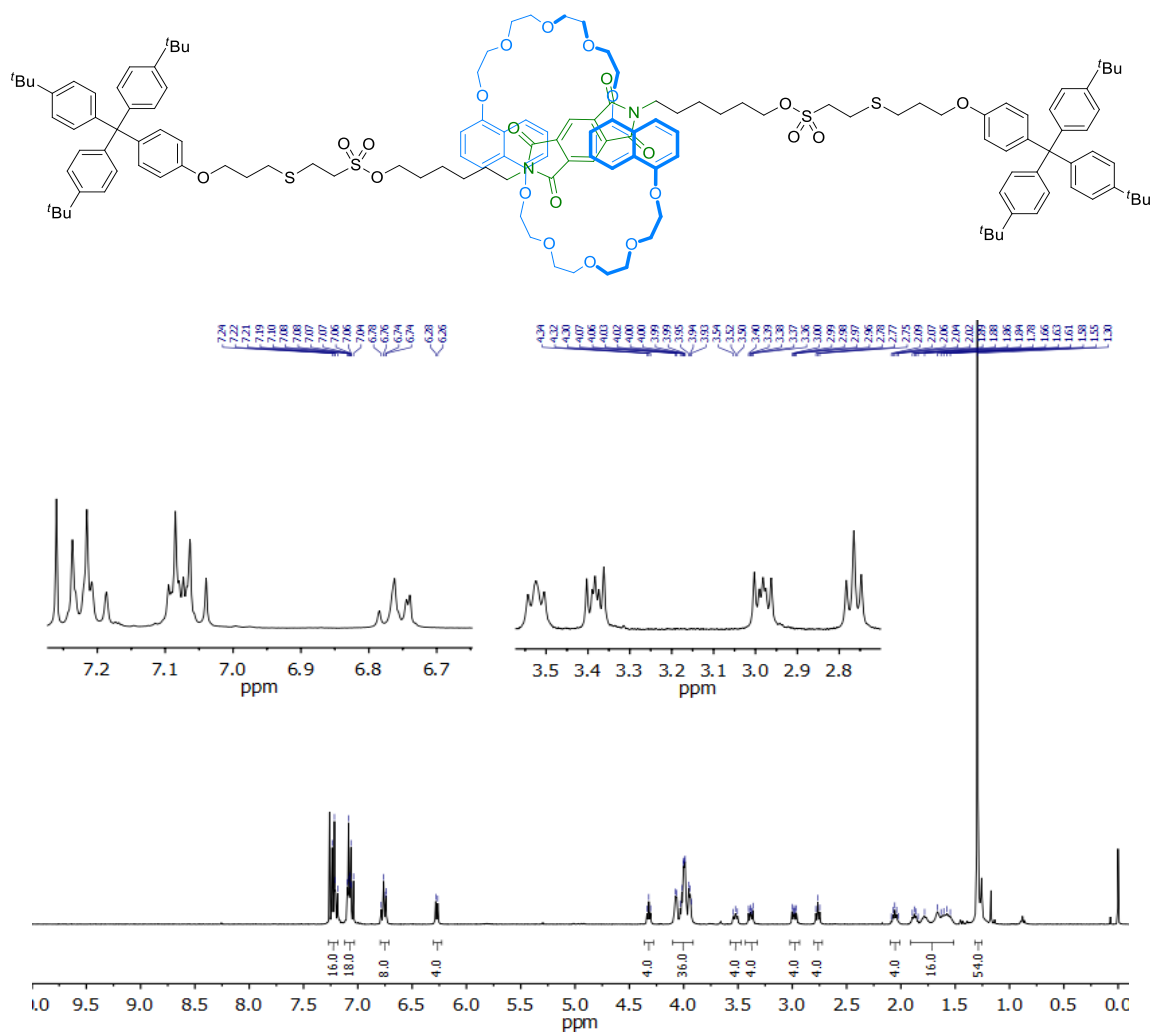
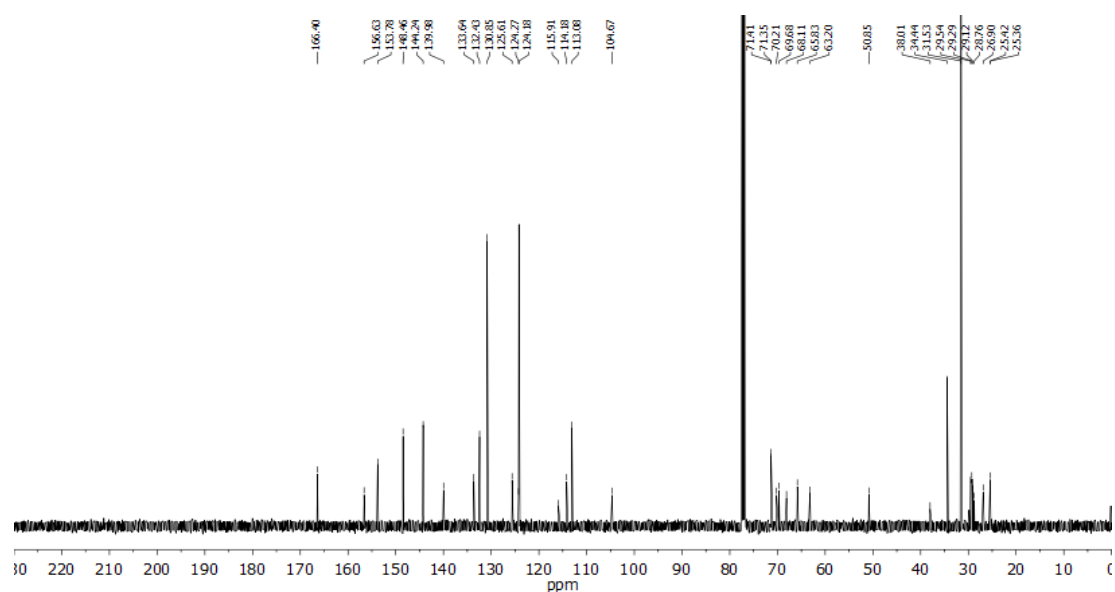


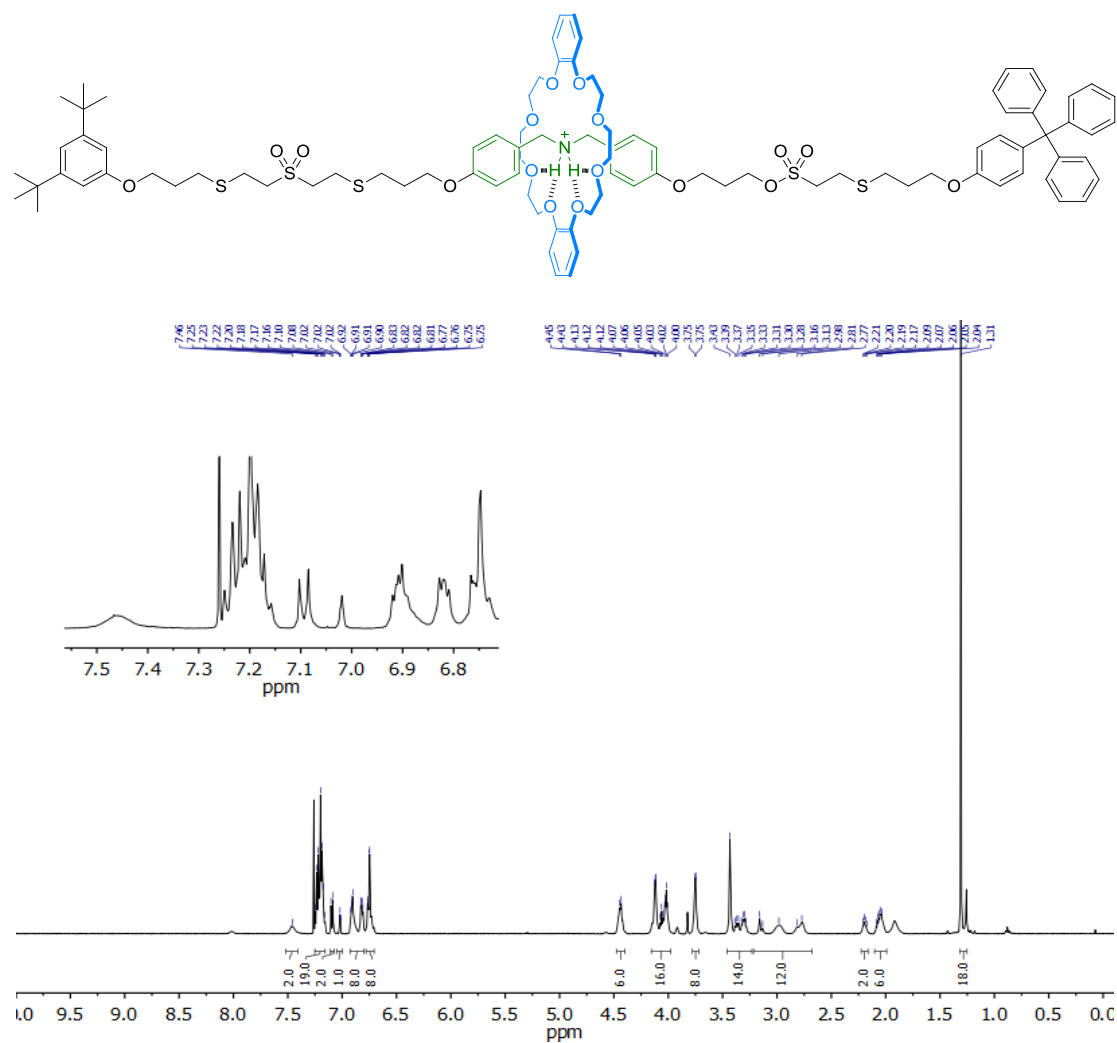
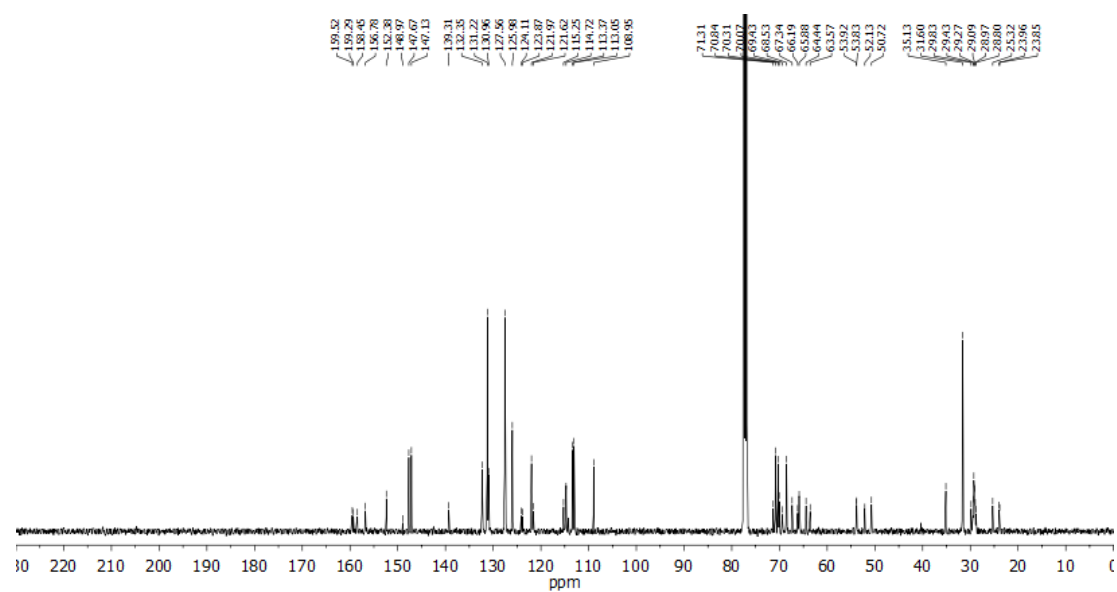
Figure 106. ¹³C NMR (126 MHz, CDCl₃) spectrum of 100c.

Compound 100d:

Figure 107. ^1H NMR (500 MHz, CDCl_3) spectrum of 100d.Figure 108. ^{13}C NMR (126 MHz, CDCl_3) spectrum of 100d.

Compound 106:

Figure 111. ¹H NMR (400 MHz, CDCl₃) spectrum of 106.Figure 112. ¹³C NMR (126 MHz, CDCl₃) spectrum of 106.

Compound **121**·PF₆⁻:Figure 115. ¹H NMR (500 MHz, CDCl₃) spectrum of **121**·PF₆⁻.Figure 116. ¹³C NMR (126 MHz, CDCl₃) spectrum of **121**·PF₆⁻.

Compound **137-H⁺·PF₆⁻**:

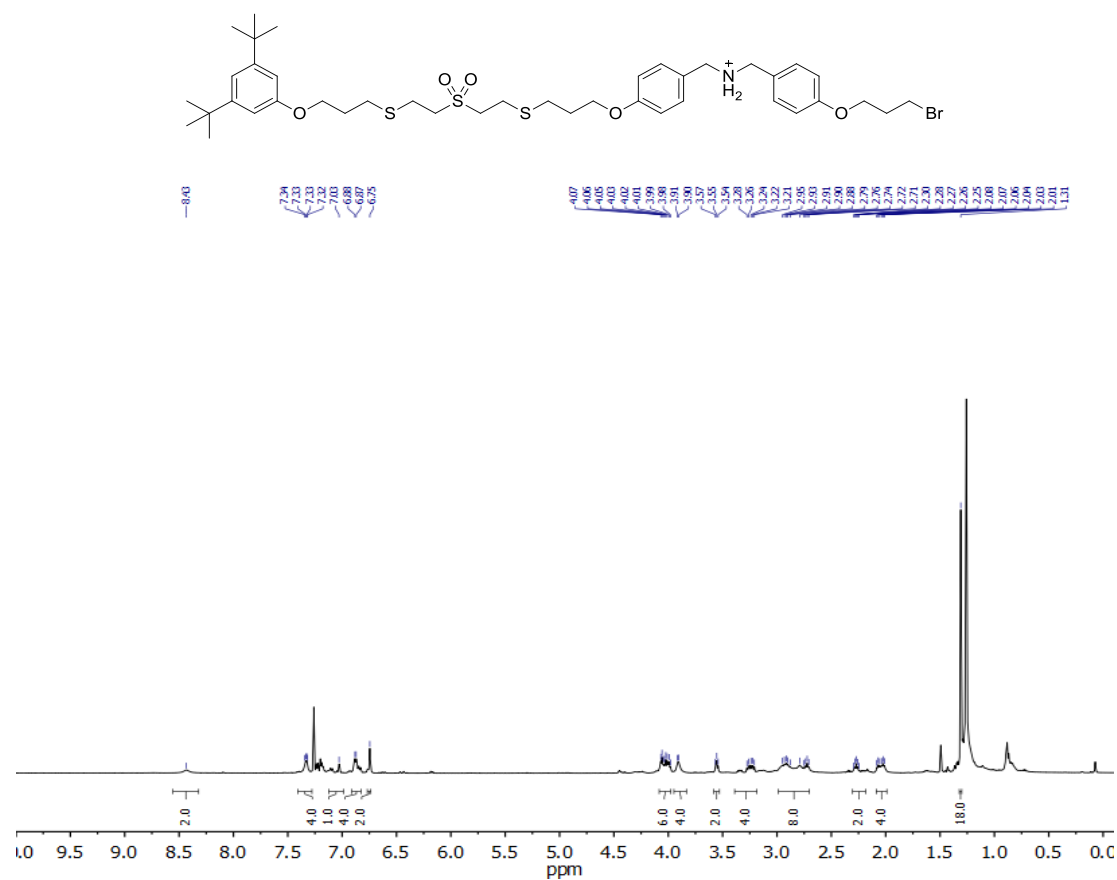


Figure 117. ¹H NMR (500 MHz, CDCl₃) spectrum of **137-H⁺·PF₆⁻**.

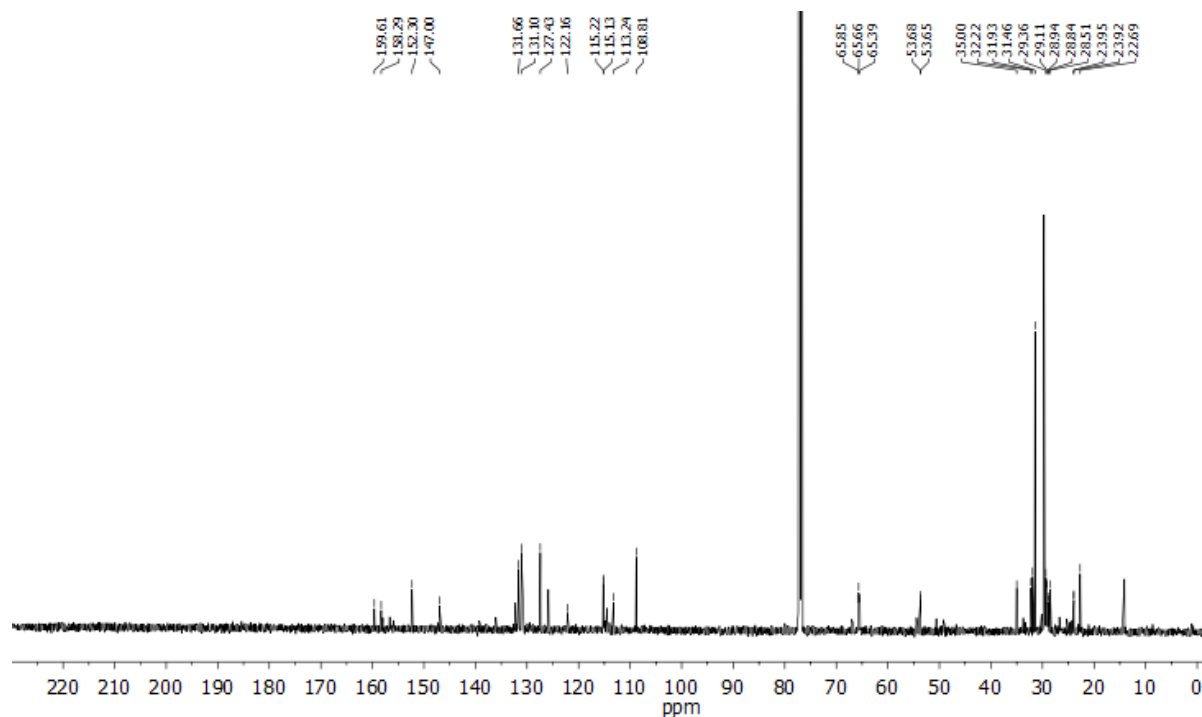


Figure 118. ¹³C NMR (126 MHz, CDCl₃) spectrum of **137-H⁺·PF₆⁻**.

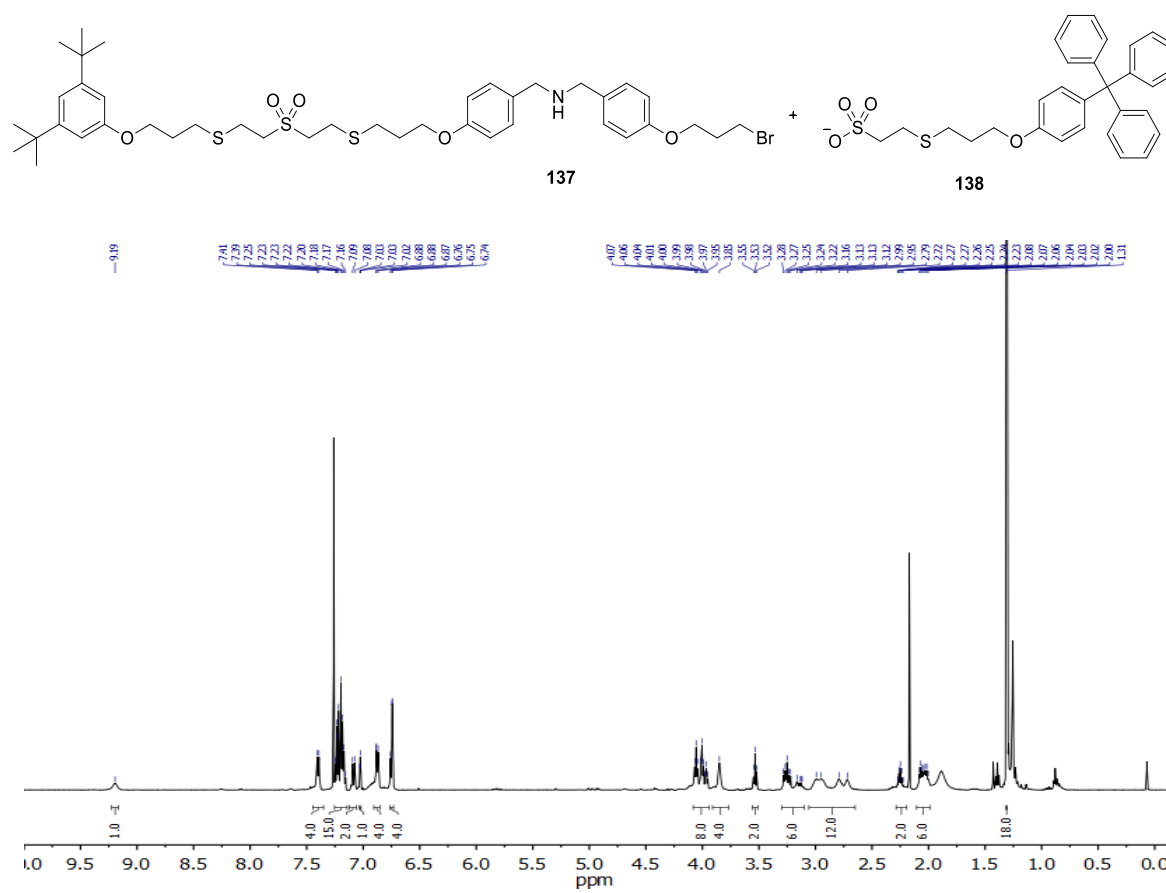
Mixture of compounds **137/138** (1:1):

Figure 119: ^1H NMR (500 MHz, CDCl_3) spectrum of a mixture of compounds **137/138** (1:1) from the cleavage of rotaxane **121**· PF_6^- .

**Chapter 2: An “ON/OFF” circularly polarized
luminescence switch based on a rotaxane architecture**

1. Background

1.1. Chiroptical properties

Chiroptical properties are optical properties specific of chiral systems that imply interactions with circularly polarized light. For the study of these properties, it is important to know that circularly polarized light has two handedness. The left-handed component is identified as a counterclockwise helix, while the right-handed one describes a clockwise helix as the wave propagates towards the observer. The irradiation of chiral molecules or assemblies with circularly polarized light results in an intrinsic property of the compound called circular dichroism (CD), which is defined as the difference of absorption between the left-handed and the right-handed circularly polarized lights:

$$CD = A^l - A^r \quad (\text{Eq. 1})$$

where A^l and A^r represent the absorbances of the left-handed and the right-handed polarized light, respectively. Typically, the CD is measured in ellipticity θ (mdeg), nevertheless, it can also be given by means of $\Delta\varepsilon$, which is the difference between the molar absorptivity of the left-handed and the right-handed polarized light:

$$\Delta\varepsilon = \varepsilon^l - \varepsilon^r = \frac{A^l - A^r}{C \times l} \quad (\text{Eq. 2})$$

where ε^l and ε^r ($\text{Lmol}^{-1}\text{cm}^{-1}$) represent the molar extinction coefficient of the left-handed and the right-handed polarized light, respectively, C (M) stands for the concentration and l (cm) for the pathlength. Another convenient parameter is the dissymmetry factor, g_{abs} for the CD,²⁷⁷ defined as:

$$g_{\text{abs}} = \frac{\Delta\varepsilon}{\varepsilon} = \frac{\varepsilon^l - \varepsilon^r}{\frac{1}{2}(\varepsilon^l + \varepsilon^r)} \quad (\text{Eq. 3})$$

The great advantage of $\Delta\varepsilon$ and g_{abs} values is that they are independent of the pathlength and the concentration. Furthermore, another advantage of using g_{abs} is that it allows the comparison of the response of species featuring very different molar extinction coefficients. It is also important to emphasize that the CD spectra of two enantiomers are always perfect mirror images of opposite sign. Furthermore, the experimental CD spectrum is widely employed for structural determination as it provides information with respect to the stereochemistry of chiral assemblies or molecules.²⁷⁷

Circularly polarized luminescence (CPL) is the analogue of CD for the emission of light. Indeed, it can be described as the difference between the emission of left-handed and right-handed circularly polarized light by an emissive structure:

²⁷⁷ N. Berova, L. Di Bari, G. Pescitelli, *Chem. Soc. Rev.* **2007**, *36*, 914-931.

$$\Delta I = I^l - I^r \quad (\text{Eq. 4})$$

where I^l and I^r represent the emission of the left-handed and the right-handed polarized light, respectively. Since it is complicated to measure an absolute emission value like fluorescence, the intensity of the CPL signal of a system is usually given and evaluated through the dissymmetry factor, now represented as g_{lum} , defined as the ratio between the difference of intensities (ΔI) and the average of the total luminescence intensity (I):

$$g_{lum} = \frac{\Delta I}{I} = \frac{I^l - I^r}{\frac{(I^l + I^r)}{2}} \quad (\text{Eq. 5})$$

Thus, it can be noticed that this parameter can reach values up to +2 or -2 when the luminescence is completely left-handed or right-handed respectively. Similarly to CD, the CPL spectra of two enantiomers are mirror images of opposite sign.²⁷⁸

In order to measure the CPL signal of a compound, it is necessary to insert additional modules to a common fluorimeter. Indeed, after being excited at a given wavelength, the emitted circularly polarized light has to be differentiated between the left and the right-handed lights. This operation is performed by a photo-elastic modulator (PEM) and subsequently, the discriminated light passes through a linear polarizer with the aim of orienting this light horizontally. The latter is then detected employing a photomultiplier tube (PMT) or a photon counter as detector (Figure 120).

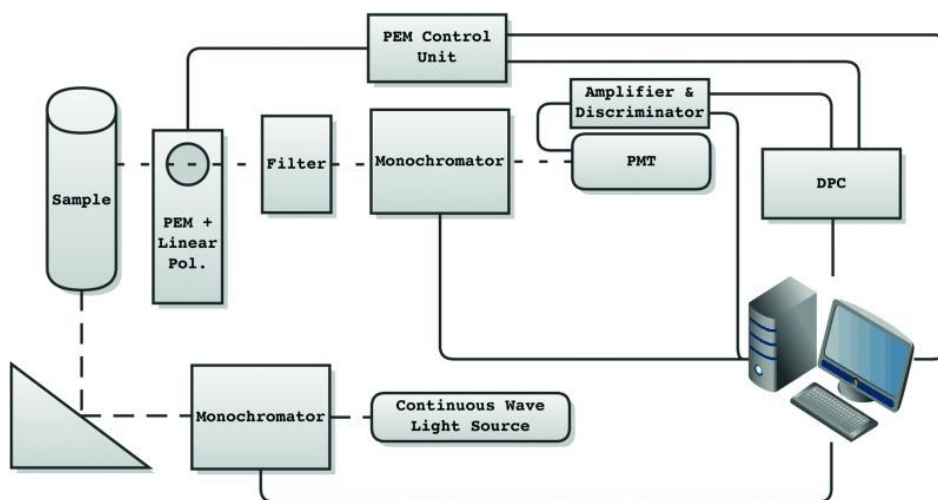


Figure 120. Schematic diagram for the instrumentation employed for implementing CPL measurements.^{278c}
Reprinted with permission from ref 278c. Copyright 2015 John Wiley and Sons.

²⁷⁸ a) J. P. Riehl, F. S. Richardson, *Chem. Rev.* **1986**, *86*, 1-16. b) F. Zinna, L. Di Bari, *Chirality* **2015**, *27*, 1-13. c) E. M. Sánchez-Carnerero, A. R. Agarrabeitia, F. Moreno, B. Maroto, G. Muller, M. J. Ortiz, S. de la Moya, *Chem. Eur. J.* **2015**, *21*, 13488-13500. d) G. Longhi, E. Castiglioni, J. Koshoubu, G. Mazzeo, S. Abbate, *Chirality* **2016**, *28*, 696-707.

1.2 CPL emitters

Among the CPL emitters based on discrete molecules, the highest responses are obtained by using lanthanide complexes,^{278b} culminating in a spectacular $|g_{lum}|$ value of 1.38 for a Eu^{III} complex in chloroform.²⁷⁹ Furthermore, numerous transition metal-based organometallic complexes exhibiting CPL signals have been reported.²⁸⁰ They mostly contain helicene units on their structures. On the other hand, CPL emitters based on organic compounds have also attracted increasing attention.^{278c,281} Thus, our group and many others exploited the chirality of luminescent cyclic ketones,²⁸² cyclophanes,²⁸³ biaryls,²⁸⁴ helicenes²⁸⁵ and bodipy groups²⁸⁶ to create a CPL signal (Figure 121). Lastly, this photophysical property was also reported for supramolecular assemblies.²⁸⁷

The interest in CPL emitting systems has risen considerably due to the numerous applications exploiting this photophysical property discovered recently, including the sensing of biomolecules²⁸⁸ or transition metals²⁸⁹ or the generation of CPL organic light-emitting diodes (OLEDs).²⁹⁰ It can also be noticed that CPL emitting compounds were incorporated in polymer²⁹¹ or cellulose films²⁹² in order to

²⁷⁹ J. L. Lunkley, D. Shirotni, K. Yamanari, S. Kaizaki, G. Muller, *J. Am. Chem. Soc.* **2008**, *130*, 13814-13815.

²⁸⁰ a) R. Aoki, R. Toyoda, J. F. Kögel, R. Sakamoto, J. Kumar, Y. Kitagawa, K. Harano, T. Kawai, H. Nishihara, *J. Am. Chem. Soc.* **2017**, *139*, 16024-16027. b) J. OuYang, J. Crassous, *Coord. Chem. Rev.* **2018**, *376*, 533-547. c) J.-R. Jiménez, B. Doistau, C. M. Cruz, C. Besnard, J. M. Cuerva, A. G. Campaña, C. Piguet, *J. Am. Chem. Soc.* **2019**, *141*, 13244-13252.

²⁸¹ H. Tanaka, Y. Inoue, T. Mori, *ChemPhotoChem* **2018**, *2*, 386-402.

²⁸² a) P. H. Schippers, J. P. M. Van der Ploeg, H. P. J. M. Dekkers, *J. Am. Chem. Soc.* **1983**, *105*, 84-89. b) G. Longhi, E. Castiglioni, S. Abbate, F. Lebon, D. A. Lightner, *Chirality* **2013**, *25*, 589-599.

²⁸³ a) S. P. Morcillo, D. Miguel, L. Alvarez de Cienfuegos, J. Justicia, S. Abbate, E. Castiglioni, C. Bour, M. Ribagorda, D. J. Cardenas, J. M. Paredes, L. Crovetto, D. Choquesillo-Lazarte, A. J. Mota, M. C. Carreno, G. Longhi, J. M. Cuerva, *Chem. Sci.* **2016**, *7*, 5663-5670. b) S. Sato, A. Yoshii, S. Takahashi, S. Furumi, M. Takeuchi, H. Isobe, *Proc. Natl. Acad. Sci. U.S.A.* **2017**, *114*, 13097-13101. c) P. Reiné, A. G. Campaña, L. Álvarez de Cienfuegos, V. Blanco, S. Abbate, A. J. Mota, G. Longhi, D. Miguel, J. M. Cuerva, *Chem. Commun.* **2019**, *55*, 10685-10688.

²⁸⁴ a) T. Amako, T. Harada, N. Suzuki, K. Mishima, M. Fujiki, Y. Imai, *RSC Adv.* **2013**, *3*, 23508-23513. b) K. Nakabayashi, T. Amako, N. Tajima, M. Fujiki, Y. Imai, *Chem. Commun.* **2014**, *50*, 13228-13230.

²⁸⁵ a) K. Nakamura, S. Furumi, M. Takeuchi, T. Shibuya, K. Tanaka, *J. Am. Chem. Soc.* **2014**, *136*, 5555-5558. b) C. M. Cruz, I. R. Márquez, I. F. A. Mariz, V. Blanco, C. Sánchez-Sánchez, J. M. Sobrado, J. A. Martín-Gago, J. M. Cuerva, E. Maçôas, A. G. Campaña, *Chem. Sci.* **2018**, *9*, 3917-3924. c) C. M. Cruz, S. Castro-Fernández, E. Maçôas, J. M. Cuerva, A. G. Campaña, *Angew. Chem. Int. Ed.* **2018**, *57*, 14782-14786.

²⁸⁶ a) H. Lu, J. Mack, T. Nyokong, N. Kobayashi, Z. Shen, *Coord. Chem. Rev.* **2016**, *318*, 1-15. b) V. G. Jiménez, F. M. F. Santos, S. Castro-Fernández, J. M. Cuerva, P. M. P. Gois, U. Pischel, A. G. Campaña, *J. Org. Chem.* **2018**, *83*, 14057-14062.

²⁸⁷ J. Kumar, T. Nakashima, T. Kawai, *J. Phys. Chem. Lett.* **2015**, *6*, 3445-3452.

²⁸⁸ K. Staszak, K. Wieszczycka, V. Marturano, B. Tylkowski, *Coord. Chem. Rev.* **2019**, *397*, 76-90.

²⁸⁹ a) P. Reiné, J. Justicia, S. P. Morcillo, S. Abbate, B. Vaz, M. Ribagorda, Á. Orte, L. Álvarez de Cienfuegos, G. Longhi, A. G. Campaña, D. Miguel, J. M. Cuerva, *J. Org. Chem.* **2018**, *83*, 4455-4463. b) Y. Imai, Y. Nakano, T. Kawai, J. Yuasa, *Angew. Chem. Int. Ed.* **2018**, *57*, 8973-8978.

²⁹⁰ a) F. Zinna, U. Giovanella, L. Di Bari, *Adv. Mater.* **2015**, *27*, 1791-1795. b) J. R. Brandt, X. Wang, Y. Yang, A. J. Campbell, M. J. Fuchter, *J. Am. Chem. Soc.* **2016**, *138*, 9743-9746. c) D. Di Nuzzo, C. Kulkarni, B. Zhao, E. Smolinsky, F. Tassinari, S. C. J. Meskers, R. Naaman, E. W. Meijer, R. H. Friend, *ACS Nano* **2017**, *11*, 12713-12722.

²⁹¹ Y. Yang, R. Correa da Costa, D.-M. Smilgies, A. J. Campbell, M. J. Fuchter, *Adv. Mater.* **2013**, *25*, 2624-2628.

²⁹² H. Zheng, W. Li, W. Li, X. Wang, Z. Tang, S. X.-A. Zhang, Y. Xu, *Adv. Mater.* **2018**, *30*, 1705948.

study the photonic applications of these materials. Furthermore, the control or modulation of the CPL signal of a certain system is relevant to encode information using light, giving rise to CPL switches whose radiation might, in the future, be correlated with a writing-and-erasing process in complex devices.

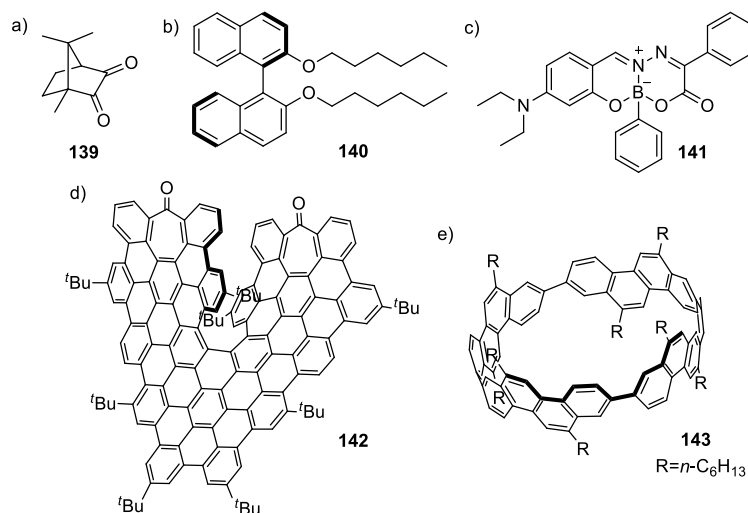


Figure 121. Selected CPL emitters based on organic molecules: a) A chiral cyclic ketone.^{282b} b) A chiral binaphthyl compound.^{284a} c) A chiral bodipy.^{286b} d) A superhelicene.^{285c} e) A chiral cyclophane.^{283b}

1.3. CPL switches

From a historical point of view, the first chiroptical switches were designed for electronic circular dichroism (ECD).²⁹³ More recently, CPL switches have started to be developed.²⁹⁴ Different types of modulation of the CPL response can be accomplished upon the application of external stimuli. Indeed, the signal can change between positive and negative sign, can be activated or deactivated, or it can also undergo a bathochromic or a hypsochromic shift.

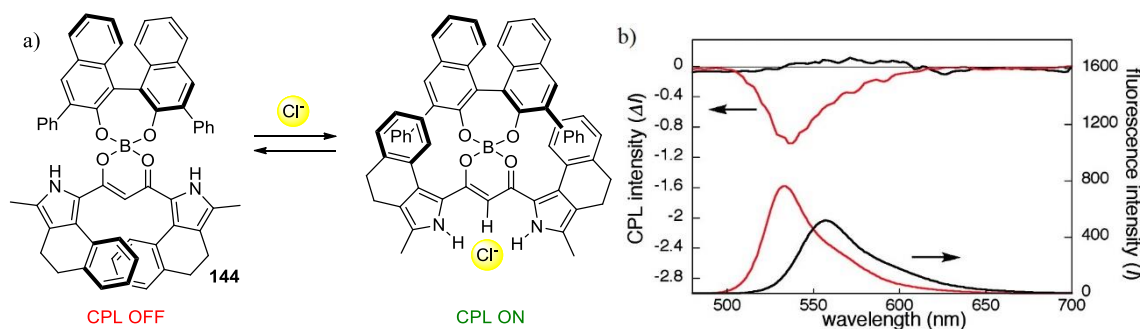


Figure 122. a) An anion-triggered CPL switch. b) CPL (top) and fluorescence (bottom) spectra of **144** in absence (black line) or in the presence of 200 equivalents of tetrabutylammonium chloride (red line).²⁹⁵ Reprinted with permission from ref 295. Copyright 2011 American Chemical Society.

²⁹³ B. L. Feringa, R. A. van Delden, N. Koumura, E. M. Geertsema, *Chem. Rev.* **2000**, *100*, 1789-1816.

²⁹⁴ J.-L. Ma, Q. Peng, C.-H. Zhao, *Chem. Eur. J.* **2019**, *25*, 15441-15454.

In 2011, Maeda and co-workers reported the first chemically-controllable CPL switch employing a molecule containing a BINOL-boron moiety and dipyrrolyldiketone units. Thus, the addition of chloride anions induced a change of conformation, since the pyrrole derivatives flipped, resulting in the modulation of the magnitude of the CPL signal (Figure 122).²⁹⁵ Similarly, this modulation consisting in increasing or decreasing the CPL signal strength can be accomplished by cation binding to *ortho*-oligo(phenylene)ethynyls (Figure 123),^{283a,296} crown ethers²⁹⁷ or a pyrene-based ligand containing imidazole units.²⁹⁸ Other stimuli such as a photo-switching²⁹⁹ or pH modification were also successfully applied (Figure 124).³⁰⁰

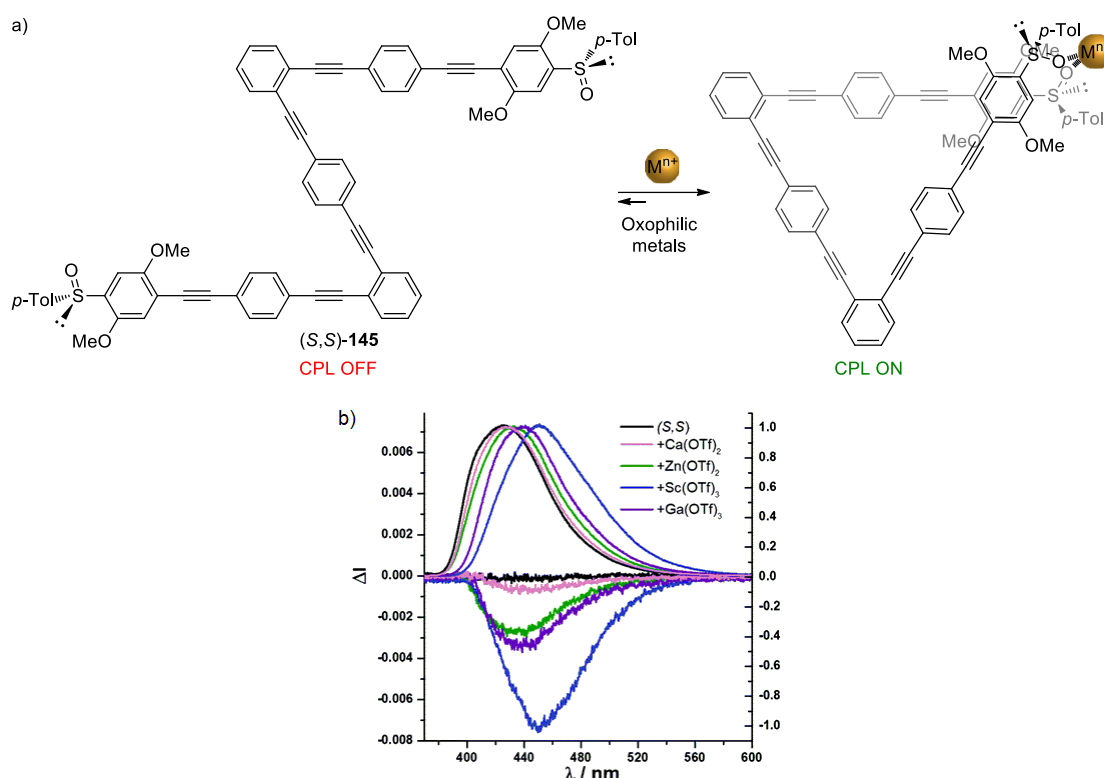


Figure 123. a) A cation-based "ON-OFF" CPL switch. b) CPL and fluorescence spectra of (S,S)-145 in presence and in absence of different oxophilic metals.²⁹⁶ Reprinted with permission from ref 296. Copyright 2018 Royal Society of Chemistry.

²⁹⁵ H. Maeda, Y. Bando, K. Shimomura, I. Yamada, M. Naito, K. Nobusawa, H. Tsumatori, T. Kawai, *J. Am. Chem. Soc.* **2011**, *133*, 9266-9269.

²⁹⁶ P. Reiné, A. M. Ortuño, S. Resa, L. Álvarez de Cienfuegos, V. Blanco, M. J. Ruedas-Rama, G. Mazzeo, S. Abbate, A. Lucotti, M. Tommasini, S. Guisán-Ceinós, M. Ribagorda, A. G. Campaña, A. Mota, G. Longhi, D. Miguel, J. M. Cuerva, *Chem. Commun.* **2018**, *54*, 13985-13988.

²⁹⁷ A. Homberg, E. Brun, F. Zinna, S. Pascal, M. Górecki, L. Monnier, C. Besnard, G. Pescitelli, L. Di Bari, J. Lacour, *Chem. Sci.* **2018**, *9*, 7043-7052.

²⁹⁸ Y. Imai, J. Yuasa, *Chem. Commun.* **2019**, *55*, 4095-4098.

²⁹⁹ a) Y. Hashimoto, T. Nakashima, D. Shimizu, T. Kawai, *Chem. Commun.* **2016**, *52*, 5171-5174. b) W. Miao, S. Wang, M. Liu, *Adv. Funct. Mater.* **2017**, *27*, 1701368.

³⁰⁰ a) S. Pascal, C. Besnard, F. Zinna, L. Di Bari, B. Le Guennic, D. Jacquemine, J. Lacour, *Org. Biomol. Chem.* **2016**, *14*, 4590-4594. b) K. Takaishi, M. Yasui, T. Ema, *J. Am. Chem. Soc.* **2018**, *140*, 5334-5338.

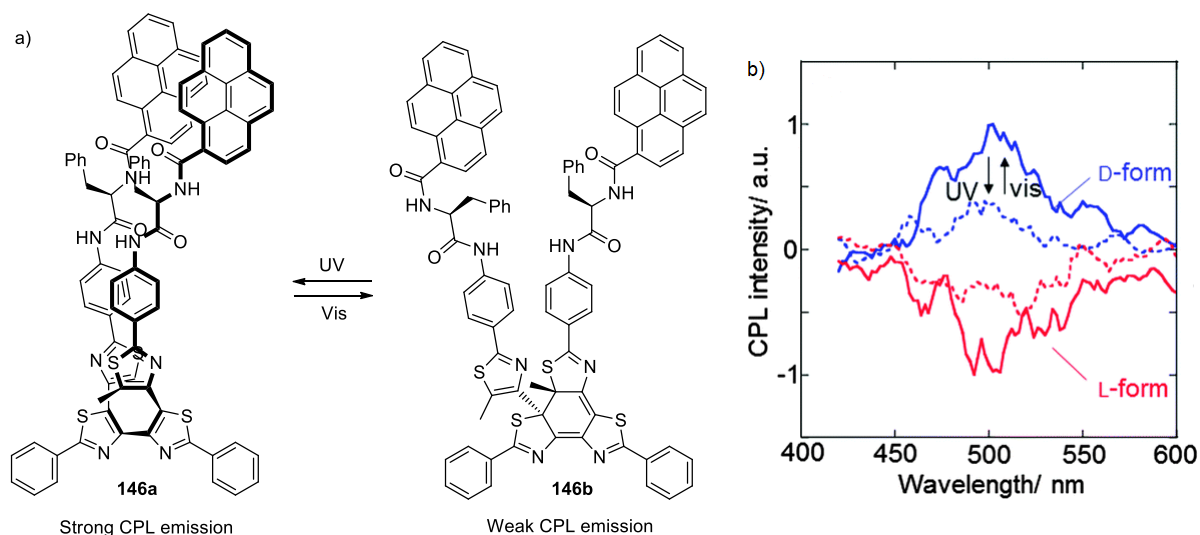
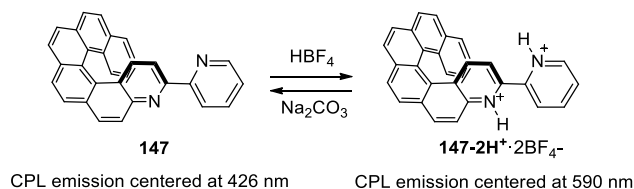


Figure 124. a) A photo-driven CPL switch. b) CPL spectra of **146a** and **146b** showing a difference of magnitude of the CPL emission.^{299a} Reprinted with permission from ref 299a. Copyright 2016 Royal Society of Chemistry.

Furthermore, Autschbach and Crassous designed an azahelicene-bipyridine molecule whose emission can suffer a bathochromic shift upon the addition of an acid. Consequently, their CPL spectra underwent an identical bathochromic shift in acidic medium and then recovered their original responses in basic medium (Scheme 71).³⁰¹ The same phenomenon occurred in other azahelicenes by the same pH change³⁰² or using Zn^{2+} as stimulus.³⁰³



Scheme 71. A pH-triggered CPL switch.³⁰¹

Regarding the switching of the handedness, it is known that the CPL signal of aggregates or polymers can be sign-inverted depending on the solvent,³⁰⁴ or for a simple compound according to the solid state matrices employed.³⁰⁵ Recently, Ito, Imai and Asami described a diamine bearing two pyrene

³⁰¹ N. Saleh, B. Moore II, M. Srebro, N. Vanthuyne, L. Toupet, J. A. G. Williams, C. Roussel, K. K. Deol, G. Muller, J. Autschbach, J. Crassous, *Chem. Eur. J.* **2015**, *21*, 1673-1681.

³⁰² T. Otani, A. Tsuyuki, T. Iwachi, S. Someya, K. Tateno, H. Kawai, T. Saito, K. S. Kanyiva, T. Shibata, *Angew. Chem. Int. Ed.* **2017**, *56*, 3906-3910.

³⁰³ a) H. Isla, M. Srebro-Hooper, M. Jean, N. Vanthuyne, T. Roisnel, J. L. Lunkley, G. Muller, J. A. G. Williams, J. Autschbach, J. Crassous, *Chem. Commun.* **2016**, *52*, 5932-5935. b) H. Isla, N. Saleh, J.-K. Ou-Yang, K. Dhbaibi, M. Jean, M. Dziurka, L. Favereau, N. Vanthuyne, L. Toupet, B. Jamoussi, M. Srebro-Hooper, J. Crassous, *J. Org. Chem.* **2019**, *84*, 5383-5393.

³⁰⁴ a) A. Satrijo, S. C. J. Meskers, T. M. Swager, *J. Am. Chem. Soc.* **2006**, *128*, 9030-9031. b) Y. Nagata, T. Nishikawa, M. Sugimoto, *Chem. Commun.* **2014**, *50*, 9951-9953. c) M. Okazaki, T. Mizusawa, K. Nakabayashi, M. Yamashita, N. Tajima, T. Harada, M. Fujiki and Y. Imai, *J. Photochem. Photobiol. A* **2016**, *331*, 115-119.

³⁰⁵ T. Kimoto, T. Amako, N. Tajima, R. Kuroda, M. Fujiki, Y. Imai, *Asian J. Org. Chem.* **2013**, *2*, 404-410.

fluorophore units that can switch between the monomer and the excimer CPL emission depending on the concentration of molecule. Thus, in diluted conditions, the monomer CPL emission prevails while at high concentrations, the excimer CPL emission, which displays an inverted sign compared to that of the monomeric emission, dominates (Figure 125).³⁰⁶

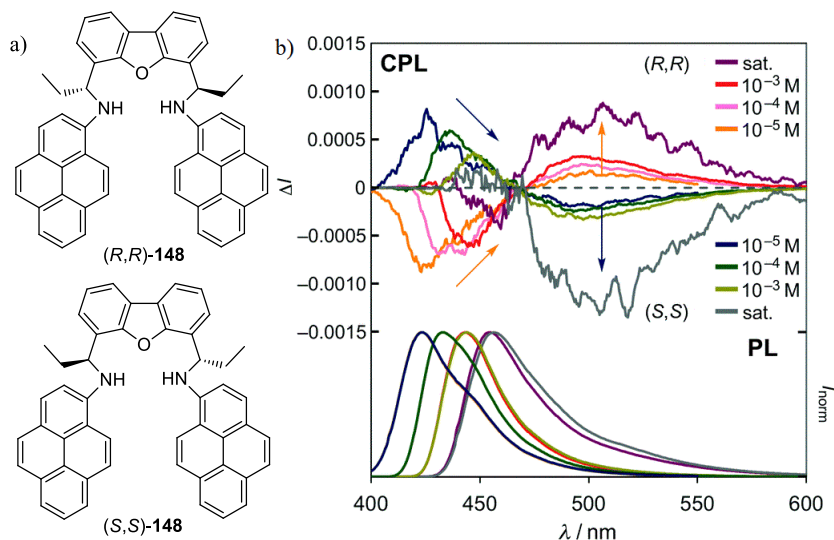


Figure 125. a) Structure of an emissive chiral diamine. b) CPL (top) and fluorescence (bottom) spectra of both enantiomers of compound **148** in toluene at different concentrations.³⁰⁶ Reprinted with permission from ref 306. Copyright 2017 Royal Society of Chemistry.

1.4. Chiral rotaxanes

As shown in the general introduction, a considerable work was dedicated to the synthesis of rotaxanes and their application as molecular machines over the years. However, the introduction of chirality in those MIMs and its use in the development of new applications was significantly less investigated. Nonetheless, recently, the synthesis and study of chiral rotaxanes and their applications started to attract more attention.³⁰⁷

In the early days of rotaxane synthesis, the introduction of chiral covalent stereogenic units was carried out employing sugars. Indeed, a cyclodextrin macrocycle, composed by glucose groups, is by itself chiral and was widely used in the preparation of rotaxanes.⁶¹ Furthermore, rotaxanes bearing glucose stoppers were also reported (Figure 126).³⁰⁸ Following these examples, other chiral covalent elements,

³⁰⁶ S. Ito, K. Ikeda, S. Nakanishi, Y. Imai, M. Asami, *Chem. Commun.* **2017**, 53, 6323-6326.

³⁰⁷ E. M. G. Jamieson, F. Modicom, S. M. Goldup, *Chem. Soc. Rev.* **2018**, 47, 5266-5311.

³⁰⁸ A. Archut, W. M. Müller, S. Baumann, M. Habel, F. Vögtle, *Liebigs. Ann./Recl.* **1997**, 495-499.

mainly based on BINOL^{29a,309} and amino acids.^{165a,310} were introduced in the structure of rotaxanes, either on the stoppers, the thread or the macrocycle.

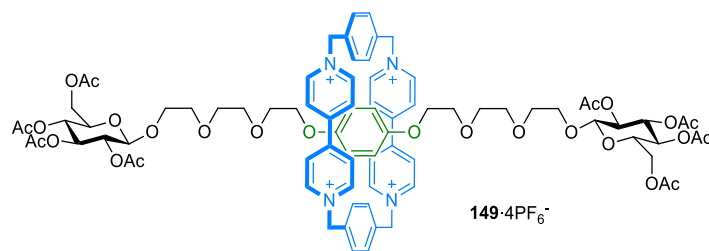
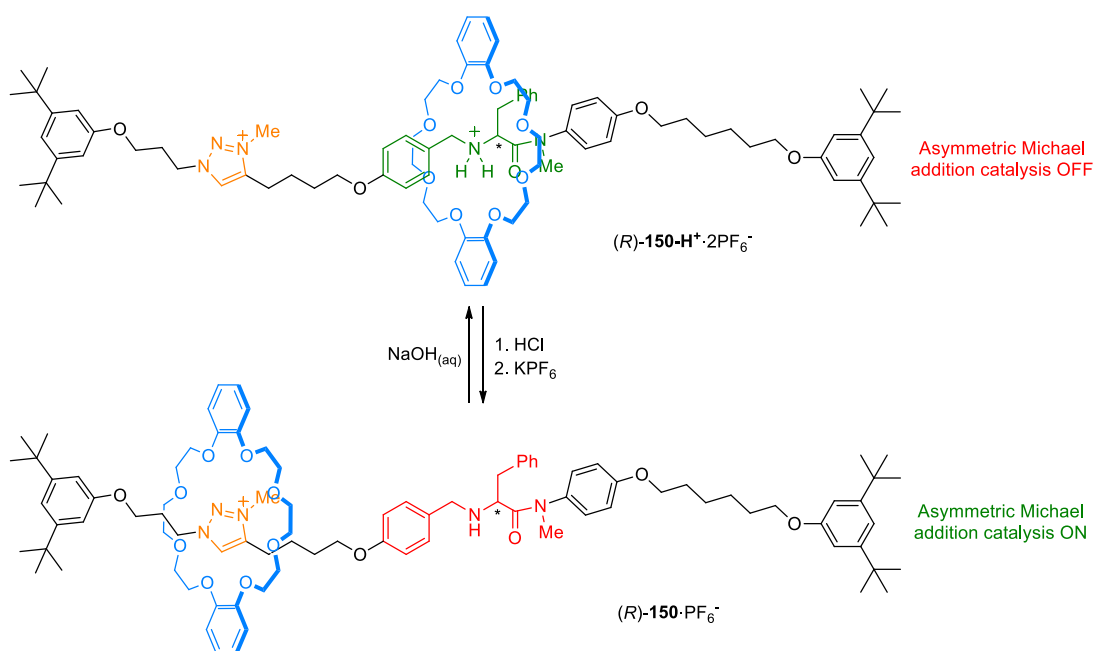


Figure 126. A chiral rotaxane stoppered by per-acetylated β -D-glucose.³⁰⁸



Scheme 72. A chiral rotaxane for asymmetric “ON-OFF” switchable catalysis.^{165a}

The introduction of covalent point chirality in rotaxanes led to relevant applications such as chiral anion recognition^{309b,311} or asymmetric organocatalysis. Thus, in 2004, Takata employed a different [2]rotaxanes featuring a chiral BINOL moiety to perform an asymmetric benzoin condensation.³¹² Following this breakthrough, chiral rotaxanes were constructed to execute asymmetric Michael addition,^{165,313} aldol reaction,^{165b} *O*-benzoylation of a *meso*-1,2-diol³¹⁴ catalysis (Scheme 72). In

³⁰⁹ a) Y. Tachibana, N. Kihara, Y. Ohga, T. Takata, *Chem. Lett.* **2000**, 29, 806-807. b) J. Y. C. Lim, I. Marques, V. Félix, P. D. Beer, *Angew. Chem. Int. Ed.* **2018**, 57, 584-588.

³¹⁰ a) I. Smukste, D. B. Smithrud, *J. Org. Chem.* **2003**, 68, 2547-2558. b) X. Bao, I. Isaacsohn, A. F. Drew, D. B. Smithrud, *J. Org. Chem.* **2007**, 72, 3988-4000.

³¹¹ J. Y. C. Lim, I. Marques, V. Félix, P. D. Beer, *J. Am. Chem. Soc.* **2017**, 139, 12228-12239.

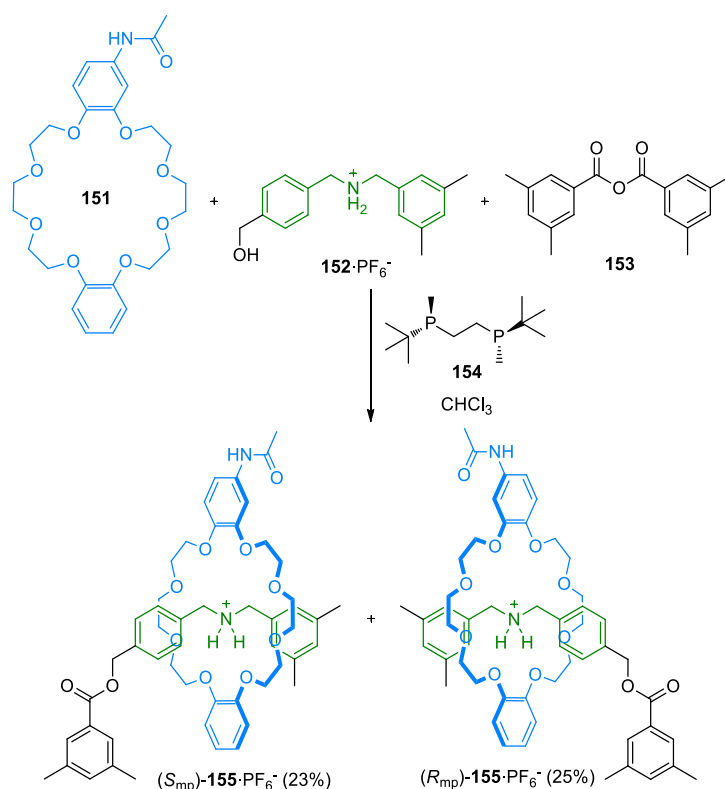
³¹² Y. Tachibana, N. Kihara, T. Takata, *J. Am. Chem. Soc.* **2004**, 126, 3438-3439.

³¹³ A. Martinez-Cuezva, M. Marin-Luna, D. A. Alonso, D. Ros-Ñiguez, M. Alajarin, J. Berna, *Org. Lett.* **2019**, 21, 5192-5196.

³¹⁴ K. Xu, K. Nakazono, T. Takata, *Chem. Lett.* **2016**, 45, 1274-1276.

addition, a rotaxane with this type of chiral element on its structure can act as a chiral ligand for stereoselective transition metal catalysis.³¹⁵

Rotaxanes featuring mechanical planar chirality properties consist generally in architectures featuring a non-symmetrical axle and a non-symmetrical macrocycle. Thus, in 1991, Kaifer and co-workers designed the first rotaxane exhibiting this kind of chirality by employing an α -D-cyclodextrin wheel and a non-symmetrical thread. They formed a mixture of two diastereoisomers (D,S_{mp}) and (D,R_{mp}) depending on the orientation of the cyclodextrin.⁶⁰ Later, in 1997, Okamoto and Vögtle prepared a mechanically planar chiral [1]rotaxane and were able to separate both enantiomers by HPLC.³¹⁶ Furthermore, it is possible to synthesize a mechanically planar chiral rotaxane in a stereoselective manner (Scheme 73).³¹⁷



Scheme 73. Enantioselective synthesis of a mechanically planar chiral [2]rotaxane.^{317a}

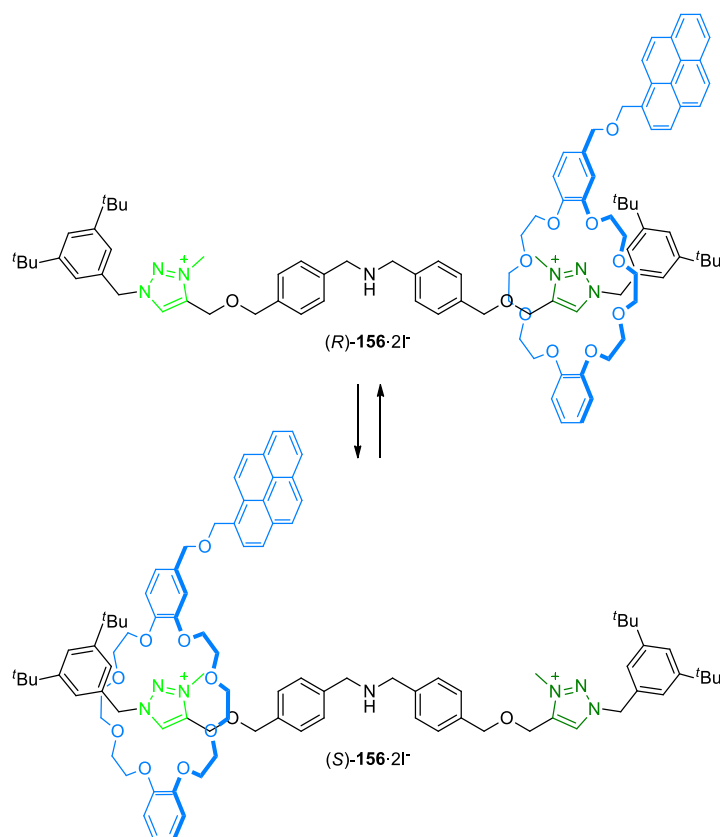
Regarding co-conformational stereogenic units, they can be divided in two categories: co-conformational covalent point or planar chiral units. Applied to rotaxanes, the latter consists in having a [3]rotaxane containing a symmetrical axle and two non-symmetrical macrocycles, affording a pair of

³¹⁵ S. Hoekman, M. O. Kitching, D. A. Leigh, M. Papmeyer, D. Roke, *J. Am. Chem. Soc.* **2015**, *137*, 7656-7659.

³¹⁶ C. Yamamoto, Y. Okamoto, T. Schmidt, R. Jäger, F. Vögtle, *J. Am. Chem. Soc.* **1997**, *119*, 10547-10548.

³¹⁷ a) Y. Makita, N. Kihara, N. Nakakoji, T. Takata, S. Inagaki, C. Yamamoto, Y. Okamoto, *Chem. Lett.* **2007**, *36*, 162-163. b) M. A. Jinks, A. de Juan, M. Denis, C. J. Fletcher, M. Galli, E. M. G. Jamieson, F. Modicom, Z. Zhang, S. M. Goldup, *Angew. Chem. Int. Ed.* **2018**, *57*, 14806-14810. c) C. Tian, S. D. P. Fielden, B. Pérez-Saavedra, I. J. Vitorica-Yrezabal, D. A. Leigh, *J. Am. Chem. Soc.* **2020**, *142*, 9803-9808.

enantiomers (*R,R*), (*S,S*) and a meso compound (*R,S*). This property of chiral rotaxanes was reported by Vögtle and co-workers in 1999. Indeed, they were able to separate those diastereoisomers by HPLC.³¹⁸ In addition, it is also possible to form a co-conformational planar chiral [2]rotaxane by combining a symmetrical axle and a non-symmetrical macrocycle. Thus, if the macrocycle is centered in the middle of the molecule, the rotaxane is achiral, nevertheless, if the macrocycle is displaced on either one side or the other of the thread, it becomes chiral. This kind of chirality can be found, for example, in cyclodextrin-based rotaxanes³¹⁹ or in hydrogen bonding-based rotaxanes (Scheme 74).³²⁰



Scheme 74. A co-conformationally mechanically planar chiral [2]rotaxane.³²⁰

Regarding co-conformationally covalent point chiral rotaxanes, they are usually achieved by building a thread owning a prochiral centre which is the desymmetrized. This is achieved transforming one of the enantiotopic substituents, which means in this case inserting a symmetrical macrocycle on one of these substituents. This type of chirality was mainly identified in benzylic amide ring-based [2]rotaxanes (Figure 127).^{248a,321}

³¹⁸ R. Schmieder, G. Hübner, C. Seel, F. Vögtle, *Angew. Chem. Int. Ed.* **1999**, *38*, 3528-3530.

³¹⁹ M. R. Craig, T. D. W. Claridge, M. G. Hutchings, H. L. Anderson, *Chem. Commun.* **1999**, 1537-1538.

³²⁰ S. Corra, C. de Vet, J. Groppi, M. La Rosa, S. Silvi, M. Baroncini, A. Credi, *J. Am. Chem. Soc.* **2019**, *141*, 9129-9133.

³²¹ Y. Cakmak, S. Erbas-Cakmak, D. A. Leigh, *J. Am. Chem. Soc.* **2016**, *138*, 1749-1751.

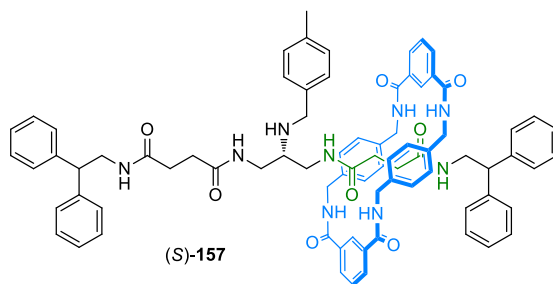


Figure 127. A co-conformationally covalent point chiral [2]rotaxane by Leigh.³²¹

It is worth noting that rotaxanes owning a mechanical planar or a co-conformational mechanical planar or covalent point chirality were employed to design molecular information ratchets,^{248a,b} asymmetric organocatalysts^{167,321} or chiral ligands for enantioselective catalysis.³²²

1.5. Chiroptical properties of rotaxanes

The implementation of chiral elements in rotaxane structures allowed the study of their chiroptical properties. Thus, in 1997, Okamoto and Vögtle achieved the first observation of a ECD signal in a rotaxane architecture employing a mechanically planar chiral [1]rotaxane (Figure 128).³¹⁶ Subsequently, Vögtle and co-workers were able to modify the ECD signal of this type of [1]rotaxanes as a function of the nature or the length of the linker employed.³²³ In addition, other mechanically planar chiral rotaxanes incorporating cyclodextrin,³²⁴ crown ether³²⁵ or pillar[n]arene³²⁶ macrocycles or prepared *via* active metal template^{317b,327} displayed an ECD response. It is also possible to detect a ECD signal from a polymer exhibiting rotaxanes with this chiral property.³²⁸

Furthermore, Vögtle was able to record an ECD spectrum of a simple [2]rotaxane containing two glucose stoppers as chiral covalent stereogenic units.³²⁹ Later, this chiroptical property was also observed in a variety of rotaxanes incorporating other classical covalent chiral elements like an amino

³²² A. W. Heard, S. M. Goldup, *Chem* **2020**, *6*, 994-1006.

³²³ a) C. Reuter, A. Mohry, A. Sobanski, F. Vögtle, *Chem. Eur. J.* **2000**, *6*, 1674-1682. b) C. Reuter, C. Seel, M. Nieger, F. Vögtle, *Helv. Chim. Acta* **2000**, *83*, 630-640.

³²⁴ a) J. W. Park, H. J. Song, *Org. Lett.* **2004**, *6*, 4869-4872. b) Q.-C. Wang, X. Ma, D.-H. Qu, H. Tian, *Chem. Eur. J.* **2006**, *12*, 1088-1096.

³²⁵ N. Kameta, K. Hiratani, Y. Nagawa, *Chem. Commun.* **2004**, 466-467.

³²⁶ T. Ogoshi, D. Yamafuji, T. Aoki, K. Kitajima, T.-A. Yamagishi, Y. Hayashi, S. Kawauchi, *Chem. Eur. J.* **2012**, *18*, 7493-7500.

³²⁷ R. J. Bordoli, S. M. Goldup, *J. Am. Chem. Soc.* **2014**, *136*, 4817-4820.

³²⁸ F. Ishiwari, K. Nakazono, Y. Koyama, T. Takata, *Angew. Chem. Int. Ed.* **2017**, *56*, 14858-14862.

³²⁹ T. Schmidt, R. Schmieder, W. M. Müller, B. Kiupel, F. Vögtle, *Eur. J. Org. Chem.* **1998**, 2003-2007.

acid group,³³⁰ a BINOL group,³³¹ a cyclodextrin ring,³³² a knot³³³ or an oligonucleotide chain.³³⁴ An ECD signal was also identified on polymers owning [2]rotaxanes with a BINOL unit on the macrocycle.³³⁵

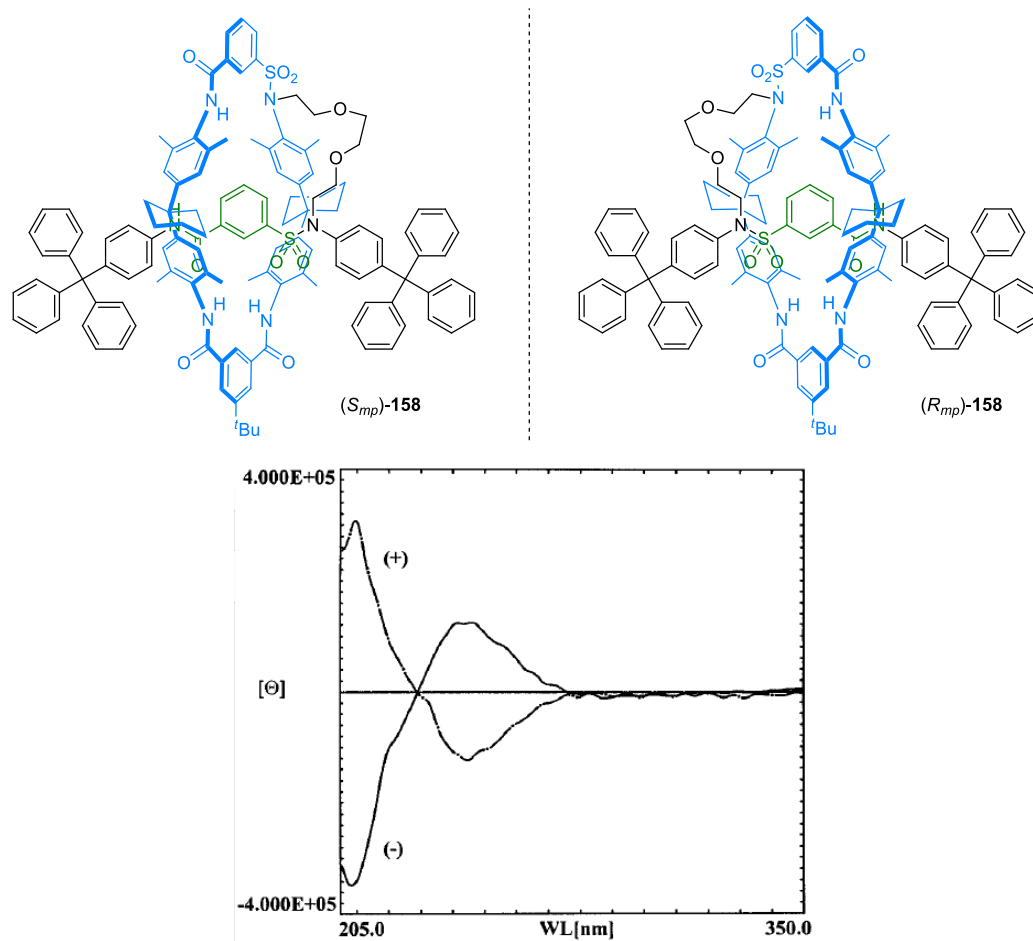


Figure 128. Mechanically planar chiral enantiomers of [1]rotaxane **158** (top) and their ECD spectra (bottom).³¹⁶ Reprinted with permission from ref 316. Copyright 1997 American Chemical Society.

In 1999, Vögtle and co-workers recorded the ECD spectra of co-conformationally mechanically planar rotaxanes after the separation of enantiomers and diastereoisomers by HPLC.³¹⁸ Following this

³³⁰ M. Asakawa, G. Brancato, M. Fantì, D. A. Leigh, T. Shimizu, A. M. Z. Slawin, J. K. Y. Wong, F. Zerbetto, S. Zhang, *J. Am. Chem. Soc.* **2002**, *124*, 2939-2950.

³³¹ a) W. Yang, Y. Li, J. Zhang, N. Chen, S. Chen, H. Liu, Y. Li, *Small* **2012**, *8*, 2602-2607. b) S. Saito, Y. Hirano, Y. Mutoh, T. Kasama, *Chem. Lett.* **2015**, *44*, 1509-1511.

³³² Z. Yan, Q. Huang, W. Liang, X. Yu, D. Zhou, W. Wu, J. J. Chruma, C. Yang, *Org. Lett.* **2017**, *19*, 898-901.

³³³ O. Lukin, T. Kubota, Y. Okamoto, F. Schelhase, A. Yoneva, W. M. Müller, U. Müller, F. Vögtle, *Angew. Chem. Int. Ed.* **2003**, *42*, 4542-4545.

³³⁴ A. Acevedo-Jake, A. T. Ball, M. Galli, M. Kukwikila, M. Denis, D. G. Singleton, A. Tavassoli, S. M. Goldup, *J. Am. Chem. Soc.* **2020**, *142*, 5985-5990.

³³⁵ F. Ishiwari, K.-I. Fukasawa, T. Sato, K. Nakazono, Y. Koyama, T. Takata, *Chem. Eur. J.* **2011**, *17*, 12067-12075.

progress, other rotaxanes including this kind of chirality or co-conformational covalent point chirality generated a preferential absorption of circularly polarized light (Figure 129).^{321,336}

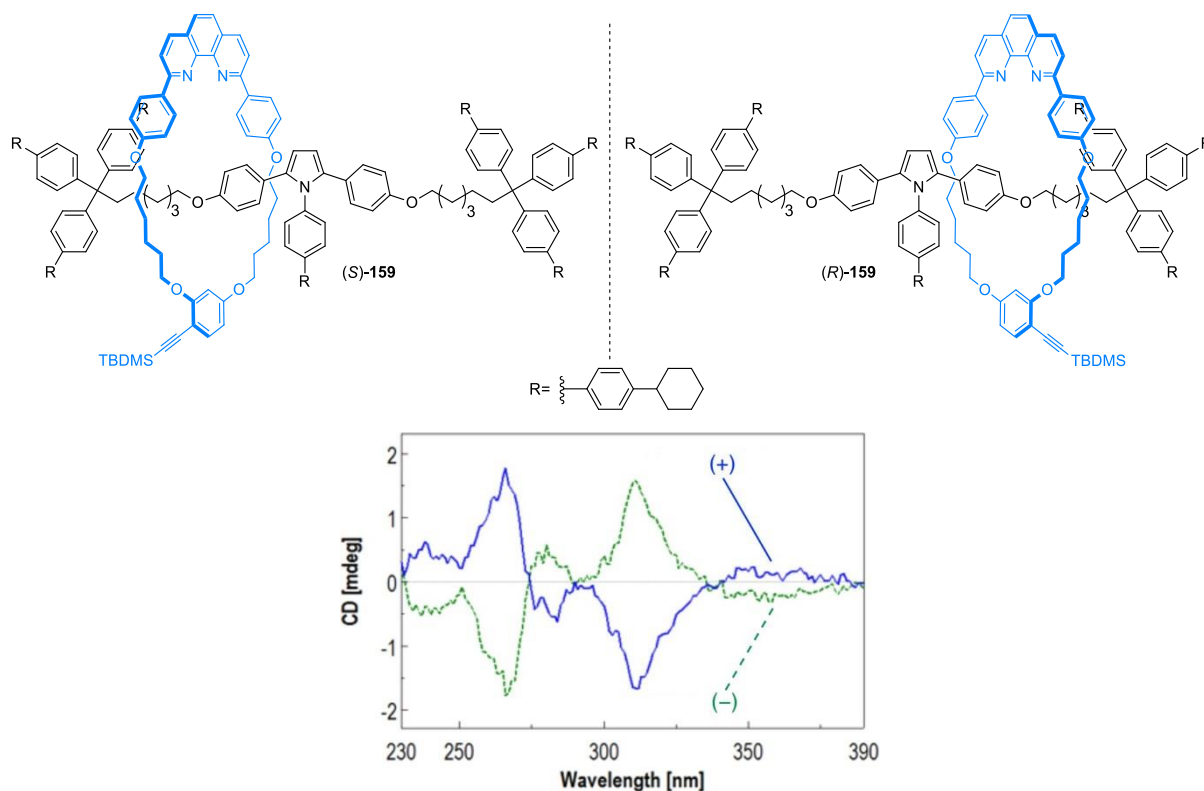


Figure 129. Co-conformationally mechanically planar enantiomers of [2]rotaxane **159** reported by Saito (top) and their ECD spectra (bottom).^{336b} Reprinted with permission from ref 336b. Copyright 2017 American Chemical Society.

Although it is quite frequent to find MIMs displaying CD properties, MIMs exhibiting CPL emission characteristics are very rare. Indeed, the CPL response has been described only for two doubly-threaded γ -cyclodextrin-based [4]rotaxanes, reported by Inouye and co-workers. The CPL signal emanates from the excimers constituted by pyrene or perylene moieties, present on each of the axles, formed inside the cavity of two γ -cyclodextrin macrocycles. Thus, these rotaxanes containing both chiral covalent and co-conformational planar chiral stereogenic elements show quite high $|g_{lum}|$ values: 1.5×10^{-2} at 480 nm for (D,D,R,R)-**160a** and 2.1×10^{-2} at 573 nm for (D,D,R,R)-**160b** respectively (Figure 130).³³⁷ As illustrated here, the study of the CPL emission of catenanes or rotaxanes remains

³³⁶ a) M. R. Kishan, A. Parham, F. Schelhase, A. Yoneva, G. Silva, X. Chen, Y. Okamoto, F. Vögtle, *Angew. Chem. Int. Ed.* **2006**, *45*, 7296-7299. b) Y. Mochizuki, K. Ikeyatsu, Y. Mutoh, S. Hosoya, S. Saito, *Org. Lett.* **2017**, *19*, 4347-4350.

³³⁷ a) M. Inouye, K. Hayashi, Y. Yonenaga, T. Itou, K. Fujimoto, T.-A. Uchida, M. Iwamura, K. Nozaki, *Angew. Chem., Int. Ed.* **2014**, *53*, 14392-14396. b) K. Hayashi, Y. Miyaoka, Y. Ohishi, T.-A. Uchida, M. Iwamura, K. Nozaki, M. Inouye, *Chem. Eur. J.* **2018**, *24*, 14613-14616.

minimally explored. At this early stage, it becomes essential to design other systems and investigate their properties.

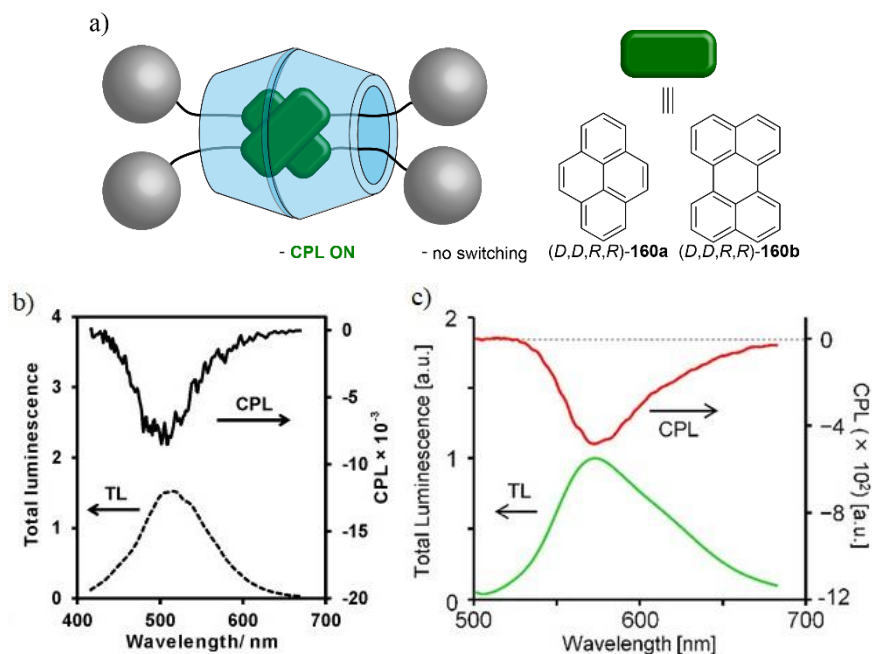


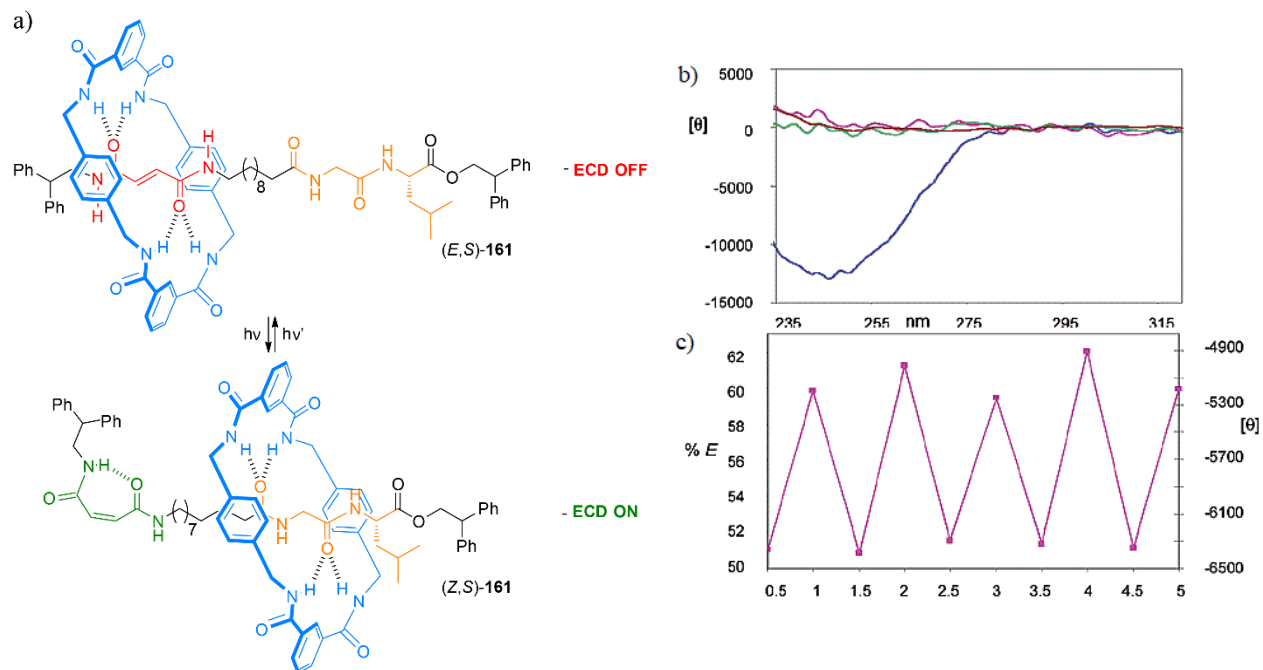
Figure 130. a) Graphical representation of γ -cyclodextrin-based doubly-threaded [4]rotaxanes reported by Inouye.³³⁷ b) CPL (black line) and fluorescence (black dashed line) spectra of (D,D,R,R)-**160a** in H₂O with NH₃ at ca. pH 9.5 at 298K.^{337a} Reprinted with permission from ref 337a. Copyright 2014 John Wiley and Sons. c) CPL (red line) and fluorescence (green line) spectra of (D,D,R,R)-**160b** in H₂O with NH₃ at ca. pH 9.5 at 298K.^{337b} Reprinted with permission from ref 337b. Copyright 2018 John Wiley and Sons.

The switching of chiroptical properties in MIMs has been clearly underdeveloped so far, as only few examples of ECD switching have been reported. In 2002, Leigh and Zerbetto created a series of benzylic amide-based [2]rotaxanes bearing amino acids and were able to modulate the ECD response of the rotaxane depending on the solvent.³³⁰ One year later, Leigh and co-workers designed a bistable photo-switch with a fumaramide/glycyl-L-leucine system. By irradiating the rotaxane at different wavelengths, they were capable to turn “on” or “off” the ECD signal as result of the control of the position of the macrocycle on the thread, since the ECD response was only observed when the macrocycle was on a chiral glycyl-L-leucine station. Moreover, they performed the switching of the ECD signal of this rotaxane for five complete cycles (Figure 131).³³⁸ In addition, the ECD response of a polymer owning pendant bistable rotaxanes can be modulated and controlled by distinct additions of acid and base.³³⁹ Therefore, it is worth to emphasize that there is still a very limited number of ECD

³³⁸ G. Bottari, D. A. Leigh, E. M. Pérez, *J. Am. Chem. Soc.* **2003**, *125*, 13360-13361.

³³⁹ a) F. Ishiwari, K. Nakazono, Y. Koyama, T. Takata, *Chem. Commun.* **2011**, *47*, 11739-11741. b) S. Suzuki, F. Ishiwari, K. Nakazono, T. Takata, *Chem. Commun.* **2012**, *48*, 6478-6480.

switches based on a rotaxane architecture. Beyond that, to the best of our knowledge, no examples of the modulation of the CPL emission neither in a catenane nor in a rotaxane have been reported.



2. Objectives

In this context, we propose to develop an "ON/OFF" CPL switching system based on a rotaxane architecture, a type of structure well-known to afford efficient shuttles and switches. Thus, we aim to modulate the chiroptical properties, especially the CPL, of these interlocked molecules by the control of the position of an emissive macrocycle between a chiral and achiral bindings sites on the thread through the application of external stimuli (Figure 132). In addition, we believe that the luminescence of the fluorophore could be maintained in both states.

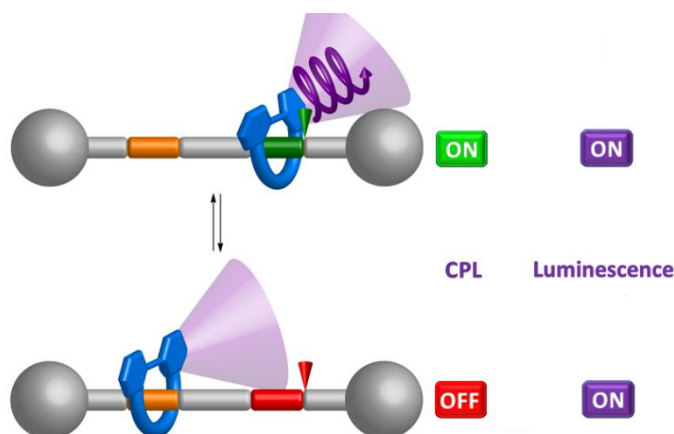


Figure 132. Graphical representation of the proposed "ON/OFF" CPL switching system based on a rotaxane structure.

The design of the target switch is based on a [2]rotaxane composed by a crown ether macrocycle bearing a 2,2'-bipyrene group, which is the fluorophore, and an axle including a triazolium salt and a chiral ammonium salt derived from an enantiopure amino acid (L- or D-phenylalanine) as switching system (Figure 133). The thread structure is similar to that generated for an asymmetric switchable catalyst.^{165a}

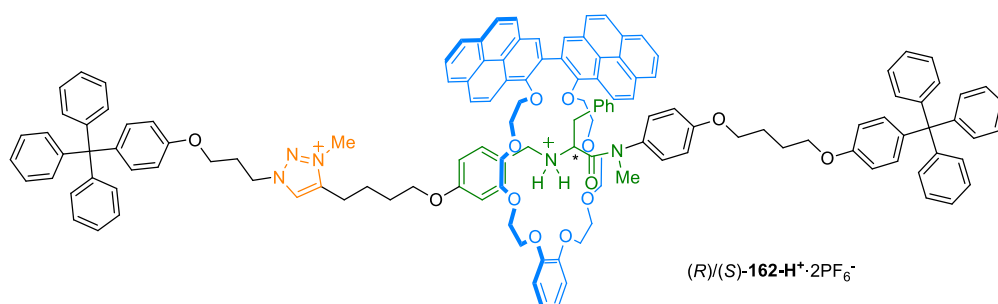


Figure 133. Proposed structure of the CPL switch.

The proposed CPL emission property of this molecular machine relies on the chiral information transfer from the chiral secondary amine unit of the axle to the emissive 2,2'-bipyrene macrocycle. We hypothesize that the chirality transfer would induce a preferential spatial arrangement of the

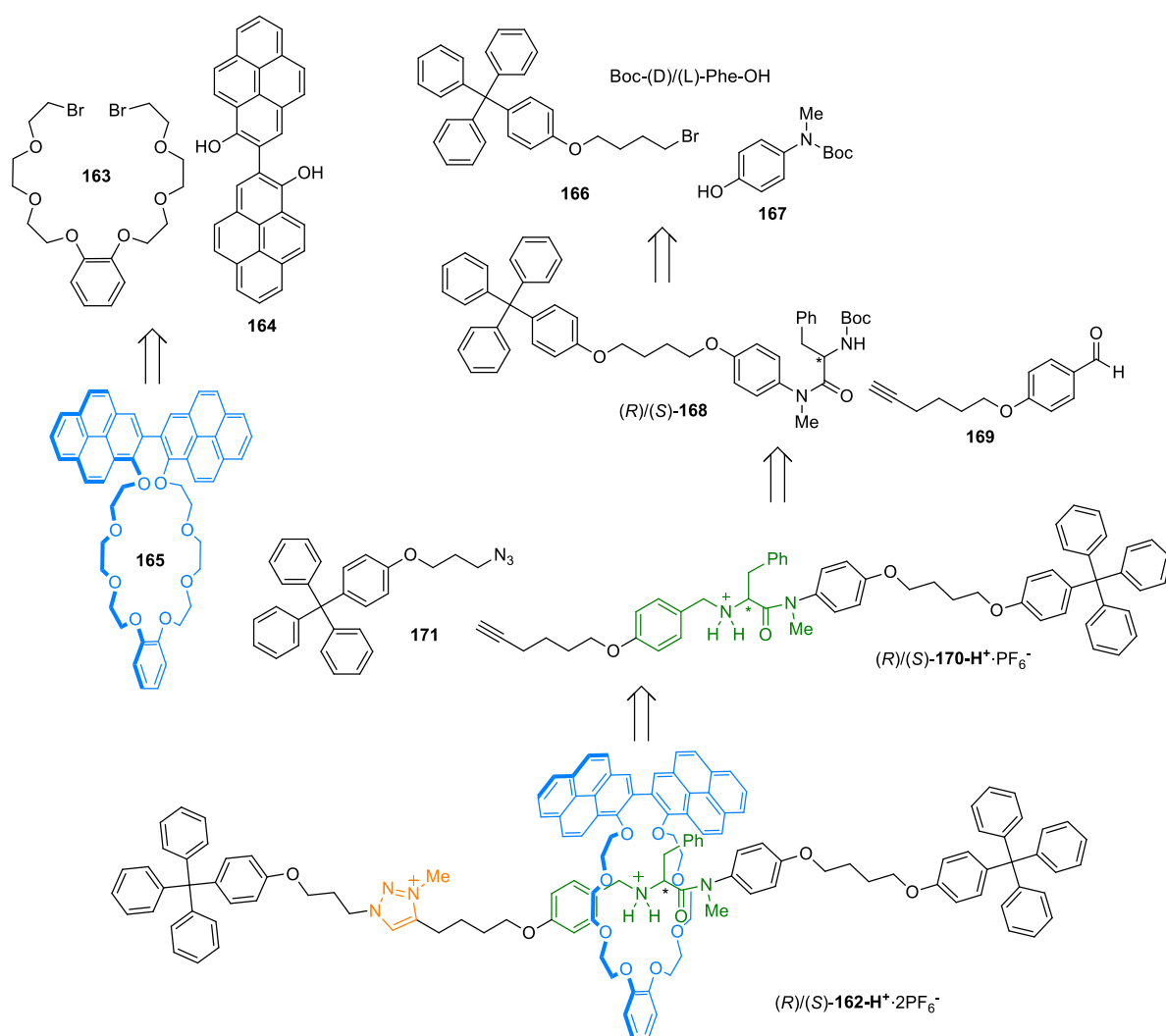
luminescent wheel, especially of its two pyrene rings, due to its proximity to the chiral source of the molecule: the amino acid. If this transmission of chirality occurs, then a CPL signal should be detected. It is important to highlight that such chirality transfer has already been noticed in a similar system. Indeed, in pseudorotaxanes formed by a biphenyl containing crown ether macrocycle and a chiral ammonium salt, a transmission of chirality was monitored by ECD spectroscopy.³⁴⁰

³⁴⁰ S. Kuwahara, R. Chamura, S. Tsuchiya, M. Ikeda, Y. Habata, *Chem. Commun.* **2013**, 49, 2186-2188.

3. Results and discussion

3.1. Synthesis and characterization

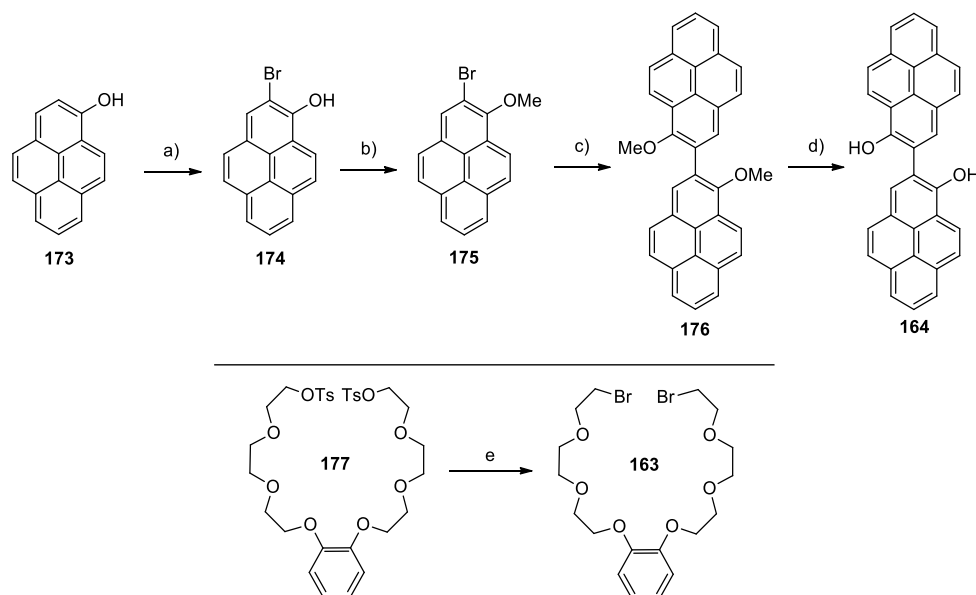
With the aim of synthesizing the target rotaxane $(R)/(S)\text{-162-H}^+\cdot 2\text{PF}_6^-$, we could proceed through a final CuAAC reaction between azide stopper **171** and mono-stoppered alkyne $(R)/(S)\text{-170-H}^+\cdot \text{PF}_6^-$ in the presence of benzo-1,1'-bipyreno-26-crown-8 (**165**) followed by methylation of the resulting triazole. The crown ether macrocycle could be constructed by a Williamson reaction between dibromide functionalized cathecol derivative **163** and a 2,2'-bipyrene derivative **164** bearing two phenol moieties. Alkyne $(R)/(S)\text{-170-H}^+\cdot \text{PF}_6^-$ could be prepared from the reductive amination between aldehyde **169** and chiral amine $(R)/(S)\text{-168}$. This could be synthesized from stopper **166**, phenol **167** and an enantiopure Boc-protected phenylalanine (Scheme 75).



Scheme 75. Retrosynthetic plan to synthesize rotaxanes $(R)/(S)\text{-162-H}^+\cdot 2\text{PF}_6^-$.

3.1.1 Synthesis of the macrocycle

To prepare target macrocycle **165**, we initially treated phenol **173** with Br₂ in the presence of ^tBuNH₂ to yield 2-bromo-1-hydroxypyrene (**174**) in 67% yield.³⁴¹ The latter was protected as methyl ether using MeI to give **175** in 83% yield (Scheme 76).



Scheme 76. Synthesis of macrocycle precursors **163** and **164**. Reagents and conditions: a) Br₂, ^tBuNH₂, toluene, -78 °C to r.t., 6 h, 67%. b) MeI, K₂CO₃, acetone, 0 °C to reflux, 18 h, 83%. c) ^tBuLi, Pd(dba)₂, XPhos, toluene, r.t., 20 h, 79%. d) BF₃·SMe₂, CH₂Cl₂, r.t., 6 h, 26%. e) LiBr, acetone, reflux, O/N, 92%.

The next reaction was the key step of our synthetic route to generate the 2,2'-bipyrene unit. First, we wanted to generate an organometallic derivative from compound **175** to enable a cross-coupling reaction. Thus, attempts to create the corresponding boronic ester or acid, a Grignard reagent, an organotin or a silane derivative in order to try the planned cross-coupling were unsuccessful as in all cases **175** was reduced to afford 1-methoxypyrene. Subsequently, we tested a nickel-catalyzed homocoupling of aryl bromides in the presence of Zn or Mn but we found that this strategy either reduced **175** to 1-methoxypyrene or the starting material remained intact depending on the procedure employed. After these failures, several other less usual approaches were explored, some of which resulted not reproducible. However, an attractive strategy caught our attention. Indeed, a coupling developed by Feringa, consisting on a Pd-catalyzed cross-coupling of organolithium and aryl halides,³⁴² allows the reaction of sterically hindered aryllithium and aryl halides³⁴³ and also the dimerization of

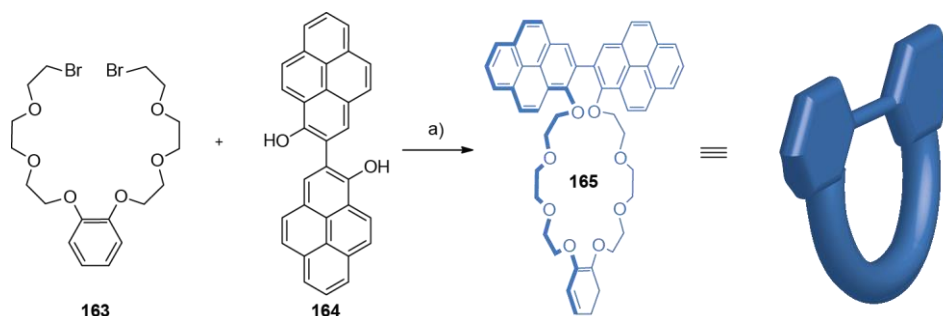
³⁴¹ Compound **174** was prepared according to Koreeda's procedure: M. Koreeda, R. Gopalaswamy, *J. Am. Chem. Soc.* **1995**, *117*, 10595-10596.

³⁴² M. Giannerini, M. Fañanás-Mastral, B. L. Feringa, *Nat. Chem.* **2013**, *5*, 667-672.

³⁴³ a) M. Giannerini, V. Hornillos, C. Vila, M. Fañanás-Mastral, B. L. Feringa, *Angew. Chem. Int. Ed.* **2013**, *52*, 13329-13333. b) C. Vila, V. Hornillos, M. Giannerini, M. Fañanás-Mastral, B. L. Feringa, *Chem. Eur. J.* **2014**, *20*, 13078-

aryl bromide derivatives mediated by $t\text{BuLi}$ in good yields, even when they are substituted in *ortho* position.³⁴⁴ Thus, by slightly modifying the $t\text{BuLi}$ -mediated dimerization reaction employing $\text{Pd}(\text{dba})_2$ as catalyst with XPhos as ligand, the target 2,2'-bipyrene derivative **176** was generated in good yield (79%) in a reproducible manner. The last step was the deprotection of the methyl ether protective groups using $\text{BF}_3\cdot\text{SMe}_2$ to prepare the building block **164**, one of the reagent for macrocyclization reaction (Scheme 76). On the other hand, the catechol derived ditosylate **177** was treated with LiBr in refluxing acetone to afford dibromide derivative **163** in good yield (92%) (Scheme 76).

Finally, the macrocyclization reaction between **163** and **164** was achieved in dioxane at 0.6 mM employing KPF_6 as template and $t\text{BuOK}$ as base to deprotonate the phenol, affording macrocycle **165** in a reasonable 34% yield (Scheme 77). It is important to emphasize that this Williamson ether reaction did not proceed with potassium, nor cesium carbonate as base. Moreover, the use $t\text{BuOK}$ in refluxing THF was not successful either. Therefore, dioxane was chosen because of its higher boiling point.



Scheme 77. Synthesis of benzo-1,1'-bipyreno-26-crown-8 macrocycle (**165**). Reagents and conditions: a) $t\text{BuOK}$, KPF_6 , $n\text{Bu}_4\text{NI}$, 0.6 mM, dioxane, r.t. to reflux, 24 h, 34%.

This crown ether macrocycle easily formed a complex with potassium cations to give $\mathbf{165}\subset\text{K}^+$, which allowed the growth of single crystals. Their study by X-ray diffraction confirmed the structure of the macrocycle,³⁴⁵ which displayed the 2,2'-bipyrene moiety with both pyrene units twisted with a torsion angle of 59.7° . The formation of the complex with a potassium ion promoted the adoption of a twisted conformation around it that allows the coordination of the O atoms from the crown ether to K^+ with K–O distances within 2.45–2.61 Å (Figure 134). Furthermore, the solid-state structure showed two possible conformational enantiomers without any preferential conformation due to the absence of a chiral environment.

13083. c) L. M. Castelló, V. Hornillos, C. Vila, M. Giannerini, M. Fañanás-Mastral, B. L. Feringa, *Org. Lett.* **2015**, *17*, 62-65.

³⁴⁴ J. Buter, D. Heijnen, C. Vila, V. Hornillos, E. Otten, M. Giannerini, A. J. Minnaard, B. L. Feringa, *Angew. Chem. Int. Ed.* **2016**, *55*, 3620-3624.

³⁴⁵ The refinement of the X-ray diffraction structure of $\mathbf{165}\subset\text{K}^+$ was performed by Dr V. Blanco.

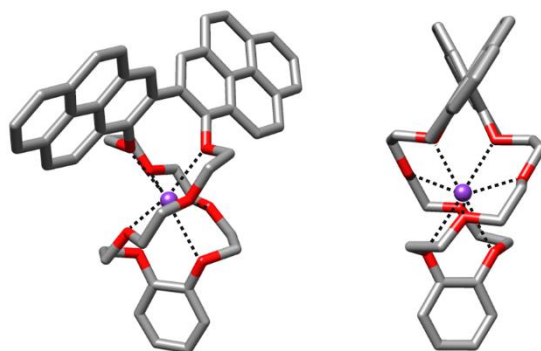
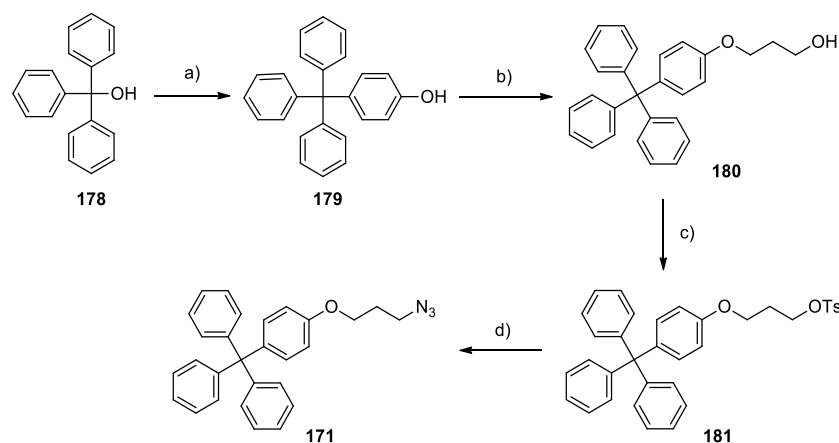


Figure 134. Front (left) and side (right) views of the stick representation of the X-ray diffraction structure of $165\cdot K^+$. The coordination bonds between K and the crown ether O atoms are shown with dashed lines. Hydrogen atoms and the PF_6^- counterion have been omitted for clarity. Only one of the isomers is represented. Color coding: C, grey; O, red; K, purple.

3.1.2. Synthesis of the thread precursors

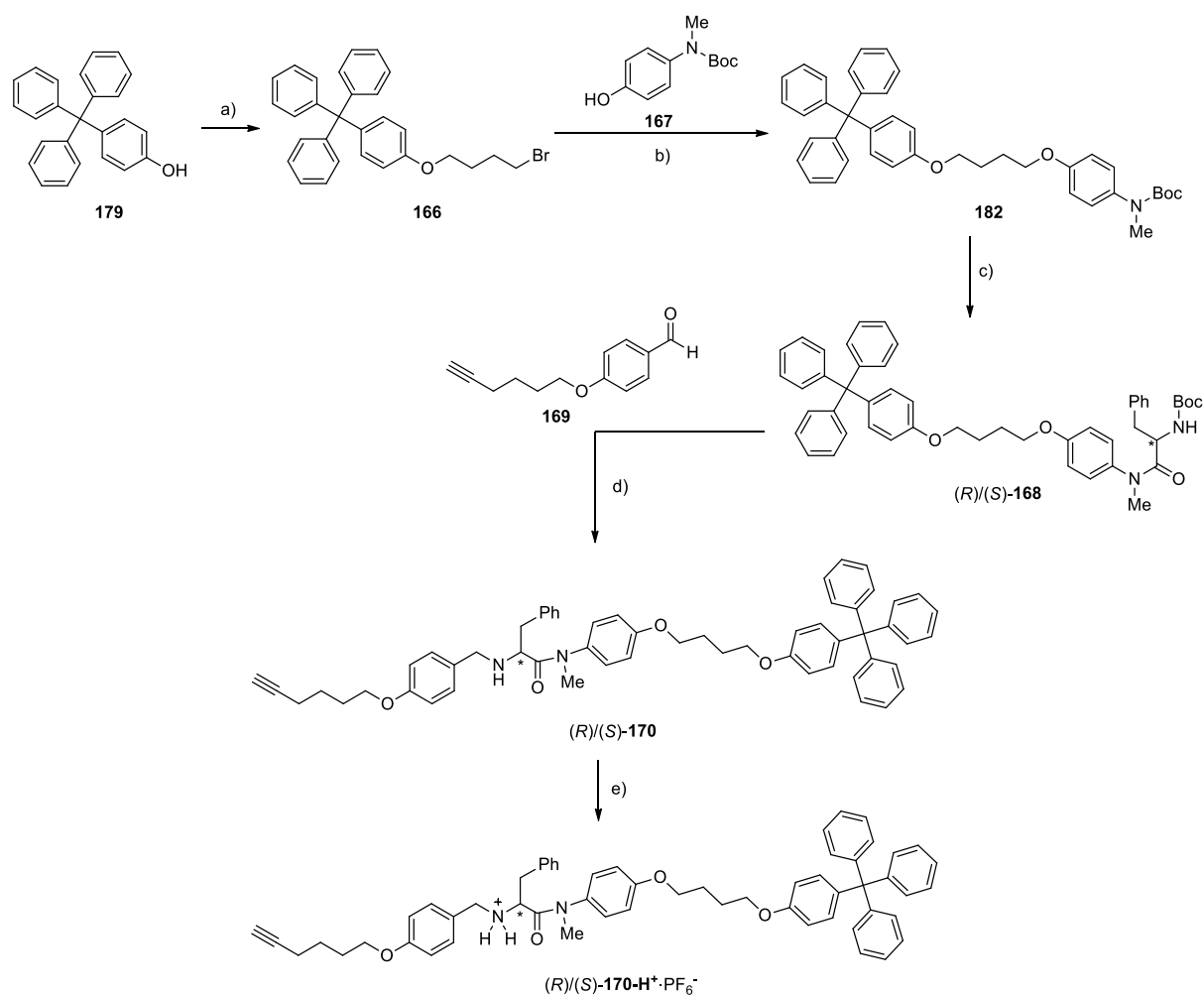
To obtain the target rotaxane, we selected a capping strategy. Thus, we tackled the synthesis of azide stopper **171**. Initially, triphenylcarbinol (**178**) was treated on a large scale (around 50 g) with phenol in acidic medium to give 4-tritylphenol (**179**) in 60% yield. Subsequently, **179** underwent a Williamson ether reaction with 3-bromo-1-propanol to afford derivative **180** in an excellent yield (98%). Its alcohol group was then transformed into a tosylate leaving group to give intermediate **181** in good yield (87%). Finally, the stopper owning a tosylate moiety was reacted with NaN_3 to yield the desired azide stopper **171** in 73% yield (Scheme 78).



Scheme 78. Synthesis of stopper **171**. Reagents and conditions: a) Phenol, $HCl_{(aq)}$ (37%), 160 °C, 6 h, 60%. b) K_2CO_3 , 3-Bromo-1-propanol, acetone, reflux, 24 h, 98%. c) TsCl, Et_3N , DMAP_(cat.), CH_2Cl_2 , r.t., O/N, 87%; d) NaN_3 , DMF, 70 °C, 15 h, 73%.

Regarding the synthesis of the monostoppered chiral ammonium salt (*R*)/(*S*)-**170-H⁺**· PF_6^- , we followed synthetic route similar to that of one of the precursors of the switchable catalysts developed by Leigh and co-workers.^{165a} It started with a Williamson ether reaction between 4-tritylphenol (**179**) and 1,4-dibromobutane to obtain alkyl bromide derivative **166** in moderate yield (54%). Treatment with **167** in

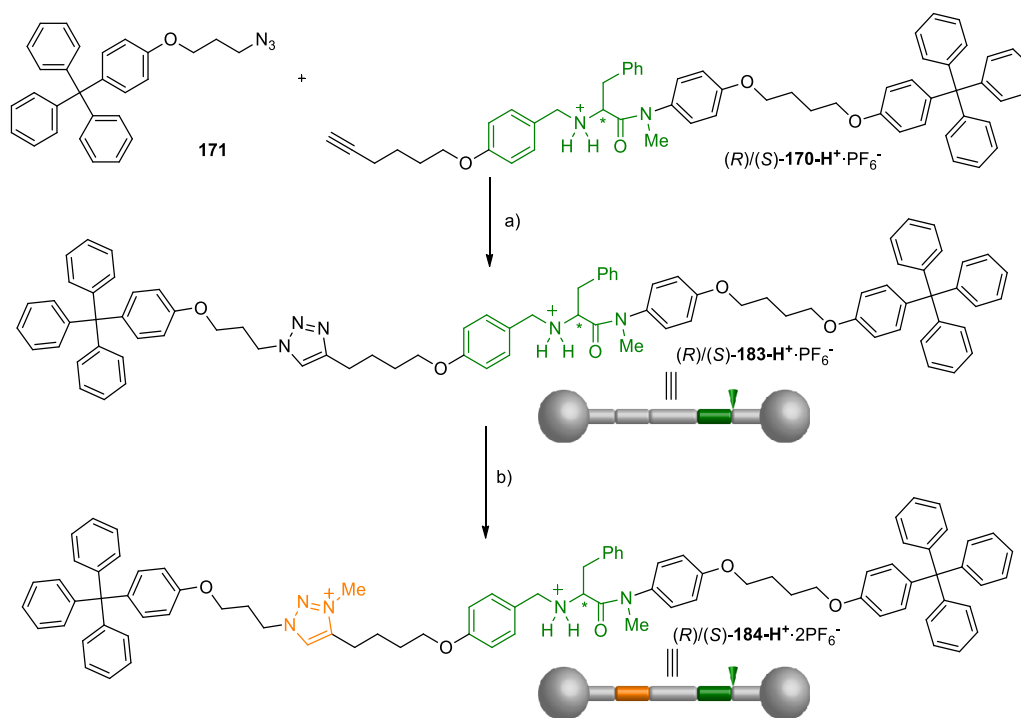
the presence of Cs_2CO_3 at 70°C gave intermediate **182** having a Boc-protected secondary amine. This was deprotected using trifluoroacetic acid to give the free amine that underwent a peptide coupling with enantiopure Boc-D/L-phenylalanine to afford (*R*)/(*S*)-**168** respectively in good yield (60-66%). Subsequently, the protecting group of the amino acid was enabling the reductive amination with aldehyde **169** to yield compound (*R*)/(*S*)-**170**, featuring a chiral secondary amine and a terminal alkyne group, in 32-34% yield. Finally, protonation of the chiral secondary amine and counterion exchange allowed us to achieve the synthesis of the chiral axle precursor (*R*)/(*S*)-**170-H⁺·PF₆⁻** in excellent yield (91-98%) (Scheme 79).



Scheme 79. Synthesis of compounds (*R*)/(*S*)-**170-H⁺·PF₆⁻**. Reagents and conditions: a) 1,4-Dibromobutane, K_2CO_3 , CH_3CN , 75°C , O/N, 54%. b) Cs_2CO_3 , DMF, 70°C , O/N, 59%. c) 1. $\text{CF}_3\text{CO}_2\text{H}$, CH_2Cl_2 , r.t., 4 h; 2. Boc-D-phenylalanine (or Boc-L-phenylalanine), HOBt, EDCl, DIPEA, CH_2Cl_2 , 0°C to r.t., 19 h, 60% (for *R*)-**168**) and 66% (for *S*)-**168**). d) 1. $\text{CF}_3\text{CO}_2\text{H}$, CH_2Cl_2 , r.t., 4 h; 2. **169**, Et_3N , MeOH, r.t., 24 h; 3. NaBH_4 , THF, r.t., 18 h, 32% (for *R*)-**170**) and 34% (for *S*)-**170**). e) 1. HCl (1.0 M in Et_2O), CH_2Cl_2 , r.t., 8 h; 2. KPF_6 , CH_2Cl_2 /acetone/ H_2O , r.t., 16 h, 98% (for *R*)-**170-H⁺·PF₆⁻**) and 91% (for *S*)-**170-H⁺·PF₆⁻**).

3.1.3. Synthesis of threads and rotaxanes

With every compound in hand, we first synthesized the free threads, as usual. In this case, using the CuAAC reaction between azide **171** and alkyne (*R*)/(*S*)-**170-H⁺**·PF₆⁻, we obtained free axes (*R*)/(*S*)-**183-H⁺**·PF₆⁻ in good yield (59-95%). Subsequently, the triazole ring was methylated in neat MeI and the counterion changed to PF₆⁻ in order to obtain the target threads (*R*)/(*S*)-**184-H⁺**·2PF₆⁻ in good yield (58-98%) (Scheme 80).

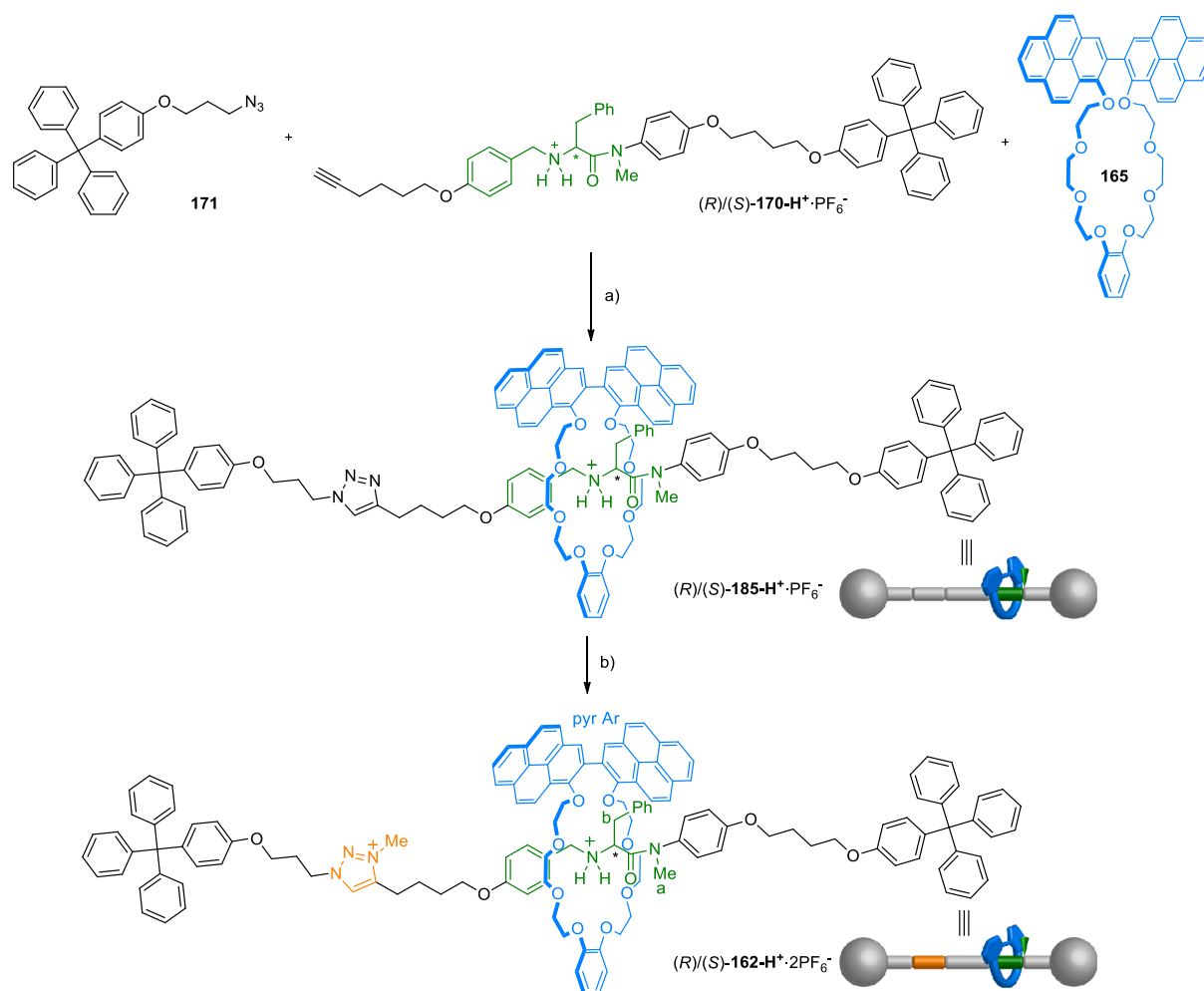


Scheme 80. Synthesis of free threads (*R*)/(*S*)-**184-H⁺**·2PF₆⁻. Reagents and conditions: a) Cu(CH₃CN)₄PF₆, TBTA, CH₂Cl₂, r.t., 48 h, 95% (for *R*)-**183-H⁺**·PF₆⁻) and 59% (for *S*)-**183-H⁺**·PF₆⁻). b) 1. MeI, r.t., 4 d; 2. KPF₆, CH₂Cl₂/acetone/H₂O, r.t., 18 h, 58% (for *R*)-**184-H⁺**·2PF₆⁻) and 98% (for *S*)-**184-H⁺**·2PF₆⁻).

For the synthesis of the chiral rotaxanes, the CuAAC reaction between the monostoppered alkyne-functionalized chiral ammonium salts ((*R*)/(*S*)-**170-H⁺**·PF₆⁻) and azide stopper **171** was performed in the presence of the benzo-1,1'-bipyreno-26-crown-8 macrocycle (**165**) and afforded enantiopure rotaxanes (*R*)/(*S*)-**185-H⁺**·PF₆⁻ in moderate yields (19-35%). Following this achievement, the rotaxanes were treated with neat MeI to form the triazolium salts. The counterion was exchanged to PF₆⁻ to generate the desired rotaxanes (*R*)/(*S*)-**162-H⁺**·2PF₆⁻ in good yields (55-68%) (Scheme 81).

These rotaxanes were characterized by means of NMR spectroscopy. Both rotaxanes (*R*)/(*S*)-**162-H⁺**·2PF₆⁻ and (*R*)/(*S*)-**185-H⁺**·PF₆⁻ display very complex patterns both in the aliphatic and aromatic regions with a high number of signals that are sometimes broad or overlap. This phenomenon can be related to the presence of chirality in the structure of the rotaxanes which induces a loss of symmetry. This increasing complexity of the NMR spectra of chiral MIMs is a known drawback that can exist in

such architectures.³⁰⁷ Nevertheless, the signal of the *N*-methyl group is a characteristic signal that can be identified, by HSQC NMR, and followed easily in the ¹H NMR of both rotaxanes (Figures 135 and 136).



Scheme 81. Synthesis of chiral rotaxanes $(R)/(S)\text{-162-H}^+\cdot 2\text{PF}_6^-$: Reagents and conditions: a) $\text{Cu}(\text{CH}_3\text{CN})_4\text{PF}_6$, TBTA, CH_2Cl_2 , r.t., 3 d, 35% (for $(R)\text{-185-H}^+\cdot\text{PF}_6^-$) and 19% (for $(S)\text{-185-H}^+\cdot\text{PF}_6^-$). b) 1. MeI, r.t., 4 d; 2. KPF_6 , $\text{CH}_2\text{Cl}_2/\text{acetone}/\text{H}_2\text{O}$, r.t., 5 h, 68% (for $(R)\text{-162-H}^+\cdot 2\text{PF}_6^-$) and 55% (for $(S)\text{-162-H}^+\cdot 2\text{PF}_6^-$).

Indeed, the latter undergoes a significant upfield shift ($\Delta\delta_{\text{Ha}} = -0.90$ ppm) in $\text{185-H}^+\cdot\text{PF}_6^-$ with respect to the free thread (Figure 135) which is due to shielding induced by the presence of the macrocycle encircling the ammonium salt. Moreover, the DOSY NMR of this rotaxane shows that every component diffuses as a whole (Figure 137a), which is consistent with the interlocked nature of the compound. Finally, the HMRS spectrum of the product exhibits a peak ($m/z = 2038.9519$) whose isotopic distribution and exact mass correspond perfectly to the calculated $[\text{M-PF}_6^-]^+$ ion which confirms the existence of the desired MIM.

For rotaxane $\text{162-H}^+\cdot 2\text{PF}_6^-$, the *N*-methyl hydrogens suffer a similar shielding effect ($\Delta\delta_{\text{Ha}} = -0.87$ ppm) when compared to the thread ones (Figure 135). Thus, this characteristic signal demonstrates that the

crowns ether wheel remains on the ammonium salt station. Furthermore, the DOSY NMR experiment displays again this time a unique diffusion coefficient for all signals which agrees with the presence of a rotaxane architecture. Finally, HRMS undoubtedly confirmed the presence of the target compound since three main peaks in the spectra ($m/z = 1026.9816$, 2052.9675 , and 2198.9368), which correspond to the $[M-2PF_6^-]^{2+}$, $[M-H^+-2PF_6^-]^+$, and $[M-PF_6^-]^+$ ions, were identified and their exact masses and isotopic distributions match nicely the theoretical ones (Figure 137b).

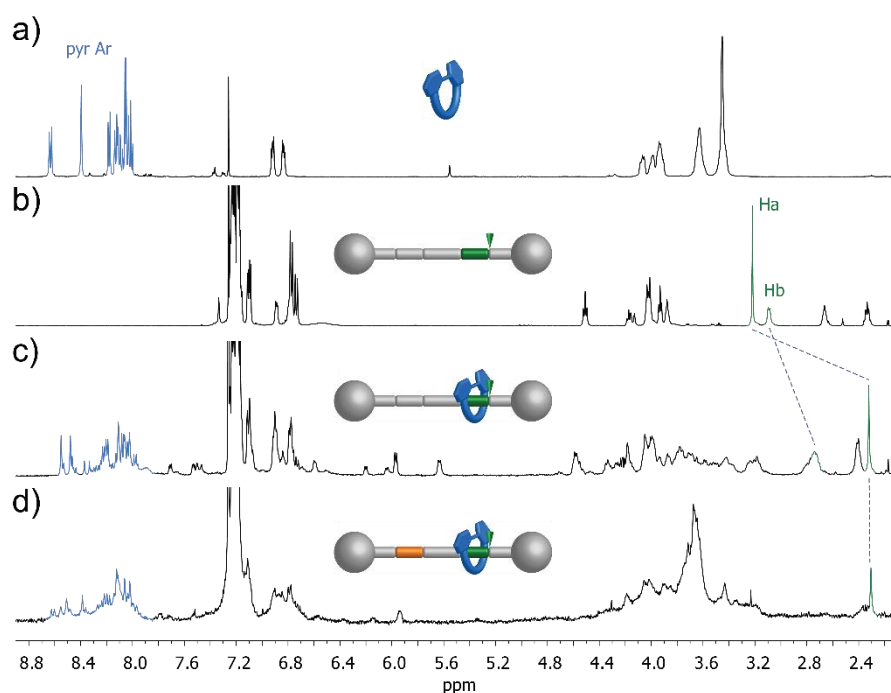


Figure 135. Partial ^1H NMR spectra (CDCl₃) of: a) Macrocycle **165** (500 MHz). b) Thread **183-H⁺**·PF₆⁻ (500 MHz). c) Rotaxane **185-H⁺**·PF₆⁻ (500 MHz). d) Rotaxane **162-H⁺**·2PF₆⁻ (400 MHz). Lettering coding is defined in Scheme 81.

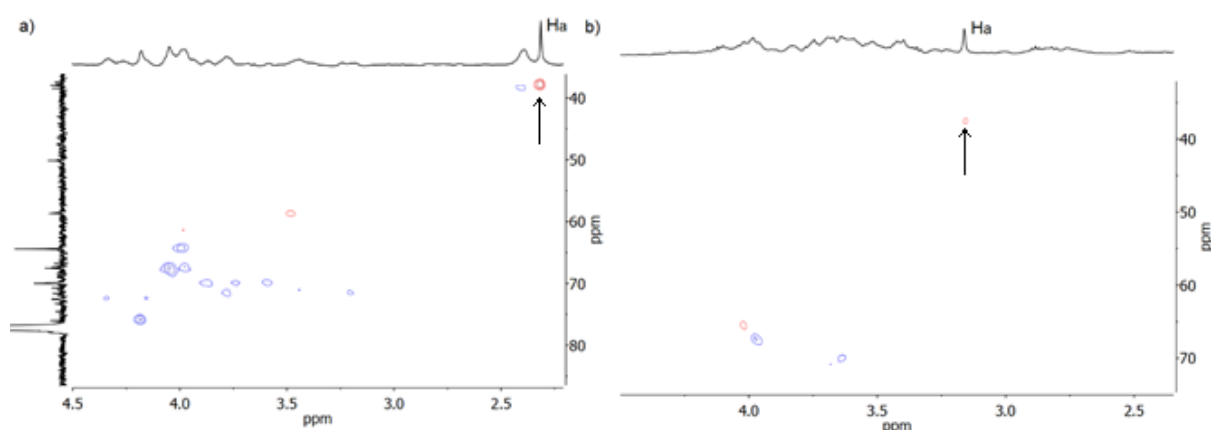


Figure 136. Partial HSQC NMR (500 MHz and 126 MHz, CDCl₃) spectra of: a) Rotaxane **185-H⁺**·PF₆⁻ showing a signal at 2.3 ppm in the CH/CH₃ phase, supporting its assignment as the *N*-methyl amide group Ha. b) Rotaxane **162**·PF₆⁻ showing a signal at 3.15 ppm in the CH/CH₃ phase, supporting its assignment as the *N*-methyl amide group Ha. Lettering coding is defined in Scheme 81.

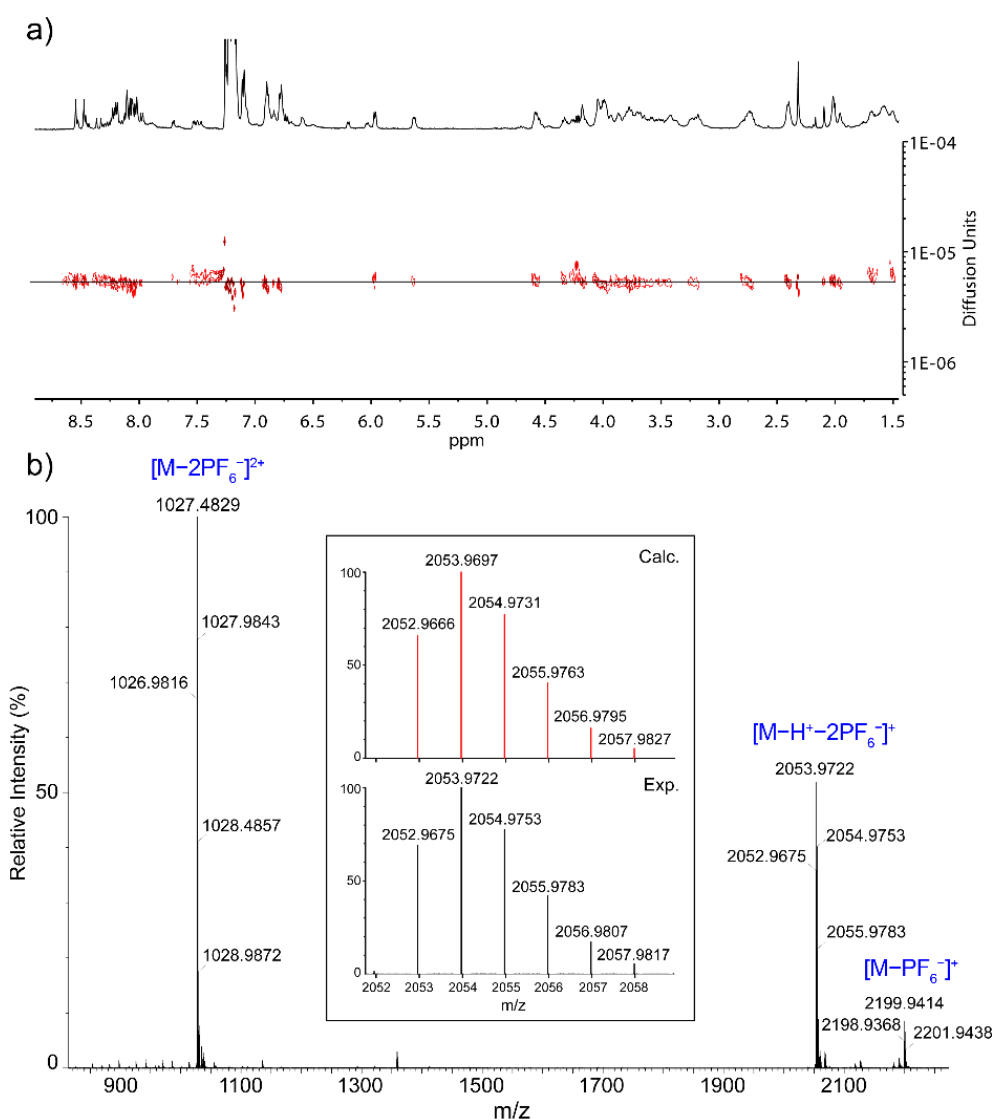


Figure 137. a) DOSY NMR spectra (500 MHz, CDCl₃) of rotaxane **185-H⁺·PF₆⁻**. b) HRMS (ESI⁺-TOF) spectrum of rotaxane **162-H⁺·2PF₆⁻**. Inset: Experimental (bottom) and calculated (top) isotopic distributions for the peak corresponding to the ion [M-H⁺-2PF₆⁻]⁺.

In order to fully demonstrate the purity of these rotaxanes despite their complex ¹H NMR spectra, a HPLC analysis was performed. Employing the same separation method, the chromatograms of every analysed product displayed a unique peak at different retention time. Thus, it has been proved that there is no contamination of thread, macrocycle or stopper on the rotaxane fractions (Figure 138).

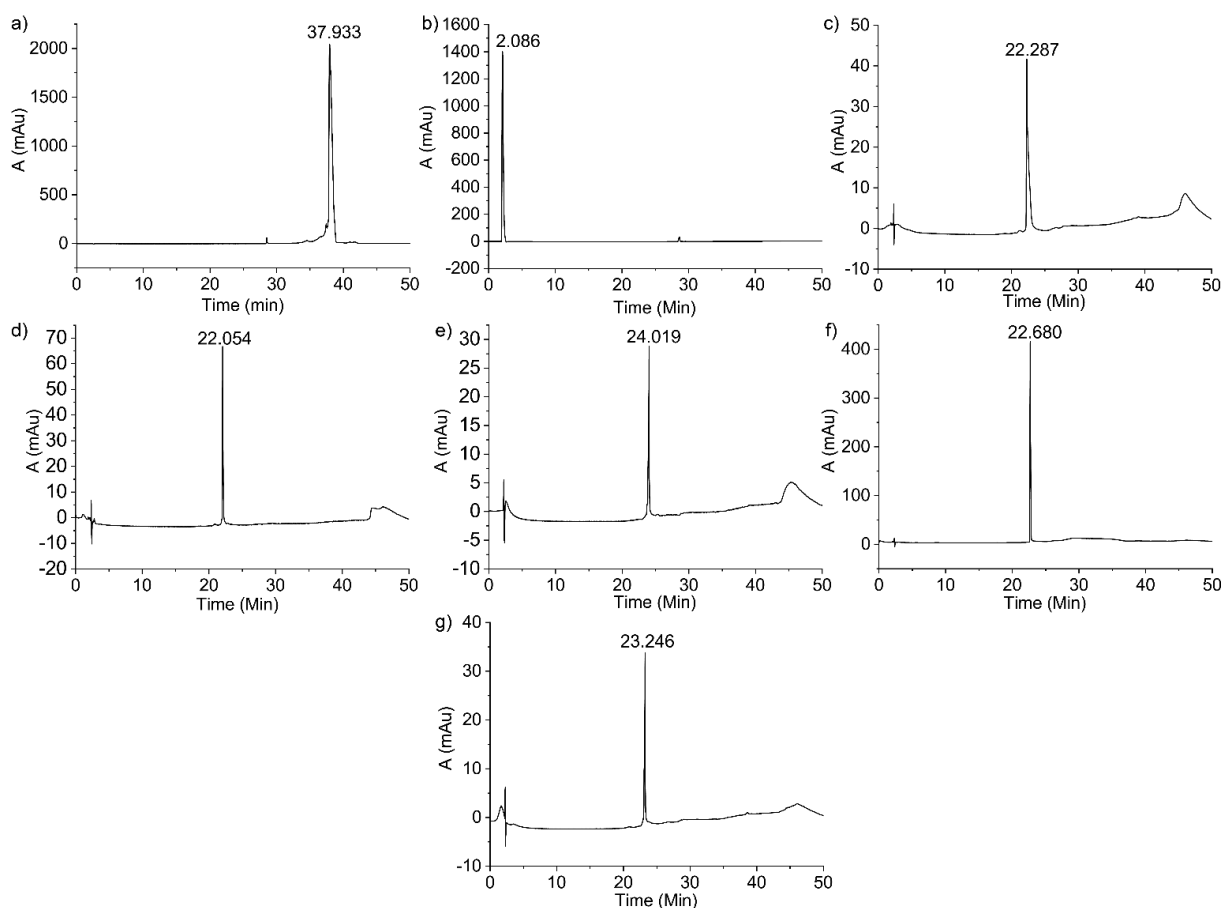


Figure 138. HPLC chromatograms of: a) Macrocycle **165**. b) Stopper **171**. c) Axle **170-H⁺·PF₆⁻**. d) Free thread **183-H⁺·PF₆⁻**. e) Free thread **184-H⁺·2PF₆⁻**. f) Rotaxane **185-H⁺·PF₆⁻**. g) Rotaxane **162-H⁺·2PF₆⁻**.

3.2. Study and switching of the chiroptical properties

As shown in the general introduction, the proposed pH-driven switching system is well-known and has proven its efficiency throughout the years. Consequently, in acidic medium, the luminescent macrocycle will be encircling the chiral ammonium station, the chirality transfer would be enabled and a CPL spectrum would be recorded. Conversely, in basic medium, the macrocycle will shuttle towards the triazolium station and, therefore, the distance between the amino acid unit and the macrocycle will be expanded. This modification would cause a diminution of the influence of the chirality source of the rotaxane to the spatial arrangement of the macrocycle and no preferential configuration would be adopted. The absence of a chiral environment near the emissive unit of the system would generate a loss of the CPL signal while keeping a fluorescence emission essentially unchanged (Figure 139).

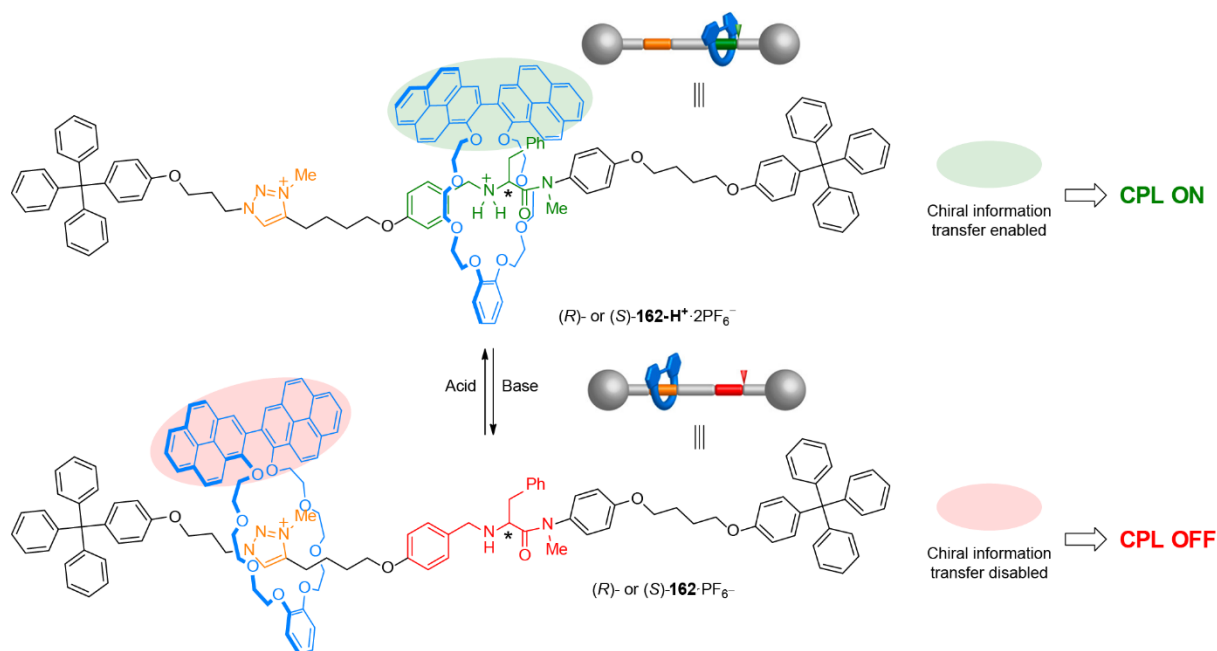


Figure 139. Proposed CPL switching mechanism based on a pH-driven [2]rotaxane molecular shuttle by activation and deactivation of the chiral information transfer between the thread and the emissive macrocycle.

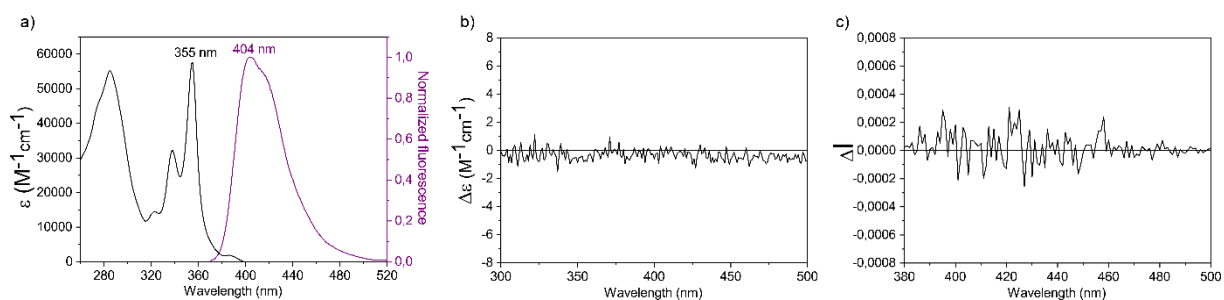


Figure 140. a) UV-Vis absorption (black line) and emission (purple line, $\lambda_{exc} = 355$ nm) spectra of macrocycle **165** (CHCl_3 , 20°C , $ca. 1 \times 10^{-5}$ M). b) ECD spectrum of macrocycle **165** showing the absence of response (CHCl_3 , 20°C , $ca. 1 \times 10^{-5}$ M). c) CPL ($\lambda_{exc} = 355$ nm) spectrum of macrocycle **165** (CHCl_3 , 20°C , $ca. 1 \times 10^{-5}$ M) demonstrating the absence of response.

Before evaluating the switching of the CPL properties of our molecular switch, it was necessary to measure the optical and chiroptical properties of the different species synthesized. In this sense, we started studying macrocycle **165**, which exhibits an absorption band between 320 and 400 nm with a maximum centered at 355 nm ($\epsilon = 57\,494\text{ M}^{-1}\text{cm}^{-1}$) and a small shoulder at 386 nm ($\epsilon = 1989\text{ M}^{-1}\text{cm}^{-1}$) in CHCl_3 (Figure 140a). Its fluorescence spectrum ($\lambda_{exc} = 355$ nm) shows an emission band at 404 nm ($QY = 0.18$) corresponding to the 2,2'-bipyrene unit of the macrocycle (Figure 140a). However, as expected, it did not display any ECD or CPL signals (Figures 140b,c) due to its low racemization barrier and the absence of a chiral environment. Conversely, enantiopure free axes (R)/(S)-**183-H**⁺·PF₆⁻ and (R)/(S)-**184-H**⁺·2PF₆⁻ have a UV-Vis spectra with an absorption between 240 and 325 nm (Figures 141a and 142a) and do not display any fluorescence properties because of the absence of a fluorophore in their structure (Figures 141b and 142b). However, the ECD spectra of both enantiomers of the

compounds were recorded and exhibit signals, only below 300 nm (Figures 141c and 142c). As (*R*)/(*S*)-**183-H⁺**·PF₆⁻ and (*R*)/(*S*)-**184-H⁺**·2PF₆⁻ were not found to be emissive, no CPL spectra were recorded.

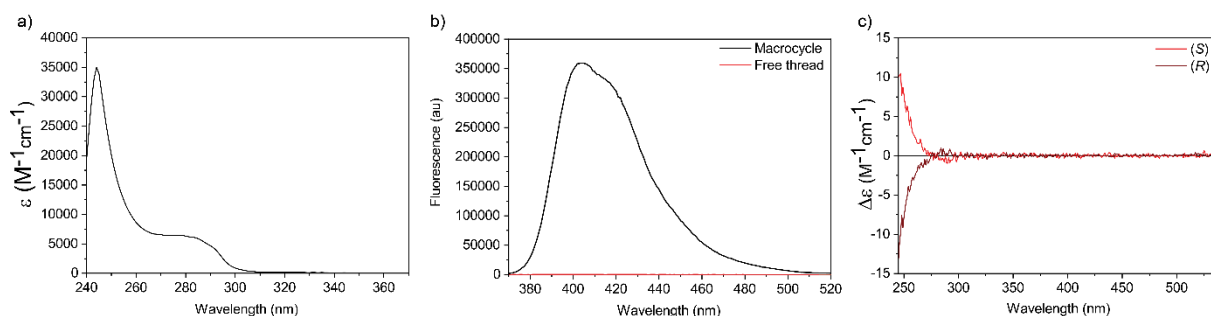


Figure 141. a) UV-Vis absorption spectrum of thread **183-H⁺**·PF₆⁻ (CHCl₃, 20 °C, *ca.* 1 × 10⁻⁴ M). b) Emission (λ_{exc} = 355 nm) spectra of macrocycle **165** (CHCl₃, 20 °C, *ca.* 1 × 10⁻⁵ M) and thread **183-H⁺**·PF₆⁻ (CHCl₃, 20 °C, *ca.* 1 × 10⁻⁴ M) showing no fluorescence response for the thread. c) ECD spectra of threads (*R*)/(*S*)-**183-H⁺**·PF₆⁻ (CHCl₃, 20 °C, *ca.* 1 × 10⁻⁴ M).

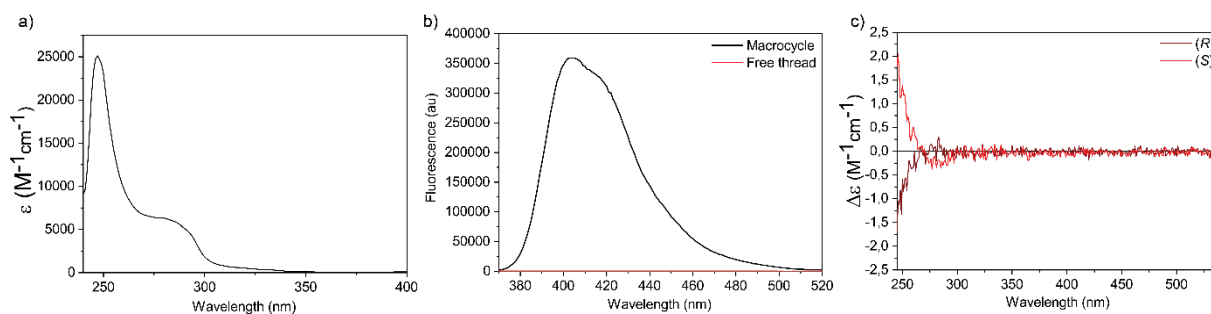


Figure 142. a) UV-Vis absorption spectrum of thread **184-H⁺**·2PF₆⁻ (CHCl₃, 20 °C, *ca.* 1 × 10⁻⁴ M). b) Emission (λ_{exc} = 355 nm) spectra of macrocycle **165** (CHCl₃, 20 °C, *ca.* 1 × 10⁻⁵ M) and thread **184-H⁺**·2PF₆⁻ (CHCl₃, 20 °C, *ca.* 1 × 10⁻⁴ M) showing no fluorescence response for the thread. c) ECD spectra of threads (*R*)/(*S*)-**184-H⁺**·2PF₆⁻ (CHCl₃, 20 °C, *ca.* 1 × 10⁻⁴ M).

When it comes to rotaxanes (*R*)/(*S*)-**185-H⁺**·PF₆⁻, their UV-Vis absorption spectrum shows two main bands, one centered at 273 nm and the another one between 320 and 400 nm whose maximum is situated at 355 nm ($\epsilon = 55\,230\text{ M}^{-1}\text{cm}^{-1}$) (Figure 143a). The structure of the latter possesses a similar shape to that of macrocycle **165**. This rotaxane displays a fluorescence spectrum ($\lambda_{exc} = 355\text{ nm}$) whose emission band is centered at 404 nm (QY = 0.19) (Figure 143a). Again, its shape and wavelength range (380–500 nm) are comparable to those of the spectrum of macrocycle **165**, demonstrating that it results from the fluorophore of the macrocycle, 2,2'-bipyrene group. Furthermore, unlike threads (*R*)/(*S*)-**183-H⁺**·PF₆⁻, the ECD spectra of rotaxanes (*R*)/(*S*)-**185-H⁺**·PF₆⁻ exhibit several bands within 300–425 nm that can be credited to the 2,2'-bipyrene subunit. The ECD spectra of both rotaxanes are mirror images and show $|g_{abs}|$ values up to 0.5×10^{-3} at 402 nm ($|\Delta\epsilon| \approx 0.8\text{ M}^{-1}\text{cm}^{-1}$) (Figures 143b). Moreover, upon excitation with UV-Vis light ($\lambda_{exc} = 355\text{ nm}$), CPL signals of both enantiomers are observed between, approximately, 390 and 470 nm. The CPL signals are mirror image and their sign

matches that of the ECD band of the lowest energy transition (Figure 143c). This system yields a $|g_{lum}|$ value of 0.5×10^{-3} which is in agreement with those previously obtained for biaryl structures.³⁴⁶

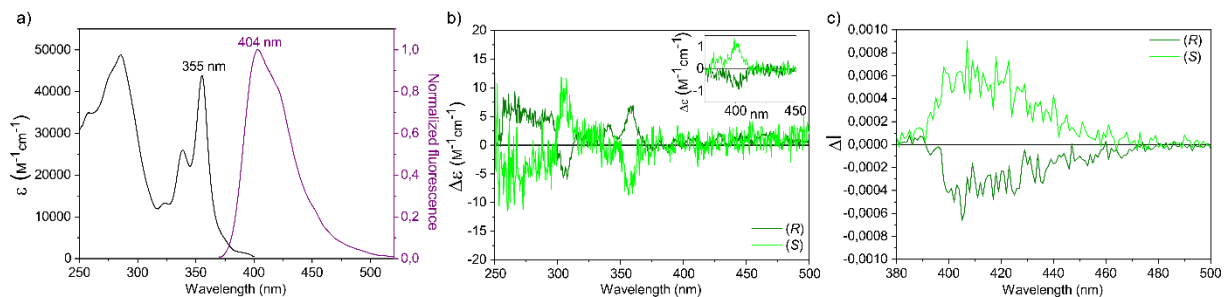


Figure 143. a) UV-Vis absorption (black line) and emission (purple line, $\lambda_{exc} = 355$ nm) spectra of rotaxane **185-H⁺·PF₆⁻** (CHCl₃, 20 °C, *ca.* 1×10^{-5} M). b) ECD spectra of rotaxanes (R)/(S)-**185-H⁺·PF₆⁻** (CHCl₃, 20 °C, *ca.* 1×10^{-5} M). Inset: Partial ECD spectra of rotaxanes (R)/(S)-**185-H⁺·PF₆⁻** (CHCl₃, 20 °C, *ca.* 1×10^{-4} M). c) CPL ($\lambda_{exc} = 355$ nm) spectra of rotaxanes (R)/(S)-**185-H⁺·PF₆⁻** (CHCl₃, 20 °C, *ca.* 1×10^{-5} M).

Regarding rotaxanes (R)/(S)-**162-H⁺·2PF₆⁻**, their UV-Vis absorption and emission spectra are very similar to those of rotaxanes (R)/(S)-**185-H⁺·PF₆⁻**, with the only difference of a quantum yield value of 0.11. Also, the ECD and CPL spectrum are analogous to those recorded for rotaxanes (R)/(S)-**185-H⁺·PF₆⁻** (Figure 144a). Its absorption dissymmetry factor $|g_{abs}|$ range between 7×10^{-5} at 355 nm ($|\Delta\epsilon| \approx 4 \text{ M}^{-1} \text{ cm}^{-1}$) and 3×10^{-4} for the lowest energy transition at 400 nm ($|\Delta\epsilon| \approx 0.5 \text{ M}^{-1} \text{ cm}^{-1}$) while its emission dissymmetry factor $|g_{lum}|$ reaches 0.5×10^{-3} .

These results demonstrate that a preferential conformation is induced to the macrocycle, and therefore to the 2,2'-bipyrene unit, due to its proximity with the enantiopure amino acid derivative which gives rise to CPL and ECD signals. Moreover, control experiments were carried out by studying the chiroptical properties of an equimolar mixture of macrocycle **165** with free axle (S)-**184-H⁺·2PF₆⁻** or thread precursor (S)-**170-H⁺·PF₆⁻**, resulting in an absence of ECD or CPL responses (Figure 145). Therefore, it is clear that a mechanical bond is necessary to obtain such signals employing our system.

After having demonstrated that our target rotaxane ((R)/(S)-**162-H⁺·2PF₆⁻**) was a CPL emitter, we tackled the evaluation of its "ON-OFF" chiroptical switching properties. Thus, the addition of an excess of K₂CO₃ afforded rotaxane (R)/(S)-**162·PF₆⁻** whose ECD and CPL responses associated to the 2,2'-bipyrene unit disappeared, while its UV-Vis absorption and emission spectra as well as its quantum yield (0.11) remained essentially unaltered (Figure 144b and Scheme 82). Conversely, the addition of CF₃CO₂H to (R)/(S)-**162·2PF₆⁻** had the effect to restore the ECD and CPL signals. Again, the UV-Vis

³⁴⁶ a) T. Amako, T. Kimoto, N. Tajima, M. Fujiki, Y. Imai, *Tetrahedron* **2013**, *69*, 2753-2757. b) T. Sato, N. Tajima, H. Ueno, T. Harada, M. Fujiki, Y. Imai, *Tetrahedron* **2016**, *72*, 7032-7038. c) T. Kitatobe, Y. Mimura, S. Tsujimoto, N. Tajima, M. Fujiki, Y. Imai, *Tetrahedron* **2017**, *73*, 6856-6862.

absorption and emission spectra and its quantum yield were maintained during the re-protonation process (Figure 144c and Scheme 82).

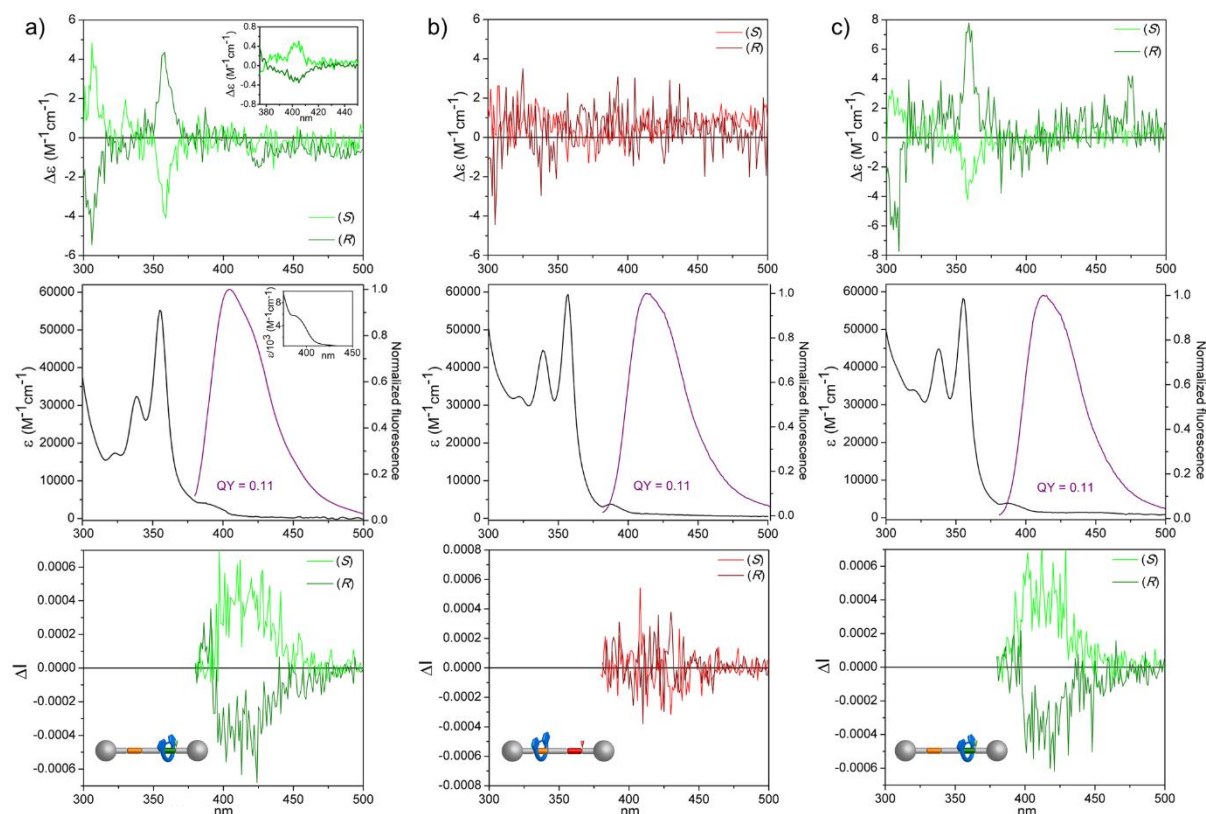


Figure 144. ECD ($ca. 1 \times 10^{-5}$ M) (top), UV-vis absorption (black line) and fluorescence ($\lambda_{exc} = 355$ nm) (purple line) ($ca. 1 \times 10^{-5}$ M) (middle), and CPL in normalized ΔI scale ($\lambda_{exc} = 355$ nm) ($ca. 1 \times 10^{-5}$ M) (bottom) spectra ($CHCl_3$, 20 °C) of: a) **162-H⁺·2PF₆⁻**. b) **162·PF₆⁻**. c) **162-H⁺**, obtained by protonation of **162·PF₆⁻** with a solution of CF_3CO_2H in $CHCl_3$. Inset (a): Partial ECD ($ca. 1 \times 10^{-4}$ M) spectrum showing the lowest energy band (top) and partial UV-vis spectrum ($ca. 1 \times 10^{-4}$ M) showing the longest wavelength absorption (bottom).

For the switching mechanism monitored by ECD, other bases such as, NaOH, Et_3N , DBU and a phosphazene-bound base (BEMP resin) were tested in addition to the selected K_2CO_3 . The phosphazene resin and NaOH lead to the decomposition of the rotaxane and, consequently, were rejected. For Et_3N , the ECD measurements displayed that 50 equivalents were needed to fully deprotonate the ammonium salt. After the re-protonation, it generated an abundant amount of salts that potentially could affect the fluorescence and, therefore, it was discarded. Finally, DBU and K_2CO_3 afforded very similar results, however we decided to employ K_2CO_3 since it was more convenient. Indeed, this solid shows a very poor solubility in $CHCl_3$ and can be easily filtered when the ammonium salt is deprotonated. For this reason, upon acidification, it will only generate a reasonable amount of salts.

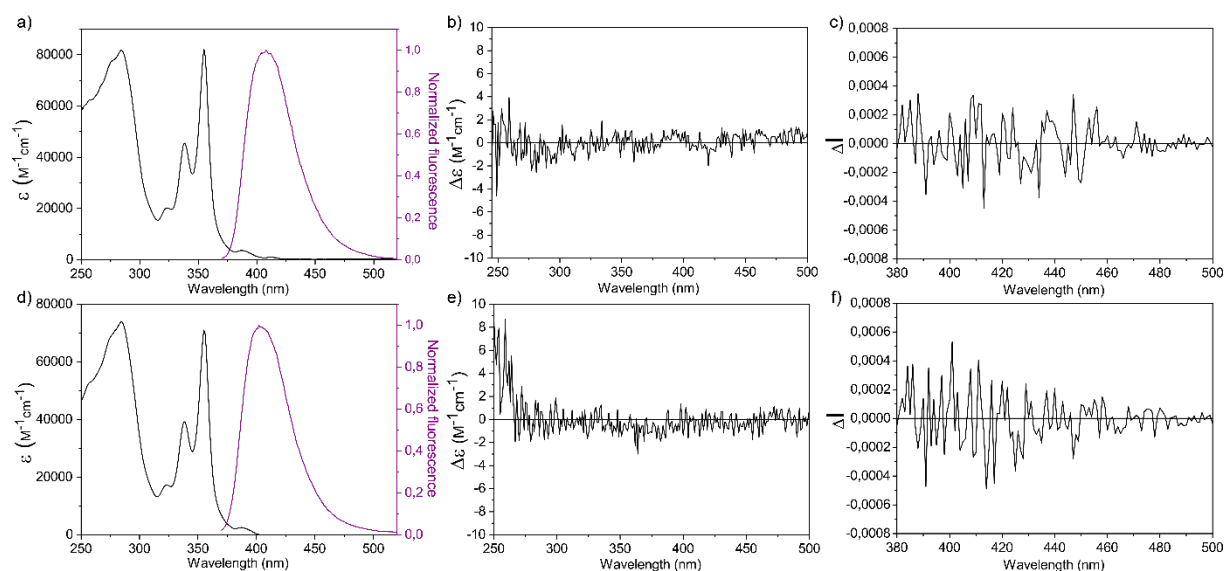
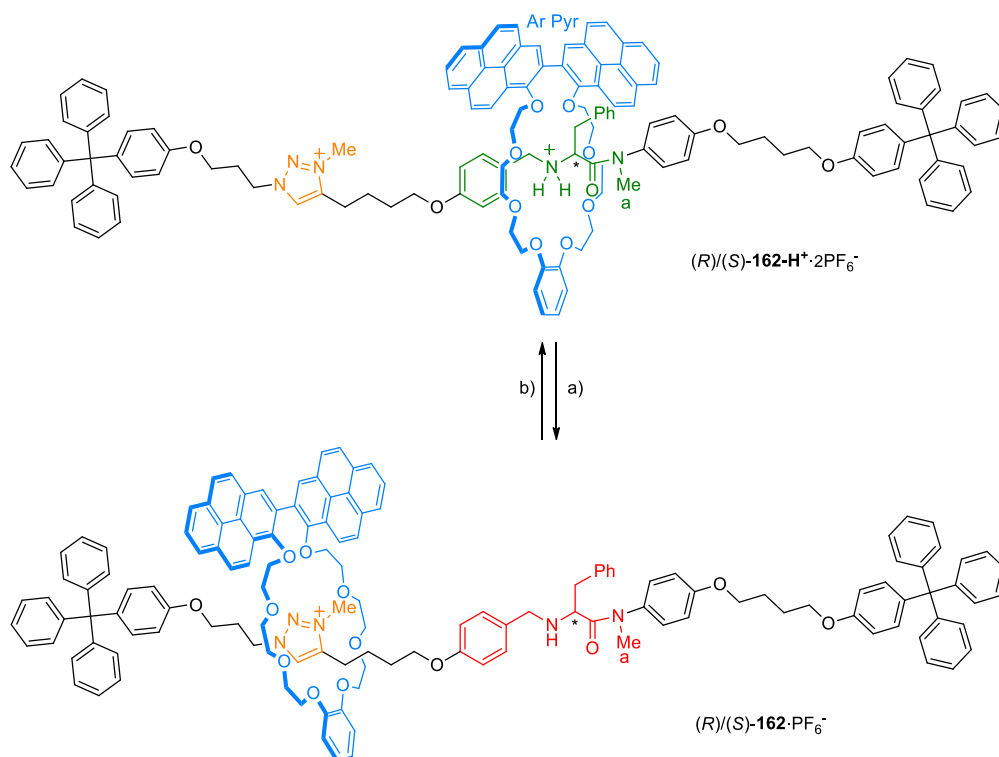


Figure 145. UV-Vis absorption (a, black line), emission (a, purple line, $\lambda_{exc} = 355$ nm), ECD (b) and CPL (c) spectra (CHCl_3 , 20 °C) of an equimolar solution of thread (*S*)-**184-H⁺**· 2PF_6^- and macrocycle **165** (*ca.* 1×10^{-5} M). UV-Vis absorption (d, black line) and emission (d, purple line, $\lambda_{exc} = 355$ nm), ECD (e) and CPL (f) spectra of an equimolar solution of (*S*)-**170-H⁺** and macrocycle **165** (*ca.* 1×10^{-5} M).



Scheme 82. Switching of rotaxanes (*R*)/(*S*)-**162**. Reagents and conditions: a) K_2CO_3 , CHCl_3 , r.t., 1 min. b) $\text{CF}_3\text{CO}_2\text{H}$, CHCl_3 , r.t., 1 min.

The switching process can also be analysed by ^1H NMR spectroscopy. Indeed, by looking at the characteristic *N*-methyl protons (H_a) after the addition of K_2CO_3 , a significant downfield shift ($\Delta\delta_{\text{H}_a} = 0.85$ ppm) was noticed in comparison to that of the protonated rotaxanes (*R*)/(*S*)-**162-H⁺**· 2PF_6^- (Figures 136b, 146b,c). Moreover, the chemical shifts of these hydrogens ($\delta_{\text{H}_a} = 3.16$ ppm) are very much alike

those of the free thread (*R*)/(*S*)-**184**-H⁺·2PF₆⁻ (Figures 146c,d). This behaviour is similar to the switchable catalyst owning the same binding stations developed by Leigh and co-workers.^{165a} Therefore, these evidences support the translation of the macrocycle from the chiral ammonium salt to the triazolium station in basic medium (Scheme 82).

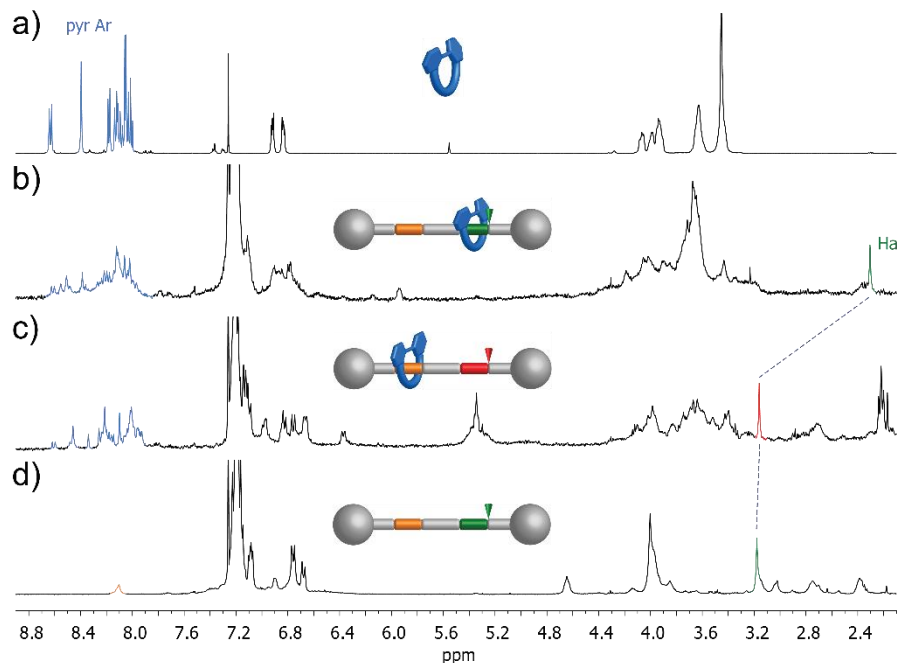


Figure 146. Partial ¹H NMR spectra (CDCl₃) of: a) Macrocycle **165** (500 MHz). b) Rotaxane **162**-H⁺·2PF₆⁻ (400 MHz). c) Rotaxane **162**·PF₆⁻ (400 MHz). d) Thread **184**-H⁺·2PF₆⁻ (400 MHz). Lettering coding is defined in Scheme 82.

Finally, we undertook the *in situ* switching of the CPL signal in order to determine how many reversible cycles could be accomplished with our molecular device. For this purpose, CPL spectra of (*S*)-**162**-H⁺·2PF₆⁻ were recorded after consecutive addition of K₂CO₃ and CF₃CO₂H in order to regulate the position of the fluorescent macrocycle on the axle and, therefore, turn on and off the CPL response. The measured data show that the deprotonation disabled the CPL response ($g_{lum} \approx 0$) while the addition of acid restored it throughout three complete cycles (Figure 147). Furthermore, it is important to highlight that the fluorescence spectra of the rotaxane remains essentially unaffected during this process (around 10% variation).

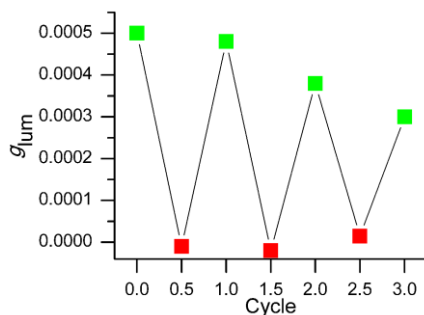


Figure 147. *In situ* "ON-OFF" switching of the CPL emission of (S)-**162-H**⁺·2PF₆⁻ after consecutive addition of base (K₂CO₃, red square) and acid (CF₃CO₂H, green square).

As can be seen on Figure 147, some decrease of the CPL response can be noticed over the cycles. We attribute this decline to some degradation of the deprotonated rotaxane. Indeed, we found that it was crucial to perform the CPL measurement of the deprotonated rotaxane in the absence of oxygen, otherwise, the CPL response would not be recovered by the addition of trifluoroacetic acid. We assumed that an *N*-oxidation occurred on the secondary amine while recording the spectra. To minimize this degradation, the measurements were carried out under Argon; however, it was not fully suppressed. In any case, despite this deterioration of the CPL signal, statistical tests were performed on each state of each cycle showing that the "ON" states are significantly different with higher $|g_{lum}|$ values than those of the "OFF" states and can be easily identified.

4. Conclusions

In this chapter, the first CPL “ON-OFF” switch based on a MIM, precisely a rotaxane, has been synthesized. Its chiroptical properties are based on a chiral information transfer between a thread owning an ammonium station including an enantiopure amino acid and a luminescent crown ether macrocycle bearing a 2,2'-bipyrene group. Consequently, when the macrocycle resides on this station, the 2,2'-bipyrene unit adopts a preferential spatial configuration that allows the observation of a CPL signal upon irradiation with UV-Vis light. Moreover, using a pH-driven switch, this CPL response can be turned off by the translation of the macrocycle towards an achiral triazolium station and restored when it comes back to its original position. Furthermore, it has been demonstrated that three complete “ON-OFF” cycles can be accomplished by consecutive additions of base and acid.

Remarkably, the rotaxane architecture provides a very efficient switching system that does not modify the absorption and the fluorescence profiles or the corresponding quantum yield of the device throughout the switching process.

These proof-of-concept results expand the numerous applications of molecular machines and provide a new architecture for future CPL switches which is relevant, efficient and robust. This new strategy could be explored in the future, to build other chiroptical switching systems, to be implemented in photonic materials or to operate in optoelectronic or sensing applications.

5. Experimental section

5.1. General details

Unless otherwise noted, commercially available reagents, solvents and anhydrous solvents were used as purchased without further purification. Anhydrous THF was freshly distilled over Na/benzophenone.

Pd(dba)₂,³⁴⁷ Boc-L-phenylalanine,³⁴⁸ compounds **167**,³⁴⁹ **169**,^{165a} **173**³⁴¹ and **177**³⁵⁰ were synthesized according to literature procedures.

TLC was performed on Merck Silica gel 60 F₂₅₄ aluminium sheets or Sigma-Aldrich (silica gel matrix, with fluorescent indicator 254 nm). The TLC plates were stained with potassium permanganate (1% w/v in water), cerium molybdate stain (Hanessian's stain) or phosphomolybdic acid (5% ethanol solution), or observed under UV light when applicable.

Flash column chromatography was performed with Silica gel 60 (Merck, 40-63 μm, 230–400 mesh ASTM, or Scharlab, Spain, Silica gel 60 (230-400 mesh) or VWR, 40-63 μm). Silica gel G preparative TLC plates were purchased from ANALTECH (20×20cm, 2000 micron) or from Silicycle (20×20cm, 1000 micron). Gel permeation chromatography was performed with Biobeads® SX-1 or Biobeads® SX-3 resin beads.

¹H and ¹³C NMR spectra were recorded at room temperature on a Varian Inova Unity (300 MHz), Varian Direct Drive (400 MHz or 500 MHz), Bruker Avance III HD NanoBay (400 MHz) or Bruker Avance Neo (400 MHz or 500 MHz) spectrometers at a constant temperature of 298 K. Chemical shifts are given in ppm and referenced to the signal of the residual protiated solvent (¹H: δ=7.26 for CDCl₃, δ=2.55 for DMSO-*d*₆ at room temperature) or the ¹³C signal of the solvents (¹³C: δ=77.16 for CDCl₃, δ=39.52 for DMSO-*d*₆) or to the signal of the residual TMS (¹H: δ=0.00). Coupling constant (*J*) values are given in Hz. Abbreviations indicating multiplicity were used as follow: m = multiplet, p = quintet, q = quartet, t = triplet, d = doublet, s = singlet, br = broad. Signals were assigned by means of 2D NMR spectroscopy (COSY, HSQC, HMBC).

UV-Vis absorption, fluorescence, electronic circular dichroism (ECD) and circularly polarized luminescence (CPL) spectra were recorded on an Olis DSM172 spectrophotometer equipped with a 150 W Xenon lamp.

³⁴⁷ Y. Takahashi, Ts. Ito, S. Sakai, Y. Ishii, Y., *J. Chem. Soc. D* **1970**, 1065-1066.

³⁴⁸ N. Naganna, N. Madhavan, *J. Org. Chem.* **2014**, *79*, 11549-11557.

³⁴⁹ A. Vlasceanu, M. Jessing, J. P. Kilburn, *Bioorg. Med. Chem.* **2015**, *23*, 4453-4461.

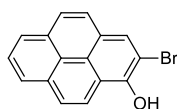
³⁵⁰ S. J. Cantrill, G. J. Youn, J. F. Stoddart, D. J. Williams, *J. Org. Chem.* **2001**, *66*, 6857-6872.

HPLC experiments were carried out using an HPLC Agilent 1200 Infinity Series with a LiChroCART® 250-4 LiChrospher® 100 RP-8 (5 µm) analytical column. The column temperature was set at 20.0 °C. The wavelength selected for the peak detection was 280 nm and the flow was constant during the operation: 1.000 mL/min.

Electrospray (ESI) HRMS spectra were recorded on a Waters Xevo G2-XS QTOF or a WATERS LCT Premier XE. Electronic impact (EI) HRMS spectra were recorded on a Bruker Maxis II spectrometer. MALDI mass spectra were recorded on a Bruker Ultraflex III mass spectrometer. IR spectra were recorded with a Perkin-Elmer Spectrum Two FTIR ATR spectrometer. Optical rotations were recorded on a Perkin-Elmer 341 polarimeter.

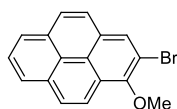
5.2. Synthetic procedures and characterization details

Compound 174:



To a degassed solution of ^tBuNH₂ (1.50 mL, 14.5 mmol) in anhydrous toluene (20 mL) at –30 °C was added rapidly Br₂ (400 µL, 7.95 mmol). The solution was stirred for 30 min at –30 °C and cooled to –78 °C. In another round-bottom flask, a solution of **173** (1.58 g, 7.23 mmol) and ^tBuNH₂ (0.750 mL, 7.23 mmol) in anhydrous toluene (150 mL) was stirred for 20 min at –78 °C. The bromine solution was then added to the pyrene solution. The resulting mixture was stirred for 30 min at –78 °C and then warmed up slowly to room temperature over 6 h. To this mixture was added EtOAc (200 mL). The organic layer was washed with H₂O (2 × 200 mL) and brine (200 mL). The organic layer was dried over anhydrous Na₂SO₄ and the solvent was evaporated under vacuum. The crude material was purified by column chromatography (SiO₂, CH₂Cl₂/hexane 40:60) to afford **174** (1.45 g, 67%) as a yellow solid. ¹H NMR (300 MHz, acetone-*d*₆) δ = 8.87 (s, 1H), 8.47 (d, *J* = 9.3 Hz, 1H), 8.44 (s, 1H), 8.25 – 8.15 (m, 3H), 8.05 (d, *J* = 7.6 Hz, 1H), 8.02 (m, 2H). Spectral data agree with those previously reported.³⁴¹

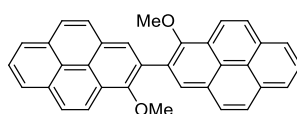
Compound 175:



Under inert atmosphere, to a solution of **174** (744 mg, 2.50 mmol) in anhydrous acetone (50 mL), at 0 °C, were added K₂CO₃ (1.70 g, 12.5 mmol) and iodomethane (315 µL, 5.00 mmol). The solution was stirred for 30 min at 0 °C and then, refluxed for 18 h. The solvent was removed under reduced pressure and the solid was dissolved in a mixture of CH₂Cl₂/H₂O (1:1, 150 mL). Layers were separated and the

aqueous one was extracted with CH₂Cl₂ (75 mL). The combined organic layers were dried over anhydrous Na₂SO₄ and the solvent was evaporated under vacuum. The crude material was purified by column chromatography (SiO₂, CH₂Cl₂/hexane 20:80) to give **175** (650 mg, 83%) as a yellow solid. ¹H NMR (500 MHz, CDCl₃): δ = 8.32 – 8.27 (m, 2H), 8.13 (m, 2H), 8.07 (d, *J* = 9.1 Hz, 1H), 8.01 – 7.93 (m, 2H), 7.84 (d, *J* = 9.0 Hz, 1H), 4.14 (s, 3H). ¹³C NMR (126 MHz, CDCl₃): δ = 150.89, 130.97, 130.95, 129.12, 128.52, 128.45, 127.55, 126.46, 126.05, 125.57, 125.55, 125.45, 125.07, 124.60, 121.21, 115.17, 62.42. IR (neat): ν = 3046, 2934, 1588, 1480, 1421, 1254, 1107, 1003, 840, 826, 783, 737. HR-MS (EI⁺): *m/z*: 310.0007 [M]⁺ (calcd for C₁₇H₁₁OBr: 309.9993).

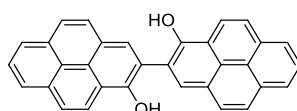
Compound 176:



Caution! The ^tBuLi solution in pentane is a pyrophoric liquid as ^tBuLi catches fire spontaneously if exposed to air. Although we did not experience any problem, this reagent should be handled with care under inert atmosphere and adequate safety measures should be taken during the synthesis. Moreover, the reaction should not be scaled up.

175 (602 mg, 1.94 mmol), Pd(dba)₂ (333 mg, 0.581 mmol) and XPhos (553 mg, 1.16 mmol) were dissolved in degassed anhydrous toluene (20 mL). To this solution was added ^tBuLi (1.6 M in pentane, 1.80 mL, 2.90 mmol) over 2 h using a syringe pump at room temperature. The solution was further stirred for 18 h at room temperature. The mixture was concentrated and the crude was purified by column chromatography (SiO₂, CH₂Cl₂/hexane 40:60) to yield **176** (362 mg, 79%) as a yellow solid. ¹H NMR (400 MHz, CDCl₃): δ = 8.54 (d, *J* = 9.2 Hz, 2H), 8.43 (s, 2H), 8.26 – 8.16 (m, 6H), 8.13 – 8.02 (m, 6H), 3.69 (s, 6H). ¹³C NMR (101 MHz, CDCl₃): δ = 152.67, 131.53, 131.48, 130.17, 128.22, 127.84, 127.78, 127.35, 126.83, 126.42, 125.92, 125.13, 125.05, 125.03, 124.54, 122.03, 62.46. IR (neat): ν = 2924, 2852, 1730, 1597, 1464, 1246, 1006, 842, 830, 760. HR-MS (ESI⁺): *m/z*: 463.1685 [M+H]⁺ (calcd for C₃₄H₂₃O₂: 463.1698).

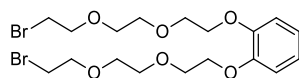
Compound 164:



Under an Ar atmosphere, to a solution of **176** (833 mg, 1.80 mmol) in dry CH₂Cl₂ (80 mL) was added BF₃·SMe₂ (2.30 mL, 21.6 mmol). The solution was stirred for 6 h at room temperature and then diluted with CH₂Cl₂ (200 mL). The mixture was washed with HCl_(aq) (5%, 200 mL). Layers were separated and

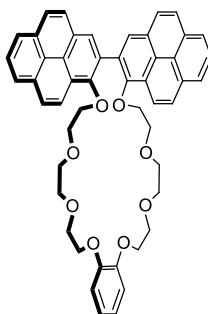
the aqueous one was extracted with CH_2Cl_2 (2×200 mL). The combined organic layers were dried over anhydrous Na_2SO_4 and the solvent was evaporated under reduced pressure. The crude material was purified by column chromatography (SiO_2 , CH_2Cl_2 /hexane 1:1 to 1:0, then acetone). Fractions containing the product were combined and concentrated. The resulting solid was washed with CHCl_3 , filtered and collected to yield **164** (202 mg, 26%) as a brown solid. ^1H NMR (400 MHz, $\text{DMSO}-d_6$): δ = 9.79 (br, 2H), 8.55 (d, J = 9.2 Hz, 2H), 8.32 (s, 2H), 8.25 – 8.09 (m, 8H), 8.01 (m, 4H). ^{13}C NMR (101 MHz, $\text{DMSO}-d_6$): δ = 149.88, 131.32, 131.18, 128.89, 127.50, 126.23, 125.87, 125.07, 125.02, 124.40, 124.32, 124.11, 124.00, 123.75, 122.04, 119.37. IR (neat): ν = 2923, 2853, 1728, 1462, 1275, 1123, 841, 750. HR-MS (ESI^-): m/z : 433.1226 $[\text{M}-\text{H}]^-$ (calcd for $\text{C}_{32}\text{H}_{17}\text{O}_2$: 433.1229).

Compound 163:



Under Ar, to a solution of **177** (455 mg, 0.666 mmol) in anhydrous acetone (5 mL) was added LiBr (1.13 g, 13.0 mmol). The suspension was refluxed overnight. The mixture was diluted with EtOAc (100 mL) and washed with brine (2×100 mL). The organic layer was dried over anhydrous Na_2SO_4 and the solvent was removed under vacuum. The crude material was purified by column chromatography (SiO_2 , gradient from hexane/EtOAc 90:10 to 30:70) to afford **163** (307 mg, 92%) as a yellow oil. ^1H NMR (500 MHz, CDCl_3): δ = 6.89 (m, 4H), 4.14 (t, J = 6.2 Hz, 4H), 3.84 (t, J = 6.2 Hz, 4H), 3.78 (t, J = 6.3 Hz, 4H), 3.72 (m, 4H), 3.66 (m, 4H), 3.44 (t, J = 6.3 Hz, 4H). ^{13}C NMR (126 MHz, CDCl_3): δ = 148.97, 121.65, 114.97, 71.18, 70.79, 70.57, 69.86, 68.89, 30.44. IR (neat): ν = 2871, 1592, 1502, 1254, 1114, 1051, 930, 747. HR-MS (ESI^+): m/z : 521.0145 $[\text{M}+\text{Na}]^+$ (calcd for $\text{C}_{18}\text{H}_{28}\text{Br}_2\text{O}_6\text{Na}$: 521.0150).

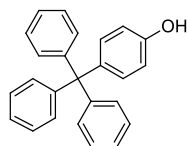
Compound 165:



To a degassed solution of **164** (41 mg, 0.094 mmol) in anhydrous dioxane (150 mL) was added $^t\text{BuOK}$ (42 mg, 0.38 mmol). The solution was stirred for 20 min at room temperature and subsequently, were added **163** (47 mg, 0.094 mmol), KPF_6 (17 mg, 0.094 mmol) and a catalytic amount of $^n\text{Bu}_4\text{NI}$. The mixture was refluxed for 24 h. The solvent was removed under reduced pressure, the solid was

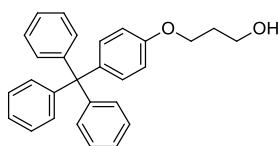
dissolved in CH₂Cl₂ (150 mL) and an excess of KPF₆ was added. The mixture was filtered and the solvent was evaporated under vacuum. The crude material was purified by column chromatography (SiO₂, CH₂Cl₂/MeOH 96:4), then by preparative TLC (SiO₂, CH₂Cl₂/MeOH 97:3) and finally by gel permeation chromatography (Bio-Beads® SX-1, CH₂Cl₂). The resulting solid was dissolved in CH₂Cl₂ (30 mL) and washed with an aqueous solution of Na₄EDTA (0.1 M, 5 × 50 mL) and H₂O (3 × 50 mL). The organic layer was dried over anhydrous Na₂SO₄ and the solvent was removed under vacuum to give **165** (25 mg, 34%) as a brown solid. ¹H NMR (500 MHz, CDCl₃): δ = 8.63 (d, *J* = 9.0 Hz, 2H), 8.40 (s, 2H), 8.18 (d, *J* = 7.6 Hz, 2H), 8.14 – 7.99 (m, 10H), 6.92 (m, 2H), 6.83 (m, 2H), 4.09 – 3.89 (m, 8H), 3.63 (m, 6H), 3.45 (m, 10H). ¹³C NMR (126 MHz, CDCl₃): δ = 151.49, 149.13, 131.48, 131.40, 130.23, 129.33, 128.27, 127.73, 127.70, 127.28, 126.76, 126.34, 125.73, 125.02, 124.99, 124.90, 122.31, 121.61, 114.64, 74.21, 70.90, 70.85, 70.39, 69.79, 69.20. IR (neat): ν = 3040, 2924, 2869, 1593, 1502, 1452, 1347, 1255, 1209, 1120, 1047, 844, 764, 749. HR-MS (ESI⁺): *m/z*: 795.2936 [M+Na]⁺ (calcd for C₅₀H₄₄O₈Na: 795.2934); 811.2678 [M+K]⁺ (calcd for C₅₀H₄₄O₈K: 811.2673)

Compound 179:



To a solution of **178** (63.7 g, 0.245 mol) and phenol (350 g) at 160 °C, was added HCl_(aq.) (37%, 12 mL). The mixture was further stirred for 6 h at 160 °C. Subsequently, toluene (500 mL) was added while the mixture was hot and the suspension was allowed to precipitate overnight at room temperature. The resulting solid was collected, washed with toluene (500 mL), cold Et₂O (300 mL) and dried under vacuum to give **179** (49.1 g, 60%) as a white solid. ¹H NMR (400 MHz, DMSO-*d*₆): δ = 7.27 (t, *J* = 7.6 Hz, 6H), 7.21 – 7.10 (m, 9H), 6.90 (d, *J* = 8.8 Hz, 2H), 6.68 (d, *J* = 8.8 Hz, 2H). ¹³C NMR (101 MHz, DMSO-*d*₆): δ = 155.26, 146.84, 136.57, 131.56, 130.46, 127.55, 125.80, 114.37, 63.74. IR (neat): ν = 3549, 3027, 1611, 1592, 1507, 1262, 1177, 1161, 764, 750, 701. HR-MS (ESI⁻): *m/z*: 335.1435 [M-H]⁻ (calcd for C₂₅H₁₉O: 335.1436).

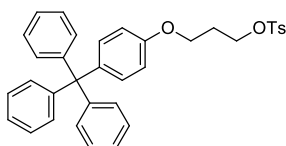
Compound 180:



Under inert atmosphere, to a solution of **179** (1.00 g, 2.97 mmol) in anhydrous acetone (100 mL) were added K₂CO₃ (2.06 g, 14.9 mmol) and 3-bromo-1-propanol (340 μL, 3.87 mmol). The suspension was

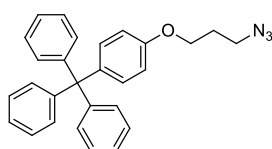
refluxed for 24 h. The mixture was filtered and the solvent was removed under reduced pressure. The resulting solid was dissolved in a mixture of $\text{CH}_2\text{Cl}_2/\text{H}_2\text{O}$ (1:1, 100 mL). Layers were separated and the aqueous one was extracted with CH_2Cl_2 (50 mL). The combined organic phases were dried over anhydrous Na_2SO_4 and the solvent was removed under vacuum. The crude material was purified by column chromatography (SiO_2 , CH_2Cl_2) to afford **180** (1.15 g, 98%) as a white solid. ^1H NMR (500 MHz, CDCl_3): δ = 7.27 – 7.17 (m, 15H), 7.11 (d, J = 8.9 Hz, 2H), 6.79 (d, J = 8.9 Hz, 2H), 4.11 (t, J = 5.9 Hz, 2H), 3.85 (t, J = 5.9 Hz, 2H), 2.04 (p, J = 5.9 Hz, 2H). ^{13}C NMR (126 MHz, CDCl_3): δ = 156.80, 147.14, 139.36, 132.37, 131.25, 127.56, 125.99, 113.37, 65.84, 64.45, 60.81, 32.14. IR (neat): ν = 3323 (br), 1605, 1507, 1264, 1248, 1183, 1058, 1034, 825, 748, 700. HR-MS (ESI^+): m/z : 417.1830 $[\text{M}+\text{Na}]^+$ (calcd for $\text{C}_{28}\text{H}_{26}\text{O}_2\text{Na}$: 417.1830).

Compound 181:



Under an Ar atmosphere, to a solution of **180** (2.00 g, 5.07 mmol) in CH_2Cl_2 (200 mL) were added Et_3N (2.80 mL, 20.3 mmol), TsCl (1.93 g, 10.1 mmol) in three portions and a catalytic amount of DMAP. The solution was stirred overnight at room temperature. The solvent was removed under reduced and the crude material was purified by column chromatography (SiO_2 , hexane/ CH_2Cl_2 60:40 to 40:60) to afford **181** (2.41 g, 87%) as a white solid. ^1H NMR (500 MHz, CDCl_3): δ = 7.75 (d, J = 8.3 Hz, 2H), 7.27 – 7.17 (m, 17H), 7.08 (d, J = 8.9 Hz, 2H), 6.64 (d, J = 8.9 Hz, 2H), 4.23 (t, J = 6.1 Hz, 2H), 3.94 (t, J = 5.9 Hz, 2H), 2.35 (s, 3H), 2.10 (p, J = 6.0 Hz, 2H). ^{13}C NMR (126 MHz, CDCl_3): δ = 156.54, 147.12, 144.89, 139.44, 132.98, 132.28, 131.23, 129.98, 128.03, 127.59, 126.03, 113.34, 67.26, 64.45, 63.15, 29.06, 21.76. IR (neat): ν = 3056, 1598, 1508, 1362, 1251, 1187, 1176, 948, 750, 702. HR-MS (ESI^+): m/z : 571.1923 $[\text{M}+\text{Na}]^+$ (calcd for $\text{C}_{35}\text{H}_{32}\text{SO}_2\text{Na}$: 571.1919).

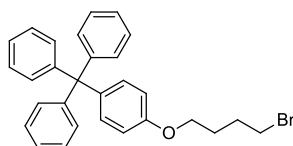
Compound 171:



Caution! NaN_3 is very toxic if swallowed, in contact with skin (readily absorbed) or inhaled. Therefore this reagent should be handled with care and adequate safety measures should be taken during the synthesis and large scale reactions should be avoided. Moreover, it forms explosive metal azides if it reacts with lead or copper.

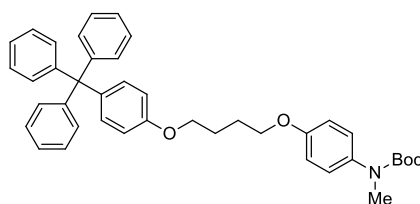
Under Ar, to a solution of **181** (309 mg, 0.563 mmol) in anhydrous DMF (15 mL) was added NaN₃ (109 mg, 1.68 mmol). The suspension was stirred for 15 h at 70 °C. The mixture was diluted with CH₂Cl₂ (30 mL) and washed with H₂O (3 × 30 mL). Subsequently, the aqueous phase was extracted with CH₂Cl₂ (2 × 70 mL). The combined organic layers were dried over anhydrous Na₂SO₄ and the solvent was evaporated under reduced pressure. The crude material was purified by column chromatography (SiO₂, hexane/CH₂Cl₂ 60:40) to give **171** (172 mg, 73%) as a white solid. ¹H NMR (400 MHz, CDCl₃): δ = 7.27 – 7.15 (m, 15H), 7.10 (d, *J* = 8.9 Hz, 2H), 6.77 (d, *J* = 8.9 Hz, 2H), 4.02 (t, *J* = 5.9 Hz, 2H), 3.51 (t, *J* = 6.7 Hz, 2H), 2.03 (p, *J* = 6.3 Hz, 2H). ¹³C NMR (101 MHz, CDCl₃): δ = 156.74, 147.14, 139.41, 132.37, 131.25, 127.57, 126.00, 113.38, 64.48, 64.46, 48.42, 28.98. IR (neat): ν = 3056, 2096, 1606, 1508, 1248, 1183, 764, 749, 701. Spectral data agree with those previously reported values.¹⁰⁰

Compound 166:



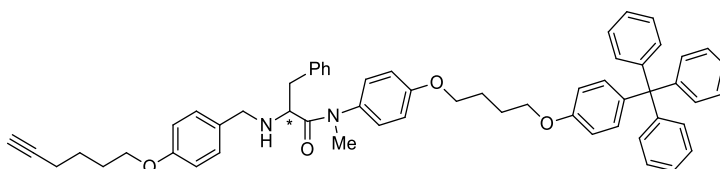
Under inert atmosphere, to a solution of **175** (5.00 g, 14.9 mmol) in anhydrous CH₃CN (150 mL) were added K₂CO₃ (10.3 g, 74.5 mmol) and 1,4-dibromobutane (8.85 mL, 74.1 mmol). The suspension was stirred overnight at 75 °C. The solvent was then removed under vacuum and the solid was dissolved in a mixture of CH₂Cl₂/H₂O (1:1, 400 mL). Layers were separated and the organic one was washed with H₂O (2 × 200 mL). The organic phase was dried over anhydrous Na₂SO₄ and the solvent was evaporated under reduced pressure. The crude material was purified by column chromatography (SiO₂, gradient from hexane to hexane/CH₂Cl₂ 90:10) to afford **166** (3.78 g, 54%) as a white solid. ¹H NMR (400 MHz, CDCl₃): δ = 7.27 – 7.16 (m, 15H), 7.10 (d, *J* = 8.9 Hz, 2H), 6.76 (d, *J* = 8.9 Hz, 2H), 3.97 (t, *J* = 6.0 Hz, 2H), 3.48 (t, *J* = 6.6 Hz, 2H), 2.06 (m, 2H), 1.93 (m, 2H). ¹³C NMR (101 MHz, CDCl₃): δ = 156.96, 147.18, 139.22, 132.36, 131.26, 127.56, 125.99, 113.35, 66.83, 64.47, 33.63, 29.68, 28.12. IR (neat): ν = 3055, 1607, 1507, 1251, 1183, 1035, 827, 764, 750, 702. HR-MS (EI⁺): *m/z*: 470.1245 [M]⁺ (calcd for C₂₉H₂₇OBr: 470.1245).

Compound 182:



^1H NMR (500 MHz, CDCl_3): δ = 7.26 – 7.16 (m, 20H), 7.11 (d, J = 8.7 Hz, 2H), 6.95 (d, J = 5.5 Hz, 2H), 6.84 – 6.68 (m, 4H), 5.20 (d, J = 9.1 Hz, 1H), 4.52 (q, J = 7.9 Hz, 1H), 4.03 (m, 4H), 3.17 (s, 3H), 2.89 (dd, J = 13.3, 7.4 Hz, 1H), 2.71 (dd, J = 13.3, 7.4 Hz, 1H), 1.98 (m, 4H), 1.38 (s, 9H). ^{13}C NMR (126 MHz, CDCl_3): δ = 172.19, 158.54, 157.02, 154.85, 147.15, 139.07, 136.78, 135.27, 132.32, 131.23, 129.55, 128.47, 128.41, 127.52, 126.74, 125.95, 115.39, 113.34, 79.47, 67.80, 67.36, 64.42, 52.20, 39.96, 37.83, 28.43, 26.15, 26.13. IR (neat): ν = 3307, 2922, 2852, 1711, 1652, 1509, 1245, 1172, 764, 750, 702. HR-MS (ESI⁺): m/z : 783.3771 [$\text{M}+\text{Na}$]⁺ (calcd for $\text{C}_{50}\text{H}_{52}\text{N}_2\text{O}_5\text{Na}$: 783.3774); 761.3951 [$\text{M}+\text{H}$]⁺ (calcd for $\text{C}_{50}\text{H}_{53}\text{N}_2\text{O}_5$: 761.3954). Spectral data are similar for both enantiomers except for the optical rotation: (*R*)-**168**: $[\alpha]_D^{20}$ = -4.2° (c 1, CH_2Cl_2); (*S*)-**168**: $[\alpha]_D^{20}$ = $+4.0^\circ$ (c 1, CH_2Cl_2).

Compounds (*R*)/(*S*)-**170**:



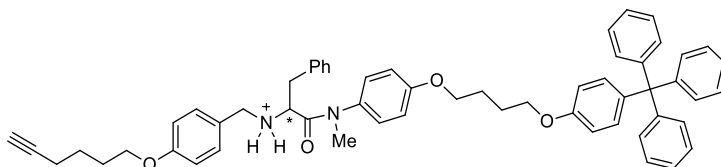
For the synthesis of (*R*)-**170**: To a solution of (*R*)-**168** (226 mg, 0.297 mmol) in CH_2Cl_2 (10 mL) was added $\text{CF}_3\text{CO}_2\text{H}$ (4 mL). The mixture was stirred for 4 h at room temperature and the solvent was evaporated under reduced pressure. The solid was dissolved in anhydrous MeOH (15 mL). Under an Ar atmosphere, Et_3N (1.6 mL) and **169** (60 mg, 0.297 mmol) were added. The mixture was stirred for 24 h at room temperature. Subsequently, NaBH_4 (50 mg, 1.33 mmol) and dry THF (5 mL) were added. The solution was stirred for 18 h at room temperature. Then, H_2O (15 mL) was added and the solution was stirred for another 30 min at room temperature. The product was extracted with CH_2Cl_2 (3 \times 30 mL). The combined organic phases were dried over anhydrous Na_2SO_4 and the solvent was evaporated under vacuum. The crude material was purified by column chromatography (SiO_2 , Hexane/EtOAc 40:60 to 20:80) to yield (*R*)-**170** (80 mg, 32%) as a white solid.

For the synthesis of (*S*)-**170**: This enantiomer was synthesized following the same procedure starting from (*S*)-**168** (163 mg, 0.214 mmol) and affording (*S*)-**170** (62 mg, 34%) as a white solid.

^1H NMR (500 MHz, CDCl_3): δ = 7.26 – 7.15 (m, 20H), 7.11 (m, 4H), 6.99 (d, J = 6.4 Hz, 2H), 6.77 (d, J = 8.3 Hz, 4H), 6.64 (d, J = 8.4 Hz, 2H), 4.03 – 3.93 (m, 6H), 3.70 (d, J = 12.6 Hz, 1H), 3.49 – 3.40 (m, 2H), 3.16 (s, 3H), 2.84 (dd, J = 12.9, 8.3 Hz, 1H), 2.77 (dd, J = 13.0, 6.2 Hz, 1H), 2.26 (td, J = 7.1, 2.6 Hz, 2H), 1.99 – 1.83 (m, 7H), 1.71 (p, J = 7.2 Hz, 2H). ^{13}C NMR (126 MHz, CDCl_3): δ = 174.83, 158.26, 158.12, 156.99, 147.13, 139.13, 138.28, 135.57, 132.33, 132.13, 131.21, 129.72, 129.27, 128.57, 128.30, 127.53, 126.50, 125.97, 115.10, 114.40, 113.31, 84.21, 68.78, 67.84, 67.42, 67.36, 64.42, 59.38, 51.22, 40.61, 37.67, 28.44, 26.13, 25.19, 18.29. IR (neat): ν = 3297, 2923, 2852, 1658, 1509, 1245, 1180, 1032,

831, 750, 701. HR-MS (ESI⁺): m/z : 847.4476 [M+H]⁺ (calcd for C₅₈H₅₉N₂O₄: 847.4475). Spectral data are similar for both enantiomers except for the optical rotation: (*R*)-**170**: $[\alpha]_D^{20} = -32.8^\circ$ (c 0.5, CH₂Cl₂); (*S*)-**170**: $[\alpha]_D^{20} = +32.1^\circ$ (c 0.5, CH₂Cl₂).

Compounds (*R*)/(*S*)-170-H⁺·PF₆⁻:

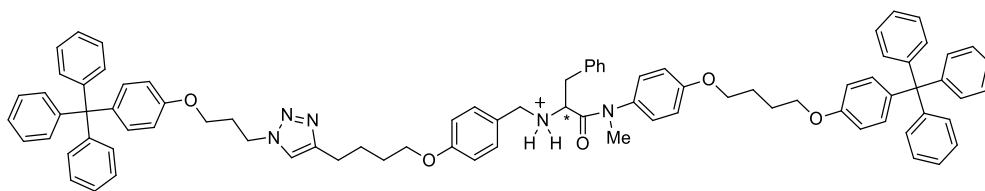


For the synthesis of (*R*)-**170-H⁺·PF₆⁻**: Under an Ar atmosphere, to a solution of (*R*)-**170** (80 mg, 0.094 mmol) in CH₂Cl₂ (5 mL) was added HCl (1.0 M in Et₂O, 1.4 mL, 1.4 mmol). The solution was stirred for 8 h at room temperature. Subsequently the solvent was removed under reduced pressure and the solid was dissolved in CH₂Cl₂ (5 mL). To this solution were added acetone (10 mL), H₂O (10 mL) and an excess of KPF₆. The mixture was stirred for 16 h at room temperature. The resulting mixture was diluted with H₂O (50 mL) and extracted with CH₂Cl₂ (3 × 50 mL). The combined extracts were dried over anhydrous Na₂SO₄ and the solvent was evaporated under vacuum to yield (*R*)-**170-H⁺·PF₆⁻** (92 mg, 98%) as a white solid.

For the synthesis of (*S*)-**170-H⁺·PF₆⁻**: This enantiomer was synthesized following the same procedure starting from (*S*)-**170** (134 mg, 0.158 mmol) and yielding (*S*)-**170-H⁺·PF₆⁻** (143 mg, 91%) as a white solid.

¹H NMR (500 MHz, CDCl₃): $\delta = 7.27 - 7.14$ (m, 22H), 7.11 (d, $J = 8.9$ Hz, 2H), 6.86 – 6.76 (m, 8H), 4.17 (d, $J = 13.0$ Hz, 1H), 4.11 – 3.91 (m, 8H), 3.21 (s, 3H), 3.07 (d, $J = 6.9$ Hz, 2H), 2.26 (td, $J = 7.0, 2.6$ Hz, 2H), 2.03 – 1.85 (m, 7H), 1.69 (p, $J = 7.1$ Hz, 2H). ¹³C NMR (126 MHz, CDCl₃): $\delta = 167.17, 160.47, 159.42, 157.01, 147.16, 139.17, 132.97, 132.90, 132.36, 131.40, 131.24, 129.48, 129.46, 128.28, 128.20, 127.56, 125.99, 120.87, 116.11, 115.49, 113.34, 84.06, 68.97, 68.15, 67.62, 67.37, 64.45, 58.74, 51.44, 38.82, 36.56, 28.28, 26.15, 26.13, 25.09, 18.30$. IR (neat): $\nu = 3295, 2937, 1648, 1509, 1248, 1181, 837, 750, 701$. HR-MS (ESI⁺): m/z : 847.4479 [M-PF₆⁻]⁺ (calcd for C₅₈H₅₉N₂O₄: 847.4475). Spectral data are similar for both enantiomers except for the optical rotation: (*R*)-**170-H⁺·PF₆⁻**: $[\alpha]_D^{20} = -46.8^\circ$ (c 0.25, CH₂Cl₂); (*S*)-**170-H⁺·PF₆⁻**: $[\alpha]_D^{20} = +42.7^\circ$ (c 0.25, CH₂Cl₂).

Compounds (*R*)/(*S*)-183-H⁺·PF₆⁻:

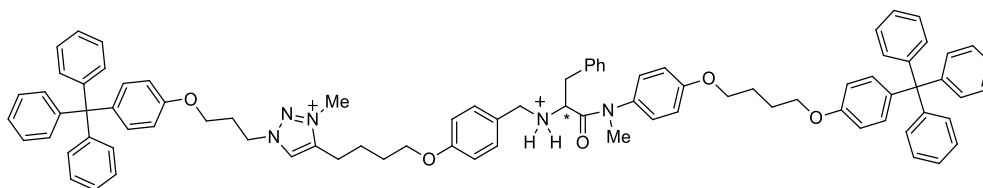


For the synthesis of (*R*)-**183-H⁺**·PF₆⁻: To a degassed solution of (*R*)-**170-H⁺**·PF₆⁻ (14 mg, 0.014 mmol) in anhydrous CH₂Cl₂ (3 mL) were added **171** (12 mg, 0.028 mmol), Cu(CH₃CN)₄PF₆ (3 mg, 0.007 mmol) and TBTA (4 mg, 0.007 mmol). The solution was stirred for 48 h at room temperature. The mixture was diluted with CH₂Cl₂ (40 mL) and washed with an aqueous solution of Na₄EDTA (0.1 M, 3 × 25 mL). The organic layer was dried over Na₂SO₄ and the solvent was removed under reduced pressure. The crude material was purified by gel permeation chromatography (Bio-Beads® S-X1, CH₂Cl₂). The resulting solid was dissolved in CH₂Cl₂ (10 mL) and HCl (1.0 M in Et₂O, 1.0 mL) was added under inert atmosphere. The solution was stirred for 3 h at room temperature. The solvent was then evaporated under vacuum. Subsequently, the solid was dissolved in CH₂Cl₂ (5 mL) and acetone (10 mL), H₂O (10 mL) and an excess of KPF₆ were added. The mixture was stirred overnight at room temperature. The resulting mixture was diluted with H₂O (20 mL) and extracted with CH₂Cl₂ (2 × 25 mL). The combined organic layers were dried over anhydrous Na₂SO₄ and concentrated to dryness to yield (*R*)-**183-H⁺**·PF₆⁻ (19 mg, 95%) as a white solid.

For the synthesis of (*S*)-**183-H⁺**·PF₆⁻: This enantiomer was obtained following the same procedure starting from (*S*)-**170-H⁺**·PF₆⁻ (62 mg, 0.062 mmol) and yielding (*S*)-**183-H⁺**·PF₆⁻ (52 mg, 59%) as a white solid.

¹H NMR (500 MHz, CDCl₃): δ = 7.33 (s, 1H), 7.25 – 7.15 (m, 37H), 7.10 (m, 4H), 6.89 (m, 2H), 6.81 – 6.71 (m, 8H), 4.51 (t, *J* = 6.9 Hz, 2H), 4.19 – 4.12 (m, 2H), 4.06 – 3.85 (m, 9H), 3.22 (s, 3H), 3.09 (d, *J* = 7.2 Hz, 2H), 2.66 (br, 2H), 2.33 (p, *J* = 6.4 Hz, 2H), 1.98 (br, 4H), 1.74 (br, 4H). ¹³C NMR (126 MHz, CDCl₃): δ = 167.11, 160.43, 159.37, 157.04, 156.54, 147.78, 147.17, 147.08, 139.59, 139.12, 133.12, 132.94, 132.40, 132.34, 131.50, 131.27, 131.24, 131.20, 129.58, 129.37, 128.23, 128.18, 127.57, 127.55, 126.02, 125.98, 121.70, 121.06, 116.11, 115.43, 113.36, 68.14, 67.76, 67.40, 64.44, 64.19, 59.12, 51.41, 47.31, 38.74, 36.72, 30.12, 29.84, 28.64, 26.14, 26.10, 25.92, 25.18. IR (neat): ν = 2936, 1658, 1608, 1509, 1275, 1257, 1182, 844, 764, 750, 702. HR-MS (ESI⁺): *m/z*: 1266.6466 [M–PF₆]⁺ (calcd for C₈₆H₈₄N₅O₅: 1266.6472). Spectral data are similar for both enantiomers except for the optical rotation: (*R*)-**183-H⁺**·PF₆⁻: [α]_D²⁰ = –22.3° (c 0.33, CHCl₃); (*S*)-**183-H⁺**·PF₆⁻: [α]_D²⁰ = +22.1° (c 0.33, CHCl₃).

Compounds (*R*)/(*S*)-**184-H⁺**·2PF₆⁻:

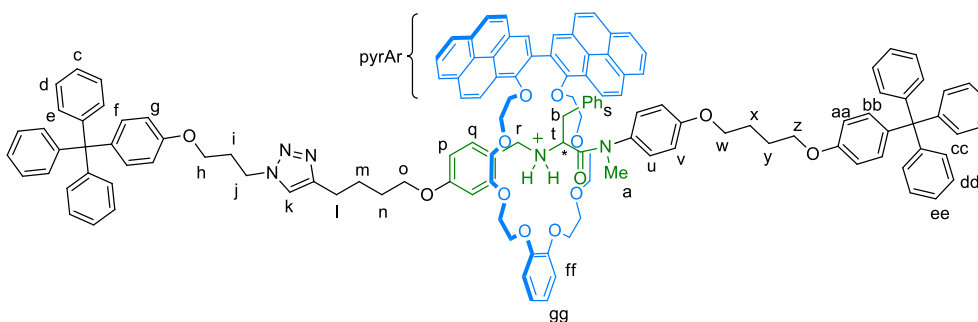


Compounds (*R*)- and (*S*)-**184-H⁺**·2PF₆⁻ were prepared adapting the method reported by Zhu.³⁵¹ For the synthesis of (*R*)-**184-H⁺**·2PF₆⁻: Under Ar, a solution of (*R*)-**183-H⁺**·PF₆⁻ (17 mg, 12 μmol) in iodomethane (4 mL) was stirred for 4 days at room temperature. The solvent was removed under reduced pressure. Then, the solid was dissolved in CH₂Cl₂ (5 mL) and acetone (10 mL), H₂O (10 mL) and an excess of KPF₆ were added. The mixture was stirred for 18 h at room temperature. The resulting mixture was diluted with H₂O (25 mL) and extracted with CH₂Cl₂ (3 × 30 mL). The combined extracts were dried over anhydrous Na₂SO₄ and were concentrated to dryness. The crude material was purified by preparative TLC (SiO₂, CH₂Cl₂/MeOH 98:2). The resulting solid was dissolved in CH₂Cl₂ (10 mL) and HCl (1.0 M in Et₂O, 1.0 mL) was added under inert atmosphere. The solution was stirred for 5 h at room temperature. The solvent was then evaporated under vacuum. Subsequently, the solid was dissolved in CH₂Cl₂ (2.5 mL); acetone (5 mL), H₂O (5 mL) and an excess of KPF₆ were added. The mixture was stirred overnight at room temperature. The mixture was diluted with H₂O (10 mL) and extracted with CH₂Cl₂ (2 × 20 mL). The combined organic layers were dried over anhydrous Na₂SO₄ and the solvent was evaporated under vacuum to yield (*R*)-**184-H⁺**·2PF₆⁻ (11 mg, 58%) as a white solid.

For the synthesis of (*S*)-**184-H⁺**·2PF₆⁻: This enantiomer was synthesized following the same procedure starting from (*S*)-**183-H⁺**·PF₆⁻ (21 mg, 15 μmol) and affording (*S*)-**184-H⁺**·2PF₆⁻ (23 mg, 98%) as a white solid.

¹H NMR (500 MHz, CDCl₃): δ = 8.12 (s, 1H), 7.25 – 7.13 (m, 37H), 7.09 (m, 4H), 6.94 (br, 2H), 6.79 – 6.66 (m, 8H), 4.67 (t, *J* = 7.0 Hz, 2H), 4.08 – 3.83 (m, 14H), 3.20 – 3.13 (m, 5H), 2.76 (t, *J* = 7.7 Hz, 2H), 2.40 (m, 2H), 1.96 (br, 4H), 1.81 (m, 4H). ¹³C NMR (126 MHz, CDCl₃): δ = 166.82, 160.24, 159.35, 157.06, 156.30, 147.18, 147.08, 144.83, 139.69, 139.09, 133.11, 132.86, 132.38, 132.33, 131.59, 131.24, 131.17, 129.63, 129.41, 128.19, 128.09, 127.60, 127.56, 126.01, 125.98, 116.10, 115.58, 113.38, 113.36, 68.11, 67.46, 67.25, 64.46, 63.87, 59.58, 51.37, 47.74, 38.75, 37.32, 32.07, 29.60, 29.51, 29.42, 29.09, 28.12, 26.15, 26.09. IR (neat): ν = 2925, 1654, 1608, 1509, 1275, 1259, 1182, 837, 764, 750, 702, 558. HR-MS (ESI⁺): *m/z*: 1280.6637 [M–H⁺–2PF₆⁻]⁺ (calcd for C₈₇H₈₆N₅O₅: 1280.6629); 1426.6366 [M–PF₆⁻]⁺ (calcd for C₈₇H₈₇N₅O₅PF₆: 1426.6349). Spectral data are similar for both enantiomers except for the optical rotation: (*R*)-**184-H⁺**·2PF₆⁻: [α]_D²⁰ = –5.5° (c 0.3, CHCl₃); (*S*)-**184-H⁺**·2PF₆⁻: [α]_D²⁰ = +3.9° (c 0.3, CHCl₃).

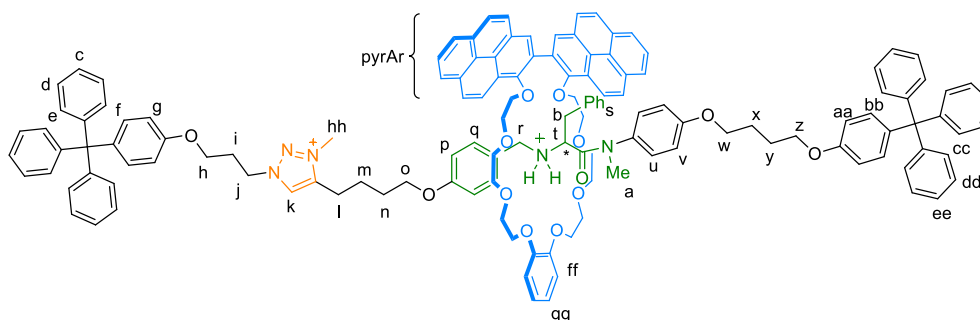
³⁵¹ S. Chen, Y. Wang, T. Nie, C. Bao, C. Wang, T. Xu, Q. Lin, D.-H. Qu, X. Gong, Y. Yang, L. Zhu, H. Tian, *J. Am. Chem. Soc.* **2018**, *140*, 17992-17998.

Compounds (R)/(S)-185-H⁺·PF₆⁻:

For the synthesis of (*R*)-**185-H⁺·PF₆⁻**: A solution of (*R*)-**170-H⁺·PF₆⁻** (17 mg, 0.017 mmol) and **165** (26 mg, 0.034 mmol) in CH₂Cl₂ (8 mL) was stirred for 10 min at room temperature. The solvent was removed under reduced pressure and the solid was redissolved in CH₂Cl₂ (1.5 mL). Under Ar, to this solution were added **171** (14 mg, 0.034 mmol), Cu(CH₃CN)₄PF₆ (3 mg, 0.008 mmol) and TBTA (5 mg, 0.008 mmol). The mixture was stirred for 3 days at room temperature. The resulting solution was diluted with CH₂Cl₂ (25 mL) and washed with an aqueous solution of Na₄EDTA (0.1 M, 2 × 25 mL). The organic layer was dried over Na₂SO₄ and the solvent was evaporated under vacuum. The crude material was purified by gel permeation chromatography (Bio-Beads® S-X1, CH₂Cl₂) to afford (*R*)-**185-H⁺·PF₆⁻** (13 mg, 35%) as a brown solid.

For the synthesis of (*S*)-**185-H⁺·PF₆⁻**: This enantiomer was synthesized following the same procedure starting from (*S*)-**170-H⁺·PF₆⁻** (17 mg, 0.017 mmol) and affording (*S*)-**185-H⁺·PF₆⁻** (7 mg, 19%) as a brown solid.

¹H NMR (500 MHz, CDCl₃) δ = 8.57 – 8.45 (m, 2H, H_{pyrAr}), 8.38 – 7.86 (m, 14H, H_{pyrAr}), 7.48 (m, 1H, H_k), 7.28 – 7.15 (m, 37H, H_{c+d+e+q+s+u+cc+dd+ee}), 7.09 (m, 4H, H_{f+bb}), 6.94 – 6.57 (m, 12H, H_{g+aa+ff+gg+p/v/s}), 5.97 (d, *J* = 7.1 Hz, 1H, H_{p/v/s}), 5.63 (d, *J* = 7.9 Hz, 1H, H_{p/v/s}), 4.58 (br, 2H, H_i), 4.36 – 3.08 (m, 35H, H_{macCH2+h+o+r+t+w+z}), 2.75 (br, 4H, H_{l+b}), 2.41 (m, 2H, H_i), 2.32 (s, 3H, H_a), 2.05 – 1.93 (m, 4H, H_{x+y}), 1.71 – 1.48 (m, 4H, H_{m+n}). ¹³C NMR (126 MHz, CDCl₃) δ = 165.98, 159.65, 158.67, 157.01, 156.63, 152.46, 150.52, 147.89, 147.13, 146.94, 139.44, 139.22, 132.37, 131.76, 131.22, 130.00, 129.60, 128.92, 128.66, 128.13, 127.86, 127.56, 127.19, 127.05, 126.91, 126.78, 126.60, 125.99, 125.76, 125.61, 125.44, 125.29, 125.17, 124.88, 124.71, 124.35, 122.46, 122.33, 122.20, 121.60, 114.08, 113.89, 113.44, 113.34, 76.00, 74.54, 73.28, 72.60, 71.63, 70.72, 70.00, 67.54, 67.42, 66.80, 64.43, 58.68, 50.12, 38.44, 37.95, 37.80, 37.44, 32.07, 30.30, 29.84, 28.64, 26.28, 25.37. IR (neat): ν=2924, 1599, 1505, 1451, 1275, 1258, 1118, 1046, 843, 764, 750, 702. HR-MS (ESI⁺): *m/z*: 2038.9519 [M-PF₆⁻]⁺ (calcd for C₁₃₆H₁₂₈N₅O₁₃: 2038.9509). Spectral data are similar for both enantiomers except for the optical rotation: (*R*)-**185-H⁺·PF₆⁻**: [α]_D²⁰ = -2.9° (c 0.2, CH₂Cl₂); (*S*)-**185-H⁺·PF₆⁻**: [α]_D²⁰ = +4.7° (c 0.2, CH₂Cl₂).

Compounds (R)/(S)-162-H⁺·2PF₆⁻:

For the synthesis of (*R*)-**162-H⁺·2PF₆⁻**: Under inert atmosphere, a solution of (*R*)-**185-H⁺·PF₆⁻** (4 mg, 1.9 μmol) in iodomethane (4 mL) was stirred for 4 days at room temperature protected from light. The solvent was evaporated under vacuum. Subsequently, the solid was dissolved in CH₂Cl₂ (2 mL); acetone (5 mL), H₂O (5 mL) and an excess of KPF₆ were added. The mixture was stirred for 5 h at room temperature protected from light. The resulting mixture was diluted with H₂O (10 mL) and extracted with CH₂Cl₂ (3 × 25 mL). The combined organic layers were dried over anhydrous Na₂SO₄ and the solvent was removed under reduced pressure. The crude material was purified by preparative TLC (SiO₂, CH₂Cl₂/MeOH 96:4) to yield (*R*)-**162-H⁺·2PF₆⁻** (3 mg, 68%) as a brown solid.

For the synthesis of (*S*)-**162-H⁺·2PF₆⁻**: This enantiomer was synthesized following the same procedure starting from (*S*)-**185-H⁺·PF₆⁻** (5 mg, 2.3 μmol) and affording (*S*)-**162-H⁺·2PF₆⁻** (3 mg, 55%) as a brown solid.

¹H NMR (400 MHz, CDCl₃) δ = 8.64 – 7.96 (m, 17H, H_{pyrAr+k}), 7.34 – 7.04 (m, 41H, H_{c+d+e+f+g+h+i+j+k+l+m+n+o+p+q+r+s+t+u+v+w+x+y+z}), 6.95 – 6.69 (m, 12H, H_{g+aa+ff+gg+p/v/s}), 5.94 (br, 2H, H_{p/v/s}), 4.33 – 3.15 (m, 44H, H_{macCH2+h+j+l+o+r+t+b+w+z+hh}), 2.36 (m, 2H, H_i), 2.31 (s, 3H, H_a), 2.06 – 1.95 (m, 4H, H_{x+y}), 1.66 (br, 4H, H_{m+n}). ¹³C NMR (126 MHz, CDCl₃) δ = 147.17, 147.12, 132.52, 132.41, 132.38, 132.21, 131.49, 131.44, 131.24, 131.05, 130.21, 129.61, 128.63, 127.81, 127.59, 127.40, 127.32, 127.22, 127.09, 126.05, 125.98, 125.78, 125.08, 125.03, 124.98, 124.94, 122.35, 113.72, 113.67, 113.34, 113.23, 74.21, 72.66, 70.87, 70.72, 70.43, 69.85, 64.46, 64.28, 61.40, 40.32, 37.96, 32.08, 30.29, 29.85, 29.51, 28.63, 26.30, 22.86. IR (neat): ν = 2922, 2853, 1660, 1506, 1456, 1254, 1109, 841, 753, 702, 558. HR-MS (ESI⁺): *m/z*: 2052.9675 [M–H⁺–2PF₆⁻]⁺ (calcd for C₁₃₇H₁₃₀N₅O₁₃: 2052.9665); 2198.9368 [M–PF₆⁻]⁺ (calcd for C₁₃₇H₁₃₁N₅O₁₃PF₆: 2198.9385). Spectral data are similar for both enantiomers except for the optical rotation: (*R*)-**162-H⁺·2PF₆⁻**: [α]_D²⁰ = +14.1° (c 0.1, CHCl₃); (*S*)-**162-H⁺·2PF₆⁻**: [α]_D²⁰ = –14.2° (c 0.1, CHCl₃).

Compound 162·PF₆⁻

To obtain **162·PF₆⁻** for the NMR experiments: An excess of K₂CO₃ was added to a degassed solution of **162-H⁺·2PF₆⁻** (1.2 mg, 0.51 μmol) in CDCl₃ (400 μL). The suspension was shaken for 1 min and subsequently filtered through a 0.2 μm filter to remove the excess of base. The resulting solution was analyzed by NMR.

5.3. HPLC method

The mobile phase gradient used is shown in the following table.

Table 11. Solvent gradient used for the HPLC analysis.

Time (min)	CH ₂ Cl ₂	Methanol
0	100	0
15	99	1
20	98	2
25	96	4
30	95	5
35	92	8
40	90	10
43	85	15
47	93	7
50	100	0

5.4. Photophysical properties

The spectra were recorded at *ca.* 1 × 10⁻⁵ M (for (R)/(S)-**162-H⁺·2PF₆⁻**, (R)/(S)-**162·PF₆⁻**, **165** and (R)/(S)-**185-H⁺·PF₆⁻**), and *ca.* 1 × 10⁻⁴ M (for (R)/(S)-**184-H⁺·2PF₆⁻**, (R)/(S)-**183-H⁺·PF₆⁻** and the partial UV-Vis and ECD spectra of (R)/(S)-**162-H⁺·2PF₆⁻** and (R)/(S)-**185-H⁺·PF₆⁻**) in HPLC grade CHCl₃ at 20 °C. For absorbance and fluorescence measurements, a fixed slit-width of 1 mm and 0.5 s of integration time were selected. For ECD measurements, a fixed slit-width of 1.000 mm and 0.5 s of integration time were selected. The ECD spectra shown correspond each one to an average spectrum of 30 scans. For CPL measurements, a fixed slit-width of 3.000 mm, a fixed excitation wavelength of 355 nm and 1.0 s of integration time were selected. Each CPL spectra correspond to an average spectrum calculated after 200 scans. UV-Vis absorption, fluorescence, ECD and CPL spectra of (R)/(S)-**162-H⁺·2PF₆⁻**, (R)/(S)-**162·PF₆⁻**, (R)/(S)-**162-H⁺** (from the protonation of (R)/(S)-**162·PF₆⁻**) and the switching experiments were carried out under Ar with degassed solvent.

Quantum yields were determined by measuring both absorbance and fluorescence of compounds **162-H⁺·2PF₆⁻**, **162·PF₆⁻**, **162-H⁺** (from the protonation of **162·PF₆⁻**), **165**, **185-H⁺·PF₆⁻** in CHCl₃, using anthracene in EtOH as standard ($\Phi_r = 0.27$).³⁵² For the relative determination of the fluorescence quantum yield Φ in a series of solvents, the following equation was used:³⁵³

$$\Phi_x = \Phi_r \times \frac{F_x}{F_r} \times \frac{1 - 10^{-A_r(\lambda_{ex})}}{1 - 10^{-A_x(\lambda_{ex})}} \times \frac{n_x^2}{n_r^2} \quad (\text{Eq. 6})$$

The subscripts x and r refer respectively to the sample and a reference (standard) fluorophore with known quantum yield Φ_r in a specific solvent; F stands for the spectrally corrected, integrated fluorescence spectra; $A(\lambda_{ex})$ denotes the absorbance at the used excitation wavelength λ_{ex} ; and n represents the refractive index of the solvent (in principle at the average emission wavelength). To minimize inner filter effects, the absorbance at the excitation wavelength λ_{ex} was kept under 0.3. The measurements were performed using 10×10 mm cuvettes on non-degassed samples for **165** and **185-H⁺·PF₆⁻** and on degassed samples for **162-H⁺·2PF₆⁻**, **162·PF₆⁻** and **162-H⁺** (from the protonation of **162·PF₆⁻**).

Table 12. Quantum yields of rotaxanes and macrocycle.

Compound	Φ
162-H⁺·2PF₆⁻	0.11
162·PF₆⁻	0.11
162-H⁺ (from the protonation of 162·PF₆⁻)	0.11
165	0.18
185-H⁺·PF₆⁻	0.19

Switching experiments:

To obtain (S)-**162·PF₆⁻** for photophysical measurements: Under an Ar atmosphere, an excess of K₂CO₃ was added to a solution of (S)-**162-H⁺·2PF₆⁻** in CHCl₃ (1.2×10^{-5} mol L⁻¹, 2.5 mL). The suspension was shaken for 2 min and subsequently filtered through a 0.2 μ m filter to remove the excess of base.

³⁵² W. H. Melhuish, *J. Phys. Chem.* **1961**, *65*, 229-235.

³⁵³ a) B. Valeur, M. N. Berberan-Santos, *Molecular Fluorescence. Principles and Applications*, 2nd ed. Wiley-VCH: Weinheim, **2012**. b) J. Lakowicz, *Principles of Fluorescence Spectroscopy*, 3rd Ed. Springer-Verlag: New York, **2006**.

(*R*)-**162**·PF₆⁻ was obtained following the same procedure starting from (*R*)-**162**-H⁺·2PF₆⁻.

To obtain (*S*)-**162**-H⁺ for photophysical measurements: Under inert atmosphere, to a solution of (*S*)-**162**·PF₆⁻ in CHCl₃ (1.2×10^{-5} mol L⁻¹, 2.5 mL) was added a degassed solution of CF₃CO₂H in CHCl₃ (0.2 %, 17.3 μL, 15 equiv.). The resulting solution was shaken for 1 min.

(*R*)-**162**-H⁺ was obtained following the same procedure starting from (*R*)-**162**·PF₆⁻.

The *in situ* switching was carried out by repeatedly following the procedures described above on the same sample.

5.5. Statistical Analysis of the CPL data

5.5.1. Statistical analysis of the CPL spectra of rotaxane (*S*)-**162**

For the statistical analysis of the CPL spectra of (*S*)-**162**-H⁺·2PF₆⁻, (*S*)-**162**·PF₆⁻ and (*S*)-**162**-H⁺ obtained by reprotonation of (*S*)-**162**·PF₆⁻ with CF₃CO₂H we used the data of non-normalized ΔI (i. e. $I_L - I_R$) as recorded. The different CPL spectra represented in ΔI before normalization are shown in the following figure. It is important to highlight that each spectrum is the average of 200 scans.

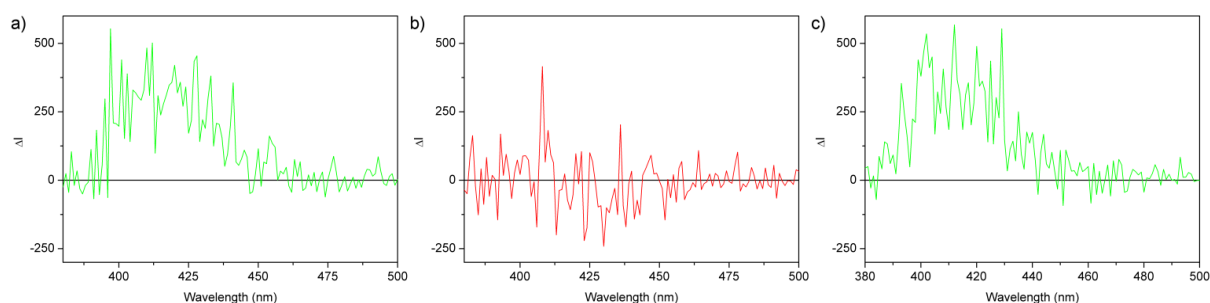


Figure 148. CPL ($\lambda_{\text{exc}} = 355$ nm) (*ca.* 1×10^{-5} M) spectra in non-normalized ΔI scale (CHCl₃) of: a) (*S*)-**162**-H⁺·2PF₆⁻. b) (*S*)-**162**·PF₆⁻. c) (*S*)-**162**-H⁺, obtained by protonation of **162**·PF₆⁻ with a solution of CF₃CO₂H in CHCl₃.

In this case, two different approaches were used, one based on the areas of the different spectra and the second one based on the ΔI values in a region of 26 nm width around the emission λ_{max} .

5.5.1.1. Statistical analysis based on the area

For this approach, we divided the spectra of the 200 scans recorded into 10 groups of 20 scans and calculated the corresponding average areas. With this 10 area values, a mean area and their standard deviations for the spectra of each compound were calculated. The data are shown in the following table and figure.

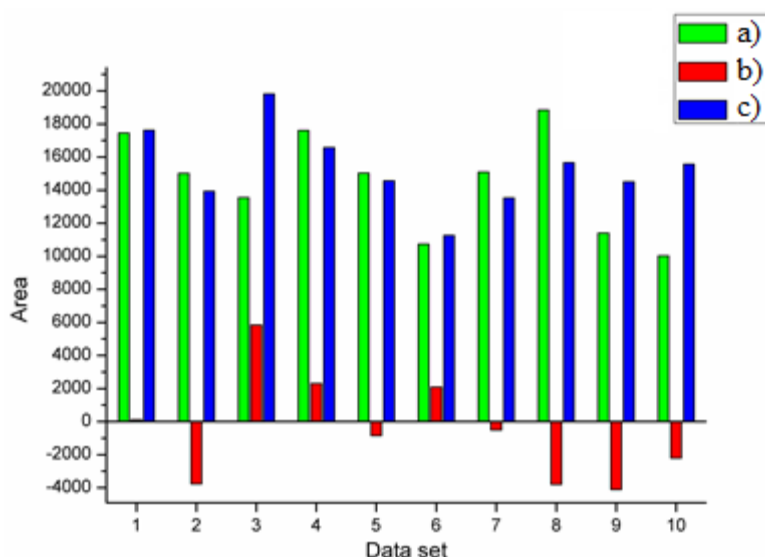


Figure 149. CPL ($\lambda_{\text{exc}} = 355 \text{ nm}$) (ca. $1 \times 10^{-5} \text{ M}$) spectra in non-normalized ΔI scale of: a) (S)-**162**-H⁺·2PF₆⁻. b) (S)-**162**·PF₆⁻. c) (S)-**162**-H⁺, obtained by protonation of **162**·PF₆⁻ with a solution of CF₃CO₂H in CHCl₃.

Table 13. Statistic parameters for the areas obtained from CPL spectra

	(S)- 162 -H ⁺ ·2PF ₆ ⁻	(S)- 162 ·PF ₆ ⁻	(S)- 162 -H ⁺ after reprotonation
Average area (\bar{x})	14469.250	-488.960 ^a	15300.45
Standard deviation (s)	3034.379	3209.730	2362.28
Variance (s ²)	9207455,916	10302366,673	5580366,798
Number of data	10	10	10

^a As the CPL signals can be positive or negative, negative values indicate that the spectra delimits a net area in the negative part of the scale.

- F-test

$$F = \frac{s_1^2}{s_2^2} \quad (s_1 > s_2)$$

$H_0 \equiv s_1^2 = s_2^2$ ($F_{\text{calc}} < F_{\text{tab}}$) Variances are not significantly different

$H_1 \equiv s_1^2 \neq s_2^2$ ($F_{\text{calc}} \geq F_{\text{tab}}$) Variances are significantly different

Table 14. F-test for the area data^a

	F _{calc}	Conclusion
(S)- 162 -H ⁺ ·2PF ₆ ⁻ vs (S)- 162 ·PF ₆ ⁻	1.119	$F_{\text{calc}} < F_{\text{tab}} \rightarrow H_0$
(S)- 162 ·PF ₆ ⁻ vs (S)- 162 -H ⁺ after reprotonation	1.846	$F_{\text{calc}} < F_{\text{tab}} \rightarrow H_0$
(S)- 162 -H ⁺ ·2PF ₆ ⁻ vs (S)- 162 -H ⁺ after reprotonation	1.650	$F_{\text{calc}} < F_{\text{tab}} \rightarrow H_0$

^a $F_{\text{tab}} (\alpha = 0.05; n_1 = n_2 = 10; df_1 = df_2 = 9) = 3.18$

Therefore, in all cases is concluded that the variances do not significantly differ.

- **t-test**

$$t = \frac{|\bar{x}_1 - \bar{x}_2|}{s_p \sqrt{\frac{1}{n_1} + \frac{1}{n_2}}} \quad (s_p = \sqrt{\frac{(n_1-1)s_1^2 + (n_2-1)s_2^2}{n_1 + n_2 - 2}})$$

- Comparison between "on" and "off" states

$H_0 \equiv \bar{X}_1 \text{ (on)} \leq \bar{X}_2 \text{ (off)}$ ($t_{\text{calc}} < t_{\text{tab}}$) Means are not significantly different

$H_1 \equiv \bar{X}_1 \text{ (on)} > \bar{X}_2 \text{ (off)}$ ($t_{\text{calc}} \geq t_{\text{tab}}$) Means are significantly different with the "on" state ((S)-162-H⁺) giving a higher signal than the "off" state ((S)-162-PF₆⁻)

Table 15. t-test for the area data of "on" and "off" states^a

	t_{calc}	Conclusion
(S)-162-H ⁺ ·2PF ₆ ⁻ vs (S)-162-PF ₆ ⁻	10.71	$t_{\text{calc}} > t_{\text{tab}} \rightarrow H_1$
(S)-162-PF ₆ ⁻ vs (S)-162-H ⁺ after reprotonation	12.53	$t_{\text{calc}} > t_{\text{tab}} \rightarrow H_1$

^a t_{tab} (one-tailed, 0.05; $n_1=n_2= 10$; $df = 18$) = 1.734; t_{tab} (one-tailed, 0.001; $n_1=n_2= 10$; $df = 18$) = 3.610

Therefore, the tests show that, at 95% confidence, and even at 99.9%, the signals observed for (S)-162-H⁺·2PF₆⁻ ("on I" state) and (S)-162-H⁺ obtained by protonation of 162·PF₆⁻ with a solution of CF₃CO₂H ("on II" state) are significantly higher from the signals of (S)-162-PF₆⁻ ("off" state).

- Comparison between "on" states

We also compared the signals of (S)-162-H⁺·2PF₆⁻ and (S)-162-H⁺ after reprotonation with CF₃CO₂H.

Table 16. t-test for the area data of (S)-162-H⁺·2PF₆⁻ and reprotonated (S)-162-H⁺

	t_{calc}	Conclusion
(S)-162-H ⁺ ·2PF ₆ ⁻ vs (S)-162-H ⁺ after reprotonation	0.68	$t_{\text{calc}} < t_{\text{tab}} \rightarrow H_0$

^a t_{tab} (two-tailed, 0.05; $n_1=n_2= 10$; $df = 18$) = 2.101; t_{tab} (two-tailed, 0.001; $n_1=n_2= 10$; $df = 18$) = 3.922

On the contrary, at the same level of confidence as the comparison between "on" and "off states" there are no significant differences between the signals of both "on" states ((S)-162-H⁺·2PF₆⁻ and reprotonated (S)-162-H⁺).

If we assume that due to the degradation, the signal of (S)-**162-H**⁺ after reprotonation can only diminish due to the degradation, then $H_1 \equiv \bar{X}_1 > \bar{X}_2$, and a one-tailed test would be the appropriate and the reference t values would have to be considered. However, the conclusion of the test would remain unaltered.

5.5.1.2. Statistical analysis based on the intensity

For this approach, we analyzed the non-normalized ΔI values between 400 and 425 nm (26 points). The data are shown in figure and table.

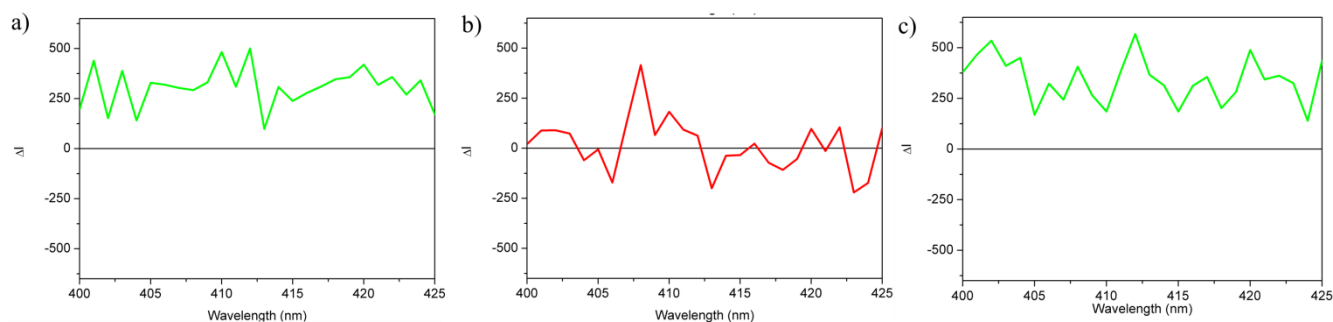


Figure 150. Partial CPL ($\lambda_{\text{exc}} = 355$ nm) (*ca.* 1×10^{-5} M) spectra in non-normalized ΔI scale (CHCl_3) of: a) (S)-**162-H**⁺·2PF₆⁻. b) (S)-**162**·PF₆⁻. c) (S)-**162-H**⁺, obtained by protonation of (S)-**162**·PF₆⁻ with a solution of CF₃CO₂H in CHCl_3 .

Table 17. Statistic parameters for the non-normalized ΔI values obtained from CPL spectra

	(S)- 162-H ⁺ ·2PF ₆ ⁻	(S)- 162 ·PF ₆ ⁻	(S)- 162-H ⁺ after reprotonation
Average ΔI (\bar{x})	308.08	15.39	342.34
Standard deviation (s)	97.56	132.92	110.97
Variance (s^2)	9517.387	17668.095	12315.404
Number of data	26	26	26

Table 18. F-test for the ΔI data^a

	F_{calc}	Conclusion
(S)- 162-H ⁺ ·2PF ₆ ⁻ vs (S)- 162 ·PF ₆ ⁻	1.856	$F_{\text{calc}} < F_{\text{tab}} \rightarrow H_0$
(S)- 162 ·PF ₆ ⁻ vs (S)- 162-H ⁺ after reprotonation	1.435	$F_{\text{calc}} < F_{\text{tab}} \rightarrow H_0$
(S)- 162-H ⁺ ·2PF ₆ ⁻ vs (S)- 162-H ⁺ after reprotonation	1.294	$F_{\text{calc}} < F_{\text{tab}} \rightarrow H_0$

^a $F_{\text{tab}} (\alpha = 0.05; n_1=n_2= 26; df_1 = df_2 = 25) = 1.96$

Therefore, in all cases is concluded that the variances do not significantly differ.

As we are comparing the data of the different (S)-**162** species, we consider the signal of the "on" state positive and higher than that of the "off" state.

Table 19. t-test for the ΔI data of "on" and "off" states^a

	t_{calc}	Conclusion
(S)- 162 -H ⁺ ·2PF ₆ ⁻ vs (S)- 162 ·PF ₆ ⁻	9.05	$t_{\text{calc}} > t_{\text{tab}} \rightarrow H_1$
(S)- 162 ·PF ₆ ⁻ vs (S)- 162 -H ⁺ after reprotonation	9.63	$t_{\text{calc}} > t_{\text{tab}} \rightarrow H_1$

^a t_{tab} (one-tailed, 0.05; $n_1=n_2= 26$; $df = 50$) = 1.676; t_{tab} (one-tailed, 0.001; $n_1=n_2= 26$; $df = 50$) = 3.262

Therefore, the tests based on ΔI bring the same conclusions than those based on the areas of the spectra. At 95% and even at 99.9% confidence level, the signal observed for (S)-**162**·PF₆⁻ ("off" state) is significantly different from the signals of (S)-**162**-H⁺·2PF₆⁻ ("on I" state) and (S)-**162**-H⁺ obtained by protonation of (S)-**162**·PF₆⁻ with a solution of CF₃CO₂H ("on II" state).

- Comparison between "on" states

Table 20. t-test for the ΔI data of (S)-**162**-H⁺·2PF₆⁻ and reprotonated (S)-**162**-H⁺

	t_{calc}	Conclusion
(S)- 162 -H ⁺ ·2PF ₆ ⁻ vs (S)- 162 -H ⁺ after reprotonation	1.18	$t_{\text{calc}} < t_{\text{tab}} \rightarrow H_0$

^a t_{tab} (two-tailed, 0.05; $n_1=n_2= 26$; $df = 50$) = 2.009; t_{tab} (two-tailed, 0.001; $n_1=n_2= 26$; $df = 50$) = 3.497

On the contrary, there are no significant differences between the signals of both "on" states ((S)-**162**-H⁺·2PF₆⁻ and reprotonated (S)-**162**-H⁺).

If we assume that due to the degradation, the signal of (S)-**162**-H⁺ after reprotonation can only diminish due to the degradation, then $H_1 \equiv \bar{X}_1 > \bar{X}_2$, and a one-tailed test would be the appropriate and the reference t values would have to be considered. However, the conclusion of the test would remain unaltered.

5.5.2. Statistical analysis of the CPL data of the operation cycles

Finally, we performed the statistical analysis of the CPL data obtained during the cycles of *in situ* switching of the CPL response. Having obtained the same conclusions either using areas or non-normalized ΔI intensities for (S)-**162**-H⁺·2PF₆⁻, (S)-**162**·PF₆⁻ and reprotonated (S)-**162**-H⁺, we used the non-normalized ΔI data between 400 and 420 nm (21 points).

Table 21 Statistic parameters for the non-normalized ΔI values obtained from CPL spectra

	Average ΔI (\bar{x})	Standard deviation (s)	Variance (s^2)	Number of data
(S)-162-H ⁺ ·2PF ₆ ⁻ (Cycle 0)	366.998	136.348	18590.7588	21
(S)-162·PF ₆ ⁻ (Cycle 0.5)	1.725	131.501	17292.6318	21
(S)-162-H ⁺ (Cycle 1)	236.414	146.668	21511.3817	21
(S)-162 (Cycle 1.5)	-15.402	122.639	15040.3481	21
(S)-162-H ⁺ (Cycle 2)	198.093	108.888	11856.5789	21
(S)-162 (Cycle 2.5)	26.115	111.771	12492.8418	21
(S)-162-H ⁺ (Cycle 3)	160.206	121.127	14671.6321	21

Table 22. F-test for the cycles ΔI data^a

"on" state vs "off" state	F _{calc}	Conclusion
Cycle 0 vs Cycle 0.5	1.075	F _{calc} < F _{tab} → H ₀
Cycle 0.5 vs Cycle 1	1.244	F _{calc} < F _{tab} → H ₀
Cycle 1 vs Cycle 1.5	1.430	F _{calc} < F _{tab} → H ₀
Cycle 1.5 vs Cycle 2	1.269	F _{calc} < F _{tab} → H ₀
Cycle 2 vs Cycle 2.5	1.054	F _{calc} < F _{tab} → H ₀
Cycle 2.5 vs Cycle 3	1.174	F _{calc} < F _{tab} → H ₀

^a F_{tab} ($\alpha = 0.05$; $n_1=n_2= 21$; $df_1 = df_2 = 20$) = 2.12

Therefore, in all cases is concluded that the variances do not significantly differ.

Table 23. t-test for the cycles ΔI data^a

"on" state vs "off" state	t _{calc}	Conclusion
Cycle 0 vs Cycle 0.5	8.84	t _{calc} > t _{tab} → H ₁
Cycle 0.5 vs Cycle 1	5.46	t _{calc} > t _{tab} → H ₁
Cycle 1 vs Cycle 1.5	6.04	t _{calc} > t _{tab} → H ₁
Cycle 1.5 vs Cycle 2	5.97	t _{calc} > t _{tab} → H ₁
Cycle 2 vs Cycle 2.5	5.05	t _{calc} > t _{tab} → H ₁
Cycle 2.5 vs Cycle 3	3.73	t _{calc} > t _{tab} → H ₁

^a t_{tab} (one-tailed, 0.05; $n_1=n_2= 21$; $df = 40$) = 1.684; t_{tab} (one-tailed, 0.001; $n_1=n_2= 21$; $df = 40$) = 3.307

Therefore, the tests performed show that at 95%, and even 99.9%, confidence level, the signals observed for different "on" states (cycle 0, 1, 2 and 3) is significantly higher than those corresponding to the "off" states (cycle 0.5, 1.5 and 2.5). Therefore, although there is a degradation of the system among these cycles, the clear difference between both CPL response states is maintained.

5.6. Single crystal X-ray diffraction analysis

Suitable crystals for X-ray diffraction analysis of **165**⊂KPF₆ were grown by slow evaporation of a solution of the complex in CHCl₃. The diffraction data were collected on a Bruker SMART APEX diffractometer equipped with an APEX detector using a Mo radiation source. The structure was solved with SHELXT³⁵⁴ 2018 and refined using the full-matrix least-squares against F^2 procedure with SHELX 2018³⁵⁵ using the WinGX32³⁵⁶ software. C–H hydrogen atoms were placed in idealized positions ($U_{eg}(H) = 1.2U_{eg}(C)$ or $U_{eg}(H) = 1.5U_{eg}(C)$) and were allowed to ride on their parent atoms.

The crystals obtained were of moderate quality, which, together with its low stability at low temperature that forced to collect the data at room temperature, meant that several restraints had to be used for some atom groups, especially for the PF₆ counterion. Hence, DANG, SADI, ISOR restraints had to be used. Moreover, for this PF₆ anion, some apparent disorder between two positions was found, which resulted in the use of PART instructions.

During the refinement the structure of the target molecule was established, but large residual electron density was still present. This electron density was located mainly in the void and corresponded to a disordered chloroform molecule, which could not be fully modeled. Therefore, the SQUEEZE³⁵⁷ routine included in PLATON³⁵⁸ was applied and a density of 446 e⁻/cell in an approximate 1476 Å³ volume was identified. Eight chloroform molecules per unit cell were introduced in the formula. This density was removed and the data refined against the model.

Summary of the X-ray diffraction measurement and refinement data: Chemical formula, C₅₂H₄₆Cl₆F₆KO₈P; M_r , 1195.66; crystal size [mm³], 0.460 × 0.340 × 0.200; temperature, 293(2) K; wavelength [Å], 0.71073 (Mo $K\alpha$), crystal system, monoclinic; space group, C2/c; a [Å], 13.3866(12); b [Å], 22.472(2); c [Å], 18.1039(17); α [°], 90; β [°], 99.497(2); γ [°], 90; V [Å³], 5371.3(9); Z , 4; ρ_{calcd} [Mg m⁻³], 1.479; μ [mm⁻¹], 0.501; $F(000)$, 2448; ϑ range [°], 1.789 to 28.053; hkl ranges, -17/17, -29/16, -23/23; reflections collected, 16688; independent reflections, 6016; R_{int} , 0.0241; completeness to $\vartheta = 25.242^\circ$, 99.9%; absorption correction, semi-empirical from equivalents; refinement method; full-matrix least-squares on F^2 ; Final R indices [$I > 2\sigma(I)$], $R_1 = 0.1142$, $wR_2 = 0.3619$; R indices (all data), $R_1 = 0.1546$, $wR_2 = 0.4004$; goodness-of-fit on F^2 , 1.343.

³⁵⁴ G. M. Sheldrick, *Acta Cryst.* **2015**, A71, 3-8.

³⁵⁵ a) G. M. Sheldrick, *Acta Cryst.* **2008**, A64, 112-122. b) G. M. Sheldrick, *Acta Cryst.* **2015**, C71, 3-8.

³⁵⁶ L. J. Farrugia, *J. Appl. Cryst.* **2012**, 45, 849-854.

³⁵⁷ A. L. Spek, *Acta Cryst.* **2015**, C71, 9-18.

³⁵⁸ A. L. Spek, *Acta Cryst.* **2009**, D65, 148-155.

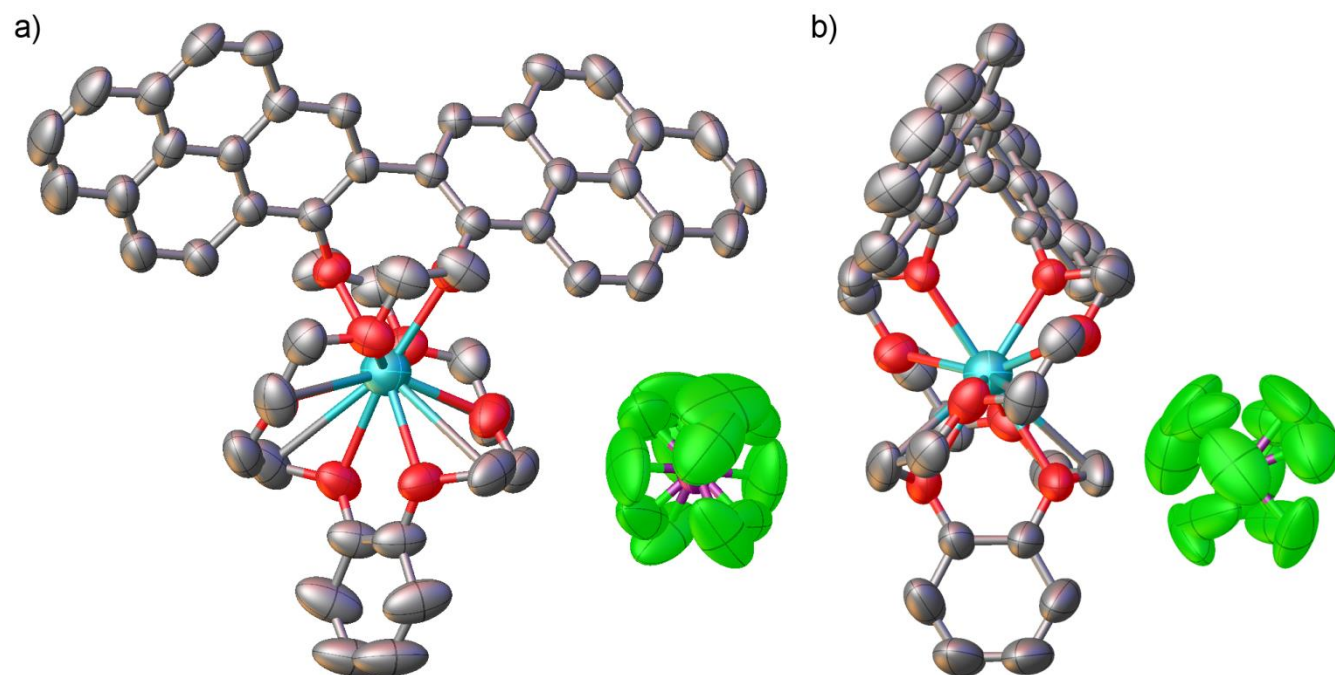


Figure 151. (a) Front and (b) side views of the ORTEP-type³⁵⁹ representation of the solid state structure of **165C**·KPF₆ showing the ellipsoids at 50% probability. Color code: C: gray, O: red, K: light blue, P: violet, Cl: green. Hydrogen atoms have been omitted for clarity.

³⁵⁹ The ellipsoid image was generated with the OLEX2 software package: O. V. Dolomanov, L. J. Bourhis, R. J. Gildea, J. A. K. Howard, H. Puschmann, *J. Appl. Cryst.* **2009**, *42*, 339-341.

5.7. NMR spectra of key compounds

Compound 165:

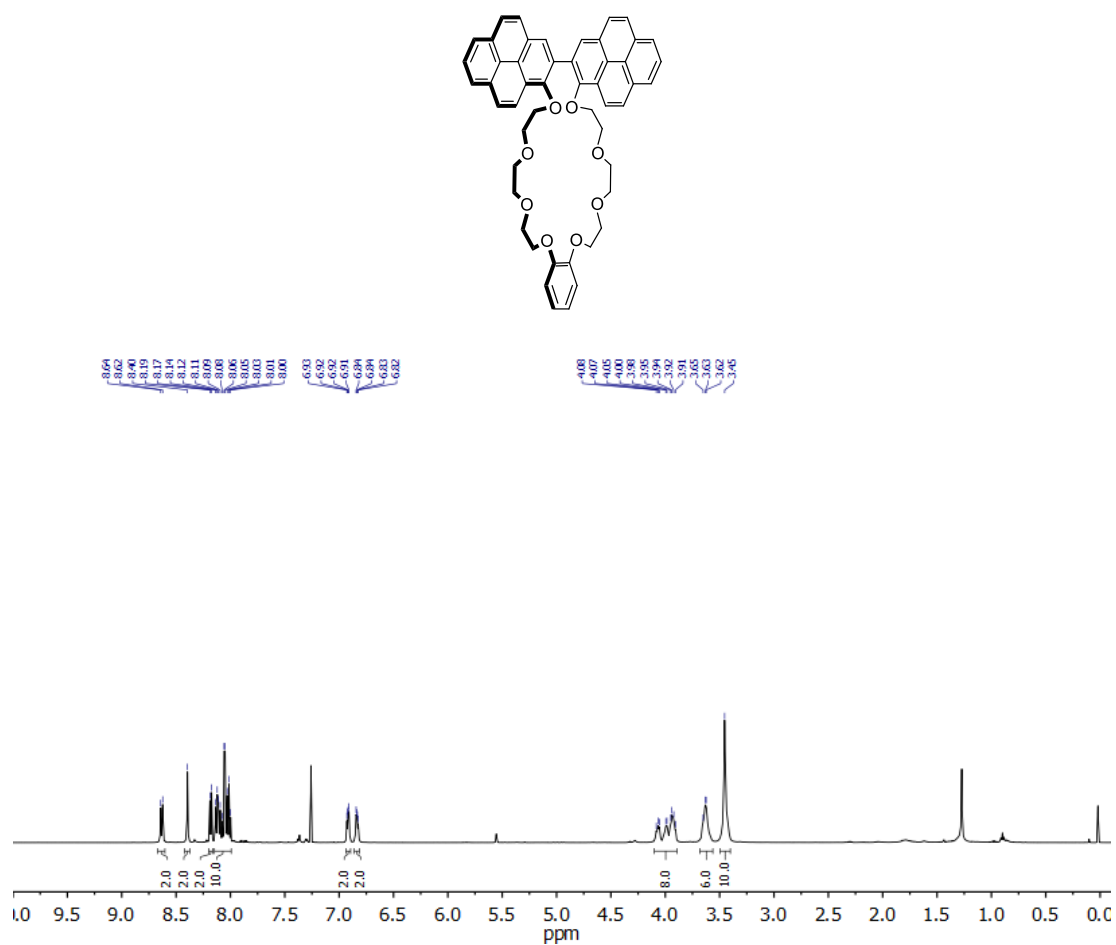


Figure 152. ^1H NMR (500 MHz, CDCl_3) spectrum of 165.

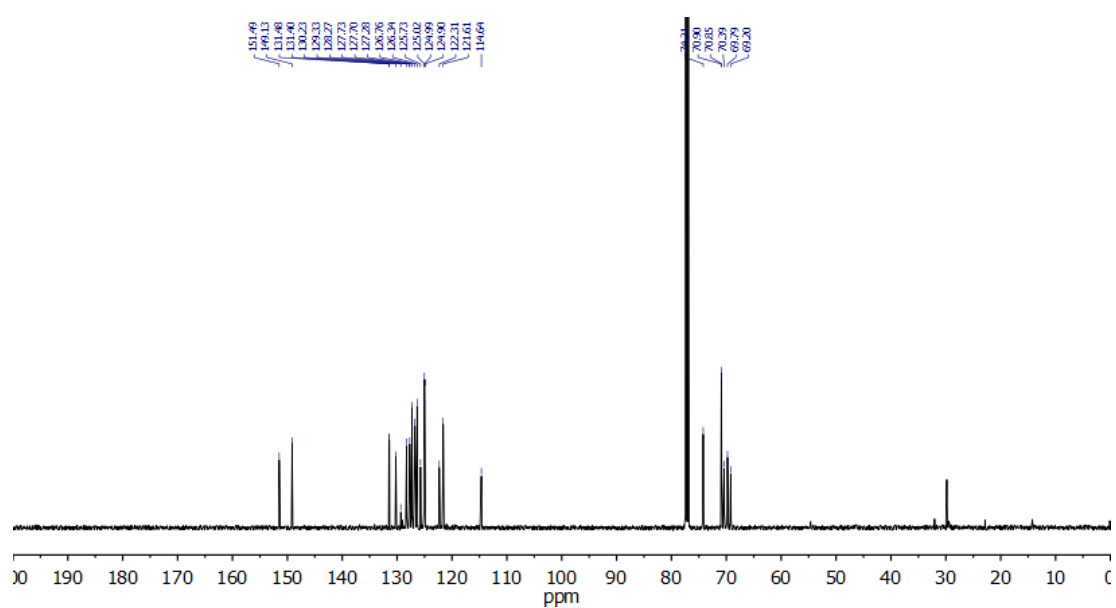
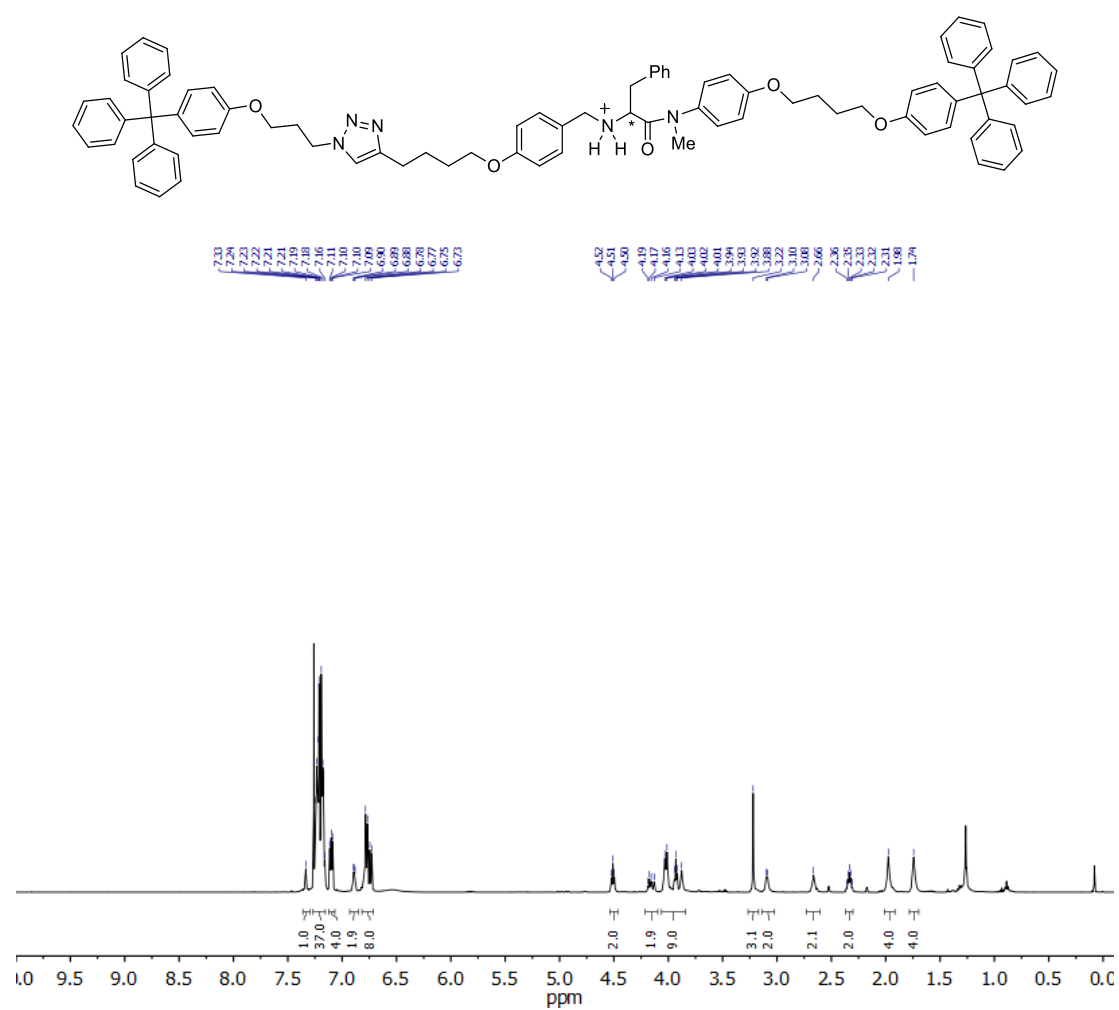
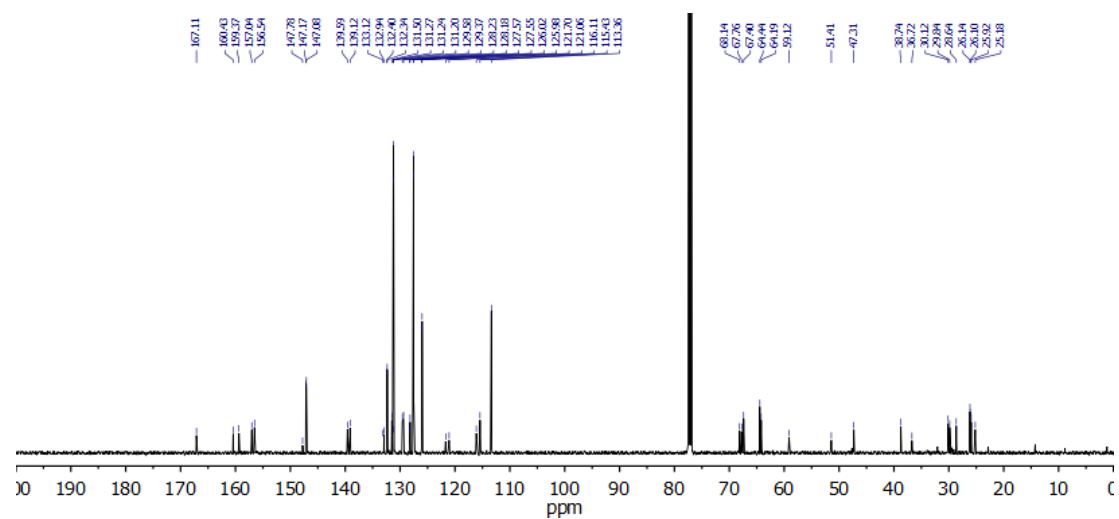


Figure 153. ^{13}C NMR (126 MHz, CDCl_3) spectrum of 165.

Compound **183-H⁺·PF₆⁻**:Figure 154. ¹H NMR (500 MHz, CDCl₃) spectrum of **183-H⁺·PF₆⁻**.Figure 155. ¹³C NMR (126 MHz, CDCl₃) spectrum of **183-H⁺·PF₆⁻**.

Compound 184-H⁺·2PF₆⁻:

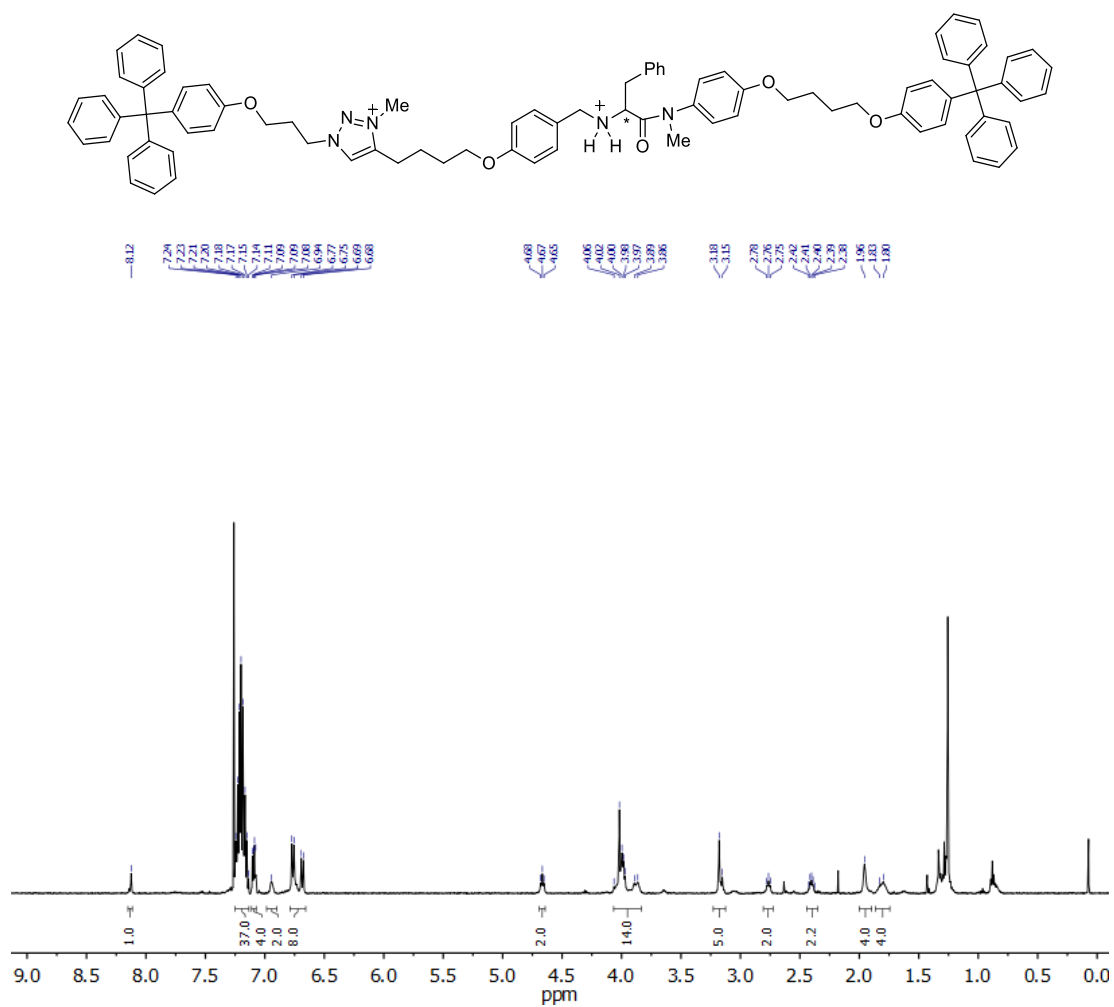


Figure 156. ¹H NMR (500 MHz, CDCl₃) spectrum of 184-H⁺·2PF₆⁻.

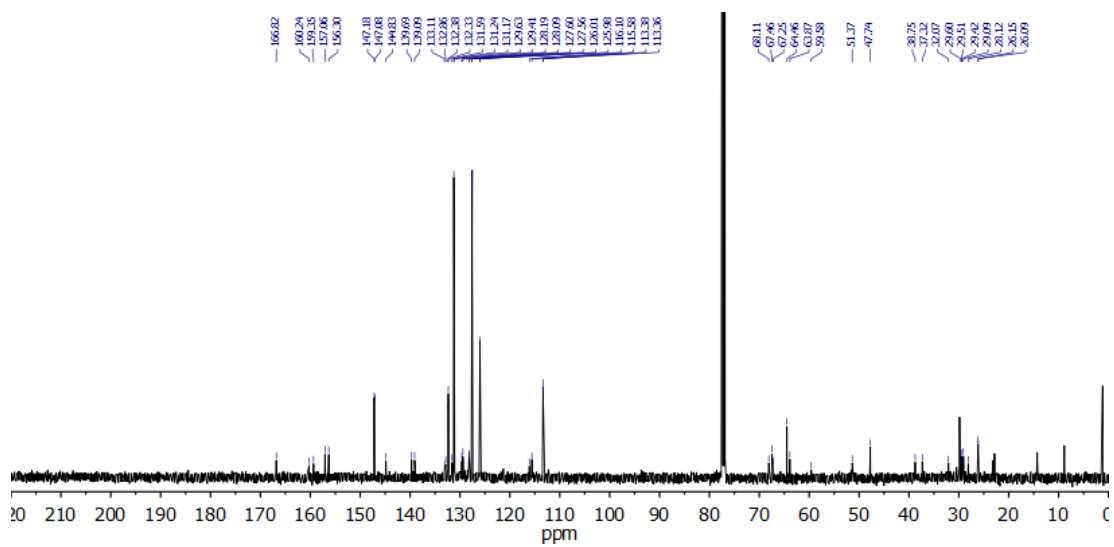
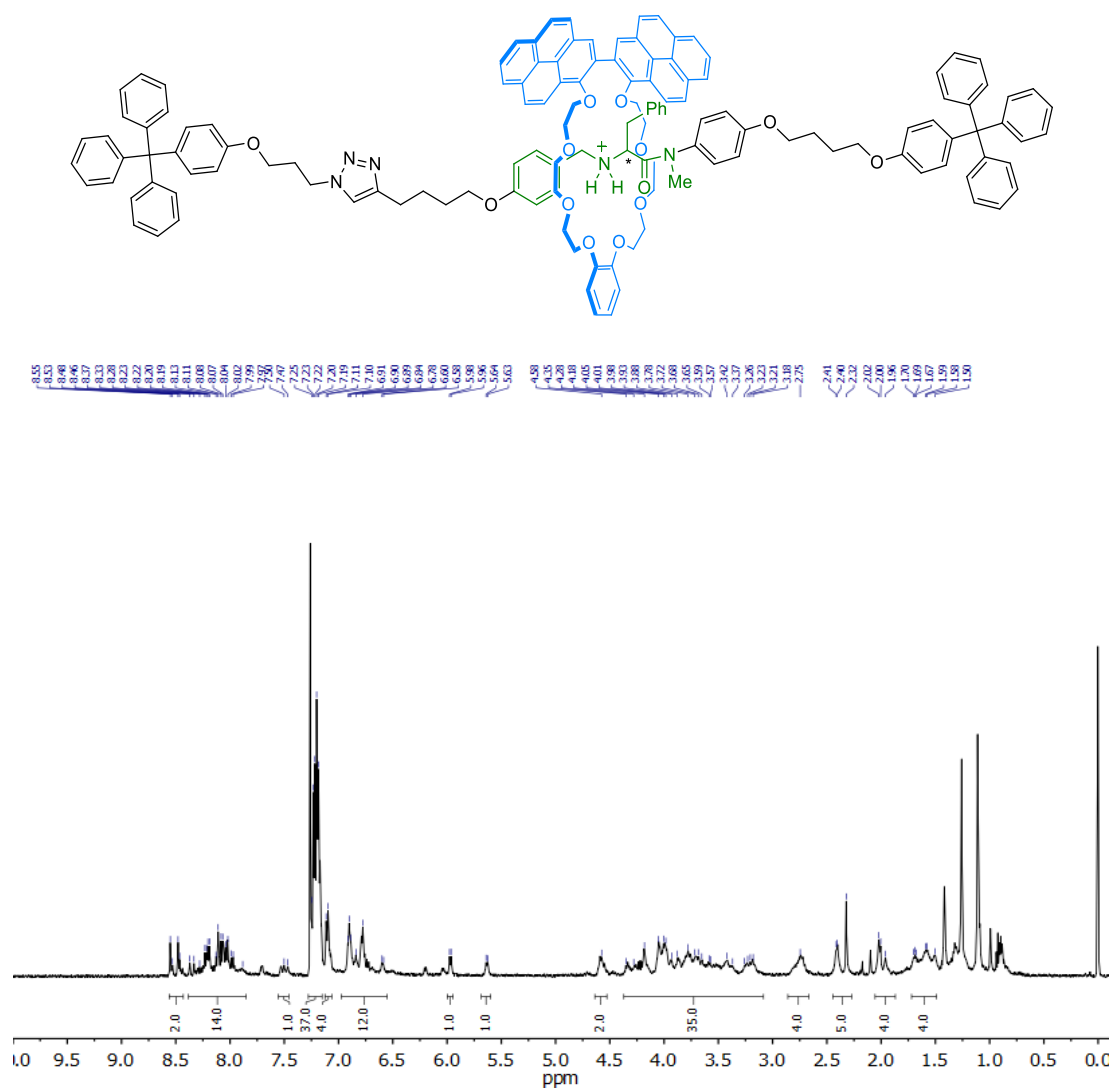
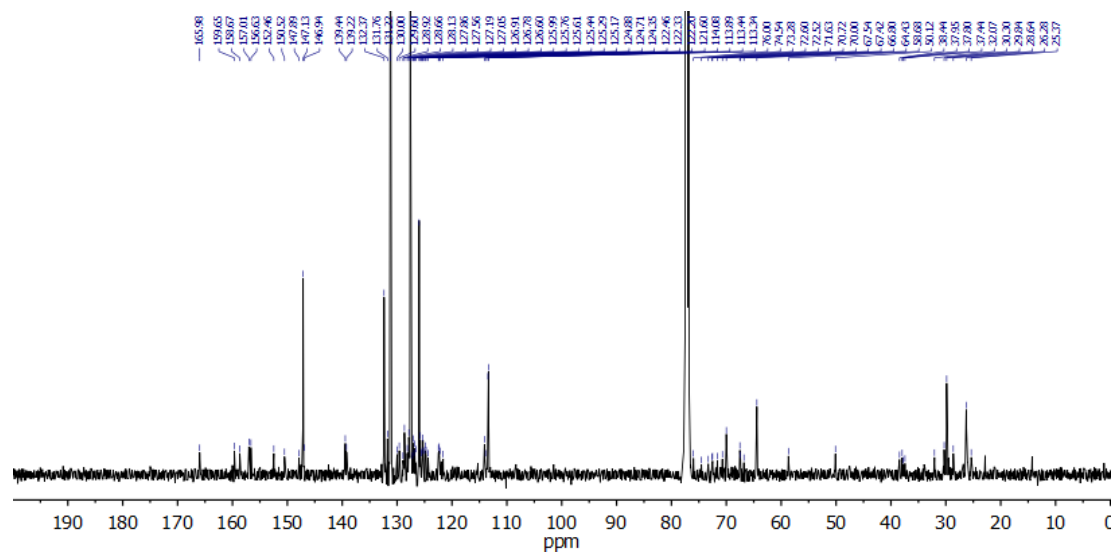


Figure 157. ¹³C NMR (126 MHz, CDCl₃) spectrum of 184-H⁺·2PF₆⁻.

Compound **185-H⁺·PF₆⁻**:Figure 158. ¹H NMR (500 MHz, CDCl₃) spectrum of **185-H⁺·PF₆⁻**.Figure 159. ¹³C NMR (126 MHz, CDCl₃) spectrum of **185-H⁺·PF₆⁻**.

Compound 162-H⁺·2PF₆⁻:

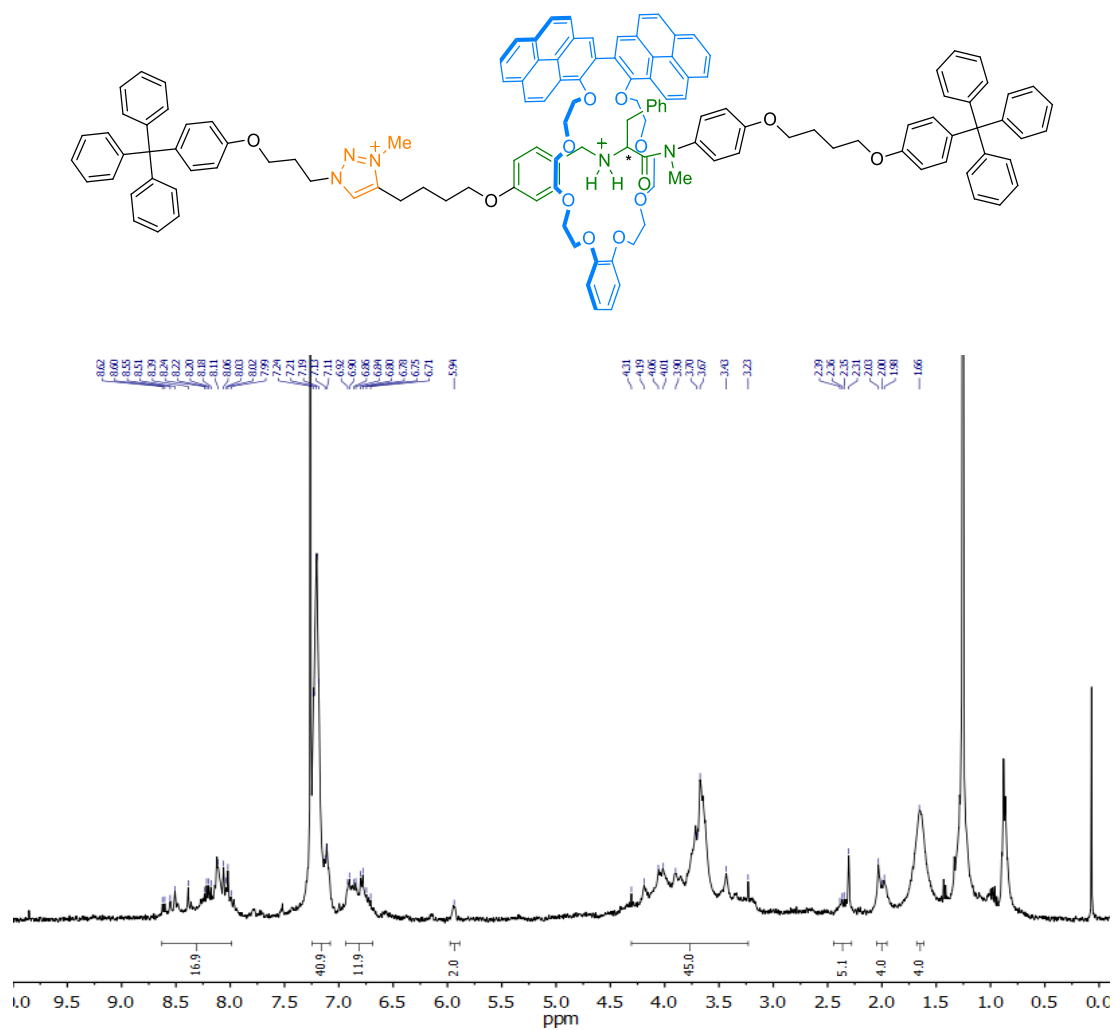


Figure 160. ¹H NMR (400 MHz, CDCl₃) spectrum of 162-H⁺·2PF₆⁻.

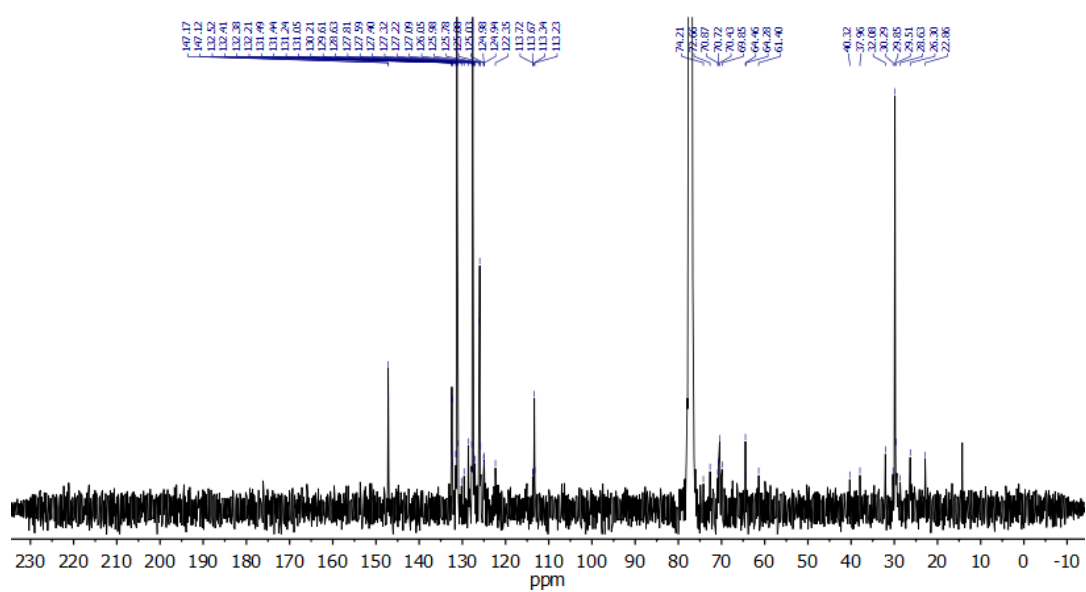


Figure 161. ¹³C NMR (126 MHz, CDCl₃) spectrum of 162-H⁺·2PF₆⁻.

Compound 162·PF₆⁻:

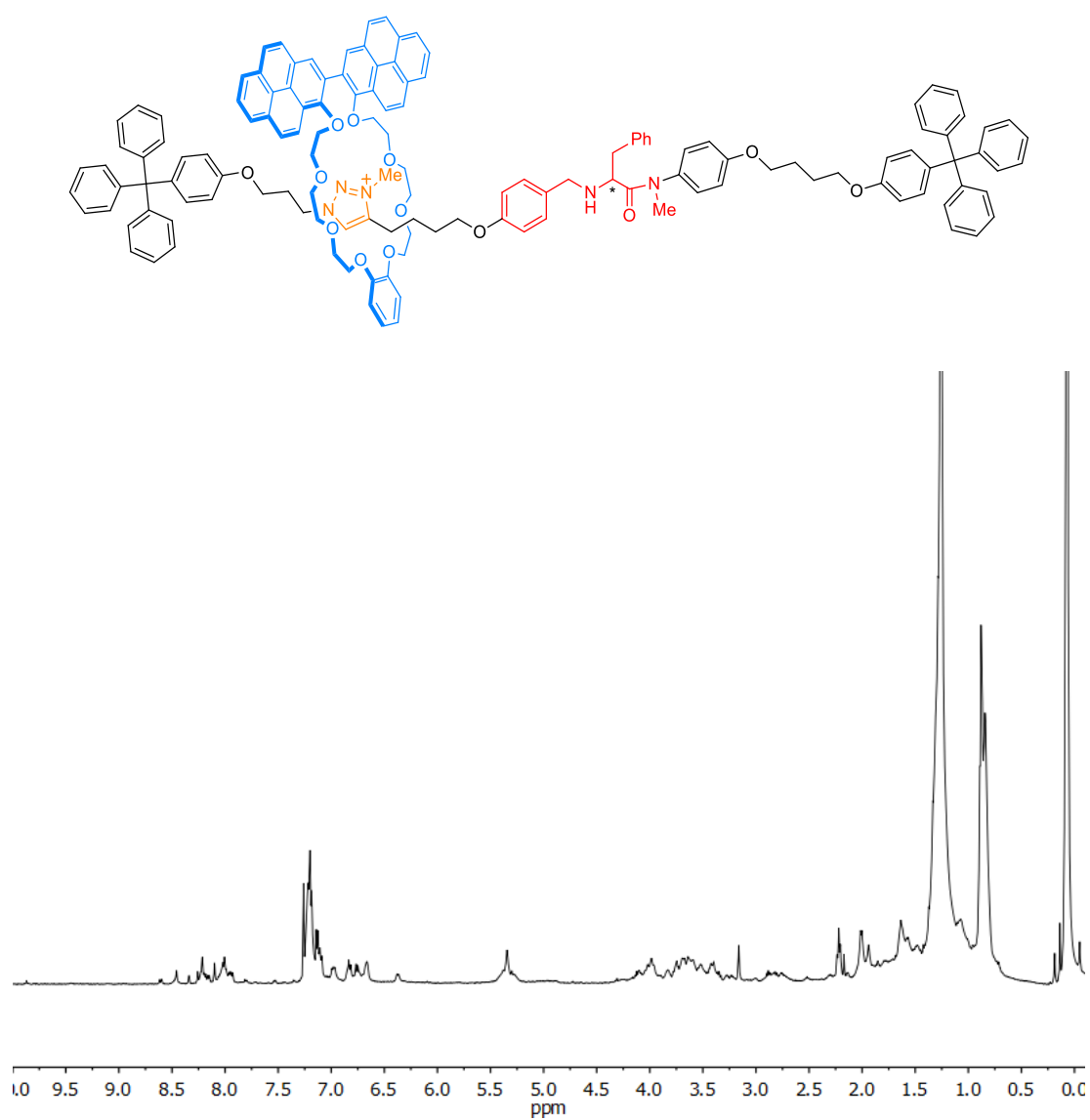


Figure 162. ¹H NMR (500 MHz, CDCl₃) spectrum of **162·PF₆⁻**.

PART B

Chapter 3: Supramolecular chemistry of saddle-shaped heptagon-containing nanographenes

1. Background

1.1 Graphene and nanographenes

Graphene is a fascinating two-dimensional material composed by a monolayer of carbon atoms bonded to three other identical carbon atoms with a sp^2 hybridization. These atoms constitute a network of hexagonal rings that resembles a honeycomb structure. This carbon allotrope was isolated and prepared in a reasonable scale for the first time in 2004 by Novoselov and Geim.³⁶⁰ Their and further studies revealed the very interesting features of this material, whose π orbitals and electrons are delocalized over its surface, providing outstanding properties associated with electric and thermal conduction but also extraordinary mechanical properties. Thus, graphene is a promising material for applications in many fields, such as electronics, energy storage, catalysis or sensing. For these reasons, Novoselov and Geim received the Nobel Prize in physics in 2010.³⁶¹

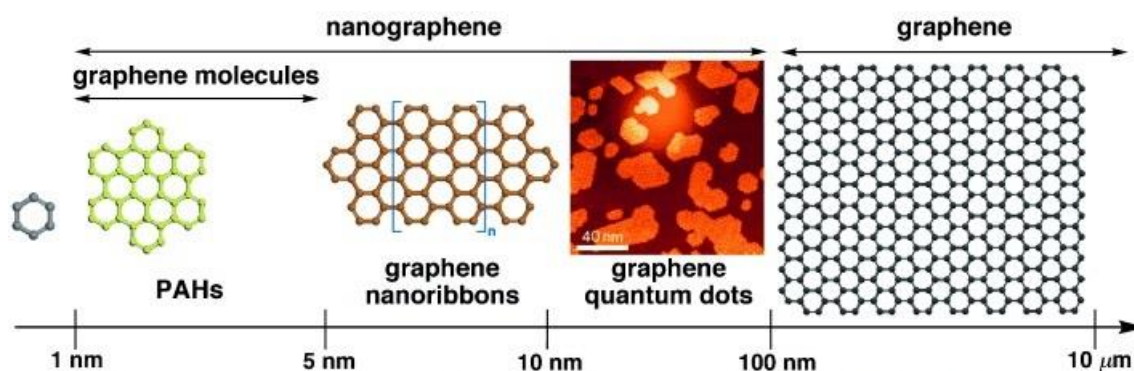


Figure 163. Illustration of graphene terminology defined depending on their size scale.³⁶³ Reprinted with permission from ref 363. Copyright 2012 John Wiley and Sons.

By tearing a graphene lattice, nanographenes whose size would range from 100 nm to 1 nm can be obtained. Therefore, the nanographene term includes graphene molecules, graphene nanoribbons and graphene quantum dots (Figure 163). These compounds can be considered as models for graphene studies, they display remarkable properties like graphene and can potentially have future applications in numerous fields such as nanoelectronics or optoelectronics.³⁶² It is important to emphasize that not all polycyclic aromatic hydrocarbons (PAHs) belong to the nanographenes group since the former are described as aromatic hydrocarbons owning two or more fused benzene rings with the occasional

³⁶⁰ K. S. Novoselov, A. K. Geim, S. V. Morozov, D. Jiang, Y. Zhang, S. V. Dubonos, I. V. Grigorieva, A. A. Firsov, *Science* **2004**, *306*, 666-669.

³⁶¹ A. K. Geim, *Angew. Chem. Int. Ed.* **2011**, *50*, 6966-6985. b) K. S. Novoselov, *Angew. Chem. Int. Ed.* **2011**, *50*, 6986-7002.

³⁶² A. Narita, X.-Y. Wang, X. Feng, K. Müllen, *Chem. Soc. Rev.* **2015**, *44*, 6616-6643.

presence of heteroatoms or non-hexagonal rings and consequently, for smaller examples their size is lower than 1 nm.³⁶³

1.2 Defects and distortion in graphene and nanographenes

Occasionally, irregularities or defects can appear in the pristine regular structure of graphene. Indeed, a wide diversity of geometrical shapes, generating non-hexagonal rings, have been detected modifying the topology of this material and its physical properties.³⁶⁴ The presence of a single five-membered or seven-membered ring results in a distortion of the graphene lattice in a bowl or a saddle shape, respectively (Figure 164).³⁶⁵ Although the presence of a single non-hexagonal ring is very rare, the inclusion of multiple odd-membered rings is quite frequent. The existence of these defects in a graphene sheet can be the consequence of vacancies,³⁶⁶ the incorporation of additional carbon atoms,³⁶⁷ or a simple rearrangement, such as the Stone-Wales defect³⁶⁸ (Figure 165).

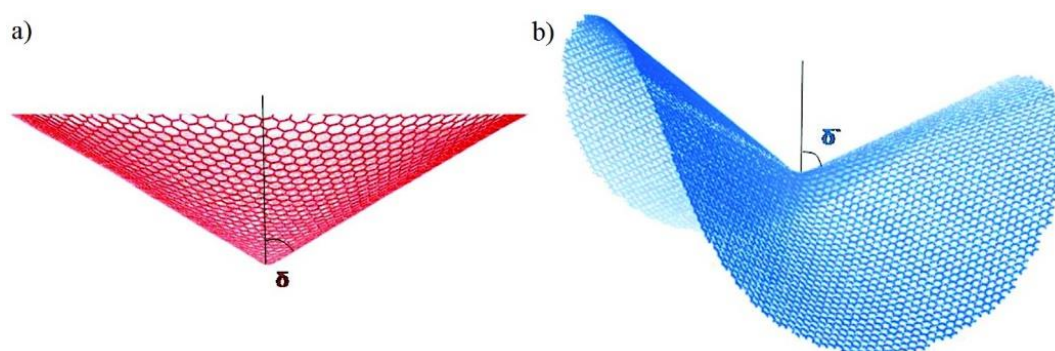


Figure 164. Graphene lattice featuring an isolated pentagon or heptagon ring displaying a bowl- (a) or a saddle- (b) shaped curvature respectively.^{365b} Reprinted with permission from ref 365b. Copyright 2010 American Chemical Society.

Theoretical studies revealed that the strain induced by non-hexagonal rings in graphene sheets considerably affects their physical properties.³⁶⁹ Thus, the synthesis of well-defined nanographene or PAHs fragments possessing non-hexagonal rings is of key importance since they can be considered as excellent models to experimentally study the modification of the physical properties induced by the introduction of topological defects in graphene.

³⁶³ L. Chen, Y. Hernandez, X. Feng, K. Müllen, *Angew. Chem. Int. Ed.* **2012**, *51*, 7640-7654.

³⁶⁴ F. Banhart, J. Kotakoski, A. V. Krasheninnikov, *ACS Nano* **2011**, *5*, 26-41.

³⁶⁵ a) O. V. Yazyev, S. G. Louie, *Phys. Rev. B* **2010**, *81*, 195420. b) Y. Liu, B. I. Yakobson, *Nano Lett.* **2010**, *10*, 2178-2183.

³⁶⁶ a) G.-D. Lee, C. Z. Wang, E. Yoon, N.-M. Hwang, D.-Y. Kim, K. M. Ho, *Phys. Rev. Lett.* **2005**, *95*, 205501. b) J. C. Meyer, C. Kisielowski, R. Erni, M. D. Rossell, M. F. Crommie, A. Zettl, *Nano Lett.* **2008**, *8*, 3582-3586.

³⁶⁷ a) A. W. Robertson, K. He, A. I. Kirkland, J. H. Warner, *Nano Lett.* **2014**, *14*, 908-914. b) O. Lehtinen, N. Vats, G. Algara-Siller, P. Knyrim, U. Kaiser, *Nano Lett.* **2015**, *15*, 235-241.

³⁶⁸ A. J. Stone, D. J. Wales, *Chem. Phys. Lett.* **1986**, *128*, 501-503.

³⁶⁹ H. Terrones, R. Lv, M. Terrones, M. S. Dresselhaus, *Rep. Prog. Phys.* **2012**, *75*, 062501.

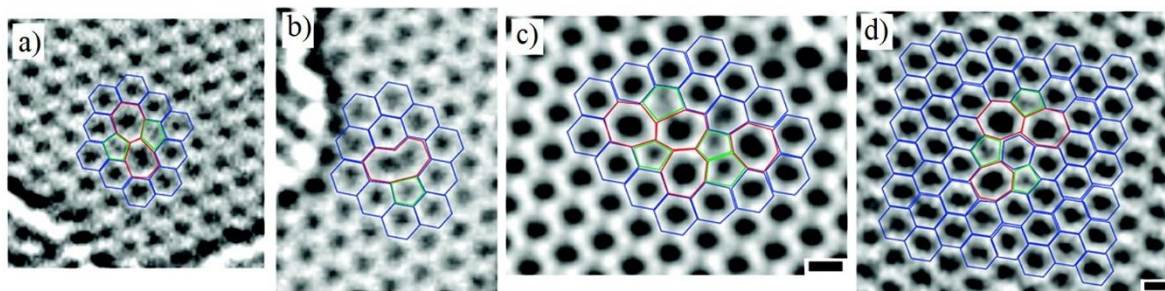


Figure 165. High-resolution transmission electron microscopy (TEM) images of a graphene lattice showing distinct defects: a) The Stone-Wales defect. b) A vacancy. c) Defect composed by four heptagons and pentagons. d) Defect displaying three pentagons and heptagons. Hexagons are shown in blue, pentagons in green and heptagons in red.^{366b} Reprinted with permission from ref 366b. Copyright 2008 American Chemical Society.

Regarding five-membered ring-containing PAHs, from the first synthesis of corannulene by Barth and Lawton in 1966,³⁷⁰ a vast number of structures containing a pentagon and therefore, a bowl-shaped positive curvature were designed and synthesized. These molecules display outstanding electrochemical, especially as electron acceptors, and photophysical properties which led to numerous applications in materials science.³⁷¹

When it comes to PAHs or nanographenes owning a heptagon on their structure, their synthesis and applications are much less explored than those of pentagon-containing systems. Although the first synthesis of [7]circulene was carried out in 1986 by Yamamoto and Nakazaki³⁷² (Figure 166), the interest of developing compounds featuring a negative saddle curvature and investigating their properties and possible applications raised only very recently.³⁷³ The benefit of building molecules possessing such curvature is their higher solubility in common organic solvents in comparison with their planar analogues, which improves and facilitates their purification and characterization. Moreover, these heptagon-containing nanographenes displayed interesting photophysical, both in chiroptical^{285b,c,374} and nonlinear optics,^{285b,c,374b,375} and relevant electronic properties since they can function as semi-conductors in thin-film transistors³⁷⁶ (Figure 166). Furthermore, theoretical

³⁷⁰ W. E. Barth, R. G. Lawton, *J. Am. Chem. Soc.* **1966**, *88*, 380-381.

³⁷¹ a) Y.-T. Wu, J. S. Siegel, *Chem. Rev.* **2006**, *106*, 4843-4867. b) E. Nestoros, M. C. Stuparu, *Chem. Commun.* **2018**, *54*, 6503-6519.

³⁷² K. Yamamoto, T. Harada, M. Nakazaki, T. Naka, Y. Kai, S. Harada, N. Kasai, *J. Am. Chem. Soc.* **1983**, *105*, 7171-7172.

³⁷³ I. R. Márquez, S. Castro-Fernández, A. Millán, A. G. Campaña, *Chem. Commun.* **2018**, *54*, 6705-6718. b) S. H. Pun, Q. Miao, *Acc. Chem. Res.* **2018**, *51*, 1630-1642.

³⁷⁴ a) T. Fujikawa, Y. Segawa, K. Itami, *J. Org. Chem.* **2017**, *82*, 7745-7749. b) C. M. Cruz, I. R. Márquez, S. Castro-Fernández, J. M. Cuerva, E. Maçôas, A. G. Campaña, *Angew. Chem. Int. Ed.* **2019**, *58*, 8068-8072.

³⁷⁵ S. Castro-Fernández, C. M. Cruz, I. F. A. Mariz, I. R. Márquez, V. G. Jiménez, L. Palomino-Ruiz, J. M. Cuerva, E. Maçôas, A. G. Campaña, *Angew. Chem. Int. Ed.* **2020**, *59*, 7139-7145.

³⁷⁶ a) K. Y. Cheung, X. Xu, Q. Miao, *J. Am. Chem. Soc.* **2015**, *137*, 3910-3914. b) X. Gu, H. Li, B. Shan, Z. Liu, Q. Miao, *Org. Lett.* **2017**, *19*, 2246-2249. c) S. H. Pun, Y. Wang, M. Chu, C. K. Chan, Y. Li, Z. Liu, Q. Miao, *J. Am. Chem. Soc.* **2019**, *141*, 9680-9686.

calculations on this type of negatively curved structure predicted unusual magnetic properties³⁷⁷ and remarkable applications in the field of electronics.³⁷⁸ This demonstrates the great potential of these saddle-shaped nanographenes and shows that there is still a lot more to explore with these molecules.

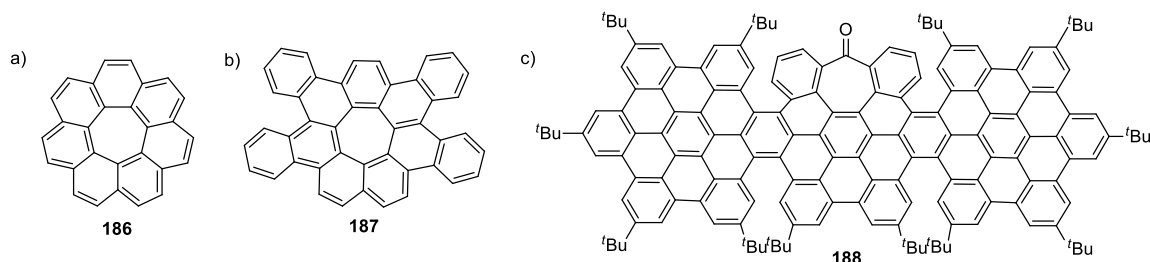


Figure 166. a) [7]Circulene reported by Yamamoto and Nakazaki.³⁷² b) A tetrabenzo[7]circulene possessing semi-conductor properties described by Miao.^{376b} c) A distorted nanographene ribbon exhibiting enhanced nonlinear optical properties reported by Maçõas and Campaña.³⁷⁵

1.3. Supramolecular chemistry of planar and curved PAHs

Besides the outstanding photophysical and electronic applications enabled by the study of planar and curved nanographenes and PAHs, their supramolecular properties were investigated and analysed, giving rise to the discovery of fascinating host-guest properties and useful supramolecular assemblies. Here, it is crucial to highlight that planar extended PAHs, such as coronene or HBC (Hexa-*peri*-hexabenzocoronene) derivatives, and bowl-shaped PAHs, such as corannulene-based molecules, have been widely studied while those incorporating a saddle shape have remained completely unexplored experimentally. Although theoretical studies suggested that, among the [n]circulenes, the stacking interactions of [7]circulene was the stronger,³⁷⁹ the only experimental supramolecular study reported for a negatively-curved PAH owning a heptagonal ring was the co-crystallization of a nanographene with C₆₀ suggesting the formation of supramolecular interactions between both species. Nonetheless, the structure was not presented by the authors due to the poor quality of the data.^{376b} Taking into account the widespread use of small PAHs motifs in supramolecular assemblies, in this section, we will only focus on the supramolecular chemistry of coronene, HBC and corannulene derivatives or PAHs bigger than those.

1.3.1. Self-association of HBC derivatives in solution

In 2004, Müllen and co-workers reported the control of the self-association of various HBCs in solution. Indeed, by ¹H NMR spectroscopy they were able to distinguish between the monomeric species of a dendronized HBC and its dimer by varying the concentration of the solution and therefore, to regulate

³⁷⁷ N. Park, M. Yoon, S. Berber, J. Ihm, E. Osawa, D. Tománek, *Phys. Rev. Lett.* **2003**, *91*, 237204.

³⁷⁸ D. Odkhuy, D. H. Jung, H. Lee, S. S. Han, S.-H. Choi, R. S. Ruoff, N. Park, *Carbon* **2014**, *66*, 39-47.

³⁷⁹ Y. Guan, M. L. Jones, A. E. Miller, S. E. Wheeler, *Phys. Chem. Chem. Phys.* **2017**, *19*, 18186-18193.

the dimer formation. Furthermore, employing ^1H NMR spectroscopy, they succeeded in estimating the monomer-dimer equilibrium constant of hexakis(4-dodecyl)-*peri*-hexabenzocoronene (**189**) (Figure 167), ranging from 188 to 457 M^{-1} depending on the association model, in $\text{C}_2\text{D}_2\text{Cl}_4$ at 333 K by analysing the change of the chemical shift of the HBC protons using a nonlinear least-squares curve fitting. It is important to notice that the HBC protons underwent an upfield shift by increasing the solution concentration due to the π - π interactions established between the HBC cores.³⁸⁰

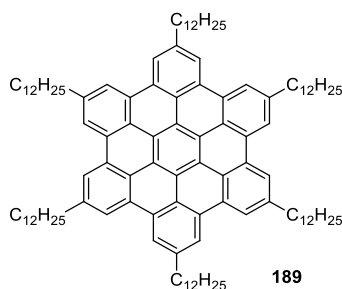


Figure 167. Structure of hexakis(4-dodecyl)-*peri*-hexabenzocoronene employed by Müllen for the first estimation of the monomer-dimer equilibrium constant of HBCs in solution.³⁸⁰

One year later, Müllen proved that the self-association of HBCs was very sensitive to their peripheral substituents and to the solvent effect. Consequently, he found out that the monomer-dimer equilibrium constant of hexakis(4-dodecyl)-*peri*-hexabenzocoronene could reach 14900 M^{-1} at 303 K when the solvent was changed to benzene- d_6 .³⁸¹ Furthermore, the shielding effect correlated to the increase in the concentration of HBC derivatives was described in several other cases, allowing for some of them the calculation of the monomer-dimer equilibrium constants with values in the range 257-1406 M^{-1} in CDCl_3 or $\text{C}_2\text{D}_2\text{Cl}_4$, depending on the substituent attached to the HBC unit (aliphatic chains, fluorenyl or nitrile groups, among others).³⁸²

The ^1H NMR spectra of some corannulene-based PAHs showed a concentration-dependent behaviour.³⁸³ Thus, by ^1H NMR spectroscopy, its monomer-dimer equilibrium constant has been estimated at $K_a = (2.0 \pm 1.0) \times 10^5 \text{ M}^{-1}$ in D_2O at 300 K for corannulenes derivatives pentasubstituted with nucleosides.^{383b}

³⁸⁰ J. Wu, A. Fechtenkötter, J. Gauss, M. D. Watson, M. Kastler, C. Fechtenkötter, M. Wagner, K. Müllen, *J. Am. Chem. Soc.* **2004**, *126*, 11311-11321.

³⁸¹ M. Kastler, W. Pisula, D. Wasserfallen, T. Pakula, K. Müllen, *J. Am. Chem. Soc.* **2005**, *127*, 4286-4296.

³⁸² a) W. W. H. Wong, C.-Q. Ma, W. Pisula, C. Yan, X. Feng, D. J. Jones, K. Müllen, R. A. J. Janssen, P. Bäuerle, A. B. Holmes, *Chem. Mater.* **2010**, *22*, 457-466. b) W. W. H. Wong, T. B. Singh, D. Vak, W. Pisula, C. Yan, X. Feng, E. L. Williams, K. L. Chan, Q. Mao, D. J. Jones, C.-Q. Ma, K. Müllen, P. Bäuerle, A. B. Holmes, *Adv. Funct. Mater.* **2010**, *20*, 927-938. c) L. Chen, X. Dou, W. Pisula, X. Yang, D. Wu, G. Floudas, X. Feng, K. Müllen, *Chem. Commun.* **2012**, *48*, 702-704.

³⁸³ a) Y.-L. Wu, M. C. Stuparu, C. Boudon, J.-P. Gisselbrecht, W. B. Schweizer, K. K. Baldrige, J. S. Siegel, F. Diederich, *J. Org. Chem.* **2012**, *77*, 11014-11026. b) M. Mattarella, L. Berstis, K. K. Baldrige, J. S. Siegel, *Bioconjugate Chem.* **2014**, *25*, 115-128.

1.3.2. Host-guest properties of PAHs bigger than coronene and corannulene

1.3.2.1. PAH-based hosts

It is not surprising that the π -surface of PAHs has been employed to bind to aromatic compounds. In 1993, Bohme and co-workers described the formation in the gas phase of a stable complex between corannulene and $(C_{60})^+$.³⁸⁴ Later, Scott reported the binding of C_{60} to simple *sym*-pentakis(arylthio) corannulenes through π - π interactions in solution. The calculated association constants (K_a) ranged from 280 to 474 M^{-1} at 298 K in toluene- d_8 .³⁸⁵ By improving the receptor design, they succeeded to enhance this binding constant ($K_a \approx 1.4 \times 10^3 M^{-1}$ at 298 K in CS_2) and to generate a complex with C_{70} ($K_a \approx 1.1 \times 10^3 M^{-1}$ at 298 K in CS_2).³⁸⁶ Using decapyrrylcorannulene hosts, the binding constant (K_a) attained $(8.3 \pm 1.0) \times 10^3 M^{-1}$ at 298 K in toluene- d_8 for C_{60} and $(5.7 \pm 0.1) \times 10^3 M^{-1}$ at 298 K in toluene- d_8 for C_{70} .³⁸⁷ In addition, the formation of co-crystals of the complex between C_{60} or C_{70} and a corannulene derivative was observed,^{387,388} exploiting the perfect geometrical match between the bowl shape of corannulene with a fullerene.

Thus, in 2007, Sygula conceived a molecular tweezer with two corannulene subunits possessing the ability to bind C_{60} ($K_a = (8.6 \pm 0.5) \times 10^3 M^{-1}$ in toluene- d_8 at 298 K) (Figure 168).³⁸⁹ Subsequently, many other molecular tweezers were reported that can act as receptors, sometimes in a selective way, for C_{60} and C_{70} .³⁹⁰ The formation of an inclusion complex with fullerenes was also accomplished using hosts owning multiple corannulene units.³⁹¹ Moreover, this geometrically complementary concave-convex

³⁸⁴ H. Becker, G. Javahery, S. Petrie, P.-C. Cheng, H. Schwarz, L. T. Scott, D. K. Bohme, *J. Am. Chem. Soc.* **1993**, *115*, 11636-11637.

³⁸⁵ Shehadeh Mizyed, Paris E. Georghiou, Mihail Bancu, Bernardo Cuadra, Amarjit K. Rai, Peichao Cheng, Lawrence T. Scott, *J. Am. Chem. Soc.* **2001**, *123*, 12770-12774.

³⁸⁶ P. E. Georghiou, A. H. Tran, S. Mizyed, M. Bancu, L. T. Scott, *J. Org. Chem.* **2005**, *70*, 6158-6163.

³⁸⁷ Y.-Y. Xu, H.-R. Tian, S.-H. Li, Z.-C. Chen, Y.-R. Yao, S.-S. Wang, X. Zhang, Z.-Z. Zhu, S.-L. Deng, Q. Zhang, S. Yang, S.-Y. Xie, R.-B. Huang, L.-S. Zheng, *Nat. Comm.* **2019**, *10*, 485.

³⁸⁸ a) L. N. Dawe, T. A. AlHujran, H.-A. Tran, J. I. Mercer, E. A. Jackson, L. T. Scott, P. E. Georghiou, *Chem. Commun.* **2012**, *48*, 5563-5565. b) A. S. Filatov, M. V. Ferguson, S. N. Spisak, B. Li, C. F. Campana, M. A. Petrukhina, *Cryst. Growth Des.* **2014**, *14*, 756-762. c) S. Lampart, L. M. Roch, A. K. Dutta, Y. Wang, R. Warshamanage, A. D. Finke, A. Linden, K. K. Baldrige, J. S. Siegel, *Angew. Chem. Int. Ed.* **2016**, *55*, 14648-14652.

³⁸⁹ A. Sygula, F. R. Fronczek, R. Sygula, P. W. Rabideau, M. M. Olmstead, *J. Am. Chem. Soc.* **2007**, *129*, 3842-3843.

³⁹⁰ Selected examples: a) C. M. Álvarez, L. A. García-Escudero, R. García-Rodríguez, J. M. Martín-Álvarez, D. Miguel, V. M. Rayón, *Dalton Trans.* **2014**, *43*, 15693-15696. b) P. L. A. Kuragama, F. R. Fronczek, A. Sygula, *Org. Lett.* **2015**, *17*, 5292-5295. c) K. G. U. R. Kumarasinghe, F. R. Fronczek, H. U. Valle, A. Sygula, *Org. Lett.* **2016**, *18*, 3054-3057.

³⁹¹ a) M. Yanney, A. Sygula, *Tetrahedron Lett.* **2013**, *54*, 2604-2607. b) C. M. Álvarez, G. Aullón, H. Barbero, L. A. García-Escudero, C. Martínez-Pérez, J. M. Martín-Álvarez, D. Miguel, *Org. Lett.* **2015**, *17*, 2578-2581. c) V. García-Calvo, J. V. Cuevas, H. Barbero, S. Ferrero, C. M. Álvarez, J. A. González, B. Díaz de Greñu, J. García-Calvo, T. Torroba, *Org. Lett.* **2019**, *21*, 5803-5807. d) S. Ferrero, H. Barbero, D. Miguel, R. García-Rodríguez, C. M. Álvarez, *J. Org. Chem.* **2020**, *85*, 4918-4926.

π - π interaction was also observed with fullerene guests in a corannulene-based cage³⁹² or in a polymer with pendant corannulenes.³⁹³

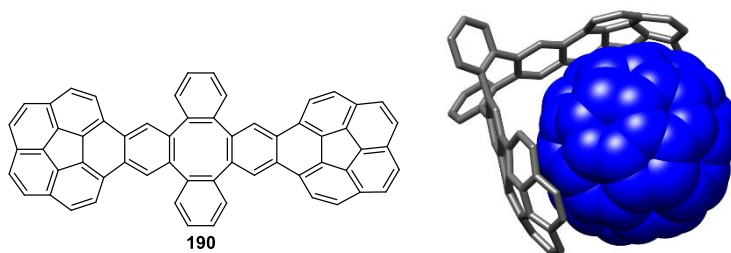


Figure 168. A molecular tweezer reported by Sygula and the representation of its X-ray diffraction structure showing its binding to C_{60} .³⁸⁹ Color coding: C, gray or blue; H, white.

Furthermore, the growth of co-crystals of C_{60} and different contorted coronene derivatives was described, evidencing the importance of the distortion to bind such curved compounds.³⁹⁴ Thus, the preparation of hosts based on non-planar coronene derivatives was achieved by synthesizing strained nano hoops³⁹⁵ or cyclophanes³⁹⁶ featuring one or more HBC units. The study of their complexation with C_{60} and C_{70} afforded association constants ranging approximately from 10^5 to 10^7 M^{-1} (Figure 169). Nevertheless, Fujita also reported a giant cage owning 24 ligands with pendant planar coronenes able to bind C_{60} .³⁹⁷

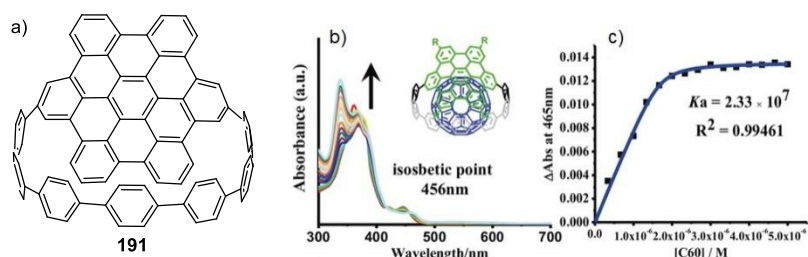


Figure 169. a) Structure of a nanobelt owning a HBC derivative reported by Yang and Du. b) UV/Vis absorption spectra of the titration of **191** with C_{60} c) Fitted binding isotherm showing the change of absorbance at 465 nm versus $[C_{60}]$ ($K_a = 2.33 \times 10^7$).^{395c} Reprinted with permission from ref 395c. Copyright 2019 John Wiley and Sons.

Besides fullerene hosting, HBC derivatives shown the ability to bind PDI dyes. Indeed, in 2009, Müllen and Samorì demonstrated the self-assembly in solution of an electron-poor molecule, perylene

³⁹² W. Sun, Y. Wang, L. Ma, L. Zheng, W. Fang, X. Chen, H. Jiang, *J. Org. Chem.* **2018**, *83*, 14667-14675.

³⁹³ M. C. Stuparu, *Angew. Chem. Int. Ed.* **2013**, *52*, 7786-7790.

³⁹⁴ a) Z. Wang, F. Dötz, V. Enkelmann, K. Müllen, *Angew. Chem. Int. Ed.* **2005**, *44*, 1247-1250. b) C.-Y. Chiu, B. Kim, A. A. Gorodetsky, W. Sattler, S. Wei, A. Sattler, M. Steigerwald, C. Nuckolls, *Chem. Sci.* **2011**, *2*, 1480-1486. c) Z. Li, Z. Hu, X. Chen, Y. Zhang, J. Zhang, *Chem. Lett.* **2012**, *41*, 1588-1590.

³⁹⁵ a) D. Lu, G. Zhuang, H. Wu, S. Wang, S. Yang, P. Du, *Angew. Chem. Int. Ed.* **2017**, *56*, 158-162. b) S. Cui, G. Zhuang, D. Lu, Q. Huang, H. Jia, Y. Wang, S. Yang, P. Du, *Angew. Chem. Int. Ed.* **2018**, *57*, 9330-9335. c) Q. Huang, G. Zhuang, H. Jia, M. Qian, S. Cui, S. Yang, P. Du, *Angew. Chem. Int. Ed.* **2019**, *58*, 6244-6249.

³⁹⁶ G. Li, T. Matsuno, Y. Han, H. Phan, S. Wu, Q. Jiang, Y. Zou, H. Isobe, J. Wu, *Angew. Chem. Int. Ed.* **2020**, *59*, 9727-9735.

³⁹⁷ K. Suzuki, K. Takao, S. Sato, M. Fujita, *J. Am. Chem. Soc.* **2010**, *132*, 2544-2545.

diimide, with an electron-rich compound, hexa-*peri*-hexabenzocoronene, through π - π interactions. The resulting 1:1 complex possessed a good association constant of $K_a = (2.1 \pm 0.3) \times 10^4 \text{ M}^{-1}$ in CHCl_3 .³⁹⁸ Following this achievement, Akine and Nabeshima synthesized a cyclophane bearing two HBC units capable of binding a PDI dye with a relatively high association constant ($K_a = 3.89 \times 10^4 \text{ M}^{-1}$, in CHCl_3).³⁹⁹

1.3.2.2. PAHs as guests

Throughout the years, many PAHs were used as guests in supramolecular chemistry taking advantage of the π -surface they offer. Regarding planar extended PAHs like coronene, they have been encapsulated a number of times by many different metal-organic⁴⁰⁰ or organic⁴⁰¹ molecular cages with walls usually incorporating aromatic cores and, more recently, antiaromatic ones.^{400d} In addition, some MOFs,⁴⁰² macrocycles⁴⁰³ or a metallacycle⁴⁰⁴ were able to trap coronene (Figure 170). It is also possible to find more exotic types of receptors for planar PAHs, such as tweezers or a nanoparticle.⁴⁰⁵

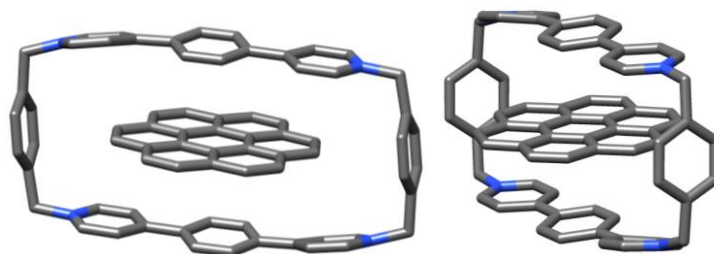


Figure 170. Selected coronene receptor: Front (left) and side (right) views of the representation of the X-ray diffraction structure of a macrocycle encircling coronene described by Stoddart.^{403a} Color coding: C, gray; H, white; N, light blue.

³⁹⁸ G. De Luca, A. Liscio, M. Melucci, T. Schnitzler, W. Pisula, C. G. Clark Jr, L. M. Scolaro, V. Palermo, K. Müllen, P. Samorì, *J. Mater. Chem.* **2010**, *20*, 71-82.

³⁹⁹ S. Akine, T. Onuma, T. Nabeshima, *New J. Chem.* **2018**, *42*, 9369-9372.

⁴⁰⁰ Selected examples: a) J. Mattsson, P. Govindaswamy, J. Furrer, Y. Sei, K. Yamaguchi, G. Süss-Fink, B. Therrien, *Organometallics* **2008**, *27*, 4346-4356. b) P. D. Frischmann, V. Kunz, F. Würthner, *Angew. Chem. Int. Ed.* **2015**, *54*, 7285-7289. c) T. K. Ronson, W. Meng, J. R. Nitschke, *J. Am. Chem. Soc.* **2017**, *139*, 9698-9707. d) M. Yamashina, Y. Tanaka, R. Lavendomme, T. K. Ronson, M. Pittelkow, J. R. Nitschke, *Nature* **2019**, *574*, 511-515.

⁴⁰¹ Selected examples: a) E. J. Dale, N. A. Vermeulen, A. A. Thomas, J. C. Barnes, M. Juríček, A. K. Blackburn, N. L. Strutt, A. A. Sarjeant, C. L. Stern, S. E. Denmark, J. F. Stoddart, *J. Am. Chem. Soc.* **2014**, *136*, 10669-10682. b) J. Samanta, R. Natarajan, *Org. Lett.* **2016**, *18*, 3394-3397.

⁴⁰² a) T. Nozaki, W. Kosaka, H. Miyasaka, *CrystEngComm* **2012**, *14*, 5398-5401. b) X.-T. Liu, K. Wang, Z. Chang, Y.-H. Zhang, J. Xu, Y. S. Zhao, X.-H. Bu, *Angew. Chem. Int. Ed.* **2019**, *58*, 13890-13896.

⁴⁰³ Selected examples: a) J. C. Barnes, M. Juríček, N. L. Strutt, M. Frascioni, S. Sampath, M. A. Giesener, P. L. McGrier, C. J. Bruns, C. L. Stern, A. A. Sarjeant, J. F. Stoddart, *J. Am. Chem. Soc.* **2013**, *135*, 183-192. b) D. Lozano, R. Álvarez-Yebra, R. López-Coll, A. Lledó, *Chem. Sci.* **2019**, *10*, 10351-10355.

⁴⁰⁴ S. Ibáñez, E. Peris, *Angew. Chem. Int. Ed.* **2020**, *59*, 6860-6865.

⁴⁰⁵ Selected examples: a) X. Liu, Y. Hu, F. Stellacci, *Small* **2011**, *7*, 1961-1966. b) Y. Tanaka, K. M.-C. Wong, V. W.-W. Yam, *Chem. Eur. J.* **2013**, *19*, 390-399.

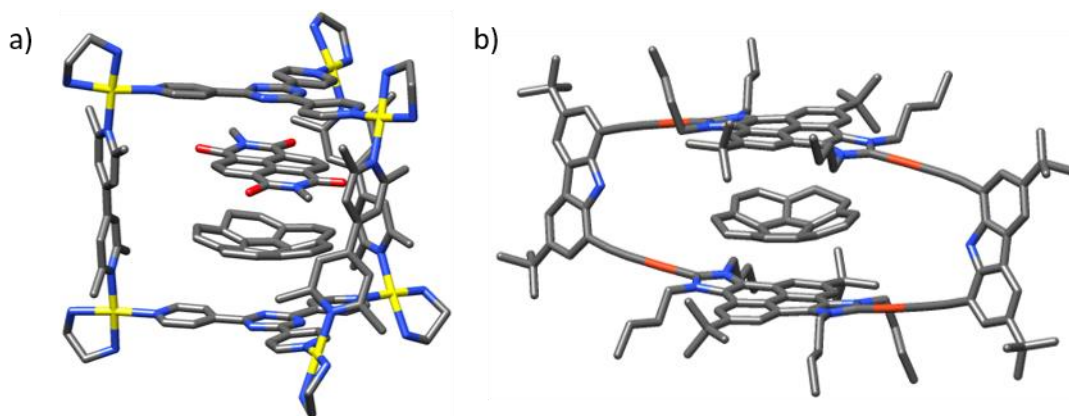


Figure 171. Representation of the X-ray diffraction structure of: a) A cage encapsulating corannulene and an NDI derivative reported by Fujita.⁴⁰⁶ b) A metallacycle binding to corannulene described by Peris.⁴⁰⁴ Hydrogen atoms and counterions have been omitted for clarity. Color coding: C, gray; N, light blue; O, red; Pd, yellow; Au, orange.

When it comes to curved PAHs, only a few cases incorporating corannulene as guest were reported. A remarkable example is the metal-organic molecular cage featuring tris(4-pyridyl)-2,4,6-triazine walls reported by Fujita, which encapsulated corannulene together with a NDI derivative (Figure 171a).⁴⁰⁶ This action can also be achieved using an antiaromatic metal-organic molecular cage.^{400b} Furthermore, macrocyclic receptors based on a cyclodextrin or a metallacycle were found to bind corannulene (Figure 171b).^{404,407} Surprisingly, no saddle shaped PAHs have been employed so far for this purpose.

1.3.3. PAH-based supramolecular materials

1.3.3.1. Liquid crystals

In 1996, Spiess and co-workers demonstrated that HBC derivatives bearing a long aliphatic chain had the ability to self-organize into columnar mesophases, thus affording discotic liquid crystalline materials.⁴⁰⁸ This breakthrough allowed the preparation of nanowires⁴⁰⁹ (Figure 172) or photovoltaic

⁴⁰⁶ B. M. Schmidt, T. Osuga, T. Sawada, M. Hoshino, M. Fujita, *Angew. Chem. Int. Ed.* **2016**, *55*, 1561-1564.

⁴⁰⁷ a) H. Joshi, S. Sreejith, R. Dey, M. C. Stuparu, *RSC Adv.* **2016**, *6*, 110001-110003. b) Q.-J. Fan, Y.-J. Lin, F. E. Hahn, G.-X. Jin, *Dalton Trans.* **2018**, *47*, 2240-2246.

⁴⁰⁸ P. Herwig, C. W. Kayser, K. Müllen, H. W. Spiess, *Adv. Mater.* **1996**, *8*, 510-513.

⁴⁰⁹ a) A. M. van de Craats, J. M. Warman, K. Müllen, Y. Geerts, J. D. Brand, *Adv. Mater.* **1998**, *10*, 36-38. b) S. Xiao, M. Myers, Q. Miao, S. Sanaur, K. Pang, M. L. Steigerwald, C. Nuckolls, *Angew. Chem. Int. Ed.* **2005**, *44*, 7390-7394.

systems.⁴¹⁰ Furthermore, the production of discotic liquid crystals can be achieved using larger nanographenes⁴¹¹ but also smaller ones such as coronene⁴¹² or ovalene⁴¹³ derivatives.

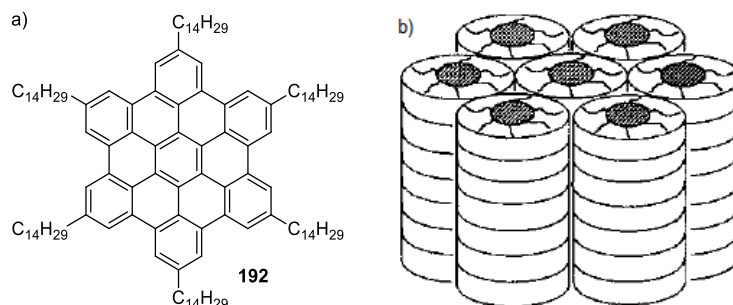


Figure 172. A HBC derivative reported by Warman (a) and a graphical representation of its hexagonal columnar mesophase (b).^{409a} Reprinted with permission from ref 409a. Copyright 1998 John Wiley and Sons.

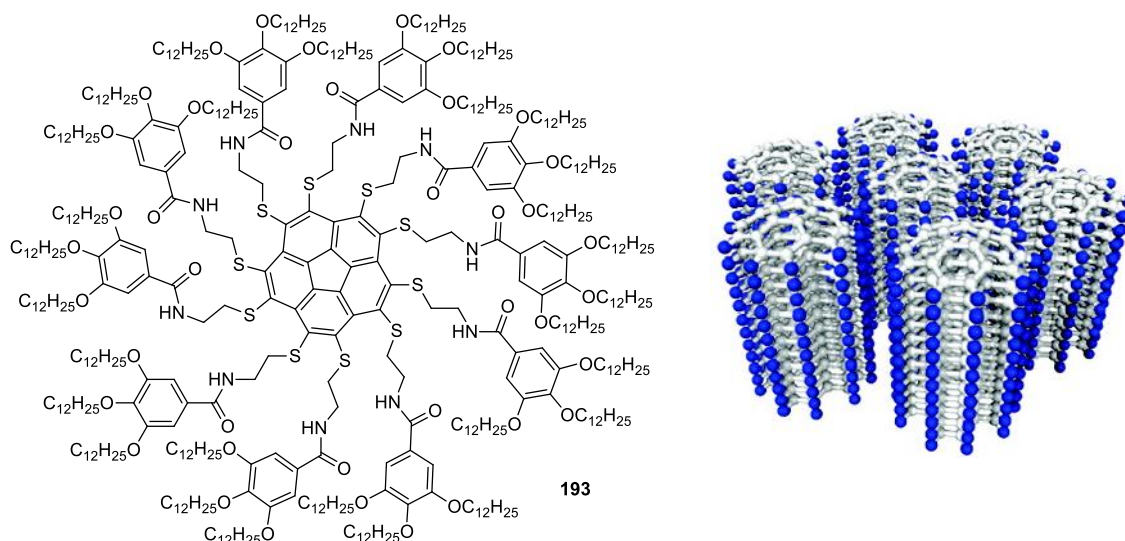


Figure 173. Corannulene derivative displaying a hexagonal columnar mesophase.⁴¹⁴ Reprinted with permission from ref 414. Copyright 2009 American Chemical Society.

When it comes to liquid crystals based on a positively curved PAHs, they were first reported by Aida and co-workers in 2009. Employing corannulene derivatives featuring long alkyl chains, they were able to identify the self-organization of these liquid crystalline materials into different mesophases, hexagonal columnar or lamellar, depending on the structure of the peripheral groups (Figure 173).⁴¹⁴

⁴¹⁰ a) L. Schmidt-Mende, A. Fechtenkötter, K. Müllen, E. Moons, R. H. Friend, J. D. MacKenzie, *Science* **2001**, 293, 1119-1122. b) W. W. H. Wong, J. Subbiah, S. R. Puniredd, B. Purushothaman, W. Pisula, N. Kirby, K. Müllen, D. J. Jones, A. B. Holmes, *J. Mater. Chem.* **2012**, 22, 21131-21137.

⁴¹¹ a) Ž. Tomović, M. D. Watson, K. Müllen, *Angew. Chem. Int. Ed.* **2004**, 43, 755-758. b) W. Pisula, Ž. Tomović, C. Simpson, M. Kastler, T. Pakula, K. Müllen, *Chem. Mater.* **2005**, 17, 4296-4303. c) X. Feng, J. Wu, M. Ai, W. Pisula, L. Zhi, J. P. Rabe, K. Müllen, *Angew. Chem. Int. Ed.* **2007**, 46, 3033-3036.

⁴¹² a) U. Rohr, P. Schlichting, A. Böhm, M. Gross, K. Meerholz, C. Bräuchle, K. Müllen, *Angew. Chem. Int. Ed.* **1998**, 37, 1434-1437. b) S. Alibert-Fouet, I. Seguy, J.-F. Bobo, P. Destruel, H. Bock, *Chem. Eur. J.* **2007**, 13, 1746-1753.

⁴¹³ S. Saïdi-Besbes, É Grelet, H. Bock, *Angew. Chem. Int. Ed.* **2006**, 45, 1783-1786.

⁴¹⁴ D. Miyajima, K. Tashiro, F. Araoka, H. Takezoe, J. Kim, K. Kato, M. Takata, T. Aida, *J. Am. Chem. Soc.* **2009**, 131, 44-45.

Later, other liquid crystals designed with a corannulene core showing lamellar, hexagonal or rectangular columnar mesophases were described.⁴¹⁵

1.3.3.2. Supramolecular nanotubular and nanofibrous assemblies

In 2004, Fukushima and Aida discovered that an amphiphilic HBC owning both ethylene glycol and long alkyl chains had the ability to self-assemble into a supramolecular electroconductive nanotube (Figure 174).⁴¹⁶ These nanotubes displayed relevant electrical conduction⁴¹⁷ and photo-conduction⁴¹⁸ properties, as well as, a one-handed helical chirality when assembled with chiral amphiphilic HBCs⁴¹⁹. Furthermore, it is possible to create supramolecular nanotubes by self-assembly of coronene bisimide⁴²⁰ or hexathienocoronene⁴²¹ amphiphiles.

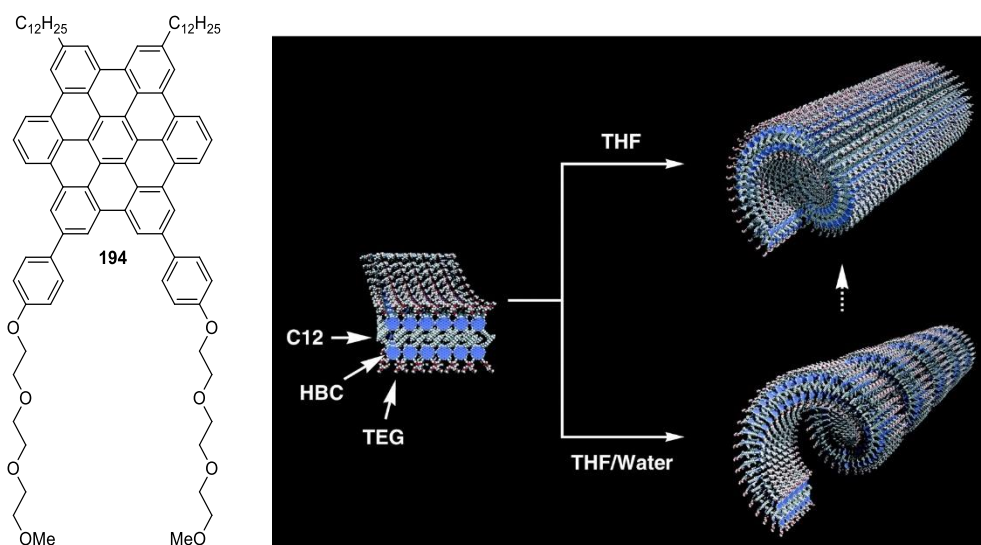


Figure 174. Amphiphilic HBC reported by Fukushima and Aida and graphical illustration of the proposed mechanism for the formation of the supramolecular nanotubes.⁴¹⁶ Reprinted with permission from ref 416. Copyright 2004 The American Association for the Advancement of Science.

⁴¹⁵ a) M. Mattarella, J. M. Haberl, J. Ruokolainen, E. M. Landau, R. Mezzeng, J. S. Siegel, *Chem. Commun.* **2013**, *49*, 7204-7206. b) Y. Bando, T. Sakurai, S. Seki, H. Maeda, *Chem. Asian J.* **2013**, *8*, 2088-2095. c) Y. Shoji, T. Kajitani, F. Ishiwari, Q. Ding, H. Sato, H. Anetai, T. Akutagawa, H. Sakurai, T. Fukushima, *Chem. Sci.* **2017**, *8*, 8405-8410.

⁴¹⁶ J. P. Hill, W. Jin, A. Kosaka, T. Fukushima, H. Ichihara, T. Shimomura, K. Ito, T. Hashizume, N. Ishii, T. Aida, *Science* **2004**, *304*, 1481-1483.

⁴¹⁷ a) Y. Yamamoto, T. Fukushima, W. Jin, A. Kosaka, T. Hara, T. Nakamura, A. Saeki, S. Seki, S. Tagawa, T. Aida, *Adv. Mater.* **2006**, *18*, 1297-1300. b) Y. Yamamoto, W. Jin, T. Fukushima, T. Minari, K. Tsukagoshi, A. Saeki, S. Seki, S. Tagawa, T. Aida, *Chem. Lett.* **2009**, *38*, 888-889.

⁴¹⁸ a) Y. Yamamoto, T. Fukushima, Y. Suna, N. Ishii, A. Saeki, S. Seki, S. Tagawa, M. Taniguchi, T. Kawai, T. Aida, *Science* **2006**, *314*, 1761-1764. b) Y. Yamamoto, T. Fukushima, A. Saeki, S. Seki, S. Tagawa, N. Ishii, T. Aida, *J. Am. Chem. Soc.* **2007**, *129*, 9276-9277. c) Y. He, Y. Yamamoto, W. Jin, T. Fukushima, A. Saeki, S. Seki, N. Ishii, T. Aida, *Adv. Mater.* **2010**, *22*, 829-832.

⁴¹⁹ W. Jin, T. Fukushima, M. Niki, A. Kosaka, N. Ishii, T. Aida, *Proc. Natl. Acad. Sci. U.S.A.* **2005**, *102*, 10801-10806.

⁴²⁰ K. V. Rao, S. J. George, *Org. Lett.* **2010**, *12*, 2656-2659.

⁴²¹ L. Chen, K. S. Mali, S. R. Puniredd, M. Baumgarten, K. Parvez, W. Pisula, S. De Feyter, K. Müllen, *J. Am. Chem. Soc.* **2013**, *135*, 13531-13537.

Additionally, the aggregation of planar nanographenes based on tetrabenzocoronene,⁴²² hexabenzocoronene⁴²³ or a larger derivative containing 132 carbons,⁴²⁴ and the self-assembly of donor-acceptor dyads featuring HBC and PDI moieties⁴²⁵ were found to afford nanofibres. These fibrous materials featured relevant electrical properties and were applied to create organic field-effect transistors.⁴²⁶ Moreover, the control of the self-assembly of smaller planar compounds like coronene⁴²⁷ or coronene bisimide derivatives⁴²⁸ generated fibres, and the introduction of chiral alkyl chains allowed for the control of the helicity of the fibres that were employed as spin filters.⁴²⁹ In addition, supramolecular nanofibrous assemblies were also constructed from the self-assembly of a π -donor coronene tetracarboxylate salt and a π -acceptor dodecyl methyl viologen and were exploited for electronic⁴³⁰ and sensing⁴³¹ applications (Figure 175).

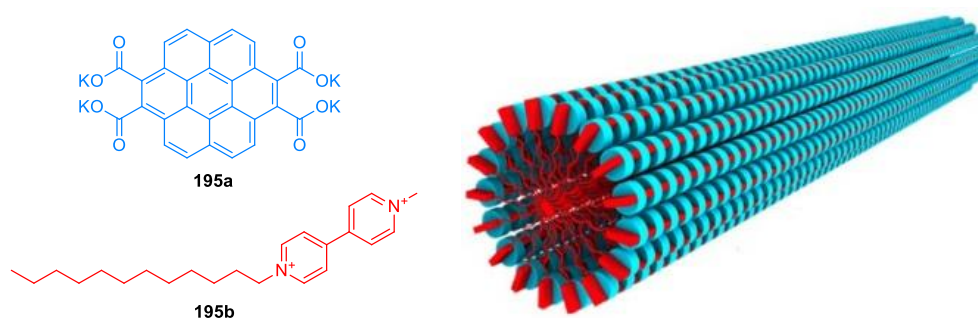


Figure 175. Graphical representation of a nanofibre achieved by self-assembly of coronene tetracarboxylate salt (**195a**) and dodecyl methyl viologen (**195b**).^{431b} Reprinted with permission from ref431b. Copyright 2017 American Chemical Society.

1.3.3.3. Supramolecular gels

According to the IUPAC, a gel can be defined as a “non-fluid colloidal network or polymer network that is expanded throughout its whole volume by a fluid.” When this material entraps an organic liquid, for example, an organic solvent, it is called an organogel. Similarly, when this liquid is water, it is a

⁴²² X. Zhang, X. Jiang, K. Zhang, L. Mao, J. Luo, C. Chi, H. S. O. Chan, J. Wu, *J. Org. Chem.* **2010**, *75*, 8069-8077.

⁴²³ a) S. Xiao, J. Tang, T. Beetz, X. Guo, N. Tremblay, T. Siegrist, Y. Zhu, M. Steigerwald, C. Nuckolls, *J. Am. Chem. Soc.* **2006**, *128*, 10700-10701. b) B. El Hamaoui, L. Zhi, W. Pisula, U. Kolb, J. Wu, K. Müllen, *Chem. Commun.* **2007**, 2384-2386.

⁴²⁴ V. Palermo, S. Morelli, C. Simpson, K. Müllen, P. Samorì, *J. Mater. Chem.*, 2006, *16*, 266–271.

⁴²⁵ J. M. Mativetsky, M. Kastler, R. C. Savage, D. Gentilini, M. Palma, W. Pisula, K. Müllen, P. Samorì, *Adv. Funct. Mater.* **2009**, *19*, 2486-2494.

⁴²⁶ M. Treier, A. Liscio, J. M. Mativetsky, M. Kastler, K. Müllen, V. Palermo, P. Samorì, *Nanoscale* **2012**, *4*, 1677-1681.

⁴²⁷ K. Takazawa, J.-I. Inoue, K. Mitsuishi, *Nanoscale* **2014**, *6*, 4174-4181.

⁴²⁸ C. Kulkarni, R. Munirathinam, S. J. George, *Chem. Eur. J.* **2013**, *19*, 11270-11278.

⁴²⁹ C. Kulkarni, A. K. Mondal, T. K. Das, G. Grinbom, F. Tassinari, M. F. J. Mabesoone, E. W. Meijer, R. Naaman, *Adv. Mater.* **2020**, *32*, 1904965.

⁴³⁰ A. A. Sagade, K. V. Rao, U. Mogera, S. J. George, A. Datta, G. U. Kulkarni, *Adv. Mater.* **2013**, *25*, 559-564.

⁴³¹ a) U. Mogera, A. A. Sagade, S. J. George, G. U. Kulkarni, *Sci. Rep.* **2015**, *4*, 4103. b) U. Mogera, M. Gedda, S. J. George, G. U. Kulkarni, *ACS Appl. Mater. Interfaces* **2017**, *9*, 32065-32070.

hydrogel. The three-dimensional network that immobilizes the fluid is composed by a solid component, called gelator, which is named organogelator or hydrogelator depending on the nature of the liquid trapped. Regarding supramolecular gels, they are formed by the assembly of low-molecular-weight gelators through non-covalent interactions.⁴³²

In 2000, Müllen and co-workers developed the first supramolecular organogel based on nanographene organogelators. For this purpose, they prepared *n*-dodecyl-functionalized dihexa-*peri*-hexabenzocoronenyldodecane or ^tBu-functionalized bishexa-*peri*-hexabenzocoronenyl nanographene that were found to form gels in toluene or *n*-heptane.⁴³³ Subsequently, Aida described that, in addition to its self-assembly into supramolecular nanotubes, his amphiphilic HBC molecule (**194**) could also lead to the formation of a gel.⁴¹⁶ Gel formation could also be achieved employing a HBC heptamer⁴³⁴ or a HBC unit functionalized with urea groups⁴³⁵ (Figure 176). Furthermore, the use of smaller PAHs gave the possibility to design organogels employing gelators based on coronene⁴³⁶ or corannulene^{415a} structures, as well as, hydrogels through the self-assembly of a coronene tetracarboxylate salt with a viologen derivative or organoclay.⁴³⁷

⁴³² X. Du, J. Zhou, J. Shi, B. Xu, *Chem. Rev.* **2015**, *115*, 13165-13307.

⁴³³ S. Ito, P. T. Herwig, T. Böhme, J. P. Rabe, W. Rettig, K. Müllen, *J. Am. Chem. Soc.* **2000**, *122*, 7698-7706.

⁴³⁴ L. Zhi, J. Wu, K. Müllen, *Org. Lett.* **2005**, *7*, 5761-5764.

⁴³⁵ X. Dou, W. Pisula, J. Wu, G. J. Bodwell, K. Müllen, *Chem. Eur. J.* **2008**, *14*, 240-249.

⁴³⁶ A. Jain, K. V. Rao, C. Kulkarni, A. George, S. J. George, *Chem. Commun.* **2012**, *48*, 1467-1469.

⁴³⁷ a) K. V. Rao, K. Jayaramulu, T. K. Maji, S. J. George, *Angew. Chem. Int. Ed.* **2010**, *49*, 4218-4222. b) K. V. Rao, K. K. R. Datta, M. Eswaramoorthy, S. J. George, *Angew. Chem. Int. Ed.* **2011**, *50*, 1179-1184.

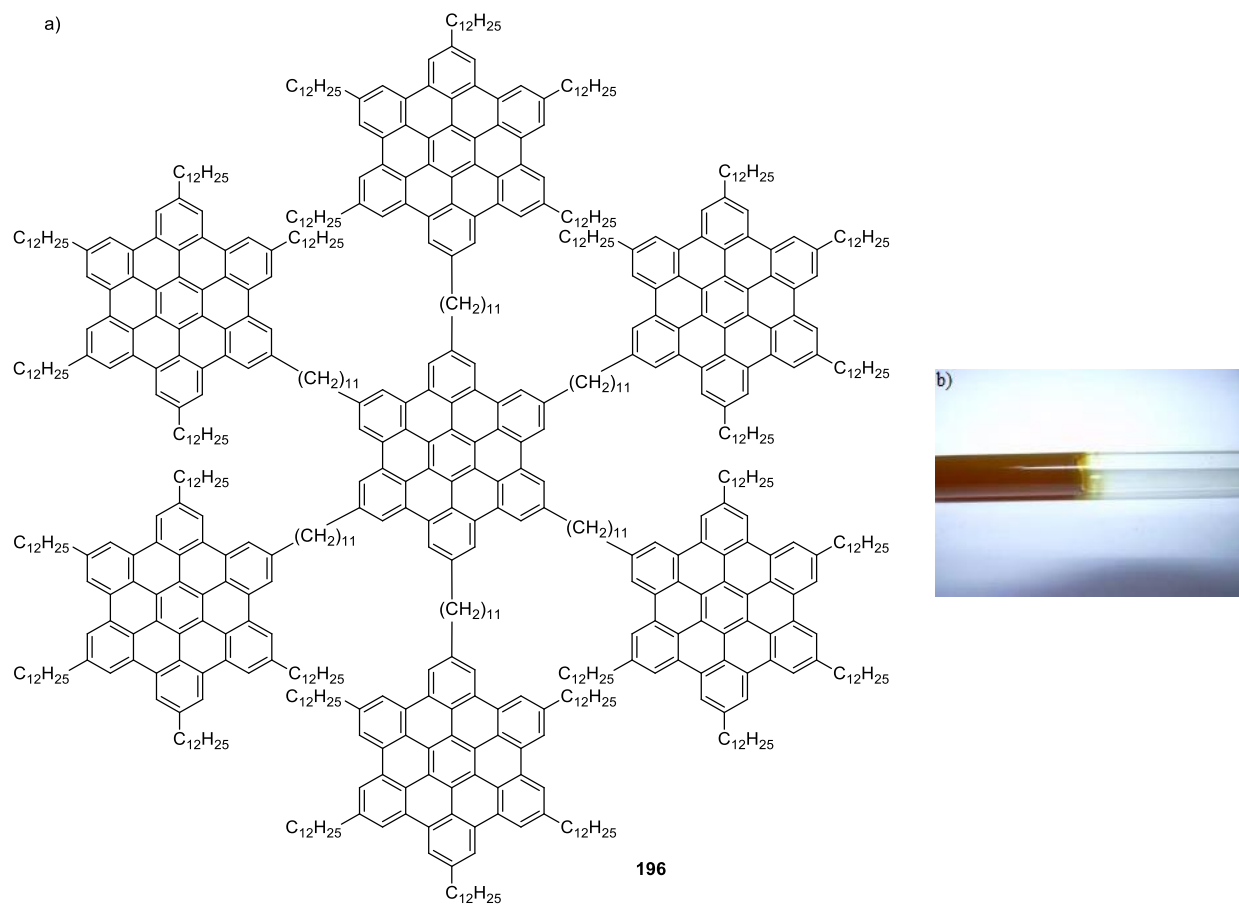


Figure 176. a) Structure of Müllen's HBC based organogelator (**196**). b) Picture of the organogel formed by **196** in toluene.⁴³⁴ Reprinted with permission from ref434. Copyright 2005 American Chemical Society.

2. Objectives

In this context, while planar and bowl-shaped PAHs exhibit very interesting host-guest and supramolecular properties those of saddle-shaped PAHs have remained almost completely unexplored. This prompted us to design a basic study of the supramolecular chemistry of saddle-shaped heptagon-containing nanographenes. To this end, we will use analogues of the well-known planar hexa-*peri*-benzocoronene (HBC) owning a heptagonal ring (hept-HBC) that will induce a saddle shape to the structure (Figure 178). This study will give us the fundamental knowledge required to address the incorporation of this kind of curved systems in more complex structures for supramolecular applications, which could lead to interesting systems taking into account the relevant properties these distorted PAHs exhibit.

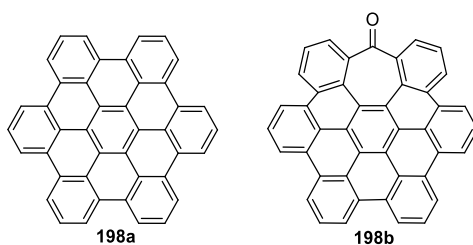


Figure 177. Planar HBC (198a) and saddle-shaped hept-HBC (198b).

For this purpose, we will start by studying the self-association in solution of a series of hept-HBC derivatives (Figure 179), trying to evaluate if the presence of the carbonyl group and/or the position and the nature of the peripheral groups have any influence on the process. Then, we will investigate their host-guest properties with a variety of aromatic derivatives.

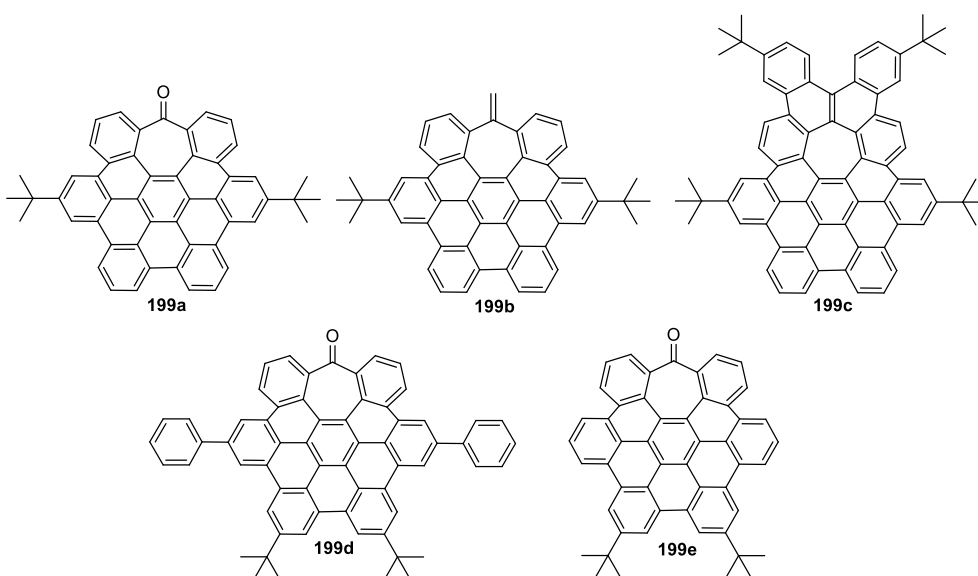


Figure 178. Designed structures of heptagon-containing PAHs for the study of their self-association and their host-guest properties with other aromatic compounds.

Furthermore, if the self-association in solution of these negatively curved nanographenes gives good results, we will design amphiphiles based on a hept-HBC structure in order to create supramolecular assemblies, that could possibly afford nanofibers or nanotubes (Figure 180).

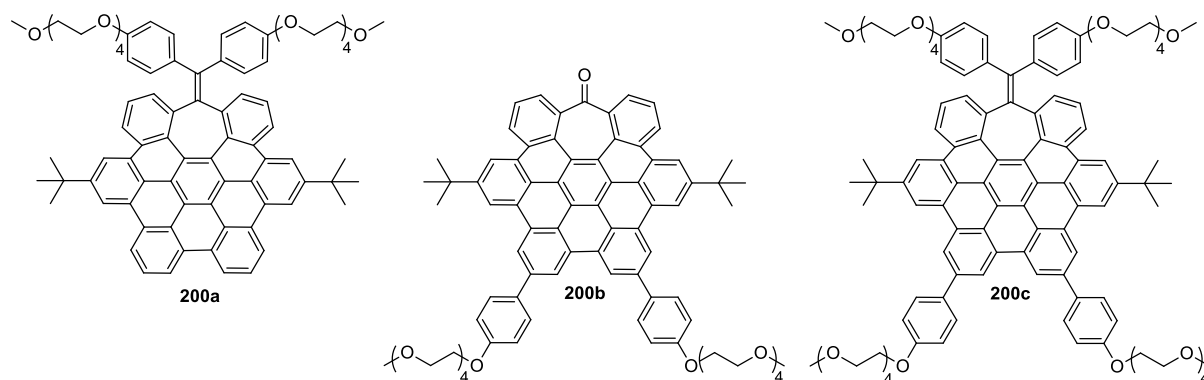


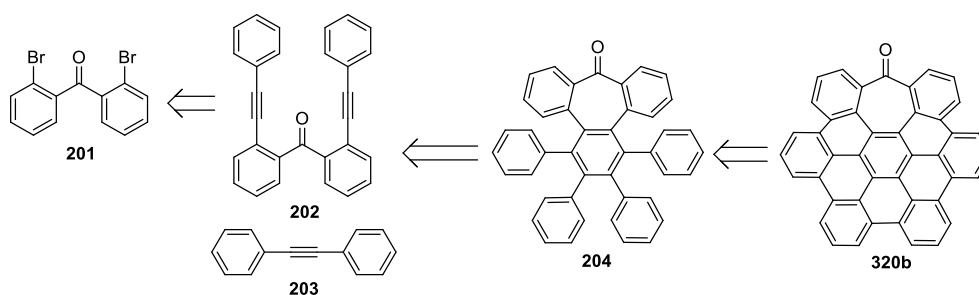
Figure 179. Proposed amphiphilic hept-HBC derivatives **200a-c**.

3. Results and discussion

3.1. Self-association and host-guest properties of heptagon-containing nanographenes

3.1.1. Synthesis and characterization

The synthesis of the proposed distorted nanographenes owning a heptagon ring was tackled employing a strategy developed by our group.⁴³⁸ With the aim of synthesizing a hept-HBC derivative such as **320b**, we will proceed to a final Scholl-type cyclodehydrogenation reaction on a tropone derivative such as **204**. This will be prepared by a Co-catalyzed cyclotrimerization using a diphenylacetylene derivative and a compound generated by Sonogashira cross-coupling reactions starting from 2,2'-dibromobenzophenone (**201**) (Scheme 83).

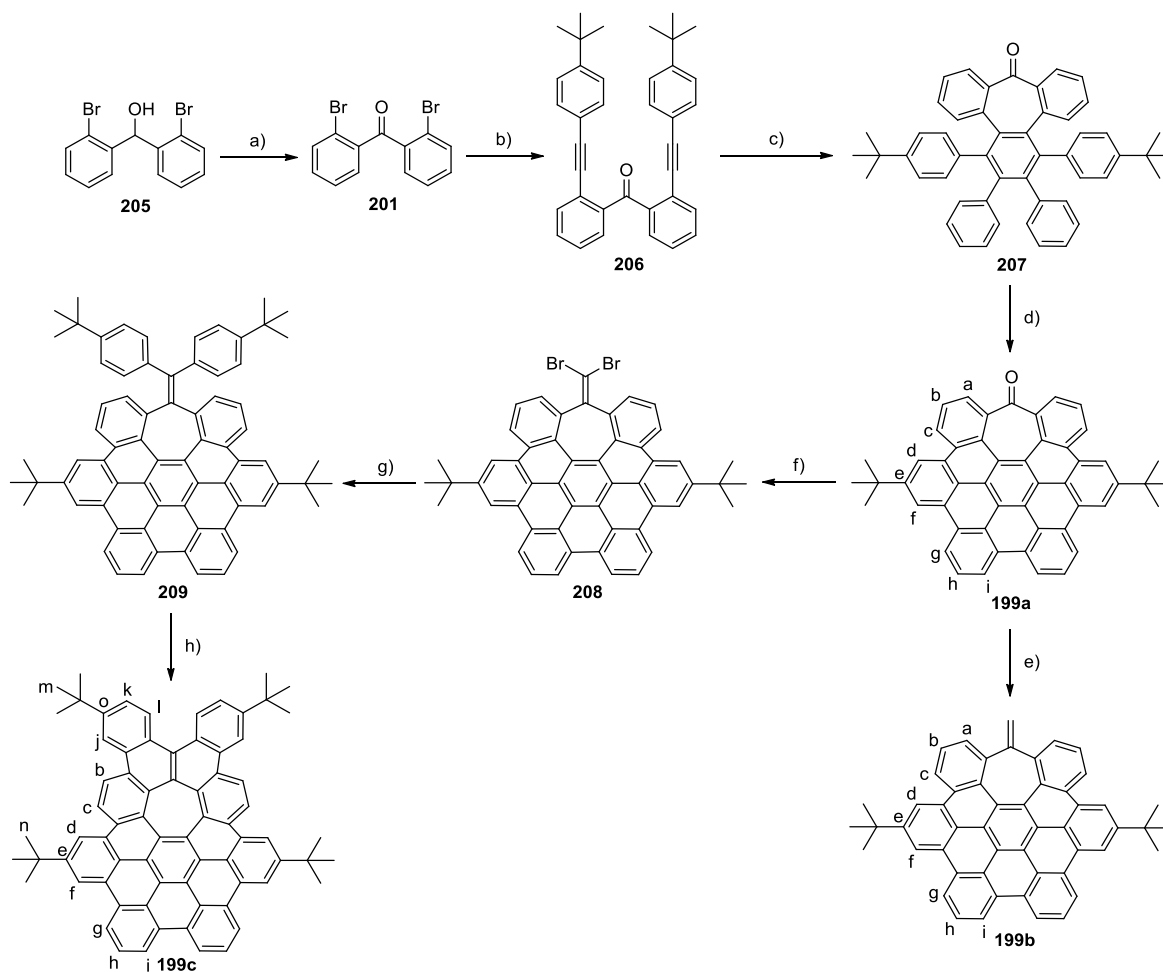


Scheme 83. Retrosynthetic plan to obtain hept-HBC derivatives.

Regarding the synthesis of nanographenes **199a-c**, **205** was treated with Dess-Martin periodinane at 0 °C yielding 2,2'-dibromobenzophenone (**201**). The latter underwent a Sonogashira coupling in the presence of 4-*tert*-butylphenylacetylene, followed by a cyclotrimerization with diphenylacetylene catalyzed by $\text{Co}_2(\text{CO})_8$ to give intermediate **207** incorporating a tropone group in moderate yield (55%). Subsequently, this compound went through a Scholl-type cyclodehydrogenation reaction employing DDQ and triflic acid to obtain nanographene **199a** in moderate yield (45%).⁴³⁹ Treatment of the **199a** with Tebbe reagent afforded nanographene **199b** which featured a terminal alkene instead of the carbonyl group in excellent yield (98%). Finally, a Wittig-like reaction on **199a** in the presence of CBr_4 and PPh_3 yielded 1,1-dibromoalkene **208** in good yield (83%). A Suzuki cross-coupling reaction with 4-*tert*-butylphenylboronic acid on intermediate **208**, followed by a cyclodehydrogenation reaction using FeCl_3 afforded the target extended nanographene **199c** in excellent yield (96%) (Scheme 84).

⁴³⁸ I. R. Márquez, N. Fuentes, C. M. Cruz, V. Puente-Muñoz, L. Sotorrios, M. L. Marcos, D. Choquesillo-Lazarte, B. Biel, L. Crovetto, E. Gómez-Bengoa, M. T. González, R. Martín, J. M. Cuerva, A. G. Campaña, *Chem. Sci.* **2017**, *8*, 1068-1074.

⁴³⁹ Compounds **199a**, **206** and **207** were prepared according to a procedure established in our group: Ref 438.

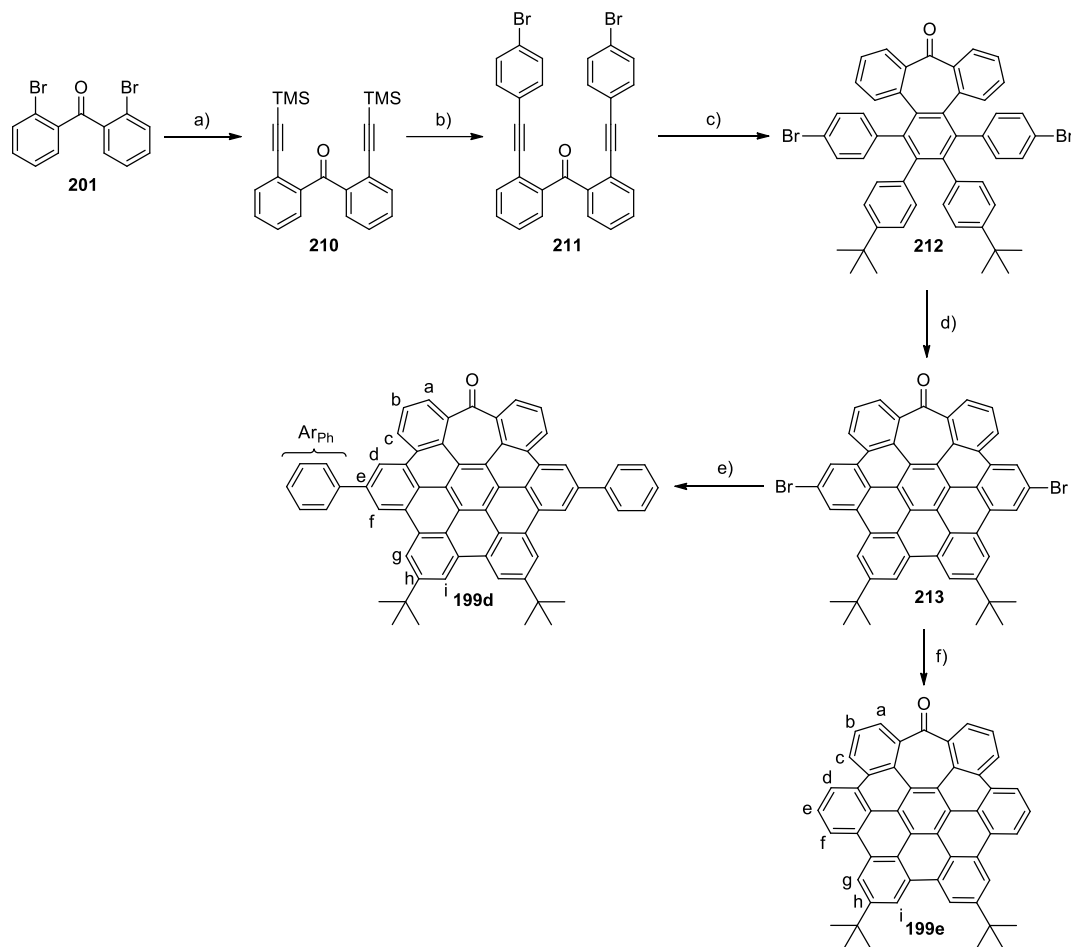


Scheme 84. Synthesis of nanographenes **199a-c**. Reagents and conditions: a) Dess-Martin periodinane, CH_2Cl_2 , 0°C , 2 h, 71%. b) 4-*tert*-butylphenylacetylene, $\text{PdCl}_2(\text{PPh}_3)_2$, $\text{P}^t\text{Bu)HBF}_4$, CuI , $^i\text{Pr}_2\text{NH}$, THF, r.t., 18 h, 98%. c) diphenylacetylene, $\text{Co}_2(\text{CO})_8$, dioxane, 100°C , 16 h, 55%. d) DDQ, $\text{CF}_3\text{SO}_3\text{H}$, CH_2Cl_2 , 0°C , 10 min, 45%. e) Tebbe reagent (0.5 M in toluene), THF, 0°C to r.t., 2 h, 98%. f) PPh_3 , CBr_4 , toluene, reflux, 28 h, 83%. g) 4-*tert*-butylphenylboronic acid, $\text{Pd}(\text{PPh}_3)_4$, K_2CO_3 , toluene, EtOH, H_2O , 100°C , 20 h, 84%. h) FeCl_3 , 1,2-dichloroethane, CH_3NO_2 , 70°C , 48 h, 96%.

Regarding the synthesis of nanographenes **199d,e**, the synthetic route started with a Sonogashira coupling between 2,2'-dibromobenzophenone (**201**) and trimethylsilylacetylene followed by a *one-pot* deprotection of the silyl group in the presence of DBU and H_2O and a Sonogashira coupling⁴⁴⁰ with 1-bromo-4-iodobenzene, which afforded intermediate **211** in moderate yield (67%). Co-catalyzed cyclotrimerization of **211** with 4,4'-di-*tert*-butyldiphenylacetylene and a subsequent cyclodehydrogenation reaction with DDQ and triflic acid gave nanographene **213**, functionalized with two Br atoms. This aryl bromide groups allow the expansion of the nanographene structure. Hence, a Suzuki cross-coupling reaction between **213** and phenyl boronic acid afforded the target nanographene **199d** in good yield (70%). Moreover, the same reaction conditions promoted, in

⁴⁴⁰ M. J. Mio, L. C. Kopel, J. B. Braun, T. L. Gadzikwa, K. L. Hull, R. G. Brisbois, C. J. Markworth, P. A. Grieco, *Org. Lett.* **2002**, *4*, 3199-3202.

absence of boronic acid, the removal of the Br atoms and the formation of the reduced nanographene **199e** in moderate yield (56%) (Scheme 85).



Scheme 85. Synthesis of nanographenes **199d,e**. Reagents and conditions: a) trimethylsilylacetylene, $\text{PdCl}_2(\text{MeCN})_2$, CuI, $\text{P}(\text{tBu})_3 \cdot \text{HBF}_4$, THF/ $i\text{Pr}_2\text{NH}$, r.t., 3 h, 90%. b) 1-bromo-4-iodobenzene, $\text{PdCl}_2(\text{PPh}_3)_2$, CuI, Et_3N , DBU, THF/ H_2O , 70 °C, 16 h, 67%. c) 4,4'-di-*tert*-butyldiphenylacetylene, $\text{Co}_2(\text{CO})_8$, toluene, 110 °C, 16 h, 56%. d) DDU, $\text{CF}_3\text{SO}_3\text{H}$, CH_2Cl_2 , 0 °C, 10 min, 52%. e) Phenyl boronic acid, $\text{Pd}(\text{PPh}_3)_4$, K_2CO_3 , toluene/ H_2O / EtOH , reflux, 20 h, 70%. f) $\text{Pd}(\text{PPh}_3)_4$, K_2CO_3 , toluene/ H_2O / EtOH , reflux, 16 h, 56%.

As expected, these curved PAHs are very soluble in organic solvents which allows their full characterisation. Indeed, the ^1H and ^{13}C NMR for nanographene **199a-e** are consistent with the proposed structures (Figures 181-182 for **199c**). Furthermore, the assignment of their ^1H signals was achieved by the analysis of 2D NMR experiments. Finally, the identity of these nanographenes was confirmed by HRMS since their exact masses and isotopic distributions of the signals observed perfectly match the theoretical ones (Figure 183 for **199b**).

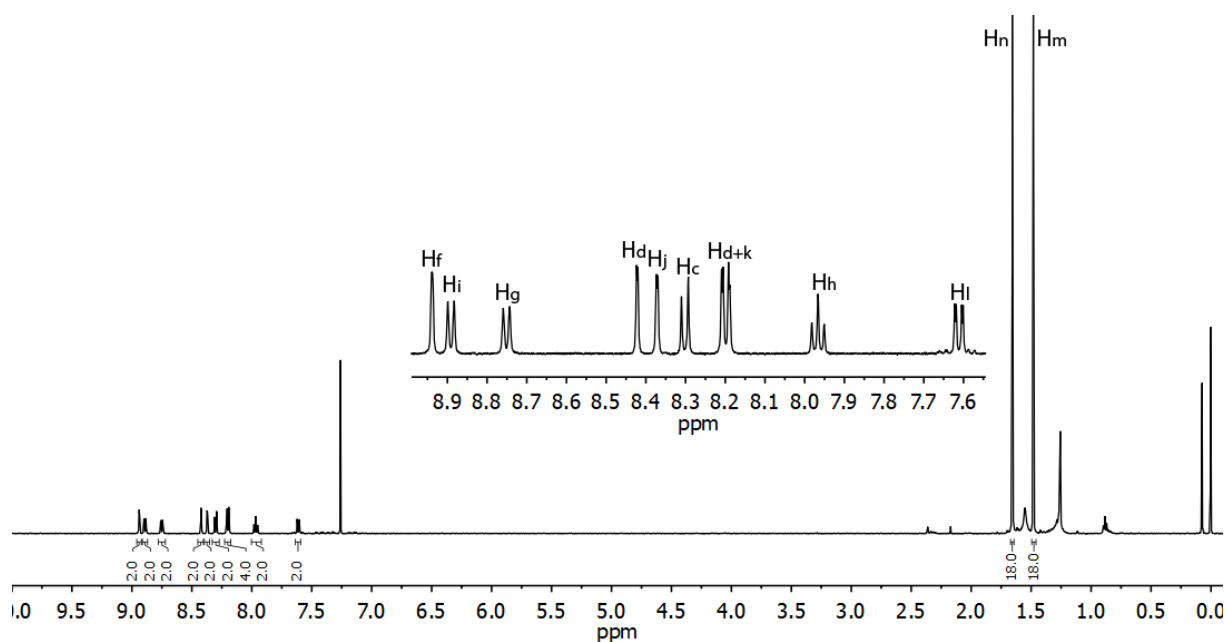


Figure 180. ^1H NMR (500 MHz, CDCl_3) spectrum of nanographene **199c** (ca. 8 mM). Lettering coding is defined in Scheme 84.

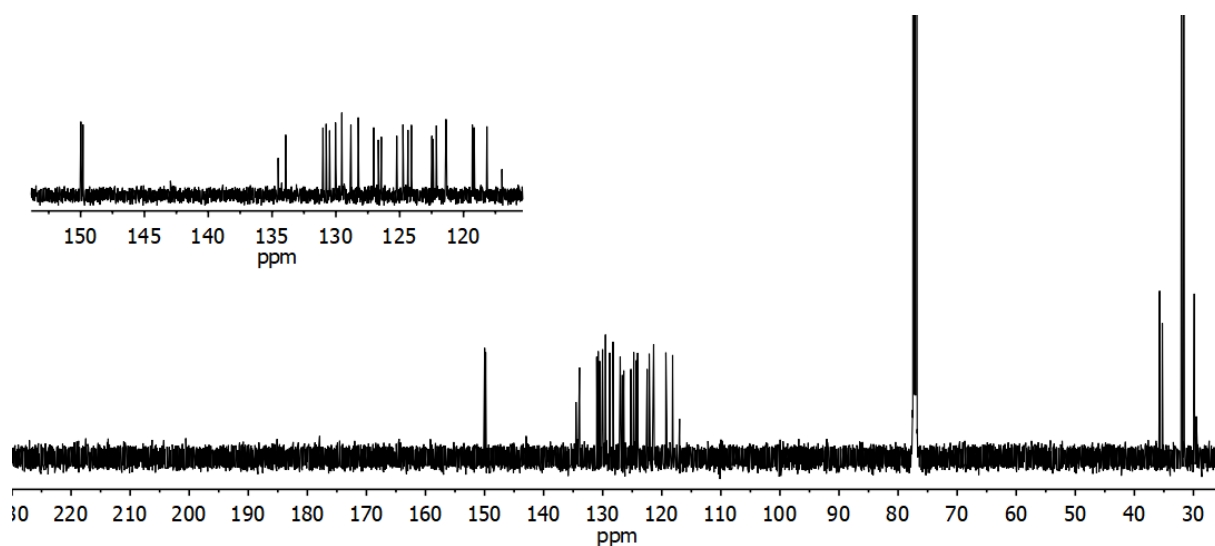


Figure 181. ^{13}C NMR (126 MHz, CDCl_3) spectrum of nanographene **199c**.

The structure of these five nanographenes **199a-e** was also studied by DFT calculations at the $\omega\text{B97XD/def2SVP}$ or B3LYP/6-31G(d,p) levels, affording both very similar results. As expected, these nanographenes exhibited a distorted structure. **199a,b,d,e** clearly displayed a saddle curvature due to the presence of the seven-membered ring while that of **199c** is twisted as a consequence of the steric hindrance induced by H_i . The size of the substituted-hept-HBC derivatives **199a,b,d,e** is approximately $11.4 \times 10.5 \text{ \AA}$ whereas that of the extended nanographene **199c** is around $16.1 \times 11.0 \text{ \AA}$ (Figure 184).

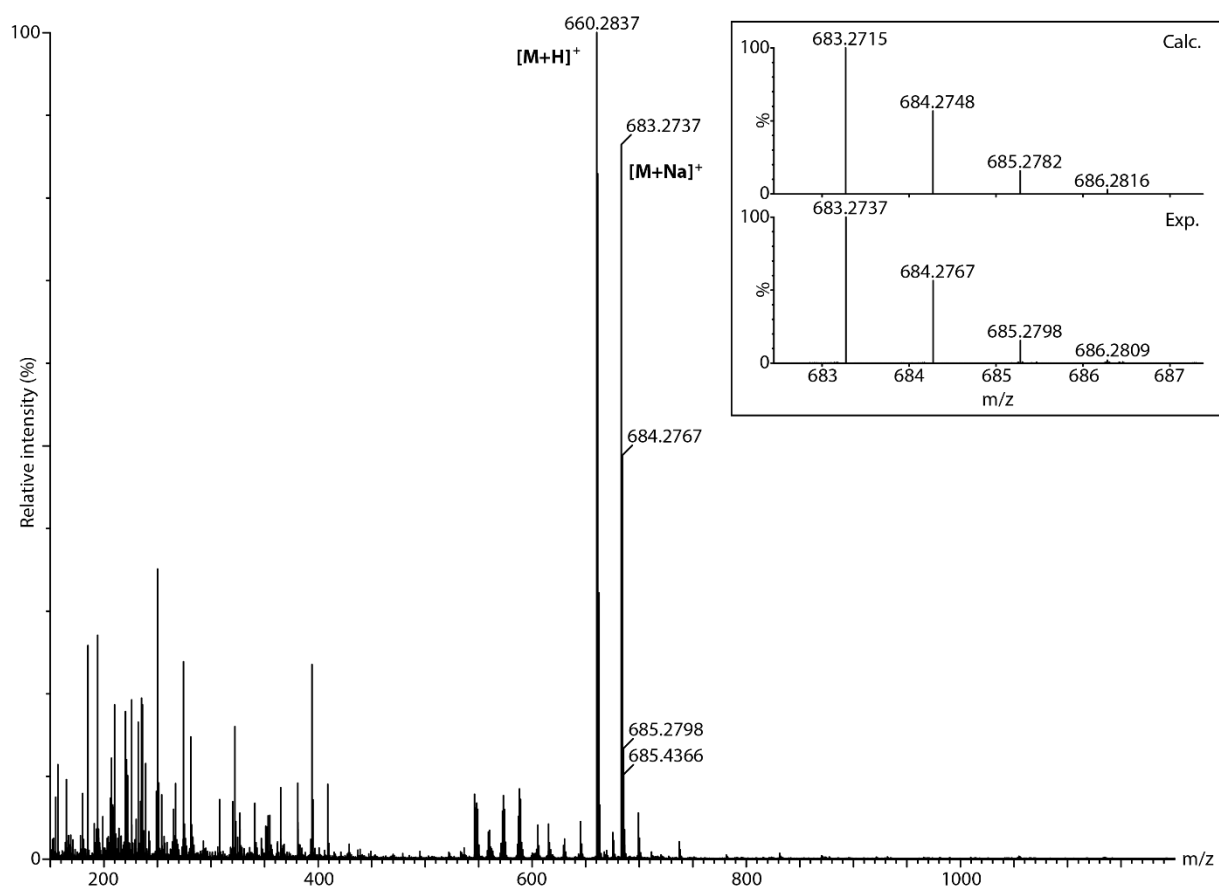


Figure 182. HRMS (ESI⁺) spectrum of nanographene **199b**. Inset: Experimental (top) and calculated (bottom) isotopic distribution for the signal corresponding to the [M+Na]⁺ ion.

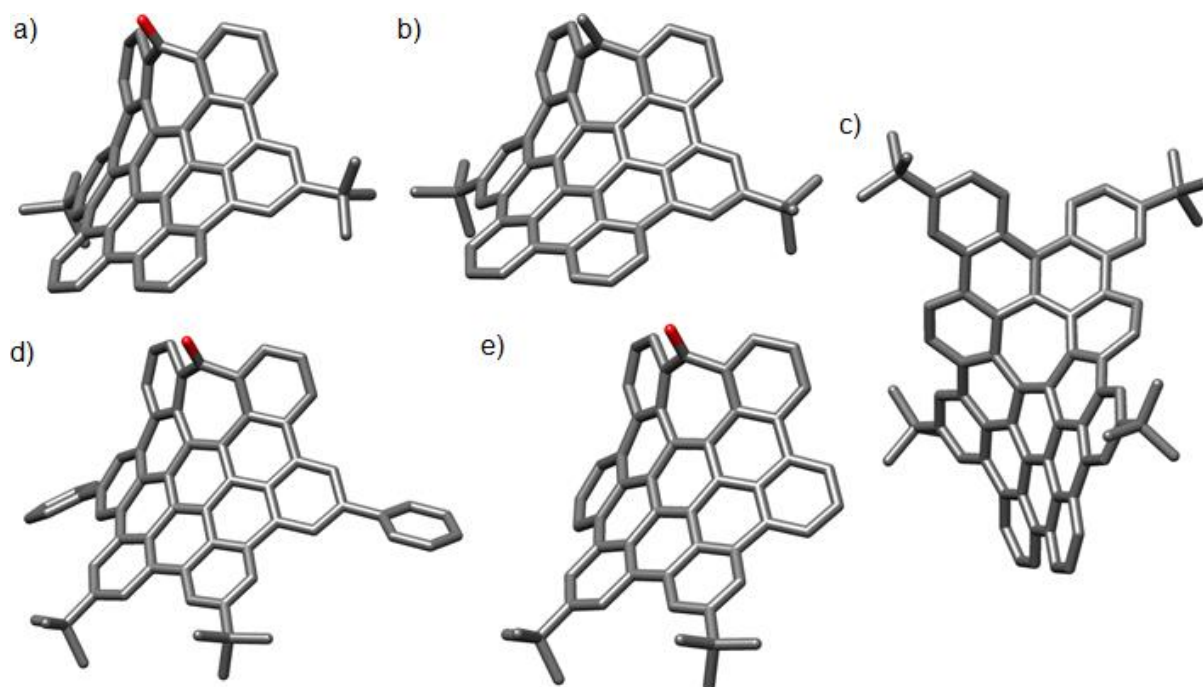


Figure 183. DFT (ω B97XD/def2SVP in CHCl₃) optimized structure of nanographenes: a) **199a**. b) **199b**. c) **199c**. d) **199d**. e) **199e**. H atoms have been omitted for clarity. Color coding: C, gray; O, red.

3.1.2. Study of the self-association

During the synthesis and the characterization process, we noticed that the chemical shifts of the nanographene protons were concentration dependent. This was a sign of self-association and therefore, of the formation of dimers or oligomers. Thus, in order to study the monomer-dimer equilibrium and estimate the association constant, we recorded various ^1H NMR spectra of nanographenes **199a-e** at different concentrations (1 mM to 100 mM) in CDCl_3 .⁴⁴¹ Subsequently, the monomer-dimer equilibrium constant (K_d) was determined by non-linear least-squares fitting using eq. 7:⁴⁴²

$$\delta = \Delta\delta \times \left(1 + \frac{1 - \sqrt{8K_d C + 1}}{4K_d C} \right) + \delta_m \quad (\text{Eq. 7})$$

The subscripts m and d refer respectively to the monomer and the dimer; C denotes the concentration; δ is the observed chemical shift; $\Delta\delta$ ($\Delta\delta = \delta_d - \delta_m$) stands for the change in chemical shift from the monomer to the dimer; and K_d represents the association constant for the dimer formation.

The experimental results nicely fit with model described by eq. 7 and the estimated values for the monomer-dimer equilibrium constant (K_d) range from 1.5 ± 0.5 to $24 \pm 4 \text{ M}^{-1}$. As can be seen on Table 5, the order of magnitude of K_d is fairly similar for every compound, except for **199d**, which shows a slightly higher constant (Figure 185, Table 24). We attribute this singularity to the phenyl ring added on the C_e position which expands the aromatic surface that can be brought into contact with the second nanographene unit in order to form the dimer.

Table 24. Monomer-dimer equilibrium constants (K_d) in CDCl_3 at 298 K of nanographenes **199a-e**.

Nanographene	199a	199b	199c	199d	199e
$K_d (\text{M}^{-1})$	3.0 ± 0.2	1.5 ± 0.5	6.7 ± 2.0	24 ± 4	6.0 ± 0.6

⁴⁴¹ Attempts to dissolve nanographene **199c** in CD_2Cl_2 , acetone- d_6 and CD_3CN and in order to obtain a 30 mM solution were unsuccessful. Thus, by adding a known proportion of CDCl_3 , **199c** dissolved. However, the recorded spectra using these mixtures of deuterated solvents ($\text{CD}_2\text{Cl}_2/\text{CDCl}_3$ (9:2), acetone- d_6/CDCl_3 (7:3) and $\text{CD}_3\text{CN}/\text{CDCl}_3$ (5:6)) were, in every case, very broad which made impossible the analysis of these data. Consequently, to allow a comparison between the data obtained for different compounds, we chose to perform this study employing CDCl_3 as solvent.

⁴⁴² M. Chu, A. N. Scioneaux, C. S. Hartley, *J. Org. Chem.* **2014**, *79*, 9009-9017.

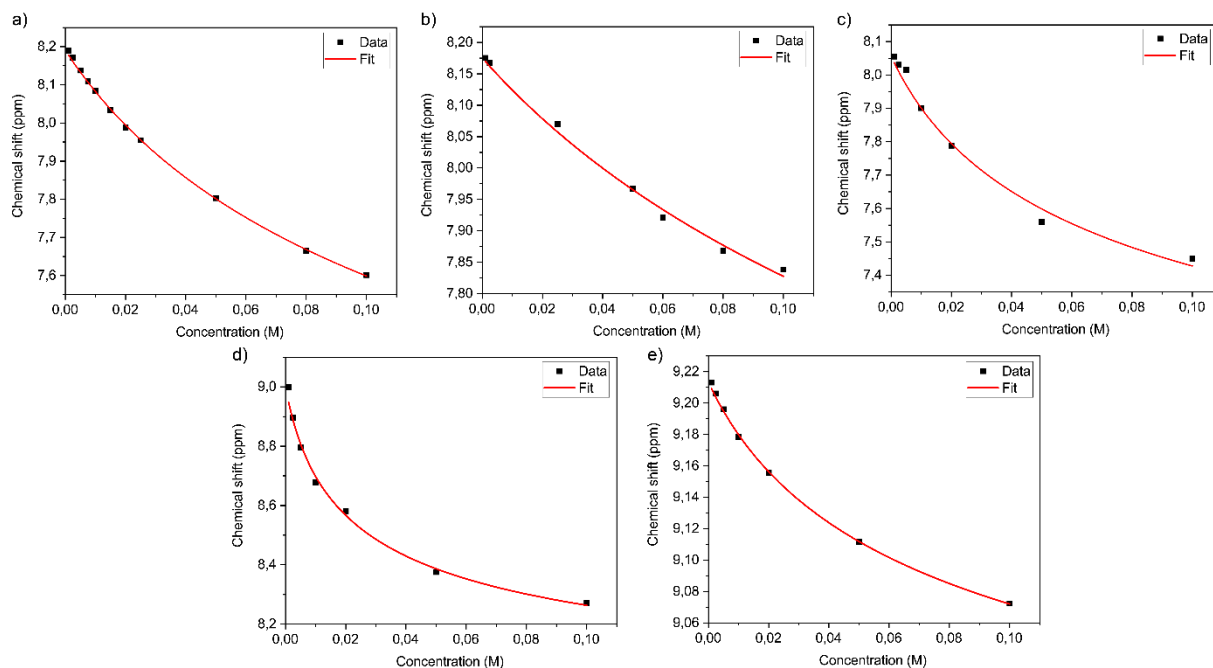


Figure 184. Non-linear least-squares fitting of the shifting of the δ (400 MHz, CDCl_3 , 298 K) upon concentration change for: a) Signal of H_h of **199a** ($K_d = 3.0 \pm 0.2 \text{ M}^{-1}$). b) Signal of H_h of **199b** ($K_d = 1.5 \pm 0.5 \text{ M}^{-1}$). c) Signal of H_h of **199c** ($K_d = 6.7 \pm 2.0 \text{ M}^{-1}$). d) Signal of H_d of **199d** ($K_d = 24 \pm 4 \text{ M}^{-1}$). e) Signal of H_i of **199e** ($K_d = 6.0 \pm 0.6 \text{ M}^{-1}$).

During these experiments, almost every proton signals underwent an upfield shift upon increase of the concentration of the nanographene. After a careful inspection of the shiftings experienced by the different signals and the identification of those most affected by the aggregation process, it became clear that the position of the ^tBu groups in these molecules had a key role in how these saddle-shaped compounds self-assemble. When the ^tBu units were located on carbons C_h, protons next to the tropone unit were very shielded ($\Delta\delta_{\text{Hc}} = -0.73 \text{ ppm}$; $\Delta\delta_{\text{Hd}} = -0.90 \text{ ppm}$; $\Delta\delta_{\text{He}} = -0.63 \text{ ppm}$ for **199e**), while the upfield shift of H located on the more planar part of the hept-HBC was weak ($\Delta\delta_{\text{Hi}} = -0.14 \text{ ppm}$ for **199e**) (Figure 186). Similar changes of chemical shift were observed for **199d**. Conversely, when the ^tBu moieties were placed on carbons C_e and C_o, the most impacted protons were situated on the more planar part of the nanographene ($\Delta\delta_{\text{Hi}} = -0.76 \text{ ppm}$; $\Delta\delta_{\text{Hh}} = -0.59$; $\Delta\delta_{\text{Hg}} = -0.48 \text{ ppm}$ for **199a**), while the modifications induced by the increase of the concentration on the protons close to the tropone moiety was minimal ($\Delta\delta_{\text{Ha}} = -0.07 \text{ ppm}$; $\Delta\delta_{\text{Hb}} = -0.16 \text{ ppm}$; $\Delta\delta_{\text{Hc}} = -0.21 \text{ ppm}$ for **199a**) (Figure 187). Similar shiftings of the ¹H signals were observed for **199b,c** demonstrating that the modification of the tropone unit and the introduction of an enhanced distortion did not influence much the self-association behaviour of these molecules. Therefore, it is obvious that the ^tBu groups are preventing the approach of the nanographene and as a result, the self-assembly of nanographenes **199d,e** takes place on the side where the tropone unit is, while for **199a-c**, the binding seems to be more intense on the other side of the molecule, where C_g, C_h and C_i are situated (Figure 188).

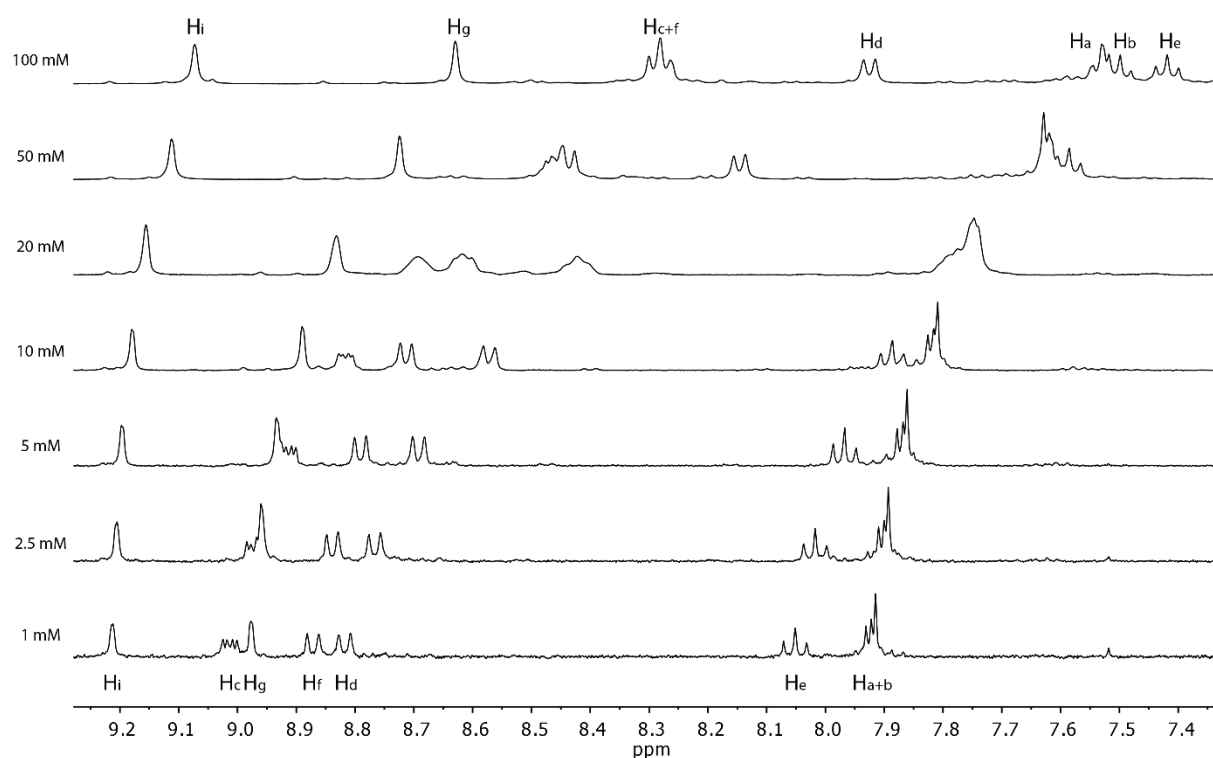


Figure 185. Self-association experiment of nanographene **199e**. Aromatic region of the ^1H NMR (400 MHz, CDCl_3) spectra of **199e** at different concentrations. Lettering coding is defined in Scheme 85.

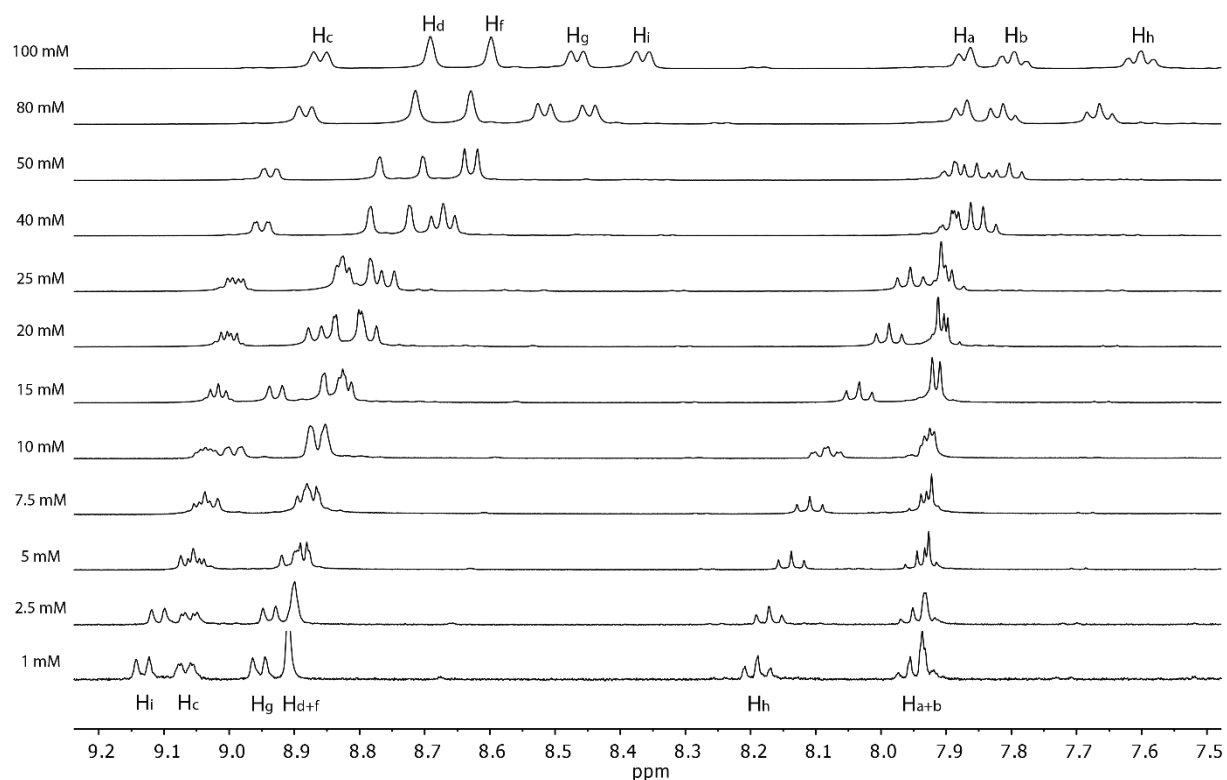


Figure 186. Self-association experiment of nanographene **199a**. Aromatic region of the ^1H NMR (400 MHz, CDCl_3) spectra of **199a** at different concentrations. Lettering coding is defined in Scheme 84.

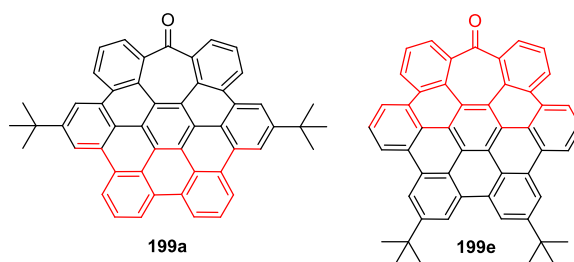


Figure 187. Structure of hept-HBC derivatives **199a,e** showing the zone where the self-assembly takes place (in red) depending of the position of ^tBu peripheral groups.

Consequently, the self-association of saddle-shaped hept-HBC nanographenes was proven. Furthermore, the position and the nature of the peripheral groups have shown to play an important role in the aggregation of these compounds. On the contrary, the enhancement of the distortion of hept-HBC derivatives or the modification of the tropone unit revealed to have a little effect on the self-association properties.

3.1.3. Study of the host-guest properties

After studying the self-association of negatively curved nanographenes **199a-e**, we turned our attention to the study of their host-guest properties in solution with different aromatics. We chose planar PAHs, such as pyrene (**214a**) or benzo[*a*]pyrene (**214b**), a π -acceptor NDI derivative **60a**, a π -donor 1,5-dialkoxynaphthalene derivative **214c** and also curved carbon structures such as corannulene and fullerenes (C₆₀ and C₇₀) as representative examples of the different aromatic systems we were interested to test (Figure 189).

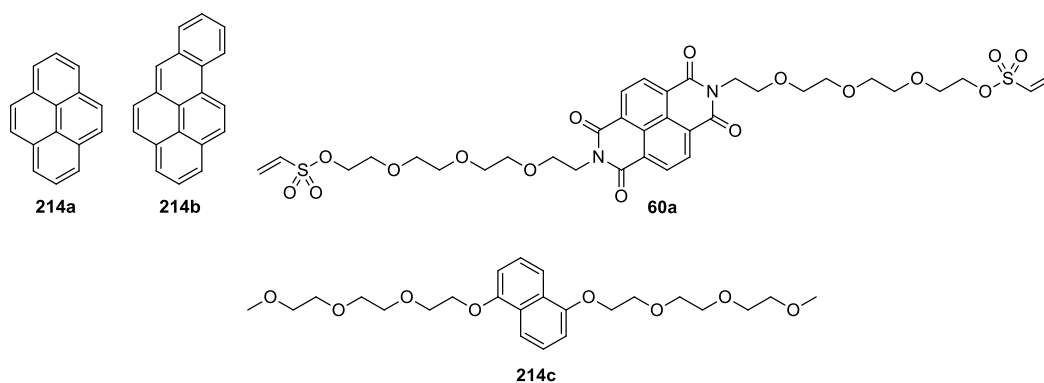
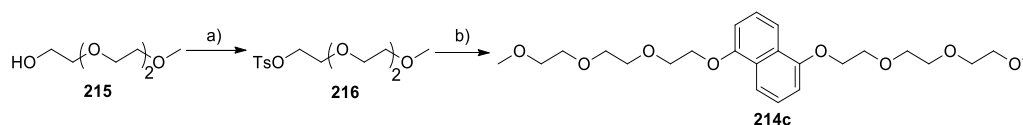


Figure 188. Planar PAHs employed to study the host-guest properties of the heptagon-containing nanographenes.



Scheme 86. Synthesis of compound **214c**. Reagents and conditions: a) TsCl, Et₃N, DMAP_(cat.), CH₂Cl₂, r.t., 20 h, 91%. b) 1,5-dihydroxynaphthalene, K₂CO₃, KI_(cat.), acetone, reflux, 20 h, 97%.

For this purpose, **214c** was synthesized through a Williamson reaction between tri(ethylene glycol) monomethyl ether tosylate and 1,5-dihydroxynaphthalene (Scheme 86).

The association constants (K_a) between nanographenes and PAHs or fullerenes were determined by ^1H or ^{13}C NMR titration experiments in CDCl_3 or $o\text{-DCB-}d_4$ at 298 K. The NMR data were analyzed using a nonlinear least-squares curve fitting procedure performed with the online software *Bindfit* (<http://supramolecular.org/>) with a 1:1 global fitting model (Nelder-Mead method).²³³

The results are summarized on Table 25. Nanographenes **199a-e** displayed higher association constants with NDI and 1,5-dialkoxynaphthalene derivatives than with pyrene and benzo[*a*]pyrene. It is worth noting that nanographenes possessing ^tBu groups on the C_h position (**199d,e**) did not bind to pyrene whereas all exhibited a similar association constant with benzo[*a*]pyrene ($3 - 6 \text{ M}^{-1}$). Regarding their binding affinity with NDI derivatives, the position of ^tBu groups is of key importance since the association constant is higher for those owning this unit on C_e ($18 - 22 \text{ M}^{-1}$) than for those substituted on C_h ($7 - 9 \text{ M}^{-1}$). Moreover, the maximum values of K_a for planar PAHs were obtained with 1,5-dialkoxynaphthalene derivative **214c** culminating at $65.7 \pm 2.1 \text{ M}^{-1}$ for nanographene **199c**. Finally, it seems that, in general, these nanographenes, except **199b**, bind more strongly to electron rich PAHs (Table 25).

By looking at the variation of chemical shift induced by the addition of those different substrates, it is clear that the interaction between pyrene, benzo[*a*]pyrene, **60a** and nanographenes **199a-e** takes place on the more planar part of those (near C_g , C_h and C_i) since the signals of H_g , H_h and H_i undergo an upfield shift while H_a , H_b , H_c , H_d or the CH_2 suffer a downfield shift (Figures 190, 191 and 192). Respect to **214c**, the changes of chemical shift observed during the titration are minimal (up to $|0.02|$ ppm) which makes difficult a precise and unequivocal spatial assignment of the interaction (Figure 193).

Table 25. Calculated association constants (K_a ; unit: M^{-1}) between nanographenes **199a-e** and different aromatic guests.

	Pyrene ^[a]	Benzo[<i>a</i>]pyrene ^[a]	NDI derivative (58a) ^[a]	1,5-dialkoxynaphthalene derivative (194c) ^[a]	Corannulene ^[a]	C_{60} ^[b]	C_{70} ^[b]
199a	20.9 ± 0.8	4.07 ± 0.08	17.7 ± 0.3	15.9 ± 0.8	13.5 ± 0.7	12.3 ± 0.2	50.2 ± 2.2
199b	8.03 ± 0.11	6.05 ± 0.06	21.8 ± 0.7	7.96 ± 0.34	13.4 ± 0.7	15.8 ± 0.2	35.3 ± 1.3
199c	8.04 ± 0.18	6.48 ± 0.13	17.7 ± 0.2	65.7 ± 2.1	10.9 ± 0.5	18.5 ± 0.3	53.1 ± 2.4
199d	< 0.01	4.73 ± 0.12	7.26 ± 0.11	18.4 ± 1.2	< 0.01	20.0 ± 0.1	3.75 ± 0.02
199e	< 0.01	3.67 ± 0.06	9.40 ± 0.13	36.6 ± 2.6	8.40 ± 0.53	8.13 ± 0.07	28.3 ± 0.7

[a] Measured by ^1H NMR in CDCl_3 . [b] Measured by ^{13}C NMR in $o\text{-DCB-}d_4$.

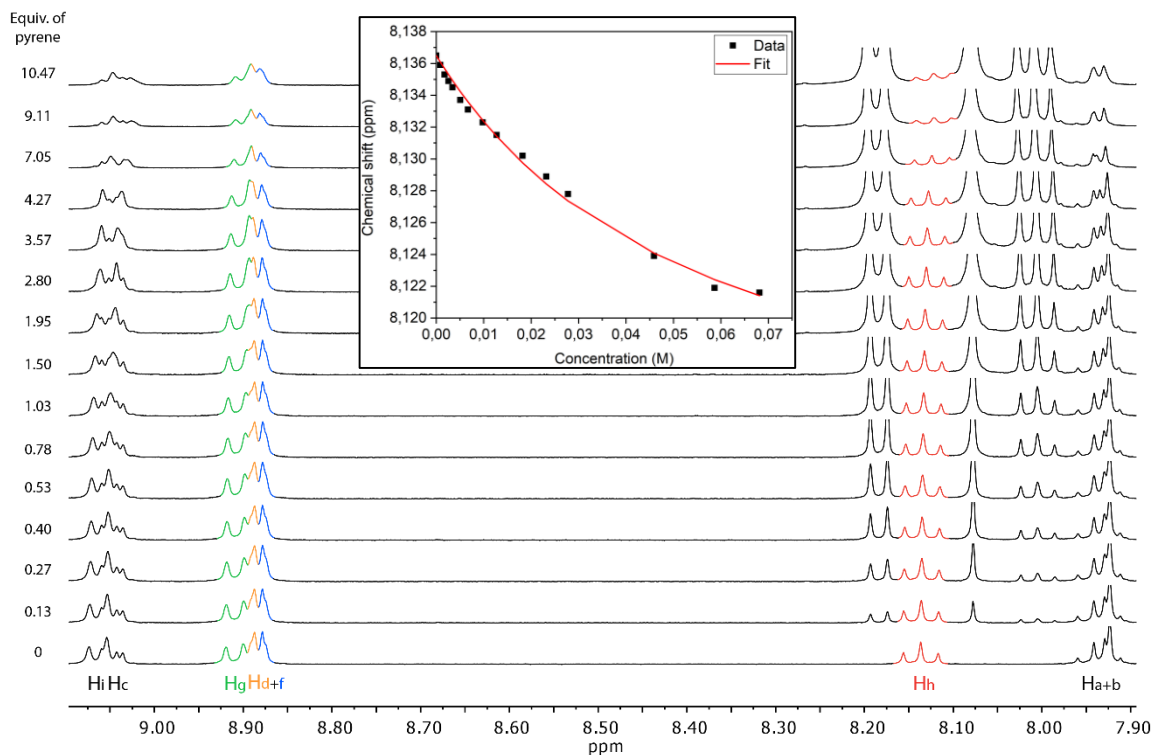


Figure 189. Aromatic region of the ^1H NMR (400 MHz, CDCl_3 , 298 K) spectra for the titration of nanographene **199a** with pyrene (0 – 10.47 equiv.). Inset: Fitted binding isotherm using a 1:1 association model ($K_a = 20.9 \pm 0.8 \text{ M}^{-1}$) showing the change in the chemical shift for H_h . Lettering coding is defined in Scheme 84.

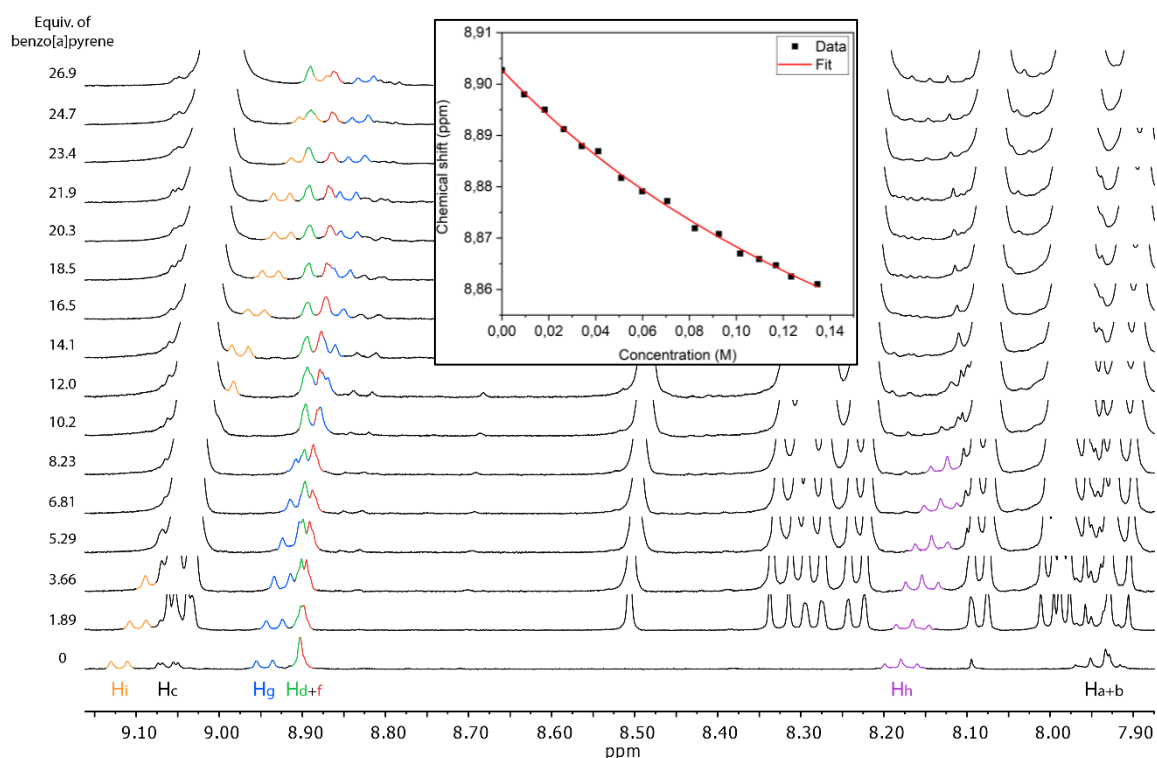


Figure 190. Aromatic region of the ^1H NMR (400 MHz, CDCl_3 , 298 K) spectra for the titration of nanographene **199a** with benzo[a]pyrene (0 – 26.9 equiv.). Inset: Fitted binding isotherm using a 1:1 association model ($K_a = 4.07 \pm 0.08 \text{ M}^{-1}$) showing the change in the chemical shift for H_f . Lettering coding is defined in Scheme 84.

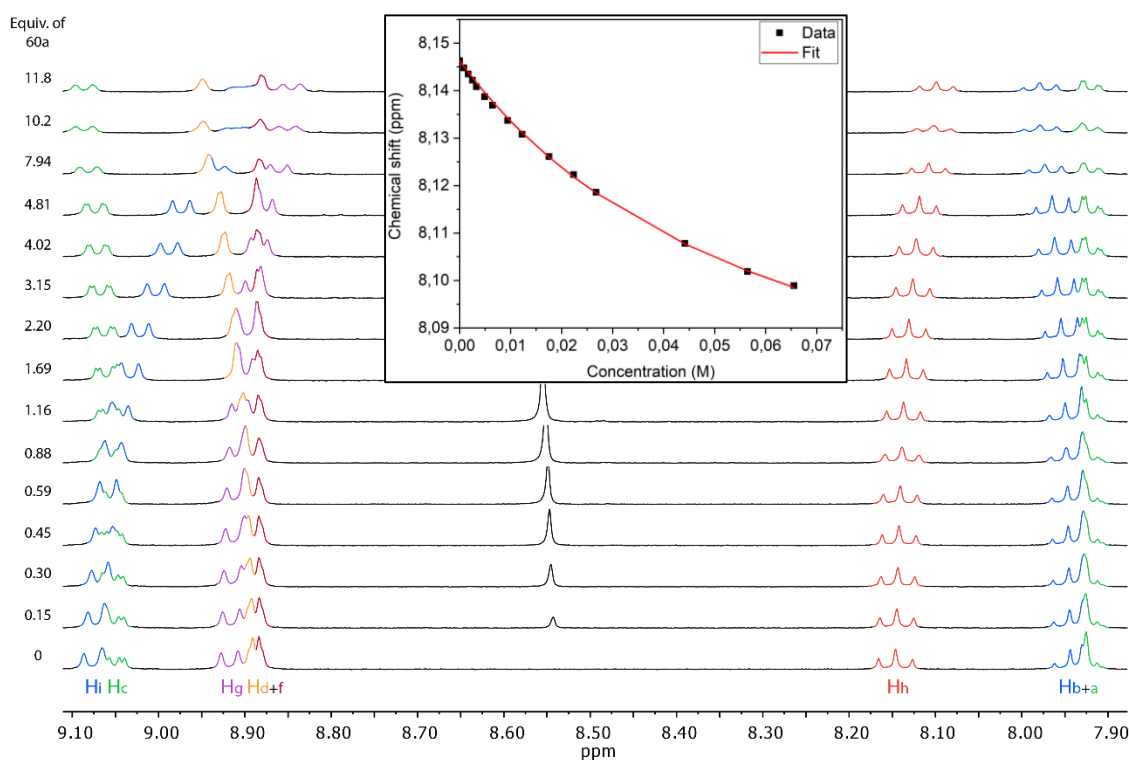


Figure 191. Aromatic region of the ^1H NMR (400 MHz, CDCl_3 , 298 K) spectra for the titration of nanographene **199a** with **60a** (0 – 11.8 equiv.). Inset: Fitted binding isotherm using a 1:1 association model ($K_a = 17.7 \pm 0.3 \text{ M}^{-1}$) showing the change in the chemical shift for H_h . Lettering coding is defined in Scheme 84.

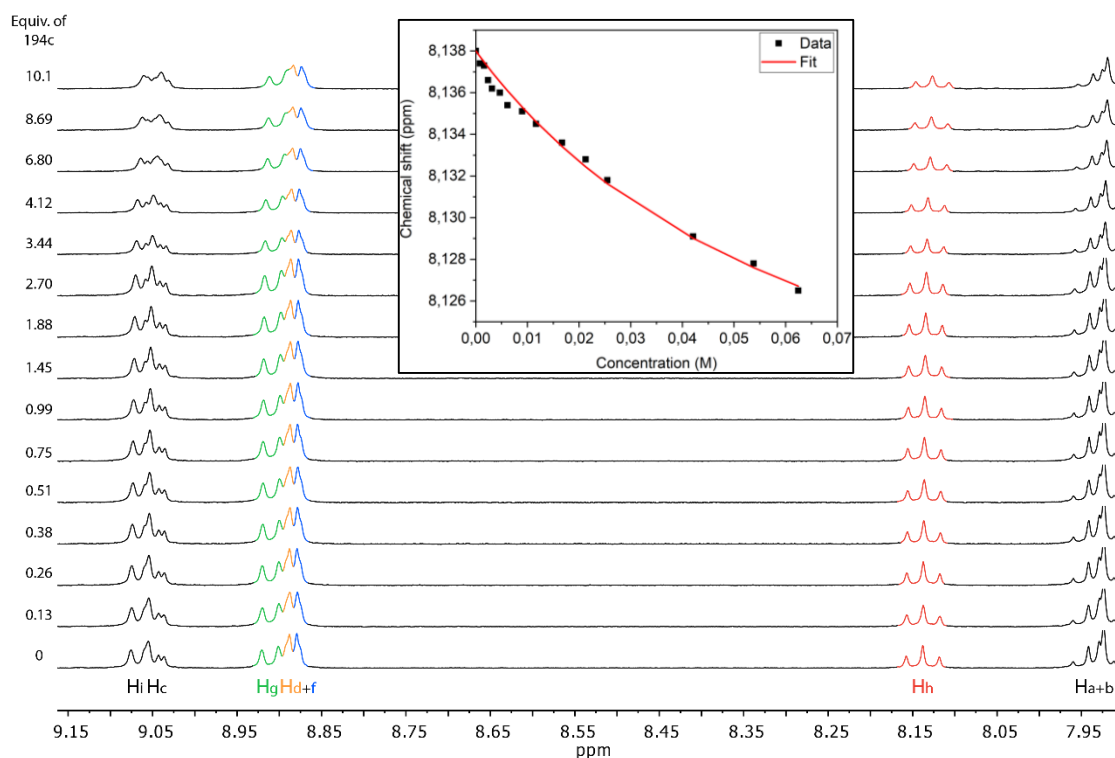


Figure 192. Aromatic region of the ^1H NMR (400 MHz, CDCl_3 , 298 K) spectra for the titration of nanographene **199a** with **214c** (0 – 10.1 equiv.). Inset: Fitted binding isotherm using a 1:1 association model ($K_a = 15.9 \pm 0.8 \text{ M}^{-1}$) showing the change in the chemical shift for H_h . Lettering coding is defined in Scheme 84.

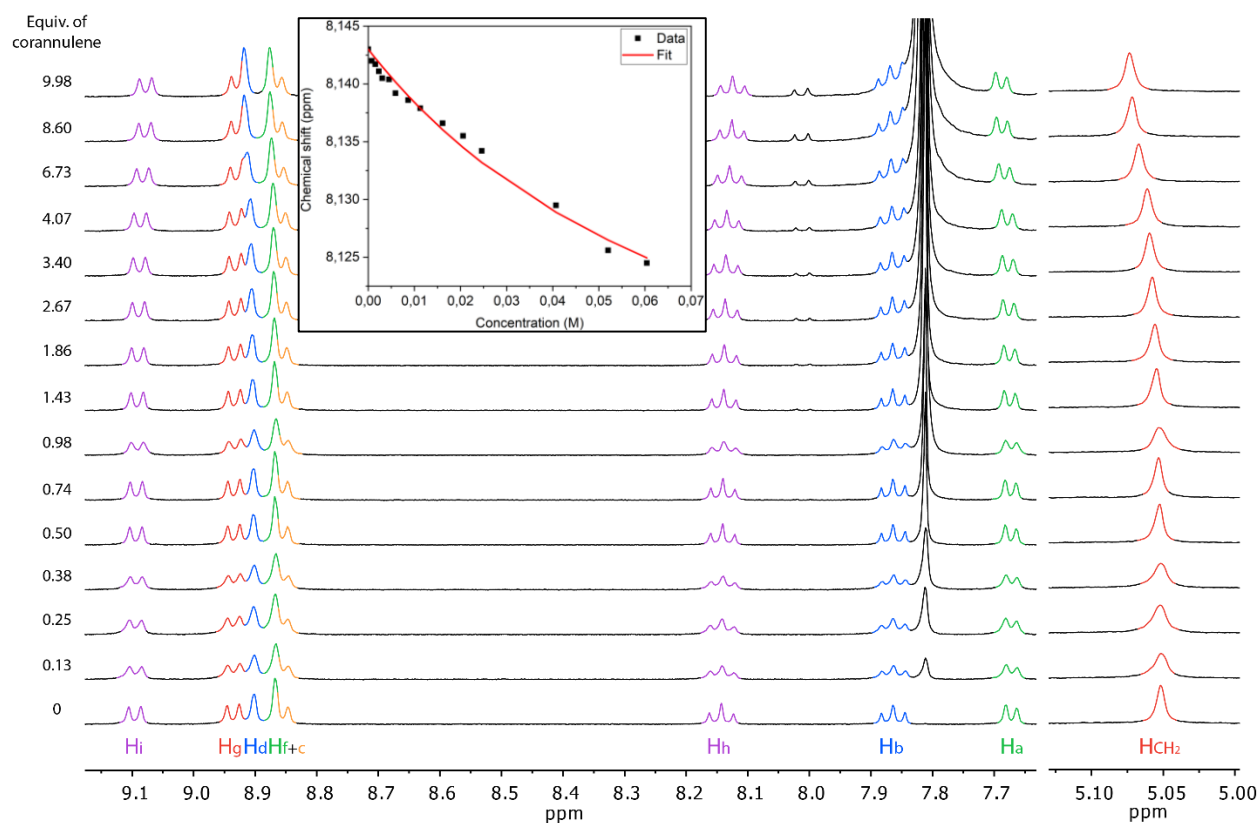


Figure 193. Partial ^1H NMR (400 MHz, CDCl_3 , 298 K) spectra for the titration of nanographene **199b** with corannulene (0 – 9.98 equiv.). Inset: Fitted binding isotherm using a 1:1 association ($K_a = 13.4 \pm 0.7 \text{ M}^{-1}$) showing the change in the chemical shift for H_h . Lettering coding is defined in Scheme 84.

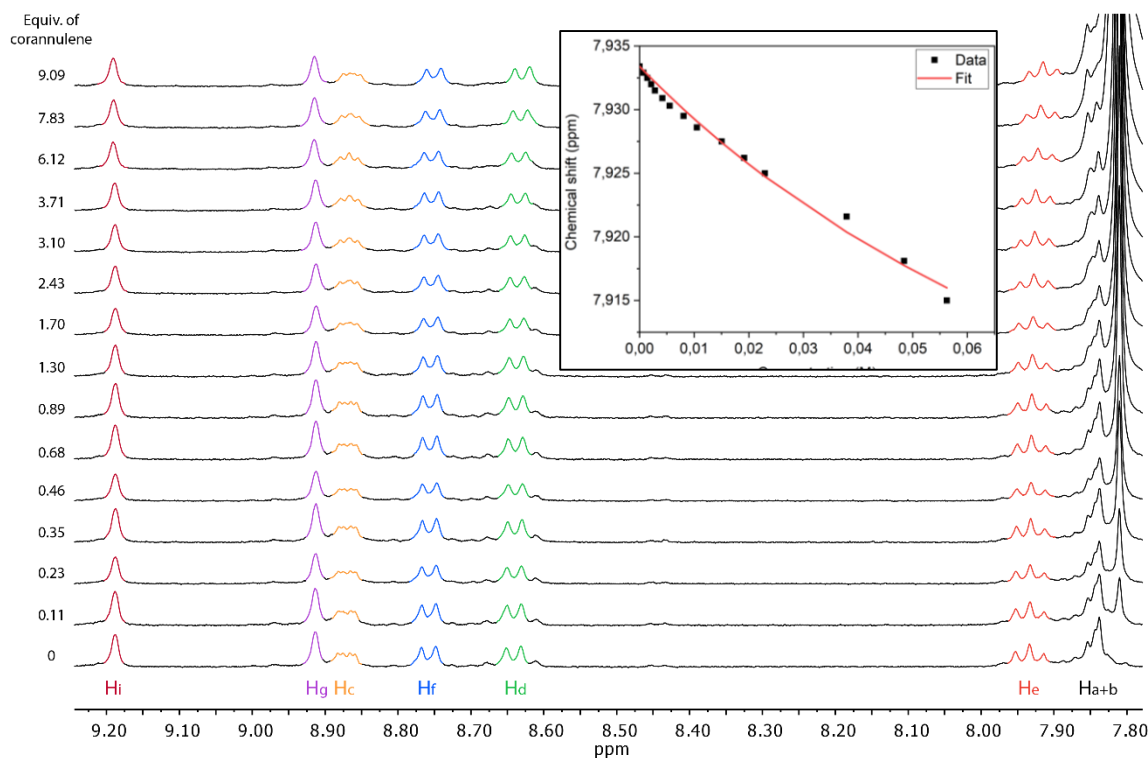


Figure 194. Aromatic region of the ^1H NMR (400 MHz, CDCl_3 , 298 K) spectra for the titration of nanographene **199e** with corannulene (0 – 9.09 equiv.). Inset: Fitted binding isotherm using a 1:1 association model ($K_a = 8.40 \pm 0.53 \text{ M}^{-1}$) showing the change in the chemical shift for H_e . Lettering coding is defined in Scheme 85.

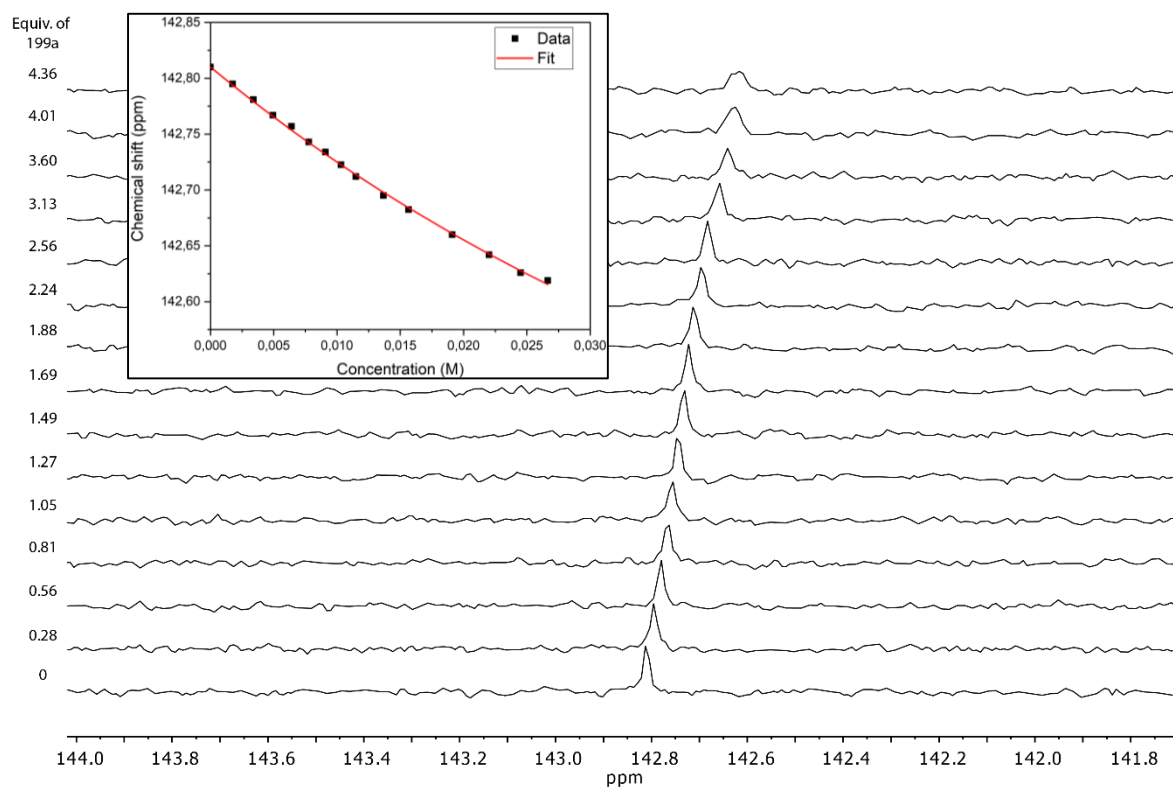


Figure 195. ^{13}C NMR (101 MHz, *o*-DCB- d_4 , 298 K) spectra for the titration of C_{60} with nanographene **199a** (0 – 4.36 equiv.). Inset: Fitted binding isotherm using a 1:1 association model ($K_a = 12.3 \pm 0.2 \text{ M}^{-1}$) showing the change in the chemical shift for C_{60} .

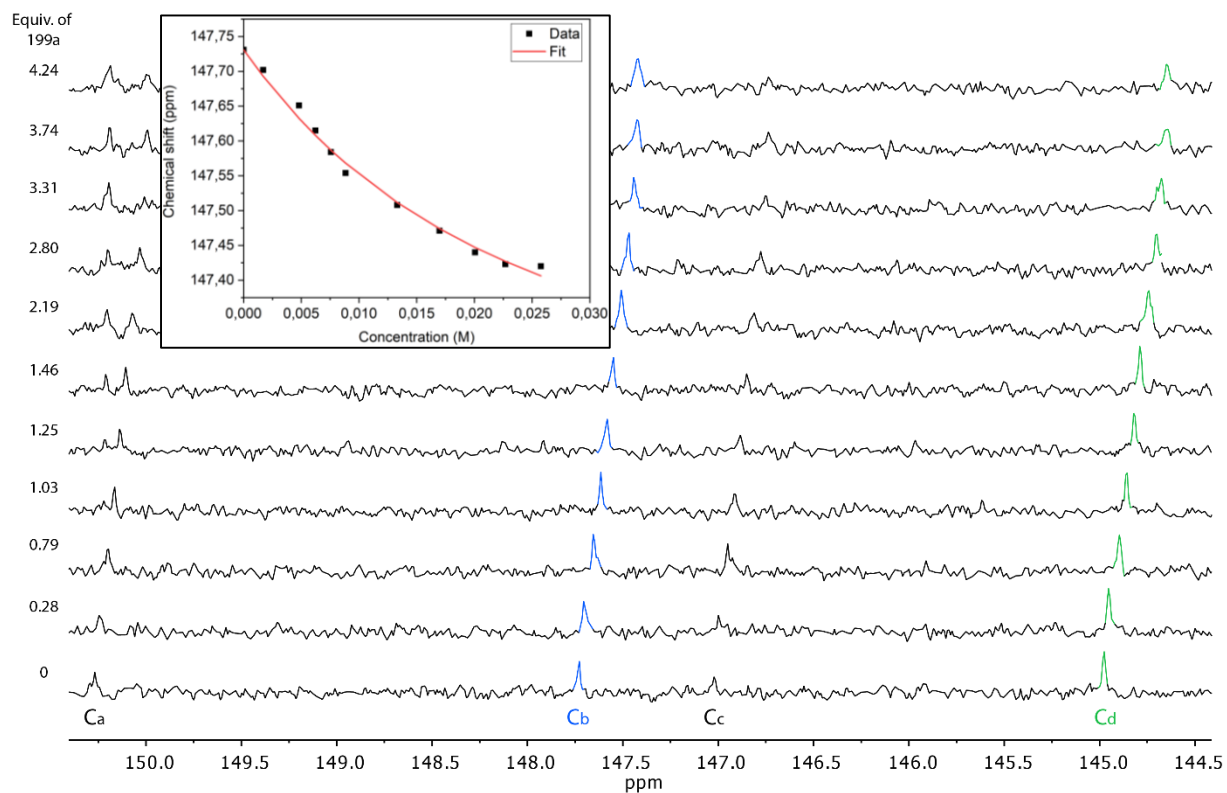


Figure 196. ^{13}C NMR (101 MHz, *o*-DCB- d_4 , 298 K) spectra for the titration of C_{70} with nanographene **199a** (0 – 4.24 equiv.). Inset: Fitted binding isotherm using a 1:1 association model ($K_a = 50.2 \pm 2.2 \text{ M}^{-1}$) showing the change in the chemical shift for C_b .

As for the ability of **199a-e** to act as hosts for the bowl-shaped corannulene, nanographene **199a-c**, all with the ^tBu group on the C_e position, show similar association constants (11 – 13 M⁻¹) with the guest that seems to be located on the more planar part of the nanographene (near C_g, C_h and C_i) as suggested for the ¹H NMR shiftings. For **199d** no interaction is observed which seems to be due to the ^tBu and the phenyl group on the C_h and C_e position, respectively, hampering the approach of corannulene. Finally, **199e** shows an association constant slightly weaker than **199a-c** (8.40 ± 0.53 M⁻¹). This might be due to the fact that the binding takes place close to the distorted tropone unit. Indeed, H_e is shielded whereas H_i and H_g are deshielded. (Table 25, Figures 194 and 195).

Regarding the binding properties between hept-HBCs **199a-e** and fullerenes, the highest association constant was estimated as 53.1 ± 2.4 M⁻¹ for the extended nanographene **199c** with C₇₀. Furthermore, it can be clearly observed that usually, nanographenes bind more strongly to C₇₀ than C₆₀ except for **199d**. Thus, we assume that this difference is due to the presence of phenyl units of the C_e position, that induce steric hindrance prohibiting the approach of C₇₀, while it seems to give more surface to interact with C₆₀. Finally, a comparison of the response of hept-HBCs **199a** and **199e**, which only differs in the position of the ^tBu unit, as hosts for fullerene shows better results for both fullerenes when the peripheral group is present on the C_e position (Table 25, Figures 196 and 197).

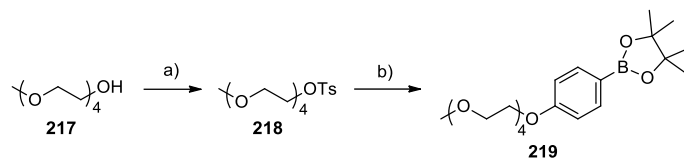
3.2. Functionalization of saddle-shaped nanographenes towards supramolecular nanostructured assemblies

3.2.1. Synthesis and characterization

As discussed in this chapter (Section 1.3.3.), nanostructured aggregates such as supramolecular nanotubes or nanofibres, as well as, supramolecular organogels can be obtained through the use of amphiphilic planar PAHs. Since we have demonstrated the self-association of hept-HBC derivatives, we hypothesized that amphiphilic negatively curved HBC derivatives could be employed to build supramolecular nanostructures, possibly nanotubes or nanofibres. In this section, we will mainly discuss the synthesis of three amphiphiles and their self-assembly capacity to afford nanomaterials will be studied in the long term (Figure 180).

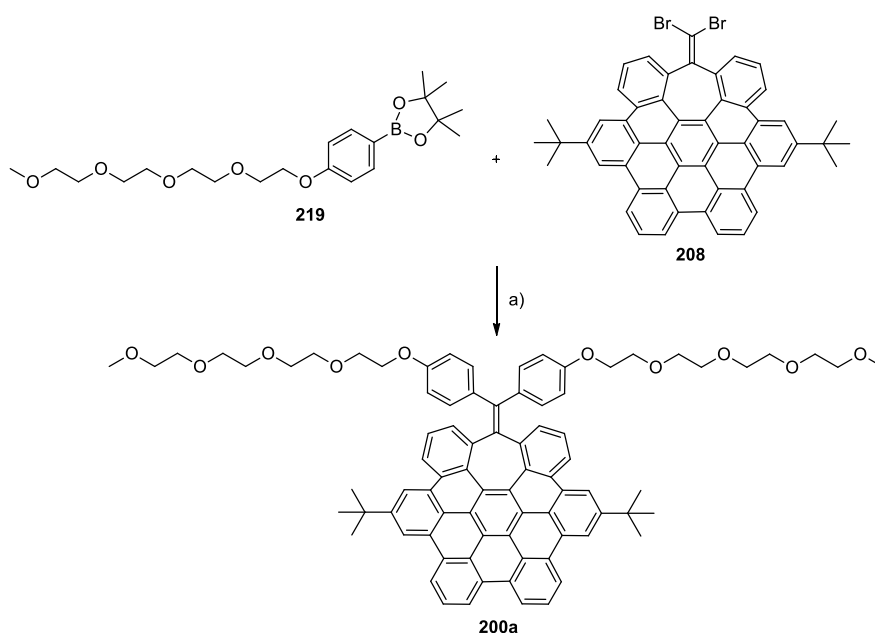
We proposed to construct amphiphilic nanographenes **200a-c** (Figure 180) *via* a Suzuki cross-coupling between hept-HBC derivatives functionalized with Br atoms and boronic ester **219** owning a tetraethylene glycol chain. First, we tackled the synthesis of boronic ester **219**. Thus, tetraethyleneglycol monomethyl ether (**217**) was treated with TsCl in basic medium to afford **218** in

an excellent yield (99%). Then, **218** underwent a Williamson reaction together with 4-hydroxyphenylboronic acid pinacol ester to yield boronic ester **219** in good yield (82%) (Scheme 87).⁴⁴³



Scheme 87. Synthesis of intermediate **219**. Reagents and conditions: a) TsCl, Et₃N, DMAP_(cat.), CH₂Cl₂, r.t., 20 h, 99%. b) 4-hydroxyphenylboronic acid pinacol ester, K₂CO₃, DMF, 80 °C, 18 h, 82%.

Boronic ester **219** was reacted with 1,1-dibromoalkene-functionalized hept-HBC **208** under Suzuki coupling reaction conditions, affording target amphiphile **200a** in 18% yield (Scheme 88).



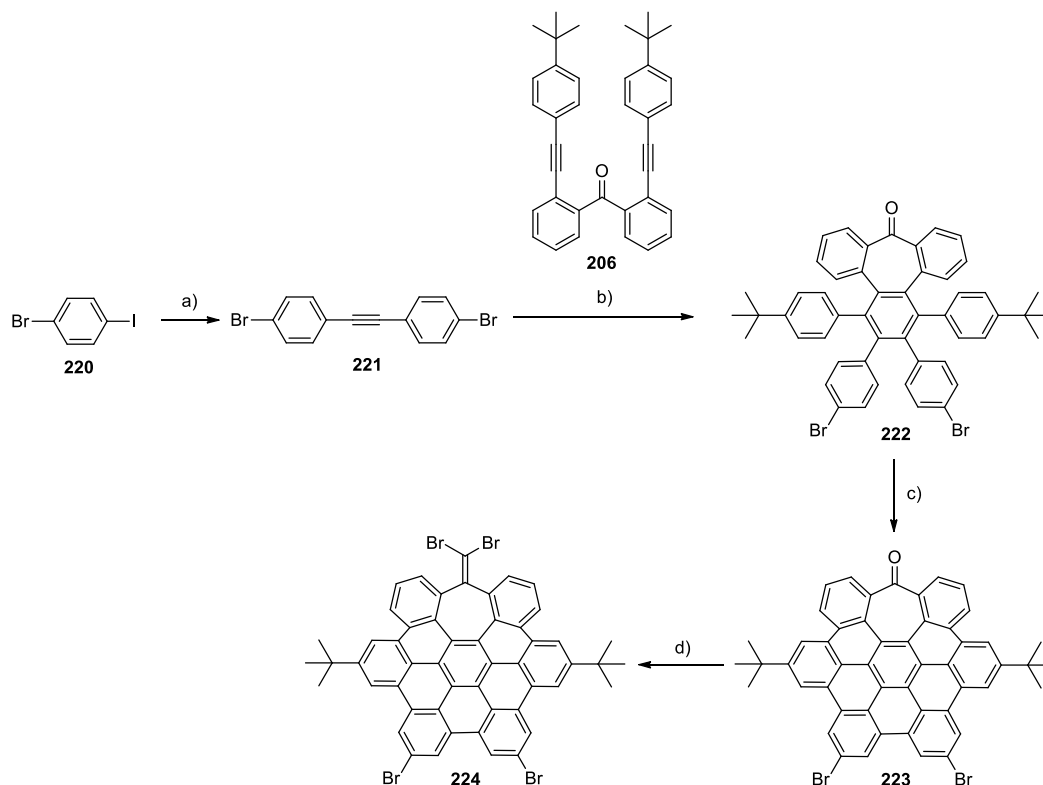
Scheme 88. Synthesis of nanographene **200a**. Reagents and conditions: a) Pd(PPh₃)₄, K₂CO₃, EtOH, H₂O, toluene, reflux, 20 h, 18%.

Regarding the synthesis of hept-HBCs **200b,c**, nanographenes **223** and **224**, functionalized with Br atoms at the adequate positions of the aromatic core, needed to be prepared. Thus, trimethylsilylacetylene underwent a double Sonogashira coupling reaction, with an intermediate alkyne deprotection, in the presence of 1-bromo-4-iodobenzene (**220**) to obtain intermediate **221** in good yield (76%).⁴⁴⁴ **221** was treated with Co₂(CO)₈ in the presence of dialkyne **206** to give compound **222** in moderate yield (40%). A cyclodehydrogenation reaction was performed on **222** employing DDQ

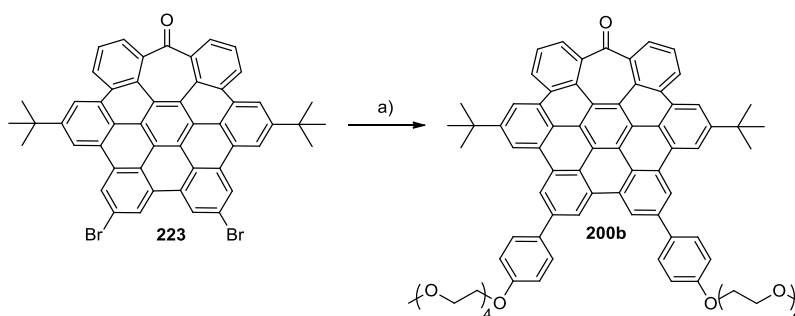
⁴⁴³ Compound **219** was prepared according to Iovine's procedure: A. L. Korich, K. M. Clarke, D. Wallace, P. M. Iovine, *Macromolecules* **2009**, *42*, 5906-5908.

⁴⁴⁴ Compound **221** was prepared according to Zhu's procedure: J. Wang, S. Zha, K. Chen, J. Zhu, *Org. Chem. Front.* **2016**, *3*, 1281-1285.

and $\text{CF}_3\text{SO}_3\text{H}$ to yield nanographene **223** in 39%.⁴⁴⁵ Treatment of **223** with CBr_4 and PPh_3 in toluene generated 1,1-dibromoalkene-functionalized hept-HBC derivative **224** in good yield (84%) (Scheme 89).



Scheme 89. Synthesis of intermediates **223** and **224**. Reagents and conditions: a) trimethylsilylacetylene, $\text{PdCl}_2(\text{PPh}_3)_2$, CuI , DBU, H_2O , CH_3CN , r.t., 20 h, 76%. b) $\text{Co}_2(\text{CO})_8$, toluene, 110 °C, 18 h, 40%. c) DDQ, $\text{CF}_3\text{SO}_3\text{H}$, CH_2Cl_2 , 0 °C, 10 min, 39 %. d) PPh_3 , CBr_4 , toluene, 120 °C, 20 h, 84%.

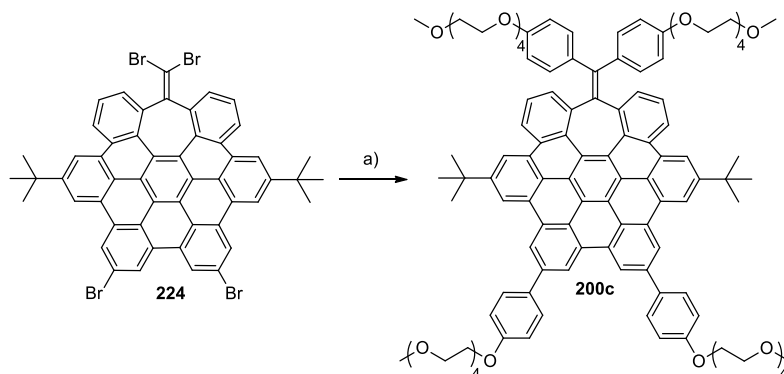


Scheme 90. Synthesis of nanographene **200b**. Reagents and conditions: a) **219**, $\text{Pd}(\text{PPh}_3)_4$, K_2CO_3 , EtOH , H_2O , Toluene, reflux, 18 h, 54%.

Finally, a double Suzuki cross-coupling reaction between nanographene **223** and boronic ester **219** afforded target amphiphile **200b** in moderate yield (54%) (Scheme 90), while a quadruple Suzuki

⁴⁴⁵ Compounds **222** and **223** were prepared according to a procedure established in our group: C. M. Cruz, Diseño, síntesis y evaluación de las propiedades físicas de nanografenos distorsionados que incluyen heptágonos, PhD dissertation, Universidad de Granada, Granada, Spain, 2020.

reaction between nanographene **224** and the same boronic ester gave desired nanographene **200c** in 15% (Scheme 91).



Scheme 91. Synthesis of nanographene **200c**. Reagents and conditions: a) **219**, Pd(PPh₃)₄, K₂CO₃, EtOH, H₂O, Toluene, reflux, 20 h, 15%.

As usual, the three hept-HBC derivatives functionalized with polar chains were characterized by means of NMR spectroscopy, obtaining ¹H and ¹³C NMR spectra in agreement with the proposed structures (Figures 198 and 199 for **200a**). Moreover, HRMS confirmed the existence of these three hept-HBCs as we observed signals whose exact masses and isotopic distributions nicely match the theoretical ones (Figures 200 for **200a**).

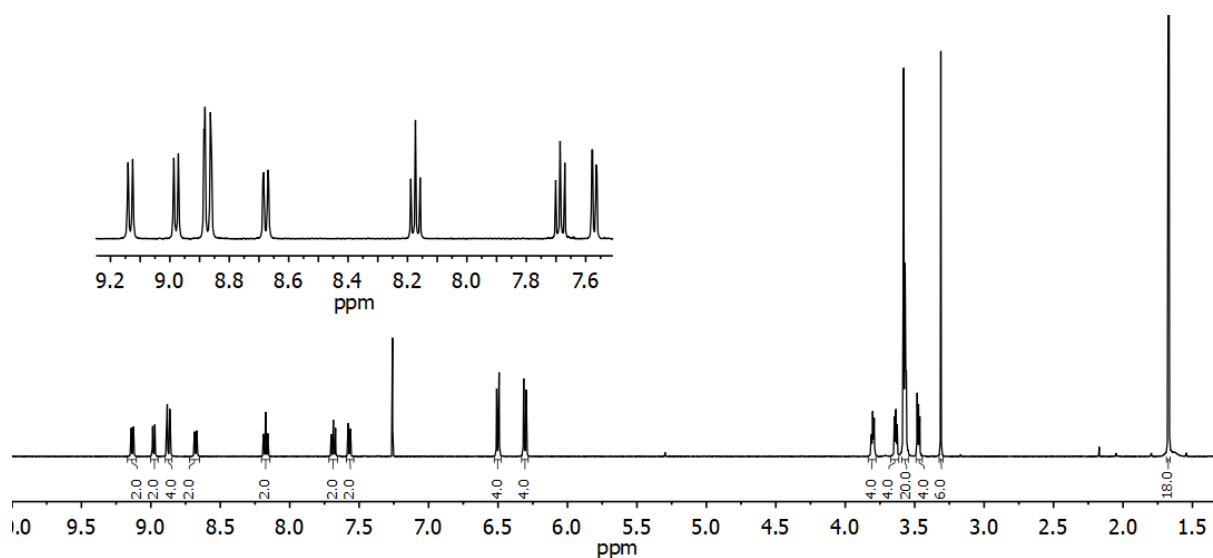


Figure 197. ¹H NMR (500 MHz, CDCl₃) spectrum of nanographene **200a**.

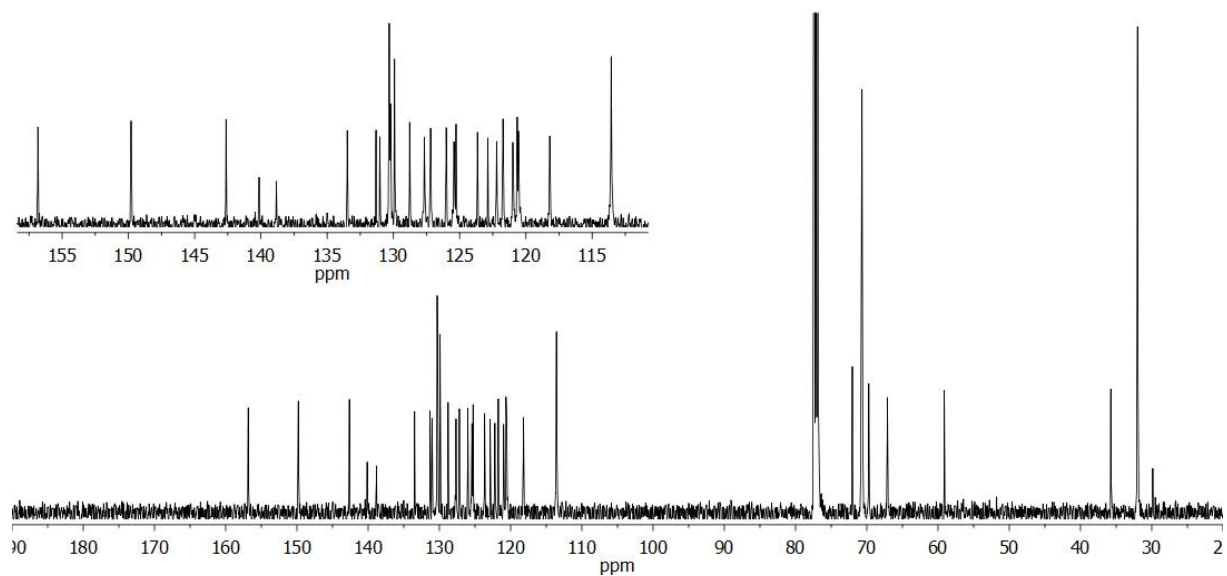


Figure 198. ^{13}C NMR (126 MHz, CDCl_3) spectrum of nanographene **200a**.

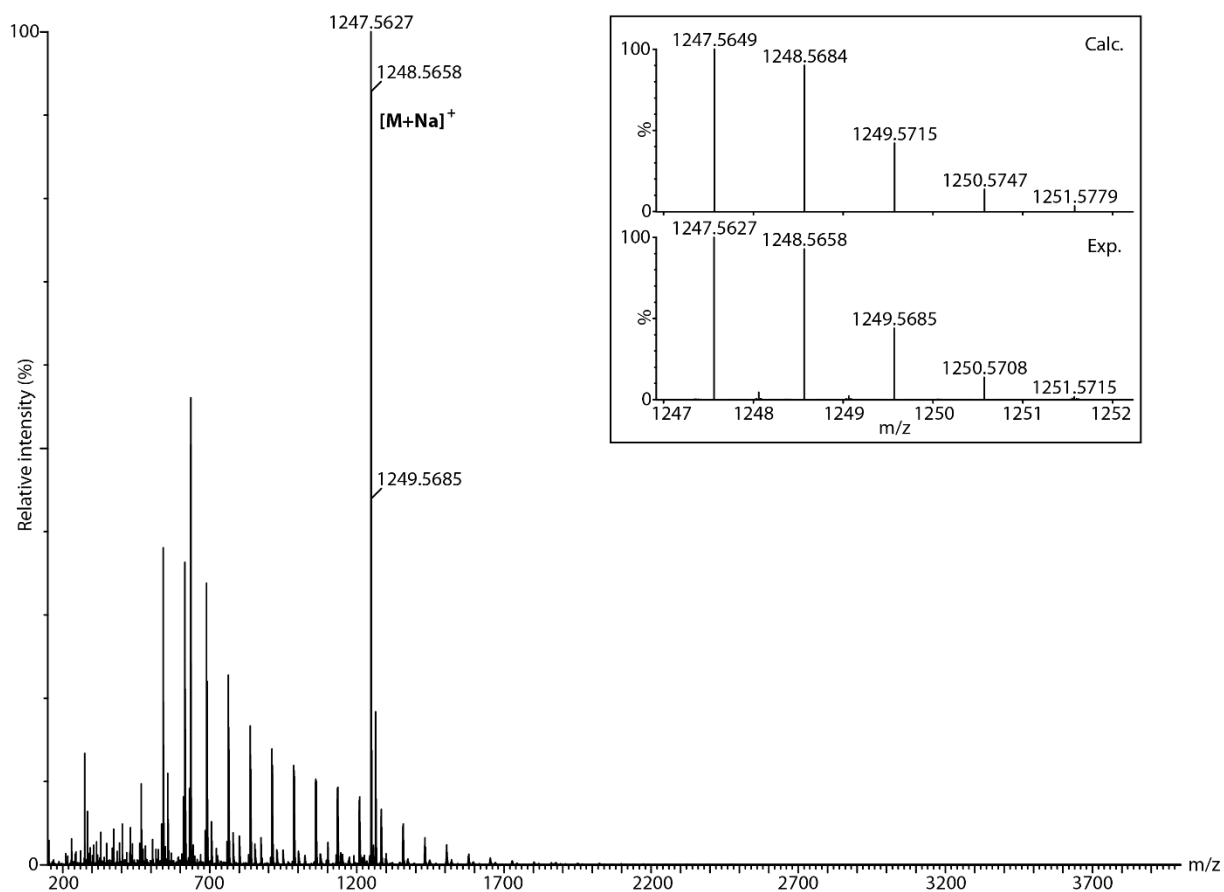


Figure 199. HRMS (ESI^+) spectrum of nanographene **200a**. Inset: Experimental (top) and calculated (bottom) isotopic distribution for $[\text{M}+\text{Na}]^+$.

3.2.2. Preliminary study to form supramolecular aggregates

Supramolecular aggregates or organogels with aromatic molecules are generally formed following a *temperature switch* protocol, that is: the molecule is disposed in a solvent in which it is not soluble at

room temperature but gets dissolved once the solvent is heated. A slowly cooling of the previous solution induces the formation of supramolecular aggregates that, in some cases, at specific concentrations can give rise to the formation of organogels. Another alternative to induce aggregation consists of a *solvent switch* protocol, in this case the stimulus to promote the aggregation consists on the addition of a precipitant agent, in this case, a solvent in which the molecule is not soluble, to a solution of the molecule.⁴⁴⁶

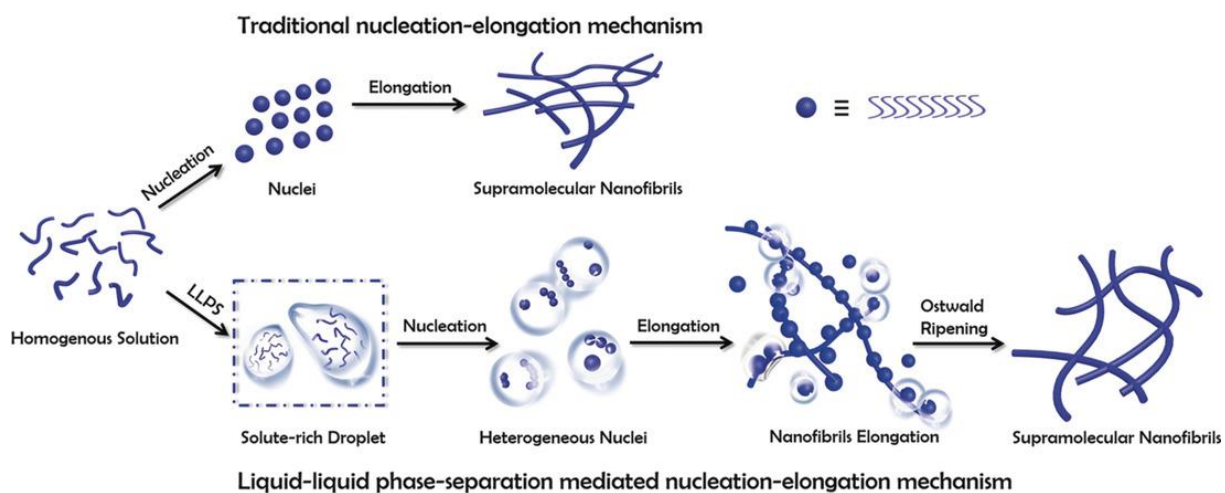


Figure 200. Graphical representation of the nucleation-elongation mechanisms for the formation of supramolecular nanostructures.⁴⁴⁷ Reprinted with permission from ref 447. Copyright 2019 John Wiley and Sons.

From a mechanistic point of view, mainly two kinds of mechanisms to build supramolecular assemblies have been described. One of them, is the *Isodesmic model*, in which the aggregation of the monomer is identical in all the steps of the polymerization process and, another model, is the *Cooperative* or *Nucleation-Elongation* process. In this second mechanism two differentiate steps having two different association constants are identified. This process implies first, the formation of nuclei, having an association constant K_n , and a posterior elongation process having a different association constant (K_e). The formation of the final supramolecular structures implies that $K_e > K_n$. Recently, it has been observed that some molecules which follow a nucleation-elongation polymerization process, are able to form a liquid-liquid separation phase before nuclei formation. This process affords droplets rich of monomer in which the formation of the nuclei is favoured. This process has been described for proteins and peptides in which the hydrophobic groups of these molecules are responsible of creating these concentrated droplets in water (Figure 201).⁴⁴⁷

⁴⁴⁶ S. S. Babu, V. K. Praveen, A. Ajayaghosh, *Chem. Rev.* **2014**, *114*, 1973-2129.

⁴⁴⁷ C. Yuan, A. Levin, W. Chen, R. Xing, Q. Zou, T. W. Herling, P. K. Challa, T. P. J. Knowles, X. Yan, *Angew. Chem. Int. Ed.* **2019**, *58*, 18116-18123.

As a first attempt to create supramolecular aggregates, heptagon-containing nanographene **200c** was dissolved in THF and H₂O was added (final concentration: $\approx 2 \times 10^{-4}$ M). In some THF/H₂O mixtures (3:7, 2:8 and 1:9) turbid solutions were formed. These solutions were then analyzed by transmission electron microscopy (TEM) (Figure 202). Images from Figure 202a,b showed the presence of dark non-defined nanospheres isolated or combined in clusters. These nanospheres were assigned to droplets of water rich in nanographene **200c**. Images from Figures 202c-f showed similar nanospheres but in this case a secondary structure was observed in the limits of the aggregates. This secondary structure was clearly seen in the image of Figure 202g. This image showed a well-defined and extremely large sheet possibly formed by strong lateral supramolecular interactions between the nanographenes **200c**. Although, at this moment, a study in detail of this aggregate has not been performed yet, the self-assembly of the nanographene **200c** into sheets is expected considering that this molecule has ethylene groups in both ends of the molecule allowing a planar 2D growth through lateral intermolecular interactions. Figure 202h showed again the presence of nanosheets although in this case the sheets appeared rolled up on themselves.

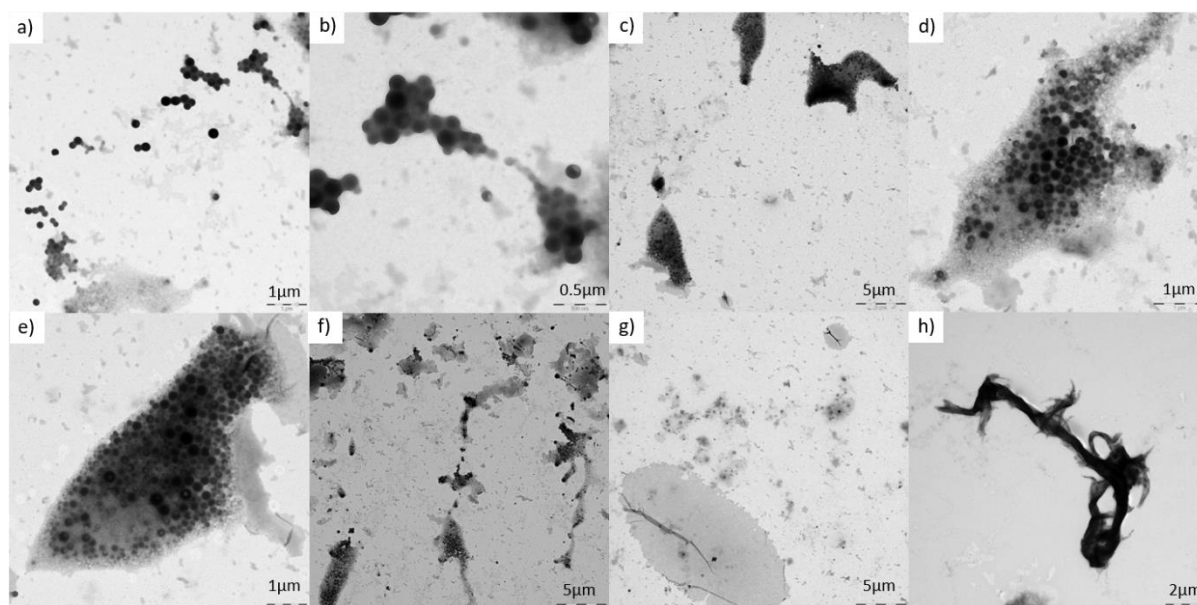


Figure 201. TEM images of solutions of **200c** in THF/H₂O mixtures: 2:8 (a, b, c, e, f, g) and 3:7 (h).

To summary, TEM images of the nanographene **200c** in mixtures of THF:H₂O have shown that this particular nanographene is able to self-assemble giving rise to supramolecular aggregates assembled into 2D sheets triggered by a solvent switch protocol. Additionally, TEM images has also confirmed the presence of water nanospheres that later evolved to the mentioned sheets. This might imply that the mechanism of polymerization goes through a nucleation-elongation process mediated by a liquid-liquid separation process, although more work is needed to verify this hypothesis.

In the light of these preliminary results, it seems that hept-HBC derivatives are promising for developing supramolecular nanostructured assemblies, however it is necessary to investigate more this topic in the future. Thus, similar experiments have to be carried out with other hept-HBC nanographenes **200a,b**. Moreover, in order to consolidate this achievement and explore different aggregation patterns, the effect of the concentration have to be investigated and some other solvent mixtures have to be tested.

4. Conclusions

In this chapter, five hept-HBC nanographenes have been synthesized to study their self-association and host-guest properties. The ^1H NMR spectra of these molecules are concentration dependant and therefore, their aggregation tendency has been demonstrated. Although the evaluated monomer-dimer equilibrium constants are modest, we found out that the nature and the position of the peripheral groups of the nanographene is of key importance for the magnitude of this constant but also for the region where they bind, while the functionalization of the tropone moiety did not influence significantly the results.

Furthermore, we studied the potential of negatively curved nanographenes to bind PAHs and fullerenes and found that they mostly bind to these species. The best outcome was attained with **199c**: C_{70} system which gave a binding constant $K_a = 53.1 \pm 2.4 \text{ M}^{-1}$. This value was attributed to the extended π -surface of nanographene **199c** owning an enhanced distorted structure. Therefore we proved that these distorted nanographene have a promising future in the field of supramolecular chemistry, especially, to bind to fullerenes and PAHs, and could be conceivably incorporated in the synthesis of aromatic receptors or MIMs. Although the association constants are modest, it worth noting that thanks to this primary study, another PhD student from the group synthesized a cyclophane owning two nanographene units that was able to bind to fullerenes.⁴⁴⁸

Since we established that the hept-HBC derivatives have the ability to constitute dimers in solution, three amphiphilic heptagon-containing nanographenes have been synthesized with the aim of developing supramolecular nanostructures with distorted building blocks. However, the study of their aggregation and the preparation of such materials is only preliminary but very promising and will be studied in depth in the future.

⁴⁴⁸ V. G. Jiménez, A. H. G. David, J. M. Cuerva, V. Blanco, A. G. Campaña. *Angew. Chem. Int. Ed.* **2020**, doi:10.1002/anie.202003785

5. Experimental section

5.1. General details

Unless otherwise noted, commercially available reagents, solvents and anhydrous solvents were used as purchased without further purification. Anhydrous THF was freshly distilled over Na/benzophenone.

Compound **205**,⁴⁴⁹ PdCl₂(MeCN)₂,⁴⁵⁰ PdCl₂(PPh₃)₂,⁴⁵¹ and Pd(PPh₃)₄,⁴⁵² were synthesized according to literature procedures.

TLC was performed on Merck Silica gel 60 F₂₅₄ aluminium sheets or Sigma-Aldrich (silica gel matrix, with fluorescent indicator 254 nm). The TLC plates were stained with potassium permanganate (1% w/v in water) or observed under UV light when applicable.

Flash column chromatography was performed with Silica gel 60 (Merck, 40-63 μm, 230–400 mesh ASTM, or Scharlab, Spain, Silica gel 60 (230-400 mesh) or VWR, 40-63 μm). Silica gel G preparative TLC plates were purchased from ANALTECH (20×20cm, 2000 micron) or from Silicycle (20×20cm, 1000 micron). Gel permeation chromatography was performed with Biobeads® SX-1 or Biobeads® SX-3 resin beads.

¹H and ¹³C NMR spectra were recorded at room temperature on a Varian Inova Unity (300 MHz), Varian Direct Drive (400 MHz or 500 MHz), Bruker Avance III HD NanoBay (400 MHz) or Bruker Avance Neo (400 MHz or 500 MHz) spectrometers at a constant temperature of 298 K. Chemical shifts are given in ppm and referenced to the signal of the residual protiated solvent (¹H: δ=7.26 for CDCl₃ and δ=5.32 for CD₂Cl₂ at room temperature) or the ¹³C signal of the solvents (¹³C: δ=77.16 for CDCl₃, δ=54.00 for CD₂Cl₂ and δ=132.39 for *o*-DCB-*d*₄) or to the signal of the residual TMS (¹H: δ=0.00). Coupling constant (*J*) values are given in Hz. Abbreviations indicating multiplicity were used as follow: m = multiplet, p = quintet, q = quartet, t = triplet, d = doublet, dd = doublet of doublets, s = singlet, br = broad. Signals were assigned by means of 2D NMR spectroscopy (COSY, HSQC, HMBC).

Electrospray (ESI) HRMS spectra were recorded on a Waters Xevo G2-XS QTOF spectrometer. MALDI mass spectra were recorded on a Bruker Ultraflex III mass spectrometer. IR spectra were recorded with a Perkin-Elmer Spectrum Two FTIR ATR spectrometer.

⁴⁴⁹ T. K. Wood, W. E. Piers, B. A. Keay, M. Parvez, *Chem. Eur. J.* **2010**, *16*, 12199-12206.

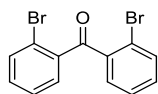
⁴⁵⁰ F. R. Hartley, S. G. Murray, C. A. McAuliffe, *Inorg. Chem.* **1979**, *18*, 1394-1397.

⁴⁵¹ H. A. Oskooie, M. M. Heravi, F. K. Behbahani, *Molecules* **2007**, *12*, 1438-1446.

⁴⁵² D. R. Coulson, L. C. Satek, S. O. Grim, *Inorg. Synth.* **1972**, *13*, 121-124.

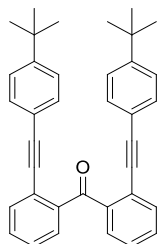
5.2. Synthetic procedures and characterization details

Compound 201:



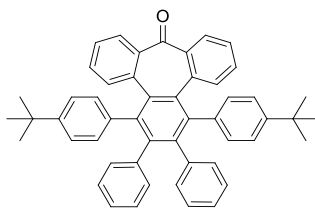
To a degassed solution of **205** (7.96 g, 23.2 mmol) in CH_2Cl_2 (100 mL), cooled in a water-ice bath, was added Dess-Martin periodinane (11.8 g, 27.9 mmol). The mixture was stirred for 2 h at 0 °C. Subsequently, the mixture was washed with an aqueous solution of NaHCO_3 (sat.)/ $\text{Na}_2\text{S}_2\text{O}_3$ (0.6 M) (1:1, 2 × 100 mL). The aqueous layer was then extracted with CH_2Cl_2 (2 × 100 mL). The combined organic layers were dried over anhydrous Na_2SO_4 and the solvent was evaporated under vacuum. The crude was purified by flash column chromatography (SiO_2 , Hexane/EtOAc 90:10) affording **201** (5.62 g, 71%) as a white solid. ^1H NMR (400 MHz, CDCl_3): δ =7.67 – 7.61 (m, 2H), 7.49 – 7.41 (m, 2H), 7.40 – 7.31 (m, 4H). ^{13}C NMR (101 MHz, CDCl_3): δ =195.48, 139.358, 134.17, 132.64, 131.40, 127.41, 121.25. These spectroscopic data agree with those previously reported.⁴⁵³

Compound 206:

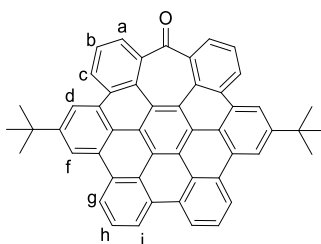


To a degassed solution of **201** (2.00 g, 5.88 mmol), $\text{PdCl}_2(\text{CH}_3\text{CN})_2$ (228 mg, 0.882 mmol), $\text{P}(\text{tBu})_3\text{HBF}_4$ (511 mg, 1.76 mmol) and CuI (167 mg, 0.882 mmol) in $i\text{Pr}_2\text{NH}$ (20 mL) was added a previously degassed solution of 4-*tert*-butylphenylacetylene (2.80 g, 17.6 mmol) in THF (40 mL). The solution was stirred for 18 h at r.t.. Subsequently, the solvent was evaporated under reduced pressure and the syrup was dissolved in CH_2Cl_2 (200 mL). The solution was washed with NH_4Cl (sat) (100 mL), the organic layer was dried over anhydrous Na_2SO_4 and the solvent was removed under vacuum. The crude material was purified by column chromatography (SiO_2 , hexane/EtOAc 95:5) to yield **206** (2.846 g, 98%) a black syrup. ^1H NMR (400 MHz, CDCl_3): δ =7.72 (dd, J = 7.8, 1.3 Hz, 2H), 7.62 (dd, J = 7.7, 1.2 Hz, 2H), 7.49 (td, J = 7.5, 1.5 Hz, 2H), 7.43 (td, J = 7.5, 1.4 Hz, 2H), 7.27 (d, J = 8.4 Hz, 4H), 7.14 (d, J = 8.5 Hz, 4H), 1.31 (s, 18H). Spectral data agree with those previously reported.⁴³⁸

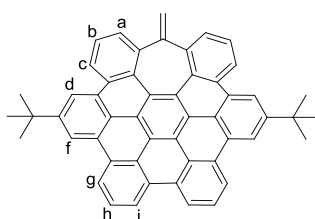
⁴⁵³ K. Kobayashi, Y. Nishimura, F. Gao, K. Gotoh, Y. Nishihara, K. Takagi, *J. Org. Chem.* **2011**, 76, 1949-1952.

Compound 207:

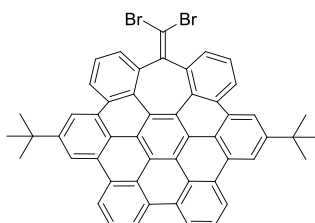
In three different flasks, a degassed solution of **206** (304 mg, 0.615 mmol) and $\text{Co}_2(\text{CO})_8$ (270 mg, 0.790 mmol) in dry dioxane (4 mL) was heated for 30 min at 100 °C. Subsequently, a degassed solution of diphenylacetylene (162 mg, 0.909 mmol) in anhydrous dioxane (4 mL) was added portionwise for 30 min. The solution was stirred for 16 h at 100 °C. The three solutions were combined and the solvent was removed under reduced pressure. The crude material was purified by column chromatography (SiO_2 , hexane/ CH_2Cl_2 1:1). Fractions containing the product were combined and concentrated. The resulting solid was washed with hexane, filtered and collected to yield **207** (676 mg, 55%) a white solid. ^1H NMR (400 MHz, CDCl_3): δ =7.41 – 7.34 (m, 4H), 7.09 – 6.92 (m, 10H), 6.77 (m, 6H), 6.66 (t, J = 7.6, 2H), 6.39 (t, J = 7.4 Hz, 4H), 1.13 (s, 18H). Spectral data agree with those previously reported.⁴³⁸

Compound 199a:

Under an Ar atmosphere, to a solution of **207** (101 mg, 0.150 mmol) and DDQ (204 mg, 0.900) in dry CH_2Cl_2 (6 mL) in a water-ice bath, was added $\text{CF}_3\text{SO}_3\text{H}$ (0.150 mL). The solution was stirred for 10 min at 0 °C and the solvent was evaporated under vacuum. The crude material was purified by column chromatography (SiO_2 , hexane/ CH_2Cl_2 1:1) to give **199a** (45 mg, 45%) a yellow solid. ^1H NMR (500 MHz, CDCl_3): δ =9.01 (t, J = 4.9 Hz, 2H, H_b), 8.94 (d, J = 7.9 Hz, 2H, H_i), 8.84 (m, 6H, H_{d+f+g}), 8.04 (t, J = 7.8 Hz, 2H, H_h), 7.91 (d, J = 4.8 Hz, 4H, H_{a+c}), 1.65 (s, 18H, $\text{H}_{t\text{Bu}}$). ^{13}C NMR (126 MHz, CDCl_3): δ =202.94, 150.17, 142.71, 131.60, 130.55, 130.13, 129.79, 128.39, 127.67, 127.43, 126.56, 124.91, 124.69, 124.03, 123.38, 123.26, 122.17, 121.76, 121.23, 120.99, 118.27, 35.74, 31.94. Spectral data agree with those previously reported.⁴³⁸

Compound 199b:

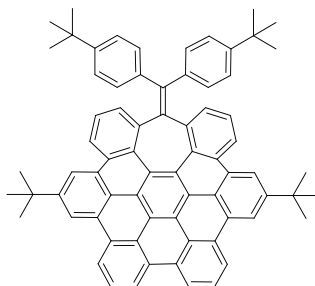
To a degassed solution of **199a** (50 mg, 0.075 mmol) in freshly distilled THF (10 mL) in a water-ice bath was added Tebbe reagent (0.5 M in toluene, 0.20 mL, 0.10 mmol). The solution was stirred for 5 min at 0 °C and 15 min at r.t. The round-bottom flask was again immersed in a water-ice bath and Tebbe reagent (0.5 M in toluene, 0.20 mL, 0.10 mmol) was added. The solution was stirred for 5 min at 0 °C and 15 min at r.t. This operation was achieved another time and the solution was stirred for 1 h at r.t. Subsequently, NaOH_(aq) (1 M; 10 mL) was added to quench the reaction. The resulting mixture was diluted with H₂O (20 mL) and extracted with CH₂Cl₂ (3 × 30 mL). The combined organic phases were dried over Na₂SO₄ and the solvent was evaporated under reduced pressure. The crude material was purified by column chromatography (SiO₂, CH₂Cl₂/hexane 10:90 then 20:80) to yield **199b** (49 mg, 98%) as a yellow solid. ¹H NMR (500 MHz, CDCl₃): δ=8.88 – 8.84 (m, 6H, H_{c+d+i}), 8.79 (m, 4H, H_{f+g}), 7.95 (t, *J* = 7.7 Hz, 2H, H_h), 7.87 (t, *J* = 7.6 Hz, 2H, H_b), 7.68 (d, *J* = 6.4 Hz, 2H, H_a), 5.08 (s, 2H, H_{CH2}), 1.64 (s, 18H, H_{tBu}). ¹³C NMR (126 MHz, CDCl₃): δ=152.92, 149.80, 143.95, 131.45, 130.57, 130.00, 129.77, 128.96, 128.64, 127.91, 126.97, 125.85, 124.90, 124.28, 123.50, 123.12, 122.53, 121.92, 121.53, 120.70, 120.40, 118.18, 115.28, 35.67, 31.95. IR (neat): ν=2956, 1613, 1588, 1462, 1368, 1256, 1078 cm⁻¹. HR-MS (ESI⁺): *m/z*: 683.2737 [M+Na]⁺ (calcd for C₅₂H₃₆Na: 683.2715).

Compound 208:

Under Argon, to a solution of **199a** (346 mg, 0.522 mmol) in anhydrous toluene (20 mL), were added PPh₃ (1.30 g, 4.95) and CBr₄ (865 mg, 2.61 mmol). The solution was refluxed for 28 h and later, the solvent was removed under reduced pressure. The crude material was purified by column chromatography (SiO₂, hexane/CH₂Cl₂ 80:20) to afford **208** (355 mg, 83%) a yellow solid. ¹H NMR (500 MHz, CDCl₃): δ= 8.91 (m, 4H), 8.81 (m, 6H), 7.94 (m, 4H), 7.77 (d, *J* = 7.2 Hz, 2H), 1.65 (s, 18H). ¹³C NMR (126 MHz, CDCl₃): δ=150.01, 147.31, 140.96, 132.14, 130.58, 130.04, 130.02, 128.30, 128.21, 127.80, 127.12, 124.81, 124.63, 123.97, 123.63, 123.09, 122.50, 122.05, 121.67, 120.87, 120.76, 118.11, 90.43,

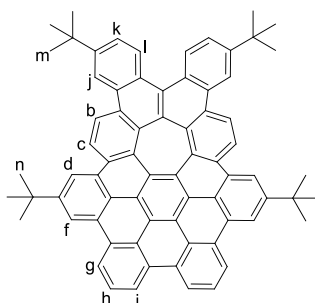
35.74, 31.97. IR (neat): $\nu=2957, 1675, 1612, 1588, 1463, 1393, 1078, 811 \text{ cm}^{-1}$. HR-MS (MALDI): m/z : 816.1015 $[M]^+$ (calcd for $C_{52}H_{34}Br_2$: 816.1022).

Compound 209:



Under an Ar atmosphere, to **208** (313 mg, 0.382 mmol), 4-*tert*-butylphenylboronic acid (680 mg, 3.82 mmol), $Pd(PPh_3)_4$ (100 mg, 76.4 μmol), K_2CO_3 (636 mg, 4.60 mmol) were added degassed toluene (50 mL), degassed EtOH (3.6 mL) and degassed H_2O (3.6 mL). The mixture was stirred for 20 h at 100 °C. The resulting mixture was diluted with H_2O (50 mL) and extracted with CH_2Cl_2 ($2 \times 50 \text{ mL}$). The combined organic phases were washed with brine (50 mL), dried over anhydrous Na_2SO_4 and the solvent was removed under vacuum. The crude material was purified by column chromatography (SiO_2 , CH_2Cl_2 /hexane 20:80) to yield **209** (296 mg, 84%) as a yellow solid. 1H NMR (400 MHz, $CDCl_3$): $\delta=9.10$ (d, $J = 7.9 \text{ Hz}$, 2H), 8.96 (d, $J = 7.9 \text{ Hz}$, 2H), 8.88 (m, 4H), 8.67 (d, $J = 6.8 \text{ Hz}$, 2H), 8.15 (t, $J = 7.8 \text{ Hz}$, 2H), 7.67 (t, $J = 7.6 \text{ Hz}$, 2H), 7.59 (dd, $J = 7.2, 1.3 \text{ Hz}$, 2H), 6.77 (d, $J = 8.3 \text{ Hz}$, 4H), 6.54 (d, $J = 8.3 \text{ Hz}$, 4H), 1.67 (s, 18H), 1.04 (s, 18H). ^{13}C NMR (101 MHz, $CDCl_3$): $\delta=149.76, 148.57, 142.76, 140.37, 139.51, 137.47, 131.34, 130.97, 130.24, 129.97, 128.92, 127.65, 127.15, 126.10, 125.52, 125.31, 124.32, 123.75, 122.89, 122.16, 121.75, 120.93, 120.68, 120.48, 118.08, 35.75, 34.27, 32.00, 31.23$. IR (neat): $\nu=2957, 1613, 1588, 1462, 1363, 1261 \text{ cm}^{-1}$. HR-MS (MALDI): m/z : 924.4688 $[M]^+$ (calcd for $C_{72}H_{60}$: 924.4690).

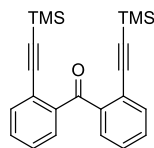
Compound 199c:



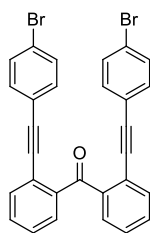
A degassed solution of **209** (128 mg, 0.138 mmol) in 1,2-dichloroethane (180 mL) was split in 6 different 50 mL round-bottom flasks. These solutions were heated to 70 °C, subsequently, in each flask was

added a degassed solution of FeCl₃ (75 mg) in dry CH₃NO₂ (500 μL) portionwise. These solutions were further stirred for 48 h at 70 °C. The 6 resulting mixtures were combined, diluted with CH₂Cl₂ (100 mL) and washed with brine (150 mL). The organic layer was then dried over Na₂SO₄ and the solvent was evaporated under vacuum. The crude material was purified by column chromatography (SiO₂, CH₂Cl₂/hexane 20:80) to give **199c** (124 mg, 96%) as an orange solid. ¹H NMR (500 MHz, CDCl₃): δ=8.94 (d, *J* = 1.8 Hz, 2H, H_f), 8.89 (d, *J* = 7.9 Hz, 2H, H_i), 8.75 (d, *J* = 8.0 Hz, 2H, H_g), 8.42 (d, *J* = 1.8 Hz, 2H, H_d), 8.37 (d, *J* = 2.0 Hz, 2H, H_j), 8.30 (d, *J* = 8.6 Hz, 2H, H_c), 8.20 (m, 4H, H_{b+k}), 7.97 (t, *J* = 7.7 Hz, 2H, H_h), 7.61 (dd, *J* = 8.8, 2.0 Hz, 2H, H_l), 1.66 (s, 18H, H_n), 1.48 (s, 18H, H_m). ¹³C NMR (126 MHz, CDCl₃): δ=149.98, 149.82, 134.53, 133.93, 131.01, 130.76, 130.49, 130.03, 130.00, 129.54, 129.53, 128.82, 128.25, 127.03, 126.68, 126.43, 125.23, 124.74, 124.35, 124.08, 122.48, 122.38, 122.13, 121.38, 121.36, 119.31, 119.16, 118.17, 116.99, 35.73, 35.27, 32.02, 31.62. IR (neat): ν=3390 (br), 2957, 2922, 2852, 1612, 1589, 1462, 1363, 1262, 1093, 1024 cm⁻¹. HR-MS (MALDI): *m/z*: 920.4383 [M]⁺ (calcd for C₇₂H₅₆: 920.4377).

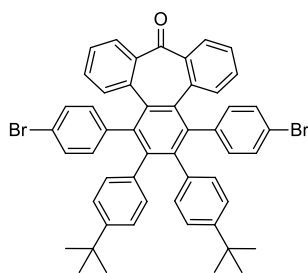
Compound 210



Under Ar, **201** (0.50 g, 1.47 mmol), PdCl₂(CH₃CN)₂ (57 mg, 0.22 mmol), CuI (42 mg, 0.22 mmol) and P(tBu)₃·HBF₄ (127 mg, 0.44 mmol) were suspended in a degassed mixture of THF/*i*Pr₂NH (2:5, 14 mL). Trimethylsilylacetylene (0.61 mL, 4.41 mmol) was added dropwise and the reaction mixture was stirred at r.t. for 3 h. The solvent was removed under reduced pressure. The crude was dissolved in CH₂Cl₂ (100 mL) and washed with NH₄Cl_(sat) (2 × 100 mL). The organic layer was dried over anhydrous Na₂SO₄ and the solvent was removed under vacuum. The crude was purified by flash column chromatography (SiO₂, Hexane/EtOAc 98:2) affording **210** (497 mg, 90%) as a yellow syrup. ¹H NMR (400 MHz, CDCl₃): δ=7.56 (dd, *J* = 7.6, 1.4 Hz, 2H), 7.51 (dd, *J* = 7.6, 1.4 Hz, 2H), 7.43 (td, *J* = 7.5, 1.6 Hz, 2H), 7.37 (td, *J* = 7.5, 1.6 Hz, 2H), 0.04 (s, 18H). ¹³C NMR (101 MHz, CDCl₃): δ=196.95, 141.88, 133.88, 131.04, 129.90, 128.38, 122.67, 102.50, 100.93, -0.13. HR-MS (ESI⁺): *m/z*: 375.1605 [M+H]⁺ (calcd. for C₂₃H₂₇OSi₂: 375.1595). IR (neat): 3069, 2964, 2159, 1667, 1247, 840 cm⁻¹.

Compound 211

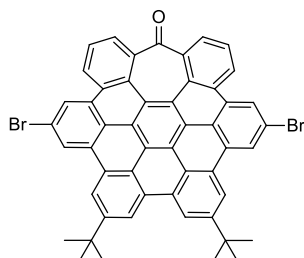
In a round bottom flask, **210** (1.51 g, 4.03 mmol), 1-bromo-4-iodobenzene (2.51 g, 8.86 mmol), PdCl₂(PPh₃)₂ (141 mg, 0.20 mmol) and CuI (77 mg, 0.40 mmol) were added and the system was purged with Ar. Subsequently, THF (32 mL), DBU (10 mL), Et₃N (5 mL) and H₂O (3 mL) were added and the mixture was heated at 70 °C under Ar atmosphere for 16 h. The resulting mixture was diluted with EtOAc (120 mL) and washed with NH₄Cl_(sat) (2 × 40 mL) and brine (15 mL). The organic layer was dried over anhydrous Na₂SO₄ and the solvent was evaporated under reduced pressure. The crude was purified by flash column chromatography (SiO₂, Hexane/EtOAc 95:5) affording **211** (1.46 g, 67%) as an orange foam. ¹H NMR (400 MHz, CDCl₃): δ=7.71 (d, *J* = 7.1 Hz, 2H), 7.60 (d, *J* = 7.1 Hz, 2H), 7.47 (m, 4H), 7.39 (d, *J* = 8.0 Hz, 4H), 7.08 (d, *J* = 8.0 Hz, 4H). ¹³C NMR (101 MHz, CDCl₃): δ=196.67, 141.14, 133.28, 133.06, 131.37, 131.31, 130.05, 128.45, 122.77, 122.36, 121.70, 94.28, 88.72. HR-MS (ESI⁺): *m/z*: 538.9644 [M+H]⁺ (calcd. for C₂₉H₁₇Br₂O: 538.9646). IR (neat): 3060, 2960, 2214, 1659, 1489, 1009, 822, 754 cm⁻¹.

Compound 212

Compound **211** (375 mg, 0.70 mmol) and Co₂(CO)₈ (308 mg, 0.90 mmol) were dissolved in anhydrous toluene (7 mL) under an Ar atmosphere. The mixture was stirred for 30 min at 110 °C. Then, 4,4'-di-*tert*-butyldiphenylacetylene (305 mg, 1.05 mmol) in anhydrous toluene (4 mL) was added over 30 min and finally the mixture was heated at 110 °C for 16 h. The solvent was removed under vacuum and the crude was purified by column chromatography (SiO₂, Hexane/CH₂Cl₂ 65:35). The resulting solid was precipitated with hexane (200 mL) yielding **212** (325 mg, 56%) as a white solid. ¹H NMR (500 MHz, CDCl₃): δ=7.41 (d, *J* = 7.6 Hz, 2H), 7.15 (m, 4H), 7.06 (d, *J* = 7.9 Hz, 2H), 7.01 (d, *J* = 8.4 Hz, 4H), 6.95 – 6.86 (m, 6H), 6.69 (d, *J* = 8.1 Hz, 2H), 6.33 (d, *J* = 8.4 Hz, 2H), 6.21 (d, *J* = 8.1 Hz, 2H), 1.11 (s, 18H). ¹³C NMR (126 MHz, CDCl₃): δ=200.14, 148.42, 146.04, 143.34, 140.38, 139.80, 136.60, 135.22, 134.50,

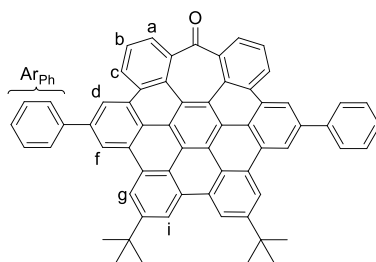
134.08, 133.14, 132.22, 131.19, 130.28, 129.73, 129.65, 128.89, 127.36, 124.38, 123.89, 122.82, 119.68, 34.13, 31.12. HR-MS (ESI⁺): m/z : 851.1520 [M+Na]⁺ (calcd. for C₅₁H₄₂Br₂ONa: 851.1495). IR (neat): 3028, 2961, 1738, 1689, 1490, 1363, 1012, 758 cm⁻¹.

Compound 213



In a round bottom flask, compound **212** (115 mg, 0.14 mmol) and DDQ (173 mg, 0.76 mmol) were dissolved in anhydrous CH₂Cl₂ (5 mL) under an Ar atmosphere. The mixture was cooled to 0 °C, then trifluoroacetic acid (0.25 mL) was added and the mixture was stirred at 0 °C for 10 min. The resulting solution was diluted with CH₂Cl₂ (4 mL) and silica gel was added. The solvent was removed under vacuum and the crude was purified by flash column chromatography (SiO₂, CH₂Cl₂/Hexane 6:4) affording **213** (59 mg, 52%) as a yellow solid. ¹H NMR (500 MHz, CDCl₃): δ=9.05 (s, 2H), 8.41 (d, J = 8.0 Hz, 2H), 8.34 (s, 2H), 7.93 (t, J = 7.7 Hz, 2H), 7.77 – 7.68 (m, 6H), 1.91 (s, 18H). ¹³C NMR (126 MHz, CDCl₃): δ = 201.88, 149.79, 141.63, 130.67, 129.35, 128.94, 128.85, 128.22, 127.30, 126.61, 125.06, 124.27, 122.75, 122.37, 122.07, 121.67, 121.44, 121.13, 120.09, 118.88, 36.03, 32.25. HR-MS (MALDI): m/z : 818.0794 [M]⁺ (calcd. for C₅₁H₃₂Br₂O: 818.0814). IR (neat): 2957, 1736, 1681, 1584, 1364, 1255, 759 cm⁻¹.

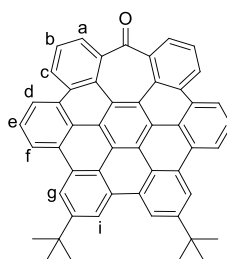
Compound 199d



Under an Ar atmosphere, **213** (42 mg, 0.051 mmol), phenyl boronic acid (62 mg, 0.51 mmol), K₂CO₃ (85 mg, 0.61 mmol) and Pd(PPh₃)₄ (30 mg, 0.026 mmol) were dissolved in degassed toluene (10 mL). Subsequently, a degassed mixture of H₂O/EtOH (1:1, 2 mL) was added. The mixture was refluxed for 20 h. The resulting suspension was diluted with H₂O (30 mL) and extracted with CH₂Cl₂ (3 × 50 mL). The combined extracts were dried over anhydrous Na₂SO₄ and the solvent was evaporated under vacuum. The crude material was purified by column chromatography (SiO₂, Hexane/CH₂Cl₂ 40:60) to yield **199d**

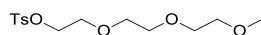
(29 mg, 70%) as a yellow solid. $^1\text{H NMR}$ (400 MHz, CDCl_3): $\delta=9.11$ (s, 2H, H_i), 8.87 (s, 2H, H_g), 8.74 (s, 2H, H_f), 8.60 (m, 2H, H_c), 8.46 (s, 2H, H_d), 7.81 (d, $J = 7.5$ Hz, 4H, H_{ArPh}), 7.61 – 7.52 (m, 8H, $\text{H}_{a+b+\text{ArPh}}$), 7.46 (t, $J = 7.3$ Hz, 2H, H_{ArPh}), 1.76 (s, 18H, H_{tBu}). $^{13}\text{C NMR}$ (126 MHz, CDCl_3): $\delta=202.27$, 150.05, 141.92, 141.20, 139.24, 130.81, 130.51, 130.02, 129.95, 129.13, 128.78, 127.83, 127.75, 127.73, 127.29, 127.20, 126.60, 124.30, 124.10, 122.85, 122.70, 121.66, 120.70, 119.65, 119.31, 118.79, 35.85, 32.07. HR-MS (ESI⁺): m/z : 837.3154 [$\text{M}+\text{Na}$]⁺ (calcd. for $\text{C}_{63}\text{H}_{42}\text{ONa}$: 837.3133); 815.3323 [$\text{M}+\text{H}$]⁺ (calcd. for $\text{C}_{63}\text{H}_{43}\text{O}$: 815.3314). IR (neat): 2921, 1677, 1464, 1256, 869, 760 cm^{-1} .

Compound 199e:



To a degassed solution of **213** (91 mg, 0.11 mmol) in toluene (6 mL) were added $\text{Pd}(\text{PPh}_3)_4$ (38 mg, 0.033 mmol), K_2CO_3 (306 mg, 2.22 mmol) and degassed mixture of EtOH/ H_2O (3:1, 4 mL). The mixture was refluxed for 16 h. Subsequently, $\text{HCl}_{(\text{aq})}$ (5%, 30 mL) was added and the resulting mixture was extracted with CH_2Cl_2 (3 \times 50 mL). The combined organic phases were dried over Na_2SO_4 and the solvent was removed under reduced pressure. The crude material was purified by column chromatography (SiO_2 , CH_2Cl_2 /hexane 60:40) to afford **199e** (41 mg, 56%) as a yellow solid. $^1\text{H NMR}$ (500 MHz, CDCl_3): $\delta=9.13$ (d, $J = 1.7$ Hz, 2H, H_i), 8.76 (d, $J = 1.7$ Hz, 2H, H_g), 8.54 (t, $J = 4.9$ Hz, 2H, H_c), 8.49 (d, $J = 7.6$ Hz, 2H, H_f), 8.23 (d, $J = 7.8$ Hz, 2H, H_d), 7.66 (m, 6H, H_{a+b+e}), 1.77 (s, 18H, H_{tBu}). $^{13}\text{C NMR}$ (126 MHz, CDCl_3): $\delta=202.60$, 149.97, 142.07, 130.89, 129.90, 129.81, 128.15, 127.24, 127.03, 126.82, 126.54, 124.76, 124.16, 123.87, 123.03, 122.71, 122.59, 120.56, 120.48, 119.45, 118.62, 35.84, 32.11. IR (neat): $\nu=2955$, 2924, 2862, 1671, 1609, 1588, 1392, 1362, 1336, 1255 cm^{-1} . HR-MS (ESI⁺): m/z : 663.2697 [$\text{M}+\text{H}$]⁺ (calcd for $\text{C}_{51}\text{H}_{35}\text{O}$: 663.2688).

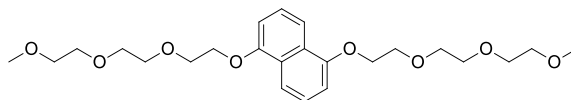
Compound 216:



To a solution of triethylene glycol monomethyl ether (1.24 g, 7.55 mmol) in anhydrous CH_2Cl_2 (30 mL) were added Et_3N (4.2 mL, 30 mmol), TsCl (2.88 g, 15.1 mmol), and a catalytic amount of DMAP. The mixture was stirred for 20 h at r.t.. Subsequently, the solution was concentrated to dryness and the crude material was purified by column chromatography (SiO_2 , hexane/EtOAc 20:80) to give **216** (2.199 g, 91%) a colorless oil. $^1\text{H NMR}$ (400 MHz, CDCl_3): $\delta=7.79$ (d, $J = 8.1$ Hz, 2H), 7.34 (d, $J = 8.0$ Hz, 2H), 4.16

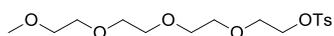
(t, $J = 4.9$ Hz, 2H), 3.68 (t, $J = 4.9$ Hz, 2H), 3.63 – 3.50 (m, 8H), 3.37 (s, 3H), 2.44 (s, 3H). Characterization data are in agreement with those from literature.⁴⁵⁴

Compound 214c:



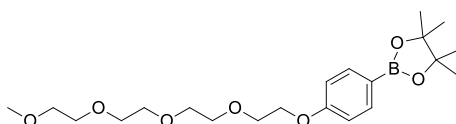
To a solution of 1,5-dihydroxynaphthalene (116 mg, 0.724) and **216** (922 mg, 2.89 mmol) in anhydrous acetone (15 mL) were added K_2CO_3 (500 mg, 3.62 mmol) and a catalytic amount of KI. The suspension was refluxed for 20 h. The solvent was removed under vacuum and the resulting crude material was purified by column chromatography (SiO_2 , hexane/EtOAc 30:70 to 10:90, then EtOAc) to yield **214c** (317 mg, 97%) a light brown solid. 1H NMR (500 MHz, $CDCl_3$): δ =7.86 (d, $J = 8.5$ Hz, 2H), 7.34 (t, $J = 8.0$ Hz, 2H), 6.84 (d, $J = 7.6$ Hz, 2H), 4.29 (t, $J = 4.6$ Hz, 4H), 3.99 (t, $J = 4.5$ Hz, 4H), 3.81 (m, 4H), 3.72 – 3.64 (m, 8H), 3.54 (m, 4H), 3.37 (s, 6H). ^{13}C NMR (126 MHz, $CDCl_3$): δ =154.48, 126.92, 125.18, 114.76, 105.80, 72.08, 71.14, 70.88, 70.74, 69.97, 68.06, 59.18. IR (neat): ν =2878, 1594, 1509, 1413, 1265, 1102, 1076, 971 cm^{-1} . HR-MS (ESI⁺): m/z : 475.2314 [$M+Na$]⁺ (calcd for $C_{24}H_{36}O_8Na$: 475.2308).

Compound 218:



To a solution of tetraethyleneglycol monomethyl ether (537 mg, 2.58 mmol) in anhydrous CH_2Cl_2 (20 mL) were added Et_3N (1.4 mL, 10 mmol), TsCl (983 mg, 5.16 mmol), and a catalytic amount of DMAP. The mixture was stirred for 20 h at r.t. Subsequently, the solution was concentrated to dryness and the crude material was purified by column chromatography (SiO_2 , hexane/EtOAc 20:80) to give **218** (921 mg, 99%) a colorless oil. 1H NMR (400 MHz, $CDCl_3$): δ =7.79 (d, $J = 7.7$ Hz, 2H), 7.34 (d, $J = 7.9$ Hz, 2H), 4.16 (m, 2H), 3.70 – 3.51 (m, 14H), 3.37 (s, 3H), 2.44 (s, 3H). Spectral data agree with those previously reported.⁴⁵⁵

Compound 219:



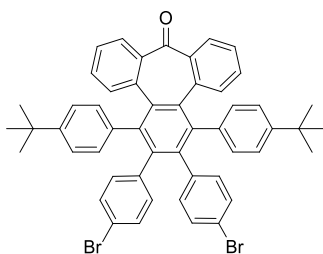
Under an inert atmosphere, to a solution of **218** (499 mg, 1.38 mmol) and 4-hydroxyphenylboronic acid pinacol ester (302 mg, 1.38 mmol) in dry DMF (8 mL) was added K_2CO_3 (190 mg, 1.38 mmol). The

⁴⁵⁴ S. Krakert, N. Ballav, M. Zharnikov, A. Terfort, *Phys. Chem. Chem. Phys.* **2010**, *12*, 507-515.

⁴⁵⁵ K. Kishimoto, T. Suzawa, T. Yokota, T. Mukai, H. Ohno, T. Kato, *J. Am. Chem. Soc.* **2005**, *127*, 15618-15623.

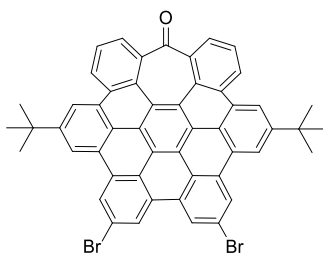
Under inert atmosphere, to 1-Bromo-4-iodobenzene (4.00 g, 14.1 mmol), PdCl₂(PPh₃)₂ (989 mg, 1.41 mmol), CuI (375 mg, 1.97 mmol), were added degassed CH₃CN (40 mL), degassed DBU (12.6 mL, 84.6 mmol) and degassed H₂O (100 μL). The solution was stirred at 70 °C for 5 min. Subsequently, trimethylsilylacetylene (1.00 mL, 7.05 mmol) was added and the solution was allowed to cool to r.t. The solution was further stirred for 20 h at r.t. and the solvent was removed under vacuum. The resulting solid was dissolved with CH₂Cl₂ (200 mL) and washed with NH₄Cl_(sat) (2 × 200 mL). The organic layer was dried over anhydrous Na₂SO₄ and the solution was concentrated to dryness. The crude material was purified by column chromatography (SiO₂, hexane/CH₂Cl₂ 80:20) to yield **221** (1.81 g, 76%) a white solid. ¹H NMR (400 MHz, CDCl₃): δ=7.49 (d, *J* = 8.2 Hz, 4H), 7.38 (d, *J* = 8.2 Hz, 4H). Spectral data agree with those previously reported.⁴⁵⁶

Compound 222:

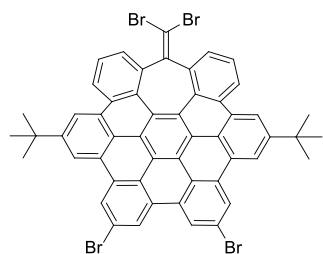


In three different flasks, a degassed solution of **206** (346 mg, 0.699 mmol) and Co₂(CO)₈ (310 mg, 0.909 mmol) in dry toluene (7 mL) was heated for 30 min at 110 °C. Subsequently, a degassed solution of **221** (352 mg, 1.05 mmol) in anhydrous toluene (4 mL) was added portionwise for 30 min. The solution was stirred for 18 h at 110 °C. The three solutions were combined and the solvent was removed under reduced pressure. The crude material was purified by column chromatography (SiO₂, hexane/CH₂Cl₂ 1:1). Fractions containing the product were combined and concentrated. The resulting solid was washed with hexane, filtered and collected to afford **222** (698 mg, 40%) a brown solid. ¹H NMR (500 MHz, CDCl₃): δ=7.39 (d, *J* = 7.5 Hz, 2H), 7.19 (s, 4H), 7.07 (t, *J* = 7.5 Hz, 2H), 7.00 – 6.91 (m, 6H), 6.84 – 6.74 (m, 6H), 6.34 (d, *J* = 8.0 Hz, 2H), 6.26 (d, *J* = 8.2 Hz, 2H), 1.15 (s, 18H). ¹³C NMR (126 MHz, CDCl₃): δ=200.38, 148.89, 146.12, 141.60, 141.29, 139.28, 137.21, 136.17, 134.80, 133.11, 133.07, 132.16, 130.43, 130.18, 129.48, 128.50, 127.12, 124.36, 124.31, 123.69, 119.96, 34.36, 31.32. IR (neat): ν=2959, 1685, 1593, 1490, 1389, 1265, 1070, 1012, 931, 835 cm⁻¹. HR-MS (ESI⁺): *m/z*: 851.1519 [M+Na]⁺ (calcd for C₅₁H₄₂OBr₂Na: 851.1500).

⁴⁵⁶ S. Cheng, L. Zong, K. Yuan, J. Han, X. Jian, J. Wang, *RSC Adv.* **2016**, *6*, 88403-88410.

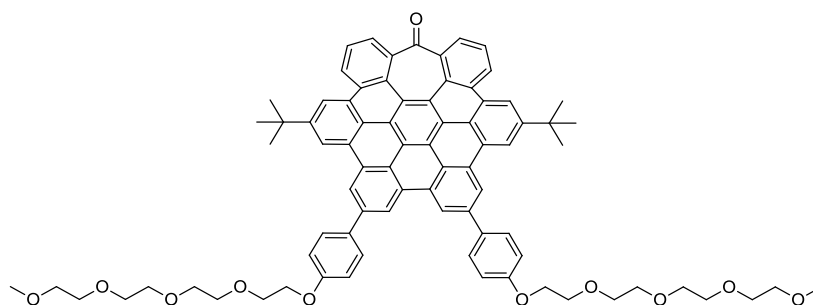
Compound 223:

In three different flasks under Ar, to a solution of **222** (115 mg, 0.138 mmol) and DDQ (173 mg, 0.761) in dry CH₂Cl₂ (6 mL) in a water-ice bath, was added CF₃SO₃H (0.250 mL). The solution was stirred for 10 min at 0 °C. The three solutions were combined and the solvent was evaporated under vacuum. The crude material was purified by column chromatography (SiO₂, hexane/CH₂Cl₂ 50:50 to 20:80) to yield **223** (132 mg, 39%) a yellow solid. ¹H NMR (500 MHz, CDCl₃): δ=8.82 – 8.75 (m, 6H), 8.69 (s, 4H), 7.84 (d, *J* = 6.5 Hz, 2H), 7.74 (t, *J* = 7.7 Hz, 2H), 1.68 (s, 18H). ¹³C NMR (126 MHz, CDCl₃): δ=202.19, 150.33, 142.47, 132.28, 131.18, 130.45, 128.39, 128.24, 127.71, 127.11, 126.26, 125.24, 125.15, 124.41, 124.35, 123.27, 123.20, 122.88, 122.31, 121.03, 120.25, 119.14, 35.81, 32.00. IR (neat): ν=2945, 2850, 1728, 1678, 1575, 1366, 1256 cm⁻¹. HR-MS (ESI⁺): *m/z*: 841.0760 [M+Na]⁺ (calcd for C₅₁H₃₂OBr₂Na: 841.0718).

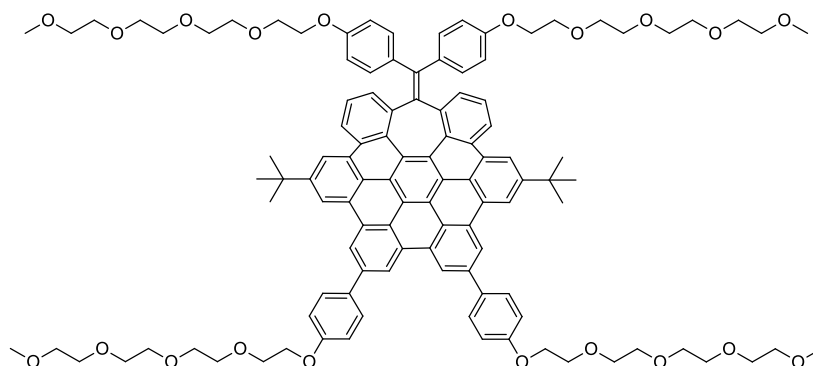
Compound 224:

In a sealed tube under Ar, a solution of **223** (26 mg, 0.030 mmol), PPh₃ (75 mg, 0.29 mmol) and CBr₄ (50 mg, 0.15 mmol) in anhydrous toluene (1.3 mL) was heated at 120 °C for 20 h. Then, the solvent was removed and the crude material was purified by column chromatography (SiO₂, hexane/CH₂Cl₂ 90:10 to 70:30) to yield **224** (25 mg, 84%) a yellow solid.

¹H NMR (500 MHz, CD₂Cl₂): δ=9.09 (d, *J* = 1.8 Hz, 2H), 9.06 (d, *J* = 1.8 Hz, 2H), 8.98 (d, *J* = 1.7 Hz, 2H), 8.95 (d, *J* = 7.5 Hz, 2H), 8.82 (d, *J* = 1.7 Hz, 2H), 7.98 (t, *J* = 7.4 Hz, 2H), 7.78 (dd, *J* = 7.3, 1.3 Hz, 2H), 1.67 (s, 19H). ¹³C NMR (126 MHz, CD₂Cl₂): δ=151.24, 147.33, 141.38, 133.14, 132.39, 131.24, 129.05, 128.77, 128.68, 128.16, 126.04, 125.53, 125.25, 124.64, 124.25, 123.96, 123.35, 123.06, 122.73, 121.61, 120.60, 119.76, 90.99, 36.20, 32.08. IR (neat): ν=2959, 2922, 2852, 1575, 1463, 1367, 1259 cm⁻¹. HR-MS (MALDI): *m/z*: 971.9226 [M]⁺ (calcd for C₅₂H₃₂Br₄: 971.9232).

Compound 200b:

To a degassed solution of **223** (21 mg, 0.024 mmol) and **219** (60 mg, 0.15 mmol) in toluene (5 mL) were added Pd(PPh₃)₄ (14 mg, 0.012 mmol), K₂CO₃ (40 mg, 0.29 mmol) and a degassed mixture of EtOH/H₂O (1:1, 1 mL). The mixture was refluxed for 18 h and was diluted with H₂O (30 mL). The aqueous layer was extracted with CH₂Cl₂ (3 × 30 mL). The combined organic layers were dried over anhydrous Na₂SO₄ and the solvent was removed under reduced pressure. The crude material was purified by column chromatography (SiO₂, CH₂Cl₂/MeOH 96:4) followed by gel permeation chromatography (Bio-Beads[®] SX1, CH₂Cl₂) and a preparative TLC (SiO₂, EtOAc) to afford **200b** (16 mg, 54%) a yellow solid. ¹H NMR (500 MHz, CDCl₃): δ=8.79 (d, *J* = 8.1 Hz, 2H), 8.69 (s, 2H), 8.61 (s, 2H), 8.43 (s, 2H), 8.01 – 7.90 (m, 4H), 7.82 (t, *J* = 7.6 Hz, 2H), 7.13 (d, *J* = 7.9 Hz, 4H), 6.71 (d, *J* = 8.0 Hz, 4H), 4.16 (t, *J* = 4.7 Hz, 4H), 3.99 (t, *J* = 4.4 Hz, 4H), 3.90 – 3.66 (m, 20H), 3.57 (m, 4H), 3.39 (s, 3H), 1.65 (s, 18H). ¹³C NMR (126 MHz, CDCl₃): δ=203.39, 158.02, 149.64, 142.67, 138.84, 133.24, 131.25, 130.39, 129.77, 129.65, 128.28, 128.09, 127.31, 126.19, 124.32, 123.63, 123.48, 123.05, 122.94, 120.84, 120.45, 120.26, 118.95, 118.12, 114.63, 72.11, 71.13, 70.95, 70.88, 70.86, 70.73, 70.03, 67.38, 59.20, 35.69, 32.07. IR (neat): ν=2955, 2889, 1682, 1608, 1514, 1455, 1371, 1247, 1115 cm⁻¹. HR-MS (ESI⁺): *m/z*: 1249.5483 [M+Na]⁺ (calcd for C₈₁H₇₈O₁₁Na: 1249.5442).

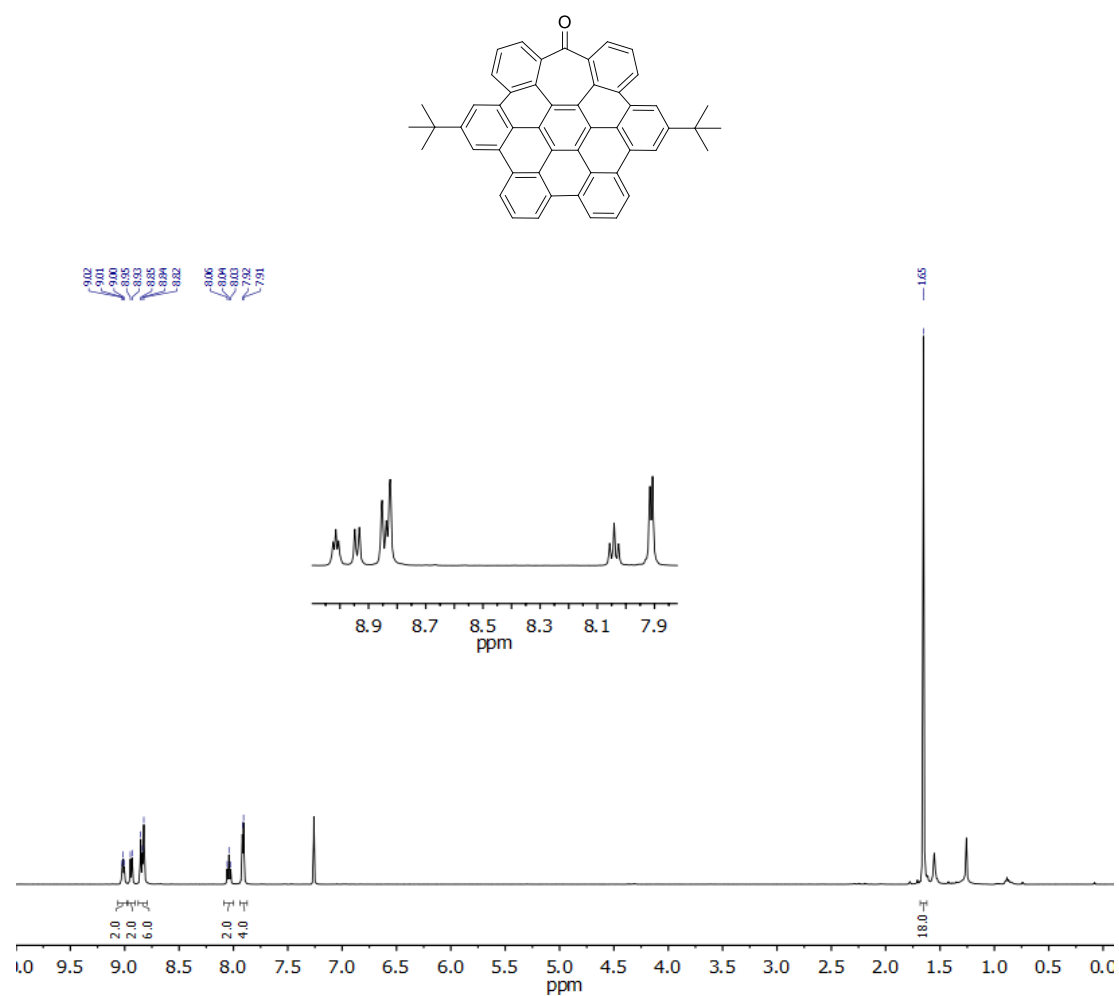
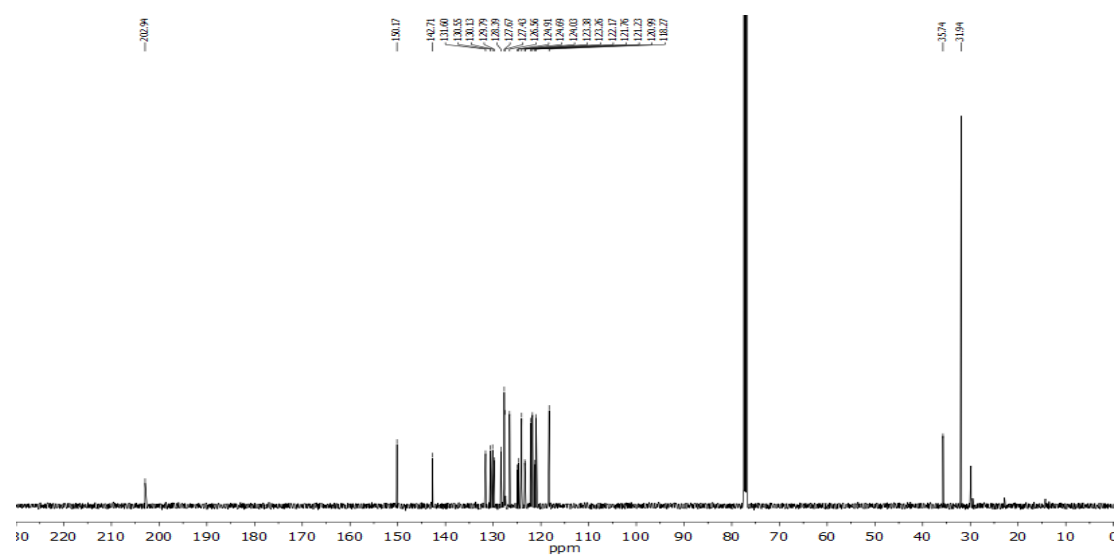
Compound 200c:

To a degassed solution of **224** (17 mg, 0.017 mmol) and **219** (85 mg, 0.21 mmol) in toluene (5 mL) were added Pd(PPh₃)₄ (16 mg, 0.014 mmol), K₂CO₃ (29 mg, 0.21 mmol) and a degassed mixture of EtOH/H₂O

(1:1, 1 mL). The mixture was refluxed for 20 h and was diluted with H₂O (50 mL). The aqueous layer was extracted with CH₂Cl₂ (3 × 30 mL). The combined organic layers were dried over anhydrous Na₂SO₄ and the solvent was evaporated under vacuum. The crude material was purified by column chromatography (SiO₂, CH₂Cl₂/MeOH 96:4) followed by two consecutive preparative TLC (firstly, SiO₂, CH₂Cl₂/MeOH 96:4; then SiO₂, EtOAc/MeOH 92:8) to give **200c** (4 mg, 13%) a yellow solid. ¹H NMR (500 MHz, CDCl₃): δ=9.37 (s, 2H), 9.12 (s, 2H), 8.95 (s, 2H), 8.88 (s, 2H), 8.68 (d, *J* = 7.5 Hz, 2H), 8.02 (d, *J* = 8.5 Hz, 4H), 7.68 (t, *J* = 7.6 Hz, 2H), 7.57 (d, *J* = 7.0 Hz, 2H), 7.25 (d, *J* = 8.5 Hz, 4H), 6.51 (d, *J* = 8.7 Hz, 4H), 6.31 (d, *J* = 8.6 Hz, 4H), 4.31 (t, *J* = 4.8 Hz, 4H), 3.98 (t, *J* = 4.9 Hz, 4H), 3.83 – 3.54 (m, 52H), 3.47 (m, 4H), 3.39 (s, 6H), 3.31 (s, 6H), 1.69 (s, 18H). ¹³C NMR (126 MHz, CDCl₃): δ=159.01, 156.85, 149.86, 142.59, 142.06, 140.20, 139.85, 138.93, 134.87, 133.53, 131.56, 131.31, 130.66, 130.31, 130.01, 129.99, 129.35, 128.87, 127.66, 126.03, 125.48, 124.34, 123.88, 122.89, 121.05, 120.63, 120.45, 120.43, 118.37, 115.52, 113.58, 72.13, 72.03, 71.08, 70.87, 70.84, 70.82, 70.72, 70.69, 70.60, 69.98, 69.73, 67.87, 67.12, 59.22, 59.13, 35.79, 32.04. IR (neat): ν=2922, 2870, 1727, 1606, 1510, 1454, 1372, 1246, 1110 cm⁻¹. HR-MS (ESI⁺): *m/z*: 1811.8667 [M+Na]⁺ (calcd for C₁₁₂H₁₂₄O₂₀Na: 1811.8584).

5.3. NMR spectra of target nanographenes

Compound 199a:

Figure 202. ^1H NMR (500 MHz, CDCl_3) spectrum of 199a.Figure 203. ^{13}C NMR (126 MHz, CDCl_3) spectrum of 199a.

Compound 199b:

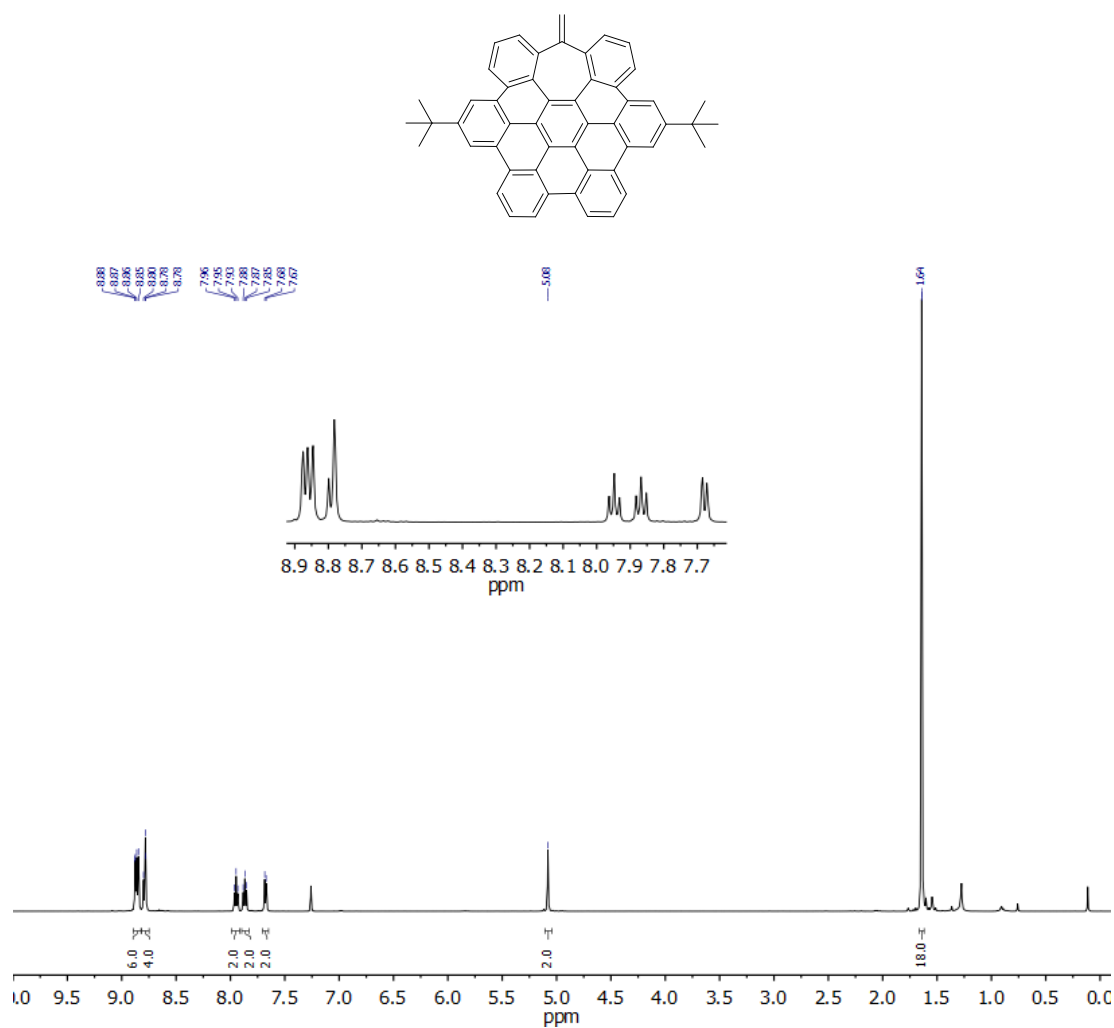


Figure 204. ^1H NMR (500 MHz, CDCl_3) spectrum of **199b**.

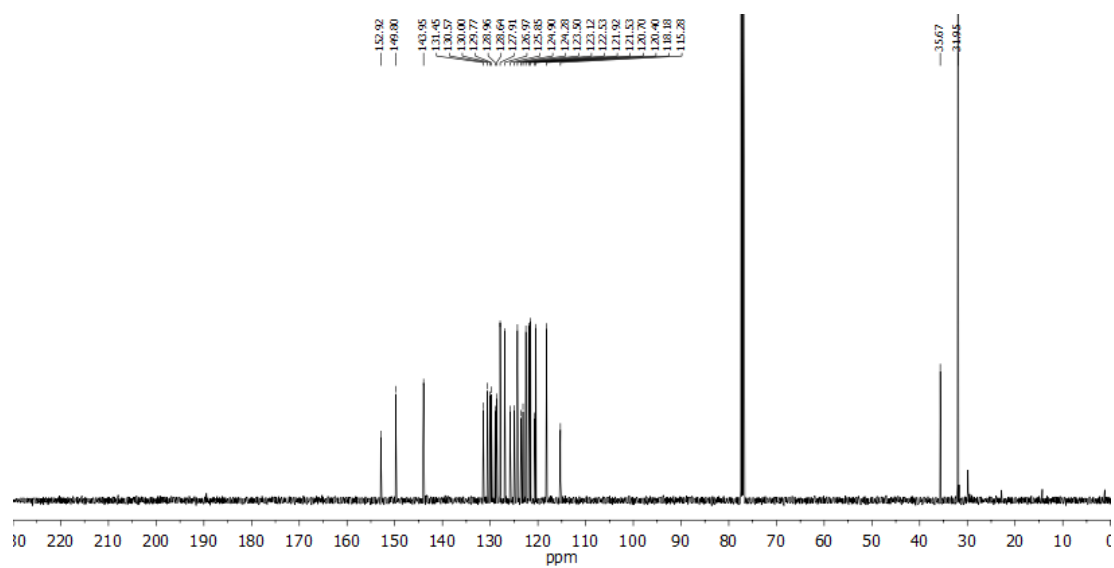
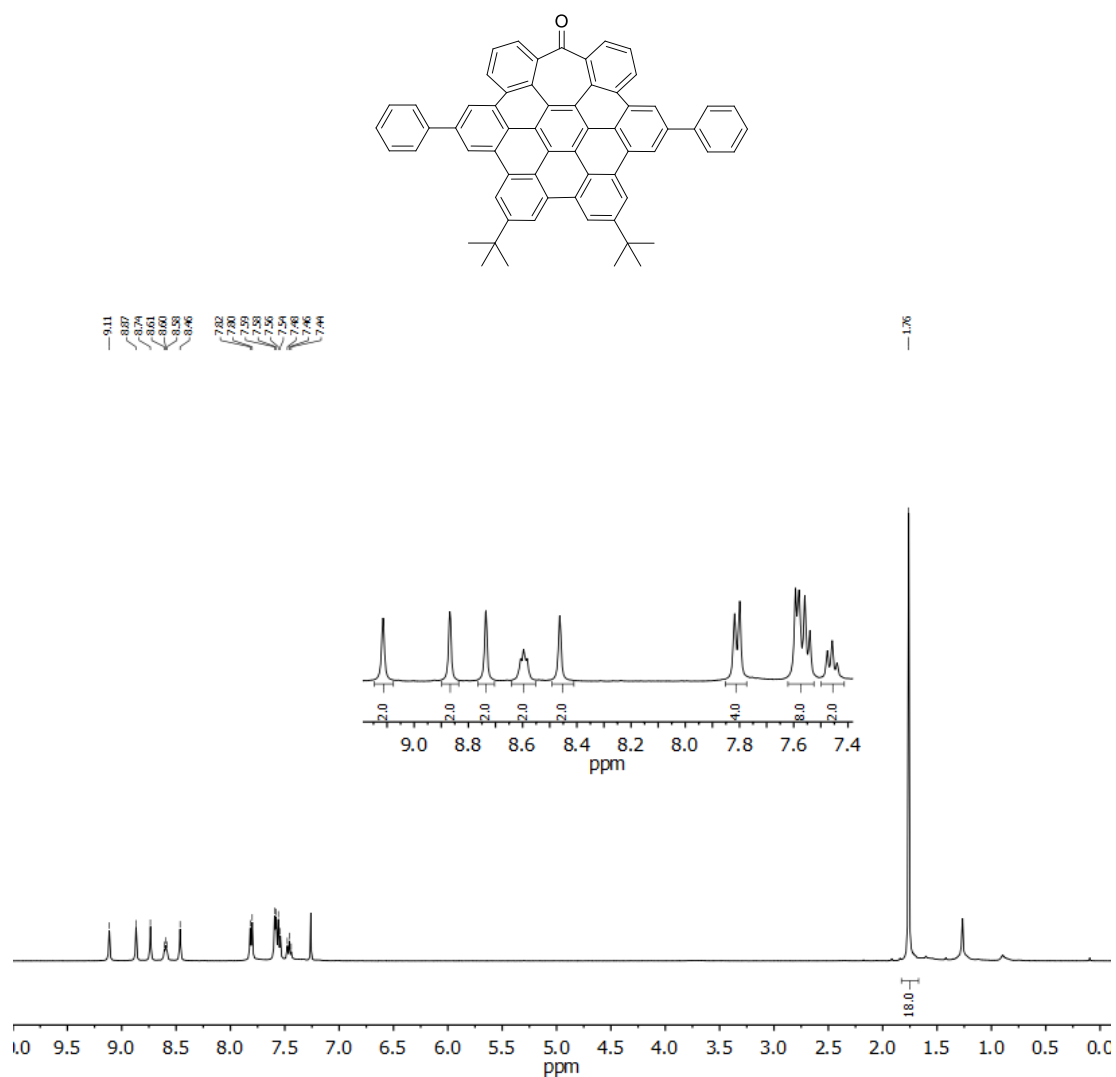
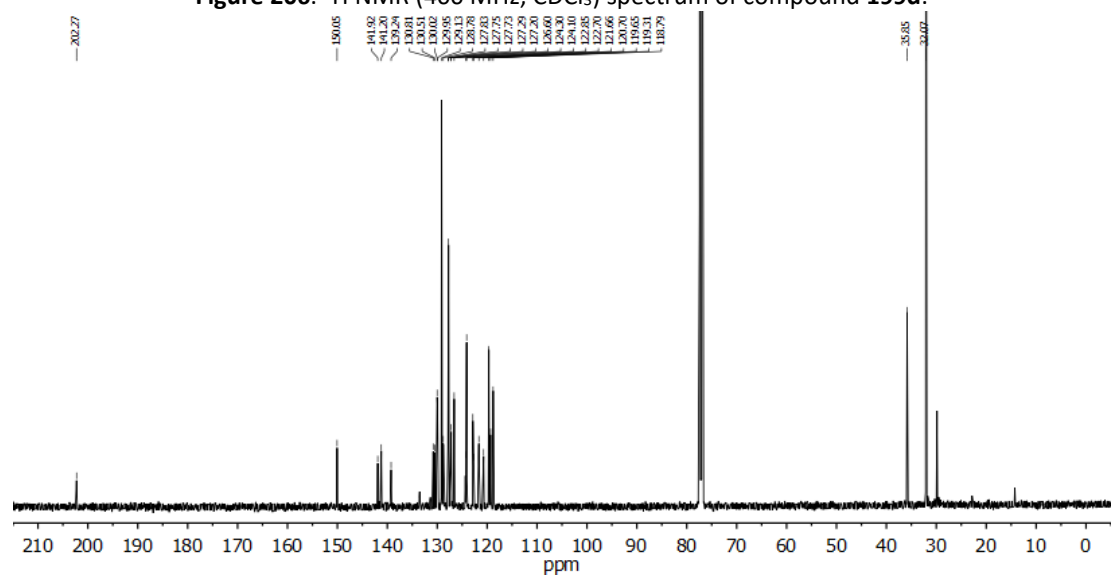


Figure 205. ^{13}C NMR (126 MHz, CDCl_3) spectrum of **199b**.

Compound 183d:

Figure 206. ^1H NMR (400 MHz, CDCl_3) spectrum of compound 199d.Figure 207. ^{13}C NMR (126 MHz, CDCl_3) spectrum of compound 199d.

Compound 183e:

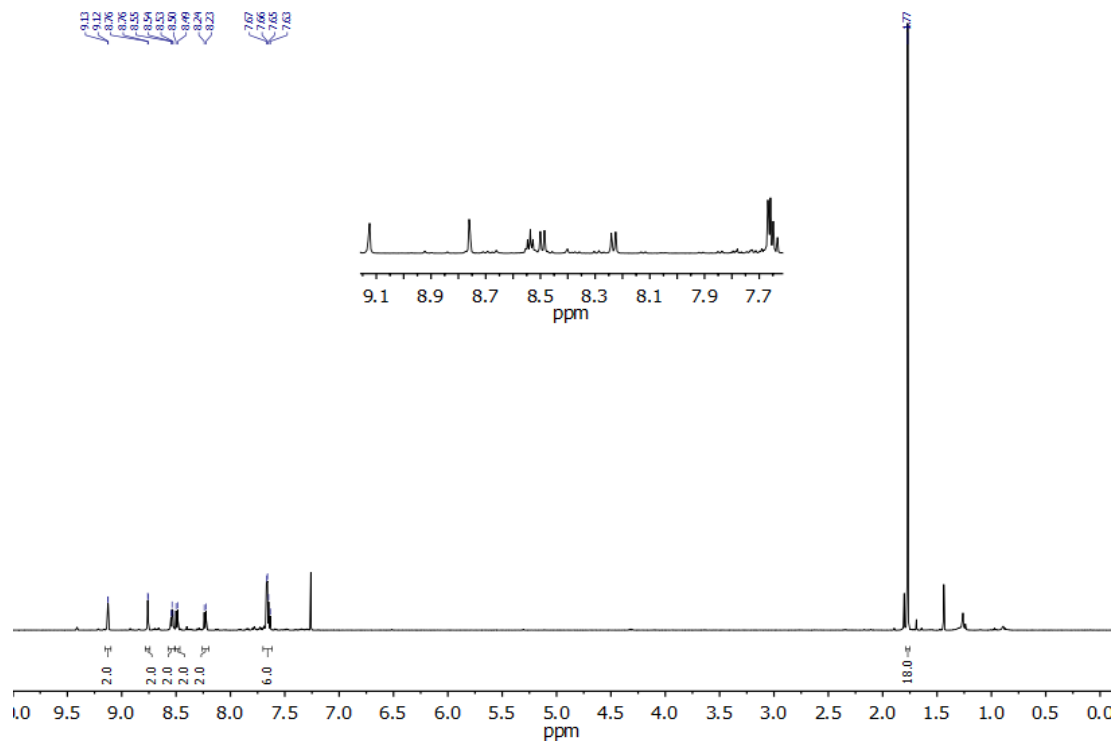
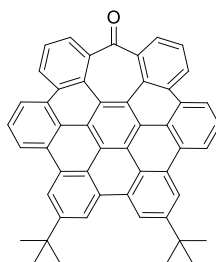


Figure 208. ^1H NMR (500 MHz, CDCl_3) spectrum of **199e**.

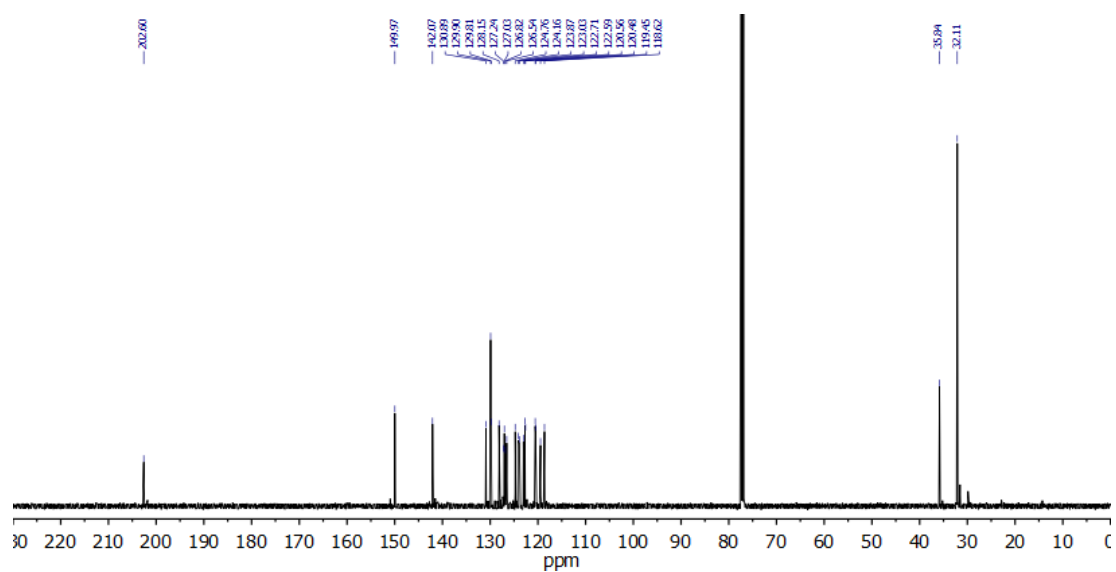


Figure 209. ^{13}C NMR (126 MHz, CDCl_3) spectrum of **199e**.

Compound 200c:

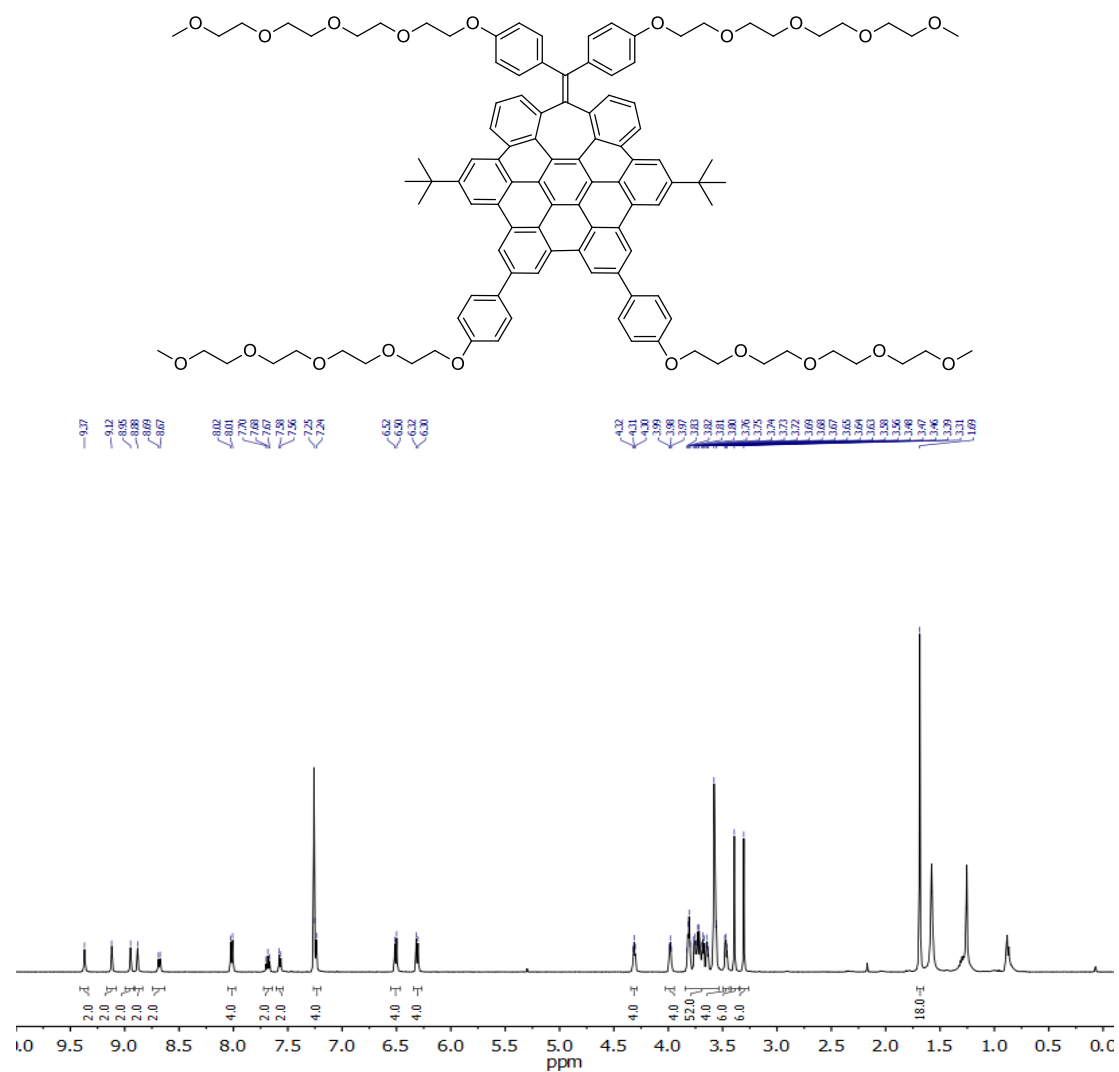


Figure 212. ^1H NMR (500 MHz, CDCl_3) spectrum of **200c**.

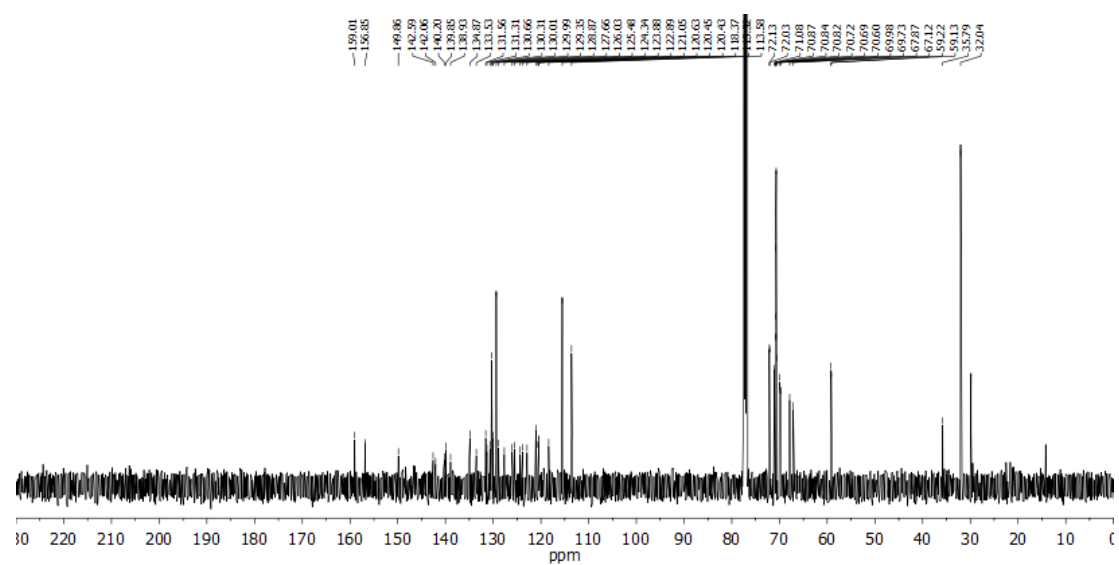


Figure 213. ^{13}C NMR (126 MHz, CDCl_3) spectrum of **200c**.

5.4. Self-association studies

Solutions of nanographenes at different concentrations (1 mM to 100 mM) were prepared in CDCl_3 using volumetric flasks and volumetric pipettes.

5.5. ^1H and ^{13}C titrations

5.5.1. PAHs binding NMR studies

For the titrations of planar PAHs, a solution of the corresponding nanographene was prepared in the CDCl_3 using a micropipette. Then, the solution of the corresponding PAH was prepared in another vial using the solution of the nanographene as solvent in order to maintain a constant concentration of nanographene during the titration experiment. The addition of the solution of PAH to the nanographene solution (450 μL) was achieved with Hamilton[®] syringes typically using the following order: 4 \times 3 μL , 2 \times 6 μL , 2 \times 12 μL , 3 \times 24 μL , 3 \times 120 μL . After each addition, the solution was shaken for 30 seconds and the ^1H NMR spectrum was recorded.

5.5.2. Fullerenes binding NMR studies

For the titrations of fullerene, a solution of the corresponding fullerene was prepared in the *o*-DCB- d_4 using a micropipette. Then, the solution of the corresponding nanographene was prepared in another vial using the solution of the fullerene as solvent in order to maintain a constant concentration of fullerene during the titration experiment. The addition of the solution of nanographene to the fullerene solution (500 μL) was achieved with Hamilton[®] syringes typically using the following order: 8 \times 16 μL , 2 \times 32 μL , 4 \times 64 μL (for C_{60}) and 1 \times 16 μL , 4 \times 32 μL , 4 \times 64 μL , 1 \times 90 μL (for C_{70}). After each addition, the solution was shaken for 30 seconds and the ^{13}C NMR spectrum was recorded.

5.6. Computational methods

DFT theoretical calculations were performed at the B3LYP/6-31G(d,p) and the $\omega\text{B97XD}/\text{def2SVP}$ levels for the five heptagon containing nanographene analogues using the Gaussian 09⁴⁵⁷ software package. Chloroform was used as a solvent, applying the polarizable continuum model with the integral

⁴⁵⁷ M. J. Frisch, G. W. Trucks, H. B. Schlegel, G. E. Scuseria, M. A. Robb, J. R. Cheeseman, G. Scalmani, V. Barone, B. Mennucci, G. A. Petersson, H. Nakatsuji, M. Caricato, X. Li, H. P. Hratchian, A. F. Izmaylov, J. Bloino, G. Zheng, J. L. Sonnenberg, M. Hada, M. Ehara, K. Toyota, R. Fukuda, J. Hasegawa, M. Ishida, T. Nakajima, Y. Honda, O. Kitao, H. Nakai, T. Vreven, J. A. Montgomery, Jr., J. E. Peralta, F. Ogliaro, M. Bearpark, J. J. Heyd, E. Brothers, K. N. Kudin, V. N. Staroverov, T. Keith, R. Kobayashi, J. Normand, K. Raghavachari, A. Rendell, J. C. Burant, S. S. Iyengar, J. Tomasi, M. Cossi, N. Rega, J. M. Millam, M. Klene, J. E. Knox, J. B. Cross, V. Bakken, C. Adamo, J. Jaramillo, R. Gomperts, R. E. Stratmann, O. Yazyev, A. J. Austin, R. Cammi, C. Pomelli, J. W. Ochterski, R. L. Martin, K. Morokuma, V. G. Zakrzewski, G. A. Voth, P. Salvador, J. J. Dannenberg, S. Dapprich, A. D. Daniels, O. Farkas, J. B. Foresman, J. V. Ortiz, J. Cioslowski, D. J. Fox, *Gaussian 09, Revision B.01, Gaussian, Inc., Wallingford CT 2010*.

equation formalism (IEFPCM) implemented in Gaussian 09.⁴⁵⁸ Frequency calculations were performed to confirm the optimized structures corresponded to an energy minimum.

⁴⁵⁸ J. Tomasi, B. Mennucci, R. Cammi, *Chem. Rev.* **2005**, *105*, 2999-3094.

General conclusions

- We developed an efficient methodology to synthesize rotaxanes based on a capping strategy employing the click aza and thia-Michael additions to vinyl sulfone or vinyl sulfonate groups (MAVS). This method showed to be versatile since it allows the formation of various [2]rotaxanes based on different recognition motifs and non-covalent interactions. It is worth noting that one of these rotaxanes, based on a pyromellitic core and a DNP38C10 macrocycle, exhibited interesting cation sensing properties. Moreover, the coupling-and-decoupling chemistry of the vinyl sulfonate group enabled the disassembly of a rotaxane previously generated through a MAVS reaction. Furthermore, the combination of both vinyl sulfone and vinyl sulfonate reactivities allowed us to perform the unidirectional transportation of a macrocycle through a rotaxane. Therefore, the MAVS reactions and the CAD chemistry of the vinyl sulfonate moiety proved to be novel, interesting and relevant tools for the field of mechanically interlocked molecules, that should be considered when designing new rotaxanes architectures.

- We demonstrated the synthesis and operation of an “ON/OFF” CPL switch based on a rotaxane architecture. For this purpose, we synthesized a fluorescence macrocycle bearing a 2,2'-bipyrene unit and incorporated it in a rotaxane featuring a chiral ammonium station and an achiral triazolium secondary station. We showed that the proximity of the ring to the chiral group of the molecule induced a preferential conformation resulting from a chiral information transfer between the macrocycle and the chiral unit of the thread. This phenomenon allowed us to evaluate the chiroptical properties of this MIM. Moreover, we examined its switching behaviour and proved that when the macrocycle went to the secondary station, the achiral triazolium salt, its chiroptical properties were turned “off” while when it returned to its original position around the chiral ammonium salt its chiroptical properties were again turned “on”. Thus, employing this pH switch, we succeeded to perform three complete “ON/OFF” cycles by consecutive additions of base and acid.

Remarkably, the fluorescence profiles and the quantum yield of this compound were essentially unaltered throughout the switching process. Therefore, the use of a rotaxane structure in order to build a CPL switch is an efficient strategy that should be taken into account for future CPL switches or other chiroptical switching systems that could be implemented in new type of materials or devices.

- Finally, we investigated for the first time the supramolecular chemistry of saddle-shaped nanographenes owning a heptagon ring on their structure. We found out that they were aggregating in solution and therefore, we were able to estimate the monomer-dimer equilibrium constant associated with this phenomenon. Furthermore, we studied their association properties with planar PAHs and fullerenes and we demonstrated that they mostly bind to them, especially to C₇₀. Thus, these molecules are promising for future supramolecular applications and could be potentially included in

MIMs or sensors. In addition, three amphiphilic negatively curved rotaxanes were also synthesized in order to study their ability to generate supramolecular materials such as nanotubes or nanofibres.

Now that we know more about this supramolecular chemistry, it is important to optimize the structure of these nanographenes, especially their peripheral substituents, in order to improve their self-association and host-guest properties. Furthermore, it is now possible to start thinking about new interlocked structures or materials that could feature these type of compounds.

LIST OF PUBLICATIONS

Part of the results presented in this thesis have been published in the papers listed below:

- “[2]Rotaxane End-Capping Synthesis by Click Michael-Type Addition to the Vinyl Sulfonyl Group”, Arthur H. G. David, Pablo García-Cerezo, Araceli G. Campaña, Francisco Santoyo-González, Victor Blanco, *Chem. Eur. J.* **2019**, *25*, 6170-6179.

Article highlighted in *Angewandte Chemie International Edition (Angew. Chem. Int. Ed.* **2019**, *58*, 6478-6482) and *Angewandte Chemie (Angew. Chem.* **2019**, *131*, 6546-6550).

- “A [2]Rotaxane-Based Circularly Polarized Luminescence Switch”, Arthur H. G. David, Raquel Casares, Juan M. Cuerva, Araceli G. Campaña, and Victor Blanco, *J. Am. Chem. Soc.* **2019**, *141*, 18064-18074.

- “A Heptagon-Containing HBC-Based Macrocyclic”, Vicente G. Jiménez, Arthur H. G. David, Juan M. Cuerva, Victor Blanco, Araceli G. Campaña, *Angew. Chem. Int. Ed.* **2020**, doi:10.1002/anie.202003785.

Article highlighted as **HOT PAPER**.